



Design Optimisation of Shape Memory Alloy Linear Actuator Applications

A thesis submitted in fulfilment of the requirements of the degree of Doctor of Philosophy

Jaronie Mohd Jani

MSc., Dipl.-Ing.(FH)

School of Aerospace, Mechanical and Manufacturing Engineering

College of Science, Engineering and Health

RMIT University

March 2016

ABSTRACT

Shape memory alloy (SMA) actuators have drawn much attention and interest in recent decades due to their unique properties; and, are expected to be increasingly integrated within commercial automotive applications. Key advantages of SMA actuators include: potentially simplified construction, whereby the SMA can act as both sensor and actuator simultaneously; compatibility with Joule heating and convective ambient cooling; and, potential mass advantages over competing actuation technologies. These attributes potentially allow for the development of simpler, more reliable and cost effective actuation systems with significant reduction in mechanical complexity and size. SMA is readily available in commercial quantities and exhibits high wear resistance and durability, which make it an ideal candidate for application in automotive grade applications. Despite these identified advantages, SMA actuators are subject to a series of technical challenges associated with:

- Relatively small strain (displacement or stroke)
- Achievable frequency (actuation speed)
- Controllability (and stability)
- Positional accuracy
- Energy efficiency

These technical challenges contribute to a relatively low success rate of commercial SMA actuator applications; and, provide motivation for this program to generate relevant research outcomes that enhance the commercialisation of SMA actuators. An extensive literature review of over 500 journal and patent documents was conducted to provide a clear roadmap for the commercial imperatives for SMA design. The formulated research methodology identifies milestones required for achieving the research objectives, which were addressed as research themes. Based on this literature review, the following research themes were identified:

- Design methods to resolve SMA actuator limitations
- Development of simple and practical numerical models for SMA actuator response
- Data for SMA linear actuator design

Specific research contributions within these themes are presented within the thesis, with the objective of enhancing the commercial application of shape memory alloy (SMA) linear actuators, and include:

- A comprehensive analysis of SMAs: history, commercial applications, strength and limitations, design challenges and opportunities.
- A novel investigation of transient heat transfer scenarios for cylindrical systems associated with their crossover and critical radii.
- Development of novel latent heat models for analytical and numerical applications, and proposal of readily applied activation and deactivation charts compatible with the requirements of SMA actuator designers.
- A novel investigation of the morphological effects of SMA-pulley systems (i.e. pulley diameter, SMA and lagging diameter) on structural and functional fatigue.

DECLARATIONS

I certify that except where due acknowledgement has been made, the work is that of the author alone; the work has not been submitted previously, in whole or in part, to qualify for any other academic award; the content of the thesis is the result of work which has been carried out since the official commencement date of the approved research program; any editorial work, paid or unpaid, carried out by a third party is acknowledged; and, ethics procedures and guidelines have been followed.

Jaronie Mohd Jani

March 2016

ACKNOWLEDGEMENTS

First and foremost, I would like to show my gratitude for the extensive support of my supervisors, Assoc. Prof. Martin Leary and Prof. Aleksandar Subic for their expertise, continuous support, advice and encouragement, which have been immensely valuable throughout my research program.

Additionally, I would also like to thank all my fellow researchers from the RMIT applied optimisation group, the technical support and workshop staffs for their advice, support and friendship.

I would like to acknowledge the support of Dr. Sunan Huang, a research fellow at RMIT University and Dr. Mark Gibson from the Commonwealth Scientific and Industrial Research Organisation (CSIRO), as well as their valuable cooperation.

Special thanks are also conveyed to Universiti Kuala Lumpur (UniKL) and Majlis Amanah Rakyat (MARA) for their financial support.

Finally, I am especially thankful to my parents and family for their relentless inspiration, support, and understanding towards the completion of this thesis.

PUBLICATIONS

The following publications are associated with this research:

Journal articles:

The critical and crossover radii on transient heating,

S Huang, **J Mohd Jani**, M Leary, A Subic,
Applied Thermal Engineering 60(1), 325-334, 2013.
DOI: 10.1016/j.applthermaleng.2013.06.052

A review of shape memory alloy research, applications and opportunities,

J Mohd Jani, M Leary, A Subic, MA Gibson,
Materials & Design 56, 1078-1113, 2014.
DOI: 10.1016/j.matdes.2013.11.084
(Top cited Materials & Design article and Top 25 Science Direct article for Engineering in 2014)

Numerical modeling of Shape Memory Alloy linear actuator,

J Mohd Jani, S Huang, M Leary, A Subic,
Computational Mechanics 53(3), 443-461, 2015.
DOI: 10.1007/s00466-015-1180-z

Fatigue of Ni-Ti SMA-pulley system using Taguchi and ANOVA,

J Mohd Jani, M Leary, A Subic, Smart Materials & Structures 25 (5), 057001, 2016.
DOI: 10.1088/0964-1726/25/5/057001

Shape memory alloy applications in automotive,

J Mohd Jani, M Leary, A Subic, Applied Mechanics and Materials 663, 248-253, 2014.
DOI: 10.4028/www.scientific.net/AMM.663.248

Analysis of convective heat transfer coefficient on shape memory alloy actuator under various ambient temperatures with finite difference method,

J Mohd Jani, S Huang, M Leary, A Subic,
Applied Mechanics and Materials 736, 127-133, 2015.
DOI: 10.4028/www.scientific.net/AMM.736.127

TABLE OF CONTENTS

1. Introduction	1
1.1 Background	1
1.2 Introduction and motivation.....	1
1.3 Research scope.....	3
1.4 Research themes.....	4
1.5 Research contributions	6
1.6 Thesis overview	7
2. Shape Memory Alloys review	10
2.1 Chapter summary	10
2.2 Shape memory alloy	10
2.3 Shape memory effect and pseudoelasticity	12
2.4 Shape memory alloy development.....	16
2.4.1 SMA development history	16
2.4.2 Recent shape memory alloy development	18
2.5 Designing with shape memory alloys.....	19
2.5.1 Design advantages	19
2.5.2 Design challenges.....	22
2.6 Other forms or types of shape memory materials	27
2.6.1 High temperature shape memory alloys.....	27
2.6.2 Magnetic shape memory alloys.....	28
2.6.3 Shape memory material thin film.....	29
2.6.4 Shape memory polymers	30
2.6.5 Miscellaneous	32
2.7 Shape memory alloys applications	33
2.7.1 Automotive applications	35
2.7.2 Aerospace applications	42
2.7.3 Robotic applications	46
2.7.4 Biomedical applications.....	50
2.8 Opportunities and future direction of shape memory alloy applications	57
2.8.1 Future trends.....	58
2.8.2 Future directions	60
2.9 Discussion	62
2.10 Conclusion.....	63
2.11 Future development.....	64
3. Design of SMA linear actuators	65

3.1	Chapter summary	65
3.2	Introduction	65
3.3	Design of SMA actuator applications	66
3.3.1	The SMA actuator design process	66
3.4	Design requirements	68
3.5	Design specifications	69
3.5.1	Material selection	69
3.5.2	Loading configurations	70
3.5.3	SMA geometry	70
3.6	SMA linear actuator basic designs	72
3.6.1	One-directional actuator design	73
3.6.2	Bias-force actuator design	73
3.6.3	Antagonistic design	75
3.7	SMA design approaches	76
3.7.1	Power improvement designs	79
3.7.2	Displacement improvement designs	82
3.7.3	Bandwidth improvement designs	87
3.7.4	Optimisation with electronic controllers	96
3.8	Discussions and conclusions	97
4.	Numerical modelling of SMA linear actuators	99
4.1	Chapter summary	99
4.2	Introduction	100
4.3	SMA linear actuators numerical modelling	100
4.3.1	One and multi-dimensional models	102
4.3.2	Heat transfer mathematical models	102
4.3.3	Stress-strain constitutive models	104
4.3.4	Hysteresis model and phase fractions	109
4.4	Numerical methods	110
4.4.1	Finite difference method	110
4.4.2	Finite element method	116
4.4.3	Finite volume method	116
4.5	Discussion	117
4.6	Conclusion	119
5.	The critical and crossover radii on transient heating	120
5.1	Chapter summary	120
5.2	Introduction	120

5.2.1	Steady-state heat transfer of cylindrical systems	123
5.2.2	Critical and crossover radii	124
5.3	Analysis	125
5.3.1	Transient heat transfer analysis of cylindrical systems	125
5.3.2	Finite difference equation model	126
5.3.3	Simulation scenario	126
5.4	Results and discussion	127
5.4.1	Validation of FDE Model	127
5.4.2	Transient solution for insulated pipe	129
5.4.3	Case A simulation ($D = 50\%$, $P = 2.0s$)	130
5.4.4	Case B Simulation ($D = 90\%$, $P = 2.0s$)	135
5.4.5	Case C Simulation ($D = 50\%$, $P = 0.2s$)	137
5.5	Conclusions	140
6.	Development of one-dimensional numerical model for SMA linear actuators	142
6.1	Chapter summary	142
6.2	Introduction	142
6.3	Existing 1-D heat transfer models	143
6.4	New 1-D numerical model development	144
6.4.1	Energy balance model	145
6.4.2	Analytical heat transfer model	148
6.4.3	Finite difference method	149
6.4.4	Alternative latent heat models	152
6.4.5	Fast prediction with simplified analytical model and graphical solution charts 153	
6.5	Process flow of numerical models	157
6.6	Experimental setup	160
6.7	Results and discussion	161
6.7.1	Identification of the modelling parameters	161
6.7.2	Numerical modelling stages	163
6.7.3	Numerical modelling validation	167
6.7.4	SMA linear actuator performance analysis	169
6.8	Conclusion	172
7.	Structural and functional fatigue of Ni-Ti SMA-Pulley system using Taguchi and ANOVA	173
7.1	Chapter summary	173
7.2	Introduction	174
7.3	Fatigue failure modes	177

7.4	Shape memory alloy actuator and pulley system.....	180
7.4.1	Drive element and pulley	181
7.5	Design of Experiments.....	184
7.5.1	Full-factorial design of experiments.....	184
7.5.2	Fractional-factorial design of experiments.....	185
7.5.3	Taguchi method and ANOVA	185
7.6	Fatigue factors and effect levels selection	187
7.7	Experimental contribution	188
7.7.1	SMA failure definition	188
7.7.2	Prediction of activation duration	189
7.7.3	Main experiment.....	190
7.7.4	Control experiment.....	191
7.7.5	Experimental apparatus	191
7.8	Results.....	192
7.8.1	Graphical results interpretations.....	193
7.8.2	Linear fit analysis	196
7.8.3	Visual and microscopy inspection on fracture surface	198
7.8.4	Taguchi method and ANOVA analysis	199
7.8.5	SMA-pulley system optimum configurations and confirmation test	206
7.10	Commercially optimal SMA-pulley configuration test.....	207
7.12	Conclusion.....	208
8.	Conclusion	209
8.1	Contribution by research theme.....	210
8.1.1	Research Theme 1: Design methods to resolve SMA actuator limitations ..	210
8.1.2	Research Theme 2: Development of simple and practical numerical models for SMA actuator response.....	211
8.1.3	Research Theme 3: Data for SMA linear actuator design	212
8.2	Future work.....	213
9.	References.....	215
10.	Appendices	254

LIST OF FIGURES

Figure 1.1 - Research Methodology	2
Figure 1.2 - Thesis Map	5
Figure 2.1 - SMA phases and crystal structures	12
Figure 2.2 - Flexinol NiTi SMA (HT) phase transformation (Dynalloy Inc., 2007).....	13
Figure 2.3 - A typical DSC thermograph of SMA (Mohd Jani <i>et al.</i> , 2015b).....	14
Figure 2.4 - SMA publications and US patents from January 1990 to June 2013.....	17
Figure 2.5 - Number of "Shape Memory Alloy" articles and patents by years-group (Mohd Jani, Leary, Subic, <i>et al.</i> , 2014)	17
Figure 2.6 - Global market forecast for smart materials for 2010 – 2016.....	19
Figure 2.7 - SMA actuator element features (S. Langbein, 2009).....	22
Figure 2.8 - Fatigue lifetime for Smartflex 76 under different stress-strain	26
Figure 2.9 - Maximum strain and specific energy versus maximum bandwidth for different classes of active materials (J Ma <i>et al.</i> , 2010)	28
Figure 2.10 - NiTi thermovisible rate (TVR) springs applications, image based on	34
Figure 2.11 - EAGLE mirror prototype (Luchetti <i>et al.</i> , 2009).....	35
Figure 2.12 - Emerging General Motors' SMA applications, image based on	38
Figure 2.13 - Other commercial SMA applications in the automotive domain, image based on (Bellini <i>et al.</i> , 2009; Brugger <i>et al.</i> , 2006; Strittmatter <i>et al.</i> , 2009; EA Williams <i>et al.</i> , 2010).....	39
Figure 2.14 - Operating temperature range for automobiles applications and the transformation temperatures for selected commercially available and developed SMAs, image based on (Beyer & Mulder, 1994; Hodgson <i>et al.</i> , 1990; D. Stoeckel, 1990; JV Humbeeck <i>et al.</i> , 1991).....	41
Figure 2.15 - Boeing's variable geometry chevron (VGC) (Oehler <i>et al.</i> , 2012).....	44
Figure 2.16 - Wing morphing with antagonistic SMA actuators.....	45
Figure 2.17 - Prosthetic hand powered by SMA actuators (Chee Siong <i>et al.</i> , 2005b)	48
Figure 2.18 - Micro-gripper with SMA actuator (Mohamed Ali & Takahata, 2010)	49
Figure 2.19 - Festo BionicOpter – Inspiration dragonfly flight (Festo, 2013)	50
Figure 2.20 - The stress versus strain relationship for superelastic nitinol, stainless steel, bone and tendon tissues (NB Morgan, 2004)	53
Figure 2.21 - a) Model of stent laser cut from nitinol tubing. b) The radial resistance force and chronic outward force as a function of superelastic hysteresis loop	54
Figure 2.22 - SMA active catheter (Y. Haga <i>et al.</i> , 1998; Tung <i>et al.</i> , 2008).....	54
Figure 2.23 - Muscle like NiTi SMA (S. Kim <i>et al.</i> , 2009; Stirling <i>et al.</i> , 2011).....	55
Figure 2.24 - Artificial heart support devices with SMA fibre (Shiraishi <i>et al.</i> , 2007)	56
Figure 2.25 - An 'alterable stiffness' implant (Pfeifer <i>et al.</i> , 2013)	56
Figure 2.26 - Comparison of stress and strain of new developed SMA with other materials (Ashby, 2011; Ji Ma & Karaman, 2010)	59
Figure 2.27 - Current situation and proposed approach for SMA in product design	61
Figure 3.1 – SMA actuator design process, modified from (Pugh, 1991).....	67

Figure 3.2 – Typical SMA linear actuator designs, image based on	72
Figure 3.3 – SMA with one-directional actuator design, image based on	73
Figure 3.4 – SMA with a bias-force actuator design, image based on	74
Figure 3.5 - Linear and revolute joint configuration of SMA with bias spring and antagonistic design, image based on (Teh, 2008)	75
Figure 3.6 - Arrangement of SMA wires on end plate, image based on.....	79
Figure 3.7 - SMA bundle current versus Voltage requirement for number of paths	80
Figure 3.8 - Influence of a sigma-shaped-pulley on the bias torque, image based on (Reynaerts & Brussel, 1998).....	81
Figure 3.9 - Linear smart actuator with curvature beams, image based on (Elwaleed <i>et al.</i> , 2007).....	82
Figure 3.10: Analytical result for end displacement with different number of segments (Elwaleed <i>et al.</i> , 2007)	83
Figure 3.11 - Mini-linear-actuator with SMA winding wire on two pulleys.....	84
Figure 3.12 - FUTURIS SMA actuator prototype	84
Figure 3.13 - Miga Motor Company modular SMA linear actuator design concept; image based on (MA Gummin <i>et al.</i> , 2007; MigaMotors)	85
Figure 3.14 - The Starsys Research & APL mini actuator versus Donellan's mini actuator (Donnellan, 2005)	86
Figure 3.15 - Flow development for an inclined cylinder, based on (Heo & Chung, 2012).....	88
Figure 3.16 - Prandtl number and air properties relationship with various ambient temperatures (Mohd Jani <i>et al.</i> , 2015a)	89
Figure 3.17 – Illustrated natural, forced and mixed convection flow scenarios near hot SMA wire, image based on (Incropera & DeWitt, 1985; Çengel & Ghajar, 2011)	92
Figure 3.18 – Surface area-to-volume ratio versus diagonal length.....	94
Figure 4.1 - Design optimisation process with numerical modelling, modified from (Bathe, 2006).....	101
Figure 4.2 - Typical stress-temperature profile for constitutive models.....	106
Figure 4.3 - Typical SMA stress-strain relationship indicating Young's Modulus (E), critical stresses (σ_{cr}), martensitic residual strain (ϵ_{res}) and maximum recoverable strain (ϵ_L) (De la Flor <i>et al.</i> , 2006; Liang & Rogers, 1997).	107
Figure 4.4 - SMA hysteresis model, based on	109
Figure 4.5 - Forward difference equation. Subscript n represent the space increments, superscript t represents time increments (red are the unknown temperature nodes) (Mohd Jani <i>et al.</i> , 2015b)	112
Figure 4.6 - Backward difference equation. Subscript n represent the space increments, superscript t represents time increments (red are the unknown temperature nodes) (Mohd Jani <i>et al.</i> , 2015b)	112
Figure 4.7 - Central difference equation. Subscript n represent the space increments, superscript t represents time increments (red are the unknown temperature nodes) (Mohd Jani <i>et al.</i> , 2015b)	113
Figure 4.8 - Sample of a matrix form for finite difference equation	114

Figure 4.9 – Comparison of 2D-grids for common numerical method on cylindrical geometry	118
Figure 5.1 - Cylindrical heat transfer system (S. Huang, JM. Jani <i>et al.</i> , 2013).	123
Figure 5.2 - Ratio of insulated to bare heat transfer rate (q_{ins}/q_{bare}) versus thermal material radius ($r_{bare} = 0.025m$).....	128
Figure 5.3 - Transient temperature of insulated pipe cross section	128
Figure 5.4 - Pipe temperature versus time (Case A, B and C)	129
Figure 5.5 - Maximum observed cycle average heat transfer rate on pipe surface for Case A, and the corresponding thermal material radius (for r in range of 0.050 to 0.060m). ...	131
Figure 5.6 - Cycle average heat transfer rate (\hat{q}) on the pipe and thermal material surface for Case A ($r_{therm} = r_{cross} = 0.1757m$).	132
Figure 5.7 - Heat transfer rate on pipe surface versus thermal material radius for Case A. Upper: $N = 1$ to 1,000 cycles, and radius range including r_{cross} . Lower: $N = 1,000$ to 6,000 cycles, and radius range including r_{cr}	134
Figure 5.8 - Maximum observed cycle average heat transfer rate on pipe surface for Case B, and the corresponding thermal material radius (for r in the range of 0.050 to 0.060 m).	136
Figure 5.9 - Cycle average heat transfer rate (\hat{q}) on the pipe and thermal material surface for Case B ($r_{therm} = r_{cross} = 0.1757m$).	136
Figure 5.10 - Heat transfer rate on pipe surface versus thermal material radius for Case B. Upper: $N = 1$ to 1,000 cycles, and radius range including r_{cross} . Lower: $N = 1,000$ to 6,000 cycles, and radius range including r_{cr}	139
Figure 6.1 - SMA geometry and boundary conditions	144
Figure 6.2 - Schematic diagram of proposed numerical model	144
Figure 6.3 - Energy balance for SMA actuator	145
Figure 6.4 - Sample of a matrix form for finite difference equation	150
Figure 6.5 – Response charts creation concept.....	156
Figure 6.6 – Process flow of simplified analytical model	157
Figure 6.7 - Process flow of analytical model.....	158
Figure 6.8 - Process flow of FDE model	159
Figure 6.9 - SMA linear actuator experimental setup	160
Figure 6.10 - Identification of stress-induced modeling parameters (C_A and C_M) from experimental data	162
Figure 6.11 - SMA numerical model fine-tuning of h with reference to experimental data	163
Figure 6.12 - SMA thermal cycle with various heat transfer models	164
Figure 6.13 - Comparison of heat transfer model responses and their effective specific heat and thermal conductivity variation during the phase transition.....	166
Figure 6.14 - SMA linear actuator under natural cooling, various ambient temperatures and pre-stresses	167
Figure 6.15 - Numerical simulation of SMA linear actuator activation duration versus current density	170

Figure 6.16 - Numerical simulation of SMA linear actuator deactivation duration versus convective heat transfer coefficient.....	170
Figure 6.17 - Forced convection effect on SMA performance.....	171
Figure 7.1 - Schematic representation of SME on SMA pulley system.....	174
Figure 7.2 - SMA pulley system advantage with approximately similar packaging size..	180
Figure 7.3 - Recommended sheave design	181
Figure 7.4 - Effect of angle of wrap on drive element with a pulley system.....	182
Figure 7.5 – Numerical results of SMA linear actuators under variable load and activation duration (based on Table 7.5)	190
Figure 7.6 - Experimental apparatus for SMA-pulley system. Actuator shown in 135° position	192
Figure 7.7 - Results of SMA fatigue test at activation duration of 1500ms.....	193
Figure 7.8 - Results of SMA fatigue test at activation duration of 1000ms.....	194
Figure 7.9 - Results of SMA fatigue test at activation duration of 750ms.....	194
Figure 7.10 – SMA fatigue test results at three activation duration levels.....	195
Figure 7.11 – Linear fit curve model	196
Figure 7.12 - Linear fit analysis on main and control experiments	197
Figure 7.13 - SEM micrograph of the rupture surface of SMA actuator with a pulley system and the illustration of the fatigue crack growth from the crack initiation point (CP).	199
Figure 7.14 - Effect of controllable factors on \bar{y} and S/N_{LTB} for structural fatigue (a) main and (b) control experiments	202
Figure 7.15 - Effect of control factors on \bar{y} and S/N_{STB} for the functional fatigue (a) main and (b) control experiments	205

LIST OF TABLES

Table 2.1 - Commercial NiTi SMA physical properties, based on (Hodgson <i>et al.</i> , 1990; K Otsuka & Wayman, 1999).....	15
Table 2.2 - Comparison of actuator performance, based on.....	20
Table 2.3 - Summary of various SMA properties and their effects.....	21
Table 2.4 - Cooling methods (Dynalloy Inc., 2007)	23
Table 2.5 - Comparison of loading configuration for SMA actuators.....	24
Table 2.6 - HTSMA groups and their properties, based on.....	27
Table 2.7 - Micro-actuators comparison, based on.....	29
Table 2.8 - Comparison of SMP and SMA properties, based on	31
Table 2.9 - Materials with SME, based on	32
Table 2.10 - Shape memory application categories, based on	33
Table 2.11 - Existing and potential SMA applications in the automotive domain, based on	36
Table 2.12 - Comparison of DC-Drive and SMA-Drive for fuel door actuator (Neugebauer <i>et al.</i> , 2010a).....	38
Table 2.13 - Typical automotive electronic components specifications.....	40
Table 2.14 - Existing and potential SMA applications in the aerospace domain, based on.....	43
Table 2.15 - Existing and potential SMA applications in the robotics domain, based on	47
Table 2.16 - Existing and potential SMA applications in the biomedical domain, based on	51
Table 2.17 - Potential SMA applications (Bogue, 2009)	57
Table 3.1 – Typical SMA applications based on material properties.....	70
Table 3.2 – Typical SMA linear actuator form and shape, based on.....	71
Table 3.3 – Basic SMA wire design approaches, based on	76
Table 3.4 - Miga Motor Company SMA linear actuator specifications (MigaMotors).....	85
Table 3.5 – Constants for SMA wire with Eishakani <i>et al.</i> correlation equation (Eisakhani <i>et al.</i> , 2011).....	90
Table 3.6 - Surface area-to-volume ratio for various forms or shapes.	95
Table 3.7 - SMA application optimisation with electronic devices	97
Table 4.1 – Comparison of phase transformation conditions, modified from	106
Table 4.2 – Node coefficients for FDE models in matrix form	114
Table 4.3 - Available Finite Difference Equation implementation.....	115
Table 4.4 - Comparison of common numerical methods.....	117
Table 5.1 - Transient analysis of pipe system.....	129
Table 5.2 - Cycle-average heat transfer rate at pipe surface, \hat{q}_{pipe} , for Case A (bare pipe radius is 0.025m). Red shaded values indicate that stabilization of \hat{q}_{pipe} has occurred at the associated thermal material radius. Green shaded values indicate that thermal energy has not yet propagated to r_{therm} . Critical radius (r_{cr}) identified in bold italics.	133
Table 5.3 - Cycle-average heat transfer rate at pipe surface, \hat{q}_{pipe} , for Case B (bare pipe radius is 0.025m). Red shaded values indicate that stabilization of \hat{q}_{pipe} has occurred at the	

associated thermal material radius. Green shaded values indicate that thermal energy has not yet propagated to r_{therm} . Critical radius (r_{cr}) identified in bold italics.....	138
Table 6.1 - SMA material properties (Dynalloy Inc., 2007; Elahinia & Ahmadian, 2005) .	160
Table 6.2 - SMA linear actuator modeling parameters (Elahinia & Ahmadian, 2005)	162
Table 6.3 - Comparison of analytical and FDE models	165
Table 6.4 - Comparison of convective heat transfer coefficients.....	168
Table 6.5 - Comparison of experimental and numerical data.....	168
Table 7.1 – Summary of SMA fatigue influential factors	178
Table 7.2 - Typical mechanical effects on fatigue life of a pulley drive element.....	183
Table 7.3 - Comparison of DOE method experimental durations.....	185
Table 7.4 - Physical and mechanical of SMA actuator.....	188
Table 7.5 - Estimated strain with heat transfer model.....	189
Table 7.6 - Experiment factors and levels for main experiment	190
Table 7.7 - Experiment factors and levels for control experiment	191
Table 7.8 - Numerical model and experiment strain level comparison for the 1 st cycle....	195
Table 7.9 - Linear fit curve analysis results.....	198
Table 7.10 - \bar{y} and S/N values for the main experiment	199
Table 7.11 - \bar{y} and S/N values for the control experiment	200
Table 7.12 - \bar{y} and S/N _{STB} values for all levels for main and control experiments for structural fatigue test.....	202
Table 7.13 - ANOVA on main and control experiments for structural fatigue test.....	203
Table 7.14 - \bar{y} and S/N _{STB} values for all levels for main and control experiments for functional fatigue test.....	205
Table 7.15 - ANOVA on main and control experiments for functional fatigue test	206
Table 7.16 - Confirmation test with optimum configuration for structural and functional fatigue of SMA-pulley system	206
Table 7.17 - Commercially optimal SMA-pulley system summary	207
Table 8.1 – Summary of publications with associated chapters in thesis	214

NOMENCLATURE

Term	Definition
3M	Three-M: man, material and method
APL	Applied Physic Laboratory
CAD	Computer Aided Design
CAE	Computer Aided Engineering
CAGR	Compound Annual Growth Rate
DARPA	Defense Advanced Research Projects Agency
DCM	Dual-Component Mechanism
DOF	Degree of Freedom
DSC	Differential Scanning Calorimetry
EDM	Electrical Discharge Machining
FDA	Food and Drug Administration
FDE	Finite Difference Equation
FDM	Finite Difference Method
FEA	Finite Element Analysis
FSMA	Ferromagnetic Shape Memory Alloy (similar: MSMA)
GM	General Motors
HTSMA	High Temperature Shape Memory Alloy
MEMS	Micro-Electro-Mechanical Systems
MIS	Minimally Invasive Surgery
MS	Mean of Square
MSMA	Magnetic Shape Memory Alloy (similar: FSMA)
NASA	National Aeronautics and Space Administration
OWSMA	One-Way Shape Memory Alloy
OWSME	One-Way Shape Memory Effect
PTM	Partial-Transition Mechanism
PWM	Pulse Width Modulation
PE	Pseudoelasticity (similar: superelasticity)
RF	Radio Frequency
SCSMA	Single-Crystal Shape Memory Alloy
SAMPSON	Smart Aircraft and Marine Propulsion System Demonstration
SE	Superelasticity (similar: pseudoelasticity)
SHM	Structural Health Monitoring
SMA	Shape Memory Alloy
SMC	Shape Memory Composite
SME	Shape Memory Effect
SMH	Shape Memory Hybrid
SMM	Shape Memory Material
SMP	Shape Memory Polymer
SMT	Shape Memory Technology
SS	Sum of Square
TWSMA	Two-Way Shape Memory Alloy
TWSME	Two-Way Shape Memory Effect
TED	Thermoelectric Device
UAV	Unmanned Air Vehicle
USPTO	United States Patent and Trademark Office
VGC	Variable Geometry Chevron

LIST OF SYMBOLS

Parameter	Description
α	Thermal diffusivity [m^2/s]
ρ_D	Density [kg/m^3]
ρ_R	Resistivity [Ωm]
\varnothing, d, D	Diameter [m]
ε	Strain [%]
ε'	Emissivity
σ	Stress [Pa]
θ	Angle of wrap [$^\circ$]
θ_T	Thermoelastic tensor [$\text{N}/\text{m}^2.\text{K}$]
Ω	Transformation tensor [N/m^2]
ξ_M	Martensite volume fraction
a, g	Gravitational acceleration [m/s^2]
A	Cross-sectional area [m^2]
A_{sf}	Surface area [m^2]
ΔH	Latent heat of phase transformation [J/kg]
∇T	Temperature gradient [K/m , $^\circ\text{C}/\text{m}$]
Δx	Stroke [mm]
$\Delta x/N$	Deformation rate [$\text{mm}/\text{number of cycles}$]
A_f	Austenite-final-temperature [$^\circ\text{C}$, K]
A_p	Austenite-peak-temperature [$^\circ\text{C}$, K]
A_s	Austenite-start-temperature [$^\circ\text{C}$, K]
B19 and B19'	Martensite or product phase (orthorhombic and monoclinic structures)
B2	Austenite or parent phase
c	Specific heat capacity [$\text{J}/\text{kg.K}$]
C_A, C_M	Stress-influenced coefficients [$\text{MPa}/^\circ\text{C}$]
dt_{Act}	Activation duration [s]
dt_{Deact}	Deactivation duration [s]
D	Duty cycle
D/d	Sheave-to-drive element diameter ratio
F	Force or tension [N]
\dot{G}	Rate of Joule heating per volume [W/m^3]
h	Convective heat transfer coefficient [$\text{W}/\text{m}^2\text{K}$]
i	Space-domain subscript $\in [0, n]$
J	Current density [A/mm^2]
k	Thermal conductivity [$\text{W}/\text{m.K}$]
K	Dimensionless constant for deadweight and bias-spring system
L	Length [m]
L_0	Characteristic length [m]
ℓ_0	Initial length [mm]
l	Time-domain subscript $\in [0, n]$
m	Mass [kg]
M_f	Martensite-start-temperature [$^\circ\text{C}$, K]
M_p	Martensite-peak-temperature [$^\circ\text{C}$, K]
M_s	Martensite-final-temperature [$^\circ\text{C}$, K]
n	Total number of observations
N	Number of cycles
N_{drift}	Number of cycles at which drift is measured
N_{int}	Intermediate cycle point
P	Cycle period [s]
\dot{Q}, q	Heat transfer rate [W]

Parameter	Description
q'	Heat flux
\dot{q}	Cycle-average heat transfer rate [W]
r	Radius [m]
R_{elec}	Electrical resistance [Ω]
R_{therm}	Thermal resistance [K/W]
R_s	Rhombohedral-start-temperature [$^{\circ}\text{C}$, K]
R_f	Rhombohedral-finish-temperature [$^{\circ}\text{C}$, K]
s	Arc of contact [mm]
s/L_{lay}	Arc of contact-to-lay length ratio
S	Spring constant [N/m]
S^2	Variance
S/N	Signal-to-noise ratio [dB]
$SA:V$	Surface area-to-volume ratio
t	Time or duration [s]
T	Temperature [K, $^{\circ}\text{C}$]
T_w	Wire temperature
T_{∞}	Ambient temperature [K, $^{\circ}\text{C}$]
U	Velocity [m/s]
ν	Kinematic viscosity [m^2/s]
ν'	Poisson's ratio
V	Volume [m^3]
y_i	Observation deviation
\bar{y}	Overall mean
E	Young's modulus [N/m^2]
Bi	Biot number
Fo	Fourier number
Gr	Grashof number
Nu	Nusselt number
Pr	Prandtl number
Ra	Rayleigh number
Re	Reynolds number
σ'	Stephen-Boltzman constant [$\text{W}/\text{m}^2\text{K}^4$]
Au	Aurum (or gold)
Co-Ni-Ga	Cobalt-Nickel-Gallium
Cu-Al-Ni	Copper-Aluminium-Nickel
Cu-Sn	Copper-Tin
Cu-Zn	Copper-Zinc
Cu-Zn-Al	Copper-Zinc-Aluminium
Hf	Halfnium
In-Tl	Indium-Thallium
Nb	Niobium
Ni-Mn-Ga	Nickel-Manganese-Gallium
NiTi	Nickel-Titanium (or nitinol)
Pd	Palladium
Pt	Platinum
Ru	Ruthenium
Ta	Tantalum
Ti	Titanium
U	Uranium
Zr	Zirconium

1. Introduction

1.1 Background

This research program was initiated to enhance the commercial application of shape memory alloy (SMA) linear actuators. Meticulous review of existing commercial and research literature combined with feedback from industry has formally identified the commercially relevant technical challenges associated with the design of SMA actuator systems. Specific opportunities for novel research contributions are subsequently identified and addressed in this thesis.

1.2 Introduction and motivation

The unique properties of SMA actuators result in a number of technical advantages including: significantly higher power-to-weight ratio than conventional electro-mechanical actuators; potentially simplified construction, whereby the SMA can act as both sensor and actuator simultaneously; and, potential cost and mass advantage competing technologies such as solenoid actuators (DC Lagoudas, 2010; Mohd Jani, Leary, Subic, & Gibson, 2014; K Otsuka & Wayman, 1999). The demand for SMA actuators in technical and engineering applications has been steadily increasing in numerous commercial fields, in particular, biomedical, automotive, aerospace and robotics (Mohd Jani, Leary, Subic, *et al.*, 2014).

As an example of the commercial opportunities for SMA actuation; in the automotive domain, the need for safer, more comfortable and enhanced vehicle performance has tremendously increased the number of sensors, actuators and microcontrollers embedded in modern vehicles. These technologies increase the mass and volume of the vehicle, result in packaging challenges and have a negative impact on fuel economy and carbon footprint. Currently, automotive applications make extensive use of conventional electromagnetic actuators (GM, 2013), which may be sub-optimal for weight, volume and reliability. Therefore, the lightweight, compact and high 'functional density' attributes of SMA actuators may provide an excellent alternative to replace the electromagnetic actuators in existing automotive applications (Borrioni-Bird, 1997; Butera, Coda, & Vergani, 2007; D. Stoeckel, 1990).

The research methodology of Figure 1.1 was formulated to strategically distil the research themes and associated research contributions; initially by completing an intensive literature review and analysis of existing SMA research and associated commercial applications; identifying associated research gaps; and, opportunities for novel, commercially relevant SMA research contributions are subsequently identified.

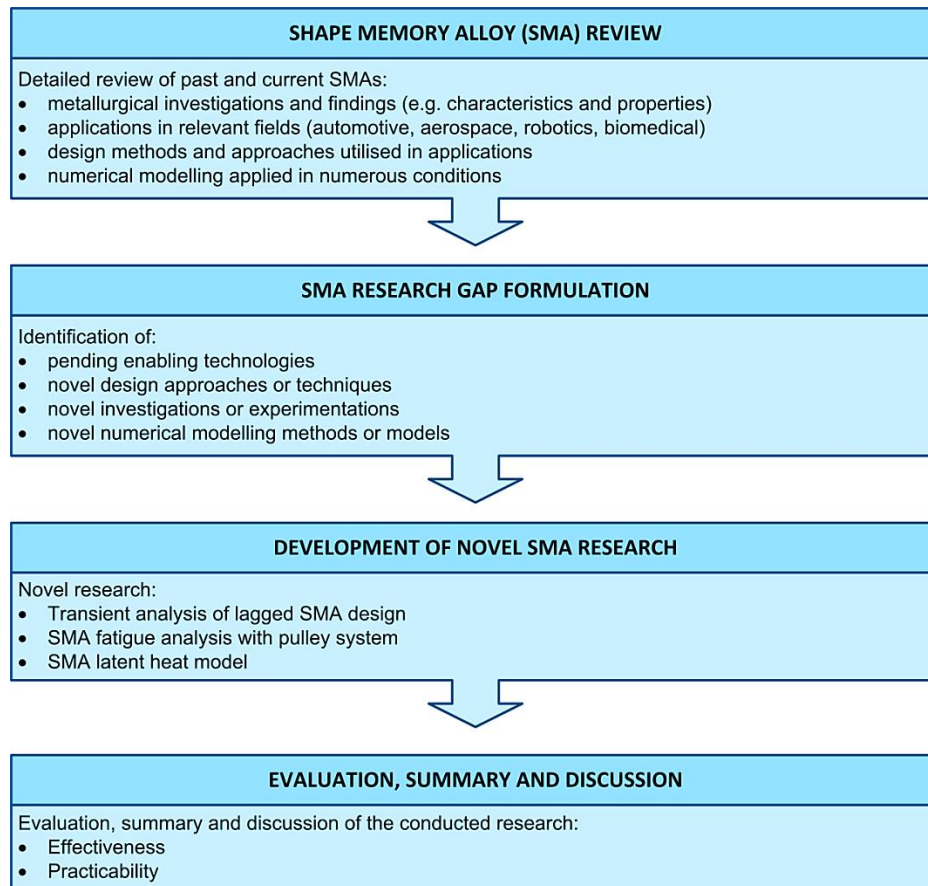


Figure 1.1 - Research Methodology

A comprehensive literature review of over 500 journal and patent documents was conducted by the author to provide a timely review of SMA based research, development and associated applications; and to provide a clear roadmap for the commercial imperatives for SMA design, and the associated research themes of this work. In summary, this literature review: describes a historical overview of SMA development and the performance attributes of relevance to SMAs actuator applications; identifies relevant design challenges faced by SMA developers due to associated technical limitations; and, summarises the recent advances and opportunities of SMA applications. This extensive review was awarded “top cited article in 2014” within Journal of Materials and Design (Mohd Jani, Leary, Subic, *et al.*, 2014); and Elsevier “top 25 downloaded Materials Engineering articles in 2014”.

Based on the literature review outcomes, it appears that the majority of existing SMA actuation research has focused on the associated metallurgical properties; whereby substantial achievements have been reported, such as: higher recovery rate and associated durability; a wider range of available operating temperatures; SMA with multiple shape conditions via SMA *programming*; and performance and functionality enhancements that increase the potential for sophisticated, multifunctional SMA actuation applications and systems (Ji Ma & Karaman, 2010). In spite of these achievements, and although more than 10,000 United States patents and over 20,000 worldwide SMA patent applications have been issued, the number of commercially successful SMA applications remains low (Vaidyanathan, 2000; Welp & Breidert, 2004; C. Zhang, Zee, & Thoma, 1996).

1.3 Research scope

Based on the extensive review of commercial and research SMA literature (Mohd Jani, Leary, Subic, *et al.*, 2014), technical and design limitations that stymie commercial SMA application were identified and may be categorised according to three fundamental factors according to the Kaizen methodology for continuous improvement: **man** (human), **material** and **machine**, (Imai, 1986; Kato & Smalley, 2012):

1) **Man (Human)**

- Lack of: design knowledge for understanding the technical requirements of SMAs; and, design methods and tools available to deploy SMAs in a robust manner to achieve the application requirements of durability and positional stability (P. Abrahamsson & Møster, 1997; AD Johnson, 1998; Sven Langbein & Czechowicz, 2012; Welp & Breidert, 2004; C. Zhang *et al.*, 1996).
- Lack of connectivity between the research outcomes of material scientists and the requirements of engineering designers; as the data and methods offered by material scientists is not always compatible with the requirements of design engineers (P. Abrahamsson & Møster, 1997; JV Humbeeck, 1997; Welp & Breidert, 2004).
 - Lack of 'smart marketing' of the commercial capabilities of SMA applications to key engineering design personnel (JV Humbeeck, Chandrasekaran, & Delaey, 1991).

2) **Material**

- Technical limitations of SMAs, associated with: usable strain, actuation frequency, controllability, and energy efficiency (Mohd Jani *et al.*, 2014).
- Potentially high material cost due to relatively small commercial sales volumes.

3) **Method**

- Relative lack of SMA research from an engineering design perspective (Mohd Jani *et al.*, 2014); thereby resulting in lack of design procedures, guidelines and tools to assist

engineers in developing SMA applications (P. Abrahamsson & Møster, 1997; Spaggiari, Mammano, & Dragoni, 2012; D. Stoeckel, 1990; JV Humbeeck, 1997; Welp & Breidert, 2004).

- Lack of models that are compatible with computer-based design and analysis methods, which are essential to enhancing the SMA design process, in particular for preliminary studies and validation of high risk and/or expensive projects.

These identified limitations define the research scope and provide the motivation to further research toward the optimisation and improvement of SMA actuators. Specific, commercially relevant SMA research objectives have been selected and subsequently addressed in this thesis as research themes.

1.4 Research themes

Significant opportunity exists for the development of enhanced methods, tools and associated data for SMA actuator design (P. Abrahamsson & Møster, 1997; Mohd Jani, Leary, Subic, *et al.*, 2014; Spaggiari *et al.*, 2012; D. Stoeckel, 1990; JV Humbeeck, 1997; Welp & Breidert, 2004). The focus of this thesis is to enhance the design of SMA actuators in response to this identified limitation. Three research themes were identified from the literature review as listed below:

1. Design methods to resolve SMA linear actuator limitations

- Improvement of activation and deactivation durations, such as lagged SMA with highly conductive materials
- Novel understanding of transient heat transfer and the effect of critical and crossover radii on cylindrical geometry for transient heating
- Durability and stability investigation (structural and functional fatigue) on SMA linear actuator with and without pulley system

2. Development of simple and practical numerical models for SMA linear actuator response

- Simplified and robust analytical and numerical models that are compatible with the requirements of design engineers
- Readily applied charts to predict SMA linear actuator response

3. Data for SMA linear actuator design

- Investigation of system design effects on SMA-pulley system fatigue performance
- Models to predict and characterise SMA structural and functional fatigue

Chapter 1	Introduction: Research Backgrounds and Motivations		
This research was initiated to optimise Shape Memory Alloy linear actuator applications, by addressing their strengths and limitations, and recommending design solutions. This work assists in the commercialisation of SMA linear actuator applications by providing useful design guidelines and tools.			
Literature Review			
Chapter 2	SMA Review	Chapter 3	Design of SMA linear actuators
<ul style="list-style-type: none">SMA overview, including associated strengths, limitations and design challenges.Current SMA research, applications and future prospects for commercial applications.<ul style="list-style-type: none">Highlighted commercial domains: Automotive, aerospace, biomedical and robotics.Important design factors and recommendations for commercialisation improvements.Identification of future development for SMA applications.		<ul style="list-style-type: none">Overview of SMA designing process, including: design requirements and specifications.Design fundamentals and factors associated with: power, displacement and bandwidth.Sample of design solutions, including: parallel, serial, telescopic and pulley systems.Convective heating and geometric effects on thermomechanical performance.	
Chapter 4	Numerical modelling of SMA linear actuators		
<ul style="list-style-type: none">Review of SMA numerical models:<ul style="list-style-type: none">Fundamentals (e.g. mathematical equations and Biot numbers).Heat transfer and constitutive models.One dimensional and multi-dimensional models.Analytical, FDM, FEM and FVM models.Comprehensive overview of FDM:<ul style="list-style-type: none">Forward, backward and central FDEs.Matrix-forms.Review of SMA numerical models.			
Research Themes			
<ul style="list-style-type: none">Design methods to resolve SMA linear actuator limitations.<ul style="list-style-type: none">Improvement of activation and deactivation durations, such as lagged SMA with highly conductive materials.Novel understanding of transient heat transfer and the effect of critical and crossover radii on cylindrical geometry for transient heating.Durability and stability investigation (structural and functional fatigue) on SMA linear actuator with and without pulley system.Development of simple and practical numerical models for SMA linear actuator response.<ul style="list-style-type: none">Simplified and robust analytical and numerical models that are compatible with the requirements of design engineers.Readily applied charts to predict SMA linear actuator response.Data for SMA linear actuator design.<ul style="list-style-type: none">Investigation of system design effects on SMA-pulley system fatigue performance.Models to predict and characterise SMA structural and functional fatigue.			
Research Contributions			
Chapter 5	The critical and crossover radii on transient heating	Chapter 6	Development of 1-D numerical model for SMA linear actuators
<ul style="list-style-type: none">Investigate the effect of transient heating on cylindrical lagged system, e.g. linear SMA actuators.Custom FDE model development.Novel critical and crossover radii analysis for the transient case.Novel conclusions of steady-state and transient scenarios for cylindrical system.Guidelines for SMA linear actuator lagged design.		<ul style="list-style-type: none">Development of novel 1-D numerical models (both analytical and FDE) with advantages in practical application over existing methods, including: novel latent heat models, and phase transitions effects.Simulation of the thermomechanical behaviour of SMA linear actuators under variable ambient and mechanical conditions with the developed numerical models.Simple charts for prediction of: SMA activation duration versus required Joule heating; and deactivation duration versus convective heat transfer coefficient.	
Chapter 7	Structural and functional fatigue of Ni-Ti SMA-pulley system using Taguchi and ANOVA		
<ul style="list-style-type: none">Investigation of the effect of pulley system parameters on structural and functional fatigue of SMA linear actuators with Taguchi and ANOVA.Optimal pulley system configurations are proposed for functional stability and durability of SMA linear actuators.Novel conclusions of the pulley system effects on SMA linear actuator and design guideline proposal.Novel multi-linear-fit model developed and validated for functional fatigue prediction.			
Chapter 8	Conclusion		
Reports on thesis outcomes and suggested future work.			

Figure 1.2 - Thesis Map

1.5 Research contributions

The overview of interconnections between the research review, identified research themes and specific contributions is presented in the associated thesis map (Figure 1.2) and categorically summarised below, according to the relevant research themes.

Research theme 1: Design methods to resolve SMA actuator limitations

Two identified impediments to the commercial application of SMA actuators is their relatively low speed (e.g. activation and deactivation durations) and challenges to positional stability (e.g. functional fatigue). In response to these identified opportunities, the following research contributions have been made:

- A novel study of the transient heat transfer behaviour of cylindrically lagged thermal systems is made to enhance the deactivation speed of SMA linear actuators. A suitable finite difference equation (FDE) is developed and presented in Chapter 5. This study quantifies the transient crossover and critical radii of the cylindrical system, and novel conclusions are drawn between the steady-state and transient scenarios (Sunan Huang, Mohd Jani, Leary, & Subic, 2013). The influence of SMA design, geometry and ambient conditions are presented, Chapter 3, (Mohd Jani, Huang, Leary, & Subic, 2015a), and (Mohd Jani, Huang, Leary, & Subic, 2015b).
- An investigation with Taguchi and ANOVA DOE was conducted to investigate the positional stability (i.e. functional fatigue) of SMA linear actuators, Chapter 7 (Mohd Jani, Leary, & Subic, 2016). This novel investigation identifies the primary factors affecting the functional fatigue of SMA linear actuators, and proposes optimal configurations for commercial SMA-pulley system applications.

Research theme 2: Development of simple and practical numerical models for SMA actuator response.

Novel numerical models are proposed to simulate the thermomechanical behaviour of SMA linear actuators in Chapter 6 (Mohd Jani *et al.*, 2015b). These developed numerical models are readily implemented in analytical and finite difference equation (FDE) models that include relevant phase transition factors, such as latent heat effect and material properties variability. Readily applied activation and deactivation charts that assist in the early design phase are also developed.

Research theme 3: Data for SMA linear actuator design

A selection of factors of influence to SMA linear actuators performance are investigated in Chapters 5, 6 and 7 to aid in optimising performance of SMA linear actuator applications. Several design approaches have been reviewed in Chapter 3, and a series of design guidelines for SMA linear actuators are stated, such as the need to consider phase transition and pre-stress for the application actuation durations in Chapter 6 (Mohd Jani *et al.*, 2015b). SMA actuators can be integrated within a pulley system for mechanical advantage and enhanced packaging; however no data exists on the influence of SMA-pulley system parameters on fatigue performance. Taguchi methods and ANOVA are used to formally assess functional and structural fatigue response for a range of relevant design parameters; including a fatigue confirmation test for a commercially optimal SMA-pulley configuration. A novel bi- and tri-linear functional fatigue model is proposed and found to characterise the experimentally observed data, Chapter 7 (Mohd Jani *et al.*, 2016).

1.6 Thesis overview

This thesis is organised into 8 chapters as illustrated in the thesis map (Figure 1.2). Chapter 1 introduces the background and motivation of this research; it summarises the research objectives, methodology, outcomes, and contributions. Chapter 2 provides a comprehensive overview of SMAs, their advantages, limitations and associated design challenges. Prospects for future commercial SMA applications, as well as opportunities and future directions for novel research are identified. The content of this chapter has contributed to the following publications:

- *A review of shape memory alloy research, applications and opportunities*,
J Mohd Jani, M Leary, A Subic, MA Gibson, Materials & Design 56, 1078-1113, 2014.
DOI: 10.1016/j.matdes.2013.11.084
- *Shape memory alloy applications in automotive*,
J Mohd Jani, M Leary, A Subic, Applied Mechanics and Materials 663, 248-253,
2014. DOI: 10.4028/www.scientific.net/AMM.663.248

Chapter 3 reviews existing approaches to SMA actuator design, while Chapter 4 reviews the numerical models applied in SMA analysis. The content of this chapter has contributed to the following publications:

- *Analysis of convective heat transfer coefficient on shape memory alloy actuator under various ambient temperatures with finite difference method*,
J Mohd Jani, S Huang, M Leary, A Subic, Applied Mechanics and Materials 736, 127-133, 2015. DOI: 10.4028/www.scientific.net/AMM.736.127
- *Numerical modeling of Shape Memory Alloy linear actuator*,
J Mohd Jani, S Huang, M Leary, A Subic, Computational Mechanics 53(3), 443-461, 2015. DOI: 10.1007/s00466-015-1180-z

Chapter 5 investigates the effect of transient heating on cylindrically lagged thermal systems such as linear SMA actuators. This is achieved by developing a one-dimensional FDE heat transfer model to simulate periodic transient heating of a cylindrical lagged SMA system under variable thermal-cycle characteristics. This investigation allows novel conclusions to be drawn between the steady-state and transient scenarios. The content of this chapter has contributed to the following publication:

- *The critical and crossover radii on transient heating*,
S Huang, **J Mohd Jani**, M Leary, A Subic, Applied Thermal Engineering 60(1), 325-334, 2013. DOI: 10.1016/j.applthermaleng.2013.06.052

Chapter 6 investigates the SMA thermomechanical behaviour under various ambient temperatures and mechanical conditions with the newly developed numerical models, where novel latent heat equations are proposed. The FDE model of Chapter 5 is further enhanced by incorporating Joule heating and latent heat effects into the model. Additionally, constitutive models are integrated into the model to accommodate pre-stress effects and to provide predictive data on the associated stress-strain relationship. These newly developed numerical models are validated with existing models and experimental data. Readily applied charts for SMA response prediction are also proposed in this chapter. The content of Chapter 6 has contributed to the following publication:

- *Numerical modeling of Shape Memory Alloy linear actuator*,
J Mohd Jani, S Huang, M Leary, A Subic, Computational Mechanics 53(3), 443-461, 2015. DOI: 10.1007/s00466-015-1180-z

Chapter 7 investigates, for the first time, the structural and functional fatigue of SMA actuators within a pulley system. This novel investigation studies the influences of the pulley system with variable pulley configurations on SMA fatigue performance. The factors affecting SMA-pulley system performance are ranked and the optimal configurations are identified using Taguchi methods and ANOVA. A confirmation test is completed to provide robust design data for a commercially optimal SMA-pulley configuration. A novel bi- and tri-linear characterisation approach for SMA functional fatigue is proposed, which will enable increased insight into the phenomena of SMA functional fatigue and predictive modelling. The content of Chapter 7 has contributed to the following publication:

- *Fatigue of Ni-Ti SMA-pulley system using Taguchi and ANOVA*,
J Mohd Jani, M Leary, A Subic, Smart Materials & Structures 25 (5), 057001, 2016.
DOI: 10.1088/0964-1726/25/5/057001.

Chapter 8 summarises the thesis outcomes and conclusions and recommends potential relevant future research and development. Appendices containing additional detail on associated SMA applications, experimental data and numerical modeling code developed by the author concludes the thesis.

2. Shape Memory Alloys review

The outcomes of this chapter have contributed to the following peer reviewed publication:

- *A review of shape memory alloy research, applications and opportunities*, J Mohd Jani, M Leary, A Subic, MA Gibson, Materials & Design 56, 1078-1113, 2014.
- *Shape memory alloy applications in automotive*, J Mohd Jani, M Leary, A Subic, Applied Mechanics and Materials 663, 248-253, 2014.

2.1 Chapter summary

This chapter presents brief summary of SMAs, their design feasibility and the variety of SMA applications that are relevant to the research outcomes of this thesis. SMA applications are divided into several sections based on the application domain, such as automotive, aerospace, robotics and biomedical, as well in other areas. The work presented here has an emphasis on nickel-titanium (NiTi) SMAs, but other forms of smart materials such as high temperature shape memory alloys (HTSMAs), magnetic shape memory alloys (MSMAs), SMM thin film (e.g. NiTi thin film) and shape memory polymers (SMPs) are also discussed. Specific opportunities for novel research contributions are identified, and further developed in subsequent chapters. A comprehensive summary of SMA applications are summarised in Appendix A to Appendix E.

2.2 Shape memory alloy

Shape memory alloy (SMA) or 'smart alloy' was first discovered by Arne Ölander (1932), and the term 'shape-memory' was first described by Vernon (1941) for his polymeric dental material. The importance of shape memory materials (SMMs) was not recognised until William Buehler and Frederick Wang revealed the shape memory effect (SME) in a nickel-titanium (NiTi) alloy in 1962 (WJ Buehler, Gilfrich, & Wiley, 1963; Kauffman & Mayo, 1997), which is also known as nitinol (derived from the material composition and the place of discovery, i.e. a combination of NiTi and Naval Ordnance Laboratory). The demand for SMAs in engineering and technical applications has been increasing in numerous commercial fields, including: consumer products and industrial applications (Hautcoeur & Eberthardt, 1997; MH Wu & LM Schetky, 2000; Zider & Krumme, 1988); structures and composites (Yasubumi Furuya, 1996); automotive (Butera *et al.*, 2007; Leo, Weddle, Naganathan, & Buckley, 1998; D. Stoeckel, 1990); aerospace (Bil, Massey, & Abdullah, 2013; Hartl & Lagoudas, 2007; Humbeeck, 1999; McDonald Schetky, 1991); mini actuators and micro-electromechanical systems (MEMS) (Hiroyuki Fujita & Toshiyoshi, 1998; Humbeeck, 1999; Kahny, Huffz, & Heuer, 1998; Kohl, 2010; Sun *et al.*, 2012); robotics (Y. Furuya & Shimada, 1991; Kheirikhah, Rabiee, & Edalat, 2011; Sreekumar, Nagarajan,

Singaperumal, Zoppi, & Molfino, 2007); biomedical (T. Duerig, Pelton, & Stöckel, 1999; Humbeeck, 1999; Machado & Savi, 2003; Mantovani, 2000; NB Morgan, 2004; Petrini & Migliavacca, 2011; C. Song, 2010; Sun *et al.*, 2012); and even in fashion (Langenhove & Hertleer, 2004). Although iron-based and copper-based SMAs, such as Fe-Mn-Si, Cu-Zn-Al and Cu-Al-Ni, are low-cost and commercially available, due to their instability, impracticability (e.g. brittleness) (Cederström & Van Humbeeck, 1995; Hodgson, Wu, & Biermann, 1990; Wilkes, Liaw, & Wilkes, 2000) and poor thermo-mechanic performance (W. Huang, 2002), NiTi-based SMAs are preferable for most applications due to their mechanical robustness. However, each SMA material has their own advantage for particular requirements or applications.

SMAs are group of metallic alloys that can return to their original form (shape or size) when subjected to a memorisation process between two transformation phases, which is temperature or magnetic field dependent. This transformation phenomenon is known as the Shape Memory Effect (SME).

The basic application of these materials is quite simple, where the material can be readily deformed by applying an external force, and will contract or recover to its original form when heated beyond a certain temperature either by external or internal heating (Joule heating); or other relevant stimuli such as a magnetic field for MSMA.

2.3 Shape memory effect and pseudoelasticity

Practically, SMAs can exist in two different phases, with three different crystal structures (i.e. twinned martensite, detwinned martensite and austenite) and six possible transformations (Mihálcz, 2001; Sun & Huang, 2009) (see Figure 2.1).

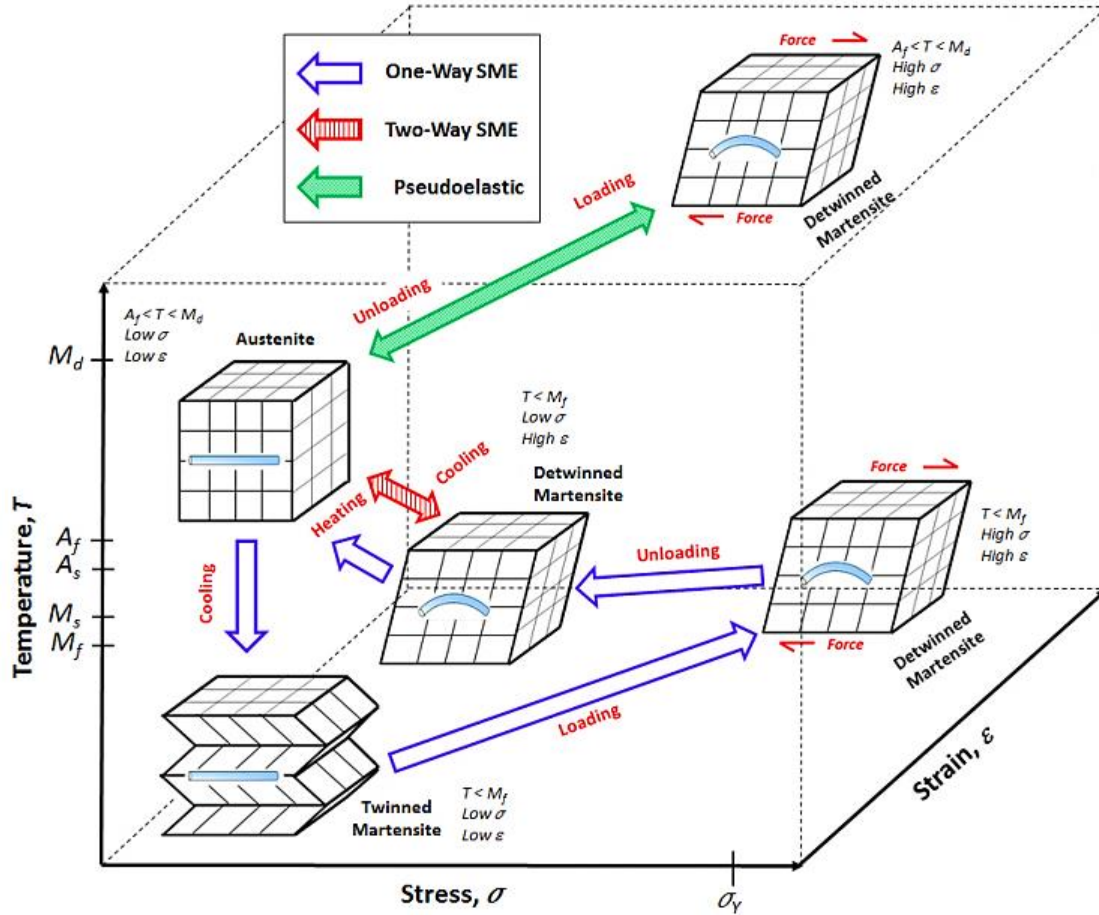


Figure 2.1 - SMA phases and crystal structures
(Mohd Jani, Leary, Subic, *et al.*, 2014)

The austenite structure is stable at high temperature, and the martensite structure is stable at lower temperatures. When a SMA is heated, it begins to transform from martensite into the austenite phase. The austenite-start-temperature (A_s) is the temperature where this transformation starts and the austenite-finish-temperature (A_f) is the temperature where this transformation is complete. Once a SMA is heated beyond A_s it begins to contract and transform into the austenite structure, i.e. to recover into its original form. This transformation is possible even under high applied loads, and therefore, results in high actuation energy densities (DC Lagoudas, 2010). During the cooling process, the transformation starts to revert to martensite at the martensite-start-temperature (M_s) and is complete when it reaches the martensite-finish-temperature (M_f) (WJ Buehler *et al.*, 1963) (see Figure 2.2 and Figure 2.3).

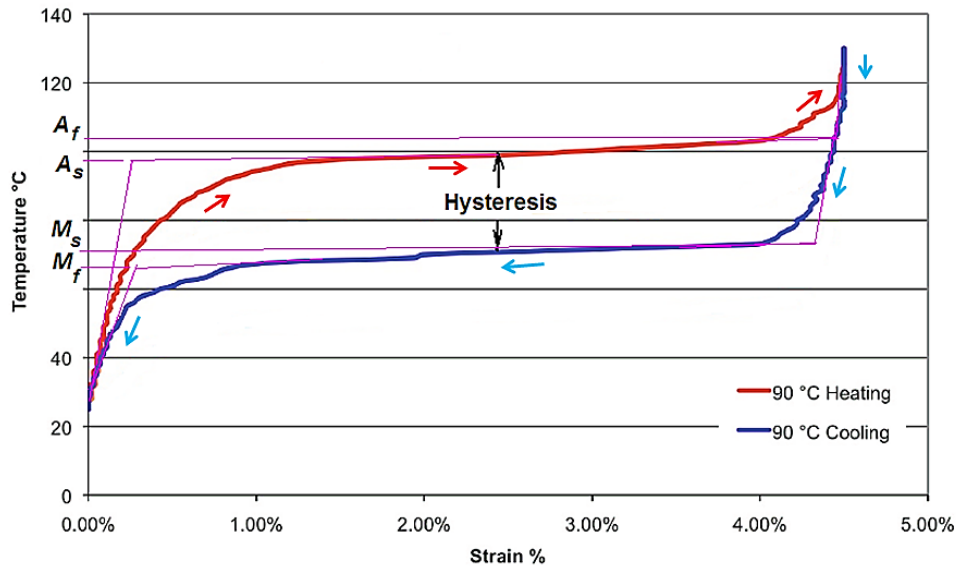


Figure 2.2 - Flexinol NiTi SMA (HT) phase transformation (Dynalloy Inc., 2007)

The highest temperature at which martensite can no longer be stress induced is called M_d , and above this temperature the SMA is permanently deformed like any ordinary metallic material (TW Duerig & Pelton, 1994). These shape change effects, which are known as the Shape Memory Effect (SME) and pseudoelasticity (or superelasticity), can be categorised into three shape memory characteristics as follows:

1) One-way shape memory effect (OWSME):

The one-way SMA (OWSMA) retains a deformed state after the removal of an external force, and then recovers to its original shape upon heating.

2) Two-way shape memory effect (TWSME) or reversible SME:

In addition to the one-way effect, a two-way SMA (TWSMA) can remember its shape at both high and low temperatures. However, TWSMA is less applied commercially due to the 'training' requirements and to the fact that it usually produces about half of the recovery strain provided by OWSMA for the same material (W. Huang & Toh, 2000; Jeff Perkins & Hodgson, 1990; Schroeder & Wayman, 1977) and its strain tends to deteriorate quickly, especially at high temperatures (J Ma, Karaman, & Noebe, 2010). Therefore, OWSMA typically provides a more reliable and economical solution (Stöckel, 1995). Various training methods have been proposed (Funakubo & Kennedy, 1987; Weiming Huang, 1999; K Otsuka & Wayman, 1999; J. Perkins *et al.*, 1990; Schroeder & Wayman, 1977; Stalmans, Van Humbeeck, & Delaey, 1991), including: spontaneous and external load-assisted induction (Vladimir Brailovski, Prokoshkin, Terriault, & Trochu).

3) Pseudoelasticity (PE) or superelasticity (SE):

The SMA reverts to its original shape after applying mechanical loading at temperatures between A_f and M_d , without the need for any thermal activation.

In addition to the ‘material TWSME’ above, a biased OWSMA actuator could also act as a ‘mechanical TWSME’ at a macroscopic (structural) level; which is more powerful, reliable and is widely implemented in many engineering applications (Sun *et al.*, 2012). In many references, the austenite and martensite phases are also known as parent (or B2) and product (or B19 and B19’ for orthorhombic and monoclinic structures) phases respectively.

Hysteresis is a measure of the difference in the transition (or transformation) temperatures between heating and cooling (i.e. $\Delta T = A_f - M_s$), which is generally defined between the temperatures at which the material is in 50% transformed to austenite upon heating and in 50% transformed to martensite upon cooling (WJ Buehler & Wang, 1968). This property is important and requires careful consideration during SMA material selection for targeted technical applications; e.g. a small hysteresis is required for fast actuation applications (such as micro-electro-mechanical systems and robotics), larger hysteresis is required to retain the predefined shape within a large temperature range (such as in deployable structures and pipe joining) (Yong Liu, 2010). In addition, the transition temperatures referred to identify the operating range of an application. These transition temperatures and the hysteresis loop behaviour are influenced by: the composition of SMA material, the thermomechanical processing tailored to the SMA and the working environment of the application itself (e.g. applied stress) (Stöckel, 1995). Transition temperatures can be directly measured with various techniques such as differential scanning calorimetry (DSC), dilatometry, electrical resistivity measurement as a function of temperature, and can be indirectly determined from a series of constant stress thermal cycling experiments (J Ma *et al.*, 2010).

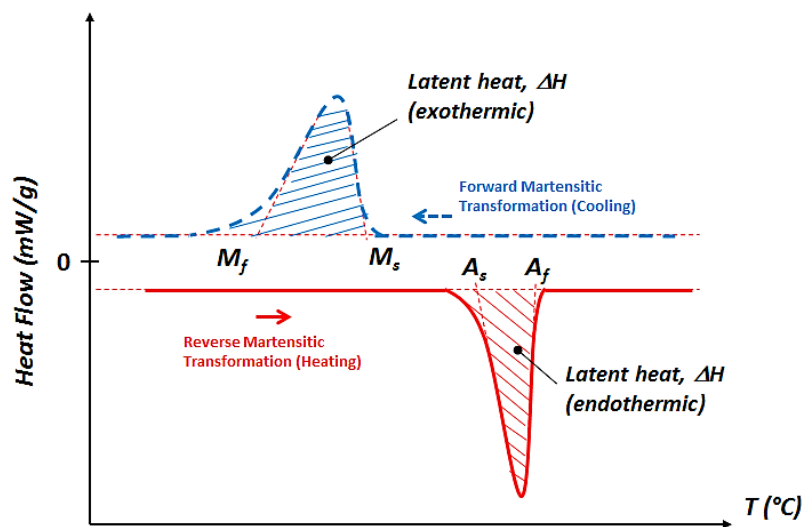


Figure 2.3 - A typical DSC thermograph of SMA (Mohd Jani *et al.*, 2015b)

SMA physical and mechanical properties also vary between these two phases, such as Young's modulus, electrical resistivity, thermal conductivity and thermal expansion coefficient (Mertmann & Vergani, 2008; Mihálcz, 2001; Sreekumar, Nagarajan, & Singaperumal, 2009). The austenite structure is relatively hard and has a much higher Young's modulus; whereas the martensite structure is softer and more malleable; i.e. can be readily deformed by application of an external force (Hodgson *et al.*, 1990; Mihálcz, 2001) (see Table 2.1).

Table 2.1 - Commercial NiTi SMA physical properties, based on (Hodgson *et al.*, 1990; K Otsuka & Wayman, 1999)

Property	Symbol	Units	Value	
			Martensite	Austenite
Corrosion Resistance	-	-	Similar to 300 series SS or Ti-alloy	
Density	ρ_D	kg/m ³	6450 ~ 6500	
Electrical Resistivity (approx.)	ρ_R	$\mu\Omega\cdot\text{cm}$	76 ~ 80	82 ~ 100
Specific Heat Capacity	c	J/kg.K	836.8	836.8
Thermal Conductivity	k	W/m.K	8.6 ~ 10	18
Thermal Expansion Coefficient	α	m/m.K ⁻¹	6.6×10^{-6}	11.0×10^{-6}
Ultimate Tensile Strength	σ_{UTS}	MPa	895 (Fully annealed) / 1900 (Hardened)	
Young's Modulus (approx.)	E	GPa	28 ~ 41	75 ~ 83
Yield Strength	σ_Y	MPa	70 ~ 140	195 ~ 690
Poisson's Ratio	ν	-	0.33	
Magnetic Susceptibility	χ	$\mu\text{emu.g}$	2.5	3.8

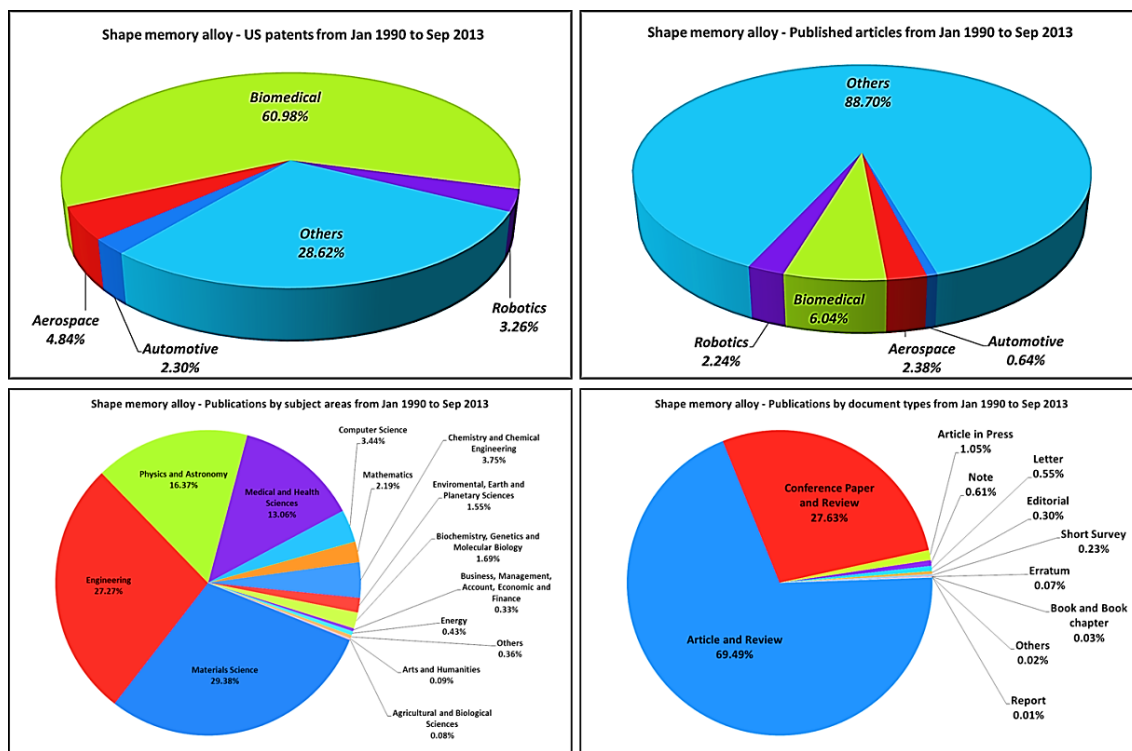
When an external stress is applied below the martensite yield strength (approximately 8.5% strain for NiTi alloys and 4-5% for copper-based alloys (Dynalloy Inc., 2007; Hodgson *et al.*, 1990; Vaidyanathan, 2000), the SMA deforms elastically with recoverable strain. However, a large non-elastic deformation (permanent plastic deformation) will result beyond this point. Most applications will restrict the strain level; e.g. to 4% or less, for NiTi alloys (Dynalloy Inc., 2007; W. Huang, 2002).

2.4 Shape memory alloy development

2.4.1 SMA development history

The solid phase transformation in SMA was first discovered by Arne Ölander (1932), a Swedish physicist who determined that the gold-cadmium (Au-Cd) alloys could be plastically deformed when cool, and returned to its original configuration when heated. Later, Greninger and Mooradian (1938) first observed the SME for copper-zinc (Cu-Zn) alloys and copper-tin (Cu-Sn) alloys. The fundamental phenomenon of the memory effect governed by the thermoelastic behaviour of the martensite phase was widely reported a decade later by Kurdjumov and Khandros (1949) and also by Chang and Read (1951). Similar affects in other alloys such In-Tl and Cu-Al-Ni were also observed in the 1950's. These discoveries had captured the interest of many researchers and inventors, but practical and industrial applications could not be realised due to high material costs, manufacturing complexity and unattractive mechanical properties.

Although the NiTi alloy was discovered by William Buehler in 1959 (Kauffman & Mayo, 1997), the potential to commercialise SMA applications only became available after the SME in NiTi alloy was revealed by William Buehler and Frederick Wang in 1962 (WJ Buehler *et al.*, 1963; Kauffman & Mayo, 1997). Nitinol alloys are cheaper to produce, easier and safer to handle, and have better mechanical properties compared to other existing SMAs at that time (WJ Buehler *et al.*, 1963; WJ Buehler & Wang, 1968). The first commercial success for a SMA application was the Raychem Corporation's CryoFit™ 'shrink-to-fit' pipe coupler in 1969 for the F-14 jet fighter built by the Grumman Aerospace Corporation, and followed subsequently by orthodontic bridge wires by George B. Andreasen in 1971 (Kauffman & Mayo, 1997). Since the 1980's, the commercial application of NiTi alloys has developed in many areas due to greater demands for lighter and more compact actuators, especially in the biomedical sector (see Figure 2.4 and Figure 2.5).



Source: SCOPUS and USPTO, accessed on 15 Sep 2013, keyword: "shape memory alloy" OR nitinol

Figure 2.4 - SMA publications and US patents from January 1990 to June 2013 (Mohd Jani, Leary, Subic, et al., 2014)

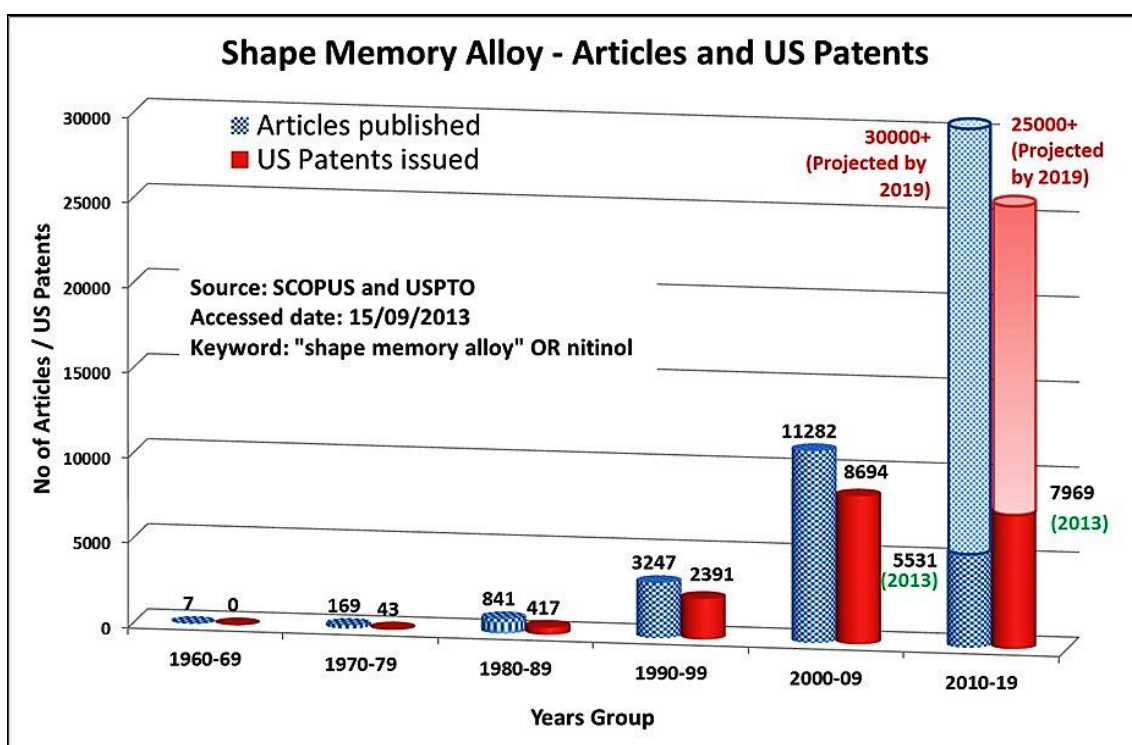


Figure 2.5 - Number of "Shape Memory Alloy" articles and patents by years-group (Mohd Jani, Leary, Subic, et al., 2014)

2.4.2 Recent shape memory alloy development

In the 1990's, the term Shape Memory Technology (SMT) was introduced into the SMM community (P Abrahamsson & Bjiimemo, 1994). SMA application design has changed in many ways since then and has found commercial application in a broad range of industries including automotive, aerospace, robotics and biomedical (Butera, 2008; Humbeeck, 1999; AD Johnson, 1998; Kumar & Lagoudas, 2008; Sreekumar *et al.*, 2007; Strittmatter & Gümpel, 2011; Sun *et al.*, 2012). Currently, SMA actuators are successfully applied in low frequency vibration (Baz, Imam, & McCoy, 1990) and actuation applications. However, much systematic and intensive research work is still needed to enhance the performance of SMAs (TW Duerig, Stockel, & Keeley, 1990; Hirose, Ikuta, & Umetani, 1988), especially to increase their bandwidth, fatigue life and stability (Karhu & Lindroos, 2010).

Recently, many researchers have taken an experimental approach to enhance the attributes of SMAs, by: improving material compositions (quantifying the SMA phase transition temperature (Choon, Salleh, Jamian, & Ghazai, 2007; Ren & Liew, 2005; Wada & Liu, 2005; ZG Wang *et al.*, 2003; ZG Wang *et al.*, 2004)) to achieve a wider operating temperature range, and better material stability; as well as to improve the material response and stroke with better mechanical design (or approach), controller systems and fabrication processes. Research into alternative SMMs, forms or shapes, such as MSMA, HTSMA, SMP, shape memory ceramic, SMM thin films, as well as hybrid or composite SMMs, are also intensively being conducted, and the number of commercial applications is growing each year (see Figure 2.5). More details of recent applications and development of SMA are described in the subsequent sections.

A detailed analysis has been carried out using Scopus and United States Patent and Trademark Office (USPTO) search engines with search keywords of 'shape memory alloy' or 'nitinol' for related areas as presented in Figure 2.4 and Figure 2.5.

The global market for smart materials is reported to be approximately USD19.6 billion in 2010 (McWilliams, 2011), estimated to approach USD22 billion in 2011, and forecast to reach over USD40 billion by 2016 with a compound annual growth rate (CAGR) of 12.8% between 2011 and 2016. The largest application segment of the market is actuators and motors, with sales of nearly USD10.8 billion (55% of the total market) in 2010 and forecasted to reach USD25.4 billion (approximately 64% of the market) by 2016 with CAGR of 15.4% between 2011 and 2016 (see Figure 2.6).

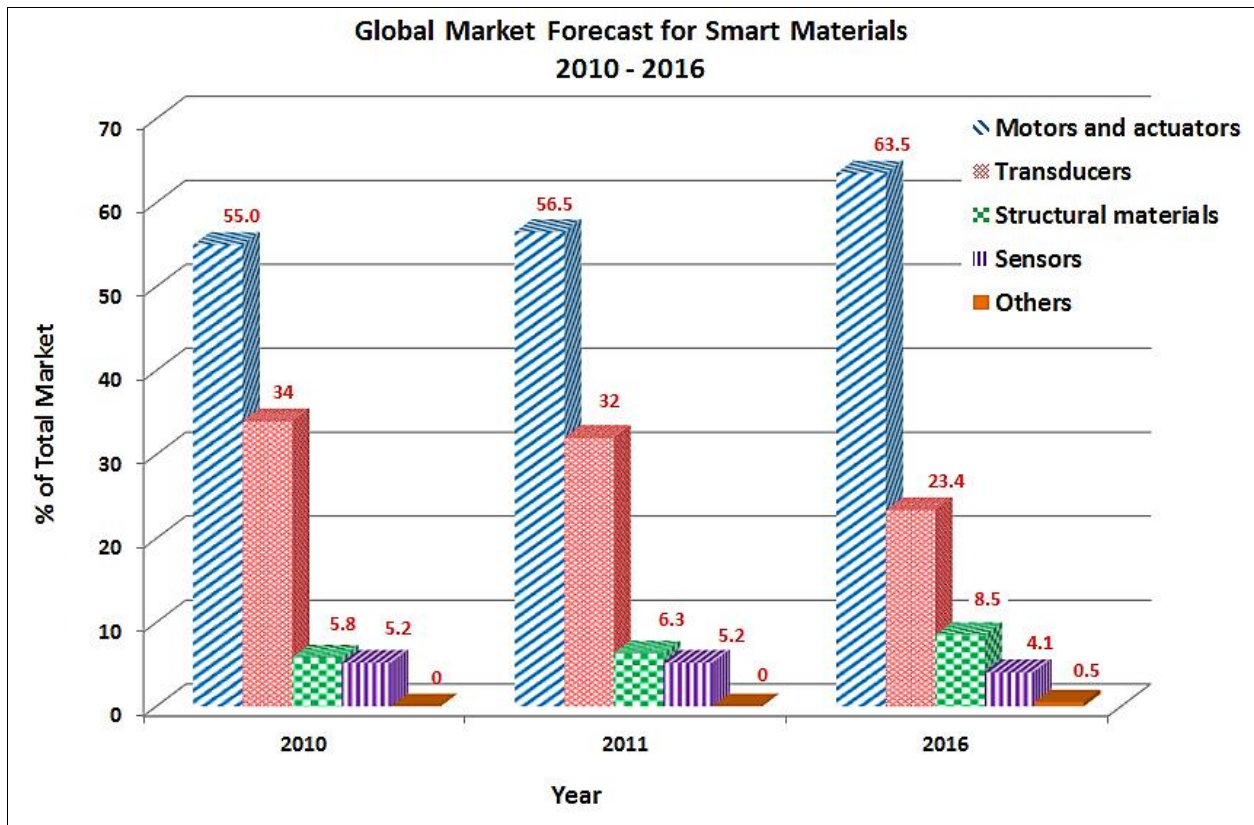


Figure 2.6 - Global market forecast for smart materials for 2010 – 2016 (McWilliams, 2011)

2.5 Designing with shape memory alloys

To date, more than 10,000 United States patents and over 20,000 worldwide patents have been issued on SMAs and their applications, but the realisation of viable products from all this intellectual property has thus far been relatively limited (Vaidyanathan, 2000; Welp & Breidert, 2004; C. Zhang *et al.*, 1996). The reason for the discrepancy between patent applications and commercial implementation lies primarily in a lack of understanding by many scientists and engineers on both the technical limitations of SMAs and the methods to apply SMAs in a robust manner to achieve technical requirements of durability and dimensional stability (P. Abrahamsson & Møster, 1997; AD Johnson, 1998; Sven Langbein & Czechowicz, 2012; Welp & Breidert, 2004; C. Zhang *et al.*, 1996).

2.5.1 Design advantages

Recent research work has shown that SMA actuators provide an excellent technological opportunity to replace conventional actuators such as electric, pneumatic and hydraulic actuators (Hartl & Lagoudas, 2007; Reynaerts & Brussel, 1998), due to their unique characteristics and ability to react directly to environmental stimuli (C. Zhang *et al.*, 1996); thus promoting the development of more advanced and cheaper actuators with a significant reduction in mechanical complexity and size (Butera *et al.*, 2007; M. Leary, Schiavone, & Subic, 2010). For example, the NiTi SMA displays one of the highest achievable actuation

work densities at 10 Jcm^{-3} (Table 2.2), which is a factor of 25 times greater than the achievable work density of electric motors (Kohl, 2010) and is able to lift more than 100 times of its own weight (Winzek *et al.*, 2004). Furthermore, NiTi SMA is bio-compatible (Mantovani, 2000; Ryhänen *et al.*, 1998), exhibits high wear resistance (WJ Buehler & Wang, 1968; Hodgson *et al.*, 1990), and the tribological behaviour has been investigated and compared to many conventional engineering materials such as steels, Ni-based and Stellite alloys (Clayton, 1993; Kohl, 2010; Richman, Rao, & Kung, 1995; JK Singh & Alpas, 1995).

Table 2.2 - Comparison of actuator performance, based on (Hunter, Hollerbach, & Ballantyne, 1991; Lederlé, 2002; Tadesse, 2013)

Actuator type	Stress [MPa]	Strain [%]	Efficiency [%]	Bandwidth [Hz]	Work per Volume [J/cm³]	Power per Volume [W/cm³]
NiTi SMA	200	10	3	3	10	30
Piezoceramic	35	0.2	50	5000	0.035	175
Single crystal piezoelectric	300	1.7	90	5800	2.55	15000
Human Muscle	0.007-0.8	1-100	35	2-173	0.035	0.35
Hydraulic	20	50	80	4	5	20
Pneumatic	0.7	50	90	20	0.175	3.5

With reference to Table 2.2, the NiTi SMA would be the obvious choice for designers of actuators that provide significant displacement and actuation force, with no critical requirements for a short response time or high efficiency. This makes NiTi SMA an attractive candidate for a variety of industrial applications, 'smart' structures and 'intelligent' systems (Angioni, Meo, & Foreman, 2011; C. Smith, Villanueva, Joshi, Tadesse, & Priya, 2011). A composite airframe with a combination of piezoelectric crystals, as the vibration sensors, and NiTi as the actuators used to counteract vibration, is an excellent example of a 'smart' structure commercial application (C. Zhang *et al.*, 1996).

Commonly, designers make use of the benefit of the engineering effects described above to design their applications, where the SME is employed for actuation and pseudo-elasticity for vibration isolation and damping (see Table 2.3). For example, the unique pseudoelastic behaviour of SMA provides a valuable commercial advantage in dampening vibrations, where its non-linear behaviour allows vibration isolation and large deformation recovery, and the associated hysteresis behaviour dissipates the vibration energy (Godard & Lagoudas, 2003; Saadat *et al.*, 2002). SMAs are also capable of actuating in a fully three-dimensional manner, allowing the fabrication of actuation components which can extend, bend and twist, in isolation or combination; and can be used in various configurations and shapes such as helical springs, torsion springs, straight wires, cantilever strips, and torsion tubes (D. Stoeckel, 1990; Waram, 1993). SMAs can provide a highly innovative approach to solve a

wide range of engineering problems and may in fact be the only viable technical option for complex applications, due to their attributes and unique advantages.

**Table 2.3 - Summary of various SMA properties and their effects
(Hartl & Lagoudas, 2007)**

SMA traits	Practical consequences
Shape memory effect	Material can be used as an actuator, providing force during shape recovery
Pseudoelasticity	Material can be stressed to provide large, recoverable deformations at relatively constant stress levels
Hysteresis	Allows for dissipation of energy during pseudo-elastic response
High actuation stress (400-700 MPa)	Small component cross-sections can provide substantial forces
High actuation strain (ca. 8%)	Small component lengths can provide large displacements
High energy density (ca. 1200 J/kg)	Small amount of material required to provide substantial actuation work
Three-dimensional actuation	Polycrystalline SMA components fabricated in a variety of shapes, providing a variety of useful geometric configurations
Actuation frequency	Difficulty in achieving high component cooling rates limits use in high frequency applications
Energy efficiency (10-15%)	Amount of thermal energy required for actuation is much larger than mechanical work output
Transformation - induced plasticity	Plastic accumulation during cyclic response eventually degrades material and leads to failure

An overview of the features and possibilities of SMA actuators is provided in Figure 2.7, which characterises the SMA actuators according to their relevant requirements and can be considered as a useful checklist for the development of SMA applications (S. Langbein, 2009). A series of charts to aid the selection of SMAs (NiTi, Cu-Zn-Al and Cu-Al-Ni) is also presented by Huang (2002), based on a number of performance indices and criteria (Ashby, 2011), with special reference to the unique features of SMA actuators.

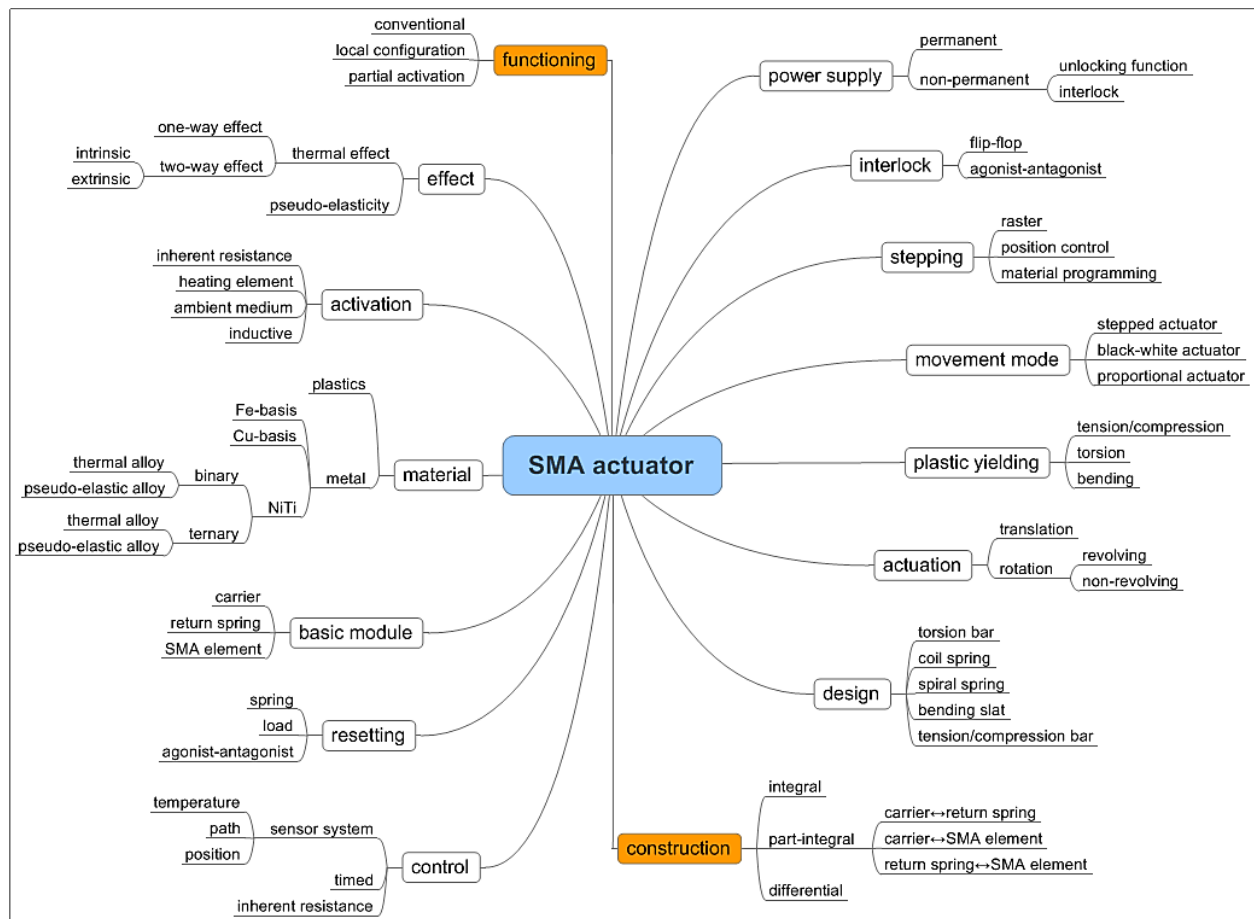


Figure 2.7 - SMA actuator element features (S. Langbein, 2009)

2.5.2 Design challenges

The challenges in designing SMA applications are to overcome their technical limitations, associated with: a relatively small strain (displacement or stroke), achievable frequency (actuation speed), controllability (and stability), positional accuracy and energy efficiency.

The major challenge for many SMA actuator applications is the low operational frequency and narrow bandwidth of SMA materials, which have a relatively high heat capacity and density, and as a result they experience difficulty in transferring the heat rapidly into and more importantly out of the active element, which leads to a severe bandwidth problem. In several studies (Chee Siong, Yokoi, & Arai, 2005b; Featherstone & Teh, 2006; Qiu, Tani, Osanai, & Urushiyama, 2001), it has been shown that rapid heating of SMA actuators can be achieved easily with several methods, such as applying large electrical currents (Joule heating) to increase the heating rate. However, without proper monitoring and control this may overheat and damage the actuator. Nonetheless, the most significant concern in bandwidth limitation is the very slow cooling process, where the heat energy removal rate is limited by the mechanisms of heat conduction and convection. The size and shape of the SMA actuator affects the actuator response time, where actuators with smaller diameter heat faster due to their higher resistivity, and cool faster due to their higher *surface area-to-*

volume ratio (SA:V) (An, Huang, Fu, & Guo, 2008; Dynalloy Inc., 2007; Lara-Quintanilla & Bersee, 2015). Therefore changing the wire diameter could change the application bandwidth dramatically (see Table 2.4). In addition, the preloading stress, loading condition and amplitude of activation also influence the response time of SMA actuators (Tadesse, Thayer, & Priya, 2010). Several strategies have been developed to improve the control of the heating process (Gorbet, Morris, & Chau, 2009; W. Huang, 2002) and to expedite the cooling process with active cooling such as forced air (Hisaaki, Kimio, Hiroyuki, & Cahoon, 1990; Howe, Kontarinis, & Peine, 1995; Tadesse *et al.*, 2010), flowing liquids (Bergamasco, Salsedo, & Dario, 1989; Mascaro & Asada, 2003; Tadesse *et al.*, 2010; Wellman, Peine, Favalora, & Howe, 1997), thermoelectric modules (i.e. Peltier or semiconductor heat pumps) (Bhattacharyya, Lagoudas, Wang, & Kinra, 1995; Brian, Kyujin, & Asada, 2006; Y. Luo, Takagi, Maruyama, & Yamada, 2000; Romano & Tannuri, 2009; Selden, Cho, & Asada, 2006; Shahin, Meckl, Jones, & Thrasher, 1994), heat sinks (Chee Siong *et al.*, 2005b; Russell & Gorbet, 1995; Tadesse *et al.*, 2010) and conductive materials (Chee Siong, Yokoi, & Arai, 2005a; S. Huang, Leary, Ataalla, Probst, & Subic, 2012; M. Leary, Schiavone, *et al.*, 2010). Table 2.4 shows the ratio of actuation speed improvement with several cooling methods (Dynalloy Inc., 2007).

Table 2.4 - Cooling methods (Dynalloy Inc., 2007)

Cooling Methods	Improvement in Speed
Increasing Stress	1.2:1
Using higher temperature wire	2:1
Using solid Heat Sink materials	2:1
Forced air	4:1
Heat conductive grease	10:1
Oil immersion	25:1
Water with Glycol	100:1
Note: Typical heating (joule heating) and cooling time (passive cooling) for HT-type (90°C) <i>Flexinol</i> wire at standard environmental condition (i.e. static air, vertical position and atmospheric pressure): <ul style="list-style-type: none"> ▪ Ø0.05mm: Heating (85mA) = 1s, Cooling = 0.3s. ▪ Ø0.51mm: Heating (4000mA) = 1s, Cooling = 14s. 	

Higher cooling rates are obtained when cooling with a fluidic medium, but this requires a special design to prevent any leakage to the environment. A small amount of air circulation around the wire is sufficient to obtain a substantial improvement compared to the natural convection case, however, several studies have also indicated that increasing the air flow would only produce a minor effect on the cooling performance and has several drawbacks such as higher energy consumption and noise production (Reynaerts & Brussel, 1998). Therefore, active cooling may not be practical in commercial applications since it contributes to increases in cost, weight, physical volume, as well the mechanical and control complexity (Gorbet *et al.*, 2009; DC Lagoudas, 2010). Alternatively, bandwidth improvement with

passive cooling is also achievable via improvements in mechanical design and control systems, such as the application of an agonist-antagonist system (Ditman, Bergman, & Tsao, 1996; Sven Langbein & Czechowicz, 2012), high surface area-to-volume ratio design (e.g. thin film SMA), and controller optimisation (e.g. gain optimisation (Gorbet *et al.*, 2009)). An assessment of transient cooling opportunities has been completed by Huang, Mohd Jani, *et al.* (2013).

The second challenge is the low associated energy efficiency. Theoretically the maximum energy efficiency of SMAs is in the range of 10-15% (Jackson, Wagner, & Wasilewski, 1972), which may fall to 10% (Jun, Rediniotis, & Lagoudas, 2007) based on the Carnot cycle efficiency in some studies, and is often less than 1% in practical applications (Humbreeck, 1999). Hence SMA actuator applications are limited to scenarios where energy efficiency is not a significant design constraint. However, it should be noted that there is a difference between SMA efficiency and actuator efficiency (i.e. efficiency of the entire system versus efficiency of SMA wire) (Thrasher, Shahin, Meckl, & Jones, 1994). Mechanically, SMA actuators come in various loading configurations. Most of the proposed actuator designs are based on a SMA spring as the active element, where large macroscopic displacements can be generated from a relatively small microscopic strain. However, the stress distribution over the cross-section of the SMA spring is not constant, and therefore requires greater material volume to generate the same force as a linear actuator, which has a negative effect on efficiency and actuator bandwidth (i.e. for the same output, a larger material volume has to be heated and cooled) (Mertmann & Vergani, 2008; Reynaerts & Brussel, 1998). Therefore, linear SMA actuators are advantageous due to the optimal use of material (i.e. more work generated from the available SMA material) (see Table 2.5).

**Table 2.5 - Comparison of loading configuration for SMA actuators
(Reynaerts & Brussel, 1998).**

Loading configuration	Efficiency (%)	Energy density (J/kg)
Tension	1.3	446
Torsion	0.23	82
Bending	0.013	4.6
<i>Note: The values in this table are calculated based on a pure elastic deformation which is acceptable as an preliminary estimate for comparing the three loading configurations.</i>		

The next challenge is the durability and reliability of SMA actuators when subjected to multiple transformation cycles, which is significantly important to be assured of long-term stability, functionality and safety for applications such as in ‘automotive safety systems’ (Strittmatter & Gümpel, 2011). Many factors influence the long-term performance and reliability of SMA actuators, including: maximum temperature, applied stress, strain and the

number of transformation cycles accumulated. SMAs have been shown to exhibit a softening of behaviour (i.e. reducing the amount of recoverable strain) as the actuator is cycled, either by heating and cooling the SMA under load (Erbstoesser, Armstrong, Taya, & Inoue, 2000; He & Sun, 2010; W. Tang & Sandström, 1993; ZG Wang *et al.*, 2004) or by mechanically cycling the wire in its super-elastic state (Iadicola & Shaw, 2002). Many researchers have concluded that thermal effects are highly relevant in determining fatigue-life, particularly for the NiTi SMA (Auguet, Isalgue, *et al.*, 2007; Auguet, Isalgue, Torra, Lovey, & Pelegrina, 2008; Auguet, Isalgué, Lovey, Martorell, & Torra, 2007; Carreras *et al.*, 2011; Carreras, Isalgue, Torra, Lovey, & Soul, 2008; Isalgue, Torra, Yawny, & Lovey, 2008; Sepulveda *et al.*, 2007; Torra *et al.*, 2010; Torra, Pelegrina, Isalgue, & Lovey, 2005). For fatigue-limited applications, the SMA actuator temperature should be controlled precisely as overheating the SMAs reduces the fatigue life considerably (Karhu & Lindroos, 2010). Recent studies (Barnes, Brei, Luntz, & LaVigna, 2007; W. Tang & Sandström, 1993; ZG Wang *et al.*, 2004) have also shown that SMA actuators with constant loading, which are higher than the recommended load (stress), experienced a reduction in stroke (strain) as the number of cycles is increased. It was also reported that overstraining of the SMA material also degraded performance, either in tension (Fumagalli, Butera, & Coda, 2009), torsion (Pieczyska, Tobushi, Date, & Miyamoto, 2010) or bending (Kitamura, Tobushi, Yoshimi, Date, & Miyamoto, 2010; Hisaaki Tobushi, Kitamura, Yoshimi, Miyamoto, & Mitsui, 2011). Increasing both stress and strain reduces the lifetime of SMA materials, and it is therefore essential to select the appropriate working boundary conditions to obtain high fatigue resistance and high reliability from SMA materials (see Figure 2.8) (Fumagalli *et al.*, 2009). In terms of fatigue performance, SMA wires were reported to be superior to SMA springs, where the recovery force and strain of SMA springs decreased by 30% after 1000 cycles and by 60% after 10,000 cycles (Tamura, Mitose, & Suzuki, 1995); in addition, the SMA springs deflection against the bias force degraded by at least 20% after ageing at 95°C for 2000 h (Michael, 1995).

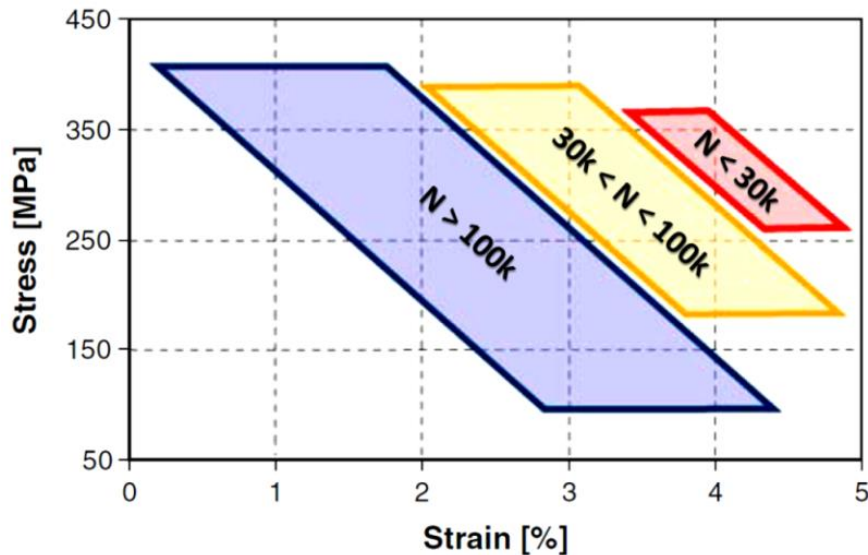


Figure 2.8 - Fatigue lifetime for Smartflex 76 under different stress-strain (Fumagalli *et al.*, 2009)

SMA actuators should be prevented from overheating, overstressing and overstraining. Generally, to guarantee the applications are designed to perform safely over a large number of cycles (about 10^6 cycles) the active elements should be prevented from overheating; and not allowed to exceed the recommended fatigue strength and strain of the SMA material (i.e. maximum load of 350 MPa (W. Huang, 2002), safe design load at 100 MPa (Reynaerts & Brussel, 1998) and 3-4% strain (Dynalloy Inc., 2007; W. Huang, 2002; Thoma, Kao, & Schmitz, 1995). The advancement in materials development and processing of commercially available SMA has reduced material degradation and fatigue, and as a result, millions of cycles are readily achievable with appropriate training and usage (Dynalloy Inc., 2007). Application of electronic controllers such as temperature sensors (Katsutoshi Kuribayashi, 1991), position feedback (Ikuta, Tsukamoto, & Hirose, 1988), resistance feedback (H. Meier, Czechowicz, Haberland, & Langbein, 2011; Schiedeck & Mojrzisch, 2011), limit curve (Bergamasco, Dario, & Salsedo, 1990), and adaptive resetting (Sven Langbein & Czechowicz, 2012) are capable of resolving overstress and overheating problems in commercial applications. Other methods to enhance SMA fatigue life include: improvement of materials (S. Miyazaki, Mizukoshi, Ueki, Sakuma, & Liu, 1999; TH Nam, Saburi, & Shimizu), fabrication processes (Jee, Han, Kim, Lee, & Jang, 2008; G. A. Porter, Liaw, Tiegs, & Wu, 2001), thermomechanical treatments (Fernandes, Mahesh, & Paula, 2013; Hornbogen, 2004; DC Lagoudas, Miller, Rong, & Kumar, 2009; M. F. X. Wagner, Nayan, & Ramamurty, 2008) and mechanical design optimisation (Sven Langbein & Czechowicz, 2012).

2.6 Other forms or types of shape memory materials

Other forms of Shape Memory Materials (SMMs) have been investigated to improve SMA performance. SMMs can be categorised in multiple forms or types, such as Co-Ni-Ga and Ni-Mn-Ga can be categorised as HTSMA and MSMA, and Ni-Ti-Pt/Pd also can be fabricated as SMM thin film.

2.6.1 High temperature shape memory alloys

Extensive research for High Temperature Shape Memory Alloys (HTSMAs) with other ternary additions to the NiTi SMA (e.g. Au, Hf, Pd, Pt and Zr) has been undertaken (Beyer & Mulder, 1994; Firstov, Van Humbeeck, & Koval, 2006; J Ma *et al.*, 2010), due to the increasing demands for high-temperature applications. Practically, HTSMAs are defined as SMAs that are operating at temperatures above 100°C, and can be categorised into three groups based on their martensitic transformation ranges (J Ma *et al.*, 2010) (see Table 2.6).

Table 2.6 - HTSMA groups and their properties, based on (H. Y. Kim, Satoru, Kim, Hosoda, & Miyazaki, 2004; Lelatko & Morawiec, 2001; J Ma *et al.*, 2010; R. Noebe *et al.*, 2005)

Group	Alloy composition	Transformation temperature range [°C]	Thermal hysteresis [°C]	Strain [%]	Recovery [%]	Comments
100 - 400°C	Ti-Ni-Pd Ti-Ni-Pt	100 – 530 110 – 1100	20 – 26 31 – 55	2.6 – 5.4 3 -4	90 ^{PE} -100 100	High work output, most commercial ready and high materials cost.
	Ni-Ti-Hf Ni-Ti-Zr	100 – 400 100 – 250	60 54	3 1.8	100 100	Reasonable SME, large hysteresis and relatively low materials cost.
	Cu-Al-Ni Cu-Al-Nb	100 – 400	21.5 59 - 170	3 – 5 ^{PE} 5.5 - 7.6	80 – 90 ^{PE} -	Low cost, poor to reasonable SME, and brittle in tension (Cu-Al-Ni).
	Co-Al Co-Ni-Al	100 – 400	121 15.5	2 5 ^{PE}	90 100 ^{PE}	Good workability, large hysteresis and high temperature PE (Co-Ni-Al)
	Ni-Al Ni-Mn Ni-Mn-Ga	100 – 300 100 – 670 100 – 400	- 20 85	- 3.9 10	- 90 70	Low materials cost, low hysteresis and poor tensile ductility.
	Zr-Cu	100 – 600	70	8	44	Good ductility and workability, but poor SME.
	Ti-Nb U-Nb	100 – 200 100 – 200	50 35	2 – 3 7	97 - 100	Good ductility and SME, but subject to oxidation and contain Uranium (U-Nb).
400 - 700°C	Ti-Pd Ti-Au	100 – 510 100 - 630	40 35	10 3	88 100	Good ductility (Ti-Pd), but high materials cost (Ti-Pt).
> 700°C	Ti-Pt-Ir	990 – 1184	66.5	10 ^{PE}	40 ^{PE}	High yield strength.
	Ta-Ru Nb-Ru	900 – 1150 425 – 900	20	4 4.2	50 88	Stable microstructural, but poor oxidation resistance and small hysteresis.

Note: PE = Pseudoelastic

Unfortunately, most HTSMAs are very difficult to process and to train due to their limited ductility or poor fatigue resistance at room temperature, making them very expensive to manufacture. Therefore, alternative low cost materials or compositions such as copper and cobalt have been researched. At present, only TiNiPd, TiNiPt, NiTiHf, NiTiZr and CuAlMnNi alloys are useful at 100-300°C, and the others have significant challenges to commercial application and require further work (J Ma *et al.*, 2010).

2.6.2 Magnetic shape memory alloys

Magnetic shape memory alloys (MSMAs), which are also known as ferromagnetic shape memory alloys (FSMAs) can actuate at higher frequencies (up to 1 kHz) because the actuation energy is transmitted via magnetic fields and is not hindered by the relatively slow heat transfer mechanism (Tellinen, Suorsa, Jääskeläinen, Aaltio, & Ullakko, 2002). FSMA strain rate is quite comparable to magnetostrictive and piezoelectrics active elements, but at strains as large as are achievable with SMAs (see Figure 2.9, (J Ma *et al.*, 2010)). FSMA can also provide the same specific power as SMAs, but this power can be delivered at higher frequencies than for SMAs (see Figure 2.9) (J Ma *et al.*, 2010). The maximum strain of FSMA is 32 times higher than the magnetostrictive Terfenol-D (TbDyFe_2), but the trade-off for the greater strain is 46 times lower (about 0.5 GPa stiffness) (Czimmek, 2004). Consequently, FSMAs are suitable to fill the technological gap between SMAs and magnetostrictive materials, and provide a commercial niche for motor and valve applications (Henry, 2002) that require significantly displacement at lower actuation force (Czimmek, 2004).

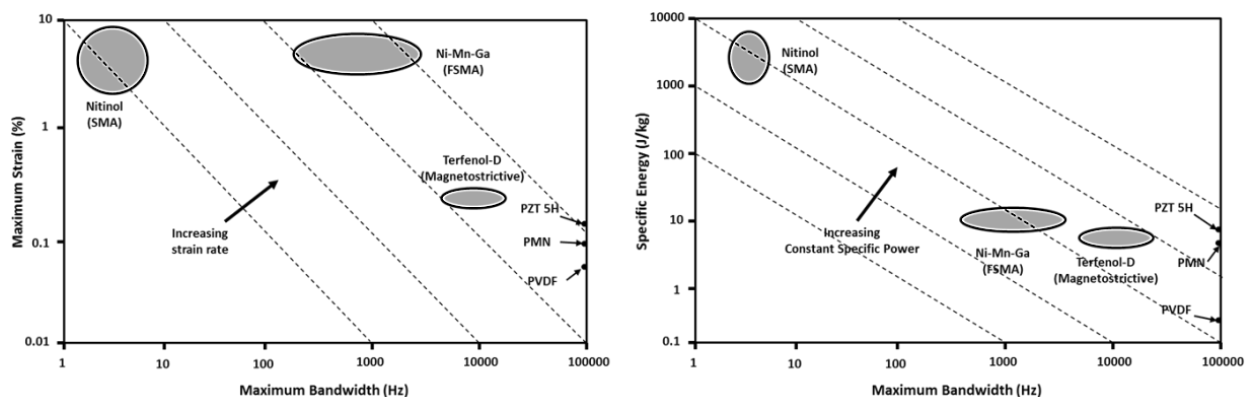


Figure 2.9 - Maximum strain and specific energy versus maximum bandwidth for different classes of active materials (J Ma *et al.*, 2010)

However, in general MSMA also experience similar design issues as described above for SMAs (Lu, Liang, & Qu, 2009). Furthermore, MSMAs are very brittle, stiff and only operable at low temperature (Czimmek, 2004; Heczko & Straka, 2003; Tsuchiya, Tsutsumi, Ohtsuka, & Umemoto, 2004). Therefore, MSMAs are difficult to shape and to form, and are not suitable for many present applications at present which require high temperatures and high force. Fundamental research continues to develop a better understanding of the constitutive behaviour of these MSMAs (such as Ni-Mn-Ga, Fe-Pd and Ni-Mn-Al) in order to further improve the materials.

2.6.3 Shape memory material thin film

SMM thin films evolved from the advancement of fabrication technology, where SMMs are deposited directly onto micro-machined materials or as stand-alone, thin film micro-actuators (Fu, Du, Huang, Zhang, & Hu, 2004; Gabriel, Mehregany, & Walker, 1989; AD Johnson, 2009; Krulevitch *et al.*, 1996; S. Miyazaki & Ishida, 1999; Winzek *et al.*, 2004). Moreover, in the rapidly growing field of micro-electro-mechanical systems (MEMS), NiTi thin films have become the actuator of choice at the micro-scale level, due to the attributes as described earlier (i.e. higher actuation force and displacement), but at relatively low frequency (up to 100 Hz) and efficiency, as well as the non-linear behaviour (Fu *et al.*, 2004; Kahny *et al.*, 1998; Krulevitch *et al.*, 1996; S. Miyazaki & Ishida, 1999) (see Table 2.7). The versatility of NiTi thin film with multiple degrees of freedom and compact structure, expand the potential of NiTi in biomedical, aerospace, automotive, and consumer products applications. Miniature NiTi actuated devices based on sputtered NiTi films are anticipated to capture a significant market share, especially for medical micro-devices and implantable applications (Fu *et al.*, 2004).

**Table 2.7 - Micro-actuators comparison, based on
(Fu *et al.*, 2004; Krulevitch *et al.*, 1996; S. Miyazaki & Ishida, 1999)**

<i>Micro-actuators</i>	<i>Maximum Energy Density (J/m³)</i>	<i>Maximum Frequency (Hz)</i>	<i>Efficiency (%)</i>
NiTi thin film	2.5×10^7	<100	1
Electrostatic	1.8×10^5	<10000	50
Electromagnetic	4.0×10^5	<1000	< 1
Piezoelectric	1.2×10^5	<5000	30
Bimetallic	4.0×10^5	<100	0.01
Thermo-pneumatic	5.0×10^5	<100	10
Conductive polymer	3.4×10^6	<1000	60

2.6.4 Shape memory polymers

Shape memory polymers (SMPs) are relatively easy to manufacture and fast to train (or program) as well being able to be tailored for a variety of applications. SMPs are claimed to be a superior alternative to SMAs due to their low associated cost (at least 10% cheaper than SMAs), higher efficiency, biodegradable properties, and robust mechanical properties (see Table 2.8) (Lendlein & Kelch, 2002; C. Liu, Qin, & Mather, 2007; Ochonski, 2010; Voit *et al.*, 2010; Witold, Annick, Shunichi, L'Hocine, & Jean, 2007). In addition, SMPs can sustain two or more shape changes (Bellin, Kelch, Langer, & Lendlein, 2006; Hu, Zhu, Huang, & Lu, 2012; Xie, 2010) when triggered by thermal heating (WM Huang *et al.*, 2012) or cooling (CC Wang, Huang, Ding, Zhao, & Purnawali, 2012), electrical (Yanju Liu, Lv, Lan, Leng, & Du, 2009), magnetic field (Mohr *et al.*, 2006), light (Lendlein, Jiang, Jünger, & Langer, 2005), chemical solutions (Lv, Leng, Liu, & Du, 2008; WM Huang *et al.*, 2012) or water (WM Huang, Yang, An, Li, & Chan, 2005; Leng, Lv, Liu, & Du, 2008). Generally, there are three categories of SMPs (K Otsuka & Wayman, 1999), and most of them are naturally either thermo- or chemo-responsive (WM Huang *et al.*, 2012). When one considers the vast commercial application of polymer products, it is apparent that SMPs have significant commercial application (Behl & Lendlein, 2007; Hu *et al.*, 2012; Ratna & Karger-Kocsis, 2008; Sun *et al.*, 2013), including smart fabrics (Hu, 2007), self-repairing (or seal-healing) plastic components (CC Wang, WM Huang, Z. Ding, Y. Zhao, H. Purnawali, *et al.*, 2012), spacecraft sails (Campbell, Lake, Scherbarth, Nelson, & Six), biomedical devices (Baer, Wilson, Matthews, & Maitland, 2007; Gall *et al.*, 2005; Hayashi; Witold *et al.*, 2007) and intelligent structures. The characteristics of SMPs are summarised in Table 2.8.

There are three basic working mechanisms for the SME in polymeric materials: Dual-state mechanism, dual-component mechanism (DCM) and partial-transition mechanism (PTM) (WM Huang *et al.*, 2012). The recovery precision of more than 99% makes SMPs suitable for highly demanding applications (Lendlein & Kelch, 2002). Similar to SMAs, the SME of SMPs varies depending on the composition of the material used, i.e. weight fraction of the switching segments and the molecular weight of the polymer-chain employed. The biodegradable nature of certain SMPs provide advantages over metal implants, where the removal of the implant after regeneration can be avoided, thus gentler, more effective and more economical treatments can be offered. However, despite the advantages described above, SMAs are still preferred for applications that require higher actuation forces and faster response.

**Table 2.8 - Comparison of SMP and SMA properties, based on
(C. Liu *et al.*, 2007; Ochonski, 2010)**

Property	SMP	SMA
Density (gcm ⁻³)	0.9 to 1.25	6 to 8
Transition breath (°C)	10 to 50	5 to 30
Phase transformations	Glass transition	Martensitic transformation
Strain (%)	up to 400, and possibly above 800	up to 8%
Young's modulus (GPa) at T < T _{Trans} at T > T _{Trans}	0.01 to 3 (0.1 to 10) x 10 ³	83 (NiTi) 28 to 41
Deform stress (MPa)	1 - 3	50 to 200
Recovery stress (MPa)	1 - 3	150 to 300
Recovery speeds (s)	< 1s to several min.	< 1s
Thermal conductivity (W/m.K)	0.15 to 0.30 W/m.K	18 (NiTi, Austenite)
Bio-compatibility and degradability	High	Not all biocompatible. Not biodegradable.
Corrosion performance	Excellent	Excellent
Condition at high temperature	Soft	Hard
Condition at low temperature	Hard	Soft
Cost	Cheap (ca. USD10/lb)	More expensive (ca. USD250/lb)
Shape training	Easy and fast	Difficult
Fabrication / Processing condition	<200°C, low pressure	>1000°C, high pressure

2.6.5 Miscellaneous

A summary of existing shape memory materials are described in Table 2.9 below.

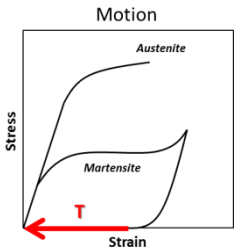
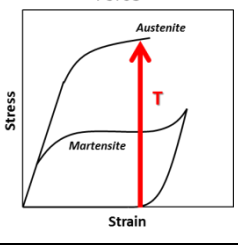
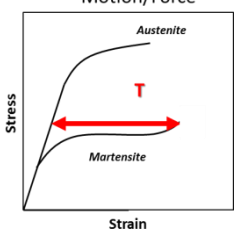
**Table 2.9 - Materials with SME, based on
(Czimmek, 2004; Kohl, 2010; C. Liu *et al.*, 2007; J Ma *et al.*, 2010)**

Materials	Examples	Notes
Metals	<p>SMA:</p> <ul style="list-style-type: none"> NiTi-based alloys: NiTi, NiTiCu, NiTiPd, NiTiFe, NiTiNb, NiFeGa, NiTiCo Cu-based alloys: CuZn, CuZnAl, CuAlNi, CuAlNiMn, CuSn... Fe-based alloys: FePt, FeMnSi, FeNiC ... Ag-based alloys: AgCd ... Au-based alloys: AuCd ... Co-based alloys: CoNiAl... 	<p>The best choice is NiTi SMA.</p> <p><u>E.g. NiTi-based:</u> Frequency: ≤ 3Hz, dia. 100μm with natural cooling (Very Slow). Strain: max. 10% (High), Recommended: 4%. Stress: up to 500 MPa (High), Recommended: 100 MPa. Max. operating temp: ca. 100°C (Low).</p>
	<p>MSMA/FSMA: NiMnGa, FePd, NiMnAl, FePt, Dy, Tb, LaSrCuO, ReCu, NiMnIn, CoNiGa...</p>	<p>NiMnGa was first discovered in 1984 (Webster, Ziebeck, Town, & Peak, 1984) and have received increasing interest since the principle of the MSMA was presented by Ullakko <i>et al.</i> (K. Ullakko, Huang, Kantner, O'Handley, & Kokorin, 1996; K. Ullakko, Huang, Kokorin, & O'Handley, 1997).</p> <p><u>E.g. NiMnGa:</u> Frequency: max. 2kHz (High), Recommended: 500 Hz Strain: max. 10% (High), Typical: 6% Stress: max. 9MPa (Low), Typical: 3.4MPa Young modulus: 0.5GPa (Very Low) Max. operating temp: 72°C. (Low), full austenite transition at 48°C.</p>
	<p>HTSMA: TiNiPd, TiNiPt, NiTiHf, NiTiZr, ZrRh, ZrCu, ZrCuNiCo, ZrCuNiCoTi, TiMo, TiNb, TiTa, TiAu, UNb, TaRu, NbRu, FeMnSi and etc.</p>	<p>So far, TiNiPd and TiNiPt produced the best results and commercially ready.</p> <p><u>E.g. TiNiPd (Bigelow, Padula, Garg, Gaydosh, & Noebe, 2010):</u> Frequency: < 1 Hz with natural cooling (Very Slow) Strain: 1.5 - 4.0% (Med) Stress: max. 295 MPa (High) Max. operating temp: 83 - 513°C (Very high)</p>
Polymers	<p>PTFE, PU, Poly-caprolactone, EVA + nitrile rubber, PE, Poly-cyclooctene, PCO-CPE blend, PCL-BA copolymer, Poly(ODVE)-co-BA, EVA + CSM, PMMA, Copolyesters, PET-PEG ...</p>	<p>First publication described SME in polymers was in 1941 (Vernon & Vernon, 1941) that is much earlier than SMA.</p> <p><u>E.g. PU-based:</u> Frequency: max 1 Hz (Very Slow) Strain: >800% (Very High) Stress: 3 MPa (Low)</p>
Ceramics	<p>ZrO₂ (PSZ), MgO, CeO₂, PLZT, PNZST ...</p>	<p>Shape memory ceramics has limited shape memory effect (below 0.5 %) (Cederström & Van Humbeeck, 1995; Swain, 1986; Uchino, 1989).</p> <p><u>E.g. PNZST:</u> Frequency: ca. 1 kHz (High) Strain: < 1 % (Very low) Stress: max.100 MPa (High), Typically: 35 MPa. Operating temp: 200 - 500°C (Very high).</p>
Others	<p>SMM thin film: NiTi, SMP and etc.</p>	<p>This technology is based on smart materials applied to a thin film to produce SME for MEMS applications (Krulvitch <i>et al.</i>, 1996).</p> <p><u>E.g. NiTi-based:</u> Frequency: <100 Hz (Med) Strain: max. 10% (High), Typically: 7%. Stress: up to 500 MPa (High), Recommended: 100-350MPa. Max. operating temp: ca. 100°C (Low).</p>

2.7 Shape memory alloys applications

Generally, shape memory applications can be divided into four categories according to the primary function of their memory element as shown in Table 2.10 (TW Duerig, 1990; Hodgson *et al.*, 1990); where the SME can be used to generate motion and forces, and the SE can store the deformation energy (Stöckel, 1995).

Table 2.10 - Shape memory application categories, based on (TW Duerig, 1990; Hodgson *et al.*, 1990; Stöckel, 1995)

Category	Description	Examples
Free recovery	<p>The sole function of the memory element is to cause <i>motion</i> or <i>strain</i> on the applications.</p> <p>Working principle: The memory element is stretched and then released (no load applied). It remains in stretched condition until heated above the transition temperature and shrink back to its original form, and subsequent cooling below the transition temperature does not cause any macroscopic shape change (e.g. OWSMA).</p>	<p>NiTi eyeglass frames (TiFlex™, TITANFlex®) and Simon IVC filter.</p> 
Constrained recovery	<p>The memory element is prevented from changing shape and thereby generates a <i>stress</i> or <i>force</i> on the applications.</p> <p>Working principle: The memory element is prevented from returning to its original form after being stretched and considerable force generated if heated above the transition temperature.</p>	<p>Hydraulic couplings, fasteners and connectors: CryoFit™, Cryocon®, UniLok®, CryOlive®, CryoFlare®, CryoTact®, Permacouple®, Tinel Lock® and BetaFlex™.</p> 
Actuator or work production (Force actuator, proportional control and two-way-effect with external reset force)	<p>There is <i>motion</i> against a <i>stress</i> and thus work is being done by the memory element on the applications. Most of applications fall in this category. Can be either OWSMA or TWSMA. Three types of actuators:</p> <p><u>Force actuator:</u> The memory element exerts force over a considerable range of motion, and often for many cycles.</p> <p><u>Proportional control:</u> The memory element used only part of its selected portion of shape recovery to accurately position the mechanism, because the transformation occurs over a range of temperatures rather than at a single temperature.</p> <p><u>Two-way-effect with external reset force:</u> The memory element generates motion to overcome the opposing force, and thus do work. The memory element contracts upon heating to lift a load, and the load will stretch the heating element and reset the mechanism upon cooling (e.g. TWSMA).</p>	<p>Electrical actuators (VEASE™, SMARt Clamp™), thermal actuators (Memrysaf®), circuit breaker, window or louvre opener, valves), and heat engines.</p> 
Superelasticity	<p>The applications are isothermal in nature and involve the storage of potential energy.</p>	<p>Eyeglass frame, orthodontic archwire, Mammelok® breast hook, guidewires, anchors and underwire brassiere.</p>

The unique behaviour of NiTi SMAs have enabled new, innovative applications in the aerospace, automotive, automation and control, appliance, energy, chemical processing, heating and ventilation, safety and security, and electronics (MEMS devices) industries. Some of these applications apply similar methods, concepts or techniques, which are also transferable to other application domains; such as the NiTi thermovaryable rate (TVR) springs, which are used to control door opening in a self-cleaning oven, and are also used to offer smooth gear shifting for Mercedes-Benz automatic transmissions, for domestic safety devices to control the hot water flow (e.g. Memrysafe® antiscald valves from Memry Corporation), and for industrial safety valves to prevent the flow of flammable and dangerous gasses (e.g. Firechek® from Memry Corporation)(TW Duerig, 1990; Dieter Stoeckel & Waram, 1992; Stöckel, 1995; MH Wu & LM Schetky, 2000)(see Figure 2.10). More interesting, in terms of commercial opportunities is the fact that these SMA actuators act as both a sensor and an actuator in these applications (MH Wu & LM Schetky, 2000).

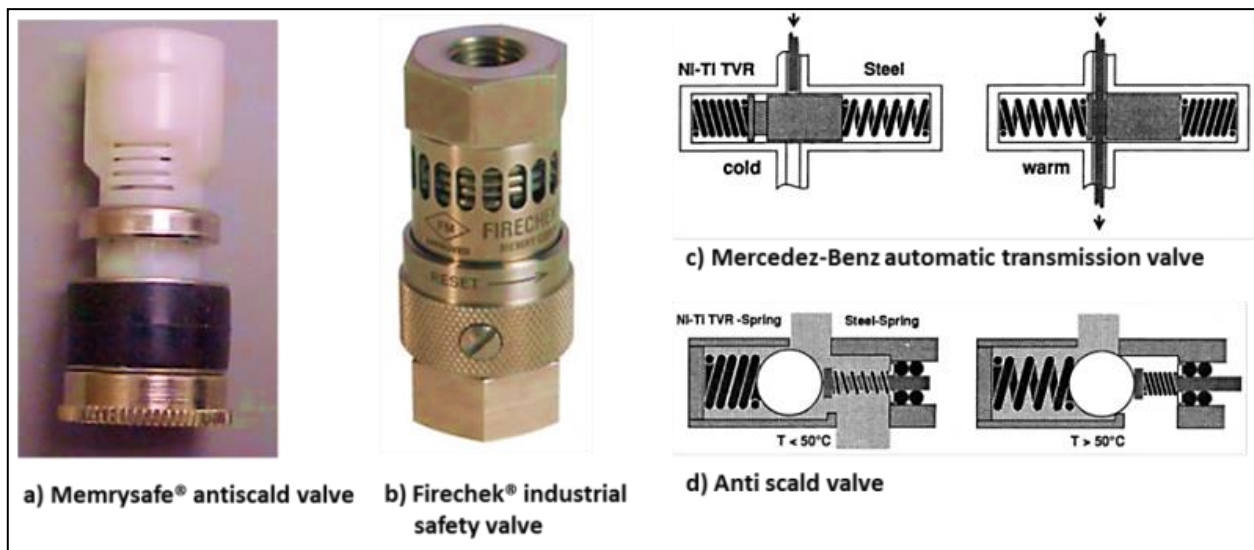


Figure 2.10 - NiTi thermovaryable rate (TVR) springs applications, image based on (Dieter Stoeckel & Waram, 1992; MH Wu & LM Schetky, 2000)

Selected state-of-the-art and relevant SMA applications and patents are presented in this section, particularly from the automotive, aerospace, robotics and biomedical domains. A brief summary of other related SMA applications and discoveries is provided in the appendices.

2.7.1 Automotive applications

In modern vehicles, the number of sensors and actuators is continuously increasing due to customer demand for safer, more comfortable vehicles with enhanced performance. For example, emerging drive-by-wire technologies, offers a wide range of opportunities for SMA actuators as an alternative to electromagnetic actuators in automotive applications (Butera, 2008; Butera *et al.*, 2007; D. Stoeckel, 1990). Existing and potential SMA applications for passenger vehicles are presented in Table 2.11, which categorises applications according to vehicle functional areas (Butera, 2008). Most of the selected components are occasional use linear actuators (e.g. rear-view mirror folding, climate control flaps adjustment and lock/latch controls) and active thermal actuators (e.g. engine temperature control, carburetion and engine lubrication, and powertrain clutches) (D. Stoeckel, 1990; Dieter Stoeckel & Tinschert, 1991). However, due to the SMA morphing capability (active and adaptive structures), commercial automotive applications are also expanding into other areas, such as aerodynamic and styling applications (Table 2.11).

The mechanical simplicity and miniaturisation possibilities associated with SMA actuators reduce the scale, weight and cost of automotive components significantly, and provide substantial performance benefits in comparison to conventional actuators. This opportunity is demonstrated by the example provided by Neugebauer *et al.* (2010b) (see Table 2.12). The versatility of SMA actuators to integrate with other design mechanisms and techniques, make it an excellent actuator for automotive applications (see Figure 2.11), for example, the electrically actuated antiglare rear-view (EAGLE) mirror by Luchetti *et al.* (2009).

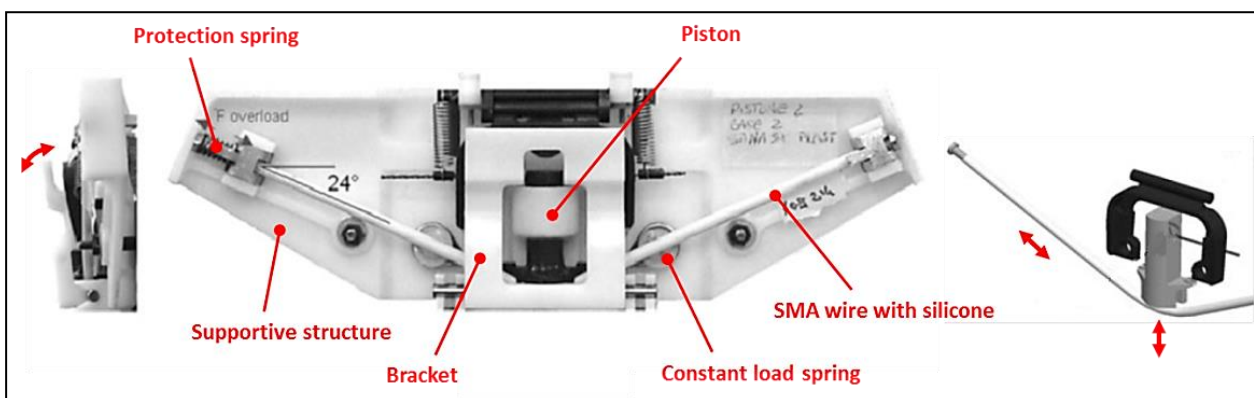
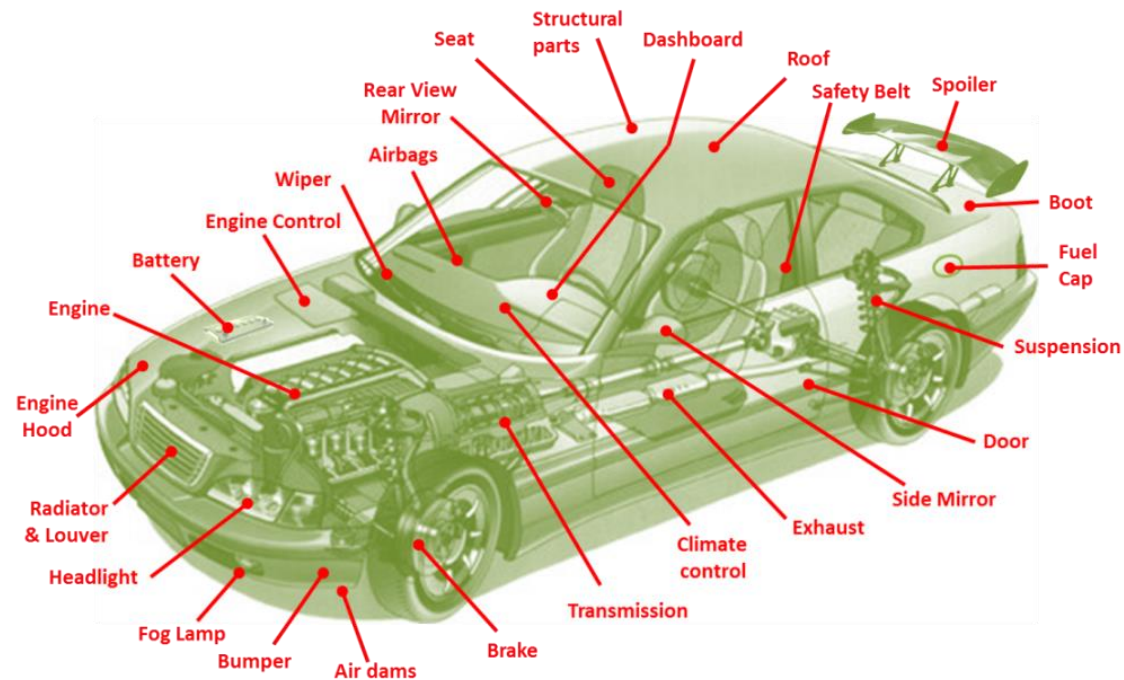


Figure 2.11 - EAGLE mirror prototype (Luchetti *et al.*, 2009)



Table 2.11 - Existing and potential SMA applications in the automotive domain, based on (Butera, 2008; R. W. Johnson, Evans, Jacobsen, Thompson, & Christopher, 2004; Mohd Jani, Leary, Subic, *et al.*, 2014; D. Stoeckel, 1990)



CATEGORIES / PARTS	REFERENCES
ENGINE ROOM / UNDERHOOD	
<i>Radiator</i>	(Aase, Browne, Johnson, & Ulicny, 2006; AL Browne & Johnson, 2009; Macgregor, Szilagyi, & Von Behrens, 2004; Mc Knight <i>et al.</i> , 2008)
<i>Fan clutch</i>	(Bohan, 2009)
<i>Engine control (sensors and actuators)</i>	(Shaw, Prince, Snyder, Willett, & Lisy, 2009)
<i>Start-up clutch</i>	(Predki & Bauer, 2010)
<i>Tumble flaps</i>	(Bellini, Colli, & Dragoni, 2009)
<i>Fuel injector / Fuel system</i>	(Allston, Knebel, & Salemi, 2000; Kilgore & Robinson, 2000; Knebel & Salemi, 2004; Wu, 1999)
<i>Piston rings</i>	(Shuichi Miyazaki, Onoda, Okada, Fujii, & Kim, 2008)
<i>Booster / Charger</i>	(D. Stoeckel, 1990)
<i>Valves</i>	(Perry & Veinotte, 2006; D. Stoeckel, 1990)
<i>Battery</i>	(Jones, Campbell, & Janmey, 2010)

CATEGORIES / PARTS	REFERENCES
DRIVETRAIN	
<i>Transmission control</i>	(AL Browne, Johnson, Mankame, <i>et al.</i> , 2009; Mitteer, 2010; D. Stoeckel, 1990)
INTERIOR / PASSENGER ROOM	
<i>Dashboard</i>	(AL Browne & Johnson, 2005)
<i>Rear view mirror</i>	(Luchetti <i>et al.</i> , 2009)
<i>Seats</i>	(Alexander, Brown, & Zolno, 2011; H. Harry Asada, Cho, & Roy, 2005; AL Browne, Johnson, Khoury, Alexander, & Carpenter, 2009; AL Browne, Johnson, & Sears, 2011; AL Browne <i>et al.</i> , 2010; Gandhi, 2010; K. R. Kennedy, Nathan, Hanlon, & Maue, 2010; Jennifer P. Lawall, McQueen, Johnson, Browne, & Alexander, 2011; RJ Yang, Le, Chou, & Tzou, 2007)
<i>Airbags</i>	(Gheorghita <i>et al.</i> , 2013; Jennifer P Lawall <i>et al.</i> , 2010)
<i>Structural parts / Impact structures</i>	(AL Browne & Johnson, 2005; AL Browne, Johnson, Chernoff, <i>et al.</i> , 2011; Melz, Seipel, Sielhorst, & Zimmerman, 2011)
BODY AND EXTERIOR	
<i>Headlights / Lamps</i>	(AL Browne, Aase, Johnson, & Keefe, 2007; Hashemi & Schickel, 2011; D. Stoeckel, 1990)
<i>Wiper</i>	(Buchanan & Victor, 1991; Kutlucinar, 2005b; D. Stoeckel, 1990)
<i>Sunroof / Sunshade</i>	(Alacqua, Capretti, Biasiotto, & Zanella, 2010; Butera, Alacqua, & Zanella, 2006; Lane, 2008; Mc Knight <i>et al.</i> , 2008)
<i>Door and locking mechanism</i>	(AL Browne, Stauffer, Mathieu, Szczerba, & Johnson, 2009; Dominique, 2003a, 2003b; Gehm, 2007; J. D. Niskanen, Daniels, & Mrkovic, 2008; D. Stoeckel, 1990)
<i>Side mirror</i>	(Suzuki, 1986; EA Williams, Shaw, & Elahinia, 2010; Zychowicz, 1992)
<i>Boot</i>	(AL Browne, Stauffer, <i>et al.</i> , 2009; GM, 2013)
<i>Engine hood</i>	(Brei <i>et al.</i> , 2006; Strittmatter, Gümpel, & Zhigang, 2009)
<i>Petrol cap</i>	(Neugebauer, Bucht, Pagel, & Jung, 2010a)
<i>Bumpers and crash structures</i>	(AL Browne & Johnson, 2005; AL Browne, Johnson, & Kramarczyk, 2006; AL Browne, Johnson, & Sears, 2011; Choi, 2011)
<i>Air dams</i>	(Gehm, 2007; Rober, Browne, Johnson, & Aase, 2010)
<i>Grill / Louver</i>	(AL Browne & Johnson, 2009; Gehm, 2007; Mc Knight <i>et al.</i> , 2008)
<i>Spoiler</i>	(AL Browne, Johnson, Rober, <i>et al.</i> , 2009)
<i>Structural parts / Panels</i>	(AL Browne, Johnson, Chernoff, <i>et al.</i> , 2011; AL Browne <i>et al.</i> , 2005; AL Browne, Mankame, Johnson, & Keefe, 2007; Mc Knight <i>et al.</i> , 2008; RJ Yang <i>et al.</i> , 2007)
SUSPENSION / STEERING / WHEEL & TYRE	
<i>Brake</i>	(AL Browne, Johnson, Mankame, <i>et al.</i> , 2009; Zimmer & Zimmer, 2006)
<i>Absorber</i>	(D. Stoeckel, 1990)
<i>Tyre</i>	(Oku, 1993)

**Table 2.12 - Comparison of DC-Drive and SMA-Drive for fuel door actuator
(Neugebauer *et al.*, 2010a)**

Parameters	DC-Drive	SMA-Drive
		
Actuation time (Complete cycle open-close)	3 sec.	2-3 sec.
Installation space	Compact	Stretched along the air duct
Acoustics emission (from drive)	Slight noise	No noise
Mechanical complexity	High	Low
Mass	approx. 65 gm.	approx. 20gm.
Positioning accuracy	$\pm 1.5^\circ$	$\pm 2.25^\circ$
Energy consumption	1 W during flap movements	1W permanent

General Motors (GM) state that their engineers have been working with SMA applications since the mid-1990s, and that SMA would be likely first implemented on their 2013 model-year cars (Weber, 2010). So far GM has lodged in the order of 250 SMA related patents, including: SMA electric generator to generate electricity from exhaust heat; a situation-dependent active louver to control the airflow into the engine compartment; on-demand air dam to reduce aerodynamic drag at highway speeds; and, an adaptive 'grab handle' to ease the opening vehicle doors (AL Browne, Alexander, *et al.*, 2011; Gehm, 2007) (Figure 2.12). Recently the seventh-generation of the Chevrolet Corvette was to be the first GM vehicle with a SMA actuator to actuate the hatch vent that releases air from the trunk for reduced trunk-lid closing effort (GM, 2013).

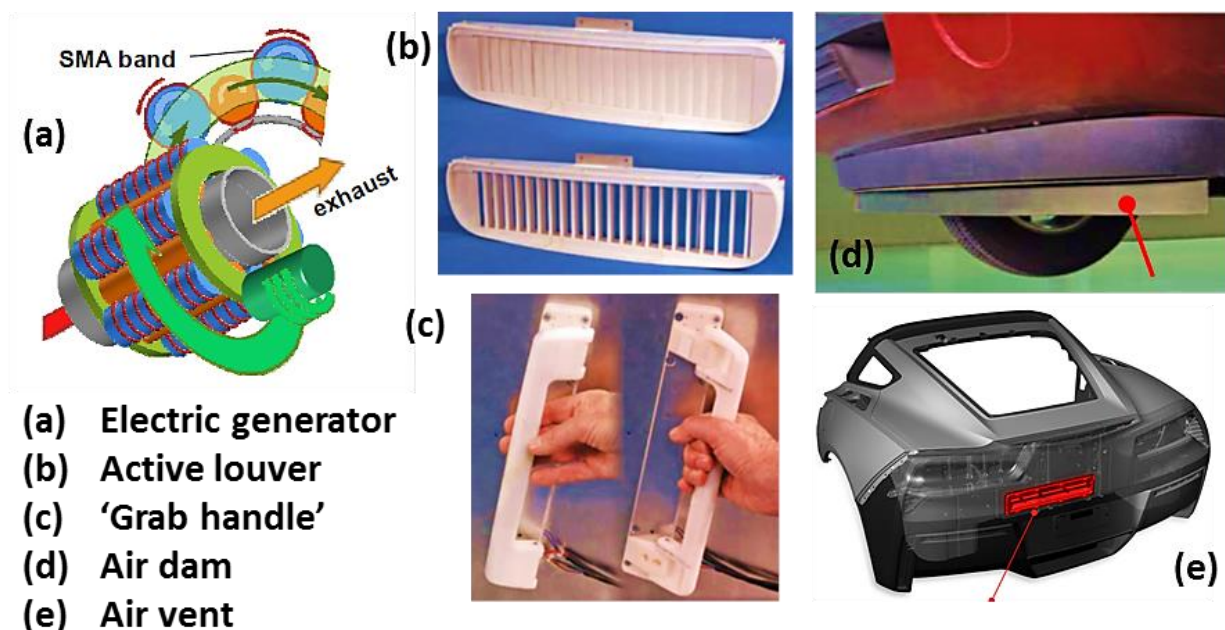


**Figure 2.12 - Emerging General Motors' SMA applications, image based on
(AL Browne, Alexander, *et al.*, 2011; Gehm, 2007; GM, 2013)**

Other commercial SMA applications developed for the automotive industry include: SMA activated automotive tumble flaps (Bellini *et al.*, 2009) to replace conventional electromagnetic and pneumatic effectors; an automatic pedestrian protection system (pop-up bonnet) to minimise pedestrian injuries during impact collisions (Strittmatter *et al.*, 2009); a cost effective side mirror actuator (Suzuki, 1986; EA Williams *et al.*, 2010; Zychowicz, 1992); and a micro-scanner system for optical sensing of an objects distance and angle with a FSMA actuator (Brugger, Kohl, Hollenbach, Kapp, & Stiller, 2006) (Figure 2.13).

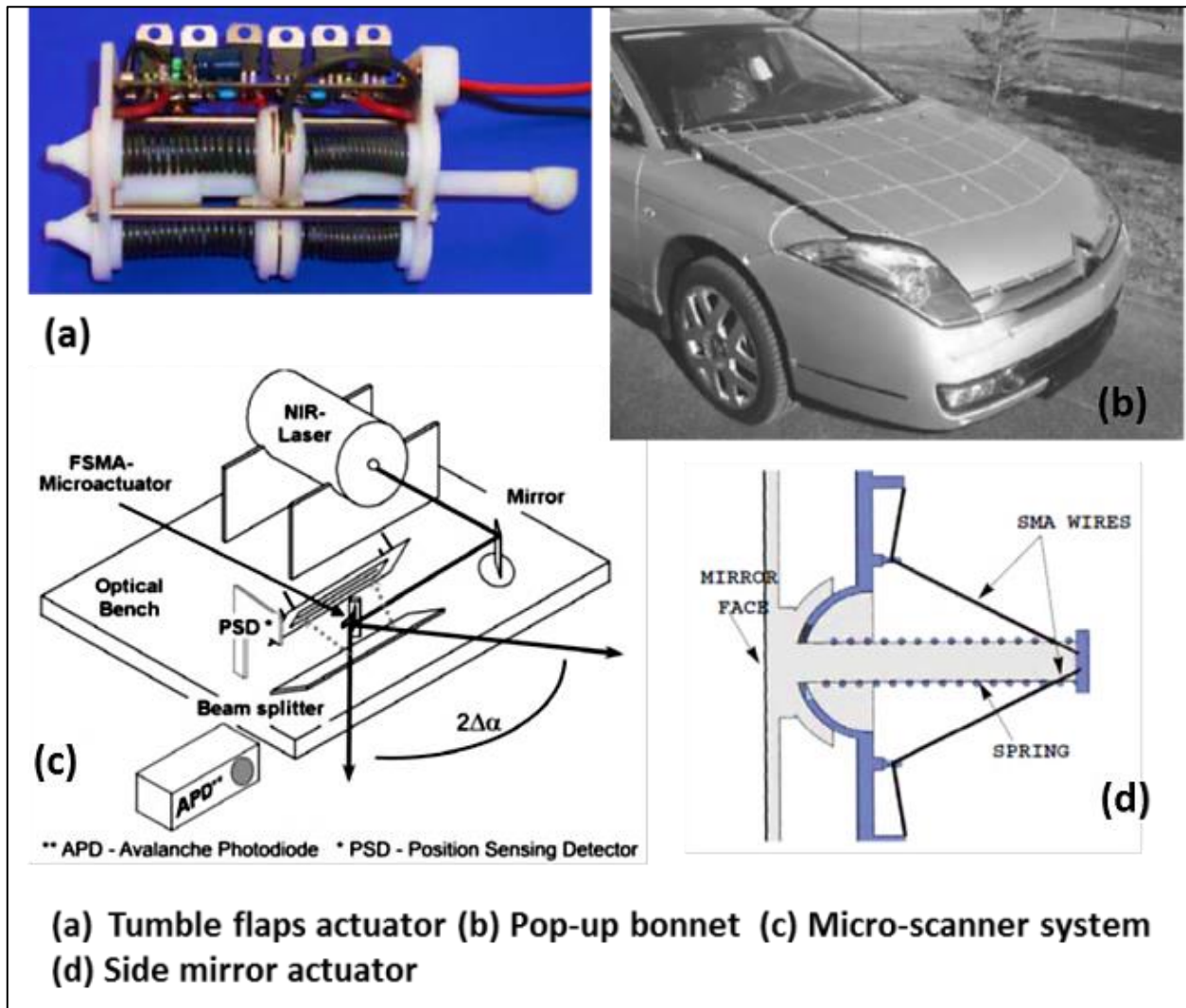


Figure 2.13 - Other commercial SMA applications in the automotive domain, image based on (Bellini *et al.*, 2009; Brugger *et al.*, 2006; Strittmatter *et al.*, 2009; EA Williams *et al.*, 2010)

There are numerous potential commercial SMA applications that have been proposed in the patent literature, and summarised in this work, however, few of these proposed actuators have actually been commercially implemented or are technically and economically feasible due to the limited range of transformation temperatures for commercial SMAs. Other technical challenges, such as durability, hysteresis width, and stability must also be considered, especially when dealing with extreme operating conditions and stringent safety and reliability requirements associated with the automotive domain (Table 2.13). One of the challenges specific to automotive applications is the compatibility of SMA with automotive batteries; this challenge is directly assessed by (M. Leary, Huang, Ataalla, Baxter, & Subic, 2013).

**Table 2.13 - Typical automotive electronic components specifications
(Leo *et al.*, 1998)**

Requirements	Engine Room	Passenger Room
Operating temperature	-40°C to +125°C (+175°C for some parts mounted to engine)	-40°C to +85°C
Storage temperature	+100°C for 500 hours	-50°C to 100°C for 500 hours
Thermal shock	100 thermal cycles	20 thermal cycles
Relative humidity	0 to 100%	95% @ +65°C for 100 hours
Shock	20g	Maximum 25g
Drop test	4 ft. drop	4 ft. drop
Vibration	50 to 2000 Hz, 10g RMS, 16 hours	50 to 2000 Hz, 4g RMS
Operating voltage	5 V, $\pm 0.5V$	12 V, $\pm 4.0V$
Reliability	95% reliable for 10 years, 120k miles	90% reliable for 10 years, 100k miles
Other	-	Minimal radiated or conducted emissions. Not susceptible to conducted/radiated emissions.
Contaminant resistance	Salt spray, engine oil, ATF, windshield washer fluid, ethylene, glycol, gasoline, power steering fluid, battery acid, engine cleaner, methanol, mud and exhaust gases.	-

The majority of these feasible applications are covered with the commercially available binary NiTi SMA, where its operational temperature range lies approximately within the standard range of environmental temperature extremes to which a passenger vehicle may be exposed during service (i.e. between -40°C to approx. +125°C, see Table 2.13 and Figure 2.14 (Leo *et al.*, 1998; D. Stoeckel, 1990)). The standard binary NiTi SMA with transformation temperatures from -50°C to approximately +110°C (Hodgson *et al.*, 1990) performs well for multiple cycles within locations of vehicle within this temperature range (D. Stoeckel, 1990), but not in locations with higher temperatures such as under the engine hood. The SMAs should have an M_f temperature well above the maximum operating

temperatures (see the red dotted lines in Figure 2.14) in order to function correctly (D. Stoeckel, 1990). The comparison of the transformation temperature ranges of the most common SMAs under development in Figure 2.14 shows that the cheaper Cu-Al-Ni SMAs can perform with the transformation with temperatures up to 200°C, but these SMAs are brittle, unstable, have low fatigue strength and not suitable for multiple cyclic operations (Firstov *et al.*, 2006; Hodgson *et al.*, 1990; D. Stoeckel, 1990; Stöckel, 1995; Wilkes *et al.*, 2000). A wide selection of HTSMAs are available, but these materials are currently expensive, and may not be compatible with the cost constraints in the automotive domain (D. Stoeckel, 1990).

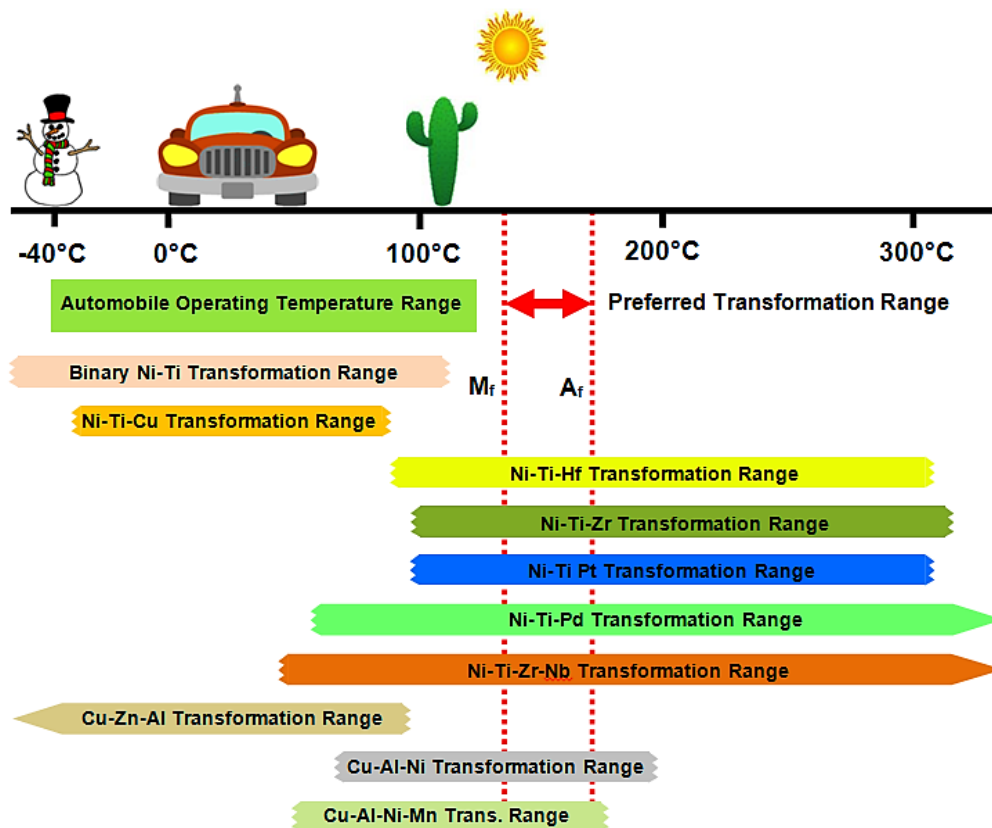


Figure 2.14 - Operating temperature range for automobiles applications and the transformation temperatures for selected commercially available and developed SMAs, image based on (Beyer & Mulder, 1994; Hodgson *et al.*, 1990; D. Stoeckel, 1990; JV Humbeeck *et al.*, 1991)

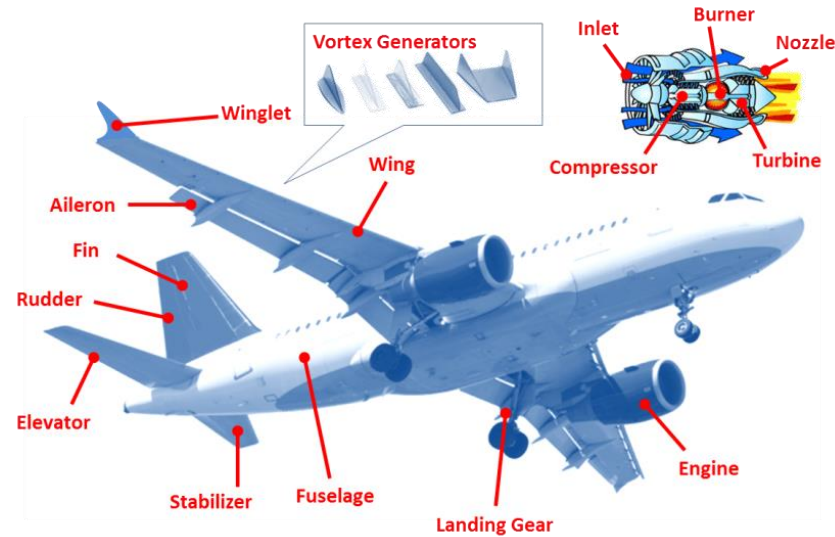
A brief review of SMAs in automotive applications was further described in (Mohd Jani, Leary, & Subic, 2014), where the automotive actuators can be generally divided into three categories. The SMA actuators are expected to be most suitable for the first category (low power actuators for comfort and bodywork functions) and practicable for the second category (high power vehicle control actuators), and are less preferred for the third category (high frequency engine control actuators) due to the low operational frequency and narrow bandwidth (Mohd Jani, Leary, & Subic, 2014).

2.7.2 Aerospace applications

Since the success of the SMA coupling for hydraulic lines in the F-14 fighter jets of the 1970s (KN Melton, 1999), the unique properties of SMAs have gathered greater interest in aerospace applications (Godard *et al.*, 2003; Humbeeck, 1999; McDonald Schetky, 1991; K. Singh & Chopra, 2002), which are subjected to high dynamic loads and geometric space constraints. A few examples of these applications are actuators (Baumbick, 2000; Hartl & Lagoudas, 2007), structural connectors, vibration dampers, sealers, release or deployment mechanisms (B. Carpenter & Lyons, 2001; Cleveland, 2008; B Huettl & Willey, 2000; Long & Vezain, 1998; Lortz & Tang, 1998), inflatable structures (Fujun, Xin-Xiang, Yan-Ru, & Ng, 2005; Roh, Han, & Lee, 2005), manipulators (Birman, 1997; Prahlad & Chopra, 2001), and the pathfinder application (Godard *et al.*, 2003; Landis & Jenkins, 1997).

In the 1990s, aerospace researchers focussed on active and adaptive SMA structures with morphing capability and system-level optimisation under various flight conditions. For example, the Defense Advanced Research Projects Agency (DARPA) program for aircraft 'smart wings' (Kudva, 2004); the Smart Aircraft and Marine Propulsion System Demonstration (SAMPSON) program for jet engines (Pitt, Dunne, White, & Garcia, 2001); and, a number of other programs (Icardi & Ferrero, 2009; Mieloszyk, Krawczuk, Zak, & Ostachowicz, 2010; Sofla, Meguid, Tan, & Yeo, 2010; Strelec, Lagoudas, Khan, & Yen, 2003). Boeing has developed an active serrated aerodynamic device with SMA actuation, known as a variable geometry chevron (VGC) that has been installed on a GE90-115B jet engine for the Boeing 777-300 ER commercial aircraft. The VGC device has proven to be very effective in reducing noise during take-off by maximising chevron deflection, and also increasing the cruise efficiency by minimising chevron deflection during the remainder of the flight (Hartl, Lagoudas, Calkins, & Mabe, 2010; Hartl, Mooney, Lagoudas, Calkins, & Mabe, 2010; Oehler, Hartl, Lopez, Malak, & Lagoudas, 2012) (Figure 2.15). The high temperature requirement for a core exhaust chevron design was resolved by the identification, testing, and validation of the new TiNiPt HTSMA at the NASA Glenn Research Center (Ronald D Noebe, Draper, Nathal, & Garg, 2009; RD Noebe, Quackenbush, & Il, 2005).

Table 2.14 - Existing and potential SMA applications in the aerospace domain, based on (Bil *et al.*, 2013; Hartl & Lagoudas, 2007; Mohd Jani, Leary, Subic, *et al.*, 2014)



CATEGORIES / PARTS	REFERENCES
FUSELAGE	
<i>Aerostructure / Composite body</i>	(Balta, Simpson, Michaud, Manson, & Schrooten, 2001; Mohammad, Jeng-Jong, & Chuh, 2002)
<i>Skin / Panel</i>	(Mani, Lagoudas, & Rediniotis, 2003)
WING / FIN / STABILIZER	
<i>Wing</i>	(Elzey, Sofla, & Wadley, 2003; Knowles & Bird, 2004; Kudva, 2004; Manzo, Garcia, Wickenheiser, & Horner, 2005; Sofla <i>et al.</i> , 2010)
<i>Winglet</i>	(Balta <i>et al.</i> , 2001)
<i>Vortex generator</i>	(Geraci, Cooper, & Amprikidis, 2003)
<i>Flap edge</i>	(Larssen & Calkins, 2010)
<i>Structure / Spars</i>	(C. Nam, Chattopadhyay, & Kim)
ENGINE	
<i>Inlet</i>	(Dunne, Hopkins, Baumann, Pitt, & White, 1999; Pitt <i>et al.</i> , 2001; Rey, Miller, Tillman, Rukus, & Kettle, 2006)
<i>Nozzle</i>	(Hartl, Lagoudas, <i>et al.</i> , 2010; Rey <i>et al.</i> , 2006; Wood & Dunne, 2008)
<i>Rotor</i>	(Birman, 1997; N. Caldwell, Gutmark, & Ruggeri, 2007; D. K. Kennedy, Straub, Schetky, Chaudhry, & Roznoy, 2000; Prahlad & Chopra, 2001; K. Singh & Chopra, 2002)
LANDING GEAR	(Kutlucinar, 2005a)
ELECTRO-MECHANICAL CONTROL	
<i>Hydraulic lines</i>	(KN Melton, 1999)

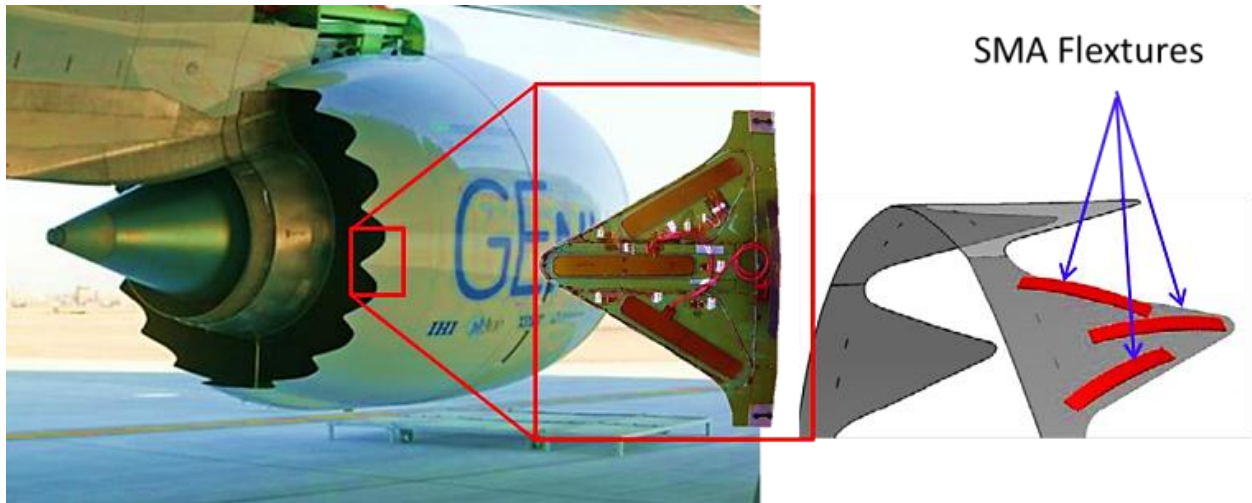


Figure 2.15 - Boeing's variable geometry chevron (VGC) (Oehler *et al.*, 2012)

Following the VGC success, new SMA based technology programs have been initiated by Boeing, DARPA, NASA and other related research agencies, as reviewed by Calkins and Mabe (2010). For example: a smart inlet that could provide aircraft with a variable engine inlet capability; a reconfigurable rotor blade, which is highly robust; and, the twist-able rotor blade that optimises rotor aerodynamic characteristics. Most recently, the variable geometry fan nozzle, which is based on the VGC technology, has demonstrated the potential to improve jet engine performance.

Sofla *et al.* (2010) have provided a comprehensive review of aircraft wing morphing technologies, and have also developed a shape morphing wing design for small aircraft. This design operates by applying antagonistic SMA-actuated flexural structural forms that enable morphing of the wing profile by bending and twisting to improve the aerodynamic performance (Figure 2.16). A preliminary design study with finite element simulations presented by Icardi and Ferrero (2009) has verified that an adaptive wing for a small unmanned aircraft (UAV), which is entirely actuated by SMA devices, could bear the associated aerodynamic pressure of realistic flight conditions, without weight increase or stiffness loss compared to conventional actuators.

There has also been significant research in rotor technology (rotorcraft) with SMAs conducted by several researchers, including rotor blade twisting (N. Caldwell *et al.*, 2007; A. Dean Jacot, Ruggeri, & Clingman, 2006; Prahlad & Chopra, 2001), rotor blade tracking tab (D. K. Kennedy *et al.*, 2000; K. Singh & Chopra, 2002), rotor control (Robert, 1997) and rotor blade tip morphing (Testa, Leone, Ameduri, & Concilio, 2005).

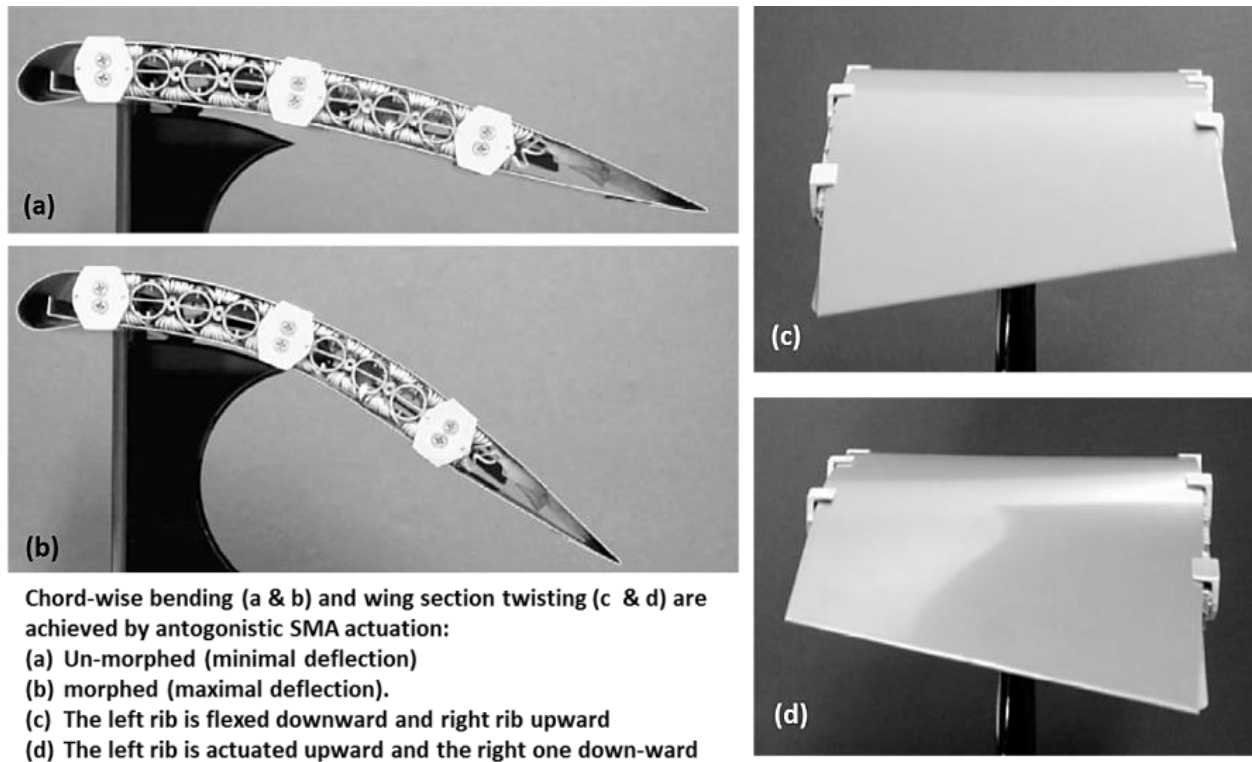


Figure 2.16 - Wing morphing with antagonistic SMA actuators (Elzey *et al.*, 2003; Sofla *et al.*, 2010)

SMA's have been used for many years in spacecraft as low-shock release mechanisms because they can be actuated slowly by gradual heating, can efficiently absorb vibration and can be fabricated in simple and compact designs, which are most suitable for average and smaller sized spacecraft (e.g. microsatellite) (Godard *et al.*, 2003; Brett Huettl & Willey; Alfred D. Johnson, 1992b). Examples of small SMA devices for aerospace applications include: the QWKNUT (Peffer, Denoyer, Fosness, & Sciulli, 2000), Frangibolt® (Alfred D. Johnson, 1992), Micro-Sep-Nut, and Rotary Latch; as described in previous reviews (Hartl & Lagoudas, 2007; B Huettl & Willey, 2000; Willey, Huettl, & Hill, 2001).

As mentioned earlier, SMA's are suitable for vibration damping and isolator applications due to their unique behaviour (Godard *et al.*, 2003; Saadat *et al.*, 2002). Considerable new research has been performed to study this opportunity in detail (DC Lagoudas, Machado, & Lagoudas, 2005; Ngo *et al.*, 2004; K. A. Williams, Chiu, & Bernhard, 2000), and several patents have been filed to exploit these advantages (Grosskrueger, Carpenter, Easom, & Draper, 2000; Renz & Kramer, 1997; Sherwin & Ulmer, 2004). Other proposed or developed SMA applications for aerospace include: a telescopic wing system (Knowles & Bird, 2004); wing span morphing (Manzo *et al.*, 2005); retractable landing gear (Kutlucinar, 2005a); jet engine components (Core, 2010; Mons, 2008; Shmilovich, Yadlin, Smith, & Clark, 2010; Gangbing Song & Ma, 2012; Wood, 2007); morphing structures (Wood & Dunne, 2008); flap edge fence (Larssen & Calkins, 2010); aircraft related actuators (Mabe, Calkins, Bushnell,

& Bieniawski, 2011) and aerostructures (Mani *et al.*, 2003; Mohammad *et al.*, 2002; Widdle *et al.*, 2009) (Table 2.14).

2.7.3 Robotic applications

Since the 1980s, SMAs have been used in a diverse range of commercial robotic systems, especially as micro-actuators or artificial muscles (DG Caldwell & Taylor, 1988; H Fujita, 1989; Honma, Miwa, & Iguchi, 1985; Katsutoshi Kuribayashi, 1986; K. Kuribayashi, 1989); as described by Furuya and Shimada (1991) and Sreekumar *et al.* (2007). Today, most of the SMA robotic applications are biologically inspired (i.e. biomechanics) and widely utilised in biomedical areas but are also used extensively in other fields as well. The primary challenges relevant to the robotics domain are: to increase the performance and miniaturisation of the hardware platform and to increase the intelligence of the integrated system (i.e. small, faster, reliable and autonomous). Several technical issues have been highlighted and need to be resolved, such as clamping difficulties, low electrical resistance, miniature electrical connection (for micro-robots), small strain output, control issues and very low efficiency. However, some of these issues have been tackled by selecting suitable modelling techniques, control techniques and feedback sensors. As an example, the resistance feedback control is ideal for micro-robots as it eliminates the necessity of additional sensors, although with limited accuracy (Sreekumar *et al.*, 2007).

As mentioned earlier, the response rate of an SMA actuator depends significantly upon its shape and size, and consequently the overall actuator size and achievable degrees of freedom of the robotic device. Resistive heating is generally used for small SMA actuators (up to 400 μm diameter), and indirect heating techniques are applied for larger diameter actuators (Sreekumar *et al.*, 2007). To increase the actuation frequency, capacitors are incorporated with thicker actuators to obtain a rapid heating response, and several cooling strategies, has been adopted as defined in Section 2.5.2, to enhance the cooling process, however these would make the device bulkier (Sreekumar *et al.*, 2007). Furthermore, to increase the degrees of freedom of the robots, the number of actuators has to be increased, which leads to complex control problems.

Table 2.15 - Existing and potential SMA applications in the robotics domain, based on (Y. Furuya & Shimada, 1991; Kheirikhah *et al.*, 2011; Mohd Jani, Leary, Subic, *et al.*, 2014; Sreekumar *et al.*, 2007)



CATEGORIES / PARTS	REFERENCES
BIOMIMETICS	
<i>Crawling / Snaking</i>	(Gambao, Hernando, & Brunete; Huitao, Peisun, & Chongzhen, 2005; Kate <i>et al.</i> , 2008; SK Lee & Kim, 2008; CY Liu & Liao, 2004; Arianna Menciassi, Accoto, Gorini, & Dario, 2006; A. Menciassi, Gorini, Pernorio, & Dario, 2004; Shiotsu <i>et al.</i> , 2005; Young Pyo, Byungkyu, Moon Gu, & Jong-Oh, 2004)
<i>Walking / Jumping</i>	(Berry & Garcia, 2008; Hoover, Steltz, & Fearing, 2008; Nishida, Tanaka, & Wang, 2006; Shiotsu <i>et al.</i> , 2005; Sugiyama & Hirai, 2006)
<i>Rolling / Skating</i>	(Chang-jun, Pei-sun, & Qin, 2004; Sugiyama & Hirai, 2006)
<i>Climbing</i>	(Menon & Sitti, 2005; Trimmer <i>et al.</i> , 2006)
<i>Swimming</i>	(Alex, Colin, & Shashank, 2011; Kyu-Jin, Hawkes, Quinn, & Wood, 2008; Liwei, Shuxiang, & Asaka, 2010; Tao, Liang, & Taya, 2006; Zhenlong, Guanrong, Yangwei, Jian, & Wei, 2008)
<i>Flying</i>	(Bunget & Seelecke, 2009; Colorado, Barrientos, Rossi, & Breuer, 2012; Festo, 2013)
<i>Others</i>	(H. L. Huang, Park, & Park, 2008)
BIOMEDICAL	
<i>Endoscopic</i>	(Cepolina & Michelini, 2004; Mi, Gong, Qian, Mi, & Shen, 2001; Reynaerts, Peirs, & Van Brussel, 1996)
HUMANOID	
<i>Fingers / Hands</i>	(Andrianesis & Tzes, 2008; Bundhoo, Haslam, Birch, & Park, 2009; Chee Siong <i>et al.</i> , 2005b; De Laurentis & Mavroidis, 2002; Hino & Maeno, 2004; Maeno & Hino, 2006; O'toole & McGrath, 2007; Price, Jnifene, & Naguib, 2007)
<i>Head / Facial expression</i>	(Hara, Akazawa, & Kobayashi, 2001; Hong & Priya, 2011)
MISCELLANEOUS	
<i>Controller</i>	(Ashrafiun, Eshraghi, & Elahinia, 2006; Katsutoshi Kuribayashi, 1986, 1991; Terauchi, Zenba, Shimada, & Fujita, 2006)
<i>Actuators</i>	(Mohamed Ali & Takahata, 2010)
<i>Sensors</i>	(Tuna, Solomon, Jones, & Hartmann, 2012)

A new SMA actuator design for a prosthetic hand was introduced by (Chee Siong *et al.*, 2005b), where two SMA actuators are used to actuate the robotic finger, instead of using the conventional push-pull type and the biased spring type (Figure 2.17). The two actuators are inserted from both ends of the outer stainless tube, which functions as a heat sink and guide simultaneously. The current is passed asynchronously through the wires via electrode points, which are located at the centre of the tube (where the wires join) and at each end of the tube. The two actuators are used to actuate the robotic finger, which can almost replicate the actions of the human finger actions (flexion and extension). A PWM controller is used to avoid overheating and excessive power usage.

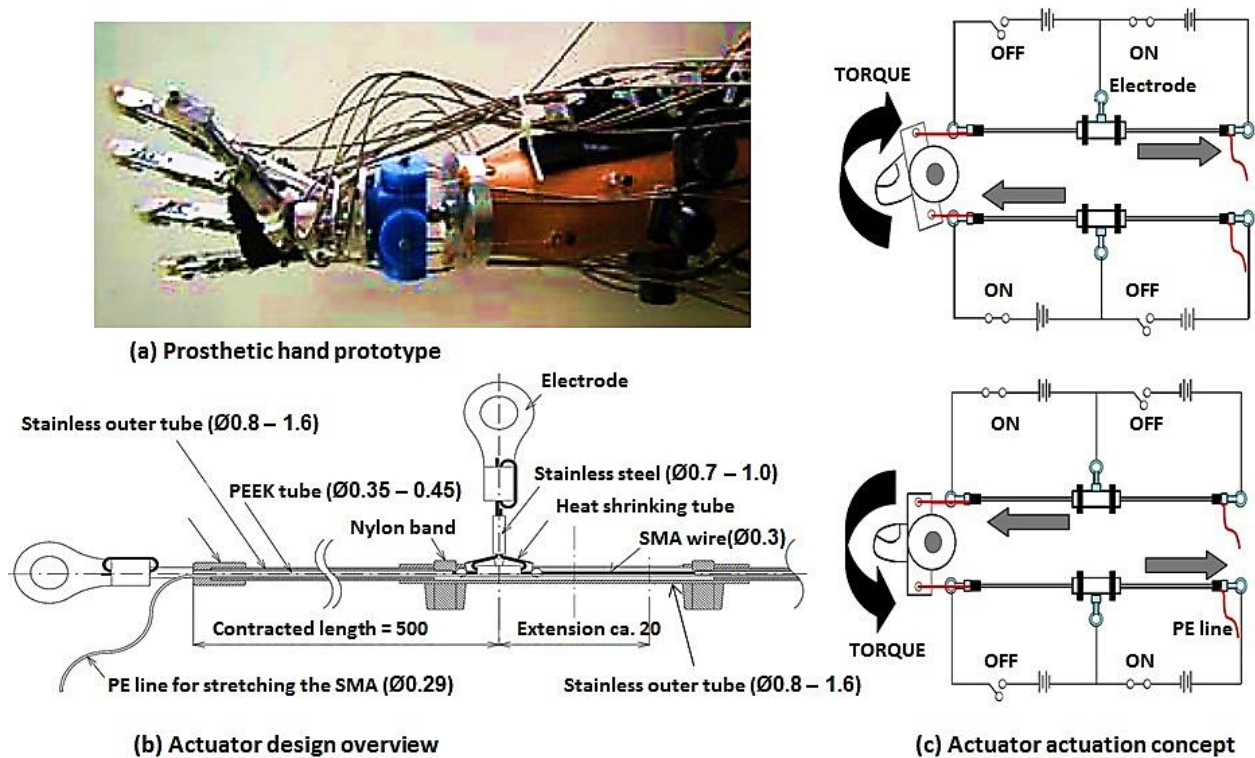


Figure 2.17 - Prosthetic hand powered by SMA actuators (Chee Siong *et al.*, 2005b)

In a recent review by Kheirikhah *et al.* (2011), robots are categorised based on their locomotion styles and applications such as crawler, jumper, flower, fish, walker, medical and biomimetic robotic hand. Many robotics researchers are more interested in developing biomimetics and humanoid robots. These robots are useful in solving problems that are challenging for humans, by providing pertinent information from underwater, space, air and land. Comprehensive details and challenges in developing these robots are summarised by several researchers, focusing on the actuation technologies, especially SMA actuators (refer Table 2.15) (Tao *et al.*, 2006) designed a robotic fish with a caudal peduncle actuator based on the concept of a FSMA hybrid mechanism that can provide fast response and a strong thrust.

Mohamed Ali and Takahata (2010) have developed passive (i.e. without internal power source) micro-grippers (i.e. about 600 μm displacement) that can be actuated wirelessly with a RF magnetic field. The fabrication of the micro-gripper is similar to the wafer fabrication processes used in the semiconductor industry, where the SMA actuator is bonded to or near an inductor-capacitor (LC) resonant circuit with photo-defined electroplating technology, and then micro-machined with a μEDM process. The working principle of the micro-gripper is quite simple. The frequency-sensitive LC resonant circuit is heated when a RF magnetic field passes through it, and it then transfers the heat energy to the SMA actuator for activation. The opportunity to control multiple selections of micro-SMA actuators is possible by applying different resonant frequencies, either selectively or simultaneously to the actuators (see Figure 2.18).

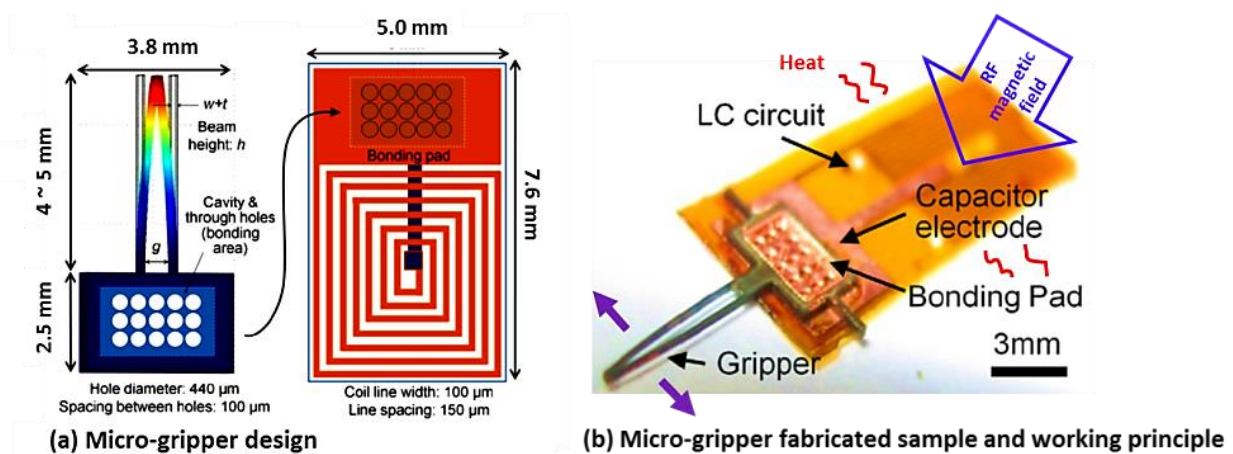


Figure 2.18 - Micro-gripper with SMA actuator (Mohamed Ali & Takahata, 2010)

A novel sensory system for robotics has been developed by researchers at Northwestern University, Illinois applying the SE characteristic of a NiTi SMA to create an artificial rat whisker, utilising the rat's sensing capabilities. The artificial whisker technology has the potential to enhance robotic sensing capabilities, and could be used to examine and navigate into small and tight interiors, or to locate and identify micro-features on surfaces (Tuna *et al.*, 2012).

Several flying robots have been developed with SMAs, such as the BATMAV (Bunget & Seelecke, 2009; Stephen, George, & Stefan, 2013) and Bat Robot (Colorado *et al.*, 2012). Recently, a 44 cm length dragonfly with a wingspan of 63 cm was developed by Festo Group, equipped with four SMA actuators to control the movements of its head from side to side and its tail up and down for flight manoeuvre and stability. The 'dragonfly', also known as 'BionicOpter', has 13 degrees of freedom, can hover in mid-air and manoeuvre in all directions (Festo, 2013) (see Figure 2.19).



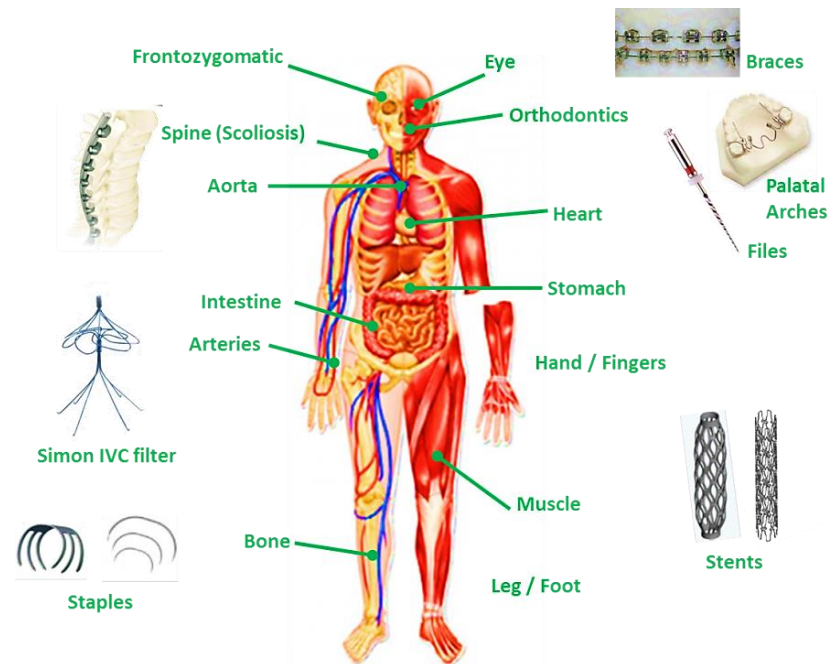
Figure 2.19 - Festo BionicOpter – Inspiration dragonfly flight (Festo, 2013)

2.7.4 Biomedical applications

After the discovery of the SME in nitinol by Buehler *et al.* in 1962, it was proposed to use this material for implants in dentistry, and in 1971, the first superelastic braces made from a NiTi alloy were introduced by Andreasen (Andreasen, 1977; Andreasen & Hilleman, 1971; Kauffman & Mayo, 1997). SMA made a significant breakthrough into biomedical field after its introduction in minimally invasive surgery (MIS) (C. Song, 2010). Additional commercial applications in the biomedical domain have been introduced into the market since the approval of the Mitek surgical product (i.e. Mitek Anchor) for orthopaedic surgery by US Food and Drug Administration (FDA) in September 1989.

Although NiTi alloys are significantly more expensive than stainless steels, SMAs may exhibit excellent behaviour for biomedical applications such as: high corrosion resistance (WJ Buehler & Wang, 1968; Hodgson *et al.*, 1990); bio-compatibility (Mantovani, 2000; Ryhänen *et al.*, 1998); non-magnetic (Mihálc, 2001); unique physical properties, which can replicate those of human tissues and bones (NB Morgan, 2004) (Figure 2.20); and can be manufactured to respond and change at the temperature of the human body (Machado & Savi, 2003). The need for precise and reliable miniature instruments to achieve accurate positioning and functioning for complex medical treatments and surgical procedures provides SMAs with substantial opportunities for further commercial application in this area. SMAs are used in medical equipment and devices in many fields including: orthopaedics; neurology; cardiology and interventional radiology (NB Morgan, 2004). Other medical applications include: endodontics (Oh *et al.*, 2010); stents (C. Song, 2010); medical tweezers; sutures; anchors for attaching tendon to bone; implants (Dahlgren & Gelbart, 2009; Pfeifer *et al.*, 2013); aneurism treatments (Maynard, 1999); eyeglass frames (Zider & Krumme, 1988) and guide wires (Lim, Park, Sugihara, Minami, & Esashi, 1996) (Table 2.16).

Table 2.16 - Existing and potential SMA applications in the biomedical domain, based on (T. Duerig *et al.*, 1999; Machado & Savi, 2003; Mohd Jani *et al.*, 2014; NB Morgan, 2004; Petrini & Migliavacca, 2011; C. Song, 2010)



FIELDS	REFERENCES
ORTHODONTIC	
Braces / Brackets	(Airoidi, Riva, & Vanelli, 1995; Andreasen & Hilleman, 1971; Torrisi, 1999)
Palatal arches	(Idelsohn <i>et al.</i> , 2004)
Files	(Sattapan, Palamara, & Messer, 2000)
ORTHOPAEDIC	
Head	(Laster, MacBean, Ayliffe, & Newlands, 2001)
Spine	(Contra, Dallolio, Franzoso, Gastaldi, & Vena, 2005; AE Sanders, Sanders, & More, 1994; J. O. Sanders, Sanders, More, & Ashman, 1993; Schmerling, Wilkov, Sanders, & Woosley, 1976; Wever, Elstrodt, Veldhuizen, & v Horn, 2002)
Bone	(Coati <i>et al.</i> , 2012; Kujala <i>et al.</i> , 2002; Pfeifer <i>et al.</i> , 2013)
Muscles	(Machado & Savi, 2003)
Hands / Fingers	(Chee Siong <i>et al.</i> , 2005b; DeLaurentis, Mavroidis, & Pfeiffer, 2000)
Legs	(Choudhary, Theruvil, & Taylor, 2004; Stirling <i>et al.</i> , 2011)

FIELDS	REFERENCES
VASCULAR	
<i>Aorta</i>	(Kaufman <i>et al.</i> , 2000; Uflacker & Robison, 2001)
<i>Arteries</i>	(Hausegger <i>et al.</i> , 1994)
<i>Vena cava filter</i>	(Asch, 2002; Bruckheimer <i>et al.</i> , 2003; Engmann & Asch, 1998; Poletti <i>et al.</i> , 1998; Simon, Kaplow, Salzman, & Freiman, 1977)
<i>Ventricular Septal Defect (VSD)</i>	(KC Chan <i>et al.</i> , 1999; Thanopoulos <i>et al.</i> , 1998; Walsh & Maadi, 2000)
<i>Vessels</i>	(Carter <i>et al.</i> , 1998; Lewis, 2008; Tyagi, Singh, Mukhopadhyay, & Kaul, 2003)
<i>Valves</i>	(Coats & Bonhoeffer, 2007; Laborde, Borenstein, Behr, Farah, & Fajadet, 2006; Levi, Kusnezov, & Carman, 2008)
BIOMEDICAL / SURGICAL INSTRUMENTS	
<i>Catheters / Snares</i>	(Cekirge, Weiss, Foster, Neiman, & McLean, 1993; W. Y. Wang, Cooper, & Eberhardt, 1999)
<i>Scopes (Ureteroscopy, endoscopy, laparoscopy)</i>	(Cuschieri, 1991; Elisa, Pietro, Marco, Arianna, & Paolo, 2009; Kourambas, Delvecchio, Munver, & Preminger, 2000; JM Smith & Stein, 2008; Sunkil <i>et al.</i> , 2008)
<i>Suture</i>	(Kujala <i>et al.</i> , 2004)
MISCELLANEOUS	
<i>Cardiology (Heart)</i>	(Shiraishi <i>et al.</i> , 2007; Yamada <i>et al.</i> , 2013)
<i>Hepatology (Liver, gallbladder, biliary tree and pancreas)</i>	(Davids, Groen, Rauws, Tytgat, & Huibregtse, 1992; Rossi <i>et al.</i> , 1994)
<i>Otorhinolaryngology (Ear, nose and throat)</i>	(Kardas, Rust, Polley, & Fabian, 2007; Rajan, Eikelboom, Anandacoomaraswamy, & Atlas, 2005; Vinograd <i>et al.</i> , 1994; Yanagihara, Mizuno, Wada, & Hitomi, 1997)
<i>Gastroenterology (Gullet, stomach and intestine)</i>	(Angueira & Kadakia, 1997; Cwikiel, Willen, Stridbeck, Lillo-Gil, & Von Holstein, 1993; Nudelman, Fuko, Greif, & Lelcuk, 2002; Pocek <i>et al.</i> , 1996; Raju & Gajula, 2004; C. Song, Frank, & Cuschieri, 2005; Tack, Gevers, & Rutgeerts, 1998)
<i>Urology (Kidneys, adrenal glands, ureters, urinary bladder, urethra and the male reproductive organs)</i>	(Chonan <i>et al.</i> , 1997; Gottfried <i>et al.</i> , 1997; Himpens, 1993; K. Mori, Okamoto, & Akimoto, 1995; M. Tanaka <i>et al.</i> , 1999; Yachia, 1993)
<i>Plastic, Reconstructive and Aesthetic Surgery</i>	(Khouri, 2002)
<i>Ophthalmology (Eye)</i>	(Olsen, Loftness, & Erdman, 2012)

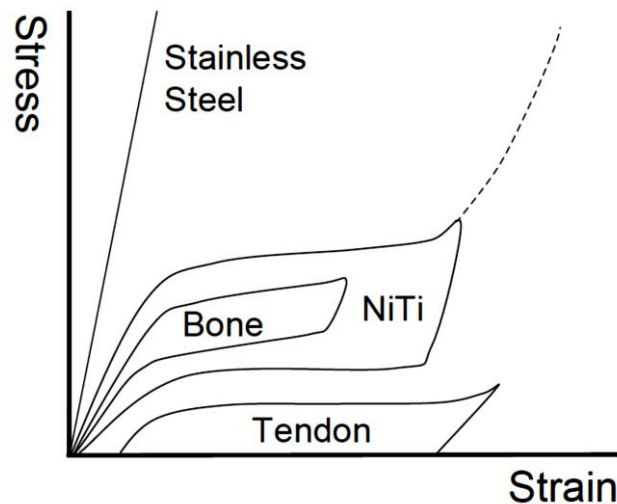


Figure 2.20 - The stress versus strain relationship for superelastic nitinol, stainless steel, bone and tendon tissues (NB Morgan, 2004)

The superelastic behaviour of SMA, which is compatible with the stress-strain behaviour of human bone and tendons, make it an excellent material to meet the challenges presented by stenting operations. SMA stents are much more compliant to bends in the vessels and contours in the lumen, whereas stainless steel stents tend to force the blood vessel to be straight. In addition, the superelastic hysteresis behaviour of SMA can resist crushing during the normal physiological process (provide radial resistive force) and exert a small outward force on the vessel during recovery, which is ideal for stenting applications (NB Morgan, 2004) (Figure 2.21). The first SMA stent was made by Dotter's group in 1983 (Dotter, Buschmann, McKinney, & Rösch, 1983), and since this initial design, SMA stents have evolved remarkably (from simple coiled wire form to complex laser cut structures), growing in a global market (nearly half of stent products are fabricated from SMA and was forecast to reach USD6.3 billion by 2010 (Terzo, 2006)), and has expanded the usage to other parts of the human body (C. Song, 2010).

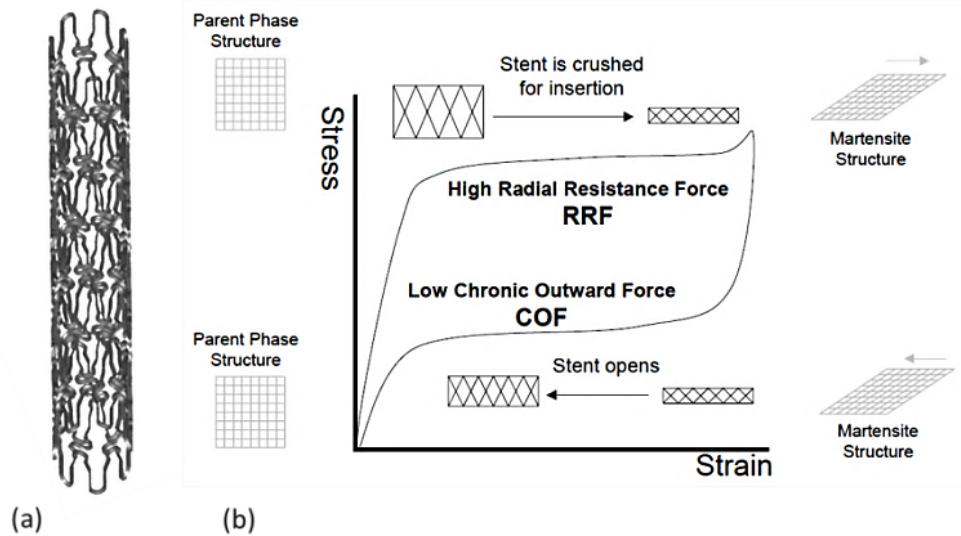


Figure 2.21 - a) Model of stent laser cut from nitinol tubing. b) The radial resistance force and chronic outward force as a function of superelastic hysteresis loop (NB Morgan, 2004)

Today, catheter-based surgeries have become increasingly popular due to the demand for MIS treatment, which will further minimise operation trauma. The application of SMAs has improved the active catheter capability to move accurately with larger bending angles, which enable novel diagnosis and therapy treatments (Y. Haga, Esashi, & Maeda, 2000; Y. Haga, Tanahashi, & Esashi, 1998; Lim *et al.*, 1996). A laser machined SMA actuator from NiTi tubing as proposed by Tung *et al.* (2008), allows for the creation of custom-tailored SMA actuators with force, elongation and size characteristics, which are not achievable with common straight wire or coil spring actuators, leading to another viable option for developing commercial actuators for steerable catheter applications (see Figure 2.22).

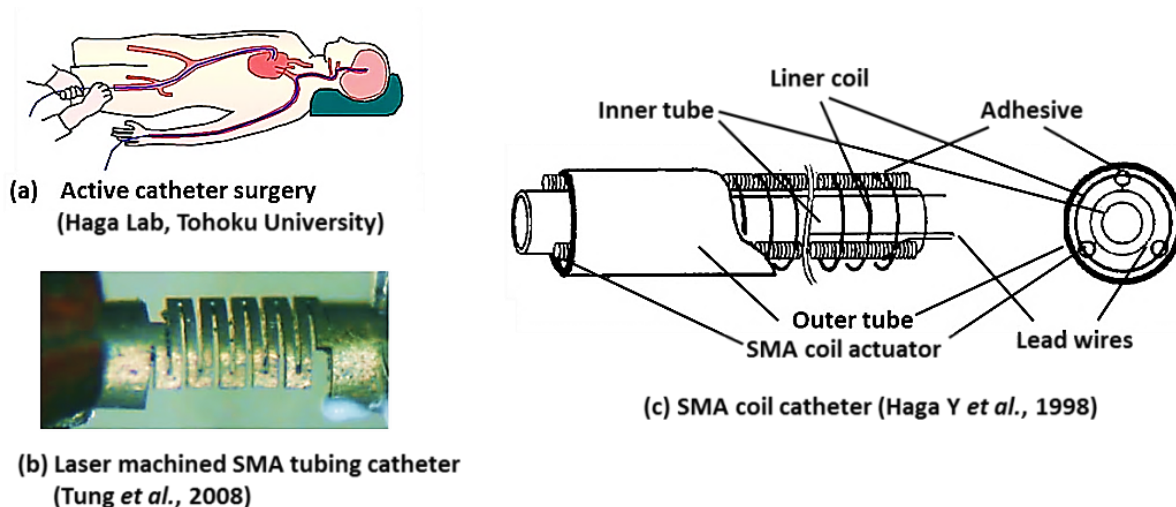


Figure 2.22 - SMA active catheter (Y. Haga *et al.*, 1998; Tung *et al.*, 2008)

A micro-muscle fibre crafted from NiTi SMA coiled springs was presented by Kim *et al.* (2009), utilising many of the SMAs attributes (resilience, high energy density, flexibility and scalability) to produce a novel mesh-worm prototype that employs a bio-inspired antagonistic actuation for its body deformation and locomotion; and this could make an excellent actuator candidate for meso-scale applications. Similar work has also been developed by Stirling *et al.* (2011), to develop an active, soft orthotic for the knee. They concluded that even though SMA springs could provide the soft characteristics as required and produce a large energy density; it was not appropriate for this application due to the poor response time and would be difficult to operate if not tethered to an external power supply. However, it could be appropriate for applications with a slower time scales or reduced forces requirements (see Figure 2.23).

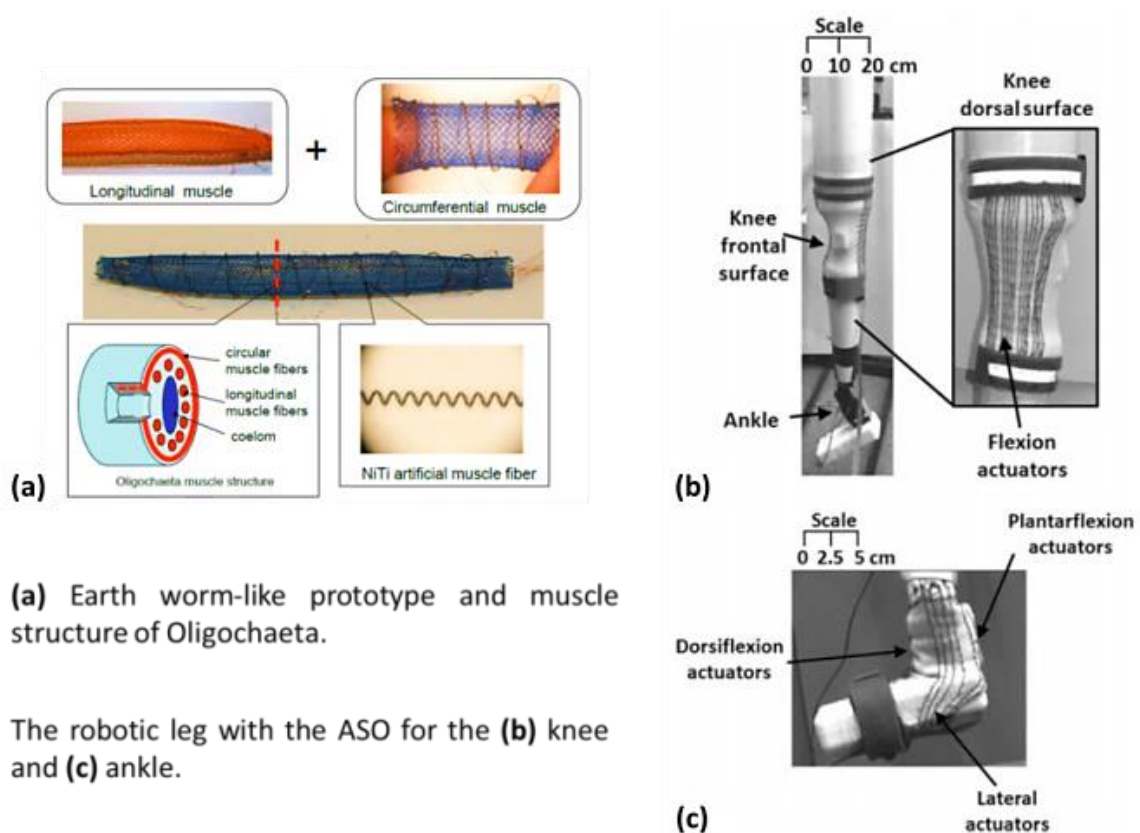


Figure 2.23 - Muscle like NiTi SMA (S. Kim *et al.*, 2009; Stirling *et al.*, 2011)

An artificial myocardium was developed by Shiraishi *et al.* (2007) using a nanotech covalent type SMA fibre with a parallel-link structured myocardial assist device, which is capable of supporting natural contractile functions from the outside of the ventricle without blood contacting the surface. They researchers concluded that their system might be applied in patients with exertional heart stroke, as well as cardiac massage during a lifesaving emergency for recovery from ventricular fibrillation. Recently, the researchers developed a mechanical circulation support device using SMA fibres for Fontan circulation to assist

pulmonary circulation in patients with congenital heart diseases (Figure 2.24) (Yamada *et al.*, 2013).

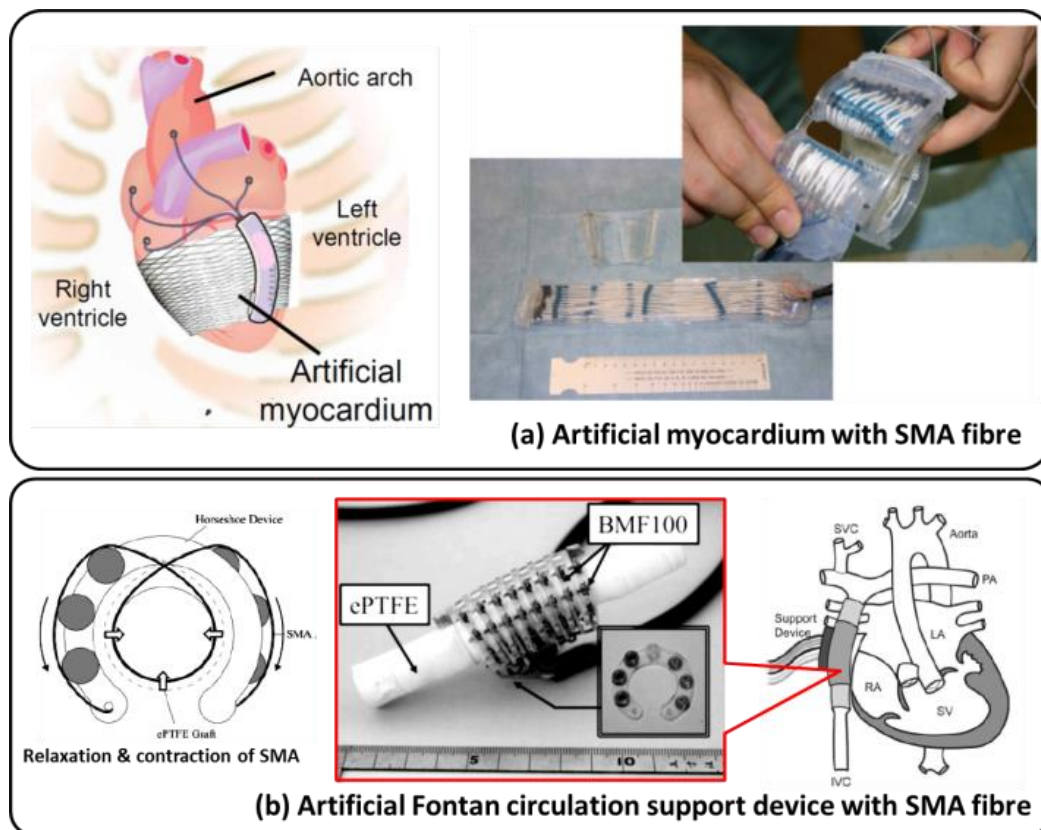
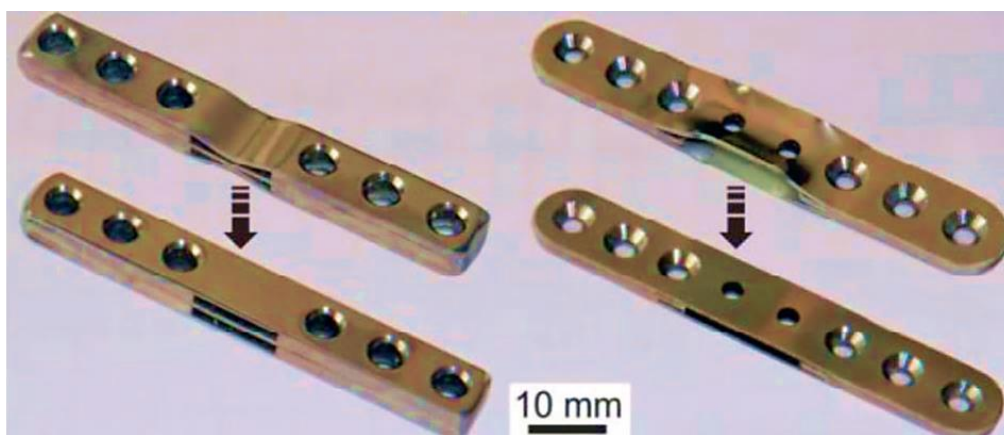


Figure 2.24 - Artificial heart support devices with SMA fibre (Shiraishi *et al.*, 2007)

An 'alterable stiffness' implant might assist bone to heal faster, and thus be able to bear weight earlier and avoid follow-on operations. Currently, this alteration is only possible with a biodegradable implant, 'fixateur externe' or a second surgery. Therefore, an 'alterable stiffness' implant made of NiTi-SMA has been developed to alter the stiffness of the implant with contactless heat induction (see Figure 2.25) (Pfeifer *et al.*, 2013).



Triggering OWSME leads to a straightening of the outer NiTi sheets, hence altering the second moment of inertia within the middle part of the implant (left: increase, right: decrease).

Figure 2.25 - An 'alterable stiffness' implant (Pfeifer *et al.*, 2013)

In recent years, there have been concerns from medical practitioners and researchers about the fatigue and fracture behaviour of SMA materials, and several observations and follow-up procedures were conducted to understand these behaviours and to enhance future biomedical applications (Allie, Hebert, & Walker; NB Morgan, 2004; Pelton *et al.*, 2008). The concern of biocompatibility of the NiTi SMAs has also been raised due to the known toxic, allergenic and carcinogenic properties of nickel, and an alternative material composition has been considered (Biesiekierski, Wang, AH Gepreel, & Wen, 2012; S. Miyazaki, Kim, & Hosoda, 2006; Pfeifer *et al.*, 2013); such as the new ideas of shaping the tissues with SMPs and SMHs (WM Huang *et al.*, 2013).

2.8 Opportunities and future direction of shape memory alloy applications

The commercial and research interests in SMMs, particularly in SMAs are rapidly increasing, and many potential new applications have been proposed, such as listed in Table 2.17 (Bogue, 2009). Opportunities for successful commercial applications can be evaluated and ranked in three different categories of applications, i.e. (JV Humbeeck *et al.*, 1991): substitution, simplification, and novel applications.

Applications with higher novelty and competitive pricing have a greater chance to penetrate the market and achieve commercial success. Examples of successful mass produced SMA applications in the market are: the underwire brassiere; the mobile-phone antenna; eyeglass frames; the SMA pneumatic valves developed by Alfmeier Präzision AG (now Actuator Solutions GmbH) for the lumbar support device in car seats; and, the Xlinea™ autofocus (AF) module for smart phones (TW Duerig, 1990; Dynalloy, 2006, 2007). However, the percentages of commercially successful SMA applications are still considered to be low (Vaidyanathan, 2000; Welp & Breidert, 2004; C. Zhang *et al.*, 1996).

Table 2.17 - Potential SMA applications (Bogue, 2009)

Configuration	Potential Applications
SMA tendons, wires and cylinders	Adaptive control and actuation of aircraft flight surfaces
Embedded SMA wires	Shape-adaptive composite materials
SMA actuators	Transmission line sag control and ice removal from overhead power lines
SMA energy absorbers and tendons	Earthquake-resistant building and bridges, bridge and structural repairs
SMA dampers	Engine mountings, structural supports
SMA wires, wings, legs, actuators, etc.	Mobile micro-robots, robot arms and grippers
SMA wires, composites, etc.	Prosthetics, artificial muscles

2.8.1 Future trends

Future trends in SMA technology can be expected to occur within the following areas (JV Humbeeck *et al.*, 1991):

- 1) development of new or improved SMAs
- 2) combination of the functional properties of SMAs with the structural properties of other materials (e.g. hybrid or composite SMMs)
- 3) search for new markets (i.e. application innovation)

The development of new and improved SMAs has significantly enhanced the achievable performance of commercial SMAs (Figure 2.26). Researchers are currently interested in '*programming*' SMMs by locally embedding multiple shape memories into SMMs to set the temporary shapes without permanently changing the material properties, instead of utilising the traditional '*training*' method (Khan, Pequegnat, & Zhou, 2013; C. Tang, Huang, Wang, & Purnawali, 2012). For example, a new process known as multiple memory material technology (MMMT) developed by researchers at University of Waterloo, Canada has transformed SMAs into multiple shapes at various temperatures (Khan *et al.*, 2013). A new single-crystal SMA (SCSMA) made of copper-aluminium-nickel (CuAlNi) developed by TiNi Aerospace has exhibited enhanced performance over NiTi SMA, i.e. higher operation temperature ($>200^{\circ}\text{C}$), fully resettable (repeatable with 100% recovery), up to one million of cycles operation, greater strain recovery (9%), wider transformation temperature range (-270°C to $+250^{\circ}\text{C}$) and very narrow loading hysteresis ($< 25^{\circ}\text{C}$) (Aerospace, 2013). Another new developed ferrous-based SMA known as NCATB alloy has exhibited maximum superelastic strain of about 13.5% and a very high tensile strength of 1200 MPa (Y. Tanaka *et al.*, 2010); and a new developed FSMA made from NiMn alloy has also been used for actuation, sensing, magnetic refrigeration, active tissue scaffolding and energy harvesting (Global, 2013; AJ Niskanen & Laitinen, 2013; Kari Ullakko, Sasaki, & Müllner, 2013).

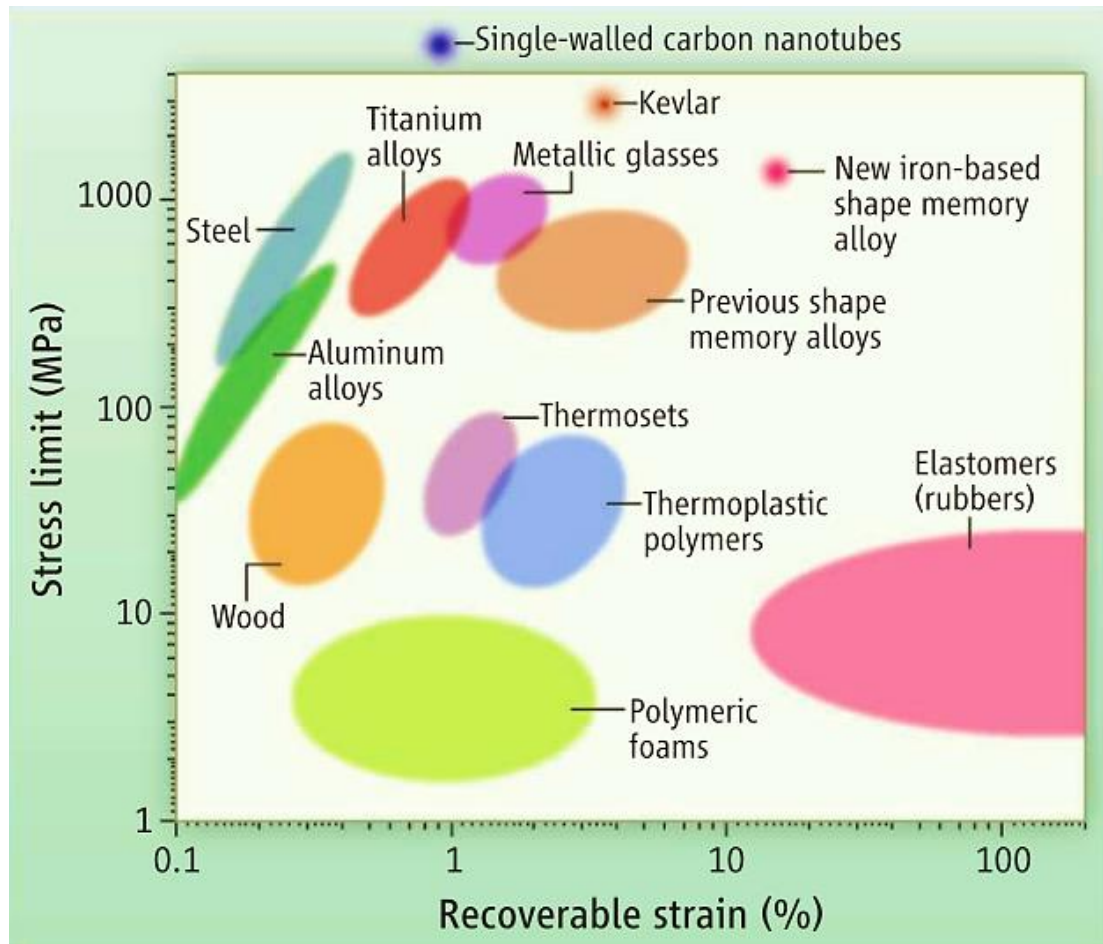


Figure 2.26 - Comparison of stress and strain of new developed SMA with other materials (Ashby, 2011; Ji Ma & Karaman, 2010)

Recently, the performance and functionality of SMAs has been augmented by integrating SMAs with other materials to form shape memory hybrids (SMHs) or shape memory composites (SMCs). Various combinations of SMAs and other materials have improved the material performance such as higher damping capacity and toughness (Yasubumi Furuya, Sasaki, & Taya, 1993; Raghavan *et al.*, 2010), active stiffening (Bidaux, Manson, & Gotthardt, 1996), triple-state changing (Ghosh, Rao, & Srinivasa, 2013) and self-healing capability (CC Wang, WM Huang, Z. Ding, Y. Zhao, H. Purnawali, *et al.*, 2012). An advanced composite structure constructed from CFRP composites with embedded SMA wires has also been employed as a structural health monitoring (SHM) system (i.e. for sensing and damage detection) with structural ice protection capacity (Fulvio, Francesco, Michele, & Umberto, 2012).

The unique properties of SMAs result in high damping, combined with the capability to resist extreme, repetitive and various loading conditions (e.g. earthquake), make SMAs highly compatible with civil engineering applications, especially in damping and vibration control (Qian *et al.*, 2010; G. Song, Ma, & Li, 2006). Several potential SMA applications in bridge and building structures are bearings, columns, beams, and connecting elements between beams and columns (Mirzaeifar, DesRoches, Yavari, & Gall, 2012). However, there exist limitations, such as high cost compared to structural steel; slower response time and larger power consumption requirement for activation due to the larger cross-section of the structure; and, difficulties in both machining and welding (Janke, Czaderski, Motavalli, & Ruth, 2005). Other new potential industries for SMA applications are oil and gas industry (Khan *et al.*, 2013; G. Song, Patil, Kocurek, & Bartos, 2010), industrial and manufacturing (MH Wu & LM Schetky, 2000), sports (Krumme & Dickinson, 2001; Maehara & Chikaraishi, 1999; Sahatjian, 1990) and arts (Descamps, 1991) (see appendices).

2.8.2 Future directions

Many potential areas and topics of SMA research have been proposed (JV Humbeeck, 1997). Most of the existing research on SMAs has focused on the associated metallurgical properties, rather than the associated design perspective. It has been suggested that to utilise SMA for commercial applications, closer collaboration between material scientists and engineering designers is essential, as the available information offered by material scientists is often not directly compatible with the requirements of design engineers (P. Abrahamsson & Møster, 1997; JV Humbeeck, 1997; Welp & Breidert, 2004). Therefore, the challenge of commercial SMA actuator design is not only the associated technical limitations, but also the effective conveyance of relevant design information and associated design tools. For example, Spaggiari *et al.* (2012) describes the three main challenges for SMA actuator design as:

- 1) Obtaining a simple and reliable material models
- 2) Increasing the stroke of the actuator
- 3) Developing design equations and associated tools, to guide the engineer in dimensioning the actuator (especially in the early design phases)

For this reason, the development of an effective information platform or database for SMA applications is important to: reduce the development time and cost; to minimise the risk of failure products; and, to identify potential applications effectively with patents screening and analysis (see Figure 2.27) (Welp & Breidert, 2004). An optimum design of SMA actuators could be realised by providing design engineers with appropriate design procedures, guidelines, and associated tools (P. Abrahamsson & Møster, 1997; Spaggiari *et al.*, 2012; D. Stoeckel, 1990; JV Humbeeck, 1997; Welp & Breidert, 2004).

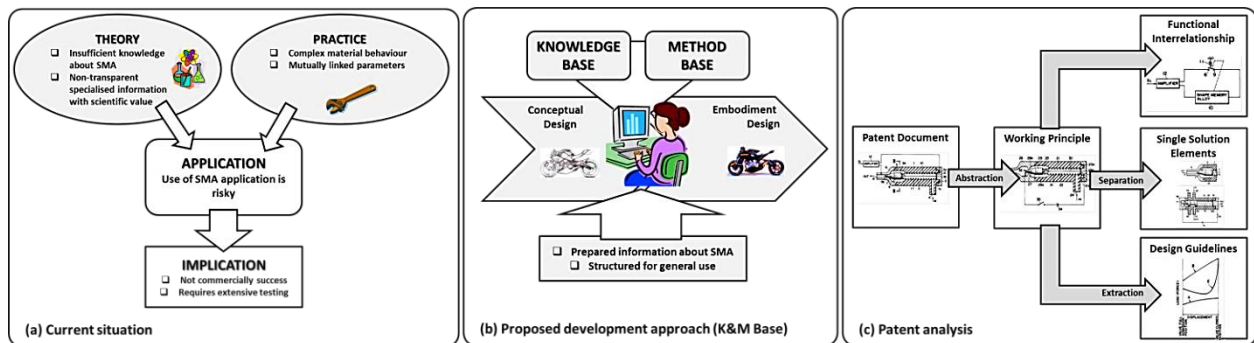


Figure 2.27 - Current situation and proposed approach for SMA in product design (Welp & Breidert, 2004)

Based on the diverse range of applications present in the patent literature, there appears to be no lack of innovation for creating novel SMA applications, however there does appear to be a limitation in associated with marketing these SMA innovations (Breidert & Welp, 2002). Involvement of marketing personnel in SMM communities essential in tailoring SMA applications to adapt to the commercial market with different approaches and strategies, where ‘smart marketing’ is key to an unconditional breakthrough (JV Humbeeck *et al.*, 1991). Standards and requirements for SMMs have been drafted by several SMM communities as guidelines in various fields and applications, such as for terminology, testings, fabrications and treatments (Materials, 1983).

Furthermore, the importance of incorporating modern computer design and analysis tools such as CAD and FEA into developing innovative and reliable SMA applications has led to an interest in more accurate 3D constitutive models and associated design tools, which are calibrated from carefully obtained material characterisation and experimental data. These are considered essential to speed up the development process, especially for preliminary studies and validation of high risk and/or expensive projects.

2.9 Discussion

More than 10,000 SMA related US patents have been proposed in many sectors (Kazuhiro Otsuka & Ren, 1999; Vaidyanathan, 2000; C. Zhang *et al.*, 1996) (Figure 2.5). Since the first commercially success SMA application as pipe coupler in 1969 (Kauffman & Mayo, 1997), the demand for SMAs has increased significantly, especially in the biomedical sector (see Figure 2.4). Consequently, major SMA manufacturers such as ATI Wah Chang Corporation, Dynalloy Inc., Johnson-Mattheys, Memory-Metalle GmbH, Memry Corporation, SAES Group and Toki Corporation have continued to grow in both size and knowledge base.

The advancement in the process and manufacturing technologies (Appendix D) has led to an increase in production quantity and quality, and at the same time reduced the material price. New SMA materials (e.g. MSMA and HTSMA) or forms (e.g. NiTi thin films, composites or hybrids) have been researched, and more promising attributes and enhancements are being offered (Section 2.8), further outweigh the associated challenges (Section 2.5.2).

Current SMA research and development trends categorised according to the selected sectors are (Section 2.7):

a) Automotive and aerospace:

- Self-healing and sensing structures/components (e.g. smart tyre and airbags).
- Morphing capability for aerodynamic and aesthetic features.
- High temperature actuators.
- Noise, vibration and harshness (NVH) dampers/isolators.
- Rotary actuators.

b) Robotics:

- Micro-sized actuators.
- High speed actuators.
- Efficient, stable and accurate actuators.
- Rotary actuators.

c) Biomedical:

- Artificial muscles.
- Shape memory implants.
- Toxic (e.g. Nickel) free SMAs.

The self-healing capability of SMHs (i.e. combination of SMAs and SMMs, particularly SMPs) (Kirkby *et al.*, 2008; X. Luo & Mather, 2013; Murphy & Wudl, 2010; CC Wang, WM Huang, Z. Ding, Y. Zhao, H. Purnawali, *et al.*, 2012) has potentially created new applications, such as healable composites, coatings and brake pads. The potential of SMAs to work as both sensor and actuator simultaneously is favourable for miniature actuators. The fabrication of mini- and micro-actuators such as NiTi thin films (Section 2.6.3) is possible with the new fabrication technologies, which further enhance SMAs design attributes and functionality.

2.10 Conclusion

In general, the critical design factors to be considered for SMA applications are:

- Operating temperature range for the actuator: Selection of SMA material and heat transfer technique to be considered.
- Force required to deform the actuator: Selection of SMA shape, size, loading configuration and design technique to be considered.
- The required speed of the actuator: Selection of SMA material, shape, size and cooling technique.
- The stroke required: Selection of SMA material, shape, size, loading configuration and design technique to be considered.
- Type of sensors and controller to incorporate with the actuator (e.g. position, temperature, force or resistance) to ensure long life and stability.
- Durability and reliability of the actuator: Selection of SMA material, size, loading configuration and number of cycles to be considered.

Proposed actions to be taken to increase the commercialisation of SMA applications:

- Increased collaboration within sectors of the SMM community (i.e. between material scientists, engineering designers and marketing personnel) and utilisation of information-sharing platforms, databases and associated design tools to share pertinent knowledge for SMA actuator design.
- Utilisation of new SMA materials, including hybrid or composite SMMs to enhance performance and functionality.
- Exploration of new markets for SMA applications.
- Incorporation of computer-based design and analysis tools (within CAD and FEA) into the design and development process.

2.11 Future development

The identified future development opportunities include:

- Development of more efficient and effective information platforms for knowledge sharing within SMM communities.
- Development of new materials (including composites and hybrid SMMs), fabrication technologies and treatment processes for SMAs, which are more stable, more durable and can be utilised in a broad range of industries.
- Development of new design approaches or guidelines for creation of novel SMA applications, in existing and new markets.
- Development of robust computational models of SMA behaviour.
- Development of integrated actuator systems (with compact, fast and intelligent controllers).

Research themes and specific research contributions identified for this work are:

1. *Design methods to resolve SMA actuator limitations*

- Improvement of activation and deactivation durations, such as lagged SMA with highly conductive materials.
- Transient heat transfer and the effect of critical and crossover radii on cylindrical geometry for transient heating.
- Stability investigation (functional fatigue) on SMA linear actuator with and without pulley system.

2. *Development of simple and practical numerical models for SMA actuator response*

- Simplified and robust analytical and numerical models that are compatible with the requirements of design engineers
- Readily applied charts to predict SMA actuator response

3. *Data for SMA linear actuator design.*

- Investigation of system design effects on SMA-pulley system fatigue performance
- Models to predict and characterise SMA functional fatigue

3. Design of SMA linear actuators

The outcomes of this chapter have contributed to the following peer reviewed publications:

- *Numerical modeling of Shape Memory Alloy linear actuator*, J Mohd Jani, S Huang, M Leary, A Subic, Computational Mechanics 53(3), 443-461, 2015, DOI: 10.1007/s00466-015-1180-z.
- *Analysis of convective heat transfer coefficient on shape memory alloy actuator under various ambient temperatures with finite difference method*, J Mohd Jani, S Huang, M Leary, A Subic, Applied Mechanics and Materials 736, 127-133, 2015, DOI: 10.4028/www.scientific.net/AMM.736.127.

3.1 Chapter summary

In the previous chapter, it was emphasised that only a few of patented SMA applications are commercially successful due to material limitations combined with a lack of material and design knowledge and associated tools. This chapter further emphasises that these limitations may be improved or even resolved with proper design approaches and techniques; thus the functionality and the reliability of SMA actuators could be realised and optimised. Brief review of the recent progress and development in optimising SMA with different design methods, techniques and/or approaches are presented and discussed in this chapter.

3.2 Introduction

As highlighted in the previous Chapter 2, SMAs can be readily obtained in commercial quantities from numerous specialised companies around the world, either as semi-finished product in various shapes and forms such as wires, rods, tubes and ribbons; or as finished product such as helical springs and wire actuators (Mohd Jani, Leary, Subic, *et al.*, 2014; Waram, 1993), at very reasonable prices. Even though thousands of patents have been issued on SMA applications, less than 1% of these are commercially successful (Mohd Jani, Leary, Subic, *et al.*, 2014; Vaidyanathan, 2000). This limited commercial success is in part due to a lack of formal guidelines and associated design tools to aid in the effective design of SMA applications. These constraints may have led to the need for further research towards optimisation and improvement of SMA actuators in any of these three categories: man, material and method (refer Chapter 1.2).

In this thesis, the optimisation of SMA applications by informed design processes is advocated. To this end, a brief summary of the SMA design process, design requirements, design specifications, and their design approaches are compiled and presented in this chapter; including: linear, rotary, agonistic and antagonistic basic SMA design; parallel and serial design; and pulley and telescopic design. Relevant factors affecting the design such as convective heating and geometric shapes are also introduced. Most of the solutions presented here are electro-mechanical design solutions, but some material solution using new and hybrid shape memory materials (SMMs) are also discussed for future references and acknowledgement.

3.3 Design of SMA actuator applications

The key to successful design is the effective management of the exploration between the 'problem space' and the 'solution space' (Cross, 2008). In this section, those two spaces are linked together to find the match and design resolutions for the intended applications.

3.3.1 The SMA actuator design process

There are many potential causes of failure in designing a commercial SMA application; these potentially include: an absence of systematic design processes; and, a failure in correctly understanding the requirements of the SMA material or the specific application (Mohd Jani, Leary, Subic, *et al.*, 2014). A systematic design process is necessary, which includes the identification of market needs, and the capability of specific SMA materials and associated actuator designs to satisfy these needs (Pugh, 1991). An overview of the SMA actuator design process is illustrated in Figure 3.1; the elements of this design process, including material selection and applicable design mechanisms, are summarised in this chapter.

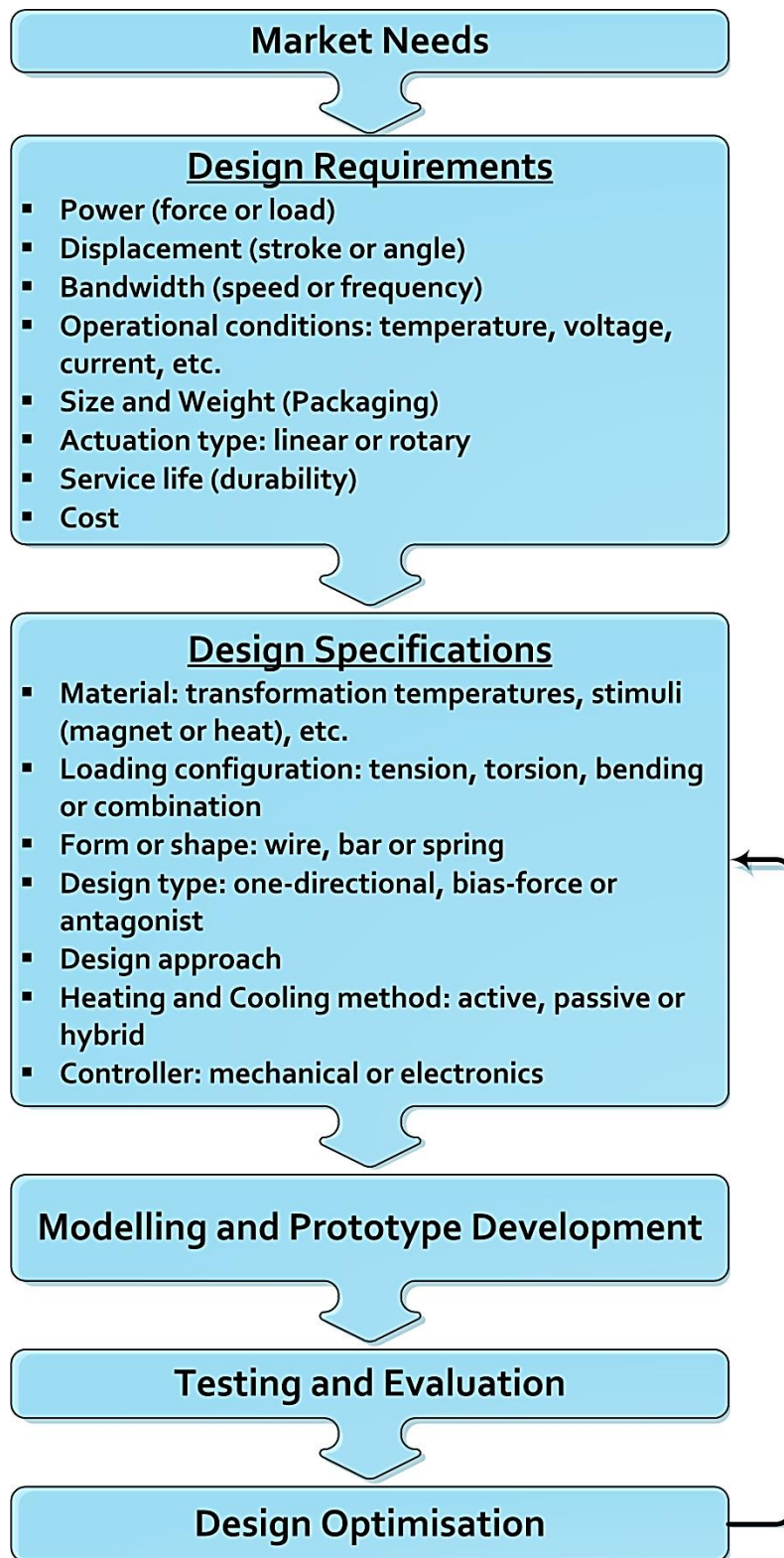


Figure 3.1 – SMA actuator design process, modified from (Pugh, 1991)

3.4 Design requirements

Based on extensive review of SMA actuator applications (Chapter 2); there exist three main technical objectives that must be addressed in any commercial SMA actuator design:

- 1) Force (or load).
- 2) Displacement (stroke or angle).
- 3) Bandwidth (speed or frequency).

Satisfaction of these potentially conflicting objectives is challenging within the constraints of one specific design or application. This challenge typically requires informed compromise between the individual requirements; for example: thin actuators actuate more rapidly than thicker actuators, but the associated actuation force is reduced; increased actuator length produce higher displacement, but requires higher heating energy and available packaging space (methods to enhance packaging space by the use of pulley systems are presented in Chapter 7). In addition to these objectives, other constraints exist in specific actuator applications including: environmental conditions; available packaging space; allowable size and weight; required positional stability and control; maintenance; cost, and durability (Figure 3.1).

Generally, the SMA actuators can be categorised as providing two types of motions:

- 1) Linear or prismatic motion.
- 2) Revolute or rotary motion.

The use of specific mechanisms such as lever and pulleys to: change direction, and type of motion (e.g. from linear to rotary and vice versa); reduce required packaging space; and, to enhance the application functionality and capability are further discussed in this chapter.

3.5 Design specifications

In response to the design requirements, a design specification is constructed to describe the details of the design and the materials used to produce the SMA application.

3.5.1 Material selection

Nitinol (NiTi) and its variations are the most frequently employed shape-memory alloys, although copper and iron based are also available for special applications (Mohd Jani, Leary, Subic, *et al.*, 2014). Nitinol is relatively expensive, due to the extremely precise composition control required for alloy preparation with specific transformation temperatures (i.e. a relative difference of 1% in Ni and Ti compositions can shift transformation temperatures by up to 150°C).

Copper based alloys are used mostly for clamps or fire detector applications. Although copper based alloys are less costly and are employed for various actuator designs, these alloys are not favourable for cyclic applications due to low fatigue strength and thermomechanical instability (Mohd Jani, Leary, Subic, *et al.*, 2014; Reynaerts & Brussel, 1998). Other potential ferrous alloys are listed and compared as in (Mellor, 1989), (Reynaerts, 1995) and (Vaidyanathan, 2000). However, these alloys have not achieved broad commercial use compared to the Ni-Ti SMA alloys that are the research focus of this work.

As described in Section 2.3, the consideration of material selection for SMA applications is typically in reference to their transformation temperatures, hysteresis and maximum stress to utilise either shape memory effect or pseudoelastic (superelastic) advantages as specified in Table 3.1 (components, 2015; Group, 2015). Low hysteresis is desirable for rapid actuation (e.g. MEMS and robotics) and large hysteresis is desirable to retain the predefined shape within a large temperature range (e.g. deployable structures and pipe joining) (Mohd Jani, Leary, Subic, *et al.*, 2014). Transformation temperatures and maximum stress are required to identify the operating range (i.e. operational temperature and load or stress limit). The operational temperature ranges for various SMMs are illustrated in Figure 2.14.

**Table 3.1 – Typical SMA applications based on material properties
(components, 2015; Group, 2015)**

Shape change effects	Austenite-final temperature, A_f [°C]	Description	Typical applications
PE	0 ~ 10	High nickel SE nitinol	Orthopaedic devices, surgical tools, orthodontic arches, cellular-phone antennas
	0 ~ 20	SE nitinol	Guidewires and mandrels
	10 ~ 20	Chromium doped SE nitinol	Stents and braided wires
PE / SME	20 ~ 40	Body temperature nitinol	Body temperature activated devices (e.g. stents and filters)
SME	45 ~ 95	Mid temperature range nitinol	Actuators, toys and demo springs
	95 ~ 115	High temperature range nitinol	Actuators
Note: PE = Pseudoelastic; SME = Shape Memory Effect			

3.5.2 Loading configurations

Mechanically, SMAs can be applied in various loading configurations. However, tension loading produces the highest efficiency and energy density for SMA actuators compared to the other types of loadings, as shown in Table 2.5, Chapter 2. Due to the associated performance advantages, most SMA applications are designed in wire form to benefit from tension type of loading.

3.5.3 SMA geometry

As mentioned earlier, SMAs can be manufactured and purchased in various shapes and forms such as wires, rods, tubes and ribbons; or as finished products such as helical springs and wire actuators (Waram, 1993). Table 3.2 describes the details and comparisons between these forms and shapes for typical SMA linear actuators (Mertmann & Vergani, 2008; Reynaerts & Brussel, 1998).

Table 3.2 – Typical SMA linear actuator form and shape, based on (Mertmann & Vergani, 2008; Reynaerts & Brussel, 1998)

Actuator form	Properties	Remarks
Wire	<ul style="list-style-type: none"> Actuation stroke up to ca. 5% strain. Actuation force up to 200 MPa (full stroke) or 350 MPa (reduced stroke) for trained NiTi actuators. Very moderate dynamic requirements (less than 1 Hz). On-Off actuation. Translational movement or rotation angles less than 90. Fatigue cycles up to 10^6. 	<ul style="list-style-type: none"> Optimal usage of material where minimal use of material for amount of work generated. Tension loading: produces highest efficiency compared to other load types.
Spring	<ul style="list-style-type: none"> Recommended to apply external heat source for heating. Any kind of stroke, but typically less than 30mm. No dynamic requirements. Actuation force up to 200 MPa (full stroke) or 350 MPa (reduced stroke) for trained NiTi actuators. Translational movement. Fatigue cycles up to 0.5×10^6 	<ul style="list-style-type: none"> Large macroscopic displacement out of a relatively small microscopic strain, but the stress distribution over the cross-section of the spring is not constant. Need greater material volume to generate the same force (low efficiency than wire). Poor dynamic response (low bandwidth) due to the larger material (low surface area-to-volume ratio). Only the outer surface actually contracts, but the inner surface acts as both heat dissipater and opposing force to the desired direction.

Studies have shown that SMA frequencies of up to 100 Hz can be achieved by increasing their associated *surface area-to-volume ratio*, such as with thin film SMA (Mohd Jani, Leary, Subic, *et al.*, 2014). Optimisation of bandwidth with this approach is described in Section 3.7.3.2.

As summarised in Table 3.2, tension loading of straight wire provides the highest efficiency compared to other load types, but it also has limited stroke or strain. Design alternatives have been proposed to overcome this limitation, such as by the application of pulley system and a serial or parallel system consisting of multiple SMA wires (Section 3.7.2). The use of a parallel SMA system is technically challenging due to the difficulty in obtaining a homogeneous stress and displacement distribution (Section 3.7.1.1). The technical utilisation of SMA pulley systems is technically challenging due to a lack of relevant design data. This limitation is addressed by the novel SMA pulley durability testing, analysis and design insight provided in Chapter 7 of this work.

3.6 SMA linear actuator basic designs

SMA applications can be divided into four categories according to their memory elements' primary functions (refer Table 2.10) (TW Duerig, 1990; Hodgson *et al.*, 1990). In this section, the SMA linear actuator applications are further explained and described into three basic SMA actuator designs, as illustrated in Figure 3.2 based on (Liang & Rogers, 1992): one-directional actuator design, bias-force actuator design and antagonist actuator design.

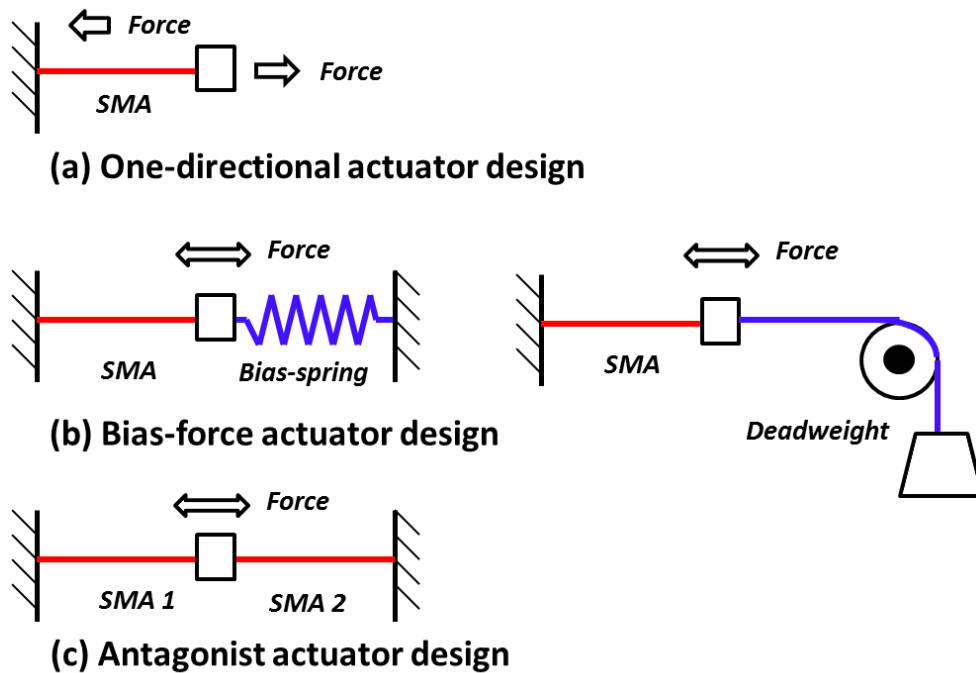


Figure 3.2 – Typical SMA linear actuator designs, image based on (Liang & Rogers, 1992)

One-directional actuator designs are commonly applied for single-use installation applications, in particular for fitting purposes such as SMA cryogenic pipe fittings (TW Duerig, 1990). Bias-force actuator designs use spring or deadweight to generate the restoring force, while antagonist actuator designs are applying an opposing SMA actuator to create an active bias force. Bias-force actuator designs (Figure 3.2b) are typically applied for SMA linear actuator applications due to its simplicity and effectiveness.

3.6.1 One-directional actuator design

For one-directional actuator design, the SMA application could be classified either as *free recovery* or *constrained recovery* (refer Table 2.10, Section 2.7).

- (a) Free recovery: The SMA actuator is stretched and then released with no (or minimal) stress applied, and shrinks back to its original form when heated.
- (b) Constrained recovery: The SMA actuator is prevented from changing shape, and generates stress when heated.

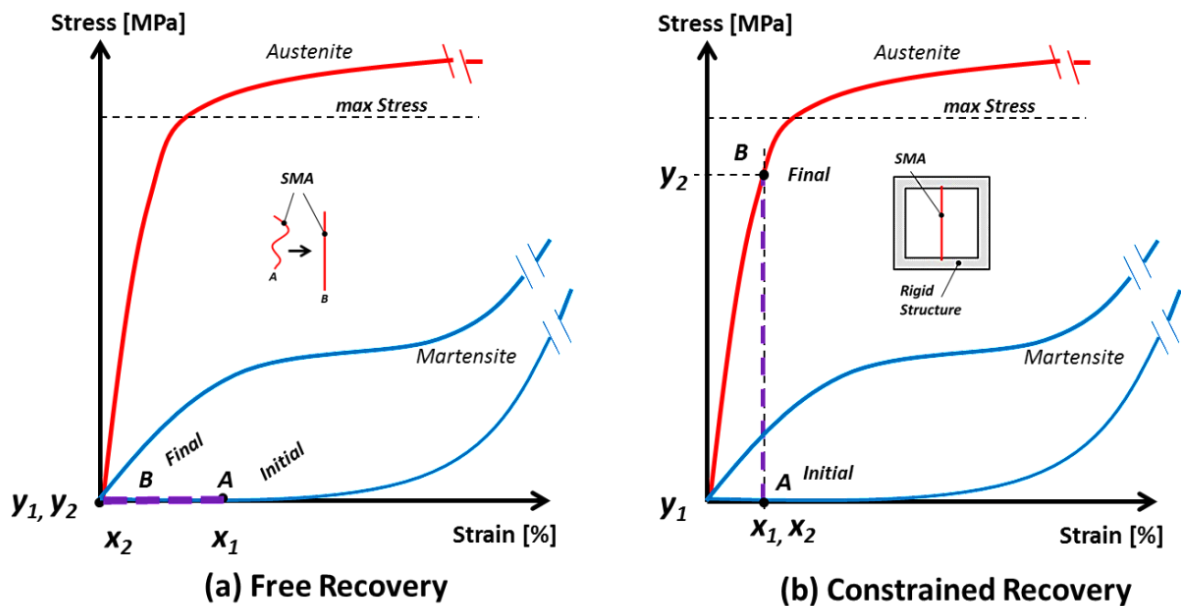


Figure 3.3 – SMA with one-directional actuator design, image based on (TW Duerig, 1990; Hodgson *et al.*, 1990; Stöckel, 1995)

These applications are suitable for single-time or low-cycle applications, such as for fitting, coupling or fastening, self-healing and deployment mechanism.

3.6.2 Bias-force actuator design

For multiple cyclic operations or actuations, the applications are require to contract and return back to their original position frequently and quickly. Since SMA linear actuators can only contract in one direction, a biasing force is necessary to return the SMA into its neutral position, by using a bias spring (or preload spring), deadweight or another SMA element in a differential arrangement. Different design approaches produce different mechanical responses from the applications.

As illustrated in Figure 3.4, SMA actuators with bias-forces are initially deformed up to x_2 % in the martensitic phase with an initial stress of y_1 MPa (pos. A in Figure 3.4). During heating, the element transforms into the austenitic phase following the characteristic of the bias-force and recovering their initial deformation, x_1 % and reaches a final stress of y_2 MPa once the

transformation has been completed. During cooling, the actuators are returned to their initial position, x_2 % by the action of the bias-forces and ready for subsequent actuation. The maximum available force during actuation develops correspondence to the maximum level of stress reached by the elastic zone of the SMA actuator during this phase change from martensite to austenite.

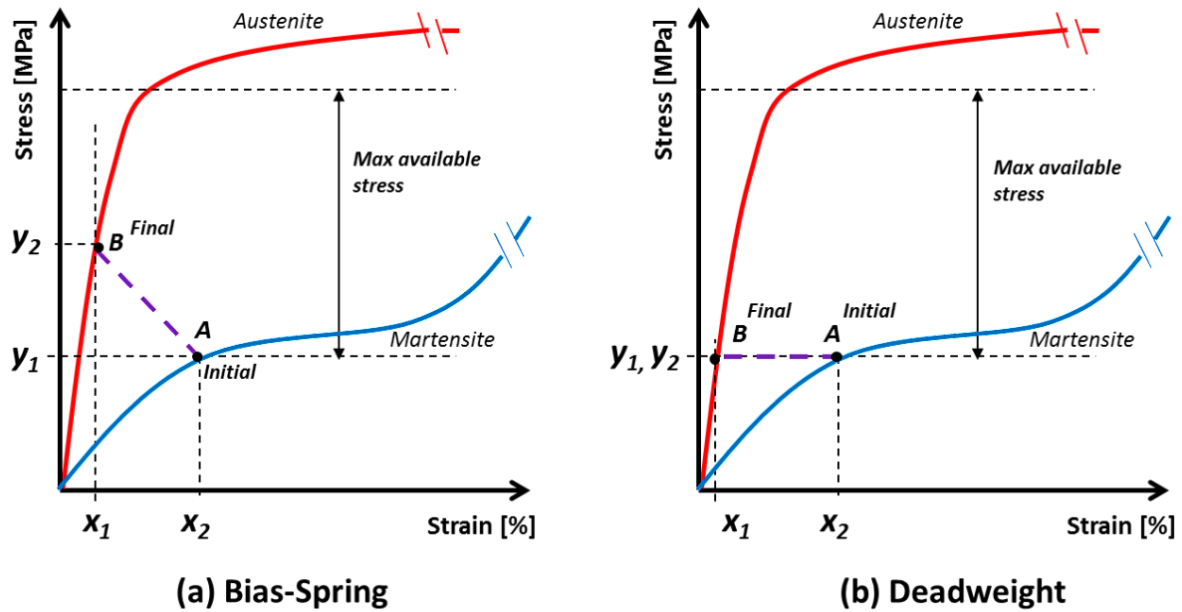


Figure 3.4 – SMA with a bias-force actuator design, image based on (Butera *et al.*, 2007)

The stress applied to the actuator by deadweight remains constant, while the stress or force applied by the bias-spring increase linearly with the displacement and is dependent on the spring constant, $F_{spring} = k_{spring} \cdot \Delta x$. Even though there is inconsistency of applied force in the bias-spring actuator design, it is often more favourable compared to the deadweight actuator design due to compactness, simplicity and lightweight.

3.6.3 Antagonistic design

In antagonistic (or differential) design approach, two SMA actuators are actuated (heated) and deactivated (cooled) alternately.

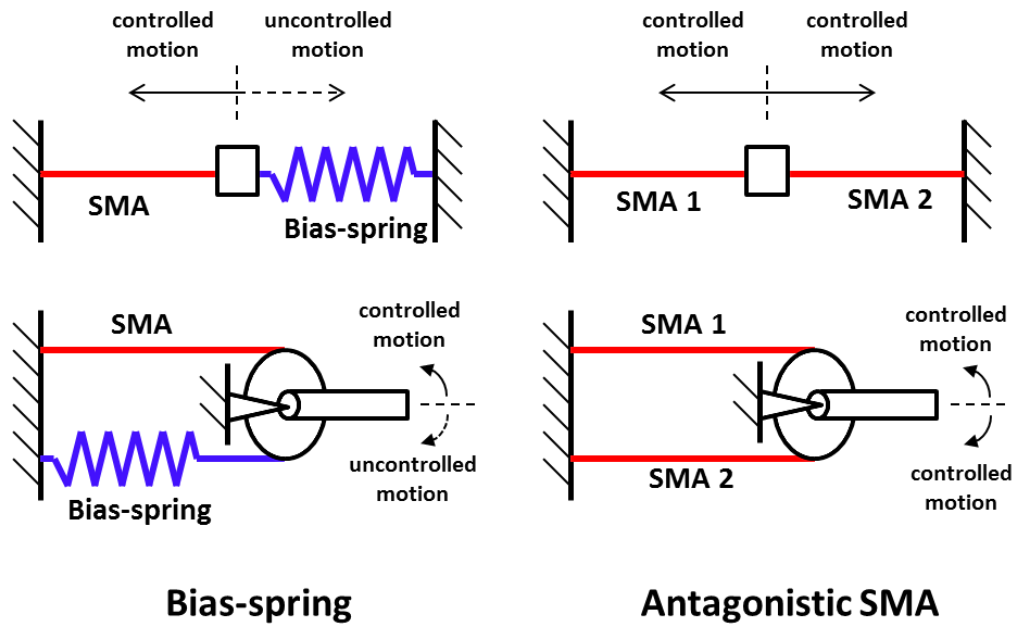


Figure 3.5 - Linear and revolute joint configuration of SMA with bias spring and antagonistic design, image based on (Teh, 2008)

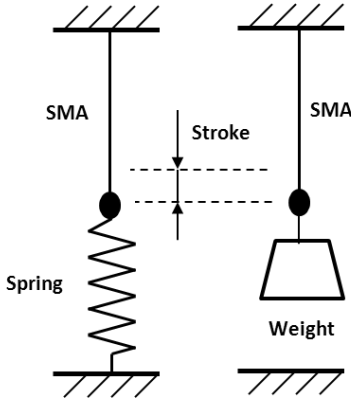
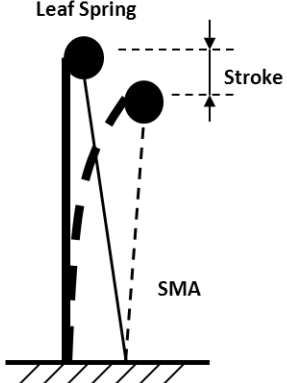
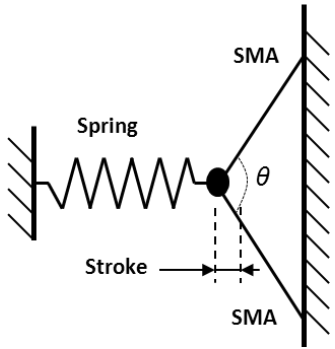
The advantage of antagonistic design over bias spring is the capability to control the movement in both directions actively, instead of only providing passive bias force. The bandwidth may also increase slightly because the heating and cooling is working alternately (Bergamasco *et al.*, 1990; W. Huang, 2002; Ikuta *et al.*, 1988; Katsutoshi Kuribayashi, 1986; Teh, 2008), but this design requires an electronic controller to control it accurately and effectively.

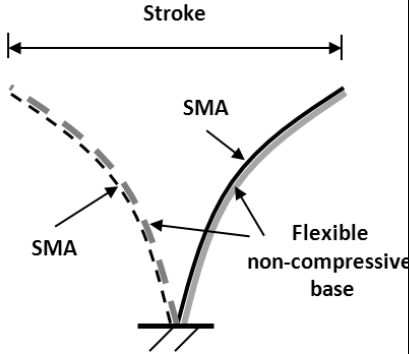
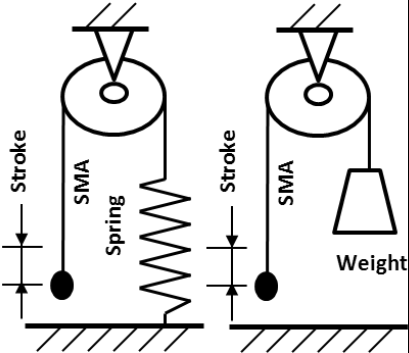
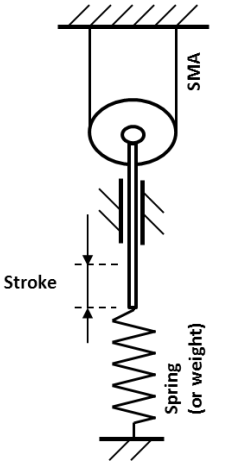
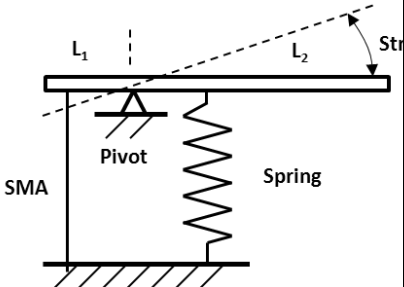
A few samples of application applying this design approach are the automotive mirror actuator (E. Williams & Elahinia, 2008), an endoscope (Ikuta *et al.*, 1988), a smart structure called an antagonistic flexural unit cell (AFC) (Sofla, Elzey, & Wadley, 2008), a braille display (Yoichi Haga *et al.*, 2005), a tactile binary display (Velázquez, Pissaloux, Szewczyk, & Hafez, 2005), an automotive tumble flap (Colli, Bellini, Concari, Toscani, & Franceschini, 2006), and the SmartServo RC-1 (Corporation).

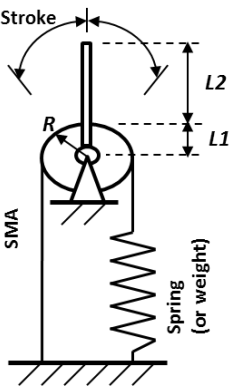
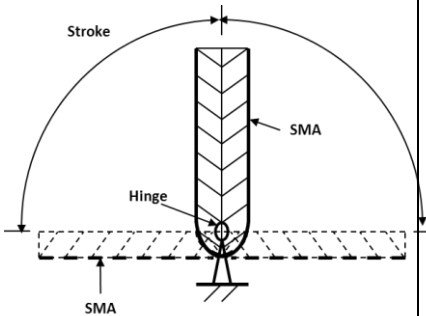
3.7 SMA design approaches

Many design approaches have been developed to optimise the SMA functionality and reliability for many applications. Recent improvements of SMA applications from the late 90's until now with electro-mechanical design solutions are discussed and presented in this chapter, such as illustrated in Dynalloy technical data sheet (Dynalloy Inc., 2007) and several others (Katsutoshi Kuribayashi, 1986; Reynaerts & Brussel, 1998). These design approaches are summarised in Table 3.3.

Table 3.3 – Basic SMA wire design approaches, based on (Dynalloy Inc., 2007; Katsutoshi Kuribayashi, 1986; Reynaerts & Brussel, 1998)

Design	Motion Types	Design Approach	Illustrations	Remarks
A	Linear	Bias spring or dead weight		<p>Stroke: $x_{\max} = 4\% \cdot L_{\text{SMA}}$</p> <p>Force: $F_{\max} = 100\% \cdot F_{\text{SMA}}$</p> <ul style="list-style-type: none"> The bias force produced by spring is proportional to the spring displacement (and spring constant, $F_{\text{Spring}} = k \cdot \Delta x$), while it is always constant with dead weight.
B	Linear	Leaf spring bias		<p>Stroke: $x_{\max} = 7\% \cdot L_{\text{SMA}}$</p> <p>Force: $F_{\max} = 100\% \cdot F_{\text{SMA}}$</p> <ul style="list-style-type: none"> Increase stroke (displacement).
C	Linear	Angled pull		<p>Stroke: $x_{\max} = 14\% \cdot L_{\text{SMA}}$</p> <p>Force: $F_{\max} = 25\% \cdot F_{\text{SMA}}$</p> <p>Formulation:</p> $\Delta x = L_{\text{SMA}} \cos \alpha - \sqrt{((L_{\text{SMA}} - \Delta L_{\text{SMA}})^2 - (L_{\text{SMA}} \cdot \sin \alpha)^2)}$ <p>where $\alpha = \theta/2$</p> <ul style="list-style-type: none"> Increase stroke (displacement) and load capacity (power).

Design	Motion Types	Design Approach	Illustrations	Remarks
D	Linear	Adjusting curvature		<p>Stroke: $x_{\max} = 110\%.L_{\text{SMA}}$</p> <p>Force: $F_{\max} = 3.8\%.F_{\text{SMA}}$</p> <ul style="list-style-type: none"> ▪ Increase stroke (displacement) and load capacity (power).
E	Linear	Simple pulley (fixed)		<p>Stroke: $x_{\max} = 4\%.L_{\text{SMA}}$</p> <p>Force: $F_{\max} = 100\%.F_{\text{SMA}}$</p> <ul style="list-style-type: none"> ▪ Increase stroke (displacement). ▪ Multiple pulleys can be used to increase stroke. ▪ May be used to change motion direction.
F	Linear	Simple pulley (moved)		<p>Stroke: $x_{\max} = 4\%.L_{\text{SMA}}/(N_{\text{pulley}}+1)$</p> <p>Force: $F_{\max} = 100\%.F_{\text{SMA}}.(N_{\text{pulley}}+1)$</p> <ul style="list-style-type: none"> ▪ Reduce stroke (displacement) and increase the load capacity (power). <p>N_{pulley} = No. of moving pulley used.</p>
G	Rotary	Simple lever		<p>Stroke: $\theta_{\max} = 120^\circ$</p> <p>Force: $F_{\max} = F_{\text{SMA}}.(L_1/L_2)$</p> <ul style="list-style-type: none"> ▪ Increase stroke (displacement) and load capacity (power).

Design	Motion Types	Design Approach	Illustrations	Remarks
H	Rotary	Simple level-pulley (fixed)		<p>Stroke: $\theta_{\max} = (180\pi R)/(4\% \cdot L_{\text{SMA}})$</p> <p>Force: $F_{\max} = F_{\text{SMA}} \cdot (L_1/L_2)$</p>
I	Rotary	Clam shell		<p>Stroke: $\theta_{\max} = 90^\circ$.</p> <p>Force: $F_{\max} = 4\% \cdot F_{\text{SMA}}$</p> <ul style="list-style-type: none"> ▪ Increase stroke (displacement) and load capacity (power).
<ul style="list-style-type: none"> ▪ The proposed value is the safe value for any design applications. ▪ L_{SMA} is the actual SMA wire length. ▪ F_{SMA} is the actual force exerted by SMA wire as indicated in (Dynalloy Inc., 2007). Example: SMA wire with diameter 0.02 inch (0.51mm), $F_{\text{SMA}} = 3560$ gram. ▪ Most of the design may replace SMA wire with SMA, but the stroke and force values would be different. 				

Other recent innovative approaches are discussed and presented into three categories, according to the main factors, as mentioned earlier in Section 3.4: power, displacement and bandwidth.

3.7.1 Power improvement designs

As mentioned earlier, thicker wires would produce higher power (load capacity), but it would also reduce the bandwidth (operational frequency range). A few design proposals to improve the application power without sacrificing the bandwidth are presented in this section.

3.7.1.1 Parallel SMA design

This design approach is implemented to increase the force (or load) capacity of SMA actuator application by arranging many SMA wires in parallel with the spaces between them. Thin SMA wires are preferable to improve the bandwidth, and the wires must remain separated to let the cooling medium such as air or liquid to flow freely around all surfaces and the advantages of the higher surface area-to-volume ratio can be realised (Laurentis, Fisch, Nikitczuk, & Mavroidis, 2002; Mosley & Mavroidis, 2000).

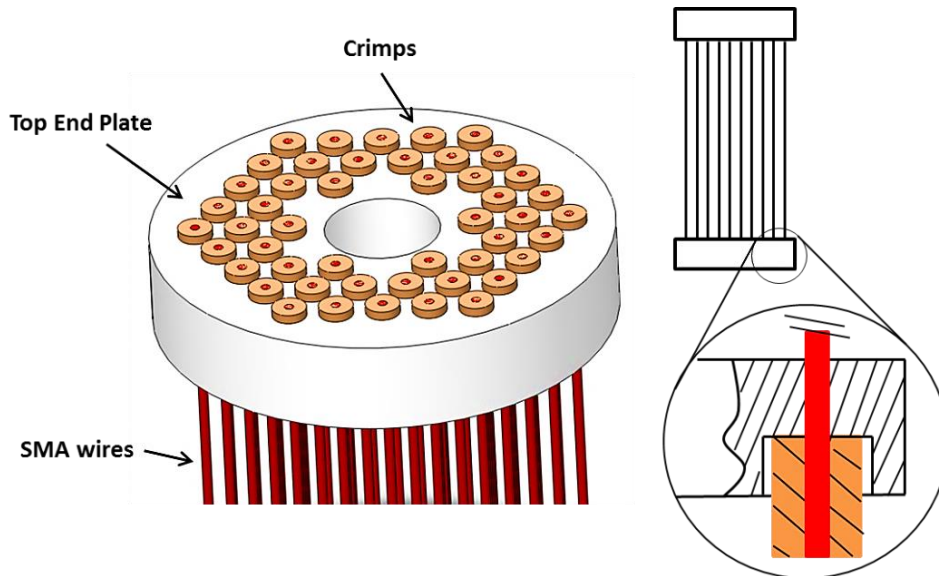


Figure 3.6 - Arrangement of SMA wires on end plate, image based on (Mosley & Mavroidis, 2000)

Referring to (Eq. 3.1) and (Eq. 3.2), the power supply would require very high amperage, I_{Total} , to actuate all the wires simultaneously if the wires are arranged in parallel circuit, due to the total resistance, R_{Total} of the system reduces as the number of wires, N increase.

As all the SMA wires are the same:

$$R_{Total} = \frac{R_{SMA}}{N} \quad (\text{Eq. 3.1})$$

$$I_{Total} = \frac{V_{Total}}{R_{Total}} = \frac{V_{Total} \cdot N}{R_{SMA}} \quad (\text{Eq. 3.2})$$

where R_{SMA} is the resistance for each single SMA wire.

However, the current supplied to each SMA wire, I_{SMA} is reduced (Eq. 3.3), and the resulting voltage drop across the system (Eq. 3.4), where the voltages are constant or same for each wire in the parallel system (see Figure 3.7).

$$I_{SMA} = \frac{I_{Total}}{N} \quad (\text{Eq. 3.3})$$

$$V_{System} = V_{SMA} = I_{SMA} \cdot R_{SMA} \quad (\text{Eq. 3.4})$$

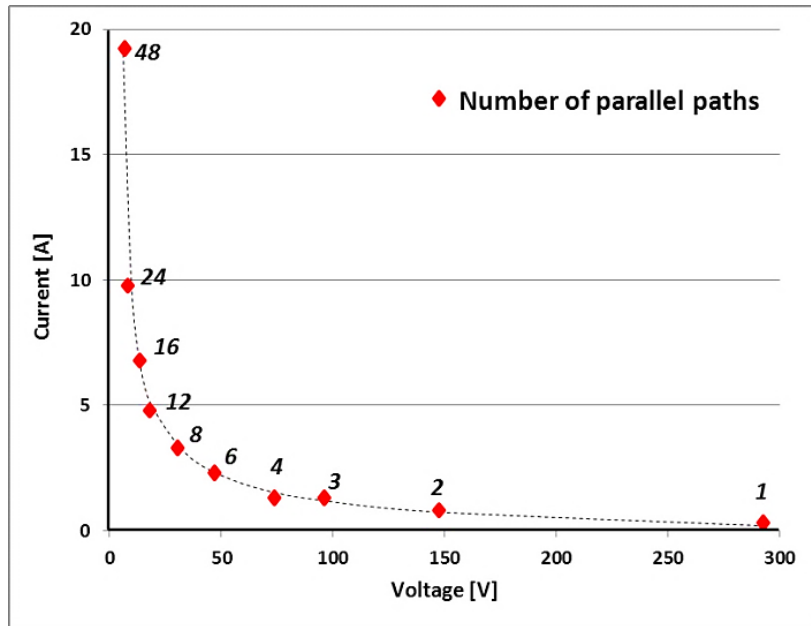


Figure 3.7 - SMA bundle current versus Voltage requirement for number of paths (Mosley & Mavroidis, 2000)

Due to this impractical power supply requirement and low power supplied to each wire, the wires are arranged mechanically in parallel, but the wires are connected electrically in series. The combination of both series and parallel circuit is necessary for a very large number of wire bundles in order to overcome the voltage restriction on power supply (Mosley & Mavroidis, 2000). One concern of using this design is it would be difficult to obtain a

homogeneous stress distribution (equal transformation temperatures) over the multiple sets of wires simultaneously.

A few applications applying this approach are the SM intramedullary nail for bone elongation by (Gümpel & Strittmatter, 2009). A further improvement suggested by (Laurentis *et al.*, 2002) to this approach is to combine wires with different diameters in series for each parallel section.

3.7.1.2 Moveable pulley system design

As illustrated in Table 3.3, Design No. F, a moveable pulley system can be utilised to increase the load capacity. For the intermediate design approach, multiple movable pulley system is utilised to increase the load capacity. The load capacity increases as the number of moveable pulley increases in the pulley system. However, the stroke reduces as the number of pulley increases. Other effects that contribute to the SMA-pulley system are reported in Chapter 7.

3.7.1.3 Torque limit with a sigma-shaped-pulley design

This design was first proposed by Hirose *et al.* (1988) to limit the torque increase due to the bias spring.

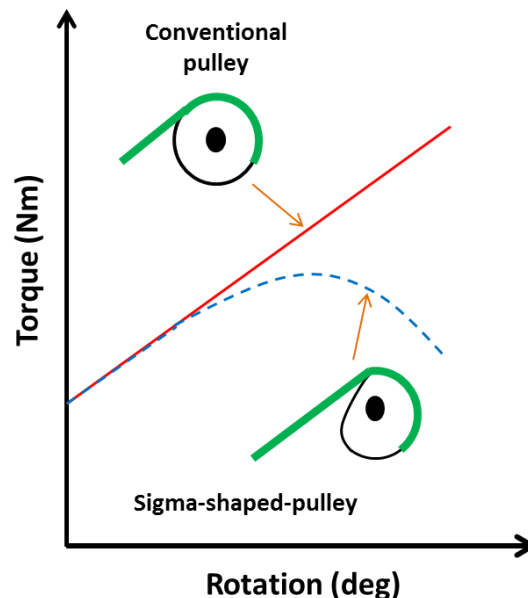


Figure 3.8 - Influence of a sigma-shaped-pulley on the bias torque, image based on (Reynaerts & Brussel, 1998)

This would be applicable for scenarios that require a certain torque limit to protect them from damage due to mechanical overload such as jams or crash stops.

3.7.2 Displacement improvement designs

As described in Section 2.5.1, NiTi SMA actuator provides the highest work densities compared to other conventional actuators. Some of the design solutions to increase the stroke (displacement) of SMA actuators are already described in previous sections. A few additional design proposals to improve the application displacement are presented in this section.

3.7.2.1 Serial SMA design

This design approach introduced by (Elwaleed, Mohamed, Nor, & Mustafa, 2007) is quite similar to the basic linear design using adjusting curvature (Design No. D, Table 3.3) with some enhancements, the SMA wires are fixed to the flexible beam in equally spaced segments, and actuated in pairs. The multiple fixed segments design offers larger displacement (up to 20mm or 280% higher) compared to the single segment design (see Figure 3.10) (Elwaleed *et al.*, 2007).

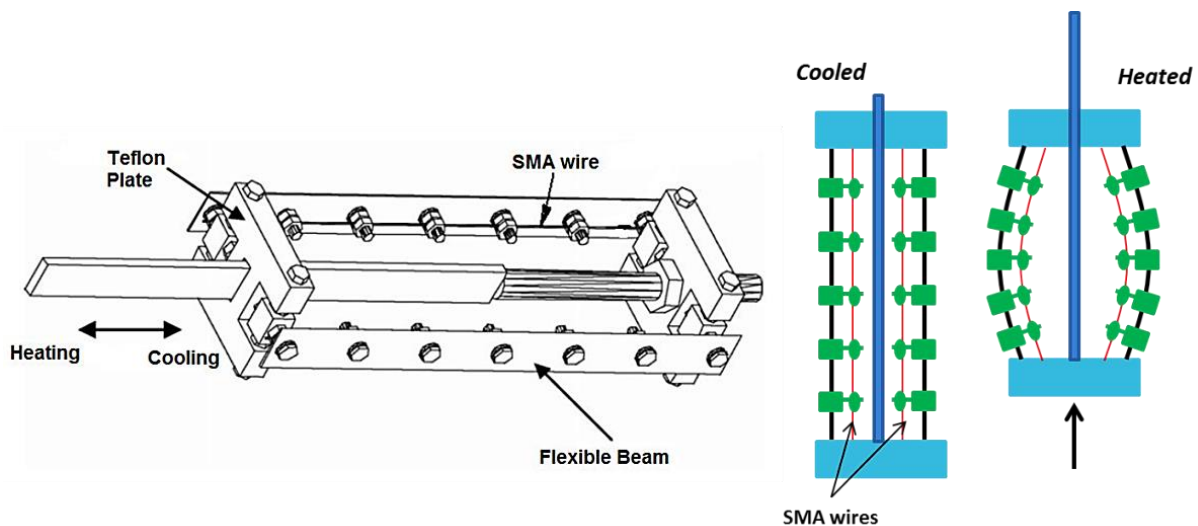


Figure 3.9 - Linear smart actuator with curvature beams, image based on (Elwaleed *et al.*, 2007)

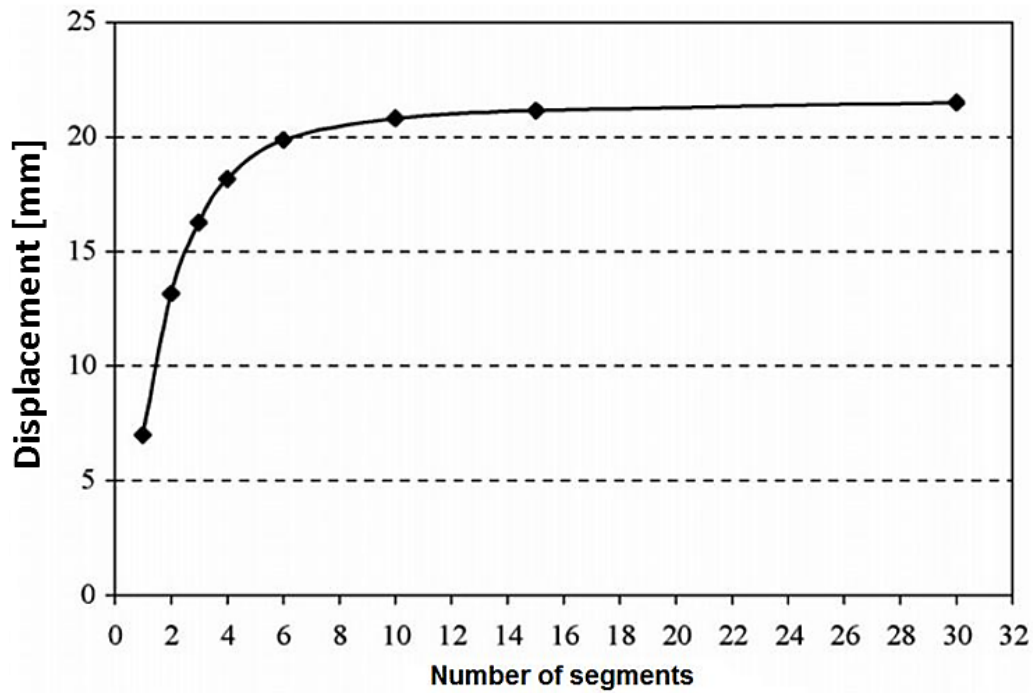


Figure 3.10: Analytical result for end displacement with different number of segments (Elwaleed *et al.*, 2007)

Adding more flexible beams in parallel could increase the load capacity (power). An electronic controller with laser displacement sensor is used in this design to optimise the actuator accuracy and stability.

3.7.2.2 Fixed pulley system design

For the intermediate design approach, a long SMA wire is wound over a multiple fixed pulleys to increase displacement capacity. This design is an enhancement of the basic design approach using simple fixed-pulley for linear motion (Table 3.3, Design No. E). Gaps or spaces may be introduced between each winding to assist SMA cooling. One recent design to utilise this approach is a medical rehabilitation device used to assist ankle stability (Pittaccio *et al.*, 2009). The SMA linear actuator for this application is constructed with a 2500 mm NiTi wire of diameter 0.25mm, winded through 2 mini-pulleys for several times, as shown in Figure 3.11.

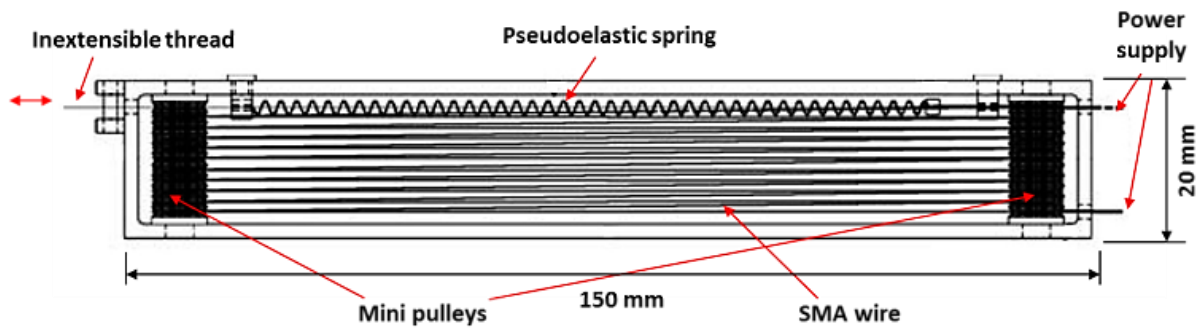


Figure 3.11 - Mini-linear-actuator with SMA winding wire on two pulleys (Pittaccio *et al.*, 2009)

The device produces a maximum of 80 mm stroke (about 3.2% wire strain) under a static load of 8.83N within 7 s (with 0.7A) and restored to initial position within 30s under natural cooling. Figure 3.12 shows another sample of a similar actuator, developed by the author in collaboration with a partner automotive supplier.



Figure 3.12 - FUTURIS SMA actuator prototype

3.7.2.3 Telescopic or multiplied displacement design

This design approach was developed by Miga Motors Company (MigaMotors) and managed to multiply the application stroke by the number of parallel telescopic modules used in its linear actuator. This approach is also known as the ‘displacement multiplied’ technique (Figure 3.13) (MA Gummin, Donakowski, & Gaines, 2007).

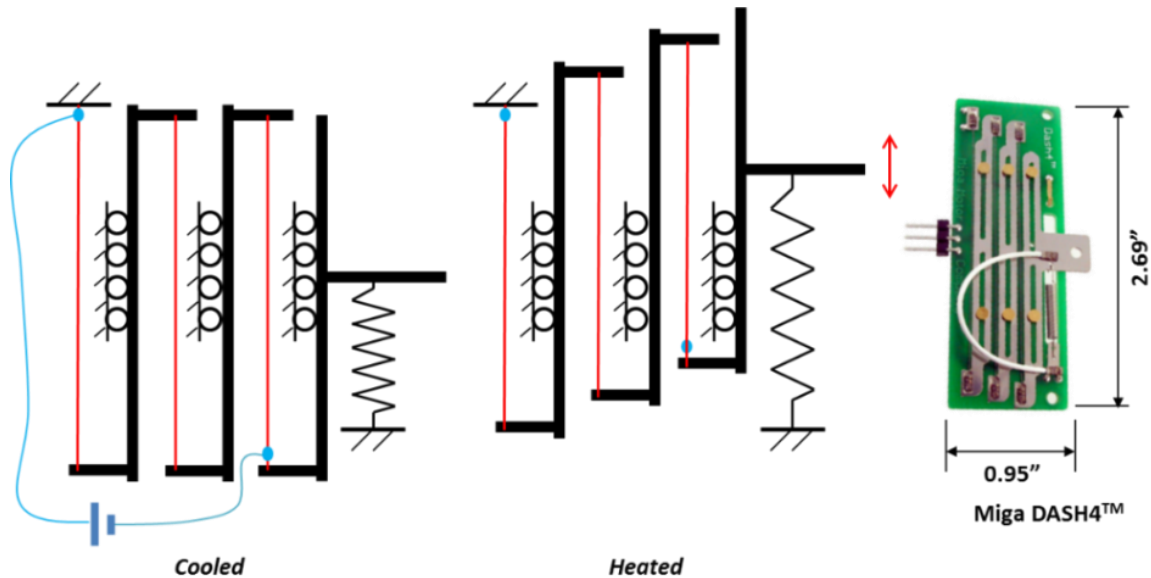


Figure 3.13 - Miga Motor Company modular SMA linear actuator design concept; image based on (MA Gummin *et al.*, 2007; MigaMotors)

The actuator load capacity could be increased with the use of larger diameter SMA wires. A variety of actuators produced by Miga Motor Company are summarised in Table 3.4. The rotary actuator versions perform bidirectional rotary motion up to 60°.

Table 3.4 - Miga Motor Company SMA linear actuator specifications (MigaMotors)

Model	Displacement [mm or °]	Output Force or Torque [N or Nmm]	No. of parallel modules	Wire diameter [inch (mm)]	Actuation duration [ms]	Dimensions [all in mm]
DM01-10	12.7mm	8.9 N	5	0.010" (0.254mm)	500 (12V, 1.6A)	21.5 x 79.4 x 7.3
DM01-12	12.7mm	12.2 N	5	0.012" (0.305mm)	500 (12V, 2.4A)	21.5 x 79.4 x 7.3
DM01-15	12.7mm	20.0 N	5	0.015" (0.381mm)	500 (12V, 4.0A)	21.5 x 79.4 x 7.3
MOBI™	3.2mm	4.5N	4	0.005" (0.127mm)	-	12.7 x 28.6 x 2.0
DASH4™	5.8mm	7.8 N	3	*0.010" (0.254mm)	250 (7V, 2.1A)	24.1 x 68.3 x 2.88
MIGAONE™	9.5mm	11.1 N	5	0.012" (0.305mm)	500 (10V, 2.7A)	72.9 x 34.8 x 2.88
NM706-Super	4.0mm	0.7 N	6	0.003" (0.076mm)	-	6.0 x 34.7 x 5.32
NM-DS-70CE 1010/1030	4mm	0.2 N	6	*0.003" (0.076mm)	400 (3.25V, 0.85A) 400 (12V, 0.28A)	12.0 x 53.0 x 10.0
NM-DS-125-CE 1010/1030	4mm	0.4 N	6	*0.003" (0.076mm)	400 (1.85V, 1.5A) 400 (12V, 0.5A)	12.0 x 53.0 x 10.0
TWA-078	2mm	4.4 N	2	0.005" (0.127mm)	150 (5V, 0.72A)	12.7 x 30.5 x 2.5
NM-RS-CE 125/70	60°	2.0 Nmm 1.2 Nmm	6	*0.003" (0.076mm)	300 (3.0V)	12.7 x 55.25 x 7.5
NM-70R 2P/6P	60°	1.2 Nmm	6	*0.003" (0.076mm)	50 (3-9V)	12.7 x 55.25 x 7.5

Note: All values are approximate. Some of the items are obsolete and replaced with new version.

***Typical size for the actuator.**

3.7.2.4 SMA form or shape replacement

Replacing SMA wire with a SMA spring configuration can significantly improve the application's stroke (Donnellan, 2005). For example the actuator developed by Starsys Research and Applied Physic Laboratory (APL) (Figure 3.14), increased actuator stroke from 0.125" to 0.28", however bandwidth was reduced by a factor of ten. Technical challenges to the use of SMA spring actuators are highlighted in Table 3.2.

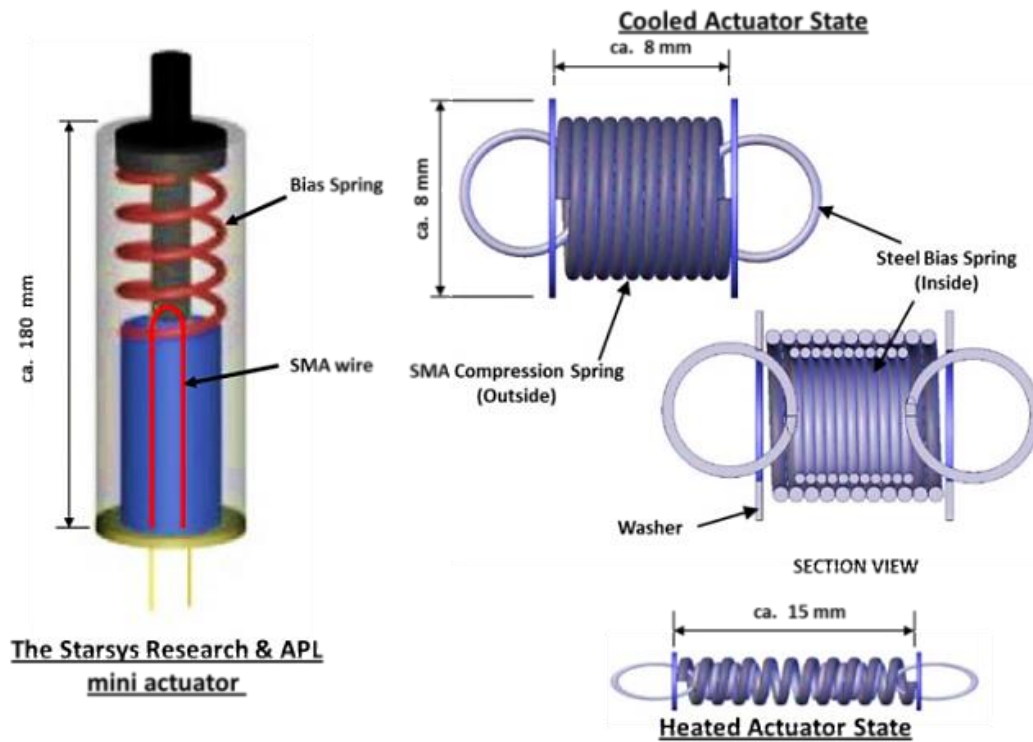


Figure 3.14 - The Starsys Research & APL mini actuator versus Donnellan's mini actuator (Donnellan, 2005)

3.7.3 Bandwidth improvement designs

One of the main reasons for the limited commercialisation of SMA actuators is the relatively poor bandwidth performance, particularly due to relatively slow cooling process, which is limited by the heat transfer mechanisms of conduction and convection (Mohd Jani, Leary, Subic, *et al.*, 2014). Vollach & Shilo (2010) revealed that SMA wire has the greatest potential for applications that require high speeds (within microseconds) and large displacements (up to 8mm) for single-use actuation, compared to other conventional actuators. Heating the SMA is not a significant technical challenge, however enhanced SMA cooling remains an open research challenge. Generally, enhanced SMA cooling strategies are achieved within two categories:

1) *Active cooling*

Active cooling is a typical cooling method, dealing with external mechanisms, including forced air, flowing liquids, heat pumps, heat sinks, and conductive materials.

2) *Passive cooling*

Passive cooling refers to cooling methods via design approach that use the system's structure or natural elements, such as shape improvement and system controller optimisation.

As discussed in Section 2.5.2, active cooling could increase the cooling performance, but may be impractical for numerous scenarios, due to relatively high energy consumption and noise production (Reynaerts & Brussel, 1998), and increased cost, mass, volume; as well as the associated mechanical and control complexity (Gorbet *et al.*, 2009; DC Lagoudas, 2010). Design solutions to enhance the cooling performance with either active or passive cooling are discussed in this section.

3.7.3.1 Natural, forced and mixed convection

Convection heat transfer mechanisms plays a critical role in typical SMA cooling processes. The convection heat transfer mechanism occurs via fluid motion, which is classified as natural (or free) and forced convection (Bergman, Lavine, Incropera, & DeWitt, 2011; Çengel & Ghajar, 2011). Fluid motion is caused by the buoyancy effect of heated air in natural convection. Fluid motion can also be motivated by external means, such as fans or pumps, in forced convection (Çengel & Ghajar, 2011). Forced convection provides a significant improvement in SMA cooling rate and associated deactivation time compared to the natural convection condition.

The rate of convective heat transfer is characterised by the convective heat transfer coefficient, h , which is dependent on many variables, including fluid properties and velocities; material surface geometry, orientation and associated roughness; and the flow type, either laminar or turbulent (Bergman *et al.*, 2011; Çengel & Ghajar, 2011). In addition, the fluid properties also depend on environmental conditions such as temperature and pressure (Figure 3.16).

The convection heat transfer is also influenced by the object's orientation due to buoyancy force moving vertically upwards (Figure 3.15). The cooling performance reduces as the object inclination increases (from horizontal to vertical) due to the decreasing of the cross-stream buoyancy force ($F_{Buoyancy} \propto g \cdot \cos\phi$) (Incropera & DeWitt, 1985; Çengel & Ghajar, 2011).

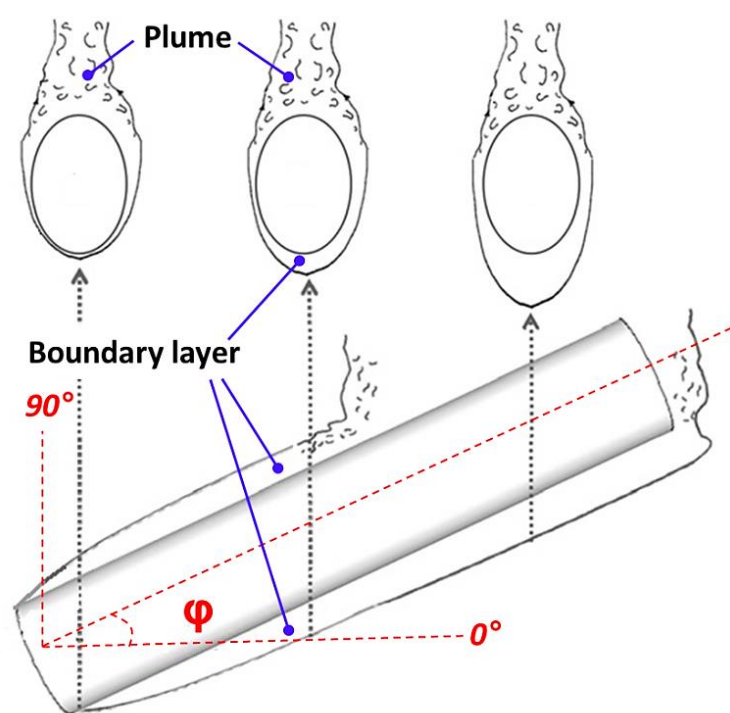


Figure 3.15 - Flow development for an inclined cylinder, based on (Heo & Chung, 2012)

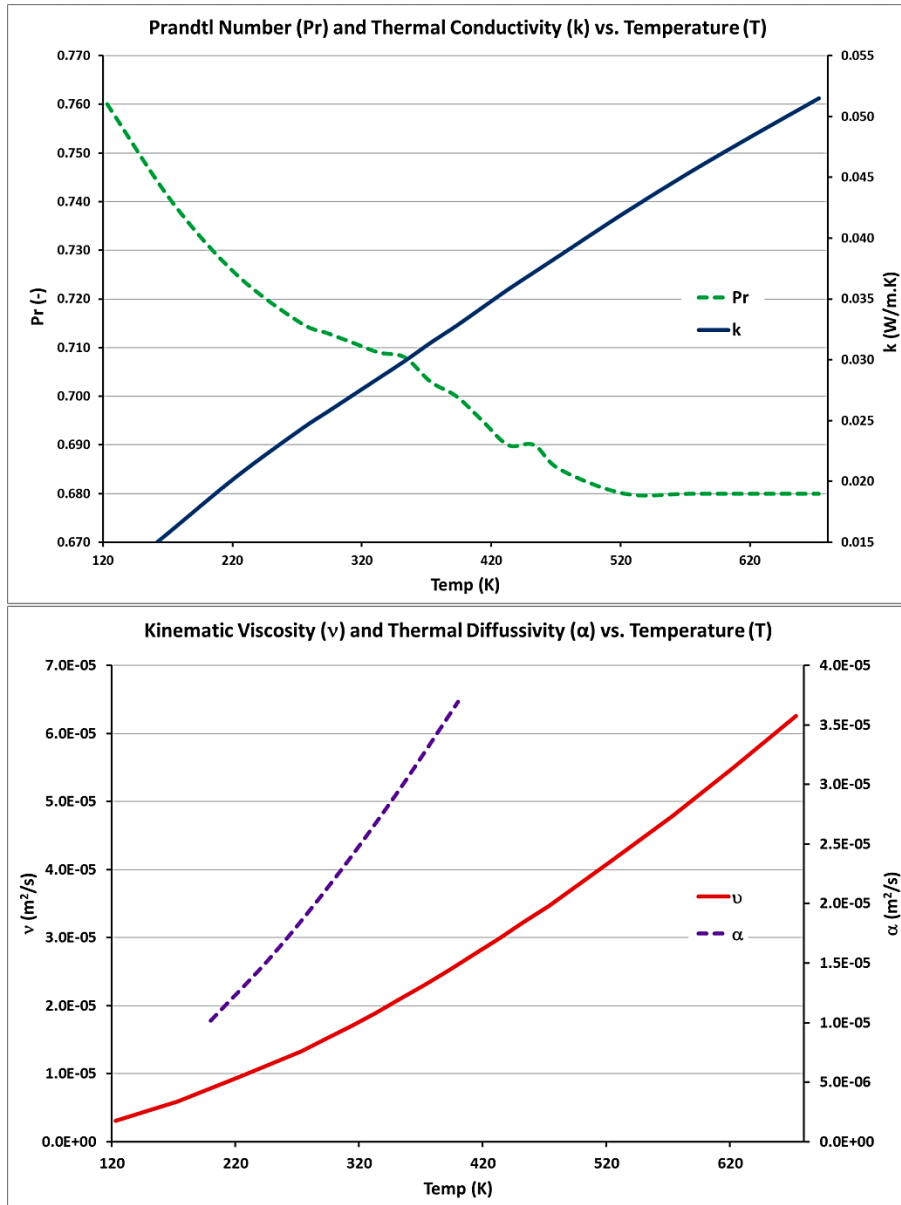


Figure 3.16 - Prandtl number and air properties relationship with various ambient temperatures (Mohd Jani *et al.*, 2015a)

The unknown convective heat transfer coefficient can be derived from the Nusselt number, Nu_D . For an isothermal long horizontal cylindrical geometry, the Nusselt number is (Bergman *et al.*, 2011; Çengel & Ghajar, 2011):

$$Nu_{cyl} = \frac{\text{Convective Heat Transfer Coefficient}}{\text{Conductive Heat Transfer Coefficient}} = \frac{h \cdot D_{cyl}}{k}, \text{ therefore } h_{cyl} = \frac{Nu_{cyl}}{D_{cyl}} \quad (\text{Eq. 3.5})$$

In Chapter 6, a finite difference equation (FDE) is developed to simulate SMA response, and calibrated with the experimental data to obtain the unknown convective heat transfer coefficient, h . Additionally, the associated advantage and limits of forced convection for commercial SMA applications are investigated and reported.

Natural convection

(SW Churchill & Chu, 1975; Çengel & Ghajar, 2011) defined the Nu_D for *natural convective* heat transfer of a long horizontal cylinder and negligible secondary effects (e.g. surface roughness) with $Ra < 10^{12}$ (Eq. 3.6); where the Rayleigh (Ra), Prandtl (Pr) and Grashof (Gr) numbers can be calculated or acquired from the standard engineering tables or graphs (Figure 3.16).

$$Nu_{cyl} = \left(0.6 + \frac{0.387 \cdot Ra^{\frac{1}{6}}}{\left[1 + \left(\frac{0.599}{Pr} \right)^{\frac{9}{16}} \right]^{\frac{8}{27}}} \right)^2 \quad (\text{Eq. 3.6})$$

Additionally, (Eisakhani, Ma, Gao, Culham, & Gorbet, 2011), had developed a correlation equation to calculate the Nusselt number for natural convective heat transfer, specifically for SMA wire experiments with various inclination angles. They defined the Nu_D for SMA wire as in (Eq. 3.7), where the constant A , C and n can be referred to as in Table 3.5.

$$Nu_D = A + C \cdot Ra_D^n \quad (\text{Eq. 3.7})$$

Table 3.5 – Constants for SMA wire with Eishakani *et al.* correlation equation (Eisakhani *et al.*, 2011)

Orientation, φ [°]	Stress-free condition			100 MPa applied load	
	A	C	n	A	C and n
0	0.190	0.820	0.170	0.810	0.16
15	0.180	0.815	0.162	0.811	0.152
30	0.169	0.797	0.154	0.798	0.144
45	0.159	0.767	0.146	0.772	0.136
60	0.148	0.724	0.139	0.732	0.129
75	0.138	0.670	0.131	0.678	0.120
90	0.127	0.603	0.123	0.610	0.113
For heat transfer correlation in the range of $2.6 \times 10^{-8} \leq Ra_D \leq 6 \times 10^{-1}$.					

Forced convection

For *forced convection* of a circular cylinder within $10^2 < Re < 10^7$ and $Re.Pr > 0.2$, the Nusselt number can be derived from the Churchill and Bernstein correlation equation (Eq. 3.8) (SW Churchill & Bernstein, 1977); where the Reynolds (Re) and Prandtl (Pr) numbers can be calculated or acquired from the standard engineering tables or graphs.

$$Nu_{cyl} = 0.3 + \frac{0.62Re^{\frac{1}{2}}Pr^{\frac{1}{3}}}{\left[1 + \left(\frac{0.4}{Pr}\right)^{\frac{2}{3}}\right]^{\frac{1}{4}}} \left[1 + \left(\frac{Re}{282000}\right)^{\frac{5}{8}}\right]^{\frac{4}{5}} \quad (\text{Eq. 3.8})$$

Alternative solutions proposed by (VDH Zijnen, 1956) (Eq. 3.9) and (MN Ozisik, 1987) (Eq. 3.10) may be sufficient to determine the Nusselt number and convective heat transfer coefficient respectively; where U and ν are the speed and kinematic viscosity of the air respectively.

$$Nu_{cyl} = 0.35 + 0.01Re + 0.5\sqrt{Re} \quad ; \quad 10^{-1} < Re < 10^5 \quad (\text{Eq. 3.9})$$

$$h_{cyl} = 0.23 \left(\frac{U}{\nu}\right)^{0.6} \frac{k_{air}}{D_{cyl}^{0.4}} \quad (\text{Eq. 3.10})$$

Mixed convection

The flow regimes in natural and forced convections are governed by the dimensionless Grashof (Gr) and Reynolds (Re) numbers, respectively. Gr represents the ratio of the buoyancy force to the viscous force acting on the fluid, while Re represents the ratio of inertia to viscous forces acting on the fluid (Incropera & DeWitt, 1985; Çengel & Ghajar, 2011).

Both natural and forced convection is involved when an object is subjected to external flow, and the influence of each mode is determined by the coefficient of Gr_L/Re_L^2 (Merkin, 1977; Sparrow & Lee, 1976). Inertia forces (i.e. forced convection) are negligible and natural convection effect dominates when $Gr_L/Re_L^2 > 10$; and buoyancy forces (i.e. natural convection) are negligible and forced convection dominates when $Gr_L/Re_L^2 < 0.1$. Neither inertia nor buoyancy forces (i.e. natural and forced convection effects) are negligible when $0.1 < Gr_L/Re_L^2 < 10$, and the combination of both convections must be considered when $Gr_L/Re_L^2 \approx 1$. This scenario is referred to as *mixed convection*. However, the natural

convection effect in mixed convection is typically ignored due to much higher fluid velocities (i.e. higher forced convection effect). At higher velocities, the error of ignoring natural convection is negligible, but should be considered at low velocities (Incropera & DeWitt, 1985; Çengel & Ghajar, 2011).

In mixed convection, the natural convection may assist or resist forced convection, depending on the relative direction of buoyancy and inertia forces. The buoyant flow motion also depends on the object's orientations, i.e. horizontal, vertical or inclined. Mixed convection can be categorised in three scenarios (Figure 3.17b) (Incropera & DeWitt, 1985; Çengel & Ghajar, 2011):

- 1) Assisting flow: Buoyant and force motions are in the same direction, thus increasing the cooling performance, e.g. upward force flow.
- 2) Opposing flow: Buoyant motion is opposing force motion, thus reducing the cooling performance, e.g. downward force flow.
- 3) Transverse flow: Buoyant motion is perpendicular to force motion, thus increasing the cooling performance, e.g. side force flow.

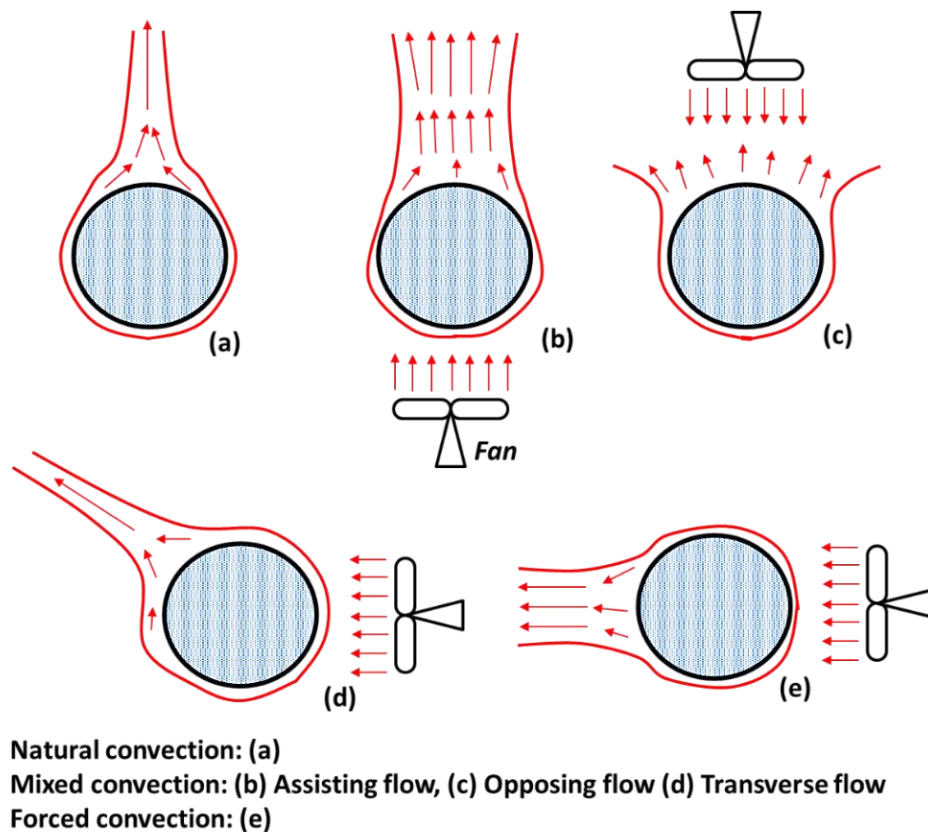


Figure 3.17 – Illustrated natural, forced and mixed convection flow scenarios near hot SMA wire, image based on (Incropera & DeWitt, 1985; Çengel & Ghajar, 2011)

The buoyancy effect can be seen clearly in laminar flow, but is difficult to distinguish in transitional flow and diminished in turbulence flow (Tam & Ghajar, 2006). For mixed convection, experimental data suggests a correlation as expressed in (Eq. 3.11) (Çengel & Ghajar, 2011), where Nu_{forced} and $Nu_{natural}$ are determined from their correlation equations, and n varies depending on the object alignment between 3 (vertical) and 4 (horizontal). The addition and subtraction signs (\pm) depend on whether both convections in the same (+) or opposite (-) directions.

$$Nu = (Nu_{forced}^n \pm Nu_{natural}^n)^{\frac{1}{n}} \quad (\text{Eq. 3.11})$$

Cooling duration

During SMA actuator cooling, thermal energy loss, E_{Loss} occurs through conduction, convection and radiation. However, radiation and conduction are negligible due to the low driving temperature difference and very small associated geometry (Bergman *et al.*, 2011; Çengel & Ghajar, 2011). Therefore, E_{Loss} can be derived from convection energy as derived in (Eq. 3.12), where h is the heat transfer coefficient; A_{sf} is the surface area; ΔT is the temperature difference between SMA actuator and ambient; and t_{cool} is the cooling duration (Bergman *et al.*, 2011; Çengel & Ghajar, 2011).

$$E_{Loss} = (h \cdot A_{sf} \cdot \Delta T) t_{cool} \quad (\text{Eq. 3.12})$$

Following the lumped capacitance model (Çengel & Ghajar, 2011), the cooling duration, t_{cool} , from object temperature, T_i , to ambient temperature, T_∞ , can be approximated with (Eq. 3.13), where m is the object mass and c is the specific heat capacity.

$$t_{cool} = -m \cdot \frac{c}{h \cdot A_{sf}} \cdot \ln\left(\frac{T_i}{T_\infty}\right) \quad (\text{Eq. 3.13})$$

However, relevant factors that affect the cooling duration, such as latent heat of transformation and induced stress are not included in (Eq. 3.13). Cooling duration estimation can be enhanced with models that include these factors, as described in Chapter 4.

3.7.3.2 Geometric shape optimisation

A critical factor in influencing SMA cooling behaviour is the contact surface. Cooling performance increases with increasing surface area-to-volume ratio (SA:V); therefore cooling performance (and thereby response time) can be enhanced by using high surface area-to-volume ratio geometries such as rectangular cross-sectional shapes, or by reducing the associated diagonal length (or diameter). Efficient cross-sectional shapes can readily increase cooling surface by 80% compared to a reference circular cross-section, while maintaining the same application strength (Reynaerts & Brussel, 1998).

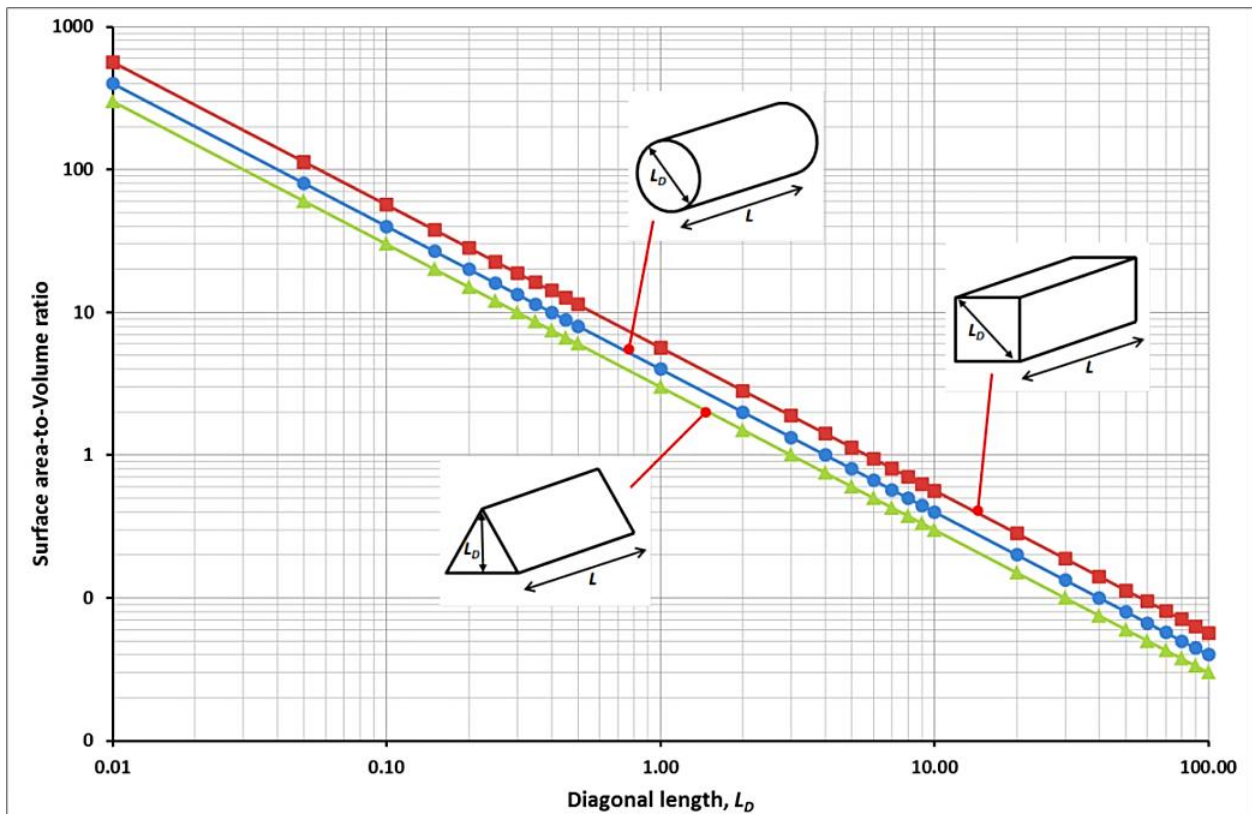
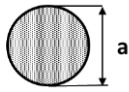
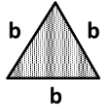
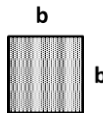
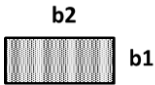
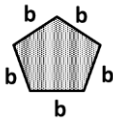
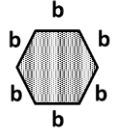


Figure 3.18 – Surface area-to-volume ratio versus diagonal length

The relationship between diagonal length of the geometry and SA:V is shown in Figure 3.18, and the comparison of the surface area-to-volume ratio of various shapes compared to the cylindrical form, while maintaining cross-sectional area (i.e. maintaining normal stress in the linear actuator, $\sigma = F/A$) is summarised in Table 3.6. SA:V decreases as the diagonal length increases, and substantial increases in surface area-to-volume ratio is achievable when the material is flattened (reduce thickness). This design approach has increased in popularity, by flat rolling SMMs or sputtering SMMs on thin films (S. Miyazaki & Ishida, 1999) for the fabrication of micro-actuators such as micro-valves, micro-switches, micro-pumps and micro-electromechanical systems (MEMS). As described in Section 2.6.3, SMA application frequency up to 100Hz is possible with this approach.

Table 3.6 - Surface area-to-volume ratio for various forms or shapes.

Shape	Illustrations	Dimension, b	Surface area	Surface area-to-volume ratio, SA:V	SA:V fraction of cylindrical form
Cylinder		-	πaL	$\frac{4}{a}$	100%
Triangle Prism		$a\sqrt{\frac{\pi\sqrt{3}}{3}}$	$3aL\sqrt{\frac{\pi\sqrt{3}}{3}}$	$\frac{12\sqrt{\frac{\pi\sqrt{3}}{3}}}{\pi a}$	129%
Square Prism		$\frac{a\sqrt{\pi}}{2}$	$2aL\sqrt{\pi}$	$\frac{8\sqrt{\pi}}{\pi a}$	113%
Rect. Prism		$b1 = \frac{a}{2}$ $b2 = \frac{a\pi}{2}$	$aL(\pi + 1)$	$\frac{4(\pi + 1)}{\pi a}$	132%
Pentagon Prism		$a\sqrt{\frac{\pi}{5(5 + 2\sqrt{5})}}$	$5aL\sqrt{\frac{\pi}{5(5 + 2\sqrt{5})}}$	$\frac{20}{\pi a}\sqrt{\frac{\pi}{5(5 + 2\sqrt{5})}}$	108%
Hexagon Prism		$\frac{a}{3}\sqrt{\frac{\pi\sqrt{3}}{2}}$	$2aL\sqrt{\frac{\pi\sqrt{3}}{2}}$	$\frac{8}{\pi a}\sqrt{\frac{\pi\sqrt{3}}{2}}$	105%
Cross-sectional area for all shapes, $A = \frac{\pi a^2}{4}$, and length, L .					

3.7.3.3 Heat sinks and lagged design

Heat sink is a passive cooling method to cool a device by absorbing heat from a device and dissipating them into the surrounding medium, or vice versa. The surrounding medium is usually air, but can also be a fluidic medium such as water, oil or gasses (e.g. refrigerants). The performance of heat sinks can be increased by maximising their surface area-to-volume ratio and the employment of active cooling methods such as heat pumps or fans (semi-active and active heat sinks), fluidic medium (liquid cooled cold plates) and heat pipes with two-phase system (phase change recirculating system) (Seri, 1995). Other factors affecting heat sink performance are choice of heat sink and medium materials, heat sink design, and surface treatment.

The selection of heat sink and associated media depends on the associated thermal diffusivity of materials (Prashant Reddy & Gupta, 2010); as well as geometric design parameters including fin geometry (length, thickness, spacing, number of fins, shape), and base plate thickness (Seri, 1995). One of most effective way of improving the SMA actuator speed (or bandwidth) is by immersing SMA actuators in fluidic or convective materials (refer Section 2.5.2) such as SMA lagged design (M. Leary, Schiavone, *et al.*, 2010; Martin Leary, Schiavone, Subic, & Miller, 2009). Response time enhancement by a factor of up to 100 is achievable with this method (Table 2.4), but requires consideration of a special design to prevent any leakage to the environment. Another crucial consideration with this cylindrical lagging design is the heat transfer performance of the designed system, in particular when dealing with continuous heating and cooling cycles of the SMA actuator. This transient heating performance for cylindrical system is reported in Chapter 5.

3.7.4 Optimisation with electronic controllers

As reported in Chapter 2, applications of electronic controllers are capable of resolving overstress and overheating problems, and enhance the accuracy and stability of SMA actuators in commercial applications. Generally, two types of electronic controllers are used:

- 1) Dynamic models: Application of mathematical models, thus requiring experimental parameters, complex calculation and high computation cost.
- 2) Closed loop feedback system: Application of sensors for a feedback signal of the control system. These controllers may perform well within the tuned control gains, but performance deteriorates dramatically once outside the standard range. May incur additional cost and size.

A summary of some of the electronic controllers utilised in SMA applications are listed in Table 3.7.

Table 3.7 - SMA application optimisation with electronic devices

Optimisation	Method	References
Stability and accurate positioning	PWM and dynamic models	(Katsutoshi Kuribayashi, 1986)
	Temperature sensor feedback	(Katsutoshi Kuribayashi, 1991)
	Electrical resistance feedback	(Ikuta <i>et al.</i> , 1988; N. Ma, Song, & Lee, 2004)
	Dynamic model: Limit curve	(Bergamasco <i>et al.</i> , 1990)
	Dynamic models: LQR and H ₂ technique	(CJ Lee & Mavroidis, 2002)
	Dynamic model: H _∞ loop shaping	(Jayender, Patel, Nikumb, & Ostojic, 2005)
	Self-tuning Fuzzy-PID controller	(Kha & Kyoung Kwan, 2006)
	Fuzzy PWM-PID and dynamic models	(Ko, Jun, Gilardi, Haslam, & Park, 2011)
	Dynamic model: Adaptive resetting	(Sven Langbein & Czechowicz, 2012)
	Inductance feedback	(Hongjip, Yongsu, Dae-young, Jung-Ik, & Kyu-Jin, 2013)
Temperature control or overheating protection	Thermoelectric device (TED) and dynamic models	(Odhner & Asada, 2006)
Energy consumption	Pulse width modulation (PWM)	(N Ma & Song, 2003)
Bandwidth	PID and dynamic models	(Gorbet <i>et al.</i> , 2009)

Due to the enhancement of electronic system technology, a combination of both the dynamic model and the closed loop feedback is viable in a single electronic controller. Therefore, the SMA application performances are further enhanced and optimised.

3.8 Discussions and conclusions

The technical challenges to SMA actuator design discussed above must be accommodated and addressed with an appropriate design development process in order to achieve a commercially successful SMA actuator design. In general, there exist three primary factors associated with SMA actuator design: load, displacement and speed. Satisfaction of these potentially conflicting factors typically informed compromise during the design process.

Two categories of SMA actuator motion identified are linear (prismatic) and revolute (rotary). The material selection of SMA actuator is determined by its operational temperatures and functional requirements (e.g. design type, actuation speed and stress applied), which influences required transformation temperatures, hysteresis and maximum allowable stress. Loading configurations (tension, torsion or bending), SMA shapes or forms and design types (one-directional, bias-force or antagonist) also critically affect the performance of SMA applications.

Poor bandwidth (low actuation speed) is one of the main reasons for the commercialisation failure of SMA applications, in particular due to slow SMA cooling performance. The optimisation of cooling performance of SMA linear actuator can be divided into two categories: i.e. passive and active optimisation approaches. Optimisation of passive SMA cooling can be achieved, for example, with geometric shape improvement towards higher surface area-to-volume ratio (SA:V), application of suitable electronic controllers, and enhanced transient thermal response (as developed in Chapter 5 of this work). The active optimisation approach is feasible with forced convection (for cooling), active thermal system (e.g. TEC) or materials (conductive substances or fluids). Recently, (Lara-Quintanilla & Bersee, 2015) revealed that cooling times increase significantly as the strain-ratio increases; where the highest frequencies are reached when the SMA is actuated in the middle- to low-strain-range.

Although numerous studies have been conducted on SMA applications, there exists a lack of formal guidelines, predictive models and design tools for the effective design of SMA actuators (Mohd Jani, Leary, Subic, *et al.*, 2014). The use of a formal systematic SMA design process is recommended, to reduce the risk of failing to understand the associated design requirements (e.g. power, displacement and speed), specifications (e.g. SMA response and form, design type, heating and cooling methods), and modelling, testing and optimisation methods available (Figure 3.1).

In order to assist in the commercialisation of SMA actuators, this work provides novel enhancements to the existing literature and design capabilities associated with:

- Numerical models of SMA response (Chapter 4 and 6)
- Transient thermal response of axisymmetric systems, such as linear SMA actuators (Chapter 5)
- Design capability associated with structural and functional fatigue of linear SMA actuators integrated with pulley systems (Chapter 7)

4. Numerical modelling of SMA linear actuators

The outcomes of this chapter have contributed to the following peer reviewed publications:

- *Numerical modeling of Shape Memory Alloy linear actuator*, J Mohd Jani, S Huang, M Leary, A Subic, Computational Mechanics 53(3), 443-461, 2015.
- *The critical and crossover radii on transient heating*, S Huang, J Mohd Jani, M Leary, A Subic, Applied Thermal Engineering 60(1), 325-334, 2013.

4.1 Chapter summary

The accurate prediction SMA actuator temperature profiles is critically important to: minimising the risk of application failure and damage due to overheating; as well as to enable optimisation of stroke and bandwidth performance. Robust, readily applied and computationally efficient SMA numerical modelling capability enables faster and more accurate SMA design predictions; thereby reducing application development cost and design time. Numerous approaches have been developed for the thermomechanical modelling of SMA linear actuators, either as one-dimensional (1D) or multi-dimensional models with various methods, such as analytical models, finite difference method (FDM), finite element method (FEM) and finite volume method (FVM). A summary of fundamental modelling theories, methods and models are reported in this chapter. A comprehensive review of finite difference equations and constitutive models are highlighted in this chapter, due to their importance for the application and development of novel numerical modelling contributions of this thesis as described in Chapters 5 and 6.

4.2 Introduction

The thermomechanical behaviour of NiTi SMA is affected by the temperature and the associated metallurgical phase, namely martensite at low temperatures and austenite at high temperatures. The SMA property that describes the shape recovery characteristic associated with the temperature changes is known as the shape memory effect (SME). The influence of environmental (e.g. ambient temperatures and air flow) and mechanical conditions (e.g. pre-stressed with bias spring or dead weight) are critical to effective SMA performance (Mohd Jani *et al.*, 2015a). This is especially true for applications with restrictive thermal circulation or extreme operating temperatures, where the application may display poor response frequency (M. Leary, Schiavone, *et al.*, 2010; Tadesse *et al.*, 2010), premature or excessive actuation (M. Leary *et al.*, 2013), or failure to recover acceptable strain for the required duty-cycle (Tadesse *et al.*, 2010).

To enable commercial application of SMA actuators it is critical to predict the thermal and mechanical response of SMA when heated with Joule heating and cooled by natural or forced convection within the operating environment. Analytical models for commercial SMA design are available to solve the mathematical equations of heat transfer problems. However, analytical models are limited to relatively simple geometries and boundary conditions; therefore, numerical methods are typically required. Numerous computational methods and numerical models are available to predict the thermomechanical behaviour of SMA; these are summarised in this chapter, including theoretical basis, strengths and limitations.

4.3 SMA linear actuators numerical modelling

Numerous analytical and numerical models have been proposed to predict and optimize SMA thermomechanical behaviour (Achenbach, 1989; Boyd & Lagoudas, 1996; S. Huang *et al.*, 2013; DC Lagoudas, 2010; Majumdar, 2005; Çengel & Ghajar, 2011). The design optimisation process with numerical modelling is illustrated in Figure 4.1.

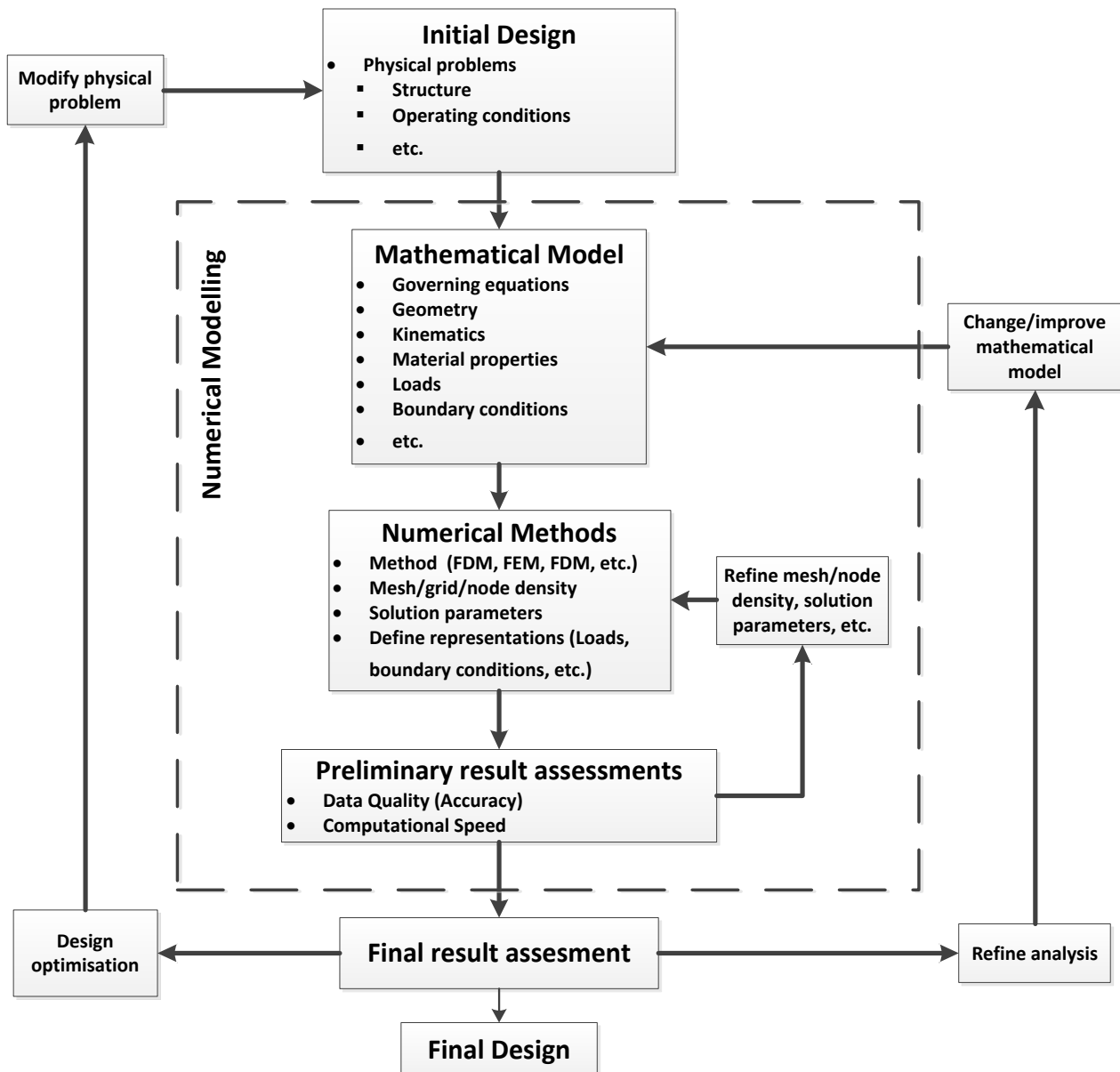


Figure 4.1 - Design optimisation process with numerical modelling, modified from (Bathe, 2006)

In initial design process, the physical problems for SMA linear actuator are identified such as the size, operating conditions (environmental conditions, design type, pre-stress value, heating and cooling modes) and design structure. For numerical modelling, the mathematical model and numerical method to be used is decided. The outcomes from the chosen mathematical model and numerical method are accessed and refined until an optimised balance between data quality and computational speed are achieved. The results from numerical modelling are further assessed and refined until a suitable mathematical model is determined for the chosen numerical method. The SMA linear actuator design is further optimised until a final design is decided.

4.3.1 One and multi-dimensional models

Multi-dimensional models are useful in solving complex problems of greater generality, while one-dimensional (1-D) numerical models are restricted in terms of boundary conditions and allowable geometry (Bonacina, Comini, Fasano, & Primicerio, 1973). Despite these limitations, 1-D models are appropriate for solving SMA linear actuator problems, and enable low computational overheads due to the mathematical simplicity of the 1-D formulation.

4.3.2 Heat transfer mathematical models

Numerous approaches have been developed for modelling SMA linear actuator heat transfer, including phenomenological, Preisach, and energy (or power) balance models (Ahn & Kha, 2008; Brinson, 1993; DC Lagoudas, 2010; Neugebauer *et al.*, 2010b). The fundamental theories of heat transfer such as heat transfer modes and Biot number are applied for all approaches.

4.3.2.1 Heat transfer modes

A temperature gradient within a media results in heat transfer by the mechanisms of conduction, convection and radiation (Bergman *et al.*, 2011). In this work, the driving temperature difference will be sufficiently low such that the effect of radiation will be ignored and heat transfer will be assumed to occur by the modes of convection and conduction.

Conduction occurs by molecular vibration from more energetic particles to less energetic particles in the absence of bulk matter transfer (Çengel & Ghajar, 2011). Fourier's Law defines the rate of heat conduction, q_{cond} , as a function of the associated area, A , thermal conductivity, k , and temperature gradient, ∇T (Eq. 4.1).

$$q_{cond} = kA\nabla T \quad (\text{Eq. 4.1})$$

The heat flux is defined as the heat transfer rate per unit area:

$$q' = \frac{q}{A} \quad (\text{Eq. 4.2})$$

Convection occurs due to the combined effects of advection and diffusion due to fluid motion as expressed by Newton's law of cooling (Eq. 4.3), where the associated heat transfer rate, q_{conv} , is a function of the convective heat transfer coefficient, h , associated area, A , and the temperature difference between the surface temperature, T_s , and ambient temperature, T_∞ (Çengel & Ghajar, 2011).

$$q_{conv} = hA(T_s - T_\infty) \quad (\text{Eq. 4.3})$$

The resistance to heat transfer is defined as the ratio of the driving potential to the resulting transfer rate (Eq. 4.4).

$$R = \frac{\Delta T}{q} \quad (\text{Eq. 4.4})$$

4.3.2.2 Biot number

In a conduction problem involving surface convection effects, the Biot number, Bi , is defined as the ratio of resistance of convection across the fluid boundary to the conduction resistance within the solid body (Eq. 4.5). The Biot number provides an indication of the temperature difference within the solid body compared to the temperature difference between the solid surface and the surrounding fluid. For $Bi \ll 1$, the conduction resistance within the body is much less than the resistance to convection across the fluid boundary, and the assumption of constant temperature within the body is reasonable. Especially for $Bi < 0.1$, the error of this assumption is less than 5% (Das, 2010; Holman, 2009). For systems where constant temperature cannot be presumed, it is necessary to accommodate variation in temperature within the solid body, where L_C is the characteristic length of the body, defined as the ratio of solid volume to surface area (Bejan, 1993; Bergman *et al.*, 2011; Das, 2010; Holman, 2009).

$$Bi = \frac{hL_c}{k} \quad (\text{Eq. 4.5})$$

For a long cylinder or sphere, L_C is defined as $r/2$ and $r/3$, respectively. However, a conservative consideration, applied in this work, defines L_C as the actual radius of the cylinder or sphere (Bergman *et al.*, 2011; Das, 2010). When considering the insulation of a cylinder, Biot number is defined as (Branco, Pinho, & Figueiredo, 2001):

$$Bi = \frac{hr_{cyl}}{k_{therm}} \quad (\text{Eq. 4.6})$$

4.3.2.3 Analytical lumped capacitance model

The lumped capacitance model is common for SMA linear actuator heat transfer modelling. However, it is only applicable when the SMA wire is of sufficiently small diameter, such that the associated internal thermal gradient is negligibly small, i.e. for Biot number, $Bi < 0.1$ (V. Brailovski, Trochu, & Daigneault, 1996; Incropera & DeWitt, 1985; Tadesse *et al.*, 2010; Velázquez & Pissaloux, 2012). Ignoring latent heat effects, the lumped capacitance model is expressed as in (Eq. 4.7) and (Eq. 4.8) for heating and cooling cycles respectively (Tadesse *et al.*, 2010; Çengel & Ghajar, 2011).

$$T_{t(heat)} = T_{\infty} + \frac{I^2 \cdot R_{tot}}{h \cdot A_{sf}} (1 - e^{-\lambda t}) \quad (\text{Eq. 4.7})$$

$$T_{t(cool)} = T_{\infty} + (T_W - T_{\infty}) e^{-\lambda t} \quad (\text{Eq. 4.8})$$

$$\lambda = \frac{h \cdot A_{sf}}{\rho_D \cdot V \cdot c} = \frac{4 \cdot h}{\rho_D \cdot c \cdot D_{SMA}} \quad (\text{Eq. 4.9})$$

Alternative numerical analysis methods such as finite difference method and finite element method maybe required when the lumped capacity model is invalid, for example with rapid resistive heating of current density higher than 100 A/mm² (V. Brailovski *et al.*, 1996).

4.3.3 Stress-strain constitutive models

Constitutive models of SMA system behaviour can be divided into two groups: micro-mechanical models and macro-mechanical (or phenomenological) models. Micro-mechanical models are based on bridging the behaviour of SMA microstructure (i.e. crystallographic transformation) to its overall stress-strain behaviour, while phenomenological models are based on thermodynamic and kinetics models. Micro-mechanical models adopt a fundamental approach and are therefore desirable due to their potentially higher accuracy. However, phenomenological models are often preferred for numerical modelling due to their compatibility with standard engineering material constants and lower complexity to apply for engineering design. In this study, phenomenological approaches are selected and discussed in detail.

4.3.3.1 Phenomenological constitutive model

The earliest SMA phenomenological model is based on kinetics equations to describe the phase transformation volume fraction as an exponential function was developed by (K. Tanaka, 1986), and further developed by (Liang & Rogers, 1997) with the cosine function (refer Section 4.3.4).

Later, (Brinson, 1993) modified Liang and Rogers's constitutive model by separating the martensitic phase fraction into stress-induced and temperature-induced components, allowing SME to be predicted at a lower range of temperature (i.e. below M_s) for twinned and detwinned martensite transformations (Figure 4.2). (Elahinia & Ahmadian, 2005) enhanced these constitutive models to predict the SMA behaviour under simultaneous change of temperature and stress loadings, such as in rotatory SMA actuators. De La Flor *et al.* (De la Flor, Urbina, & Ferrando, 2006) further improved the constitutive model based on Brinson's constitutive equation (Bekker & Brinson, 1998) and Auricchio's linear laws (1997) which can predict the SMA behaviour more accurately for wider range of temperatures and loading conditions.

Variation of transformation temperatures with stress are shown in Figure 4.2 for the constitutive models of Tanaka (1986), Liang and Roger (1997), Brinson (1993), Aurichio and Lubliner (1997), and De La Flor *et al.* (2006). The stress-influence coefficients (C_A , C_M and C_{MS}), transformation temperatures (A_s , A_f , M_s and M_f), and the critical stresses of martensite (start, σ_{cr}^s and finish, σ_{cr}^f) can be experimentally determined. Comparison between (Liang & Rogers, 1997), (Brinson, 1993) and (Elahinia & Ahmadian, 2005) phase transformation conditions is summarised in Table 4.1.

The general phenomenological constitutive equation can be expressed as (Eq. 4.10) (Liang & Rogers, 1997), where σ is the recovery stress, ε is the recovery strain, E is the elastic modulus, θ_T is the thermoelastic tensor, and Ω is the transformation tensor. E , θ_T , and Ω can be experimentally determined (Figure 4.3) (De la Flor *et al.*, 2006; Liang & Rogers, 1997).

$$(\sigma - \sigma_0) = E(\xi)(\varepsilon - \varepsilon_0) + \theta_T(T_W - T_0) + \Omega(\xi)(\xi - \xi_0) \quad (\text{Eq. 4.10})$$

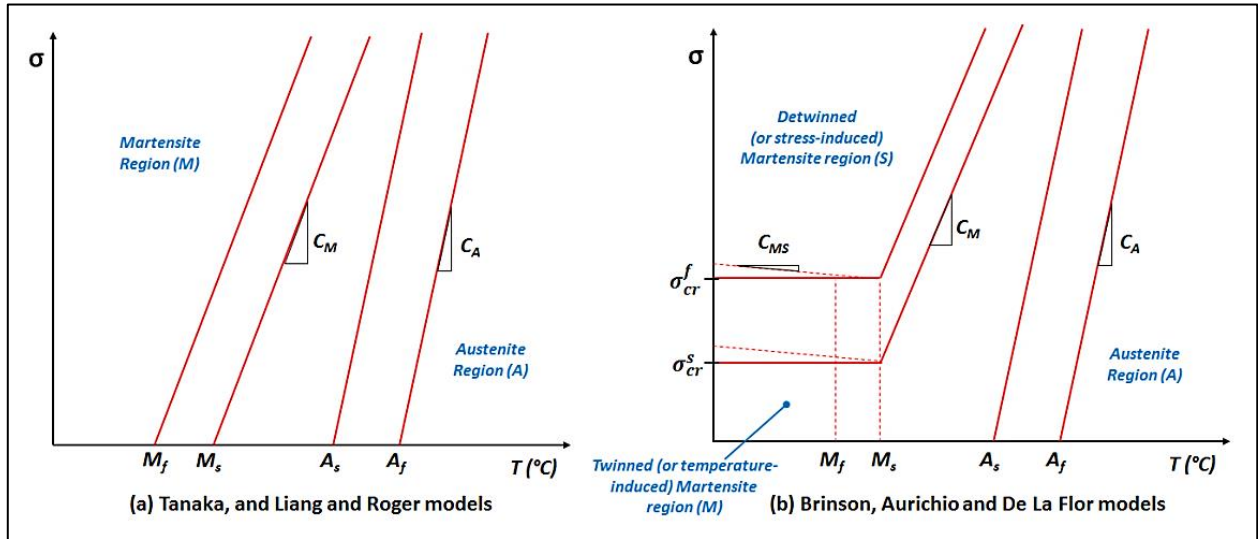


Figure 4.2 - Typical stress-temperature profile for constitutive models (Auricchio & Lubliner, 1997; Brinson, 1993; De la Flor *et al.*, 2006; Liang & Rogers, 1997; K. Tanaka, 1986)

Table 4.1 – Comparison of phase transformation conditions, modified from (Elahinia & Ahmadian, 2005)

Author	Heating cycle			Cooling cycle		
	Martensite	Martensite-Austenite	Austenite	Austenite	Austenite-Martensite	Martensite
Liang & Roger (1990)	$\dot{T} > 0$			$\dot{T} < 0$		
	$T < A_s + \frac{\sigma}{C_A}$	$A_f + \frac{\sigma}{C_A} > T \geq A_s + \frac{\sigma}{C_A}$	$T \geq A_f + \frac{\sigma}{C_A}$	$T > M_s + \frac{\sigma}{C_M}$	$M_s + \frac{\sigma}{C_M} \geq T > M_f + \frac{\sigma}{C_M}$	$T \leq M_f + \frac{\sigma}{C_M}$
Brinson (1993)	$\dot{\sigma} < 0$			$\dot{\sigma} > 0$		
	$\sigma > C_A(T - A_s)$	$C_A(T - A_s) \geq \sigma > C_A(T - A_f)$	$\sigma \leq C_A(T - A_f)$	$\sigma < C_M(T - M_s)$	$C_M(T - M_f) \geq \sigma \geq C_M(T - M_s)$	$\sigma \geq C_M(T - M_f)$
Elahinia & Ahmadian (2005)	$\dot{T} - \frac{\dot{\sigma}}{C_A} > 0$			$\dot{T} - \frac{\dot{\sigma}}{C_A} < 0$		
	$T < A_s + \frac{\sigma}{C_A}$	$A_f + \frac{\sigma}{C_A} > T \geq A_s + \frac{\sigma}{C_A}$	$T \geq A_f + \frac{\sigma}{C_A}$	$T > M_s + \frac{\sigma}{C_A}$	$M_s + \frac{\sigma}{C_A} \geq T > M_f + \frac{\sigma}{C_A}$	$T \leq M_f + \frac{\sigma}{C_A}$

The modulus of elasticity as a function of martensite volume fraction, $E(\xi)$, and the phase transformation coefficient, $\Omega(\xi)$, can be expressed as in (Eq. 4.11) and (Eq. 4.12) respectively, where ξ is the martensite volume fraction, E_A and E_M are the elastic modulus in austenite and martensite state respectively, and ε_L is the maximum recoverable strain.

$$E(\xi) = E_A + \xi(E_M - E_A) \quad (\text{Eq. 4.11})$$

$$\Omega(\xi) = -\varepsilon_L E(\xi) = -\varepsilon_L [E_A + \xi(E_M - E_A)] \quad (\text{Eq. 4.12})$$

As reported in Section 2.7 and 3.6, SMA applications are divided into four categories of primary functions and three categories of basic designs. For one-directional actuator design, the actuators are divided into free recovery and constrained recovery, while for the bias-force actuators, the actuators are divided into deadweight and bias-spring. The constitutive equation for SMA linear actuator with deadweight and bias-spring systems can be expressed as (Eq. 4.13) and (Eq. 4.14) (Liang & Rogers, 1997), respectively, where A is the SMA cross-sectional area, S is the spring constant, and L is the SMA length. Refer to Appendix H for the authors Matlab code to implement the Liang and Roger constitutive model.

$$(\sigma - \sigma_0) = [E_A + \xi(E_M - E_A)](\varepsilon - \varepsilon_0) + \theta_T(T_W - T_0) + \Omega(\xi)(\xi - \xi_0) \quad (\text{Eq. 4.13})$$

$$\left(1 + A \frac{E(\xi)}{S \cdot L}\right)(\sigma - \sigma_0) = \theta_T(T_W - T_0) + \Omega(\xi)(\xi - \xi_0) \quad (\text{Eq. 4.14})$$

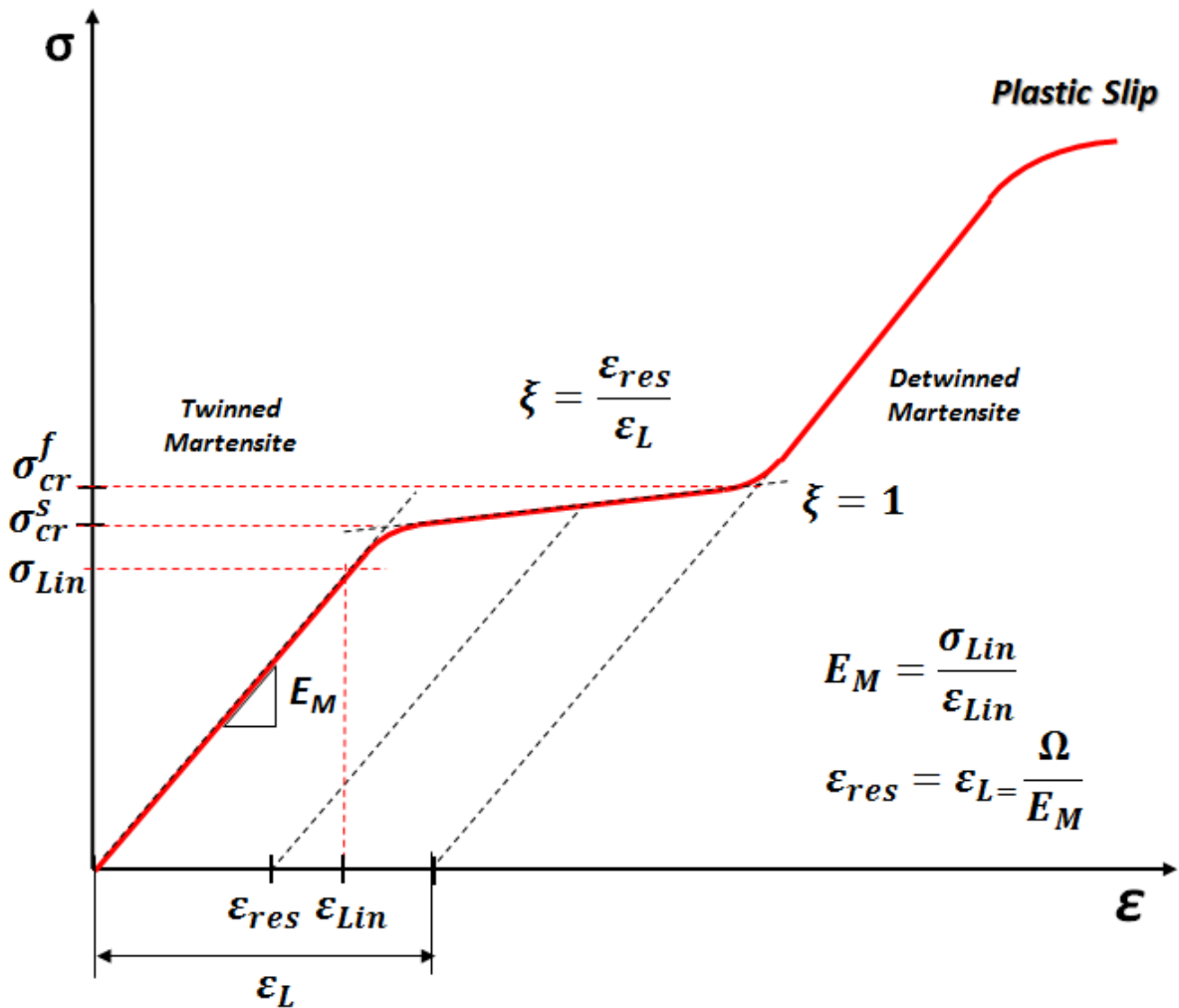


Figure 4.3 - Typical SMA stress-strain relationship indicating Young's Modulus (E), critical stresses (σ_{cr}), martensitic residual strain (ε_{res}) and maximum recoverable strain (ε_L) (De la Flor *et al.*, 2006; Liang & Rogers, 1997).

Therefore the stress and strain for SMA systems (deadweight and bias-spring) can be derived from (Eq. 4.15) and (Eq. 4.16) respectively (Liang & Rogers, 1997).

$$\sigma = \underbrace{\sigma_0 + [E_A + \xi(E_M - E_A)](\varepsilon - \varepsilon_0) + \theta_T(T_W - T_0) + [-\varepsilon_L E(\xi)](\xi - \xi_0)}_{\text{Deadweight}} + \underbrace{\frac{\theta_T(T_W - T_0) + \Omega(\xi)(\xi - \xi_0)}{\left(1 + A \frac{E(\xi)}{S.L}\right)}}_{\text{Bias-spring}} \quad (\text{Eq. 4.15})$$

$$\varepsilon = \underbrace{\frac{\sigma - \sigma_0}{E(\xi)}}_{\text{Deadweight}} = \underbrace{\frac{\sigma - \sigma_0}{\frac{S.L}{A}}}_{\text{Bias-spring}} \quad (\text{Eq. 4.16})$$

New transformation temperatures and stresses

A dimensionless constant, K , is introduced to fulfil both deadweight and bias-spring systems, where $K=1$ for deadweight system and as derived in (Eq. 4.17) for bias-spring system (Liang & Rogers, 1997).

$$K = 1 + \left(\frac{AE(\xi)}{S.L}\right) \quad (\text{Eq. 4.17})$$

Applying Liang and Roger constitutive model (1997), the new transformation temperatures and stresses are calculated with (Eq. 4.18) to (Eq. 4.25).

$$A_{S(new)} = \frac{A_s \cdot C_{As} - \frac{\theta_M}{K_M} T_\infty + \sigma_{Pre-Stress}}{C_{As} - \frac{\theta_M}{K_M}} \quad (\text{Eq. 4.18})$$

$$\sigma_{As(new)} = \frac{\theta_M}{K_M} (A_{S(new)} - M_f) + \sigma_{Pre-Stress} \quad (\text{Eq. 4.19})$$

$$A_{f(new)} = \frac{A_f \cdot C_{Af} - \frac{\theta_A}{K_A} A_{S(new)} - \frac{\Omega_A}{K_A} + \sigma_{As(new)}}{C_{Af} - \frac{\theta_A}{K_A}} \quad (\text{Eq. 4.20})$$

$$\sigma_{Af(new)} = \frac{\theta_A}{K_A} (A_{f(new)} - A_{s(new)}) - \frac{\Omega_A}{K_A} + \sigma_{As(new)} \quad (\text{Eq. 4.21})$$

$$M_{S(new)} = \frac{M_S \cdot C_{Ms} - \frac{\theta_A}{K_A} A_{f(new)} + \sigma_{Af(new)}}{C_{Ms} - \frac{\theta_A}{K_A}} \quad (\text{Eq. 4.22})$$

$$\sigma_{Ms(new)} = \frac{\theta_A}{K_A} (M_{s(new)} - A_{f(new)}) + \sigma_{Af(new)} \quad (\text{Eq. 4.23})$$

$$M_{f(new)} = \frac{M_f \cdot C_{Mf} - \frac{\theta_M}{K_M} M_{S(new)} + \frac{\Omega_M}{K_M} + \sigma_{Ms(new)}}{C_{Mf} - \frac{\theta_M}{K_M}} \quad (\text{Eq. 4.24})$$

$$\sigma_{Mf(new)} = \frac{\theta_M}{K_M} (M_{f(new)} - M_f) + \frac{\Omega_M}{K_M} + \sigma_{Ms(new)} \quad (\text{Eq. 4.25})$$

4.3.4 Hysteresis model and phase fractions

Hysteresis (see Figure 4.4) is commonly applied in constitutive models to describe the dynamic behaviour of shape memory alloys, based on the martensite volume fraction (ξ_M) and associated transition temperatures (i.e. A_s , A_f , M_s and M_f).

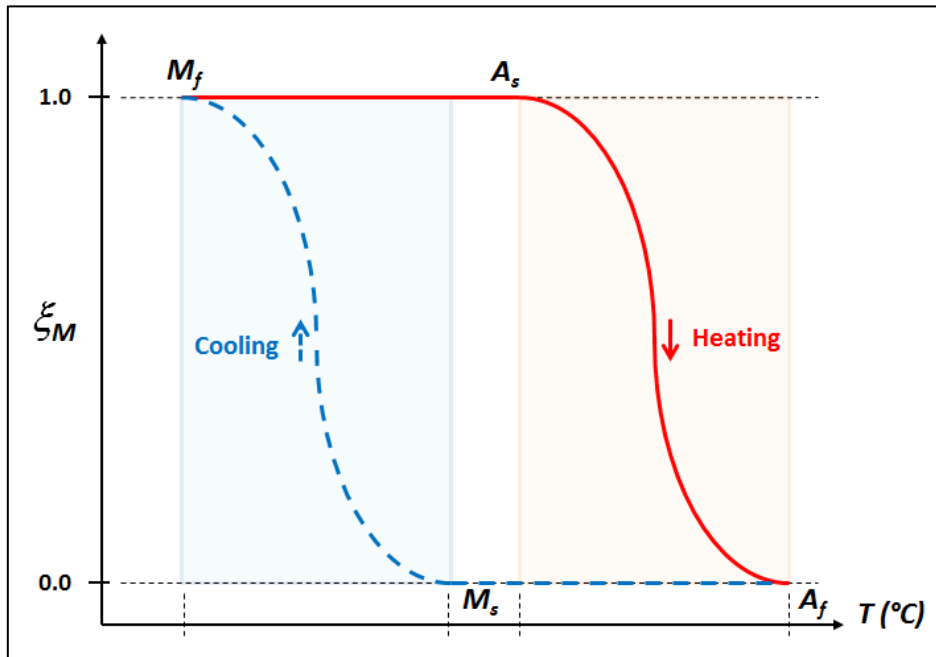


Figure 4.4 - SMA hysteresis model, based on (Bekker & Brinson, 1998; Liang & Rogers, 1997)

The martensitic volume fraction, ξ_M , accommodates the effect of phase dependent material properties, such as resistivity (see (Eq. 6.4)), thermal conductivity and Young's modulus. Martensitic volume fraction can be obtained empirically, or predicted with hysteresis models of SMA as a function of temperature (Figure 4.4). During the phase transition, the martensite volume fraction for stress-induced conditions can be expressed by cosine function (Eq. 4.26)(Brinson, 1993; Elahinia & Ahmadian, 2005; Liang & Rogers, 1997), or with an exponential function as reported by Tanaka (Eq. 4.27) (1986).

$$\xi = \underbrace{\frac{\xi_M}{2} \left[\cos \left(\pi \frac{(T_w - A_s - \frac{\sigma}{C_A})}{(A_f - A_s)} \right) + 1 \right]}_{\text{Heating cycle}} \quad (Eq. 4.26)$$

$$= \underbrace{\frac{1 - \xi_A}{2} \left[\cos \left(\pi \frac{(T_w - M_f - \frac{\sigma}{C_M})}{(M_s - M_f)} \right) \right]}_{\text{Cooling cycle}} + \frac{1 + \xi_A}{2}$$

$$\xi = \underbrace{\xi_M \exp \left[\left(\frac{\ln(100 \cdot \xi_M)}{C_A(A_f - A_s)} \right) (C_A(A_s - T_w) + \sigma) \right]}_{\text{Heating cycle}} \quad (Eq. 4.27)$$

$$= \underbrace{(1 - \xi_A) \exp \left[\left(\frac{\ln(100 \cdot \xi_A)}{C_M(M_f - M_s)} \right) (C_M(M_s - T_w) + \sigma) \right]}_{\text{Cooling cycle}}$$

4.4 Numerical methods

The development of modern numerical modelling commenced with the rise of the digital computer in the early 1950s. The common numerical methods are finite difference method (FDM), finite element method (FEM) or finite volume method (FVM), where FDM is the oldest between these three methods.

4.4.1 Finite difference method

FDM probably originated from Newton, Leibniz and the Bernoulli brothers in 1600s, improved by Euler and Clairaut in 1700s with their variational calculus and implicit differential equations respectively; further refined by Cauchy in 1824 with his convergence theorem, and become established after the fundamental theories behind finite differences was published by Courant, Friedrichs and Lewy in 1928 (Hairer, Nørsett, & Wanner, 1993).

For solving heat transfer problems, FDM is based on the differential equation of heat conduction, which is transformed into a difference equation to calculate the temperature values at the nodes within the geometry (N. Ozisik, 1994). The mathematical modelling of FDM starts with consideration of conservation equation in differential form by approximation and replacing the partial derivate in nodal values forms resulting in one algebraic equation per grid node (Sarbu & Popina, 2001). FDM is the most readily applied of the numerical methods considered here. However, FDM is restricted to simple geometries (i.e. structured grids) and does not enforce conservation laws (e.g. conservation of momentum, energy or mass) in its procedure (Forsythe & Wasow, 1960; Richtmyer & Morton, 1994; GD Smith, 1985).

4.4.1.1 FDM equations

The finite difference method (FDM) provides an opportunity to approximate a continuous function by point-wise discretization. The associated finite difference equations (FDEs) are typically derived by the Taylor series method for a two-variable function $u(x, y)$ (Crank & Nicolson, 1947; Majumdar, 2005; N. Ozisik, 1994). The transient heat conduction equation for 1-D solid cylindrical system with heat generation can be expressed in polar coordinates, where $\alpha = \frac{k}{\rho_D c}$ is the thermal diffusivity (Eq. 4.28) (Majumdar, 2005; N. Ozisik, 1994).

$$\frac{1}{\alpha} \frac{\partial T(r, t)}{\partial t} = \frac{1}{r} \frac{\partial T(r, t)}{\partial r} + \frac{\partial^2 T(r, t)}{\partial r^2} \quad (\text{Eq. 4.28})$$

In FDE, the solid object is divided into a discrete array of nodes with specific boundary conditions, and this allows prediction of the associated temperatures for specific material properties. When subjected to constant boundary conditions, the temperature field will stabilize to the steady-state condition, resulting in a closed-form steady-state solution (Bergman *et al.*, 2011).

The Taylor series can be rearranged to represent the forward, backward, and central difference equations for the first and second derivatives into two groups of known and unknown temperature nodes (Crank & Nicolson, 1947; Majumdar, 2005; N. Ozisik, 1994). Therefore, temperatures at known nodes can be used to predict the temperature at unknown nodes, which is simplified as the Fourier number, $F_o = \frac{\alpha \Delta t}{\Delta r^2}$.

4.4.1.2 Forward (explicit) FDE model

The forward difference equation is used to predict the unknown nodal temperature (T^{t+1}_n) from known nodal temperatures (T^t) (Figure 4.5). The Taylor series for forward difference equation is represented and rearranged into two groups of known and unknown temperature nodes (Eq. 4.30).

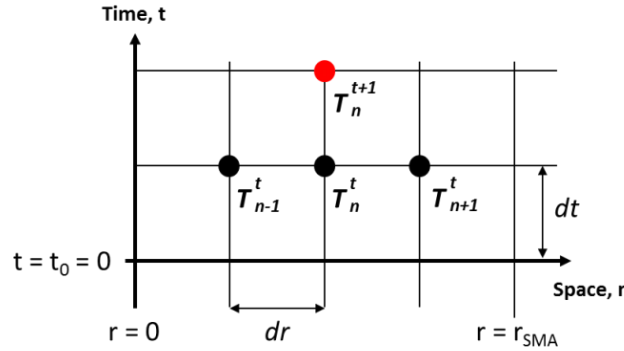


Figure 4.5 - Forward difference equation. Subscript n represent the space increments, superscript t represents time increments (red are the unknown temperature nodes) (Mohd Jani *et al.*, 2015b)

$$\frac{T_n^{t+1} - T_n^t}{\alpha \cdot \Delta t} = \frac{T_{n+1}^t - 2T_n^t + T_{n-1}^t}{(\Delta r)^2} \quad (\text{Eq. 4.29})$$

$$\underbrace{T_n^{t+1}}_{\text{Unknown nodes}} = \underbrace{Fo \cdot T_{n+1}^t + (1 - 2Fo)T_n^t + Fo \cdot T_{n-1}^t}_{\text{Known nodes}} \quad (\text{Eq. 4.30})$$

4.4.1.3 Backward (implicit) FDE model

The backward difference equation is used to predict the unknown nodal temperatures (T^{t+1}_n) from known nodal temperature (T^t_n) (Figure 4.6). The Taylor series for forward difference equation is represented and rearranged into two groups of known and unknown temperature nodes as in (Eq. 4.32).

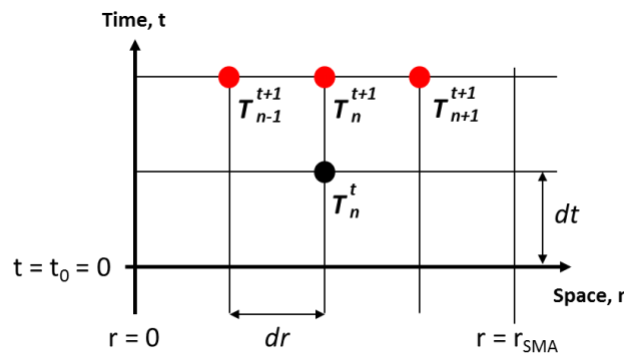


Figure 4.6 - Backward difference equation. Subscript n represent the space increments, superscript t represents time increments (red are the unknown temperature nodes) (Mohd Jani *et al.*, 2015b)

$$\frac{T_n^{t+1} - T_n^t}{\alpha \cdot \Delta t} = \frac{T_{n+1}^{t+1} - 2T_n^{t+1} + T_{n-1}^{t+1}}{(\Delta r)^2} \quad (\text{Eq. 4.31})$$

$$\underbrace{-Fo \cdot T_{n+1}^{t+1} + (1 + 2Fo)T_n^{t+1} - FoT_{n-1}^{t+1}}_{\text{Unknown nodes}} = \underbrace{T_n^t}_{\text{Known nodes}} \quad (\text{Eq. 4.32})$$

4.4.1.4 Central (Crank-Nicholson) FDE model

The Central difference equation is used to predict the unknown nodal temperatures (T^{t+1}) from known nodal temperatures (T^t) (Figure 4.7). The Taylor series for forward difference equation is represented and rearranged into two groups of known and unknown temperature nodes as in (Eq. 4.34).

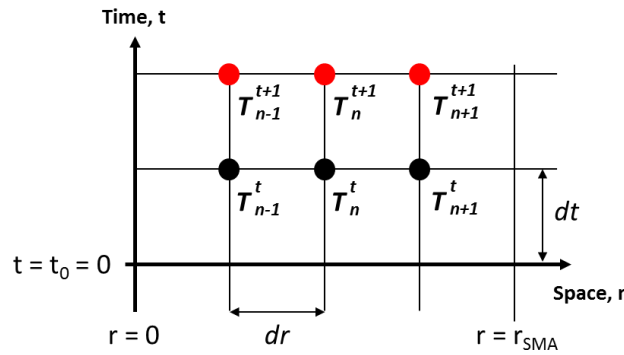


Figure 4.7 - Central difference equation. Subscript n represent the space increments, superscript t represents time increments (red are the unknown temperature nodes) (Mohd Jani *et al.*, 2015b)

$$\frac{T_n^{t+1} - T_n^t}{\alpha \cdot \Delta t} = \underbrace{\frac{T_{n+1}^t - 2T_n^t + T_{n-1}^t}{2(\Delta r)^2}}_{\text{explicit}} + \underbrace{\frac{T_{n+1}^{t+1} - 2T_n^{t+1} + T_{n-1}^{t+1}}{2(\Delta r)^2}}_{\text{implicit}} \quad (\text{Eq. 4.33})$$

$$\underbrace{-\frac{Fo}{2}T_{n+1}^{t+1} + (1 + Fo)T_n^{t+1} - \frac{Fo}{2}T_{n-1}^{t+1}}_{\text{Unknown nodes}} = \underbrace{\frac{Fo}{2}T_{n+1}^t + (1 - Fo)T_n^t + \frac{Fo}{2}T_{n-1}^t}_{\text{Known nodes}} \quad (\text{Eq. 4.34})$$

4.4.1.5 Matrix form of FDE models

The unknown nodal temperatures are calculated from the known nodal temperatures directly (for forward FDE) or by the matrix inversion technique (for backward and centre FDEs) (Crank & Nicolson, 1947; Majumdar, 2005; N. Ozisik, 1994) (Figure 4.8). The node coefficients for each FDE model are summarized in Table 4.2.

$$\underbrace{\begin{bmatrix} b_1 & c_1 & 0 & 0 & \dots & \dots & 0 \\ a_1 & b_2 & c_2 & 0 & \dots & \dots & 0 \\ 0 & a_2 & b_3 & c_3 & 0 & \dots & 0 \\ 0 & 0 & \ddots & \ddots & \ddots & \ddots & \vdots \\ \vdots & \vdots & \ddots & \ddots & \ddots & \ddots & 0 \\ 0 & \dots & \dots & \ddots & \ddots & b_{N-1} & c_{N-1} \\ 0 & 0 & \dots & \dots & 0 & a_N & b_N \end{bmatrix}}_{\mathbf{A}} \underbrace{\begin{bmatrix} d_1 \\ d_2 \\ d_3 \\ \vdots \\ d_{N-1} \\ d_N \end{bmatrix}}_{\mathbf{B}} = \underbrace{\begin{bmatrix} f_1 & g_1 & 0 & 0 & \dots & \dots & 0 \\ e_1 & f_2 & g_2 & 0 & \dots & \dots & 0 \\ 0 & e_2 & f_3 & g_3 & 0 & \dots & 0 \\ 0 & 0 & \ddots & \ddots & \ddots & \ddots & \vdots \\ \vdots & \vdots & \ddots & \ddots & \ddots & \ddots & 0 \\ 0 & \dots & \dots & \ddots & \ddots & f_{N-1} & g_{N-1} \\ 0 & 0 & \dots & \dots & 0 & e_N & f_N \end{bmatrix}}_{\mathbf{C}} \underbrace{\begin{bmatrix} h_1 \\ h_2 \\ h_3 \\ \vdots \\ h_{N-1} \\ h_N \end{bmatrix}}_{\mathbf{D}} + \mathbf{E}$$

Figure 4.8 - Sample of a matrix form for finite difference equation

Table 4.2 – Node coefficients for FDE models in matrix form

For $i = 2, 3, \dots, N-1$	\mathbf{A}			\mathbf{B}	\mathbf{C}			\mathbf{D}	Matrix Solution
	a_i	b_i	c_i	d_i	e_i	f_i	g_i	h_i	
Explicit (Forward)	Fo	$1-2Fo$	Fo	T_i	-	-	-	T^{t+1}_n	$D=AB$
Implicit (Backward)	$-Fo$	$1+2Fo$	$-Fo$	T^{t+1}_n	-	-	-	T_i	$B=A^{-1}D$
Central (Crank-Nicolson)	$-Fo/2$	$1+Fo$	$-Fo/2$	T^{t+1}_n	$Fo/2$	$(1-Fo)$	$Fo/2$	T_i	$B=A^{-1}CD$
Boundary conditions: $b_1 = 1$, $c_1 = 0$, $d_1 = T^n_i$, $a_N = 0$ or -1 , $b_N = 1$ and $d_N = T^n_N$. T^{t+1}_n are unknown nodes (bold/red coloured), and \mathbf{E} is an additional set of matrix solution.									

The boundary conditions for the heat transfer problem are defined in node b_1 , c_1 , d_1 , a_N and d_N , where the nodes are from 1 (centre of SMA) to N (outer radius), as illustrated in Figure 4.9(a). Refer Appendix J to Appendix M for the Matlab codes.

4.4.1.6 FDE data quality and speed

The data quality (i.e. accuracy and consistency) and simulation duration of an FDM solution depends on the selected discretization equations and the associated step size. The quality of the solution increases significantly with smaller step size (Iserles, 1996; B. Wang, Han, & Sun, 2012), and subsequently increases the simulation duration. In addition, the time step must be sufficiently small that the movement of the phase boundary is confined to occur within the node region (CK Chun, 2000). Therefore, a compromise between data quality and simulation duration is necessary for a practical solution. In many scenarios, large time steps (dt) are preferred to increase simulation speed, however excessive time steps induce numerical instabilities that affect data quality (Hoffman & Frankel, 2001; Jaluria & Atluri, 1994).

Stability analysis methods can be applied to assess numerical stability; this is such as the von Neumann method (also known as Fourier stability analysis) (Hoffman & Frankel, 2001; Jaluria & Atluri, 1994; Majumdar, 2005; GD Smith, 1985) which is expressed as a Fourier number, $F_o = \frac{\alpha \Delta t}{\Delta r^2}$. The recommended Fourier number required to achieve numerical stability is summarised in Table 4.3. The central difference method is selected for this work due to its unconditional stability, highest accuracy and discretization flexibility (Crank & Nicolson, 1947; Majumdar, 2005; N. Ozisik, 1994).

**Table 4.3 - Available Finite Difference Equation implementation
(Crank & Nicolson, 1947; Iserles, 1996; M. Leary, Mac, Mazur, Schiavone, & Subic, 2010; Majumdar, 2005)**

FDE implementation	Approximation Error (Space & Time)	Recommendations*	Remark
Explicit (Forward)	$O(\Delta x^2, \Delta t)$	$0 \leq Fo \leq 0.5$	Least accurate and unstable, but easiest to be implemented and least numerical intensive.
Central (Crank-Nicolson)	$O(\Delta x^2, \Delta t^2)$	$0 < Fo$	Most accurate (i.e. less truncation error) and <i>unconditionally stable</i> . Execute the highest computational duration. Provides maximum flexibility in the choice of discretization.
Implicit (Backward)	$O(\Delta x^2, \Delta t)$	$0 < Fo$	<i>Unconditionally stable</i> for all time steps, thus the best for large time steps. Higher computational duration than forward difference method.
*Based on von Neumann stability analysis (Charney, Fjörtoft, & Von Neumann, 1950)			

4.4.2 Finite element method

The Finite Element Method (FEM) was pioneered by aerospace industry researchers in the 1950s. The seminal researchers who established the “technology transfer” from aerospace industry to wider range of engineering applications between 1950s and 1960s are J. H. Argyris, R. W. Clough, H. C. Martin, and O. C. Zienkiewicz (Clough, 2004). In 1956, a paper by (Turner, Clough, Martin, & Topp, 1956) is recognized as initiating the FEM era, which was further established by (Zienkiewicz & Cheung, 1965) to analyse FEM field problems with their function minimization techniques in 1965.

For solving conductive heat transfer problems, the FEM is based on the integral equation of heat conduction, which is obtained from differential equation by applying variational calculus. The mathematical modelling of FEM starts with dividing the solution domain into *unstructured meshes* (typically with triangulation meshes; refer Figure 4.9b), calculating the temperature values on the nodes, the finite elements, and the entire domain based on the weight function and the integral of the conservation law (Anand *et al.*, 2014; Patankar, 1980; Sarbu & Popina, 2001). The primary limitation of FEM is that the linearised equations of the matrices are not well organised for *unstructured meshes*, and therefore, require higher computational performance to solve the mathematical models.

4.4.3 Finite volume method

In 1971, McDonald (1971) introduced the fundamental theory of FVM to predict two-dimensional pressure distribution in gas turbine cascades for aerodynamic efficiency by interpretation of integral forms from conservation laws (mass, momentum or energy). FVM is one of the most popular methods in the computational fluid dynamics (CFD) area, but there are relatively few works available for computational solid mechanics (CSM), such as for structural and heat transfer analysis. Three common approaches for FVM are *cell-centred*, *vertex-centred* and *cell-vertex*.

For solving heat transfer problems, FVM subdivides the solution domain into a number of *cells*, and from these *cells*, forming continuous number of *cell control volumes* with denoted *centroids* (refer Figure 4.9c). The mathematical modelling of FVM starts with representing each cell control volume by its *centroid*, calculating the relation between its neighbours with the integral form of the conservation equation (or transport equations) to each *cell control volume*, and *interpolating* the *cell surface* variable values. Then, a suitable *quadrature formula* is used to approximate the cell surface and control volume integrals, resulting in an algebraic equation for each *cell control volume* (Jakobsen, 2014).

FVM is the best for solving conservative law in integral form, and can solve discontinuous solutions, applicable for any type of *mesh* and suitable for complex geometries, with the condition that the represented convective and diffusive fluxes of the surface integrals are the same on the shared *cell volume* boundaries. The main limitations of FVMs are low rate of convergence and accuracy (Jakobsen, 2014).

4.5 Discussion

FDM, FEM and FVM involve subdividing the domain solution into a finite number of nodes, elements, and control volumes, respectively, and then solving the associated thermomechanical problem with applicable mathematical relationships. A comparison of these numerical methods are summarised in Table 4.4.

Table 4.4 - Comparison of common numerical methods

	Finite difference method	Finite Element method	Finite volume method
Mathematical model	Differential.	Integral and conservation of mass, momentum or energy.	Integral and conservation of mass, momentum or energy.
Feasible geometry	Simple	Complex	Complex
Computational requirements	Low	High	High
Programming requirement	Low	High	Moderate
Node/Grid/Mesh technique	Structured grids. Dependant values are stored at the nodes.	Structured and unstructured grids. Dependant values are stored at the element nodes.	Structured and unstructured grids. Dependant values are stored in the centre of the control volume.
Discretization technique	Approximate <i>differential forms of the PDE</i> (typically derived from a Taylor series expansion) in term of nodal points, resulting in one algebraic equation per grid node.	Equation of solution is multiplied for weight function and then integrated over entire domain by <i>integral form of the conservation equation</i> , resulting in a set of non-linear algebraic equations.	<i>Integral form of PDE</i> is solved with conservation equations, and applied to cell surfaces to establish relation between the control volume cells.
Solution	Discrete solutions at nodal points.	Continuous (up to a point) solutions.	Discrete solutions at cell or face centres.

The comparison of grid techniques between these three methods is illustrated in Figure 4.9. Cell-centred FVM approach is applied for Figure 4.9c.

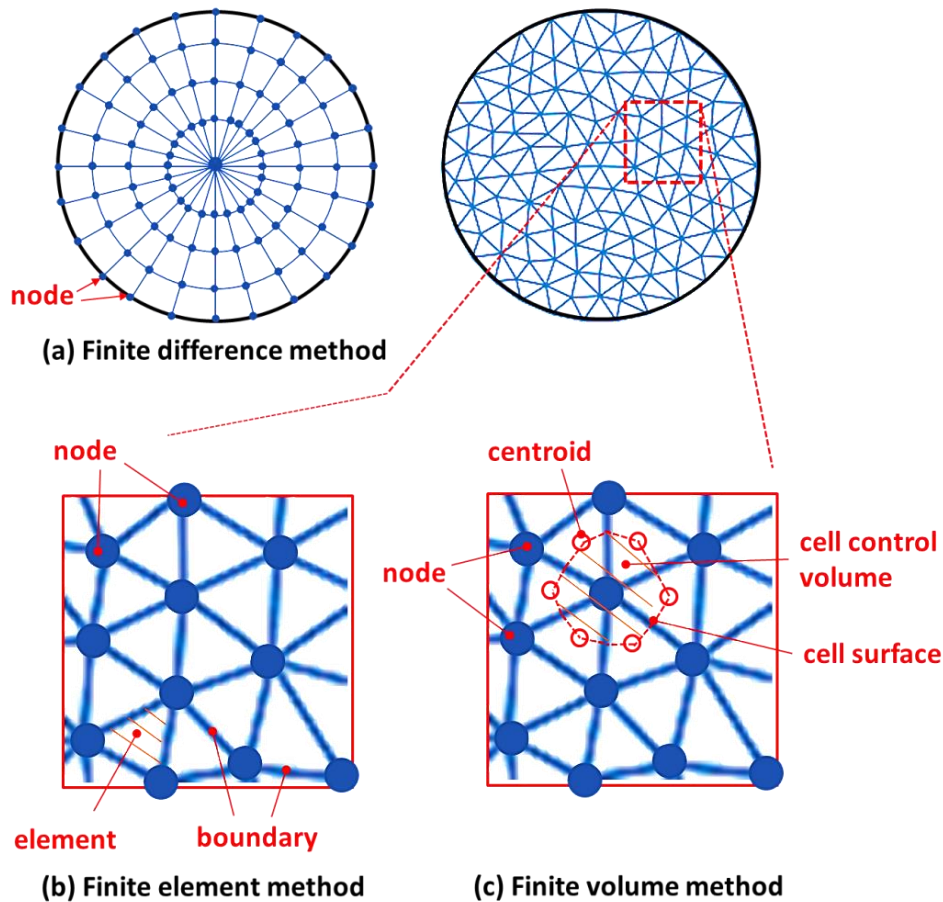


Figure 4.9 – Comparison of 2D-grids for common numerical method on cylindrical geometry

All methods involve subdividing the entire domain into a large number of nodes, finite elements or control volumes, and then solving the governing equations with their respective derivative methods. FEM and FVM allow unstructured and non-equispaced grids, and therefore, are applicable for complex geometries; meanwhile FDM is only recommended for simple geometries (structured grids). For structured grid, typically three types of grids are available, i.e. Cartesian, spherical polar and curvilinear. The higher the grid resolution, the higher the associated solution accuracy that may be obtained, and the higher the associated computational cost required.

FVM has become a popular method of deriving discretization of PDEs than FDM, due to its preservation of the conservation properties of PDEs (Jakobsen, 2014) and freedom to modify the shape and location of associated control volumes (Manna, 1992). However, FVM is more difficult to develop in 3D than FDM for solutions with higher than second order, where the two-levels approximation considers the interpolation and integration processes, while FDM requires only the approximations of the derivatives and interpolation (Jakobsen, 2014).

FVM is more robust than FEM in solving discontinuity problems and capturing shock such as in transonic and supersonic flows in fluid mechanics due to its flexibility to define interpolating functions between elements (Limache & Idelsohn, 2007); therefore, FVM is popular in fluid mechanics. Nowadays, hybrid methods (FDM, FVM and FEM) have been developed to analyse fluid and structural mechanics problems, and are found to perform better than conventional methods; e.g. FVM-FEM hybrid method to investigate the radiative heat transfer in graded index medium (L. Zhang, Zhao, Liu, & Wang, 2012), FDM-FEM hybrid method to simulate the 3D casting processes (Si, Cho, & Kwahk, 2003), and FDM-FVM hybrid method to investigate the conduction-radiation problems in cylindrical medium (Mishra, Kim, Das, Ajith, & Uppaluri, 2009). Hybrid methods are considered in recent research works to solve multi-physics problems (i.e. coupling between thermal, electrical, fluid, solids and chemical problems), due to higher data quality (accuracy) and speed.

4.6 Conclusion

Three common numerical methods are FDM, FEM and FVM. FDM and FEM are typically applied for solving SMA actuator heat transfer problems, and phenomenological constitutive models are favourable due to their simplicity and compatibility with standard engineering material constants. FVM and FEM are more flexible than FDM in allowing the solution of complex geometries and boundaries. However, FDM is favourable for relatively simple geometries, such as SMA linear actuators, due to the lower associated computational cost and programming complexity. For a simple SMA linear actuators (or wires), one-dimensional FDM models suffice. The central (Crank-Nicholson) FDE model is proven to be unconditionally stable, produces highest accuracy and discretization flexibility, and is therefore utilised in this work.

5. The critical and crossover radii on transient heating

The outcomes of this chapter have contributed to the following peer reviewed publication:
The critical and crossover radii on transient heating, S Huang, JM Jani, M Leary, A Subic, Applied Thermal Engineering 60(1), 325-334, 2013

5.1 Chapter summary

Cylindrical thermal systems often apply thermal material (known as lagging) to control heat transfer to the environment. SMA linear actuators for which the cooling time (and thereby response time) is to be minimised, can potentially apply thermal material cylindrically to *maximize* heat transfer; for these scenarios the critical radius defines the optimal radius for a specific scenario. For systems that intend to *minimize* heat transfer (for example an SMA actuator that was designed to remain contracted for an extended time period), the crossover radius defines the radius required to achieve an equal heat transfer rate to the un-insulated scenario; with any further increase in radii resulting in a monotonic reduction in the associated heat transfer rate.

The critical radius is well defined for the steady-state scenario, and recently the steady-state crossover radius has also received attention. However, the literature does not provide clarity for the transient scenario in terms of either crossover or critical radius. This lack of clarity results in uncertainty for SMA actuator designers that intend to utilise thermal material to control SMA actuator response time. This work overcomes this identified limitation by quantifying, for the first time, the crossover and critical radii of a transient cylindrical system. In particular, this work identifies that the cycle-average heat transfer rate can stabilize to a quasi-static value in response to transient heating. These outcomes enable greater certainty in SMA actuator design when applying thermal material to influence actuation speed, such as (Chee Siong *et al.*, 2005a) and (Martin Leary *et al.*, 2009).

5.2 Introduction

The heat transfer rate for planar, cylindrical and spherical systems is well understood for steady-state thermal loading. For planar systems, the resistance to heat transfer increases monotonically with increasing insulation thickness. For cylindrical and spherical systems, the resistance to heat transfer varies non-linearly, and it is therefore of significant importance that the radius of thermal material be matched to the associated heat transfer objective.

Transient thermal loading of cylindrical or spherical systems is an important design scenario for applied thermal engineering. For example, all thermal systems are in a transient state from when a heat load is initially applied to the time of temperature stabilisation; and, thermal systems are also often transient during normal operation. For example, heating or cooling by cylindrical piping is often either: applied in a transient manner, or is applied at near constant temperature to a system with a transient heat load. A practical example of the former case is domestic hot water that is intermittently delivered by piping, resulting in transient heat transfer. An example of the latter case is cooling water that is delivered to a moulding die at a constant inlet temperature; however, fluctuation of the die temperature through the manufacturing process results in transient heat transfer rates.

For steady-state thermal systems that intend to maximize heat transfer, for example SMA actuators that intend to minimise deactivation time, the critical radius defines the optimal radius for a specific thermal material. However, for systems that intend to minimize heat transfer, the critical radius does not provide robust design guidance. For systems that intend to minimize heat transfer, the crossover radius defines the minimum radius required to achieve equal heat transfer to the uninsulated case; where any further increase in radius results in a monotonic reduction in the associated heat transfer rate.

The crossover radius has received attention in recent literature (M. Kulkarni & Nelson, 2006; M. R. Kulkarni, 2004), due to its importance in design optimisation for systems that intend to minimize heat transfer; however, the results are only developed for the steady-state scenario. This study investigates the crossover and critical radii of a transient cylindrical system. In particular, a method for evaluating the transient heat transfer associated with cylindrical systems is developed, and used to draw novel conclusions between the steady-state and transient heat transfer scenarios. These conclusions provide previously unavailable design guidance for the optimisation of cylindrical systems subject to transient thermal loading. For example in SMA actuator designs that apply thermal material to influence actuation speed, such as (Chee Siong *et al.*, 2005a) and (Martin Leary *et al.*, 2009).

In addition to providing direct design guidance for scenarios that are known to be transient, the contributions of this work allow reverse engineering of a given cylindrical heat transfer scenario, in order to identify the range of design scenarios for which the system response will be either transient, or quasi-static. Furthermore, the computational cost of the proposed method may be relatively high for scenarios with relatively large thermal radius, or number

of applied cycles, as may be commonly of interest in SMA actuator design. This work identifies novel opportunities to overcome this limitation and reduce the associated computational cost, thereby enabling design outcomes of relevance to practical SMA actuator design.

The unique characteristics of SMA actuators providing an excellent technological opportunity to replace conventional actuators with reduction in mechanical complexity and size (Mohd Jani, Leary, Subic, *et al.*, 2014). However, SMA actuators produce low operational frequency due to technical heat transfer challenges, leading to challenges associated with deactivation time and associated bandwidth. In previous chapters, it was identified that the SMA linear actuator size and shape are of significance to actuator response time, where actuators with higher *surface area-to-volume ratio* (SA:V) deactivate more rapidly due to enhanced convection (An *et al.*, 2008; Dynalloy Inc., 2007; Lara-Quintanilla & Bersee, 2015). It was also identified that highest cooling rate are obtained with a high conductive fluidic medium (An *et al.*, 2008; Dynalloy Inc., 2007; Lara-Quintanilla & Bersee, 2015).

In this work, the transient heat transfer behaviour of cylindrically lagged systems are investigated with a finite difference equation (FDE) model to characterise, for the first time, the transient crossover and critical radii of the system. These outcomes are applicable to SMA linear actuator systems, where the SMA wire (i.e. cylinder), is cylindrically lagged with thermal material (i.e. cylindrical pipe), as investigated by (Chee Siong *et al.*, 2005a) and (Martin Leary *et al.*, 2009), and schematically represented in Figure 5.1.

5.2.1 Steady-state heat transfer of cylindrical systems

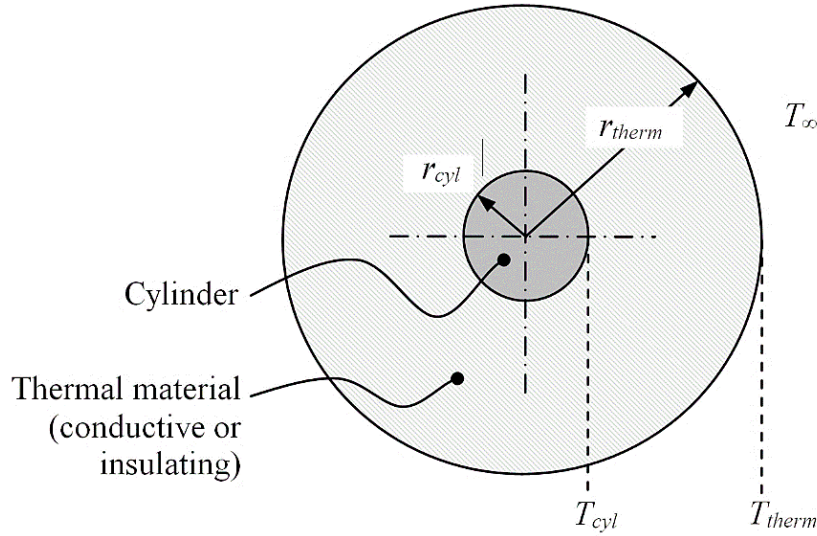


Figure 5.1 - Cylindrical heat transfer system (S. Huang, JM. Jani *et al.*, 2013).

In the presence of constant boundary conditions, and in the absence of internal heat generation, a temperature field will stabilize to a steady-state condition. The thermal resistance to heat transfer for one-dimensional conduction and convection across a cylinder shrouded by thermal material is given by (Eq. 5.1) and (Eq. 5.2), respectively (Bergman *et al.*, 2011). Where r_{cyl} is the cylinder radius, r_{therm} is the outer radius of the thermal material, L is the cylinder length, and k_{therm} is the thermal conductivity of the thermal material (Figure 5.1).

$$R_{cond} = \frac{\ln(r_{therm}/r_{cyl})}{2\pi L k_{therm}} \quad (\text{Eq. 5.1})$$

$$R_{conv} = \frac{1}{2\pi L h r_{therm}} \quad (\text{Eq. 5.2})$$

According to (Eq. 5.1) and (Eq. 5.2), the thermal resistance between a cylinder and the ambient environment is:

$$R_{cyl} = R_{cond} + R_{conv} = \frac{1}{2\pi L} \left(\frac{\ln(r_{therm}/r_{cyl})}{k_{therm}} + \frac{1}{h r_{therm}} \right) \quad (\text{Eq. 5.3})$$

According to (Eq. 4.4), the heat transfer rate can be calculated as:

$$q_{cyl} = \frac{2\pi L(T_{cyl} - T_{\infty})}{\left(\frac{\ln(r_{therm}/r_{cyl})}{k_{therm}} + \frac{1}{hr_{therm}} \right)} \quad (\text{Eq. 5.4})$$

where T_{cyl} is the temperature at the cylinder surface (Figure 5.1). From (Eq. 4.4) and (Eq. 5.4), the temperature of the thermal material at any point, T_p , can then be calculated from the absolute thermal resistance from the cylinder surface to the point of interest, R_p as:

$$T = T_{cyl} - q_{cyl}R_p \quad (\text{Eq. 5.5})$$

5.2.2 Critical and crossover radii

It is evident from (Eq. 5.3) that the addition of thermal material in a cylindrical system results in an increase in conduction resistance and a decrease in convection resistance. When considering a cylindrical system, the critical radius is defined as the outer radius of the insulation layer at which the steady-state heat transfer rate is maximized; i.e. R_{cyl} is minimized. If radiative heat transfer and variable convective heat transfer coefficients are considered, complex expressions of critical radius result (Branco *et al.*, 2001; Habib, 1982; Sahin & Kalyon, 2004; Sparrow & Kang, 1985). However, if the radiation heat transfer is negligible and the convective heat transfer coefficient is assumed to be constant, the critical radius of a cylindrical system is calculated as (Bejan, 1993; Das, 2010; Holman, 2009; M. Kulkarni & Nelson, 2006; M. R. Kulkarni, 2004):

$$r_{cr} = \frac{k_{therm}}{h} \quad (\text{Eq. 5.6})$$

The critical radius can be utilized to maximize heat transfer (M. Leary, Mac, *et al.*, 2010; M. Leary, Schiavone, *et al.*, 2010); however, it only provides a necessary condition for systems that intend to minimize the associated heat transfer rate (M. R. Kulkarni, 2004). The crossover radius, r_{cross} , is defined as the radius of the thermal layer at which the heat transfer rate from the cylinder to the ambient environment equals the heat transfer rate from the bare cylinder (M. Kulkarni & Nelson, 2006; M. R. Kulkarni, 2004):

$$\ln \left[\frac{r_{cross}}{r_{cyl}} \right] = \frac{k_{therm}}{h} \left[\frac{r_{cross} - r_{cyl}}{r_{cyl} \cdot r_{cross}} \right] \quad (\text{Eq. 5.7})$$

According to this definition the critical and crossover radii only exist for Biot number, $Bi < 1$ (M. Kulkarni & Nelson, 2006; M. R. Kulkarni, 2004) (refer Section 4.3.2.2 for Biot number).

5.3 Analysis

A transient temperature field occurs in response to time dependant boundary conditions or internal heat generation. Transient effects may be accommodated for standard geometries by graphical methods such as Heisler Charts or by numerical methods (Bergman *et al.*, 2011).

5.3.1 Transient heat transfer analysis of cylindrical systems

To accommodate the transient analysis of an insulated cylindrical system, the heat diffusion equation can be expressed in polar coordinates (Pitts & Sissom, 2002):

$$\frac{\partial^2 T}{\partial r^2} + \frac{1}{r} \frac{\partial T}{\partial r} = \frac{1}{\alpha} \frac{\partial T}{\partial t} \quad (\text{Eq. 5.8})$$

The boundary conditions for heat convection at the thermal material outer radius, r_{therm} , can be expressed as (Eq. 5.9), where T_{therm} is the temperature at the outer radius of the thermal material.

$$k_{therm} \left. \frac{\partial T}{\partial r} \right|_{r=r_{therm}} = h(T_{\infty} - T_{therm}) \quad (\text{Eq. 5.9})$$

5.3.2 Finite difference equation model

The major consideration of this model is to apply the central difference equations to (Eq. 5.8), resulting in a FDE representation of the central difference equation (Eq. 5.10) at time step, $t(l+1/2)$, and radius, $r(i)$. Where $F_0 = \alpha \Delta t / \Delta r^2$ and the associated truncation error is $O(\Delta t^2, \Delta r^2)$ (Majumdar, 2005) (refer also Section 4.4.1.4).

$$\begin{aligned} F_0 \left(1 - \frac{1}{2i}\right) T_{i-1}^l + 2(1 - F_0) T_i^l + F_0 \left(1 - \frac{1}{2i}\right) T_{i+1}^l \\ = -F_0 \left(1 - \frac{1}{2i}\right) T_{i-1}^{l+1} + 2(1 + F_0) T_i^{l+1} - F_0 \left(1 + \frac{1}{2i}\right) T_{i+1}^{l+1} \end{aligned} \quad (\text{Eq. 5.10})$$

Applying central difference equations to (Eq. 5.9) results in the discretised convection boundary conditions as indicated by (Eq. 5.11).

$$-T_{n-1}^{l+1} + \left(\frac{\Delta r h}{k_{therm}} - 1\right) T_n^{l+1} = \frac{\Delta r h}{k_{therm}} T_\infty \quad (\text{Eq. 5.11})$$

where T_n^{l+1} is the temperature of the outer surface of the thermal material at time step, $l+1$.

This model was developed in this work to study the transient heat transfer response for an insulated cylindrical system.

5.3.3 Simulation scenario

Based on the work of Kulkarni (2004), an example of steady-state cylindrical heat transfer from the classic text by Holman (2009) was used as a reference simulation scenario. In this example, a pipe of 0.025m radius is insulated by a layer of asbestos with a thermal conductivity of 0.17W/mK. The temperature of the pipe is held constant at 200°C and the ambient temperature is 20°C. The convective heat transfer coefficient on the asbestos surface is constant 3W/m²K. In this case, the associated Biot number is 0.44 (Eq. 4.6).

5.4 Results and discussion

The developed FDE model is validated prior implementation, and three cases of transient simulations were proposed in this work.

5.4.1 Validation of FDE Model

In order to validate the transient FDE model, the steady-state heat transfer of the system introduced in the example above was solved using both the steady-state analytical equation (Eq. 5.4), and the transient FDE model for a unit-length cylinder. In the FDE transient analysis, the pipe was maintained at a constant temperature of 473K (200°C), thereby heating the asbestos thermal material layer from an ambient temperature of 293K (20°C). The transient simulation continued until a near steady-state temperature field was established, based on a convergence criterion of less than 1E-6K temperature change at any radius within a period of 10s. The ratio of heat transfer rate on the thermal material surface, q_{therm} , to the heat transfer rate on an equivalent bare pipe, q_{bare} , was calculated for both analytical and FDE methods with the thermal material radius varying from the bare pipe radius (i.e. $r_{bare} = 0.025\text{m}$) to $r = 0.45\text{m}$ (Figure 5.2).

The critical radius calculated by the analytical equation is 0.0567m and the radius calculated by the numerical FDE model is 0.0568m; i.e. for the selected convergence criterion, the error is 0.0001m (less than 0.2%). The crossover radius calculated by the analytical equation is 0.1742m and the radius calculated by the FDE model is 0.1757m. The associated error is 0.0015m, i.e. less than 0.9%. This outcome confirms the validity of the proposed FDE model.

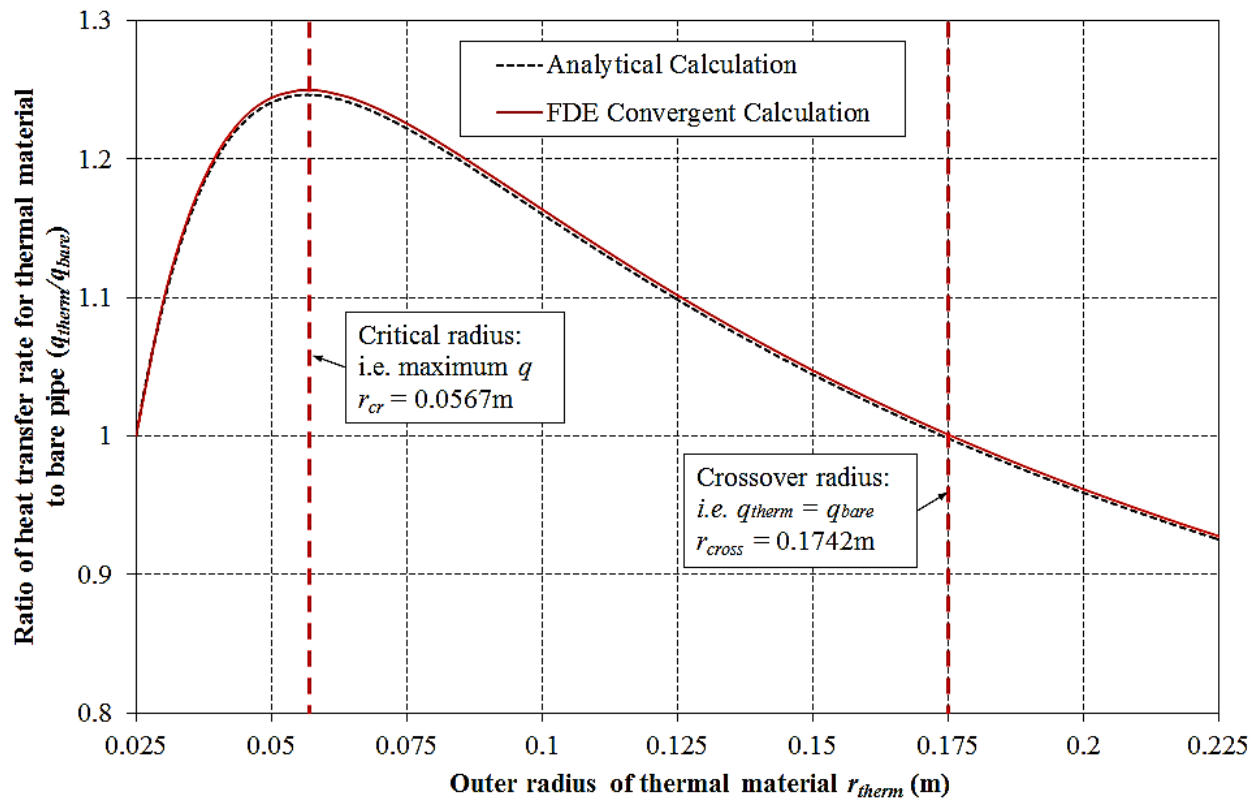


Figure 5.2 - Ratio of insulated to bare heat transfer rate (q_{ins}/q_{bare}) versus thermal material radius ($r_{bare} = 0.025m$)

Figure 5.3 shows the convergence of the insulated pipe over time for the scenario of interest. The convergence criterion is satisfied at 133,790s.

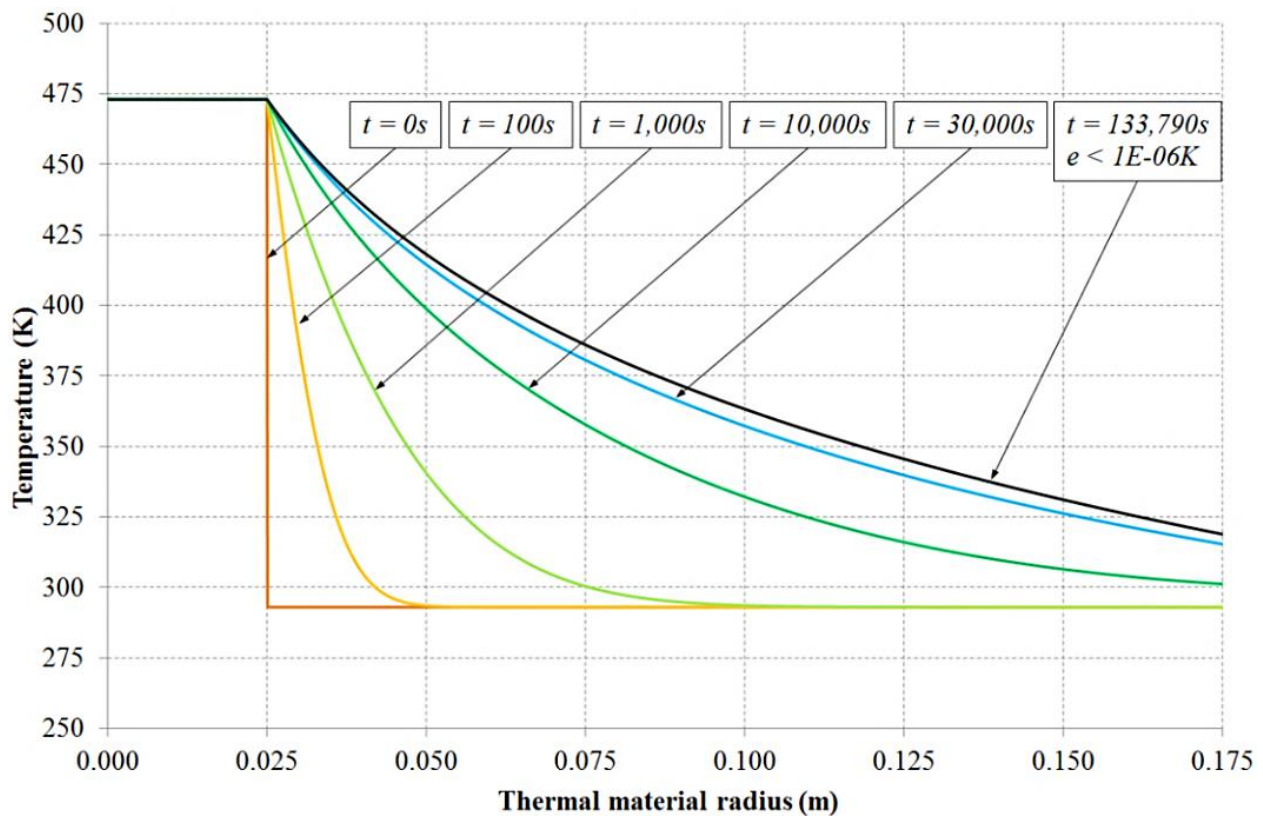


Figure 5.3 - Transient temperature of insulated pipe cross section

5.4.2 Transient solution for insulated pipe

In order to optimize the insulated pipe system undergoing cycling heating and cooling, a transient heat transfer analysis was conducted for scenarios with specific duty cycle, D , and period, P (Eq. 5.12). To provide insight into the effect of duty cycle and period: case A and B have a common period and varying duty cycle; and, case A and C have a common duty cycle and varying period.

$$D = \frac{t_{heat}}{t_{heat} + t_{cool}} = \frac{t_{heat}}{P} \quad (\text{Eq. 5.12})$$

Table 5.1 - Transient analysis of pipe system

Parameters	Case A	Case B	Case C
Ambient temperature, T_{∞} (K)	293		
Pipe surface temperature, T_{pipe} (K)	473 (heating) 293 (cooling)		
Pipe radius, r_{bare} (m)	0.025		
Convective heat transfer rate, h (W/m ² K)	3		
Thermal conductivity, k_{therm} (W/mK)	0.17		
Maximum simulation time (s)	100,000		
Thermal material radius range, r_{therm} (m)	0.025 to 0.200		
Heating period per cycle, t_{heat} (s)	1.0	1.8	0.1
Cooling period per cycle, t_{cool} (s)	1.0	0.2	0.1
Duty cycle, D (s/s)	50%	90%	50%
Period, P (s)	2.0	2.0	0.2
Maximum number of cycles, N	50,000	50,000	500,000

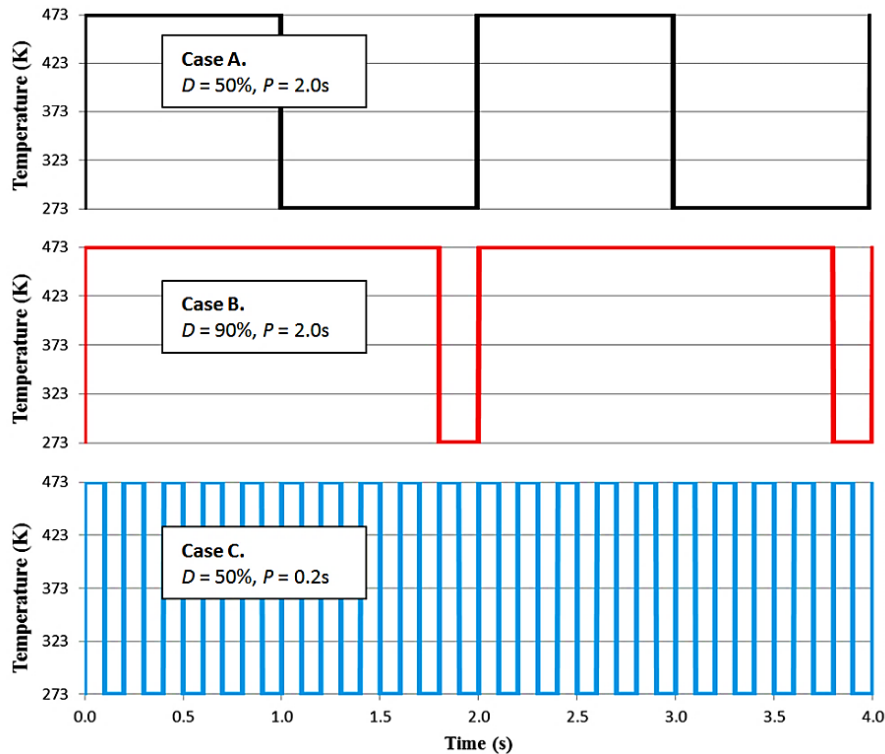


Figure 5.4 - Pipe temperature versus time (Case A, B and C)

5.4.3 Case A simulation ($D = 50\%$, $P = 2.0s$)

As a boundary condition for Case A, the pipe temperature was set as 473K with $D = 50\%$ and $P = 2.0s$ (Figure 5.4).

5.4.3.1 Identification of transient critical and crossover radii

In order to confirm whether the steady-state critical radius is applicable to Case A, the cycle-average heat transfer rate at the pipe surface, \hat{q}_{pipe} , (Eq. 5.13) was calculated for each cycle in the radius range of 0.05 to 0.06m in 0.0001m increments. This solution covers the steady-state critical radius ($r_{cr} = 0.0567$ m) at a resolution equal to the absolute error observed in the FDE method (Section 5.4.1).

The thermal material radius corresponding to the maximum cycle-average heat transfer rate at the pipe surface, \hat{q}_{max} (Eq. 5.14), is identified for each cycle of Case A (Figure 5.5). It can be seen that \hat{q}_{max} occurs for a thermal material radius of 0.06m (the maximum radii assessed) until approximately 4,100 cycles, after which \hat{q}_{max} asymptotes to the steady-state critical radius (Figure 5.5).

For N greater than approximately 6,000 cycles the convergence criterion is satisfied and the heat transfer rate stabilizes to 52.6W. This outcome confirms that for this scenario the steady-state critical radius applies to the transient system, if the number of cycles is sufficiently large to allow convergence of the cycle average heat transfer rate, \hat{q} .

$$\hat{q} = \frac{\left(\int_0^{t_{heat}} q(t)dt + \int_{t_{heat}}^{t_{heat}+t_{cool}} q(t)dt \right)}{(t_{heat} + t_{cool})} = \frac{1}{P} \left(\int_0^P q(t)dt \right) \quad (\text{Eq. 5.13})$$

$$\hat{q}_{max} = \max(\hat{q}) \quad (\text{Eq. 5.14})$$

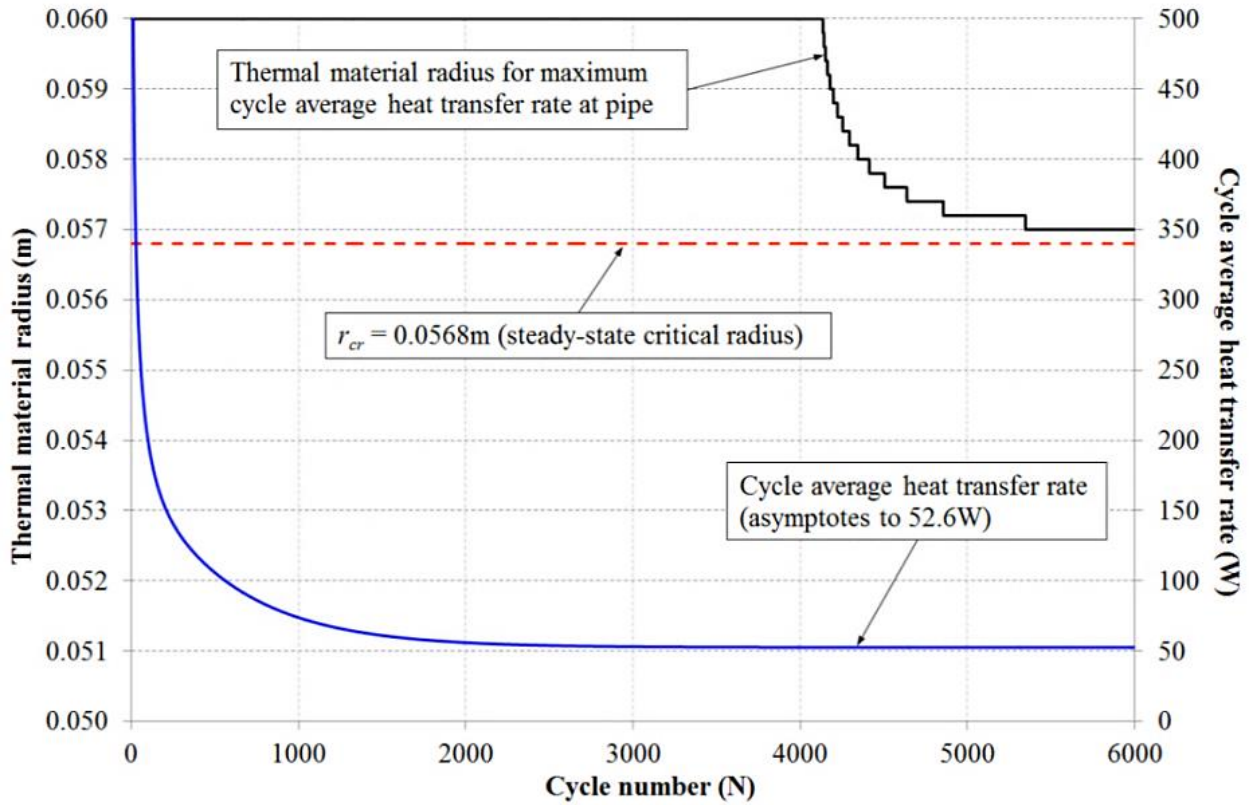


Figure 5.5 - Maximum observed cycle average heat transfer rate on pipe surface for Case A, and the corresponding thermal material radius (for r in range of 0.050 to 0.060m).

In order to confirm whether the steady-state crossover radius is applicable to the transient scenario, the cycle-average heat transfer rate on the pipe, \hat{q}_{pipe} , and thermal material surfaces, \hat{q}_{therm} , was calculated at the steady-state crossover radius ($r_{cross} = 0.1742\text{m}$, as calculated in Section 2.4). These heat transfer rates were compared with the heat transfer rate from an equivalent bare pipe surface, \hat{q}_{bare} (Figure 5.6). It can be seen that with increasing cycle number, \hat{q}_{pipe} , and \hat{q}_{therm} converge to \hat{q}_{bare} (i.e. 42.3 W). This result indicates that for the scenario investigated, the steady-state crossover radius is applicable if the number of cycles is sufficiently high to allow convergence.

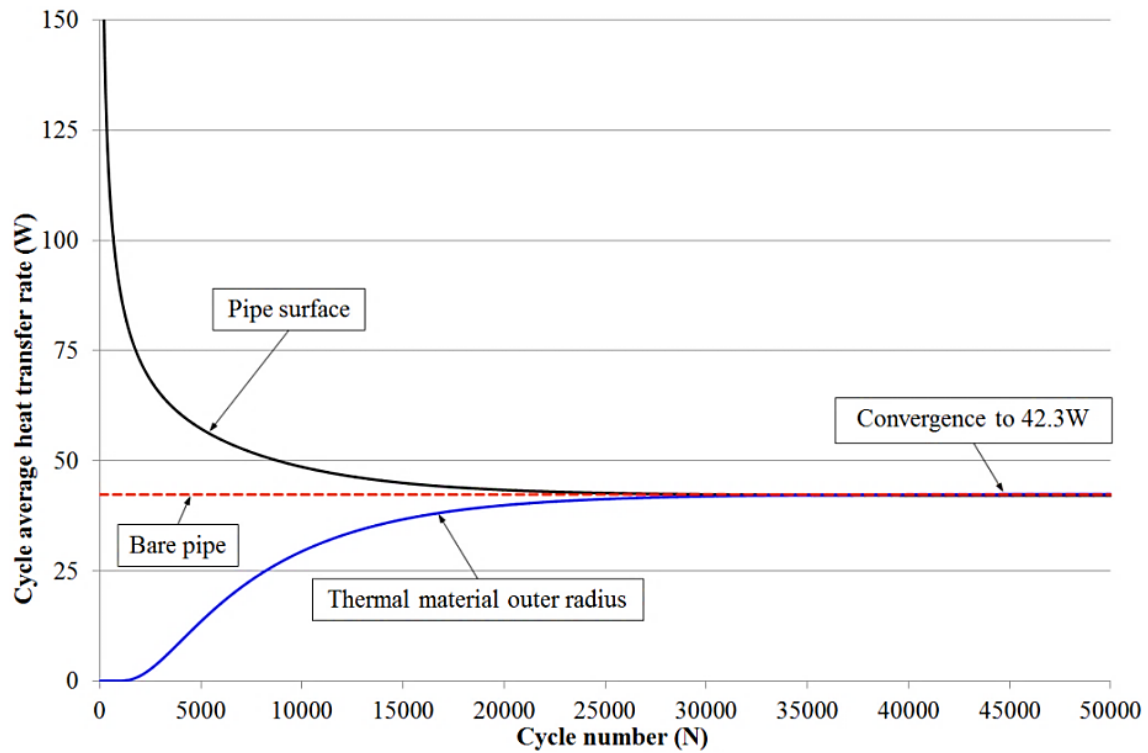


Figure 5.6 - Cycle average heat transfer rate (\dot{q}) on the pipe and thermal material surface for Case A ($r_{therm} = r_{cross} = 0.1757\text{m}$).

5.4.3.2 Transient analysis for a limited number of cycles

It was identified that the steady-state critical and crossover radii are applicable for the 50% duty cycle system when the cycle number is large enough to allow convergence (convergence criterion satisfied for N approximately greater than 6,000 cycles for the critical radius and 50,000 for the crossover radius). However, it is also useful to optimize the insulated pipe system to either maximize or minimize the heat transfer rate when N is less than required for convergence. For this case, a simulation was conducted up to 6,000 cycles in the radius range of 0.025 to 0.2m. The cycle-average heat transfer rate on the pipe surface is summarized in Table 5.2 and Figure 5.7. Note that values with high N and r_{therm} are not assessed due to the high associated computational cost.

Table 5.2 - Cycle-average heat transfer rate at pipe surface, \dot{q}_{pipe} , for Case A (bare pipe radius is 0.025m). Red shaded values indicate that stabilization of \dot{q}_{pipe} has occurred at the associated thermal material radius. Green shaded values indicate that thermal energy has not yet propagated to r_{therm} . Critical radius (r_{cr}) identified in bold italics.

Cycle Number	Thermal material radius, r_{therm} (m)													
	0.0250	0.0292	0.0333	0.0375	0.050	<i>$r_{cr}=0.0568$</i>	0.0625	0.0750	0.0875	0.1000	0.1125	0.1250	0.1375	0.2000
1	42.3	1754.3	1754.8	1754.8	1754.8	1754.8	1754.8	1754.8	1754.8	1754.8	1754.8	1754.8	1754.8	1754.8
2	42.3	1215.5	1222.8	1222.8	1222.8	1222.8	1222.8	1222.8	1222.8	1222.8	1222.8	1222.8	1222.8	1222.8
3	42.3	971.5	984.4	984.4	984.4	984.4	984.4	984.4	984.4	984.4	984.4	984.4	984.4	984.4
4	42.3	831.6	849.3	849.6	849.6	849.6	849.6	849.6	849.6	849.6	849.6	849.6	849.6	849.6
5	42.3	733.3	759.2	760.1	760.1	760.1	760.1	760.1	760.1	760.1	760.1	760.1	760.1	760.1
10	42.3	433.4	541.2	544.2	544.4	544.4	544.4	544.4	544.4	544.4	544.4	544.4	544.4	544.4
25	42.3	118.5	337.9	356.7	358.4	358.4	358.4	358.4	358.4	358.4	358.4	358.4	358.4	358.4
50	42.3	50.0	190.9	256.7	265.5	265.6	265.6	265.6	265.6	265.6	265.6	265.6	265.6	265.6
100	42.3	45.6	83.0	159.5	199.5	199.8	199.9	200.0	200.0	200.0	200.0	200.0	200.0	200.0
250	42.3	45.5	48.6	66.6	133.9	140.0	140.9	141.1	141.2	141.2	141.2	141.2	141.2	141.2
500	42.3	45.5	48.0	50.6	87.5	102.2	107.7	110.6	110.9	110.9	110.9	110.9	110.9	110.9
750	42.3	45.5	48.0	49.9	67.6	81.4	89.1	95.9	97.1	97.2	97.2	97.3	97.3	97.3
1000	42.3	45.5	48.0	49.9	58.9	69.4	76.9	85.9	88.4	88.9	88.9	88.9	89.0	89.0
1500	42.3	45.5	48.0	49.9	53.6	58.3	63.4	72.5	76.9	78.4	78.8	78.9	78.9	78.9
2000	42.3	45.5	48.0	49.9	52.6	54.6	57.3	64.4	69.2	71.6	72.4	72.7	72.8	72.8
2500	42.3	45.5	48.0	49.9	52.4	53.3	54.7	59.4	63.8	66.5	67.8	68.3	68.4	68.5
3000	42.3	45.5	48.0	49.9	52.4	52.9	53.5	56.4	59.9	62.6	64.1	64.8	65.2	65.3
3500	42.3	45.5	48.0	49.9	52.4	52.7	52.9	54.5	57.2	59.5	61.2	DATA NOT ASSESSED DUE TO HIGH COMPUTATIONAL COST		
4000	42.3	45.5	48.0	49.9	52.4	52.7	52.7	53.4	55.2	57.2	58.7			
4500	42.3	45.5	48.0	49.9	52.4	52.7	52.6	52.7	53.8	55.4	56.8			
5000	42.3	45.5	48.0	49.9	52.4	52.6	52.6	52.3	52.9	54.0	55.2			
5500	42.3	45.5	48.0	49.9	52.4	52.6	52.5	52.1	52.2	52.9	53.8			
6000	42.3	45.5	48.0	49.9	52.4	52.6	52.5	51.9	51.7	52.0	52.7			

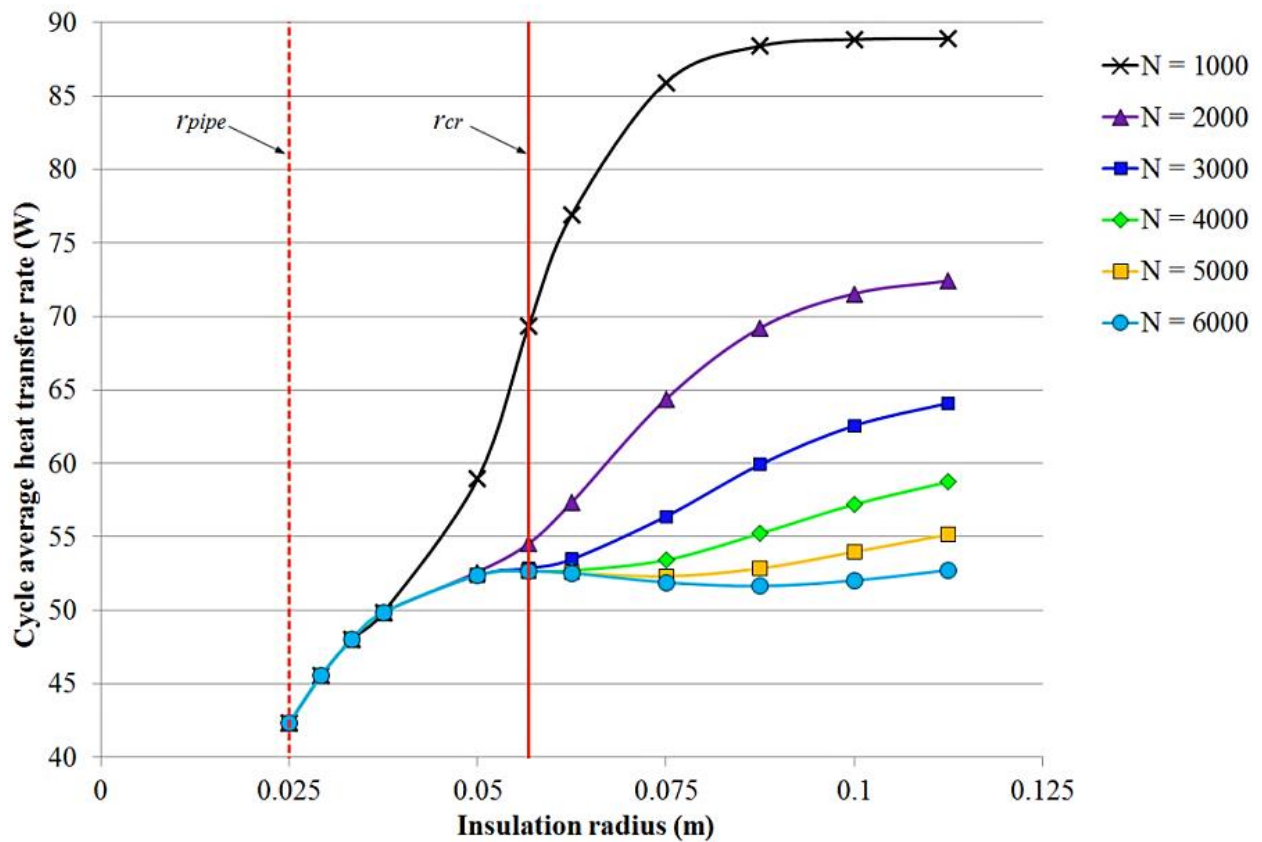
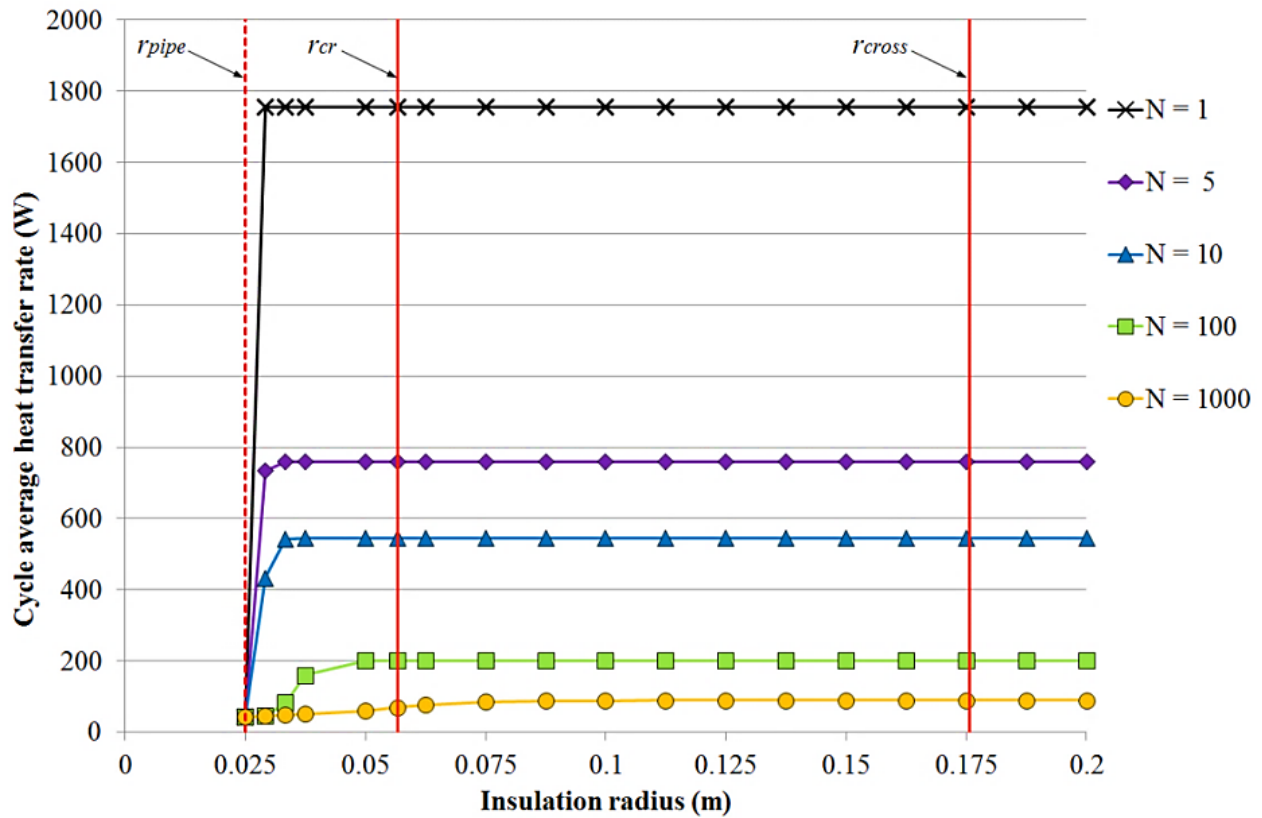


Figure 5.7 - Heat transfer rate on pipe surface versus thermal material radius for Case A. Upper: $N = 1$ to 1,000 cycles, and radius range including r_{cross} . Lower: $N = 1,000$ to 6,000 cycles, and radius range including r_{cr}

Figure 5.7 and

Table 5.2, the convergence of \hat{q}_{pipe} with increasing N . It can be seen that three zones exist:

- For high r_{therm} and low N , \hat{q}_{pipe} does not vary with increasing r_{therm} ; indicating that thermal energy is yet to propagate from the pipe to r_{therm} . For such cases much of the thermal material does not actively contribute to \hat{q}_{pipe} for *either* objective of minimising or maximising \hat{q}_{pipe} .
- For low r_{therm} and high N , \hat{q}_{pipe} stabilizes to a constant value, indicating that thermal energy has propagated from the pipe to r_{therm} , and that sufficient time has elapsed for the system to stabilise.
- For conditions between these two zones, \hat{q}_{pipe} is transient, and is a function of r_{therm} and the associated cycle number.
- The number of cycles required for stabilization increases with thermal radius, therefore the steady-state critical radius stabilizes more quickly than the crossover radius.

5.4.4 Case B Simulation ($D = 90\%$, $P = 2.0s$)

As for Section 5.4.3.1, a transient heat transfer analysis was conducted for Case B, i.e. $D = 90\%$ and $P = 2.0s$ (Figure 5.8).

5.4.4.1 Identification of transient critical and crossover radii

It can be seen that the radius at which \hat{q}_{max} occurs is identical for Case A and B (Figure 5.5). However, the magnitude of the associated cycle-average heat transfer rate is greater for Case B (94.8W). By inspection, the ratio of heat transfer rates varies in proportion to the ratio of duty cycles, i.e. $94.8W = (90\%/50\%) * 52.6W$.

In order to confirm whether the steady-state crossover radius is applicable to this transient system, the cycle-average heat transfer rate was calculated as for Case A (Figure 5.9). The results for Case B vary in proportion to the results of Case A, and convergence to the crossover radius occurs at approximately 50,000 cycles. As for the critical radius, the cycle-average heat transfer rate at convergence (76.2W) varies in proportion to the ratio of duty cycles, i.e. $76.2W = (90\%/50\%) * 42.3W$.

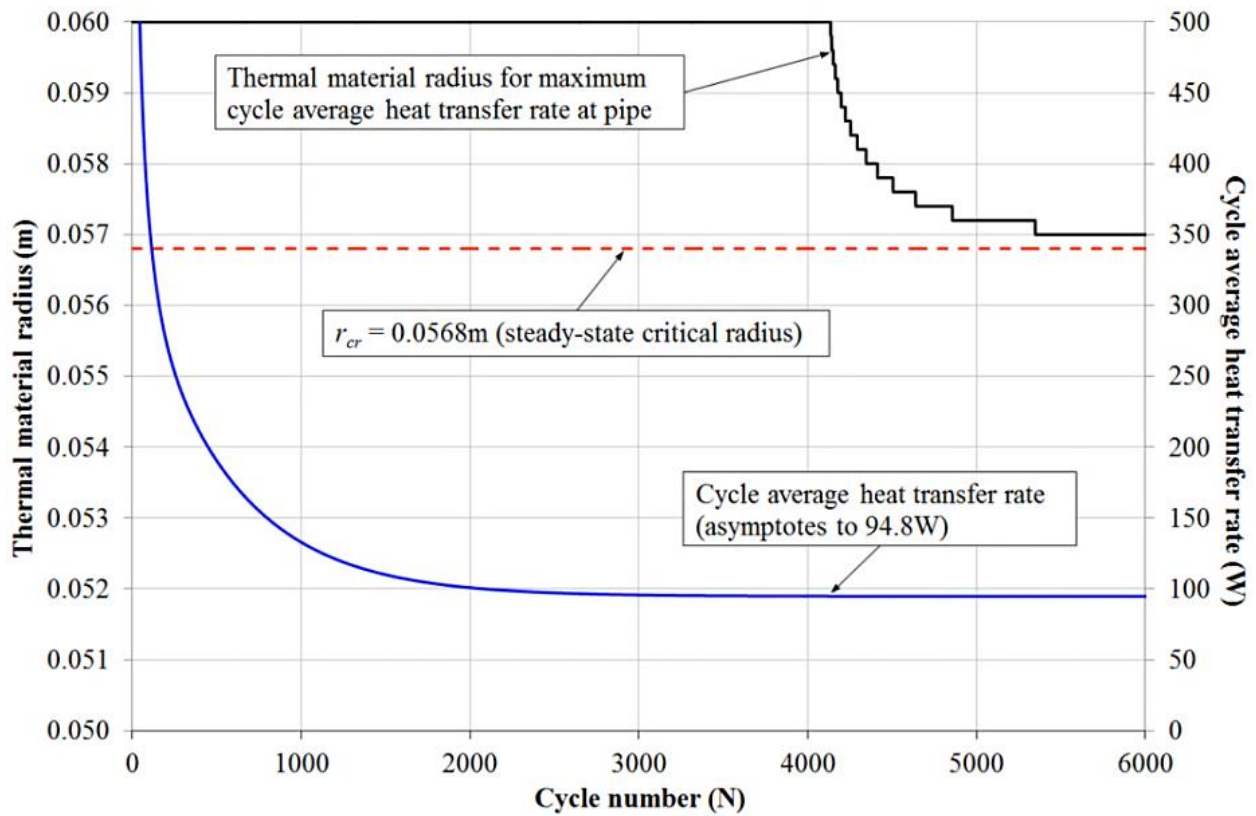


Figure 5.8 - Maximum observed cycle average heat transfer rate on pipe surface for Case B, and the corresponding thermal material radius (for r in the range of 0.050 to 0.060 m).

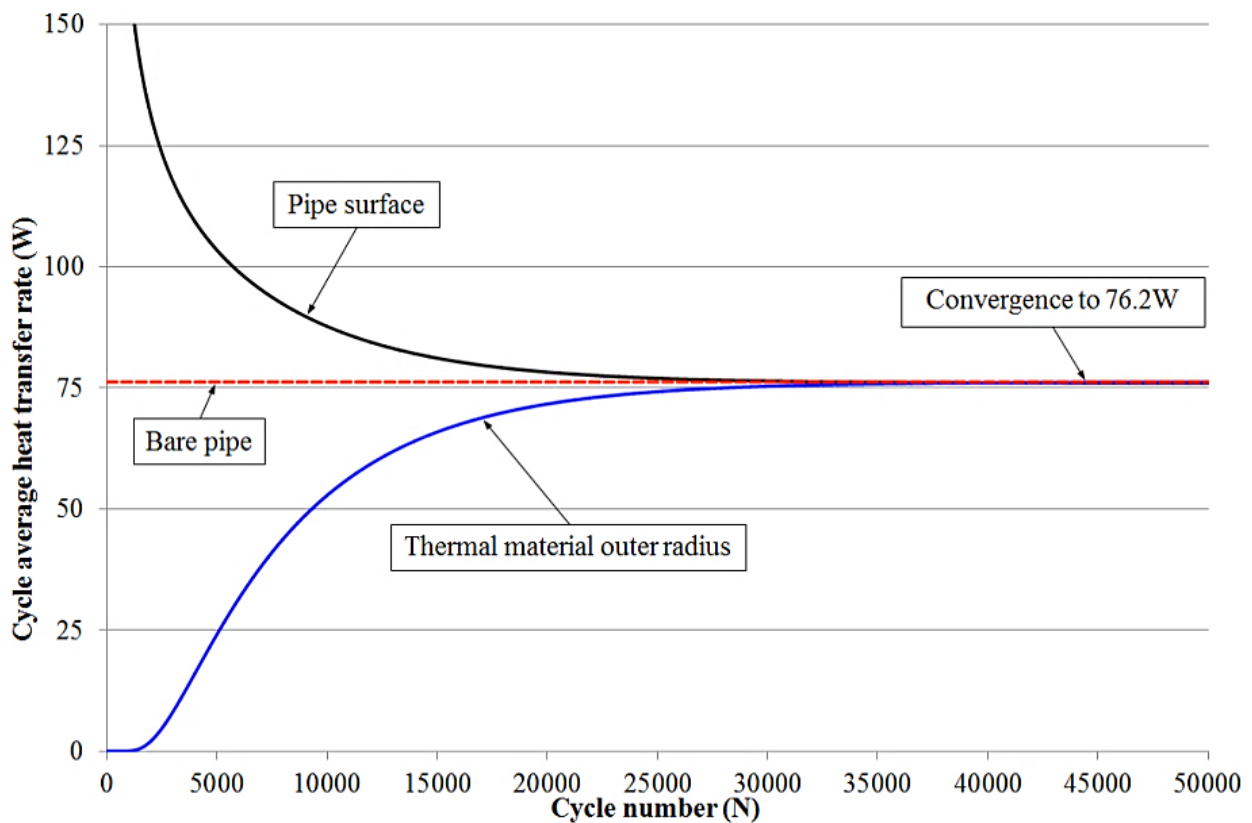


Figure 5.9 - Cycle average heat transfer rate (\dot{q}) on the pipe and thermal material surface for Case B ($r_{therm} = r_{cross} = 0.1757\text{m}$).

5.4.4.2 Transient analysis for a limited number of cycles

A simulation was conducted for Case B with cycle number up to 6,000 in the radius range from 0.025 to 0.2m. The cycle-average heat transfer rate on the pipe surface is summarized in Table 5.3 and Figure 5.10. These results are also proportional to the results of Case A, and vary by the ratio of associated duty cycles.

5.4.5 Case C Simulation ($D = 50\%$, $P = 0.2s$)

Case C provides an opportunity to assess the effect of cycle period on the associated transient heat transfer characteristics. The simulation scenarios completed for Case A and B were repeated for Case C with the following outcomes:

- As for Case A and B, the cycle-average heat transfer rate associated with Case C converges to the steady-state critical and crossover radii if the number of cycles is sufficiently high.
- The number of cycles required to stabilize to the critical and crossover radii is approximately 60,000 and 500,000 cycles respectively, i.e. ten-times that of Case A and B. Given that the period of Case C is one-tenth that of Case A and B, it is apparent that the total time required for stabilization is identical for all cases investigated.
- The cycle-average heat transfer rate converges to the same value as for Case A, which also has a duty cycle of 50%.

Table 5.3 - Cycle-average heat transfer rate at pipe surface, \hat{q}_{pipe} , for Case B (bare pipe radius is 0.025m). Red shaded values indicate that stabilization of \hat{q}_{pipe} has occurred at the associated thermal material radius. Green shaded values indicate that thermal energy has not yet propagated to r_{therm} . Critical radius (r_{cr}) identified in bold italics.

Cycle Number	Thermal material radius, r_{therm} (m)													
	0.025	0.0292	0.0333	0.0375	0.050	<i>$r_{cr}=0.0568$</i>	0.0625	0.0750	0.0875	0.1000	0.1125	0.125	0.1375	0.2000
1	76.2	4214.1	4214.6	4214.6	4214.6	4214.6	4214.6	4214.6	4214.6	4214.6	4214.6	4214.6	4214.6	4214.6
2	76.2	2343.9	2354.2	2354.2	2354.2	2354.2	2354.2	2354.2	2354.2	2354.2	2354.2	2354.2	2354.2	2354.2
3	76.2	1821.4	1842.8	1842.9	1842.9	1842.9	1842.9	1842.9	1842.9	1842.9	1842.9	1842.9	1842.9	1842.9
4	76.2	1541.9	1571.7	1572.2	1572.2	1572.2	1572.2	1572.2	1572.2	1572.2	1572.2	1572.2	1572.2	1572.2
5	76.2	1353.0	1396.3	1397.6	1397.6	1397.6	1397.6	1397.6	1397.6	1397.6	1397.6	1397.6	1397.6	1397.6
10	76.2	796.3	983.9	989.2	989.6	989.6	989.6	989.6	989.6	989.6	989.6	989.6	989.6	989.6
25	76.2	216.2	611.3	644.5	647.5	647.5	647.5	647.5	647.5	647.5	647.5	647.5	647.5	647.5
50	76.2	90.3	345.1	463.0	478.7	478.9	478.9	478.9	478.9	478.9	478.9	478.9	478.9	478.9
100	76.2	82.0	149.8	287.6	359.4	360.0	360.2	360.2	360.2	360.2	360.2	360.2	360.2	360.2
250	76.2	82.0	87.4	120.0	241.0	252.0	253.6	254.1	254.2	254.2	254.2	254.2	254.2	254.2
500	76.2	82.0	86.5	91.1	157.6	184.0	193.9	199.2	199.6	199.7	199.7	199.7	199.7	199.7
750	76.2	82.0	86.5	89.8	121.6	146.6	160.5	172.7	174.7	175.0	175.1	175.1	175.1	175.1
1000	76.2	82.0	86.5	89.8	106.1	124.9	138.5	154.7	159.1	160.0	160.1	160.1	160.1	160.1
1500	76.2	82.0	86.5	89.8	96.5	104.9	114.1	130.5	138.5	141.2	141.9	142.0	142.1	142.1
2000	76.2	82.0	86.5	89.8	94.7	98.2	103.2	115.9	124.6	128.8	130.4	130.8	131.0	131.0
2500	76.2	82.0	86.5	89.8	94.4	95.9	98.4	107.0	114.8	119.6	122.0	122.9	123.2	123.4
3000	76.2	82.0	86.5	89.8	94.3	95.2	96.3	101.5	107.9	112.6	115.4	116.7	117.3	117.6
3500	76.2	82.0	86.5	89.8	94.3	94.9	95.3	98.2	102.9	107.2	110.1	DATA NOT ASSESSED DUE TO HIGH COMPUTATIONAL COST		
4000	76.2	82.0	86.5	89.8	94.3	94.8	94.9	96.2	99.4	103.0	105.7			
4500	76.2	82.0	86.5	89.8	94.3	94.8	94.7	94.9	96.9	99.7	102.2			
5000	76.2	82.0	86.5	89.8	94.3	94.8	94.6	94.2	95.1	97.2	99.3			
5500	76.2	82.0	86.5	89.8	94.3	94.8	94.6	93.7	93.9	95.2	96.9			
6000	76.2	82.0	86.5	89.8	94.3	94.8	94.6	93.4	93.0	93.7	94.9			

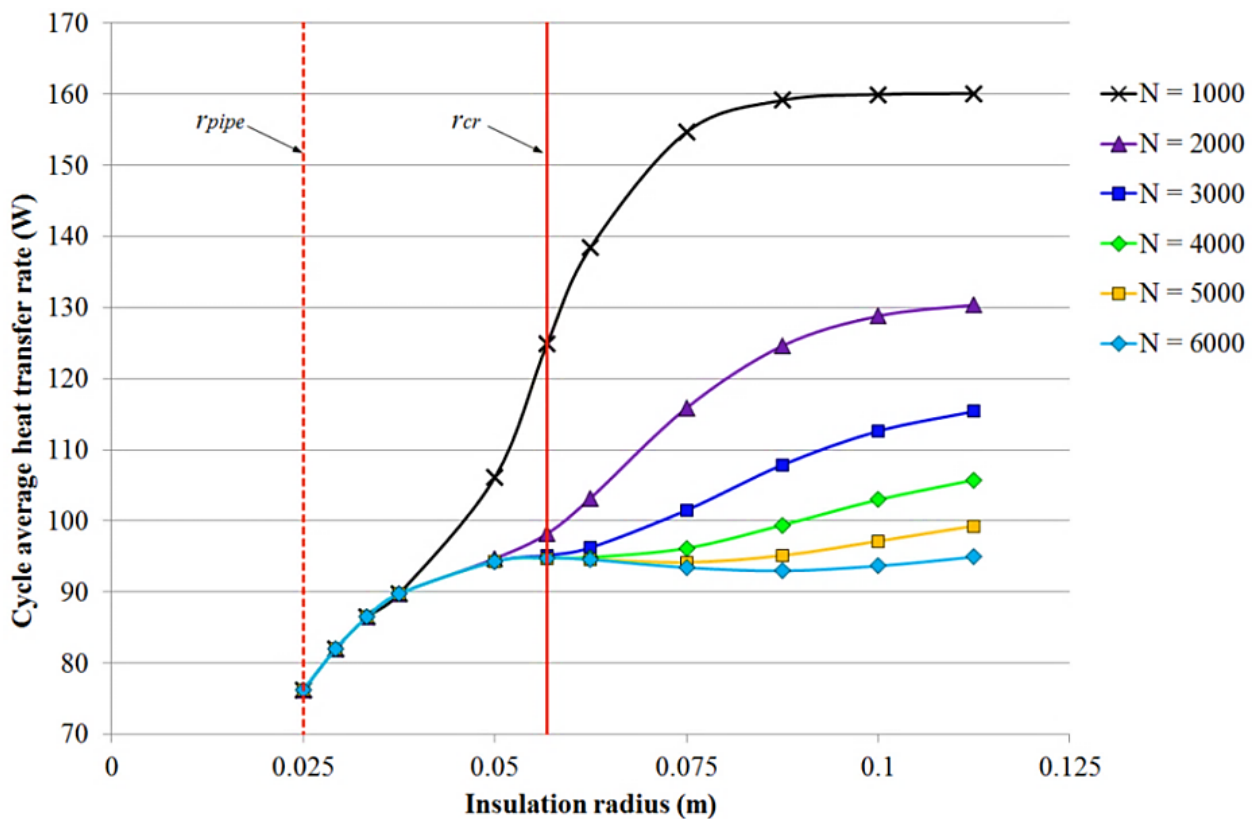
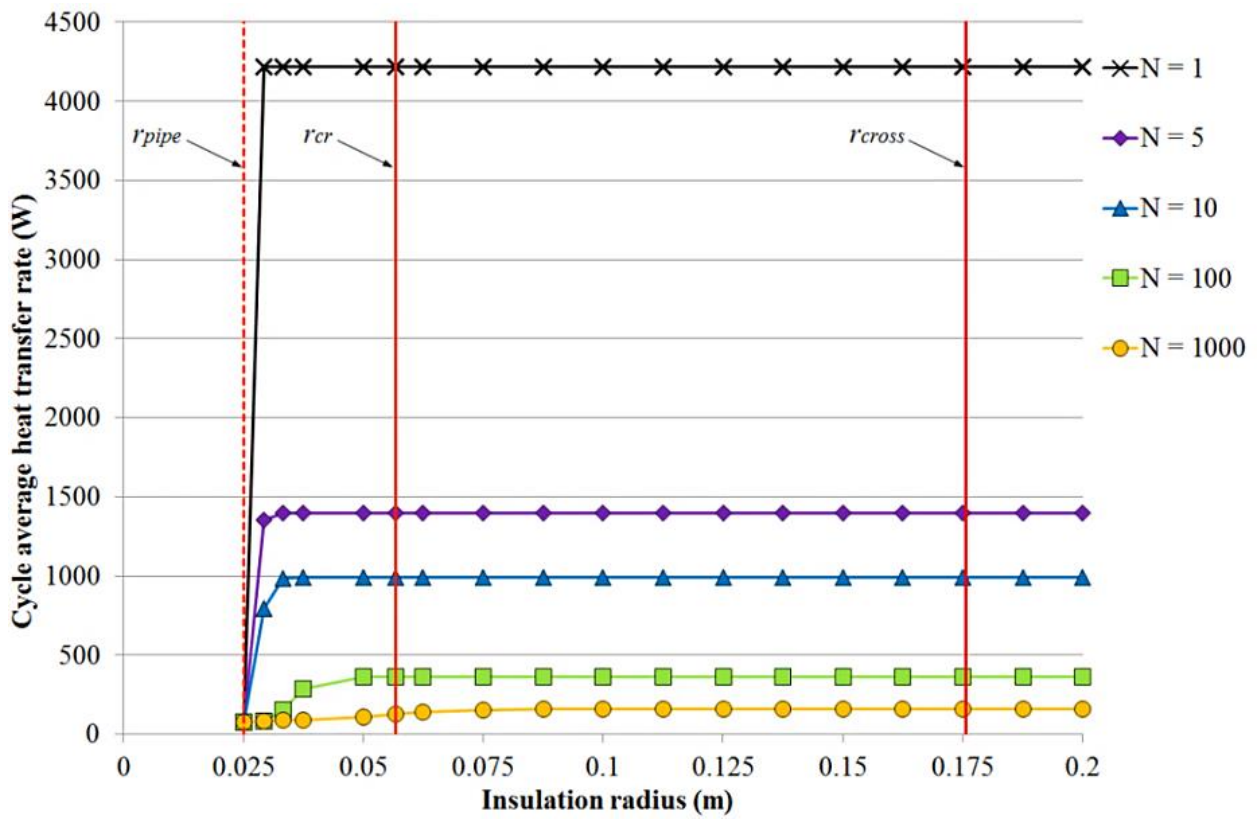


Figure 5.10 - Heat transfer rate on pipe surface versus thermal material radius for Case B. Upper: $N = 1$ to 1,000 cycles, and radius range including r_{cross} . Lower: $N = 1,000$ to 6,000 cycles, and radius range including r_{cr}

5.5 Conclusions

The FDE method developed in this work provides a flexible and useful design tool to analyse the transient heat transfer characteristics of a cylindrical system subject to transient heating. Three scenarios have been studied to draw novel conclusions between the steady-state and transient heat transfer scenarios. These conclusions are applicable generally to cylindrical thermal systems, and specifically to the design of linear SMA actuators that intend to manage cooling rates by the application of thermal lagging material. For the scenarios investigated:

- The transient thermal behaviour of the cylindrical system displays three distinct zones:
 - For relatively low thermal material radius, r_{therm} , and high N , the cycle-average heat transfer rate stabilizes to a constant value; proving that \hat{q}_{pipe} can stabilize to a quasi-static value in response to transient heating. This scenario is applicable for SMA actuators that are either cycled indefinitely, or as a worst case reference for the design of actuators for which the required number of actuation cycles is unknown.
 - For relatively high r_{therm} and low N , \hat{q}_{pipe} does not vary with increasing r_{therm} ; implying that for this zone, thermal energy is yet to propagate from the pipe to r_{therm} . This zone is of practical importance as additional thermal material does not actively contribute to \hat{q}_{pipe} for *either* objective of minimising or maximising \hat{q}_{pipe} . This zone is of practical importance for the design of SMA actuators that are infrequently actuated, or to quantify the initial response of an SMA system that is initially at ambient conditions. This reference may also allow design trade-off, whereby the initial actuator response time is initially low, and subsequent actuations, if required, may be slower.
 - For conditions between these two zones, \hat{q}_{pipe} is transient, and is a function of r_{therm} and the associated cycle number, N . For this zone, the critical and crossover radii are ill-defined. This work develops a defined method by which to assess heat transfer rates for the specific thermal material and heat transfer objective to be achieved.
- It was observed that, with increasing N : the thermal material radius, r_{therm} , required for maximum heat transfer, \hat{q}_{max} , converges to the steady-state critical radius, r_{cr} ; and, r_{therm} required for $\hat{q}_{pipe} = \hat{q}_{bare}$, converges to the steady-state crossover radius. This observation confirms that the steady state definition of both critical and crossover radius are valid for transient systems, if the number of heating-cooling cycles is sufficiently high for stabilization of the cycle-average heat transfer rate to occur. This insight enables precise lagging dimensions and materials to be specified for SMA actuator systems that

either cycle indefinitely, or as a worst case design when the required number of actuation cycles is unknown.

- For a given thermal material and system geometry, the number of heating-cooling cycles required for stabilization increases with the radius of thermal material, r_{therm} . Consequently, the critical radius stabilizes more quickly than the crossover radius.
- The total time required for stabilization is constant for a given thermal material and geometry, and is independent of duty cycle, D , and period, P , of transient heating. This insight can enable SMA manufacturers a competitive advantage by allowing the stabilization time of specific lagged SMA configurations to be formally identified and reported within the commercial literature.
- The cycle-average heat transfer rate, \hat{q} , is independent of the associated period, P , and varies linearly with the associated duty-cycle, D . From this observation, it is evident that only a single simulation is required for a given thermal material and system geometry. This data may then be extrapolated to any other duty cycle and period of interest, thereby reducing required computational cost. This could provide essential SMA design information, especially for commercial SMA suppliers. Furthermore, this insight assists in the prediction of energy requirements for intermittent joule heating control methods, (Section 3.7.4).
- When the number of transient cycles is less than that required for stabilisation, the critical and crossover radii are ill-defined. Such scenarios require explicit investigation if the associated heat transfer objective is to be achieved. These scenarios necessitate explicit simulation, and are therefore not necessarily compatible with the time constraints associated with initial design calculations; however, explicit calculation is enabled by the methods presented here, and is suitable for the detailed design phase, or to more fully understand a specific scenario of interest.
- In addition to providing direct guidance for the design of stabilised transient heat transfer scenarios, this work allow identification of the range of conditions for which the cycle average heat transfer rate is not stable, and therefore requires explicit investigation.

6. Development of one-dimensional numerical model for SMA linear actuators

The outcomes of this chapter have contributed to the following peer reviewed publication:
Numerical modeling of Shape Memory Alloy linear actuator, JM Jani, S Huang, M Leary, A Subic, Computational Mechanics 53(3), 443-461, 2015, DOI: 10.1007/s00466-015-1180-z.

6.1 Chapter summary

The demand for shape memory alloy (SMA) actuators in high-value technology applications is increasing; however, there exist technical challenges to the commercial application of SMA actuator technologies, especially associated with the prediction of actuation duration. Excessive activation duration results in actuator damage due to overheating while excessive deactivation duration is not practical for high-frequency applications. Novel analytical and finite difference equation (FDE) models were developed in this work to predict the activation and deactivation durations and associated SMA thermomechanical behaviour under variable environmental and design conditions. Relevant factors, including latent heat effects, induced stress and material property variability are accommodated. An existing constitutive model was integrated into the proposed models to generate custom SMA stress-strain curves. Strong agreement was achieved between the proposed numerical models and experimental results; confirming their applicability for predicting the behaviour of SMA actuators with variable thermomechanical conditions.

6.2 Introduction

As reported in chapter 4, numerous numerical models were developed to predict and optimize SMA thermomechanical behaviour; and to reduce the development cost and time (Achenbach, 1989; Boyd & Lagoudas, 1996; S. Huang *et al.*, 2013; DC Lagoudas, 2010; Majumdar, 2005; Çengel & Ghajar, 2011). Multi-dimensional models are favourable for solving complex problems of greater generality, while one-dimensional models are favourable for solving non-complex geometries (e.g. as typically observed in SMA linear actuators) with low computational overheads. However, the available 1-D models require numerous experimental parameters, and therefore present practical challenges to their application.

The 1-D analytical and FDE heat transfer models developed in this work allow flexibility to solve the heat transfer problem for both single (martensite and austenite) or transition (martensite-austenite) phases within a single numerical model, whereas existing methods may require multiple distinct models (refer Section 6.3). The developed heat transfer models

are further integrated with existing constitutive model (Section 4.3.3) and are compared with existing models and experimental data for verification (Section 6.7.3).

Fundamental heat transfer theories applied in the developed numerical model are summarized in Section 6.3. An overview of existing hysteresis, heat transfer, and constitutive models is presented in Chapter 4. The numerical model development is reported in Section 6.3, and discussed in Section 6.7, including: identification of modelling parameters (Section 6.7.1), numerical modelling stages (Section 6.7.2), experimental validation (Section 6.7.3) and SMA actuator performance analysis (Section 6.7.4). Finally, recommendations for future work and a summary of this work are provided in Section 6.8.

6.3 Existing 1-D heat transfer models

Many 1-D heat transfer models have been developed to predict the thermomechanical SMA behaviour (Hoffman & Frankel, 2001; Iserles, 1996; DC Lagoudas, 2010; Majumdar, 2005; N. Ozisik, 1994; GD Smith, 1985). However, most existing models use the lumped capacitance model (refer Section 4.3.2.3) for the martensitic and austenite phase calculation and a custom latent heat model for the phase transformation calculation, such as: the empirical model by Bhattacharyya *et al.* (1995); the polynomial kinetic law approach by Brailovski *et al.* (1996); the simplified analytical model by Potapov and Da Silva (2000); and, the analytical solution by Ramiro and Edwige (2012).

The Brailovski *et al.* (1996) latent heat model requires experimentally acquired coefficients, and numerous dimensionless and separable equations are employed by (Potapov & Da Silva, 2000) and (2012), respectively. The application of multiple models, prerequisite experimental coefficients and numerous equations provides a technical barrier to practical application. The models proposed and developed in this work reduce solution complexity and provides a flexible solutions that can be readily applied, especially within the early design phases.

6.4 New 1-D numerical model development

In this work, the uniform cylindrical SMA is actuated by Joule heating while the outer boundary is subject to convection (either free or forced) with the environment at constant temperature, T_∞ (Figure 6.1). As the physical size and driving temperature difference of the SMA actuators investigated is relatively low, the heating and cooling processes can be assumed to vary uniformly throughout the SMA actuator, and phase heterogeneity due to non-isothermal phase change is negligible. The numerical interactions of the proposed numerical model is schematically illustrated in Figure 6.2.

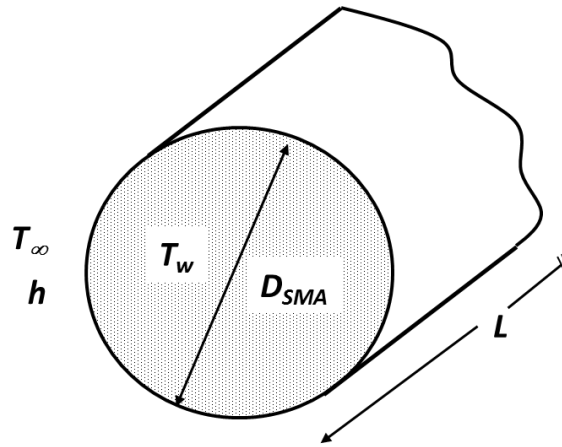


Figure 6.1 - SMA geometry and boundary conditions

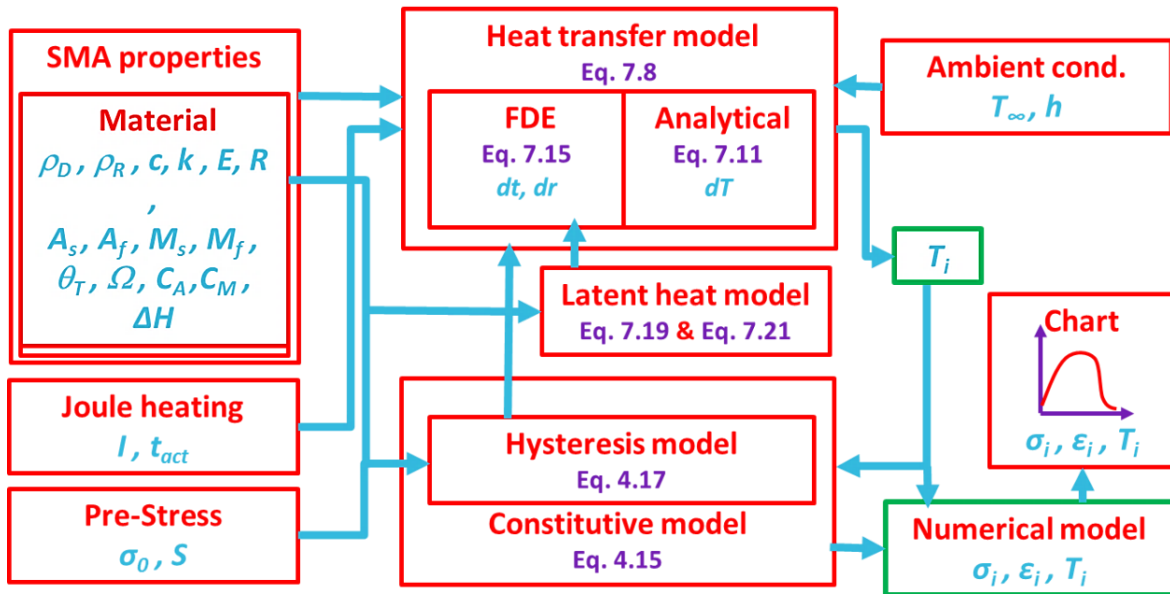


Figure 6.2 - Schematic diagram of proposed numerical model

The Liang and Rogers (1997) phenomenological model was found to be adequate for this work to generate stress-strain data from the novel heat transfer models, and (Eq. 4.14) to (Eq. 4.16) are applied for the SMA-spring system (Figure 6.3) used in this study.

6.4.1 Energy balance model

The 1-D heat transfer model developed in this thesis is based on the energy balance model (Eq. 6.1), where the energy input for SMA electrical heating (E_{elec}) is transformed into heat energy (E_{heat}), mechanical energy (E_{mech}), and energy losses (E_{loss}) (Figure 6.3).

$$\underbrace{E_{elec}}_{\text{Input energy}} = \underbrace{E_{heat} + E_{mech} + E_{loss}}_{\text{Output energy}} \quad (\text{Eq. 6.1})$$

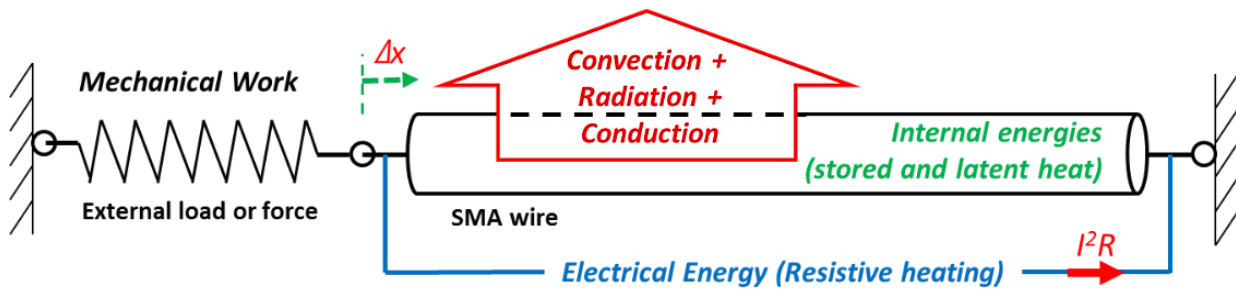


Figure 6.3 - Energy balance for SMA actuator

6.4.1.1 Resistive heating energy

Resistive heating is commonly utilized as the input energy for SMA actuation due to the associated (Kohl, 2010; K Otsuka & Wayman, 1999): control simplicity, versatility, clean operation and high efficiency of energy conversion (i.e. essentially 100% conversion efficiency). According to Joule's first law (also known as the Joule effect), heat is generated due to electron collision with atomic ions (i.e. electrical flow resistance) when a current passes through a conductor. The heat generated by Joule heating, E_{elec} , is expressed in (Eq. 6.2), where I is the electrical current supplied, R_{tot} is the total resistance and dt is the infinitesimal heating duration (Walker, 2008).

$$E_{elec} = I^2 \cdot R_{tot} \cdot dt \quad (\text{Eq. 6.2})$$

The relationship between electrical resistance, R_{tot} , and material resistivity, $\rho_{R(tot)}$, is a function of the initial length, L_o and the associated cross-section area, A , (Eq. 6.3). SMA materials with high resistivity actuate more quickly for a given input current and heating duration. Due to this thermomechanical advantage (i.e. high resistivity), NiTi SMA are preferable to iron or copper-based SMA for many commercial applications (Mohd Jani, Leary, Subic, *et al.*, 2014).

$$R_{tot} = \left[\frac{\rho_{R(tot)} \cdot L_o}{A} \right] \quad (\text{Eq. 6.3})$$

Material resistivity and resistive heating performance varies with numerous factors, including material thickness, material composition and phase change (Novák, Šittner, Dayananda, Braz-Fernandes, & Mahesh, 2008). In this work, the martensite volume fraction (ξ_M) is used to accommodate material variability (e.g. Young's modulus, thermal conductivity and resistivity) due to the phase changes, as expressed in (Eq. 6.4) for the material resistivity (Novák *et al.*, 2008); where $\rho_{R(M)}$ and $\rho_{R(A)}$ are the resistivity function of the martensite and austenite phases respectively.

$$\rho_{R(tot)} = \left[\rho_{R(M)} \xi_M + \rho_{R(A)} (1 - \xi_M) \right] \quad (\text{Eq. 6.4})$$

The resistivity of each phase can be determined from constant stress experimental trials, and is commonly provided by the SMA manufacturer, while the martensite volume fraction, ξ_M can be calculated from the hysteresis model (Section 4.3.4).

6.4.1.2 Internal heat energy

Numerous studies have demonstrated that the effect of the latent heat of transformation in SMA actuation is significant and cannot be neglected (Bekker & Brinson, 1998; DC Lagoudas & Bo, 1999). The input energy from resistive heating is transformed into internal heating energy, and consists of stored thermal energy and the latent heat of the martensitic phase transformation. This internal heat energy can be calculated as shown in (Eq. 6.5), where ρ_D is the density, V is the volume, c is the specific heat capacity, T_w is the SMA actuator temperature, T_∞ is the ambient temperature, ΔH is the integrated latent heat for transformation, and ξ_M is the martensite phase volume fraction.

$$E_{heat} = \underbrace{\rho_D \cdot V \cdot c \cdot (dT_w)}_{\text{stored thermal energy}} + \underbrace{\rho_D \cdot V \cdot (\Delta H) \cdot |d\xi_M|}_{\text{Latent heat energy}} = \rho_D \cdot V [c(dT_w) + \Delta H |d\xi_M|] \quad (\text{Eq. 6.5})$$

The latent heat energy tends to increase the heating and cooling duration of SMA actuators, and can be measured by differential scanning calorimetry (DSC) (Figure 2.3) or constant-stress experimental trials, and is commonly reported by the SMA manufacturer. The latent heat effect can be neglected for resistive heating with high current density (i.e. in excess of 2A/mm²) (V. Brailovski *et al.*, 1996), but its influence on cooling duration should always be taken into consideration.

6.4.1.3 Mechanical energy

During heating, the SMA contracts to generate useful mechanical work. The measured force, F_{act} and contraction displacement (or stroke), Δx are used to identify the mechanical energy delivered by the actuator system, (Eq. 6.6) (Neugebauer *et al.*, 2010b), where L_o is the initial length, and ε_{total} is the total strain.

$$E_{mech} = F_{act} \cdot \Delta x = F_{act} \cdot L_o \cdot \varepsilon_{tot} \quad (\text{Eq. 6.6})$$

Studies have shown that the mechanical energy affecting the thermomechanical process in the SMA linear actuator is negligible (Neugebauer *et al.*, 2010b); however, the stress dependency of SMA transformation temperatures must be considered in the numerical model (Auricchio & Lubliner, 1997; Brinson, 1993; De la Flor *et al.*, 2006; Liang & Rogers, 1997; K. Tanaka, 1986). The mechanical effect of the bias-force is incorporated within the constitutive model (Section 4.3.3).

6.4.1.4 Thermal energy loss

The thermal energy loss contributes a crucial element to the energy conversion in the system, in particular during cooling. The thermal energy loss, E_{loss} involves conductive, convective and radiation losses as expressed in (Eq. 6.7), where k is the thermal conductivity, A is the cross-sectional area, A_{sf} is the surface area, T_∞ is the ambient temperature, ε' is the emissivity, and σ' is the Stephen-Boltzmann constant. The associated heat conduction, heat convection and heat radiation may be developed from Fourier's Law, Newton's law of cooling and Stephen-Boltzmann's Law respectively (Bergman *et al.*, 2011; Carslaw & Jaeger, 1959; Walker, 2008; Çengel & Ghajar, 2011). The effect of radiation was ignored in this work due to the low associated driving temperature difference (Bergman *et al.*, 2011; Neugebauer *et al.*, 2010b; Çengel & Ghajar, 2011), as the operating temperature was below 100°C. The internal resistance of the body to heat conduction is negligible according to the lumped heat capacity method (Bergman *et al.*, 2011; V. Brailovski *et al.*, 1996; Tadesse *et al.*, 2010; Çengel & Ghajar, 2011).

$$E_{loss} = \underbrace{kA \frac{(T_w - T_\infty)}{dx} \cdot dt}_{\text{conduction energy}} + \underbrace{hA_{sf}(T_w - T_\infty) \cdot dt}_{\text{convection energy}} + \underbrace{\varepsilon' \sigma' A_{sf}(T_w^4 - T_\infty^4) \cdot dt}_{\text{radiation energy}} \quad (\text{Eq. 6.7})$$

The remaining convective energy can be calculated from the correlation equations in Section 3.7.3.1 or can be estimated with FDE simulation as described in (Mohd Jani *et al.*, 2015a).

6.4.2 Analytical heat transfer model

Referring to (Eq. 6.5), (Eq. 6.6) and (Eq. 6.7), the heat transfer relationship for a cylindrical SMA actuator can be generalized as (Eq. 6.8), where $E_{Elect} = 0$ during the cooling cycles. Mechanical energy is not included in (Eq. 6.8), but incorporated in (Eq. 6.9) and (Eq. 6.10) for the transformation temperature variations as described in Section 4.3.3.

$$\underbrace{\rho_D \cdot V [c \cdot dT_w + (\Delta H) \cdot d\xi_M]}_{E_{Heat}} = \underbrace{I^2 R_{tot} \cdot dt}_{E_{Elect}} - \underbrace{hA_{sf}(T_w - T_\infty) \cdot dt}_{E_{Loss}} \quad (\text{Eq. 6.8})$$

Substituting hysteresis equations (Eq. 4.26) into (Eq. 6.8), the heat transfer equation can be summarized as (Eq. 6.9) and (Eq. 6.10) for heating and cooling cycles respectively (Shahin *et al.*, 1994).

$$\begin{aligned} \rho_D \cdot V \left[c + \frac{\pi(\Delta H)}{2 \cdot (A_{f(new)} - A_{s(new)})} \cdot \sin \left(\pi \left(\frac{T_{w(new)} - A_{s(new)}}{A_{f(new)} - A_{s(new)}} \right) \right) \right] \cdot dT_w \\ = [I^2 R_{tot} - hA_{sf}(T_w - T_\infty)] \cdot dt \end{aligned} \quad (\text{Eq. 6.9})$$

$$\begin{aligned} \rho_D \cdot V \left[c + \frac{\pi(\Delta H)}{2 \cdot (M_{s(new)} - M_f)} \cdot \sin \left(\pi \left(\frac{T_{w(new)} - M_f}{M_{s(new)} - M_f} \right) \right) \right] \cdot dT_w \\ = -hA_{sf}(T_w - T_\infty) \cdot dt \end{aligned} \quad (\text{Eq. 6.10})$$

Thus, a flexible *analytical heat transfer model* has been developed that accommodates the latent heat of transformation and material variation for the entire thermomechanical cycle, including heating (Eq. 6.9), and cooling cycles (Eq. 6.10), as expressed in (Eq. 6.11).

$$\begin{aligned}
dt &= \frac{\rho_D \cdot V \left[c + \frac{\pi(\Delta H)}{2 \cdot (A_{f(new)} - A_{s(new)})} \cdot \sin \left(\pi \left(\frac{T_w - A_{s(new)}}{A_{f(new)} - A_{s(new)}} \right) \right) \right] \cdot dT}{\underbrace{[I^2 R_{tot} - h A_{sf} (T_w - T_\infty)]}_{\text{Heating cycle}}} dt dt \\
&= \frac{\rho_D \cdot V \left[c + \frac{\pi(\Delta H)}{2 \cdot (M_{s(new)} - M_{f(new)})} \cdot \sin \left(\pi \left(\frac{T_w - M_{f(new)}}{M_{s(new)} - M_{f(new)}} \right) \right) \right] \cdot dT}{\underbrace{[-h A_{sf} (T_w - T_\infty)]}_{\text{Cooling cycle}}} dt dt
\end{aligned} \tag{Eq. 6.11}$$

6.4.3 Finite difference method

During the heating cycle, the boundary conditions are based on the temperature increase within the SMA actuator, $0 \leq r < r_{SMA}$, due to Joule heating (Eq. 6.12), and thermal loss at the SMA actuator surface, $r = r_{SMA}$, due to convection to the ambient environment (Eq. 6.13). During the cooling cycle, no heat generation occurs within the SMA, $\dot{G}=0$, and the temperature reduces monotonically due to the convective heat losses to the ambient environment.

$$k \frac{\partial T}{\partial r} \Big|_{r \leq r_{SMA}} = \dot{G} = \left[\frac{I^2 R}{V} \right] \tag{Eq. 6.12}$$

$$k \frac{\partial T}{\partial r} \Big|_{r=r_{SMA}} = \frac{-2h[T_{Surf}-T_\infty]}{r_{SMA}} \tag{Eq. 6.13}$$

By applying Taylor series and Fourier's Law for Crank-Nicholson (central) FDE (Eq. 6.14), the equation can be separated into two groups (Eq. 6.15), associated with nodes with known and unknown temperatures (Crank & Nicolson, 1947; Majumdar, 2005; N. Ozisik, 1994), which is simplified as a Fourier number, $F_o = \frac{\alpha \Delta t}{\Delta r^2}$ (refer Section 4.4.1.1).

$$\frac{T_n^{t+1} - T_n^t}{\alpha \Delta t} = \underbrace{\frac{T_{n+1}^t - 2T_n^t + T_{n-1}^t}{2(\Delta r)^2}}_{\text{explicit}} + \underbrace{\frac{T_{n+1}^{t+1} - 2T_n^{t+1} + T_{n-1}^{t+1}}{2(\Delta r)^2}}_{\text{implicit}} + \left[\frac{I^2 R}{V} \right] \frac{1}{k} - \frac{2h \cdot [T_{surf} - T_\infty]}{k \cdot r_{SMA}} \tag{Eq. 6.14}$$

$$\begin{aligned}
\underbrace{-\frac{F_o}{2} T_{n+1}^{t+1} + (1 + F_o) T_n^{t+1} - \frac{F_o}{2} T_{n-1}^{t+1}}_{\text{Unknown nodes}} &= \underbrace{\frac{F_o}{2} T_{n+1}^t + (1 - F_o) T_n^t + \frac{F_o}{2} T_{n-1}^t}_{\text{Known nodes}} + \\
\underbrace{\frac{F_o(\Delta r^2)}{k} \left[\frac{I^2 R}{V} \right]}_{\text{Joule Heating}} &- \underbrace{\frac{F_o(\Delta r^2)}{k} \frac{2h[T_{surf} - T_\infty]}{r_{SMA}}}_{\text{Convection}}
\end{aligned} \tag{Eq. 6.15}$$

The unknown nodal temperatures are calculated from the known nodal temperatures by the matrix inversion technique (Crank & Nicolson, 1947; Majumdar, 2005; N. Ozisik, 1994), Figure 6.4, where matrix A consists of the coefficients of the known and unknown nodes, matrix B consists of the known nodes (including E, Joule heating and convection components) and matrix C consists of unknown nodes. The node coefficients for $i=2,3,\dots,N-1$ are: $a_i = c_i = -\frac{Fo}{2}$, $b_i = 1 + Fo$, $d_i = \frac{Fo}{2}T_{n-1}^t + (1 - Fo)T_n^t + \frac{Fo}{2}T_{n+1}^t$ and $E = \frac{Fo(\Delta r^2)}{k} \left[\frac{I^2 R}{V} \right] - \frac{Fo(\Delta r^2)}{k} \frac{2h[T_{surf}-T_\infty]}{r_{SMA}}$. Boundary conditions are: $b_1 = 1$, $c_1 = 0$, $d_1 = T_1^t$, $a_N = 0$, $b_N = 1$ and $d_N = T_N^t$.

$$\underbrace{\begin{bmatrix} b_1 & c_1 & 0 & 0 & \dots & \dots & 0 \\ a_2 & b_2 & c_2 & 0 & \dots & \dots & 0 \\ 0 & a_3 & b_3 & c_3 & 0 & \dots & 0 \\ 0 & 0 & \ddots & \ddots & \ddots & \ddots & \vdots \\ \vdots & \vdots & \ddots & \ddots & \ddots & \ddots & 0 \\ 0 & \dots & \dots & \ddots & \ddots & b_{N-1} & c_{N-1} \\ 0 & 0 & \dots & \dots & 0 & a_N & b_N \end{bmatrix}}_{\mathbf{A}} \underbrace{\begin{bmatrix} T_1^{t+1} \\ T_2^{t+1} \\ T_3^{t+1} \\ \vdots \\ \vdots \\ T_{N-1}^{t+1} \\ T_N^{t+1} \end{bmatrix}}_{\mathbf{C}} = \underbrace{\begin{bmatrix} d_1 \\ d_2 \\ d_3 \\ \vdots \\ \vdots \\ d_{N-1} \\ d_N \end{bmatrix}}_{\mathbf{B}} + \mathbf{E}$$

Figure 6.4 - Sample of a matrix form for finite difference equation

The proposed model is compatible with multi-dimensional models. Furthermore, the compatibility of FDE to define variable node and boundary conditions allows the model to be extended to solve a more general class of heat transfer problems, for example accommodating phase heterogeneity.

6.4.3.1 Latent heat for finite different method

During phase transition, the boundary condition at the austenite-martensite interface can be described as in (Eq. 6.16) based on the Neumann problem (S. Huang *et al.*, 2013; K. Tanaka, 1986); where T_M and T_A are the martensitic and austenitic temperatures, and k_M and k_A are the martensitic and austenitic thermal conductivities respectively.

$$k_M \frac{\partial T_M}{\partial r} - k_A \frac{\partial T_A}{\partial r} = \rho(\Delta H) \frac{dr}{dt} \quad (\text{Eq. 6.16})$$

This boundary condition (Eq. 6.16) has been utilized by numerous researchers to develop latent heat models (Bonacina *et al.*, 1973; CK Chun, 2000; Voller, Cross, & Markatos, 1987). In these models, latent heat is approximated by a finite temperature dependent thermal conductivity or/and heat capacity over the latent heat temperature range, and density across phases is assumed constant. Heat transfer models developed for FDM are: the effective specific heat method (Bonacina *et al.*, 1973) that treats latent heat as an effective specific heat in the energy equation; the enthalpy method (Voller *et al.*, 1987) where the heat conditions on the moving phase front are used in advance, and the heat conditions at the phase change are not required; and, the fixed-grid FDM (CK Chun, 2000) which eliminate temperature oscillations and phase front. Referring to (Eq. 6.9) and (Eq. 6.10), the latent heat component can be replaced by equivalent parameters for specific heat capacity and thermal conductivity.

The effective specific heat model is commonly proposed for numerical models due to its computational advantages (i.e. high speed and compatibility with numerical models) and high result accuracy (Bonacina *et al.*, 1973). The latent heat transformation effect can be derived from the equations for effective specific heat capacity, (Eq. 6.17), and effective thermal conductivity, (Eq. 6.18) (Bonacina *et al.*, 1973), where $\Delta T = \frac{A_{f(new)} - A_{s(new)}}{2} = \frac{M_{s(new)} - M_{f(new)}}{2}$ and the peak temperature, $T_p = A_{s(new)} + \Delta T = M_{f(new)} + \Delta T$.

$$c_{eff} = \frac{1}{2}(c_M + c_A) + \frac{\Delta H}{2\Delta T} \quad (\text{Eq. 6.17})$$

$$k_{eff} = k_M + \frac{k_A - k_M}{2\Delta T} [T_w - (T_p - \Delta T)] \quad (\text{Eq. 6.18})$$

A similar approach was used by Bhattacharyya *et al.* (1995) for his empirical model, where the material heat capacity is modified to accommodate latent heat effects.

6.4.4 Alternative latent heat models

In addition, two latent heat models have been developed in this work (Eq. 6.19) and (Eq. 6.20) as an alternative to the effective specific heat capacity (ESHC) model (Eq. 6.17). These models are applicable for both analytical and FDE applications, and are based on the latent heat component from (Eq. 6.9) and (Eq. 6.10), and the martensite fraction (ξ_M) from Section 4.3.4.

$$c_{eff} = \underbrace{\frac{1}{2}(c_M + c_A) + \frac{\pi \cdot \Delta H}{4\Delta T} \sin\left(\pi \left(\frac{T_w - A_{s(new)}}{A_{f(new)} - A_{s(new)}}\right)\right)}_{\text{Heating cycle}} \quad (\text{Eq. 6.19})$$

$$= \underbrace{\frac{1}{2}(c_M + c_A) + \frac{\pi \cdot \Delta H}{4\Delta T} \sin\left(\pi \left(\frac{T_w - M_{f(new)}}{M_{s(new)} - M_{f(new)}}\right)\right)}_{\text{Cooling cycle}}$$

$$c_{eff} = \frac{1}{2}(c_M + c_A) + \frac{\Delta H}{\Delta T} \sin(\pi \cdot \xi) \quad (\text{Eq. 6.20})$$

Alternatively, the martensitic phase fraction can replace the effective thermal conductivity model (Eq. 6.18) as derived in (Eq. 6.21). A similar approach has also been applied for other phase-dependant material properties (e.g. resistivity (Eq. 6.4) and Young's modulus).

$$k_{eff} = k_M \cdot \xi_M + k_A \cdot (1 - \xi_M) \quad (\text{Eq. 6.21})$$

6.4.5 Fast prediction with simplified analytical model and graphical solution charts

As discussed in Chapter 4 and previous sections in this chapter, numerous analytical and numerical models have been introduced to predict the thermomechanical behaviour of SMA linear actuators. However, these solutions are difficult to evaluate due to involvement of infinite series and implicit equations. Therefore, simplified analytical model, tabular or graphical form solutions are beneficial to designers to reduce these complex calculations and extending their practical applicability (Gurney & Lurie, 1923; Çengel & Ghajar, 2011), such as the Heisler (1947) and the Gröber (1961) charts for solving transient heat transfer of uniform geometries. Furthermore, these simplified solutions can reduce the development cost and time, and overcomes the need for applying complex modelling and accessing high performance computers.

As highlighted in Chapter 3, three critical factors in SMA actuator design are: Load, Speed and Stroke. Load requirements can typically be technically achieved by SMA actuators, due to their high power ratio compared to other conventional actuators (refer Chapter 2). The heating and cooling durations significantly influence SMA actuator speed, while optimum stroke can be achieved with optimal heating duration and an optimised design approach, for example, by the application of pulley systems (Chapter 7). In addition, correct heating duration is crucial for robust and predictable SMA response, as well as to achieve acceptable functional and structural fatigue; where excessive heating reduces fatigue life and stability, and insufficient heating compromises stroke performance (Mohd Jani *et al.*, 2016). In response to this requirement for SMA response prediction, a simplified analytical model for the estimation of SMA actuation and deactivation time is developed, as well as associated graphical solution charts. These design tools have been developed to assist in the SMA design process, especially during the early design phase, where rapidly applied models are of significant value to achieving timely and robust design outcomes.

6.4.5.1 Simplified analytical model

For SMA, the material experiences three phases during heating and cooling cycles: martensite, martensite-austenite (transition or latent heat phase) and austenite. In this work, the theoretically optimum activation and deactivation durations are the key outcomes of the simplified analytical model. Activation duration is estimated from the ambient temperature, T_∞ , to the new austenite final temperature, $A_{f(new)}$; and the deactivation duration is estimated from $A_{f(new)}$, to the new martensite final temperature, $M_{f(new)}$. The analytical model (Eq. 6.11) is further simplified into (Eq. 6.22) and (Eq. 6.23). The calculations for new transformation temperatures can be referred to in section 4.3.3.1.

$$dt_{Activation} = \underbrace{\frac{\rho_D \cdot V [c_M (A_{s(new)} - T_\infty)]}{I^2 R_M - h A_{sf} \left(\frac{A_{s(new)} + T_\infty}{2} - T_\infty \right)}}_{T_\infty \rightarrow A_{s(new)}} + \underbrace{\frac{\rho_D \cdot V (\Delta H)}{I^2 \left(\frac{R_M + R_A}{2} \right) - h A_{sf} \left(\frac{A_{f(new)} + A_{s(new)}}{2} - T_\infty \right)}}_{A_{s(new)} \rightarrow A_{f(new)}} \quad (\text{Eq. 6.22})$$

$$dt_{Deactivation} = \underbrace{\frac{\rho_D \cdot V [c_A (M_{s(new)} - A_{f(new)})]}{-h A_{sf} \left(\frac{M_{s(new)} + A_{f(new)}}{2} - T_\infty \right)}}_{A_{f(new)} \rightarrow M_{s(new)}} + \underbrace{\frac{\rho_D \cdot V (-\Delta H)}{-h A_{sf} \left(\frac{M_{f(new)} + M_{s(new)}}{2} - T_\infty \right)}}_{M_{s(new)} \rightarrow M_{f(new)}} \quad (\text{Eq. 6.23})$$

The simplified analytical model can be further expressed as current density, $J = \frac{I}{A}$, and total material resistivity, ρ_R , as derived in (Eq. 6.24) and (Eq. 6.25) for activation and deactivation durations, respectively.

$$dt_{Activation} = \underbrace{\frac{\rho_D [c_M (A_{s(new)} - T_\infty)]}{J^2 \rho_{R(M)} - \frac{4h}{D} \left(\frac{A_{s(new)} + T_\infty}{2} - T_\infty \right)}}_{a_1 = T_\infty \rightarrow A_{s(new)}} + \underbrace{\frac{\rho_D (\Delta H)}{J^2 \left(\frac{\rho_{R(M)} + \rho_{R(A)}}{2} \right) - \frac{4h}{D} \left(\frac{A_{f(new)} + A_{s(new)}}{2} - T_\infty \right)}}_{a_2 = A_{s(new)} \rightarrow A_{f(new)}} \quad (\text{Eq. 6.24})$$

$$dt_{Deactivation} = \underbrace{\frac{\rho_D [c_A (M_{s(new)} - A_{f(new)})]}{-\frac{4h}{D} \left(\frac{M_{s(new)} + A_{f(new)}}{2} - T_\infty \right)}}_{b_1 = A_{f(new)} \rightarrow M_{s(new)}} + \underbrace{\frac{\rho_D (-\Delta H)}{-\frac{4h}{D} \left(\frac{M_{f(new)} + M_{s(new)}}{2} - T_\infty \right)}}_{b_2 = M_{s(new)} \rightarrow M_{f(new)}} \quad (\text{Eq. 6.25})$$

Therefore, the SMA activation and deactivation durations can be estimated directly with this simplified analytical model.

6.4.5.2 Response charts

To assist SMA developers and designers in estimating SMA response durations with low computational complexity or direct simulation requirements, novel response charts with variable ambient temperatures are created from this simplified analytical model. (Eq. 6.24) and (Eq. 6.25) are approximated into linear equations as expressed in (Eq. 6.29) and (Eq. 6.30) for activation and deactivation durations, respectively.

For the activation duration, the response chart begins from the minimum current density, J_{min} , as derived in (Eq. 6.26).

$$J_{min} > \sqrt{\frac{4h(A_{f(new)} + A_{s(new)} - 2T_{\infty})}{D(\rho_{R(M)} + \rho_{R(A)})}} \quad (\text{Eq. 6.26})$$

The slope or gradient, $m = \frac{dt_2 - dt_1}{J_2 - J_1}$, of activation response chart can be precisely calculated with (Eq. 6.27), where $dt_{Act(J=100)}$ and $dt_{Act(J=10)}$ can be calculated from (Eq. 6.22) or (Eq. 6.24).

$$m = \left(\log \left[\frac{\rho_D [c_M (A_{s(new)} - T_{\infty})]}{10^{16} \rho_{R(M)} - \frac{4h(A_{s(new)} + T_{\infty})}{2} - T_{\infty}} + \frac{\rho_D (\Delta H)}{10^{16} \left(\frac{\rho_{R(M)} + \rho_{R(A)}}{2} \right) - \frac{4h(A_{f(new)} + A_{s(new)} - T_{\infty})}{2}} \right] - \log \left[\frac{\rho_D [c_M (A_{s(new)} - T_{\infty})]}{10^{15} \rho_{R(M)} - \frac{4h(A_{s(new)} + T_{\infty})}{2} - T_{\infty}} + \frac{\rho_D (\Delta H)}{10^{15} \left(\frac{\rho_{R(M)} + \rho_{R(A)}}{2} \right) - \frac{4h(A_{f(new)} + A_{s(new)} - T_{\infty})}{2}} \right] \right) / (\log 100 - \log 10) \quad (\text{Eq. 6.27})$$

However, based on numerous trials with the proposed predictive model, the slope of the activation response chart can be approximated as $m=-2$ and the y-intercept point at $\log (J = 1)$ can be expressed as (Eq. 6.28).

$$\log(dt)_{Act(J=1)} = \frac{-(-2)\log(\log 100 - \log 1)}{-m(\log J_{100} - \log J_1)} + \underbrace{\log \left[\frac{\rho_D [c_M (A_{s(new)} - T_{\infty})]}{10^{16} \rho_{R(M)} - \frac{4h(A_{s(new)} + T_{\infty})}{2} - T_{\infty}} + \frac{\rho_D (\Delta H)}{10^{16} \left(\frac{\rho_{R(M)} + \rho_{R(A)}}{2} \right) - \frac{4h(A_{f(new)} + A_{s(new)} - T_{\infty})}{2}} \right]}_{\log dt_{Act(J=100)}} \quad (\text{Eq. 6.28})$$

Therefore the linear equation for activation response chart can be expressed as (Eq. 6.29).

$$\log(dt)_{Act} = -2\log(J) + \log(dt)_{Act(J=1)} \quad (\text{Eq. 6.29})$$

For deactivation duration chart, the approximated linear equation can be expressed as (Eq. 6.30).

$$\log(dt)_{Deact} = -\log(h) + \log \left[\frac{\rho_D D}{2} \left(\frac{c_A (A_{f(new)} - M_{s(new)})}{-2T_{\infty} + A_{f(new)} + M_{s(new)}} + \frac{\Delta H}{-2T_{\infty} + M_{s(new)} + M_{f(new)}} \right) \right] \quad (\text{Eq. 6.30})$$

The concept of charts creation is illustrated in Figure 6.5, where the response charts may be created either with or without computational apparatus.

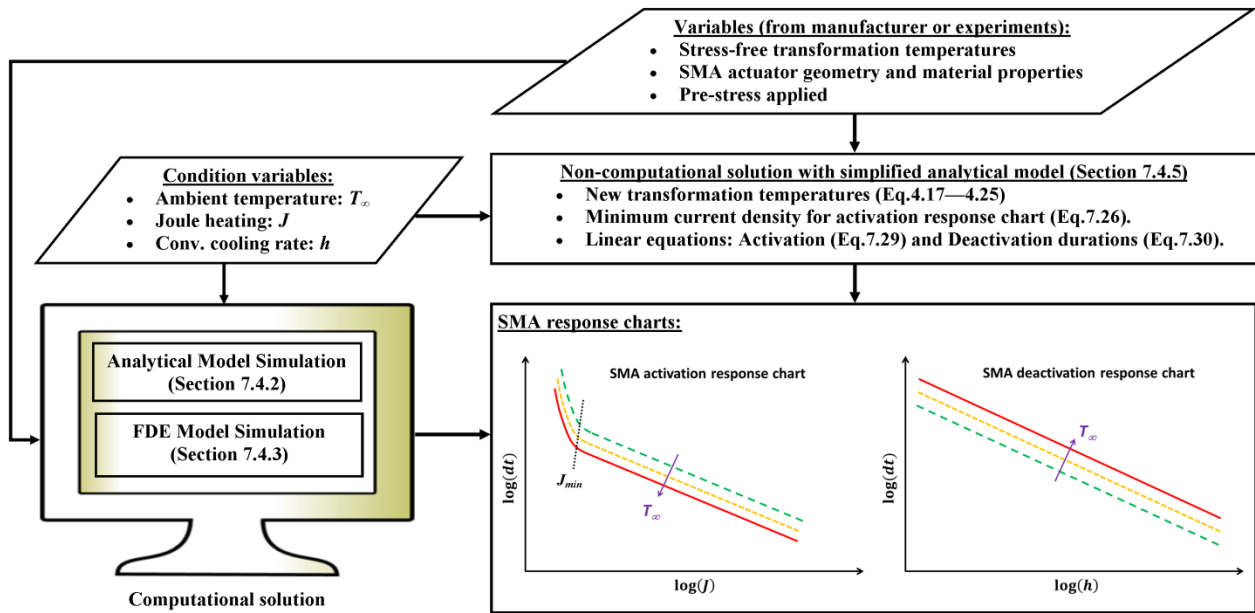


Figure 6.5 – Response charts creation concept

6.5 Process flow of numerical models

The process flows for: simplified analytical, standard analytical, and FDE models are illustrated in Figure 6.6, Figure 6.7 and Figure 6.8, respectively. These process flows assist SMA developers and designers to understand the numerical concept of these models and to develop their own numerical codes. The Matlab codes developed by the author to implement these models are available in the appendices.

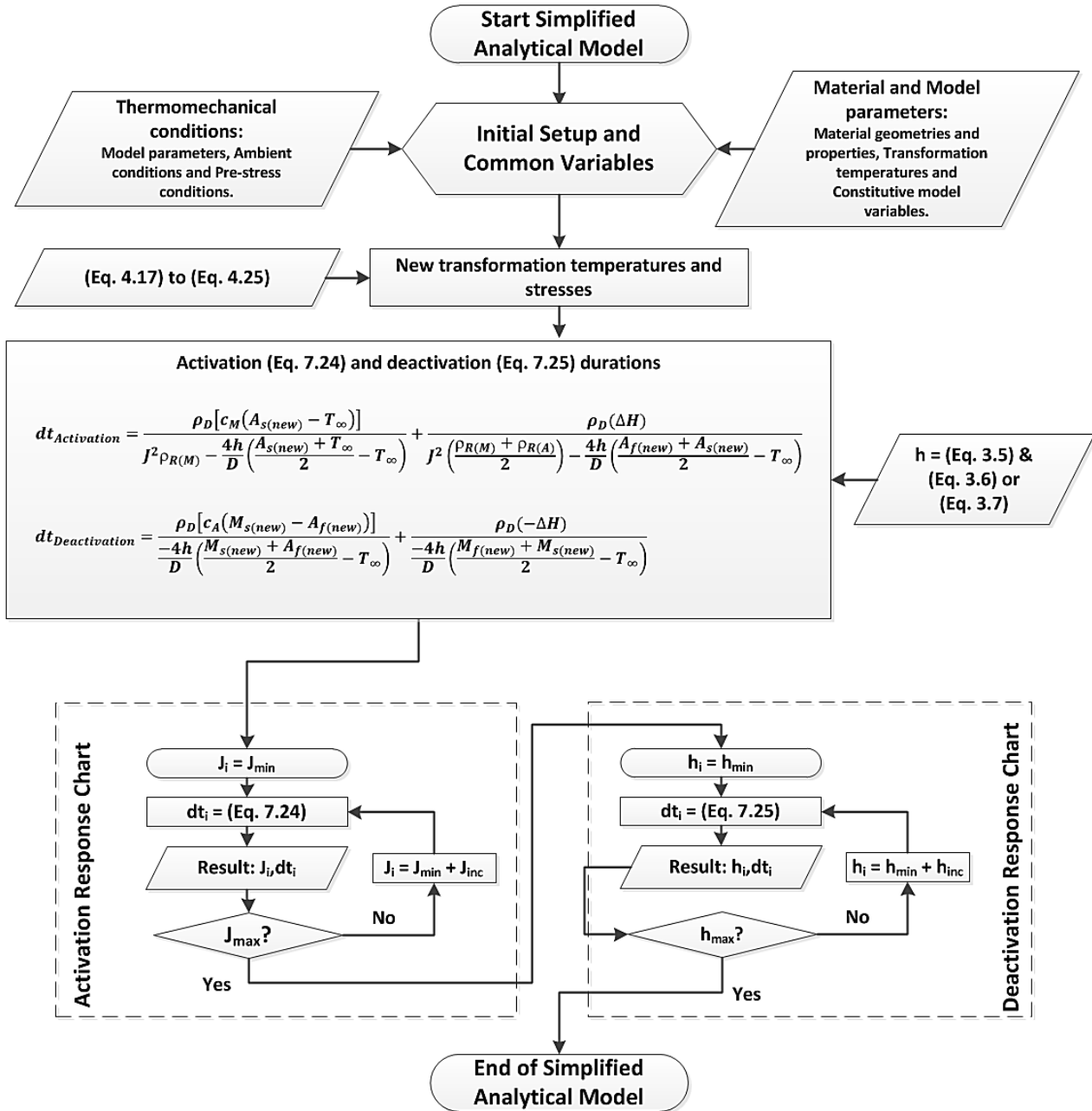


Figure 6.6 – Process flow of simplified analytical model

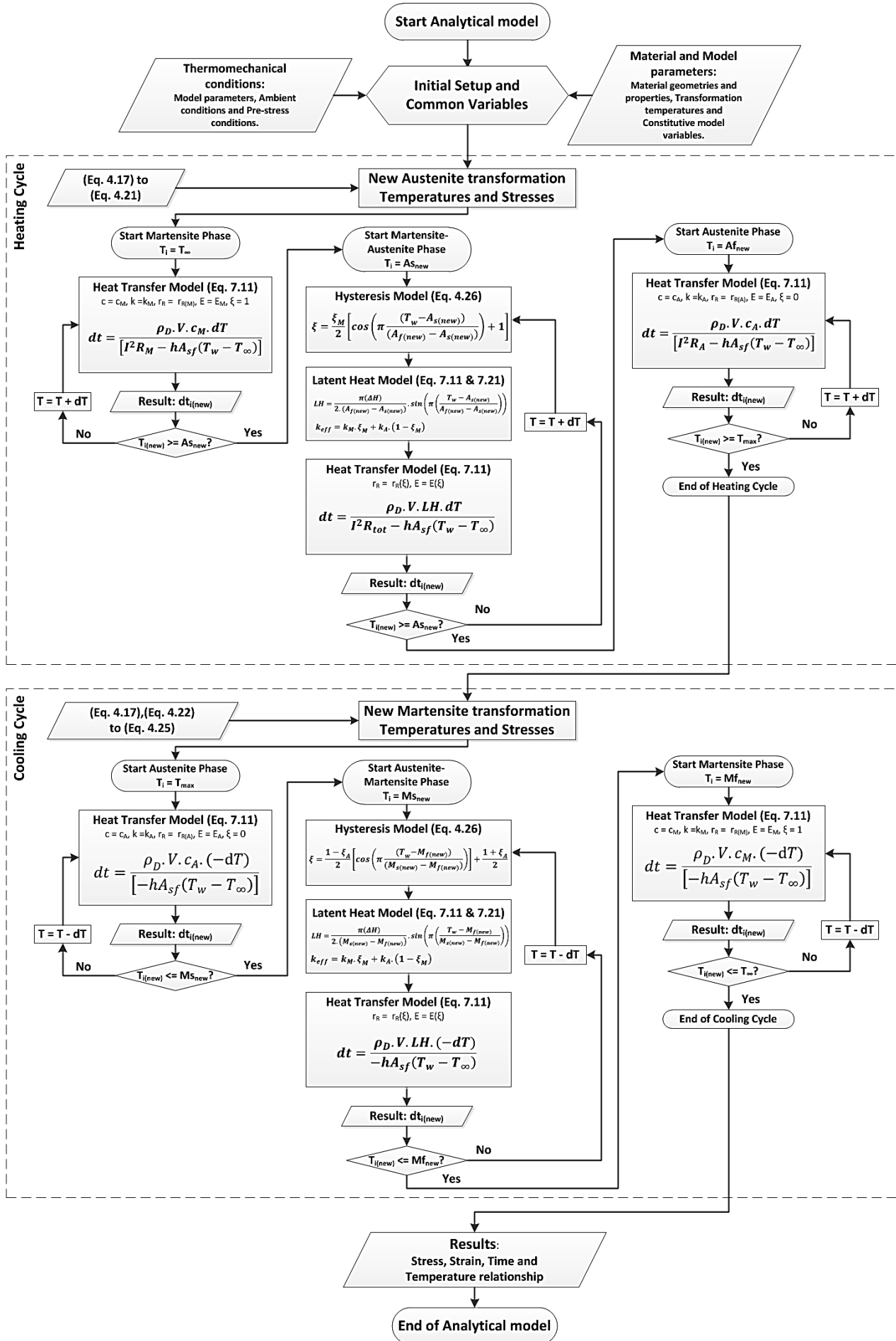


Figure 6.7 - Process flow of analytical model

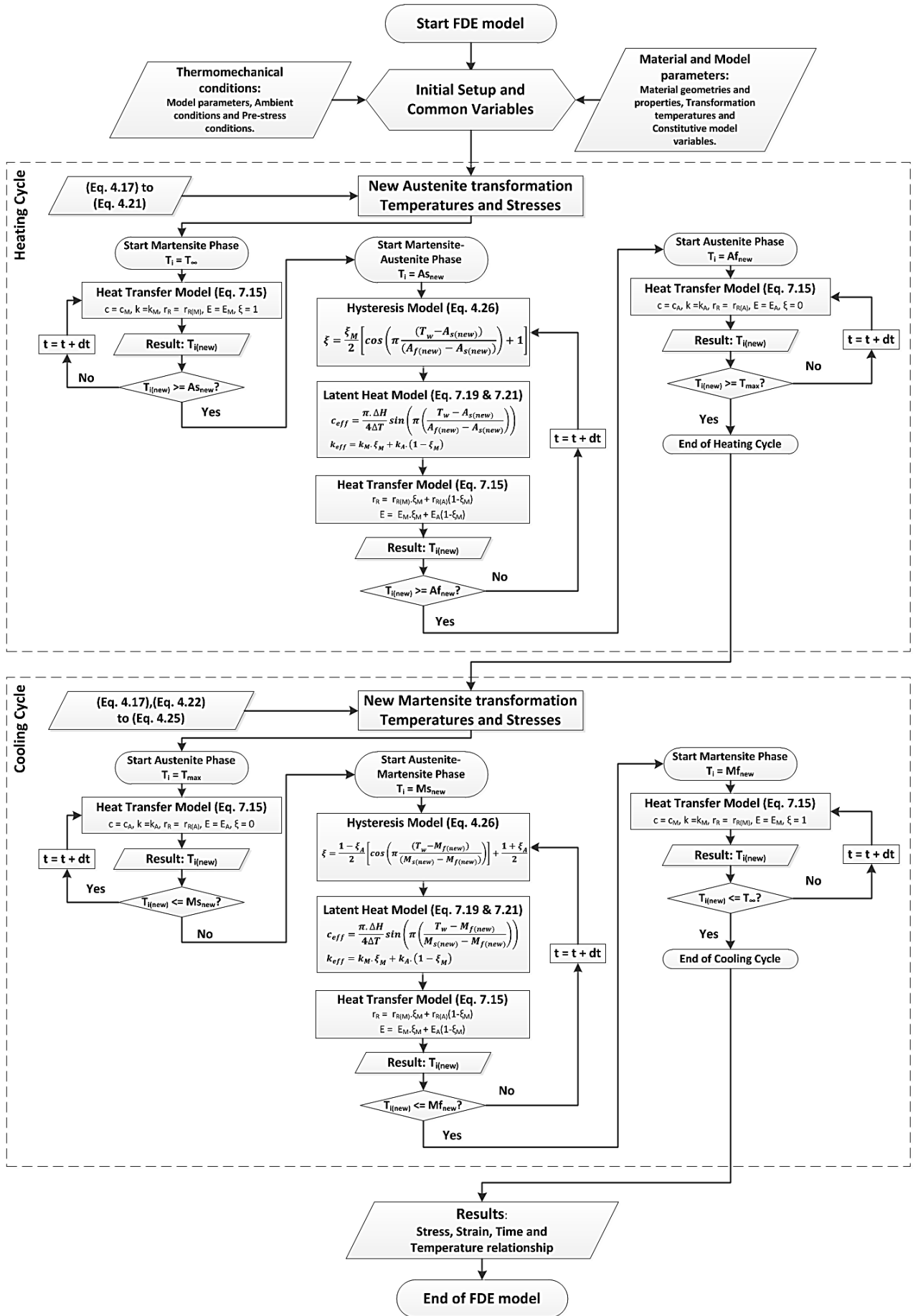


Figure 6.8 - Process flow of FDE model

6.6 Experimental setup

To confirm the predictive models, the experiment apparatus of Figure 6.9 was developed. It incorporates a TO-152F Thermoline Scientific oven at ambient pressure of 1 atmosphere, and an accuracy of $\pm 0.25^\circ\text{C}$. SMA linear actuators of length 100mm and 0.51mm diameter were assembled to the SMA fixture in a horizontal orientation inside the oven and coupled to a load cell assembly. The load cell was located remotely from the oven and actuated by a Bowden cable. A bias spring and pre-stress adjuster were coupled with the SMA actuators and load cell to adjust the SMA preload. A K-type thermocouple was used to measure the ambient oven temperature. The material properties of SMA linear actuator used in the experiment and numerical model are summarized in Table 6.1.

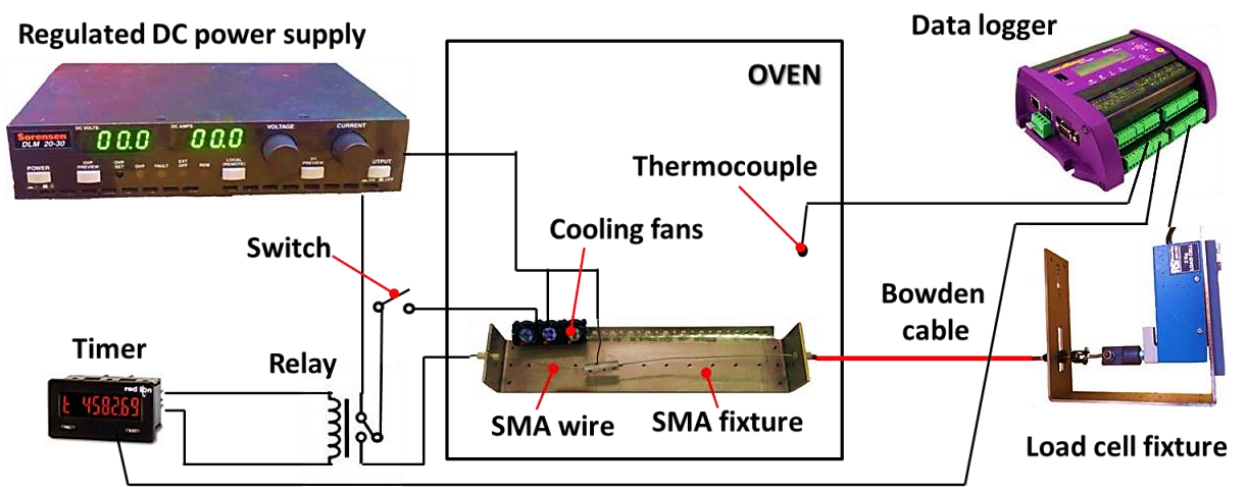


Figure 6.9 - SMA linear actuator experimental setup

Table 6.1 - SMA material properties (Dynalloy Inc., 2007; Elahinia & Ahmadian, 2005)

Name	Symbol	Unit	Value	
			Martensite	Austenite
Young Modulus	E	GPa	28	75
Density	ρ_D	kg/m ³	6450	
Specific heat capacity	c	J/kg.K	322.4	
Thermal conductivity	k	W/m.K	8	18
Resistivity	ρ_R	$\mu\Omega\text{cm}$	76	84
Latent heat of transformation	ΔH	J/kg	24180	

Two sets of experiments were performed:

Experiment 1: Stress-temperature tests with variable pre-stress conditions:

- SMA actuators were heated from 20°C to 100°C (without Joule heating), and then cooled down from 100°C to 20°C .
- Three sets of pre-stress were applied (Figure 6.10) to identify the correlation between actuation temperatures and the stress, and related stress-influenced parameters.

Experiment 2: Thermomechanical test with variable temperature and pre-stress conditions:

- The SMA actuators were activated by Joule heating (12V DC and 2A) until fully contracted (i.e. force change is less than 1% of full scale within 1 second). SMA actuators were then cooled by free or forced convection until thermal equilibrium (i.e. ambient temperature).
- Three sets of pre-stress and ambient temperature conditions were applied for free (Figure 6.14) and forced convection conditions (Figure 6.17).
- The numerical and experimental results were compared for validation (Figure 6.14 and Figure 6.17).

6.7 Results and discussion

The required modelling parameters were experimentally obtained for a range of different pre-stress configurations (Section 7.1), as shown in Figure 6.10. Two stages of modelling were conducted with these parameters (Section 6.7.2) and then compared to the experimental results (Section 6.7.3).

6.7.1 Identification of the modelling parameters

Previous studies have reported that constitutive parameters, such as the stress-influenced coefficients (C_A and C_M) may vary, depending on the actuator conditions and the number of cycles performed, and are most accurately measured at low temperatures (De la Flor *et al.*, 2006). In this work, stress-influenced coefficients were deduced from A_s and M_f from the first cycle of each experiment and projected to their respective stress-free ($\sigma_0 = 0$ MPa) transformation temperatures (from manufacturer's database and previous studies), as summarized in Table 6.2. Initially, the stress-influenced coefficients for A_f and M_s were assumed to be identical with A_s and M_f . However, after the calibration process of numerical and experimental results, the stress-influenced coefficients for M_f were adjusted as summarized in Table 6.2.

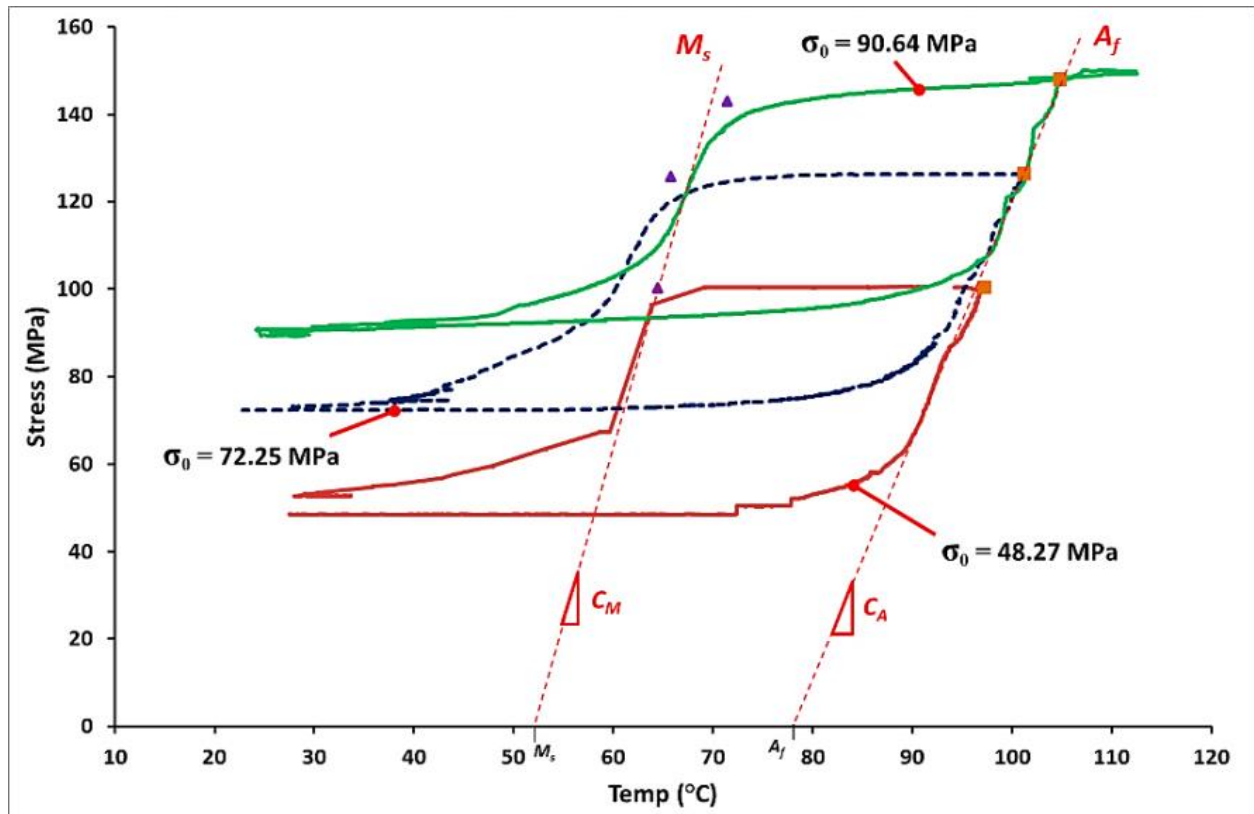


Figure 6.10 - Identification of stress-induced modeling parameters (C_A and C_M) from experimental data

Table 6.2 - SMA linear actuator modeling parameters (Elahinia & Ahmadian, 2005)

Name	Symbol	Unit	Value
Transformation temperatures:			
- Austenite start	A_s	°C	68
- Austenite final	A_f	°C	78
- Martensite start	M_s	°C	52
- Martensite final	M_f	°C	42
Thermoelastic tensor	θ_T	MPa/°C	0.55
Transformation tensor	Ω	MPa	$-E \cdot \varepsilon_L$
Stress-influenced coefficients	C_A	MPa/°C	7.0
	C_M	MPa/°C	2.5, 10.0

In this work, the method of (Mohd Jani *et al.*, 2015a) was applied to identify the unknown convective heat transfer coefficient, h . The convective heat transfer coefficient was fine-tuned with a curve-fitting analysis (root-mean-square-error (RMSE), correlation and variance test features), until correlation between FDE and experimental results were obtained (Figure 6.11), then were compared to the (SW Churchill & Chu, 1975) and (Eisakhani *et al.*, 2011) correlation equations (refer Section 3.7.3.1) for verification.

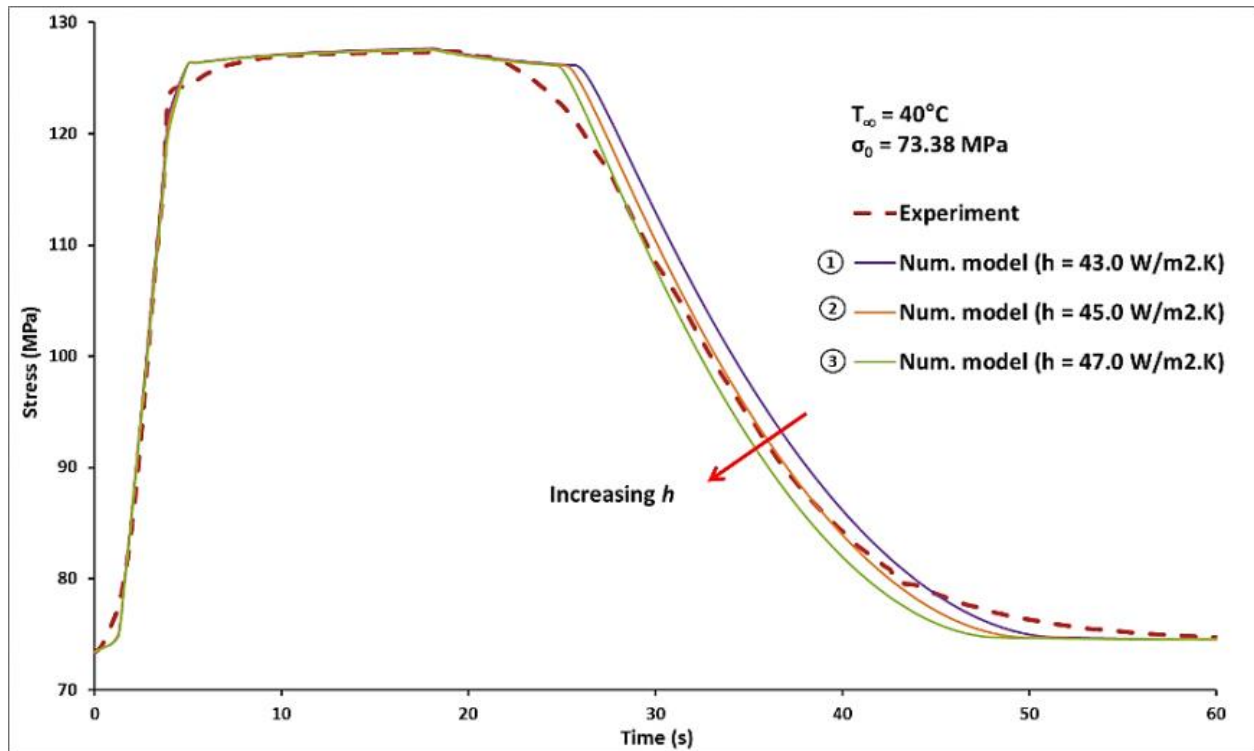


Figure 6.11 - SMA numerical model fine-tuning of h with reference to experimental data

6.7.2 Numerical modelling stages

Numerical modelling consists of two stages: heat transfer modelling of thermal response and constitutive modelling for the stress-strain analysis.

6.7.2.1 Heat transfer model

FDE model and a flexible analytical model (based on the theoretical heat transfer equation) were developed in this work and validated with the lumped capacitance model. Figure 6.12 clearly shows that the pre-stress and phase transformation are necessary and significantly influence the heat transfer results. An incorrect estimation of actuation and deactivation durations may occur if designers assume that pre-stress and phase transformation have no significant effect to the SMA linear actuator; thereby reducing the functional performance and durability of the designed device. The developed analytical and FDE models were found to closely match the lumped capacitance model, and are applicable for the robust simulation of heat transfer in SMA linear actuators, including the phase transformation effect.

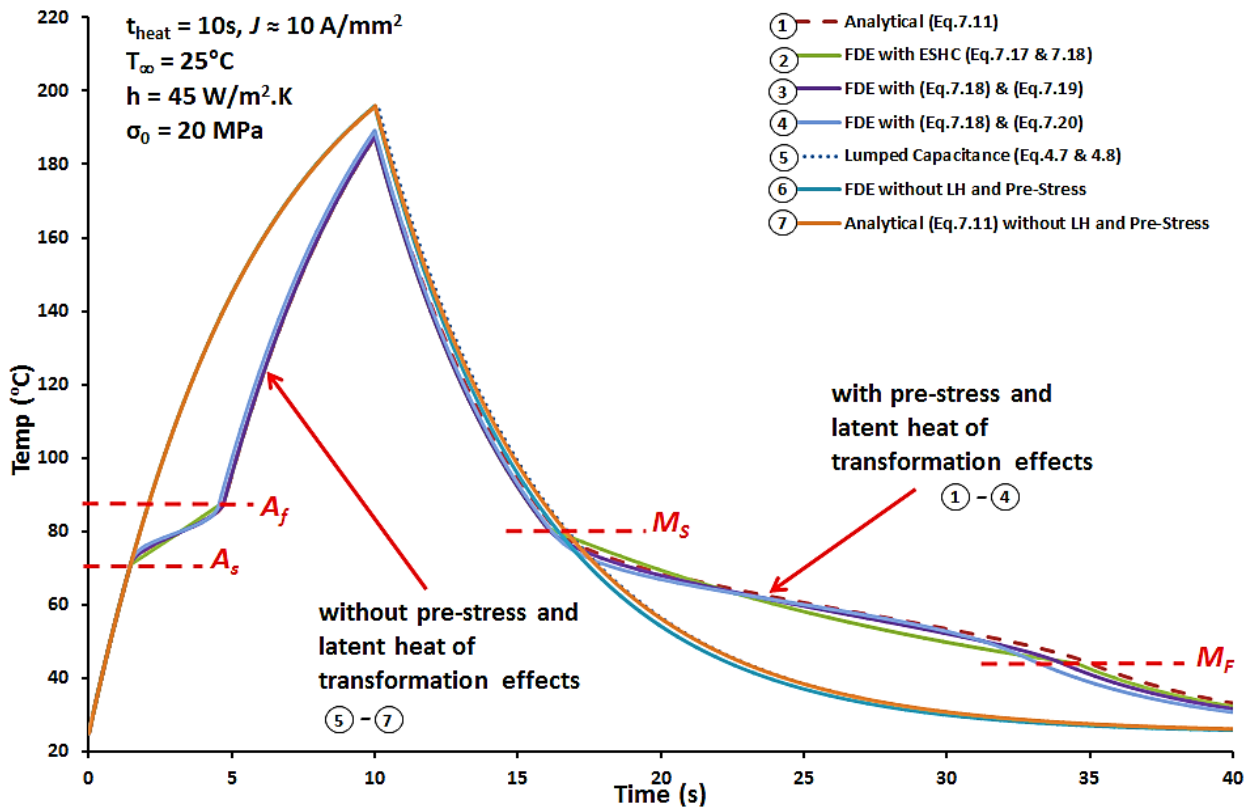


Figure 6.12 - SMA thermal cycle with various heat transfer models

Although analytical models (Eq. 6.11) may provide a more rapid estimates of the heat transfer problem (refer Table 6.3), the 1-D FDE model (Eq. 6.15) provides more accurate (i.e. lower RMSE) and comprehensive data (i.e. complete results within the nodes are available). Additionally, the FDE model can simulate higher a range of current density (e.g. the lumped capacitance model is limited up to 100 A/mm^2 (V. Brailovski *et al.*, 1996)), and can accommodate heat transfer problems with multiple layers (e.g. lagged actuator, Chapter 5). As described in Section 6.4.3, a compromise balance between data quality and simulation duration is necessary for practical applications. Larger time steps are preferable for faster simulation and smaller steps for better data quality. However, smaller steps do not guarantee improved outcomes, as shown in Table 6.3. For a robust numerical model, the space steps should be much smaller than the associated geometric geometry size.

Table 6.3 - Comparison of analytical and FDE models

Analytical model	Temperature step, dT [K]		Simulation duration [s]	RMSE [K]
	0.100		0.084	0.6801
	0.010		5.449	0.6692
	0.005		24.942	0.6701
FDE model	Time step, dt [s]	Space step, dr [m]	Simulation duration [s]	RMSE [K]
	0.100	0.00001	0.249	0.6362
	0.010	0.00001	1.775	0.6518
	0.001	0.00001	53.136	0.6526
	0.001	0.00005	52.422	1.4670
Parameters: $J \approx 10\text{A/mm}^2$, $T_\infty = 30^\circ\text{C}$, $h = 50.8\text{ W/m.K}$, $\sigma_0 = 90.61\text{MPa}$, $t_{\text{heat}} = 17.9\text{s}$, $t_{\text{cool}} = 41.7\text{s}$. Note: Root-mean-square-error (RMSE) is calculated between numerical and experimental data. Simulation: HP Compaq 8300 Elite MT: Intel Core™ i7 (3.4GHz), 8GB RAM, Windows NT (64-bit), Matlab2012b.				

Detailed investigation of the phase transformation regions (Figure 6.13a) reveals that the FDE model (Eq. 6.19), is in very close agreement with the developed analytical model (Eq. 6.11), and the other proposed models provide reasonably close agreement. There were no significant differences in applying either (Eq. 6.18) or (Eq. 6.21) as the effective thermal conductivity for the heat transfer models (Figure 6.13a). Therefore, both analytical and FDE models developed in this work are suitable for predicting the thermomechanical behaviour of a SMA linear actuator. The FDE model with combination of (Eq. 6.19) and (Eq. 6.21) as the c_{eff} and k_{eff} for the latent heat model was selected and integrated into the constitutive model due to its superior predictive capability.

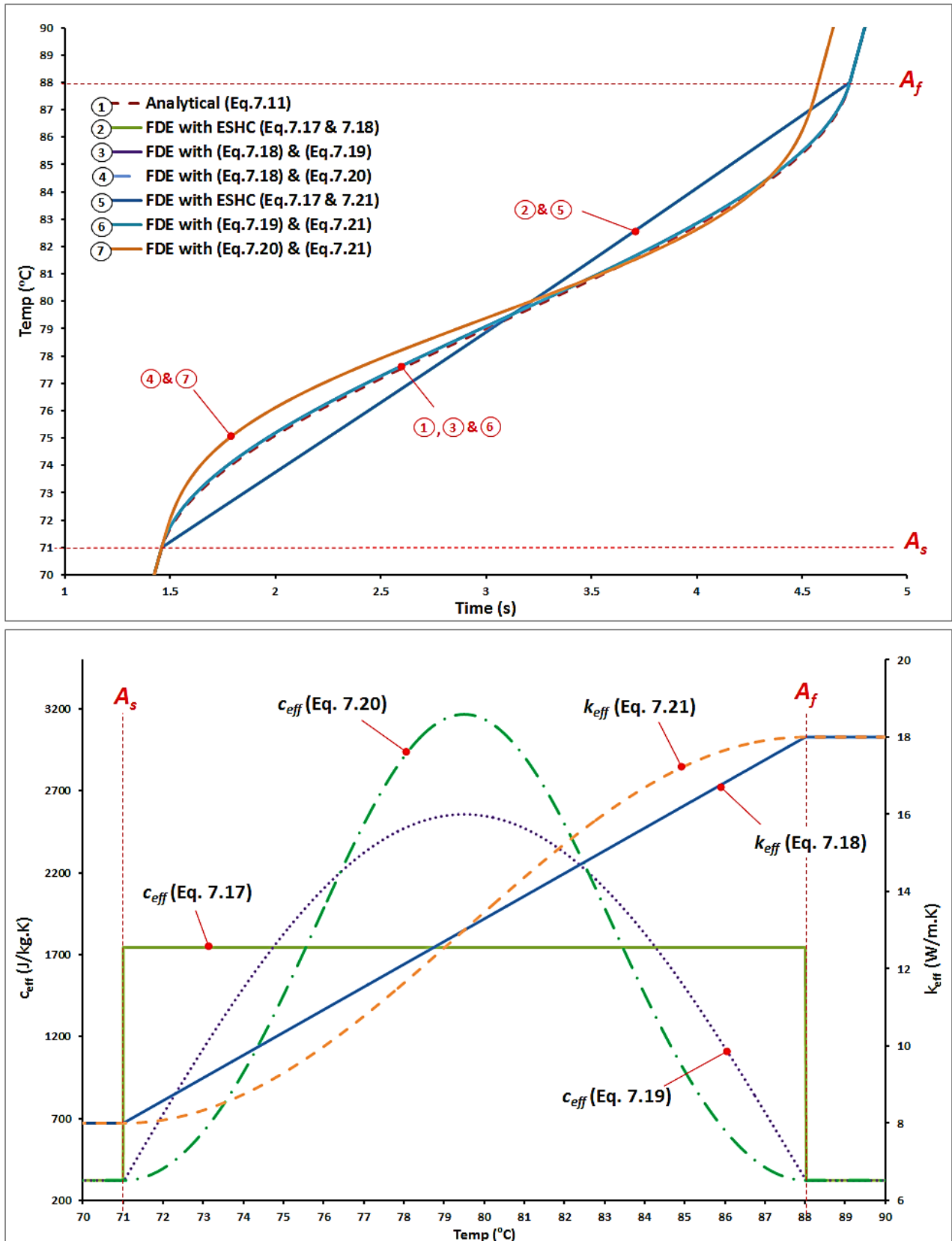


Figure 6.13 - Comparison of heat transfer model responses and their effective specific heat and thermal conductivity variation during the phase transition

6.7.2.2 Constitutive model

The thermal response data from the heat transfer model are then interpreted as stress-strain data via Liang and Roger's constitutive model and compared with the experimental results for verification, as discussed in the following sections. Other constitutive model parameters such as the tensors (θ_T and Ω) and the transformation temperatures (A_s , A_f , M_s and M_f) are obtained from previous studies and SMA manufacturer database as listed in Table 6.1 and Table 6.2.

6.7.3 Numerical modelling validation

The convective heat transfer coefficient displays significant effect on the SMA linear actuator during the cooling cycle, but is less relevant during the heating cycle (Figure 6.14 and Figure 6.17). The results of SMA linear actuator with three variable ambient temperatures and free convection cooling conditions are compiled and presented in Figure 6.14, Table 6.4 and Table 6.5. The identified convective heat transfer coefficients, h from the developed numerical models are consistent with results from existing correlation equations (Section 3.7.3.1) as summarized in Table 6.4. In addition, the experimental transformation stresses and the temperatures were experimentally measured and then compared to the numerical results (Figure 6.14 and Table 6.5).

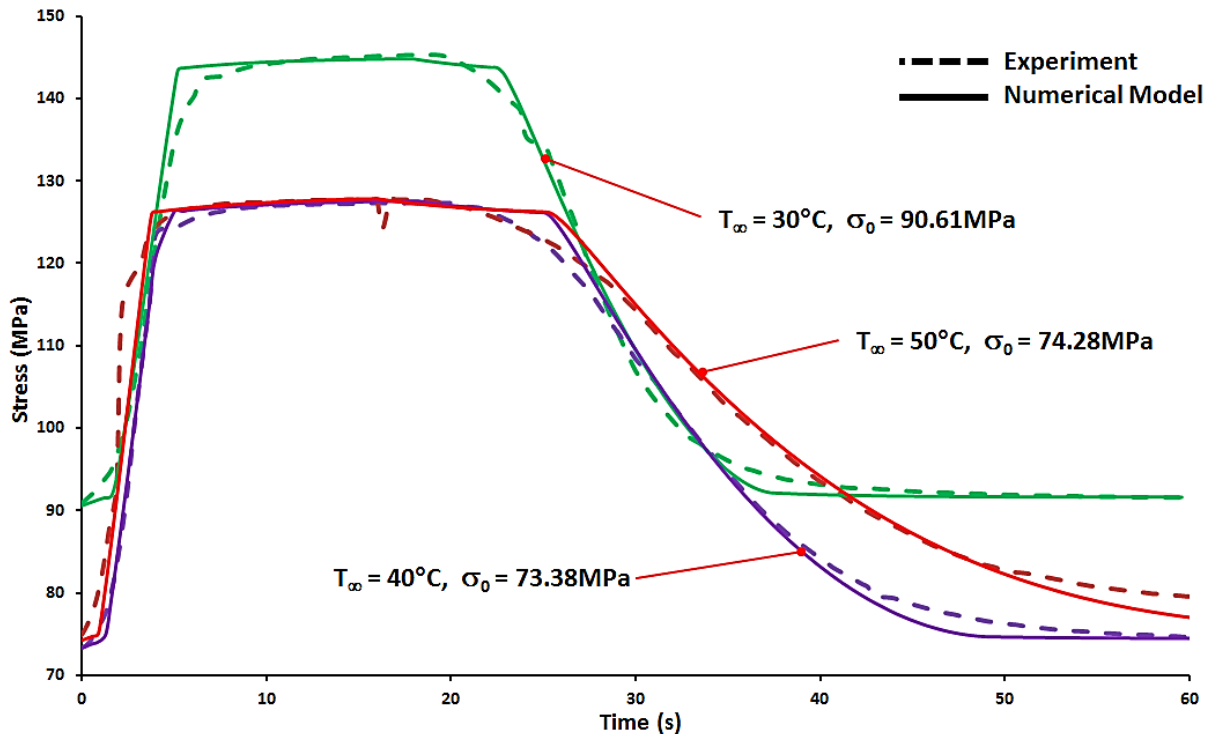


Figure 6.14 - SMA linear actuator under natural cooling, various ambient temperatures and pre-stresses

The estimated stresses, temperatures and timings for each transformation stage (A_s , A_f , M_s and M_f) from the numerical model exhibit strong agreement with the experimental data (Table 6.5), with mean error of 0.75%, 1.09% and 8.53% respectively. Therefore, the numerical models developed in this work are useful and applicable to estimate SMA linear actuator reaction under variable environmental and mechanical conditions. However, the performance of the developed models could be further enhanced to accommodate: SMA behaviour at a lower temperature range, i.e., below M_s for twinned and detwinned martensite transformation; under simultaneous temperature and stress loading variations; and, a wider range of temperatures and loading conditions could be estimated more accurately with the application of more recently developed constitutive models, for example (Auricchio & Lubliner, 1997; Brinson, 1993; De la Flor *et al.*, 2006).

Table 6.4 - Comparison of convective heat transfer coefficients

T_∞ [°C]	Convective heat transfer coefficient [W/m ² .K]		
	Eisakhani (2011)	Churchill (1975)	Num. Model
30	48.86	43.05	50.8
40	48.32	42.83	45.7
50	47.61	42.51	40.5

Table 6.5 - Comparison of experimental and numerical data

Parameter s	Unit	$T_\infty = 30^\circ\text{C}$			$T_\infty = 40^\circ\text{C}$			$T_\infty = 50^\circ\text{C}$		
		Exp.	N.M.	Err. (%)	Exp.	N.M.	Err.	Exp.	N.M.	Err. (%)
A_s	°C	81.0*	81.0	0.00	78.5*	79.0	0.64	78.6*	79.0	0.51
A_f	°C	98.5*	99.0	0.51	96.1*	96.0	0.10	96.2*	97.0	0.83
M_s	°C	110.4*	109.9	0.45	103.1*	102.0	1.07	103.3*	102.0	1.26
M_f	°C	51.3*	51.0	0.58	49.6*	49.0	1.21	49.9*	50.0	0.20
Mean		-	-	0.39	-	-	0.75	-	-	0.70
Std. Dev.		-	-	0.26	-	-	0.50	-	-	0.45
σ_{A_s}	MPa	91.0	91.9	0.99	73.5	74.3	1.09	74.4	75.0	0.81
σ_{A_f}	MPa	143.8	143.6	0.14	126.6	126.1	0.39	127.3	126.2	0.86
σ_{M_s}	MPa	146.0	143.7	1.58	127.7	126.1	1.25	128.2	126.2	1.56
σ_{M_f}	MPa	93.0	92.1	0.97	75.5	74.7	1.06	78.5	76.8	2.17
σ_{Max}	MPa	145.3	144.8	0.34	127.4	127.6	0.16	127.7	127.8	0.08
σ_0	MPa	90.6			73.4			74.3		
Mean		-	-	0.80	-	-	0.79	-	-	1.09
Std. Dev.		-	-	0.57	-	-	0.48	-	-	0.80
t_{A_s}	s	1.6	1.7	6.25	1.4	1.2	14.29	0.8	0.9	12.50
t_{A_f}	s	5.6	5.3	5.36	4.2	4.4	4.76	3.4	3.8	11.76
t_{M_s}	s	23.2	22.4	3.45	23.5	25.0	6.38	23.8	25.2	5.88
t_{M_f}	s	32.2	33.4**	3.73	41.6	40.8**	1.92	45.5	47.3**	3.96
Mean		-	-	4.70	-	-	6.84	-	-	8.53
Std. Dev.		-	-	1.34	-	-	5.30	-	-	4.25
h	W/m ² K		50.8			45.7			40.5	

Current density, $J \approx 10\text{A/mm}^2$.
Nomenclature: Exp. = Experiment, N.M. = Numerical model, Err. = Error, Std. Dev. = Standard deviation.
*Experimental temperatures were not measured, but were calculated based on the measured experimental stresses.
**Final-martensite transformation time, t_{M_f} for the numerical models were manually measured from the graphs.

6.7.4 SMA linear actuator performance analysis

By applying the developed heat transfer models (analytical or FDE), the activation and the deactivation durations was simulated to generate generalized activation and deactivation response charts (Figure 6.15 and Figure 6.16). The activation duration was simulated from T_∞ to A_f with variable current density, J , under constant h and T_∞ . Deactivation duration was simulated from A_f to T_∞ with variable h . Referring to Figure 6.15, the Joule heating supplied to the SMA should exceed the minimum current density, $J_{min(Af)}$ for complete actuation of the device to occur, otherwise convective effects dominate. These limits are dependent on the total energy induced into the SMA linear actuator (Eq. 6.5). Increases in current density reduce actuation duration, and reduce the influence of latent heat (V. Brailovski *et al.*, 1996), however caution should be taken to avoid overheating of the device.

The heat transfer models developed and associated activation and deactivation charts are useful to estimate the activation and deactivation durations of a proposed SMA linear actuator. For example, to fully actuate a 0.51mm diameter Flexinol SMA linear actuator under free convection ($h \approx 45 \text{ W/m}^2\text{K}$) and 5MPa pre-stress within 1 second, the estimated Joule heating is approximately 20 A/mm^2 (equivalent to approximately 4A) (Figure 6.15, Example 1); and the estimated cooling duration would be approximately 23 seconds (Figure 6.16, Example 1). Both determined variables were found to exhibit good agreement with the manufacturer's data (i.e. 1s with 4000mA Joule heating and 16.8s for free convection cooling (Dynalloy Inc., 2007)).

Pre-stress and latent heat effects must be considered in numerical models for optimal performance and durability. Otherwise, the SMA linear actuator may be deactivated below the actual A_f , resulting an incomplete actuation and inferior performance. As an example (Figure 6.12), if we assume that A_f and t_{Af} are unaltered (i.e. 78°C after approximately 1.72s), the device actually starts to actuate for about 0.3% strain or 8% of full actuation, where the transformation temperatures and time have shifted to approximately $A_s \approx 71^\circ\text{C}$, $t_{As} \approx 1.47\text{s}$ and $A_f \approx 88^\circ\text{C}$, $t_{Af} \approx 4.73\text{s}$ respectively due to the pre-stress and the influence of latent heat. Overheating of the SMA device might also occur when the cooling or deactivation duration is underestimated for subsequent actuation cycles.

The utilization of a constitutive model has further enhanced the heat transfer models ability to relate the temperature with the stress-strain condition. Thus, prediction of stress-strain behaviour of SMA linear actuator is achievable. For example (Table 6.5), the SMA linear actuator with $T_{\infty}=40^{\circ}\text{C}$, $h=45.7\text{ W/m}^2\text{K}$, $\sigma_0=73.4\text{ MPa}$ and $S=2.66\text{ kN/m}$, activated with 2A, 12VDC (approximately 10 A/mm^2) requires approximately 4.4 seconds to reach $\sigma_{max}=127.6\text{ MPa}$, and approximately 41 seconds to reset completely.

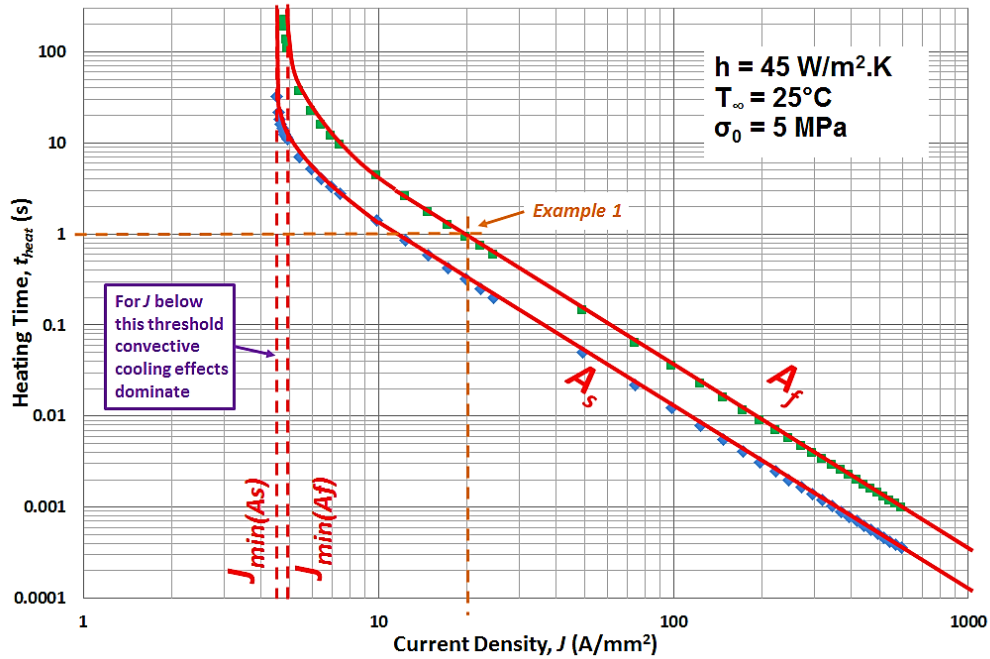


Figure 6.15 - Numerical simulation of SMA linear actuator activation duration versus current density

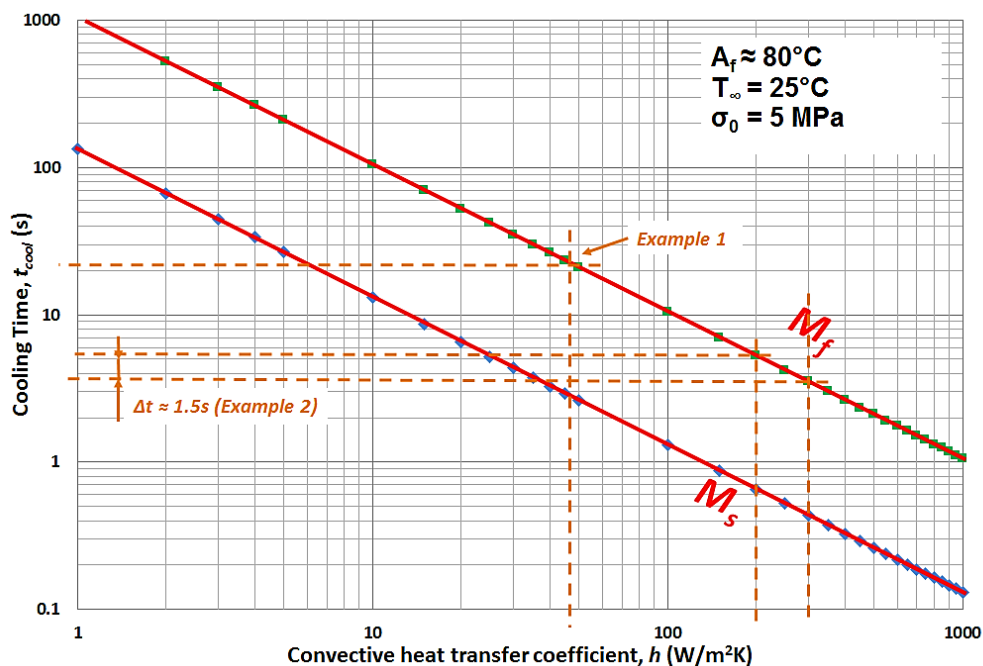


Figure 6.16 - Numerical simulation of SMA linear actuator deactivation duration versus convective heat transfer coefficient

Increased forced convection may reduce deactivation duration, but is not recommended during the heating cycle as it acts against the effect of Joule heating (Figure 6.17), consumes energy and produces noise. For example, an advantage of only approximately 1.5s is gained by increasing heat transfer coefficient from 200 W/m².K to 300 W/m².K (Figure 6.16, Example 2). The application of numerical models allows the appropriate level of forced convection to be estimated in advance, allowing the device to be configured precisely and economically (i.e. minimizing energy consumption) to enhance the actuation frequencies.

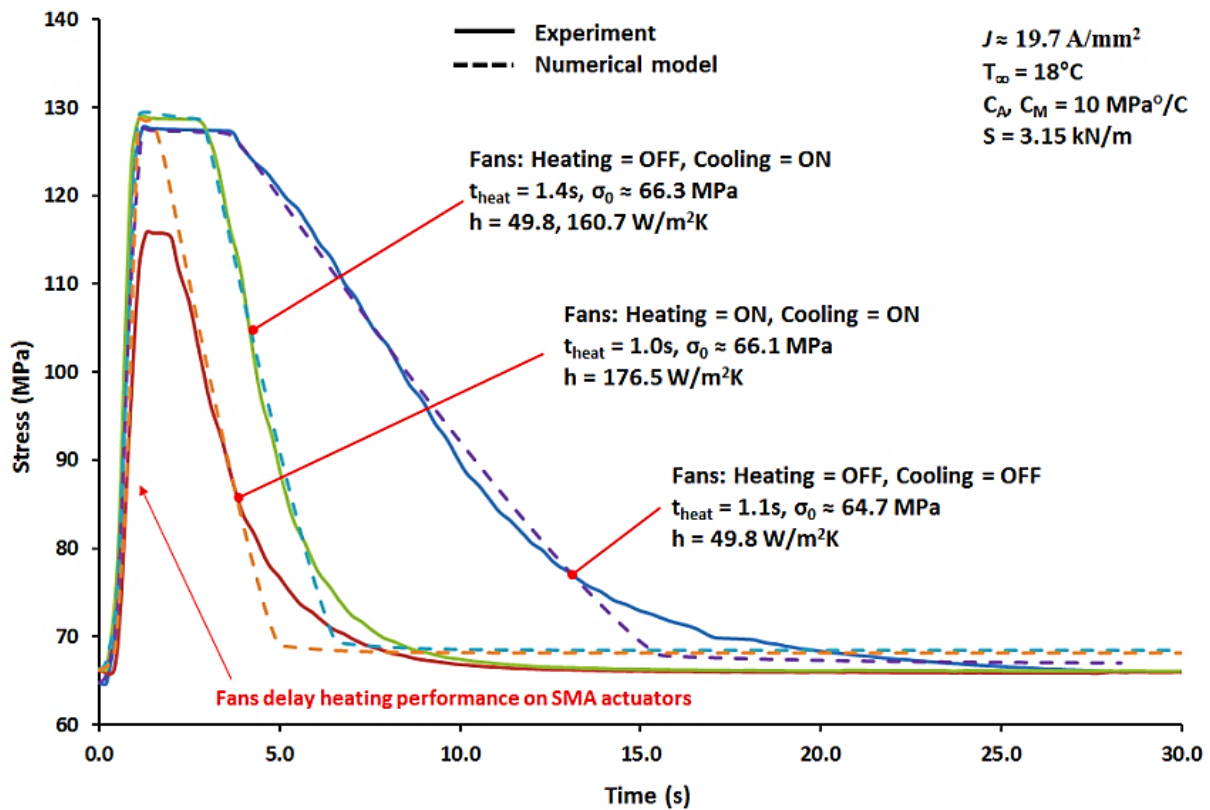


Figure 6.17 - Forced convection effect on SMA performance

Recommended future works includes:

- Extension of the numerical models developed as follows:
 - Apply recent constitutive model to predict wider range of environmental and mechanical conditions, including load and thermally induced stresses
 - To extend the models for solving multi-dimensional problems with greater geometric size and complexity.
 - To consider phase heterogeneity due to the non-isothermal phase change.
- To develop versatile activation and deactivation charts (i.e. integrate with variable factors such as h , T_{∞} , D_{SMA} , σ_0 and SMA type) for quick reference.
- To include multiple layers of simulation function for solving SMA with lagging or sandwich construction.
- To include thermal-cycling function for solving and fatigue consideration.

- To apply the developed models into finite element method.
- To extend the models for multi-dimensional, complex geometries and non-uniformity problems.

6.8 Conclusion

Both analytical and finite difference equation (FDE) models have been developed in this work to predict the linear SMA activation and deactivation durations and associated thermomechanical behaviour. The models accommodate variable environmental and design conditions, and include effects of latent heat effect, induced-stress and material property variability. Integration of the proposed models with an existing constitutive model allows the generation of custom SMA stress-strain curves. The findings of this work are summarized as:

- Strong agreement was achieved between the proposed numerical model and the experimental results. Therefore, the developed 1-D heat transfer models were concluded to be practically useful in the estimation of activation and deactivation durations for SMA linear actuators.
- For optimal performance and durability, the pre-stress and latent heat effects must be considered in heat transfer models to avoid actuator damage (i.e. due to overheating) and incomplete actuation and reset.
- The design of actuator actuation frequencies could be configured precisely and economically (i.e. minimizing energy consumption) with the numerical model.
- Despite of the analytical models are found to be faster to simulate the heat transfer problem, a 1-D FDE model is more versatile to simulate higher range of current density and heat transfer coefficient, and is more flexible to solve multiple layers (e.g. lagged actuator) heat transfer problems.
- Correct setup of FDE step parameters (e.g. dr , dt and dT) are necessary to obtain optimum data quality within reasonable simulation duration for practical application, where smaller steps does not always guarantee a better results.

7. Structural and functional fatigue of Ni-Ti SMA-Pulley system using Taguchi and ANOVA

The outcomes of this chapter have contributed to the following peer reviewed publication: “*Fatigue of Ni-Ti SMA-pulley system using Taguchi and ANOVA*”, J Mohd Jani, M Leary, A Subic, Smart Materials & Structures 25 (5), 057001, 2016, DOI: 10.1088/0964-1726/25/5/057001.

7.1 Chapter summary

Shape memory alloy (SMA) actuators can be integrated with a pulley system to provide mechanical advantage and to reduce packaging space; however, there appears to be no formal investigation of the effect of a pulley system on SMA structural or functional fatigue. In this work, cyclic testing was conducted on Nickel-Titanium (NiTi) SMA actuators on a pulley system and a control experiment (without pulley). Both structural and functional fatigue were monitored until fracture, or a maximum of 1E5 cycles were achieved for each experimental condition. The Taguchi method and analysis of the variance (ANOVA) were used to optimise the SMA-pulley system configurations. In general, one-way ANOVA at the 95% confidence level showed no significant difference between the structural or functional fatigue of SMA-pulley actuators and SMA actuators without pulley. Within the sample of SMA-pulley actuators, the effect of activation duration had the greatest significance for both structural and functional fatigue, and the pulley configuration (angle of wrap and sheave diameter) had a *greater* statistical significance than load magnitude for functional fatigue. This work identified that structural and functional fatigue performance of SMA-pulley systems is optimised by maximising sheave diameter and using an intermediate wrap-angle, with minimal load and activation duration. However, these parameters may not be compatible with commercial imperatives. A test was completed for a commercially optimal SMA-pulley configuration. These novel observations enable increased confidence in robust SMA actuator pulley system design. This outcome is of significant commercial benefit as the use of SMA-pulley systems enables a significant reduction in required packaging space; however, due to the statistical nature of SMA fatigue, and high number of influential variables, it is prohibitively expensive to complete the required system testing as part of a commercial SMA actuator design program.

7.2 Introduction

For SME transformation, the SMA actuator is initially in the martensite phase and converts to austenite phase when current is supplied to the actuator (i.e. Joule heating) and revert to the martensite phase when cooled. As illustrated schematically in the SMA pulley system of Figure 7.1, the SMA actuator begins to contract when heated beyond the austenite start temperature (A_s). Contraction continues until the austenitic transformation is complete at the austenite final temperature (A_f) (Figure 7.1, path 1-2). During the cooling cycle, the SMA actuator begins to return to its initial length when cooled below the martensite start temperature (M_s), and the martensitic transformation (MT) is complete at the martensite final temperature (M_f). The termination of Joule heating prior to A_f results in a reduced actuator deformation (Figure 7.1, path 2'-3).

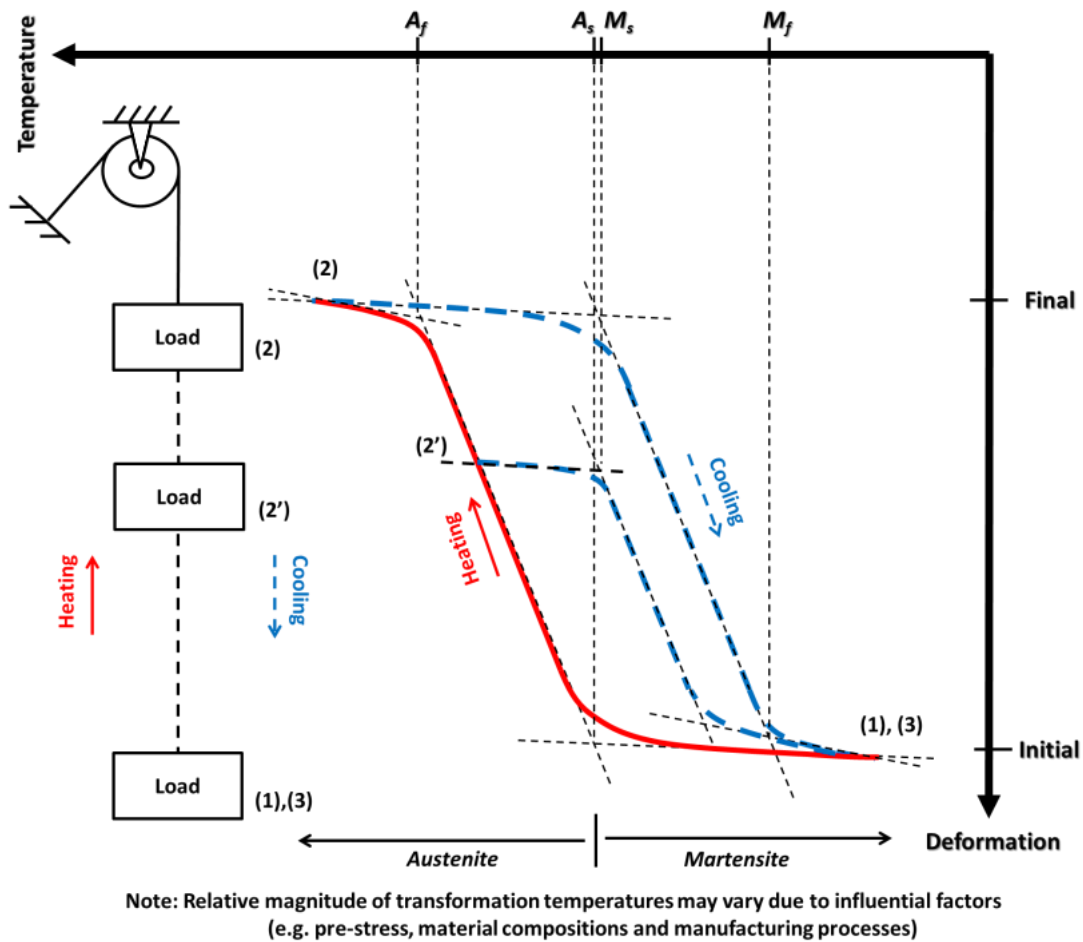


Figure 7.1 - Schematic representation of SME on SMA pulley system

NiTi SMAs are commercially favourable in comparison with copper or iron-based SMAs due to their consistency of stroke over repeated cycles and robust mechanical properties; NiTi SMAs have been commercially applied in automotive, aerospace, biomedical, robotics and structural applications (Mohd Jani, Leary, Subic, *et al.*, 2014), and will be applied in the following experimental work.

In many of commercial applications, the SMA actuator is subject to high cycle loading conditions and demanding spatial constraints. In response to these challenging design requirements, a pulley system may be utilised increase flexibility in satisfying spatial constraints while ensuring the SMA remains within the limitations of strain transformation. The following examples illustrate the commercial application of SMA-pulley systems to convert from linear to rotational motion, and to utilise mechanical advantage to achieve load or stroke amplification (Figure 7.2):

- Multiple SMA-pulley system to linearly actuate the opening area of a jet engine exhaust nozzle while achieving load and stroke amplification (Gangbing Song & Ma, 2012).
- SMA-pulley system to actuate air-dam system for vehicle aerodynamics in order to amplify actuator stroke amplification and rotational movement within the available packaging space (Rober *et al.*, 2010)
- SMA-pulley system to actuate automotive headrest assembly by converting linear to rotary motion while amplifying stroke and load (AL Browne, Johnson, Khoury, *et al.*, 2009)
- SMA-pulley system to actuate vehicle lock indicator while allowing stroke amplification and rotational movement within the available packaging space (Dominique, 2003b)

Furthermore, a variable pulley shape and diameter can be utilised to limit and control bias torque (Reynaerts & Brussel, 1998) and to reduce the SMA loading (Fumagalli *et al.*, 2009). Numerous studies have been conducted to investigate the fatigue behaviour of SMA actuators, for example:

- SMA structural and functional fatigue research was pioneered by Melton and Mercier (1979) and Miyazaki *et. al* (1986), and further discussed by Eggeler *et al.* (2004), including: uniaxial tension the fatigue of SMA wires and flat cross-section specimens, bending-rotation fatigue of SMA wires, and functional fatigue of SMA springs.
- The effects of stress, strain (e.g. temperature interval, partial and complete phase transformation) and heat treatment on the fatigue life of SMA actuators had been reported by Karhu and Lindroos (2010), and Lagoudas *et al.* (2009)
- The effects of cycling frequency on SMA fatigue life for civil engineering applications have been reported by Torra *et al.* (2010), and the fatigue behaviour of SMA with joining processes such as laser weldment (CW Chan, Man, & Cheng, 2013).
- Pappas *et al.* (2007) identified that the functional degradation of SMA is due to the number of crystalline transition performed and the main factor that affects the stress generation capability is the working temperature, where higher relaxation affects higher temperature above the austenite final temperature (A_f).

- Functional fatigue is a function of the martensitic transformation (strongly dependent on microstructure), and structural fatigue is a function of mean stress amplitude effects (Mertmann & Vergani, 2008; M. Wagner, Frenzel, & Eggeler, 2006).
- Functional fatigue under various loading conditions was investigated by Mammano and Dragoni (2014) in order to bridge the gap between the actual working conditions and laboratory conditions. Two common behaviours are commonly observed as the number of cycles increases (Eggeler *et al.*, 2004; Mahtabi, Shamsaei, & Mitchell, 2015; Maletta, Sgambitterra, Furguele, Casati, & Tuissi, 2012; S. Miyazaki *et al.*, 1986): the hysteresis loop of SMA became narrower and the stress-strain response stabilised (after approximately 100-150 cycles).
- Bending-rotation fatigue (BRF) testing was used to investigate SMA response to cyclic bending conditions (S. Miyazaki *et al.*, 1999; Pelton *et al.*, 2013; H. Tobushi, Yamada, Hachisuka, & Hashimoto, 1998), such as the one performed by a simple SMA-pulley heat engine (Hisaaki *et al.*, 1990) and coil-shaped SMA actuators (S. Miyazaki *et al.*, 1999). Two common configurations to conduct fully reversed BRF test for solid round fine wire are (ASTM, 2014; Mahtabi *et al.*, 2015): (a) rotating SMA wire with motor along guided supports and bushings to specific curvature and known radius (Eggeler *et al.*, 2004; S. Miyazaki *et al.*, 1999; H. Tobushi *et al.*, 1998), and (b) rotating SMA wire with motor around a series of fixed diameter mandrels at 90° (Pelton *et al.*, 2013). BRF has become a popular and convenient method to predict the fatigue behaviour of SMA due to their simple procedure and testing apparatus (CW Chan *et al.*, 2013; T. Duerig *et al.*, 1999; Maletta *et al.*, 2012).
- The BRF of SMA actuators under various ambient temperatures had been studied. For example, Miyazaki *et al.* (1999) assessed BRF under various rotational speeds, strains and ambient temperatures; Tobushi *et al.* (1998) studied the effects of BRF in air and water at various temperatures; and Eggeler *et al.* (2004) studied the effect of temperature on BRF for various wire diameters.
- A comprehensive review on mechanical fatigue and fracture of superelastic SMA actuators for biomedical applications had been reported by Robertson *et al.* (2012), the state-of-art and ongoing challenges on fatigue of nitinol by Mahtabi *et al.* (2015), and the microstructures analysis of thermomechanical fatigue by (Pelton, 2011). The test standards of metallic materials for fatigue behaviour can be accessed from ASTM Committee E08 (ASTM Fatigue and Fracture series of test standards).

However, the fatigue characteristics of SMA-pulley systems are ill-defined due to the limited work on SMA-pulley fatigue behaviour reported in the literature. Recently, a computer-aided shape-memory actuator development application (CASMADA) was developed to provide simulation results for the application of SMA actuator with various pulley systems (Horst Meier & Czechowicz, 2012); however this work provides no direct insight into the effect of the pulley system configurations (e.g. sheave diameter, angle of wrap, material and mechanical design) on SMA-pulley system fatigue. The current work provides novel data to address this limitation by generating robust data on the fatigue response of SMA-pulley systems that is essential for the commercialisation of NiTi SMA.

Despite the importance of pulley systems to the commercialisation of SMA systems, the authors are aware of no formal studies that specifically determine the effect of pulley system configurations on structural and functional fatigue performance of SMA actuators.

The factors and number of levels for the Taguchi method and ANOVA for structural and functional fatigue of the SMA-pulley system were selected based on previous studies (Table 7.1 and Table 7.2), and selected as reported in Section 7.6. Associated nomenclature and definitions are elaborated in Section 7.7.1.

7.3 Fatigue failure modes

Fatigue refers to the progressive degradation of a material subjected to cyclic loading. In addition to structural fatigue, SMAs are also subject to functional fatigue (Eggeler *et al.*, 2004; Karhu & Lindroos, 2010; S. Stoeckel & Simpson, 1992; W. Tang & Sandström, 1993). For SMAs subject to cyclic loading, structural fatigue refers to the loss of a SMA's ability to resist stress due to crack propagation and fracture; whereas functional fatigue results in an actuator that is physically robust, but is compromised in its ability to exhibit the SME to recover the original shape (or to regenerate mechanical stress). The fatigue behaviour of SMA is an active research area, and existing predictive of SMA fatigue may be unreliable due to: the uncertainty of SMA mechanical properties, and complexity of mechanical response under multi-axial loading conditions (Mahtabi *et al.*, 2015; SW Robertson *et al.*, 2012); as well as potential incompatibility of classical fatigue theories for accommodating mean stress effects in metals (e.g. Soderberg and Goodman) with SMA fatigue prediction (SW Robertson *et al.*, 2012; Tuissi, 2012). It is clear that many aspects and factors have to be considered in the fatigue research of shape memory alloys which cannot all be covered in this present work. Therefore, only a few influential factors were selected and summarised in Section 7.6, including: applied stress and strain, and fabrication processes (melting, hot

work, cold work, heat treatment and final finishing) (Condorelli *et al.*, 2010; Dooley, Lasley, Mitchell, Steele, & Tittelbaugh, 2012; Eggeler *et al.*, 2004; Gall *et al.*, 2008; Karhu & Lindroos, 2010; DC Lagoudas *et al.*, 2009; Mahtabi *et al.*, 2015; S. Miyazaki *et al.*, 1999; Mohd Jani, Leary, Subic, *et al.*, 2014; Pattabi & Murari, 2015; Pelton, 2011; Pelton *et al.*, 2013; SW Robertson *et al.*, 2015; Schaffer & Plumley, 2009; S. Stoeckel & Simpson, 1992; Takeda, Mitsui, Tobushi, Levintant-Zayonts, & Kucharski, 2013; H. Tobushi *et al.*, 1998; Wilkes *et al.*, 2000).

To improve the fatigue performance and reliability of SMA actuators, a number of SMA design guidelines have been developed. For example, SMA actuators should be used according to the recommended load and strain (Dynalloy Inc., 2007; W. Huang, 2002; Mohd Jani *et al.*, 2014; Reynaerts & Brussel, 1998), require highly accurate temperature control (Karhu & Lindroos, 2010), and should not be exposed to overheating or overstressing (Karhu & Lindroos, 2010; Torra *et al.*, 2010). Materials and processing development have enhanced the fatigue behaviour of SMAs, whereby the fatigue life in excess of 1E6 cycles can be reliably achieved with the appropriate design and actuator training (Mohd Jani, Leary, Subic, *et al.*, 2014). The following work contributes novel relevant data to enable the robust commercial application of NiTi SMA-pulley systems.

Table 7.1 – Summary of SMA fatigue influential factors
(Condorelli *et al.*, 2010; Dooley *et al.*, 2012; Eggeler *et al.*, 2004; Gall *et al.*, 2008; Karhu & Lindroos, 2010; DC Lagoudas *et al.*, 2009; Mahtabi *et al.*, 2015; S. Miyazaki *et al.*, 1999; Mohd Jani *et al.*, 2014; Pattabi & Murari, 2015; Pelton, 2011; Pelton *et al.*, 2013; SW Robertson *et al.*, 2015; Schaffer & Plumley, 2009; Stoeckel & Simpson, 1992; Takeda *et al.*, 2013; H. Tobushi *et al.*, 1998; Wilkes *et al.*, 2000)

Factor	Effect
Stress and Strain	<p>Stress:</p> <ul style="list-style-type: none"> Significant factor affecting fatigue life in most studies (DC Lagoudas <i>et al.</i>, 2009; Mahtabi <i>et al.</i>, 2015; Mohd Jani, Leary, Subic, <i>et al.</i>, 2014; S. Stoeckel & Simpson, 1992), but reported as minor in (Karhu & Lindroos, 2010). Effects of increasing the stress level: <ul style="list-style-type: none"> Reduces fatigue life (Karhu & Lindroos, 2010; DC Lagoudas <i>et al.</i>, 2009; Mohd Jani, Leary, Subic, <i>et al.</i>, 2014). Increases transformation temperatures (A_s, A_f, M_s and M_f) (Eggeler <i>et al.</i>, 2004; DC Lagoudas <i>et al.</i>, 2009; S. Stoeckel & Simpson, 1992). Increases initial strain (Karhu & Lindroos, 2010; DC Lagoudas <i>et al.</i>, 2009). Reduces stability (higher drift), i.e. higher stroke rate variance (Karhu & Lindroos, 2010). The plateau stresses decrease with the increasing number of cycles (Eggeler <i>et al.</i>, 2004). <p>Strain:</p> <ul style="list-style-type: none"> Strain is a quantitatively significant factor affecting fatigue life (Karhu & Lindroos, 2010). Increasing the strain level on the SMAs reduces fatigue life (Eggeler <i>et al.</i>, 2004; Karhu & Lindroos, 2010; DC Lagoudas <i>et al.</i>, 2009; Mohd Jani, Leary, Subic, <i>et al.</i>, 2014; Takeda <i>et al.</i>, 2013; H. Tobushi, Ikai, Yamada, Tanaka, & LExcellent, 1996). Partial transformation strain can increase fatigue life tremendously compared to full transformation strain (Karhu & Lindroos, 2010; DC Lagoudas <i>et al.</i>, 2009; Pelton <i>et al.</i>, 2013; H. Tobushi <i>et al.</i>, 1998). Strain is directly proportional to the heating or activation duration, i.e. longer heating duration produces higher strain and reduces fatigue life (Eggeler <i>et al.</i>, 2004; Karhu & Lindroos, 2010; DC Lagoudas <i>et al.</i>, 2009; Mohd Jani, Leary, Subic, <i>et al.</i>, 2014; H. Tobushi <i>et al.</i>, 1996). In bending-rotation fatigue (BRF), increased rotational speed, reduced actuator diameter and increased ambient temperatures increase the heating rate of SMA actuators (Eggeler <i>et al.</i>, 2004; S. Miyazaki <i>et al.</i>, 1999; H. Tobushi <i>et al.</i>, 1998), resulting in higher strain and reduced fatigue life.

Factor	Effect
Fabrication processes	<p>Material composition:</p> <ul style="list-style-type: none"> Minor factor affecting fatigue behaviour (S. Miyazaki <i>et al.</i>, 1999). Effects of increasing the ternary element on the SMA such as Cu (replacing Ni) reduces recovery stress, stress hysteresis and maximum transformation strain, resulting in fatigue life improvement; however, it may also negatively leads to brittleness (DC Lagoudas <i>et al.</i>, 2009; S. Miyazaki <i>et al.</i>, 1999). Increasing A_f with additive such as nitrogen ions may increase fatigue life (Takeda <i>et al.</i>, 2013). <p>Melting processes:</p> <ul style="list-style-type: none"> (SW Robertson <i>et al.</i>, 2015) have focused their studies to find the relationship between microstructural properties and fatigue resistance and observed that fatigue superiority increases with better or higher purity melting processes, and the purity level for each process are ranked from the highest to the lowest as follows: High purity vacuum arc remelt (VAR), process optimised vacuum induction melting (VIM) +VAR, standard VIM+VAR, standard VAR and standard VIM. <p>Hot work (Microstructure and grain size):</p> <ul style="list-style-type: none"> Crucial effect on fatigue properties (Eggeler <i>et al.</i>, 2004; Wilkes <i>et al.</i>, 2000), where the thermomechanically treated provided better functional fatigue than the annealed treated microstructures (Pelton, 2011). Finer microstructure or higher dislocation density results in greater structural and functional fatigue, due to higher dislocation of slip resistance (Mahtabi <i>et al.</i>, 2015; Pelton, 2011). <p>Cold work (Shaping):</p> <ul style="list-style-type: none"> Cold rolling shifts the transformation temperatures to higher temperatures, and heat treatments regain the SME of cold-worked SMA (Pattabi & Murari, 2015). SMA with cold work ranging from 20% - 30% lasts longer than higher cold worked specimens due to lower initial defect state (IDS), such as oxidation and inclusion (Schaffer & Plumley, 2009). The hot rolled SMA demonstrates higher fatigue than the cold-drawn one due to the higher residual stresses (Gall <i>et al.</i>, 2008). Pre-straining of SMAs in a controlled manner can increase fatigue life (Dooley <i>et al.</i>, 2012). <p>Heat treatment:</p> <ul style="list-style-type: none"> Crucial factor for functional fatigue (actuator stability), but minor for structural fatigue (Karhu & Lindroos, 2010). Effects of increasing the heat treatment temperature: <ul style="list-style-type: none"> Does not affect the surface morphology (Condorelli <i>et al.</i>, 2010), but significantly increases fatigue life (treatment at 500°C(Condorelli <i>et al.</i>, 2010) and up to 550°C (Gall <i>et al.</i>, 2008; DC Lagoudas <i>et al.</i>, 2009)). Increases plastic strain and transformation temperatures (A_s, A_f, M_s and M_f) (Gall <i>et al.</i>, 2008; Karhu & Lindroos, 2010; DC Lagoudas <i>et al.</i>, 2009). Reduces strain and stress plateau (up to 300°C (Gall <i>et al.</i>, 2008), 420°C (Karhu & Lindroos, 2010) and 550°C (DC Lagoudas <i>et al.</i>, 2009)). Hardness increases and reduces after 300°C (Gall <i>et al.</i>, 2008). Effects of increasing the heat treatment duration: <ul style="list-style-type: none"> Reduces fatigue life (above 15 minutes) (DC Lagoudas <i>et al.</i>, 2009). Increases transformation temperatures (A_s, A_f, M_s and M_f) (Karhu & Lindroos, 2010; DC Lagoudas <i>et al.</i>, 2009). Above 410°C, reduces R-phase (reduces $R_f - R_o$), and increases hysteresis (increases $A_s - R_o$) (Karhu & Lindroos, 2010). Reduces stability and transformation strain (Karhu & Lindroos, 2010). Softer material and increases initial strain (Karhu & Lindroos, 2010). <p>Final finishing or treatments:</p> <ul style="list-style-type: none"> Surface treatment such as electro (Condorelli <i>et al.</i>, 2010; SW Robertson <i>et al.</i>, 2015) and mechanical-polishing (Pelton <i>et al.</i>, 2013) increase fatigue life. The effects of surface finish quality is more obvious in BRF due to the difference in stress/strain distribution across the specimen section, where the outer layers (or outer surface) encounter higher stress/strain than inner layers (or inner surface) (Mahtabi <i>et al.</i>, 2015). Surface defects such as TiC particles, pores, laser burns and surface cracks contribute to crack initiation and fatigue failures (Eggeler <i>et al.</i>, 2004; Mahtabi <i>et al.</i>, 2015). Has limited effect on fatigue life under low strain (~1%) amplitude, but highly significant for intermediate (2%) and high strain (5-10%) amplitudes (Pelton <i>et al.</i>, 2013).
Others	<ul style="list-style-type: none"> Higher test (ambient) temperature reduces fatigue life (S. Miyazaki <i>et al.</i>, 1999; Pelton <i>et al.</i>, 2013), in particular exceeding A_f for shape memory effect (SME) materials. Fatigue life may reduce as the SMA actuator diameter increases due to higher impurities (Mahtabi <i>et al.</i>, 2015).

7.4 Shape memory alloy actuator and pulley system

Pulley systems may be used in various ways to provide technical advantage, including the amplification of force or displacement for a given work, or in transmitting power, torque and velocity from one rotating mechanism to another. Due to these advantages, pulley systems are compatible with many SMA actuator designs to increase their force and stroke capacity within the available packaging envelope, as shown in Figure 7.2. Despite the importance of pulley systems to the commercialisation of SMA systems, the authors are aware of no formal studies that specifically determine the effect of pulley system configurations on structural and functional fatigue performance of SMA actuators.

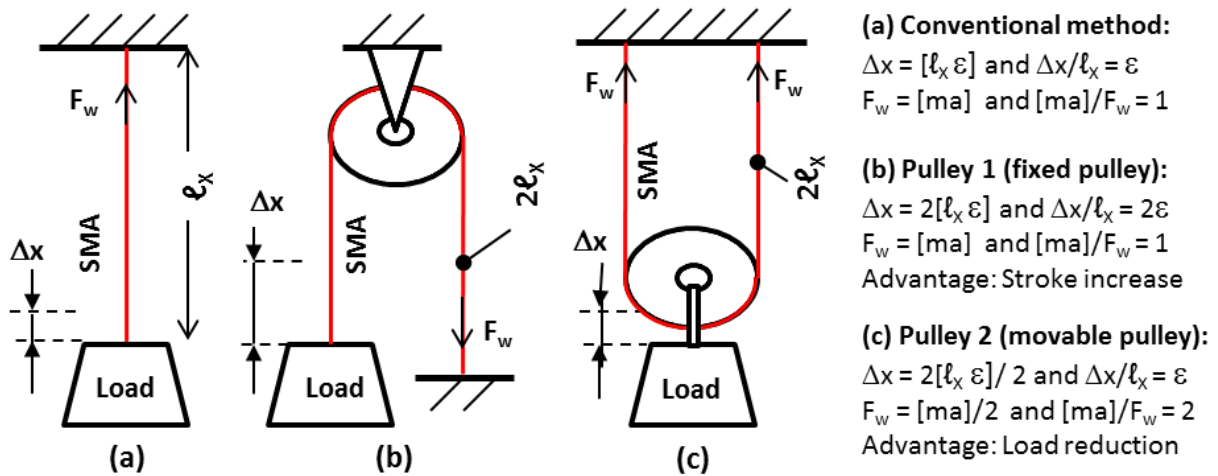


Figure 7.2 - SMA pulley system advantage with approximately similar packaging size

7.4.1 Drive element and pulley

In a pulley system, a flexible drive element such as a rope or cable is used in conjunction with a pulley (sheave). Correct sheave design is crucial for the service life of drive element (refer Figure 7.3) (Command, 1976a; Gibson, 2001; Nabijou & Hobbs, 1994). Adequate support and sufficient clearance are required to maximize load and to minimize friction (Gibson, 2001). The drive element is typically stranded or braided to increase strength, resulting in interstrand (within the drive element) and interactive (between drive element and pulley) failure modes (Nabijou & Hobbs, 1994). The impact of small wrap angle and arc of contact, $s=r\theta$ on fatigue life of braided drive elements is not clearly understood. Some evidence suggests a monotonic decrease in fatigue life for tests involving wrap angles up to one arc of contact-to-lay length ratio, s/L_{lay} (curve A, Figure 7.4); other tests conducted at specific wrap angle less than one s/L_{lay} show that the results are more damaging (curve B, Figure 7.4) below one s/L_{lay} (Command, 1976a). However, it is obvious that the fatigue damage is virtually insignificant for a braided drive element with wrap angle less than $0.1 s/L_{lay}$ and almost constant with wrap angle above one s/L_{lay} , regardless of which trend is actually correct (Command, 1976a; Gibson, 2001). There are notable exceptions and special considerations, where this factor is may also dependant on the specific drive element design, the sheave-to-drive element diameter ratio (D/d), and the operating tension (Command, 1976a; Gibson, 2001).

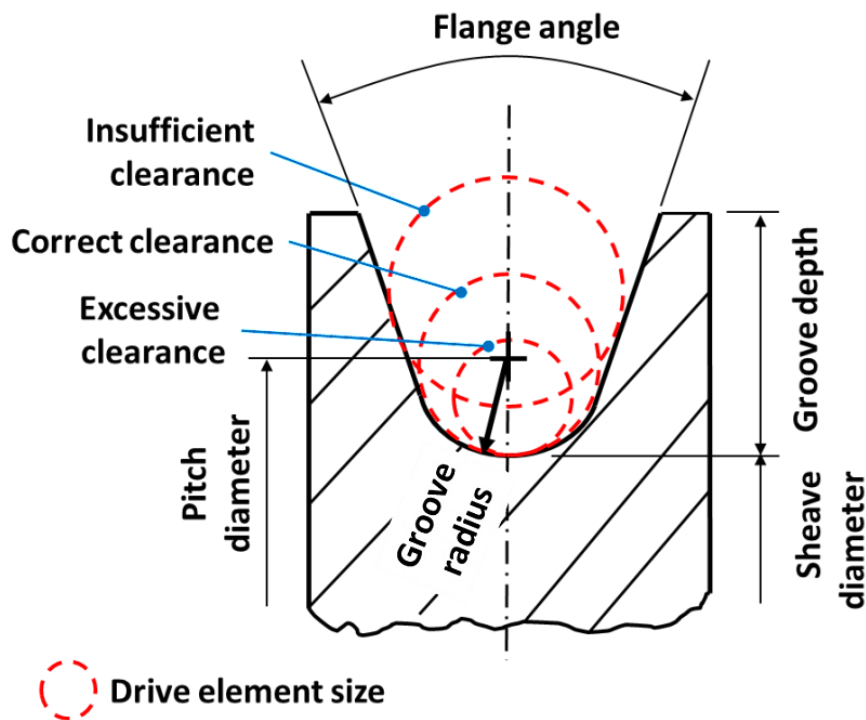


Figure 7.3 - Recommended sheave design

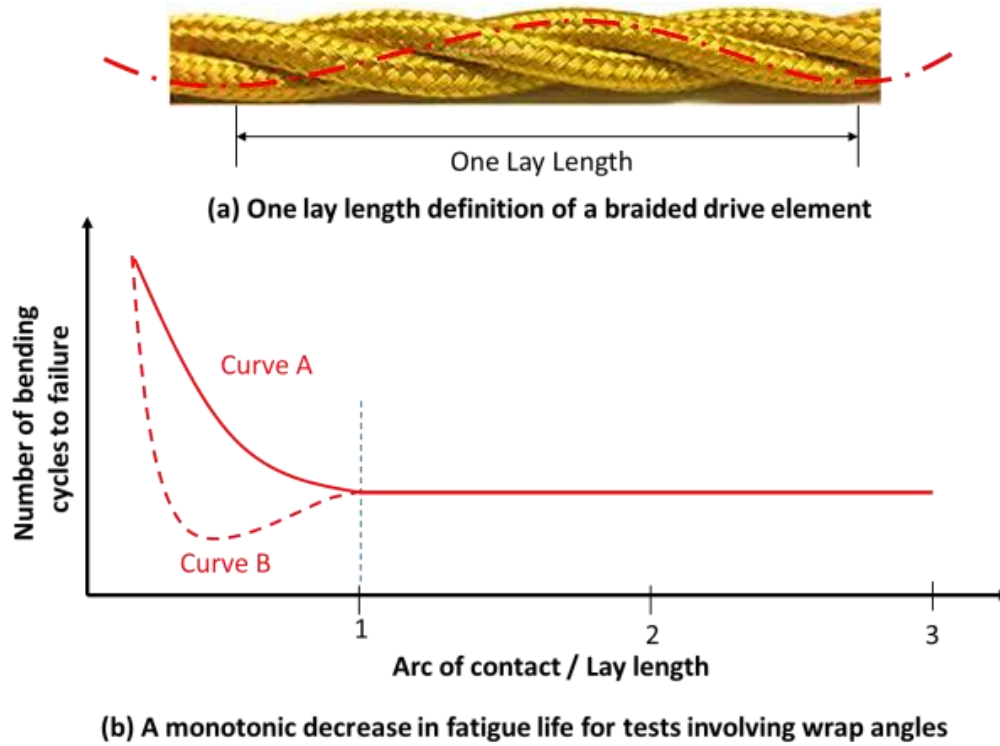


Figure 7.4 - Effect of angle of wrap on drive element with a pulley system

However, a single SMA actuator is used as the drive element in this work; therefore, the interstrand failure mode is irrelevant, and the SMA drive element of the pulley system experiences a cyclic change of stress due to repeated bending. The mechanical factors that have been identified to affect drive element fatigue in a simple pulley system are summarised in Table 7.2 (Chaplin, 2008; Command, 1976a; Gibson, 2001; Nabijou & Hobbs, 1994).

**Table 7.2 - Typical mechanical effects on fatigue life of a pulley drive element
(Chaplin, 2008; Command, 1976a; Gibson, 2001; Nabijou & Hobbs, 1994)**

Structure	Factor	Remark
Sheave	Surface roughness	<ul style="list-style-type: none"> Increased surface roughness results in reduced fatigue life due to abrasion (Command, 1976a) or fretting. The groove surface has to be smooth and clean (Gibson, 2001).
	Material	<ul style="list-style-type: none"> Non-metallic sheaves such as plastic or nylon could provide some advantages in reducing the drive element wear and contact stress. However, it is not recommended for applications with high loads, large motions or high temperatures (Command, 1976a; Gibson, 2001). Steel sheaves are recommended to be hardened to minimize material wear and deformation which can reduce the fatigue life of the drive element (Gibson, 2001).
	Diameter	<ul style="list-style-type: none"> For braided drive elements, the interactive failure predominant larger sheave-to-drive element diameter ratio ($D/d \geq 18$) or loads below 40% of the rated strength, and the interstrand failure with $D/d \leq 16$ and/or 55% or more of the rated strength (Nabijou & Hobbs, 1994). Fatigue life increases with the sheave-to-drive element diameter ratio (D/d) due to a reduction in normal and bending stress on the drive element (i.e. drive element strength increments) (Chaplin, 2008; Command, 1976a; Gibson, 2001). One of the important factors affecting fatigue life (Chaplin, 2008).
	Groove profile	<ul style="list-style-type: none"> The groove design or profile significantly influences the fatigue performance of a pulley system (Command, 1976a; Gibson, 2001; Nabijou & Hobbs, 1994) (refer Figure 7.3). The groove depth should provide adequate support and sufficient clearance for the drive element to enter and leave the sheave with minimal friction (Gibson, 2001). Generally, the groove depth and diameter should be equal or slightly larger than the diameter of the drive element when measured at zero tension, and should include an ample flange angle (Command, 1976a; Gibson, 2001). The drive element tends to flatten if clearance is excessive, resulting in deformation and reduced fatigue life. Insufficient clearance results in rubbing between drive element and sheave flange, resulting in increased friction and reduced fatigue life (Gibson, 2001).
Drive Element	Angle of wrap	<ul style="list-style-type: none"> Drive element depends on friction to grip and rotate around the sheave. This friction is associated with wrap angle, which is directly proportional to the normal and centrifugal forces acting on the pulley system. Friction and acting forces increase with wrap angle applied (Collins, Busby, & Staab, 2010). <p>For braided drive elements:</p> <ul style="list-style-type: none"> A significant increase in fatigue life can be achieved with very small angles of wrap, where the drive element does not fully conform to the sheave curvature (Chaplin, 2008) (refer Figure 7.4). Generally, the fatigue damage is virtually insignificant for a braided drive element with wrap angle less than $0.1 \pi/L_{ay}$, gradually reduces as the wrap angle increases, and almost constant with wrap angle above one π/L_{ay} (Command, 1976a; Gibson, 2001).
	Load	<ul style="list-style-type: none"> Fatigue life reduces as the load level on the driving element increases, due to the increase of abrasion on the contacted surface (i.e. normal and contact stress)(Command, 1976a). One of the important factors affecting fatigue life (Chaplin, 2008).

7.5 Design of Experiments

The design of experiments (DOE) refers to a systematic approach to quantify the effects of the identified independent variables (factors) on some dependant variable (objective function) of interest.

7.5.1 Full-factorial design of experiments

Full-factorial DOE assumes that interaction between factors may exist, and requires that all factors, k , be assessed independently at the selected number of levels, L . Full-factorial DOE allows statistically robust insight into the effect of all factors on the objective function as well as factors interactions. Full-factorial DOE requires L^k experimental evaluations, and can therefore be prohibitively expensive. The expense of full-factorial DOE is exacerbated in this work as:

- Commercial applications often requires high-cycle fatigue durability (Eggeler *et al.*, 2004; Fumagalli *et al.*, 2009), thereby necessitating a large testing time for a single experiment. For example, the SMA actuator of Table 7.4 has a minimum reported cycle time of 15 seconds; however 41 seconds are required to allow for complete cooling to ambient temperature, which requires approximately 47 days of continuous actuation to achieve 100,000 cycles for a single SMA actuator.
- Fatigue is a highly localised phenomenon with significant stochastic uncertainties (Veers, 1996), especially for high-cycle scenarios (Jahn & Maennig, 1997). This stochastic effect requires a relatively large sample size to acceptably characterise the fatigue response, thereby multiplying the total testing time; sample size considerations are discussed in Section 7.5.

For example, in this work a full-factorial DOE of the proposed designs requires approximately 2064 days of continuous testing (Table 7.3). Fractional factorial and Taguchi methods have been investigated to ameliorate test duration without excessively compromising test outcomes.

7.5.2 Fractional-factorial design of experiments

Fractional-factorial DOE eliminates elements of the full-factorial design in order to reduce the required experimental time. Fractional-factorial DOE requires L^{k-p} experiments, where p is the associated *fractional number* or *generators*. The *goodness* of the fractional-factorial DOE is indicated by the design resolution (GEP Box & Hunter, 1961) or the aberration criterion (Fries & Hunter, 1980); however these criteria do not guarantee optimal experimental design (Chen, Sun, & Wu, 1993). Fractional-factorial DOE requires fewer experiments than full-factorial. For example, for $p = 1$, the fractional factorial requires about 33% of the experimental time of the full-factorial DOE for the main experiment (Table 7.3). Further reductions in experimental time are enabled by Taguchi methods.

Table 7.3 - Comparison of DOE method experimental durations

DOE method	Number of factors, k	Number of levels, L	Number of test conditions	Number of tests	Estimated experiment duration	Time fraction of Full-factorial
Full-factorial	4 and 2	3	$3^4+3^2=81+9=90$	$(81 \times 3) + (9 \times 2) = 261$	2064 days	100%
Fractional-factorial (resolution: IV)	4 and 2	3	$3_{IV}^{4-1}+3^2=27+9=36$	$(27 \times 3) + (9 \times 2) = 99$	783 days	38%
Taguchi	4 and 2	3	$9+9=18$	$(9 \times 3) + (9 \times 2) = 45$	356 days	17%
<p>As in the experimental phase of this work (Section 7.7):</p> <ul style="list-style-type: none"> 4 factors for main experiment and 2 factors for control experiment. Both experiments have 3 levels. Duration for a single replication = $41s \times 100,000 = 4,100,000s = 47.45$ days. For each test condition: 3 replications for main experiments and 2 replications for control experiment. Each experiment using 6 multi-configurable fixtures to reduce the duration. <p>E.g. for Taguchi estimated duration:</p> <ul style="list-style-type: none"> Total experiment = $(9 \text{ test conditions} \times 3 \text{ replications}) + (9 \text{ test conditions} \times 2 \text{ replications}) = 45$ tests. Total experiment duration = $(47.45 \text{ days} \times 45 \text{ tests}) / 6 \text{ fixtures} = 356$ days. <p>Note: Estimated durations exclude confirmation tests. The number of tests required for fractional design maybe lesser than the estimated duration in this work due to lower number of replications required.</p>						

7.5.3 Taguchi method and ANOVA

Taguchi methods intend to improve real-world system performance without unnecessary experimental cost. The Taguchi method differs from full-factorial DOE in which influential factors are defined as either being controllable (control factors) or uncontrollable (noise factors). A minimum of two levels are required to estimate the factor effect, and the impact of noise factors reduces by repetitions (i.e. repeats similar test condition with more than one response). Based on the number of identified factors and desired levels, a Taguchi Orthogonal Array (OA) is selected to formally define the experimental sequence (T. Mori, 2011; Taguchi, 1987; Taguchi & Clausing, 1990). Taguchi methods assume that no interaction between factors exists, thereby allowing a significant reduction in the number of

experiments required with full-factorial DOE (T. Mori, 2011; Taguchi & Clausing, 1990). For example, in this work, the Taguchi DOE with four factors and three levels used a L9 OA which requires about 17% of the tests required for the full-factorial DOE.

Taguchi methods have been criticized as being: incompatible with highly nonlinear problems (G. Box, 1988; Nair *et al.*, 1992; Tsui, 1992) and incorrectly combining mean variance (Maghsoodloo, Ozdemir, Jordan, & Chen-Hsiu Huang, 2004). Despite these criticisms, advocates report that the significant reduction in experiment size enables a highly practical approach to the optimisation of complex and multivariate processes (Maghsoodloo *et al.*, 2004; T. Mori, 2011; Nair *et al.*, 1992; Taguchi & Clausing, 1990; Tsui, 1992). In addition, Taguchi methods are commonly combined with other statistical methods, notably Analysis of Variance (ANOVA), to statistically characterise the factor influence on the objective function and enable for a more robust design (Tsui, 1992), for example (Jong, Chen, Tsai, Chiu, & Chang, 2006; Kochure & Nandurkar, 2012).

The signal-to-noise ratio (S/N) identifies the optimum levels of each factor, depending on the associated performance objective, which can be calculated in three typical S/N conditions: minimizing the response with smaller the better (STB), maximizing the response with larger the better (LTB), or targeting the response to the standard deviations and means of samples with nominal the best (NTB). Regardless of the performance objectives, a higher S/N corresponds to better quality and the highest S/N manifest the optimal level for the identified factors. The S/N conditions are defined in (Eq. 7.1), where MSD is the Mean Square Deviation, n is the total number of observations, y_i is the deviation of the observations, \bar{y} is the overall mean, and S_y^2 is the variance of y , (Taguchi, 1987).

Taguchi practitioners typically applied ANOVA to identify which factors most influence the average response and S/N ratio statistically. Moreover, ANOVA utilises replication to test the equality of means and correlate them. Therefore, the inferential testing becomes more reliable and economical, where the responses are not divided between conditions and each response is measured under all conditions. To ensure interaction effects have not confounded the results, a confirmation experiment is typically completed to confirm the performance of the identified optimal combination of factors (Section 7.8.5).

$$S/N = -10\log(MSD) \begin{cases} -10\log \left[\frac{1}{n} \sum_{i=1}^n \frac{1}{y_i^2} \right], \text{if } LTB \\ 10\log \left[\frac{\bar{y}^2}{S_y^2} \right], \text{if } NTB \\ -10\log \left[\sum_{i=1}^n \frac{y_i^2}{n} \right], \text{if } STB \end{cases} \quad (\text{Eq. 7.1})$$

In this work, functional fatigue is optimised when the change in SME effect is minimised. Therefore, by applying the S/N ratio in the Taguchi method, functional fatigue performance is assessed with smaller-the-better (STB).

7.6 Fatigue factors and effect levels selection

Referring to the influencing factors affecting fatigue performance of a pulley system from Table 7.2, four factors are selected to be assessed in this work:

- Stress (or load)
- Strain (or stroke)
- Sheave diameter
- Angle of wrap

The other factors are not selected for the following reasons:

- A common drive element (i.e. SMA actuator) is used in all experiments. Therefore, materials and material fabrication-related factors such as material composition, melting processes, hot work, cold work, material treatments and furnishing, are insignificant.
- A common sheave material and groove design is applied and therefore it is insignificant in these experiments.
- ABS material is used for the sheave, and therefore the surface roughness effect is insignificant (confirmed by visual inspection in Section 7.8.3).

Taguchi methods have been applied to quantify the impact of pulley characteristics on fatigue performance of Ni-Ti SMA actuators subject to varying load (stress), activation duration (strain) and pulley configurations (sheave diameter and angle of wrap). For each factor, three levels of effects (i.e. low, mid and high) are selected to identify non-linearity and categorise the associated concavity, as listed in Table 7.6. For the SMA actuator specified for this work (Table 7.4), the authors' numerical model (Mohd Jani *et al.*, 2015b) was applied to estimate the required actuation duration for the SMA actuator to fulfil a partial or complete transformation cycle (Section 7.7.2).

7.7 Experimental contribution

The Ni-Ti SMA actuator specification in Table 7.4 was selected as it has a precedent of application in automotive and commercial applications (M. Leary *et al.*, 2013), and was applied in all experimental phases of this work.

**Table 7.4 - Physical and mechanical of SMA actuator
(Dynalloy Inc., 2007; Mohd Jani *et al.*, 2015a)**

Property	Symbol	Units	Value	
			Martensite	Austenite
Density	ρ_D	kg/m ³	6450	
Specific heat capacity	c	J/kg.K	322.4	
Melting point	T_m	°C	1300	
Latent heat of transformation	L	kJ/kg	24.2	
Thermal conductivity	k	W/m.K	8	18
Thermal expansion coefficient	α	m/m.K	6.6 x 10 ⁻⁶	11.0 x 10 ⁻⁶
Poisson's ratio	ν	-	0.33	
Material composition	50%Ni, 50%Ti			
Wire diameter	0.51 mm (0.02 in)			
Wire length	100 mm (pre-crimped by manufacturer)			
Wire type	HT (90°C austenite start temperature)			
Resistance	4.3 Ω /m			
Pull force	max. 3560g for 0.51mm diameter (based on 172MPa max. safe stress), 1s (with 4A)			
Heating time (approximate)				
Cooling time (approximate)	14s (at room temperature in static air, using a vertical wire)			

7.7.1 SMA failure definition

Structural fatigue of the SMA-pulley system was assessed by the number of cycles performed until fracture, or the endurance limit. An endurance limit of 1E5 cycles was selected to be compatible with the typical upper service life specification for consumer and automotive products (Eggeler *et al.*, 2004; Fumagalli *et al.*, 2009; D. Homma, 2004). Functional fatigue is defined by the measured *drift*, i.e. the change in stroke, Δx , between the initial cycle and a reference cycle, N_{drift} . In this work, N_{drift} is selected to be 3E4 cycles as structural fatigue was never observed prior to 3E4 cycles, allowing a drift value to be reported for each sample, and an observation of the experimental outcomes showed that significant fluctuation in the observed stroke is typically stabilised for $N > 3E4$ (Section 6) or earlier (Eggeler *et al.*, 2004; Mahtabi *et al.*, 2015; Maletta *et al.*, 2012; S. Miyazaki *et al.*, 1986).

7.7.2 Prediction of activation duration

The developed numerical model to predict SMA linear actuator thermomechanical behaviour under variable environmental and design conditions (Mohd Jani *et al.*, 2015b) in Chapter 6 is utilised to simulate the thermal response of SMA linear actuator with Joule heating. Necessary parameters including: ambient conditions (temperature and convective heat transfer coefficient), pre-stress applied, load condition (with deadweight), SMA properties (size, transformation temperatures, resistance, thermal diffusivity and latent heat of transformation), applied current, and constitutive model variables (i.e. stress-influenced coefficients and thermal tensors). From this input data, practical predictions of strain-heating duration relationship is generated (Figure 7.5).

For the SMA actuator specified for this work (Table 7.4), the authors numerical model was applied to estimate the actuation duration required for the SMA actuator to fulfil a partial or complete transformation cycle as follows (Figure 7.5):

- a) 750ms (low strain): Partial transformation cycle between 0 to 34% of full strain
- b) 1000ms (mid strain): Partial transformation cycle between 35 to 75% of full strain
- c) 1500ms (high strain): Complete transformation cycle ($\geq 100\%$ of full strain)

These simulated results were used as a basis for the testing levels used in this work, and predictions were found to be comparable with the experimental observations (Section 7.7).

Table 7.5 - Estimated strain with heat transfer model

<i>Applied Stress</i>	<i>A_s</i>		<i>A_f</i>		<i>Estimated strain [%]</i>		
	<i>T</i> [°C]	<i>t</i> [ms]	<i>T</i> [°C]	<i>t</i> [ms]	<i>750ms</i> <i>(Low)</i>	<i>1000ms</i> <i>(Mid)</i>	<i>1500ms</i> <i>(High)</i>
2000gm = 96.8 MPa	102	584	112	1,212	1.24	3.06	4.59
3000gm = 145.2 MPa	109	639	119	1,272	0.87	2.65	4.60
4000gm = 193.6 MPa	116	694	126	1,333	0.51	2.24	4.61
Note: Estimated strain level for SMA wire with deadweight (without pulley system) for the 1 st cycle. The temperature, T and time, t are the estimated start temperatures and activation duration for austenite phases (start and final) at ambient condition ($T_{\infty} = 23^{\circ}\text{C}$, $h = 45\text{W/m}^2.\text{K}$).							

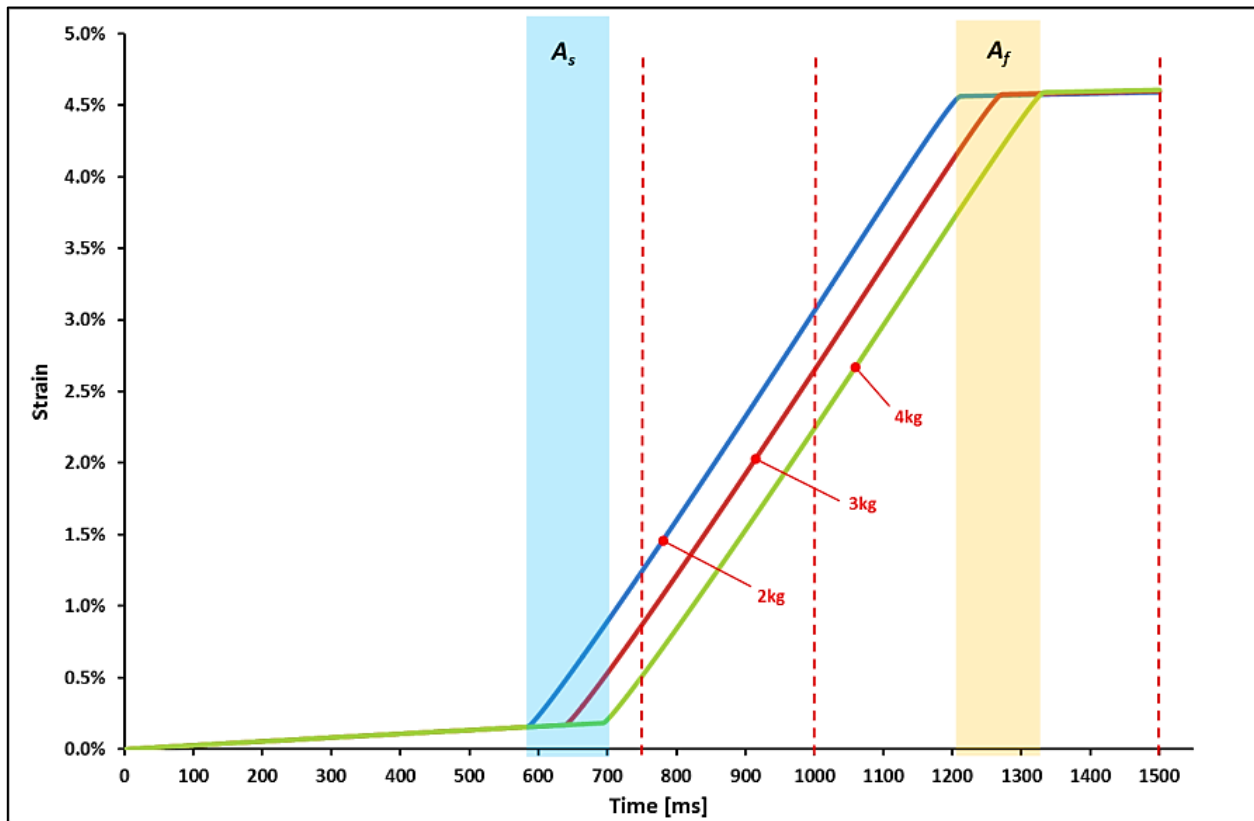


Figure 7.5 – Numerical results of SMA linear actuators under variable load and activation duration (based on Table 7.5)

7.7.3 Main experiment

The four factors and three levels identified for the main experiment are defined in Table 7.6. To determine the impact of the pulley system on the Ni-Ti SMA fatigue performance and reliability, primary factors were identified as: applied load, Joule heating duration, sheave diameter and angle of wrap. To enable the identification of non-linear effects, these factors were assessed at three levels (low, mid and high), resulting in the L9 Taguchi orthogonal array (Taguchi, 1987) (Table 7.10).

Table 7.6 - Experiment factors and levels for main experiment

<i>Factors</i>	<i>Levels</i>		
	Low	Mid	High
Sheave diameter, D_{Sheave} (mm)	15	20	30
Load (grams) / Stress, W (MPa)	2000/96.8	3000/145.2	4000/193.6
Activation duration, t_{act} (ms)	750	1000	1500
Angle of wrap, θ (°)	90	135	180

A total of 27 tests (i.e. 9 test conditions with 3 replications) were conducted in this main experiment; requiring a maximum of 214 days of continuous testing (Table 7.3).

7.7.4 Control experiment

To provide a reference baseline to compare the effects of the pulley system on the SMA fatigue, a control experiment was conducted on linear SMA actuators with no pulley system. These experiments used a freely suspended deadweight (Figure 7.2a) with two factors (applied load and Joule heating duration) at three levels (see Table 7.7), resulting in a second L9 Taguchi OA (see Table 7.11). A total of 18 tests (i.e. 9 test conditions with 2 replications) were conducted in this control experiment.

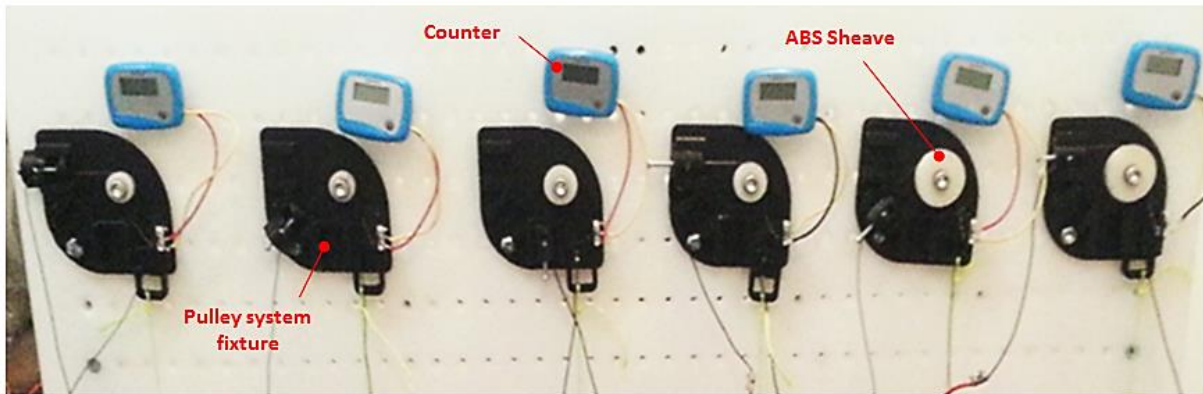
Table 7.7 - Experiment factors and levels for control experiment

<i>Factors</i>	<i>Levels</i>		
	Low	Mid	High
Load (grams) / Stress, W (MPa)	2000/96.8	3000/145.2	4000/193.6
Activation duration, t_{act} (ms)	750	1000	1500

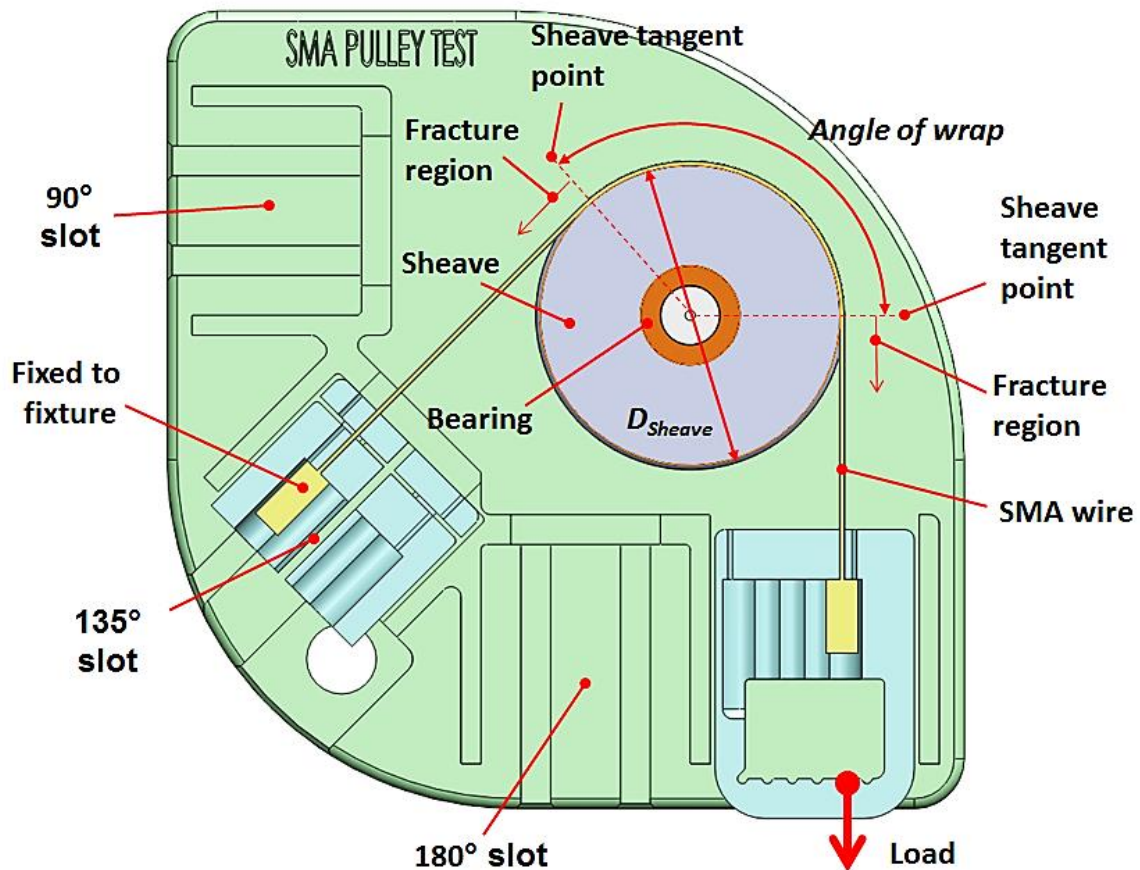
The control experiment requires a maximum of 142 days of continuous testing, which combined with the main experiment requires a total maximum of 356 days, i.e. 17% of the time required for the equivalent full-factorial DOE (Table 7.3).

7.7.5 Experimental apparatus

To reduce the test duration, an experimental apparatus was constructed with six multi-configurable fixtures (Figure 7.6), where the SMA actuators were wound over the ABS sheaves with one end ground to the fixture and the other end fixed to the constant loads (deadweight). Both ends were fixed to prevent any torsional movement of the SMA actuator about its axis. Furthermore, ABS sheaves and rolling element bearings were used to minimise friction between the sheaves with the drive elements and their shaft respectively. A microcontroller was set to actuate each SMA actuator via Joule heating with a constant power supply of 12VDC and 4A for the specified activation duration, and then permitted to cool until no extension was detected for approximately 41 seconds. Electronic counters recorded the number of SMA cycles. To minimise the impact of environmental variables (e.g. temperature and humidity), ambient conditions were maintained within the following parameters: room temperature $23\pm 2^\circ\text{C}$ and humidity $50\pm 10\%$.



a) SMA linear actuator testing bench with six multi-configurable fixtures



b) CAD Model of SMA-Pulley multi-configurable fixture

Figure 7.6 - Experimental apparatus for SMA-pulley system. Actuator shown in 135° position

7.8 Results

The experimental data was analysed graphically to allow for a general understanding of the fatigue behaviour of SMA actuators. Visual inspection was conducted on the fracture surface and location to investigate the fracture characteristic of the SMA-pulley system. Finally, the results were analysed with Taguchi and ANOVA to determine the effects and the optimal configurations when applying the pulley system on SMA actuators.

7.8.1 Graphical results interpretations

The experimental fatigue data of this work is analysed and the average stroke-number of cycle data were expressed using a novel bi- or tri-linear representation developed in this work as illustrated in Figure 7.7. In summary, the graphical result interpretations are:

- In general, the observed stroke initially decreases rapidly with increasing N . The general cyclic response showed an initially steep decrease in stroke followed by a shallow response.
- All SMA actuators with the activation duration of 750ms and 1000ms survived to the specified endurance limit of $1E5$ cycles.
- Structural fatigue failure only occurred for the activation duration of 1500ms (i.e. actuator being heated in excess of the complete transformation). In all cases structural fatigue occurred at $N > 3E4$ cycles.
- Application of pulley system reduced the SMA actuator stroke performance (comparison between main and control experiment results). For example (refer Figure 7.7b): the stroke reduced from approximately 3.23mm (C2: 2000g and 1000ms) to 2.29mm (P4: 2000g, 1000ms, $\varnothing 20$ mm and 180°).

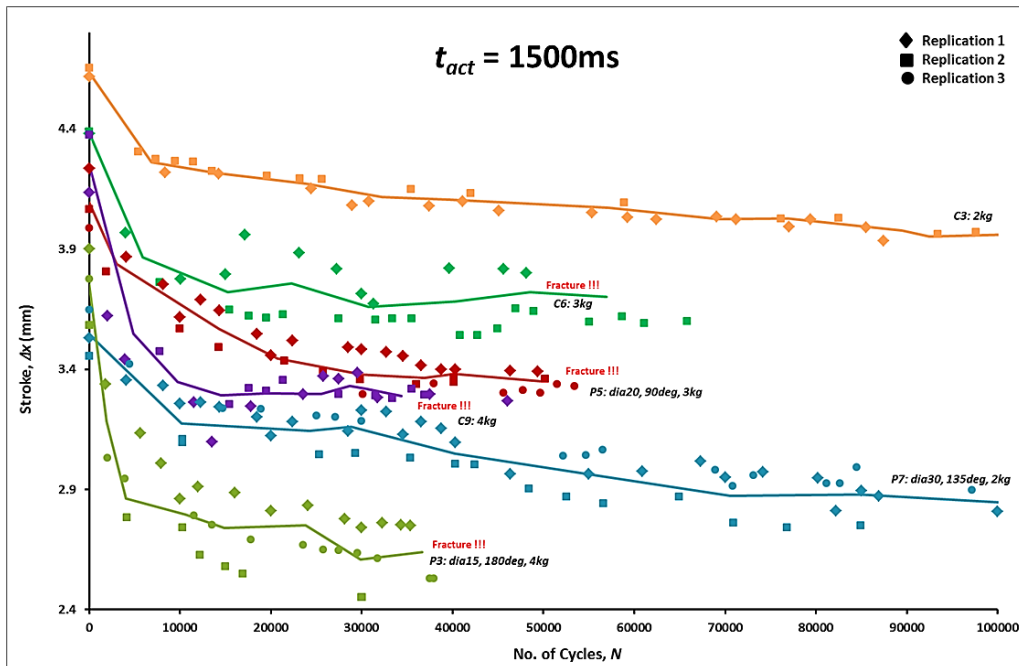


Figure 7.7 - Results of SMA fatigue test at activation duration of 1500ms

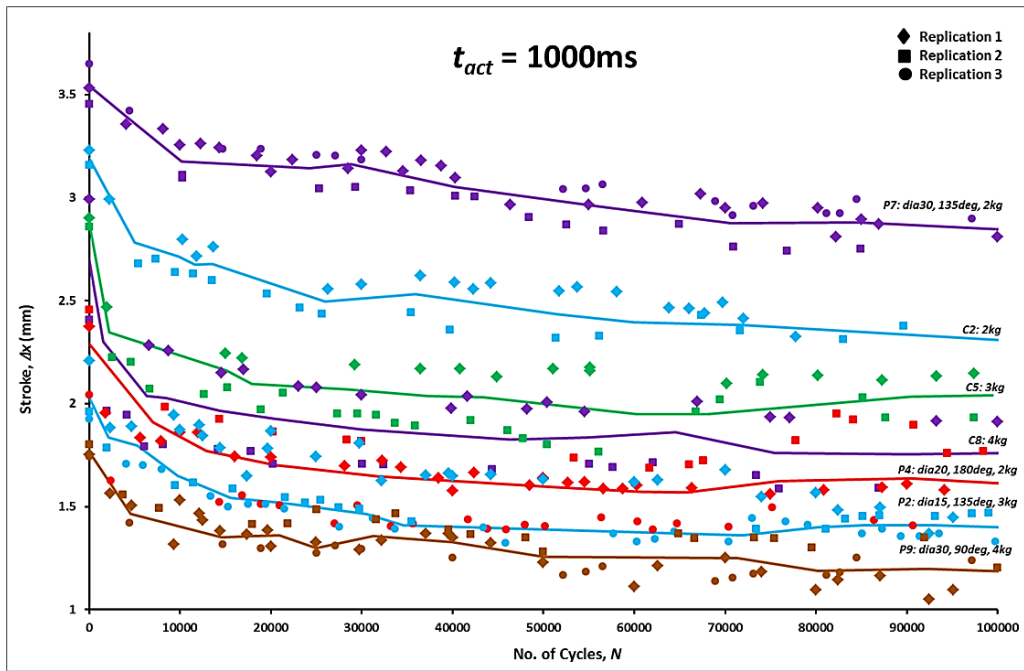


Figure 7.8 - Results of SMA fatigue test at activation duration of 1000ms

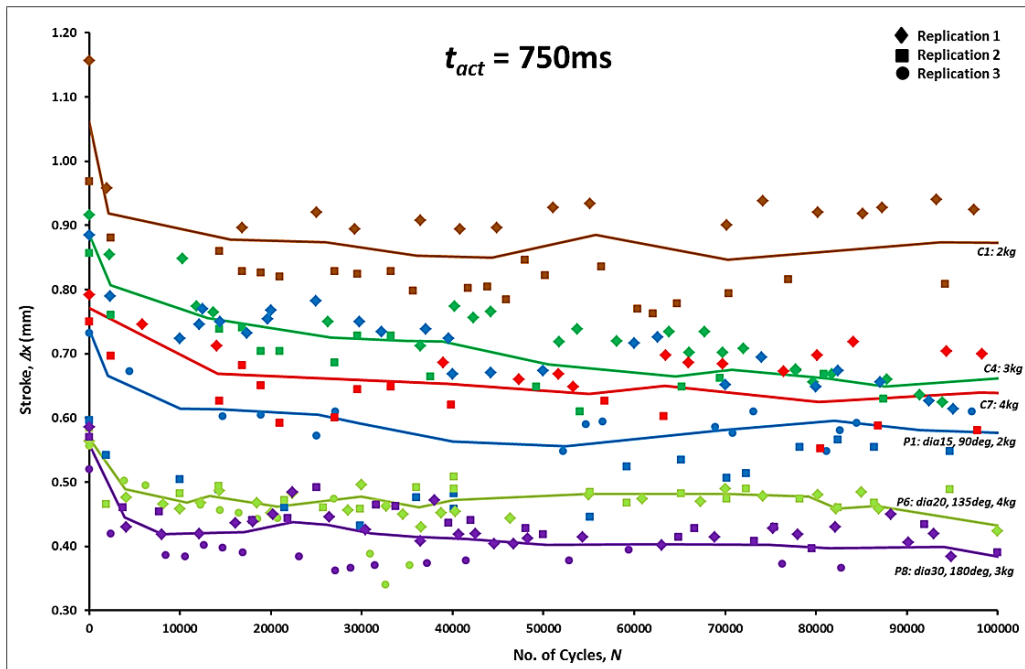


Figure 7.9 - Results of SMA fatigue test at activation duration of 750ms

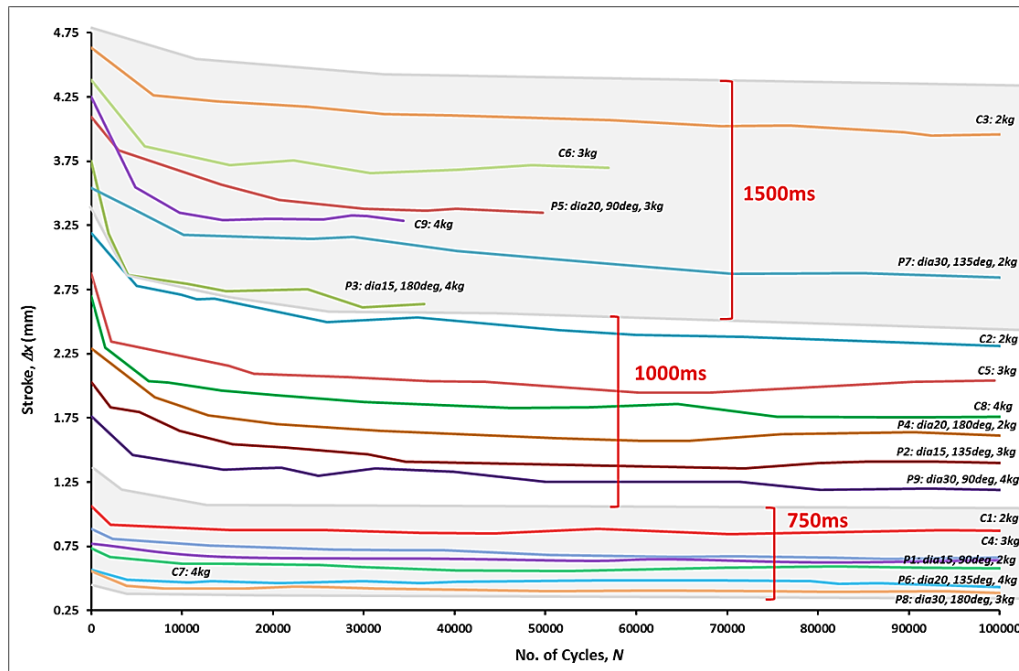


Figure 7.10 – SMA fatigue test results at three activation duration levels

Table 7.8 - Numerical model and experiment strain level comparison for the 1st cycle

Load	Strain [%]								
	$t_{act} = 750ms$			$t_{act} = 1000ms$			$t_{act} = 1500ms$		
	N. Model	Exp.	Err. (%)	N. Model	Exp.	Err. (%)	N. Model	Exp.	Err. (%)
2kg	1.24	C1: 1.10	12.73	3.06	C2: 3.16	3.16	4.59	C3: 4.61	0.43
3kg	0.87	C4: 0.89	2.25	2.65	C5: 2.81	5.69	4.60	C6: 4.44	3.60
4kg	0.51	C7: 0.59	13.56	2.24	C8: 2.70	17.04	4.61	C9: 4.24	8.73
Mean prediction Section: 7.47%, sample standard deviation in error: 5.82%.									

7.8.2 Linear fit analysis

The general cyclic response (Figure 7.11) shows an initially steep decrease in stroke followed by a shallow response. To allow general understanding of material response, and assist in the design of SMA actuators a linear curve fit model is proposed. The models are generated by performing analysis on the responses to calculate the best fit curves for stepwise linear segments that intersect at intermediate points. This hypothesis is assessed for bi-linear and tri-linear curves in in Figure 7.11 and Figure 7.12, and summarised in Table 7.9 (details in Appendix S), in summary:

- Statistically, the coefficient of determinations (R^2) for the generated bi-linear and tri-linear curves approach unity and provide excellent approximation of functional fatigue performance versus number of cycles.
- Higher correlation is obtained with tri-linear fit curves (higher R^2 and lower standard deviation for tri-linear fit curves).
- For tri-linear curve, the deformation rate (i.e. the rate of change of stroke with N) is highest during the first segment of linear fit curves, until approximately $4.3E3$ cycles, after which further reduces and stabilises beyond $3E4$ cycles.
- The intermediate point for bi-linear curve are averaging at $13.6E3$ and $16.4E3$ cycles for main (SMA-pulley system) and control experiments respectively.
- The initial stroke typically decreases with increasing load.
- As N increases, the deformation rate tends to reduce, and may asymptote towards some constant value. The identified transition borderline is also expected to show similar characteristic.

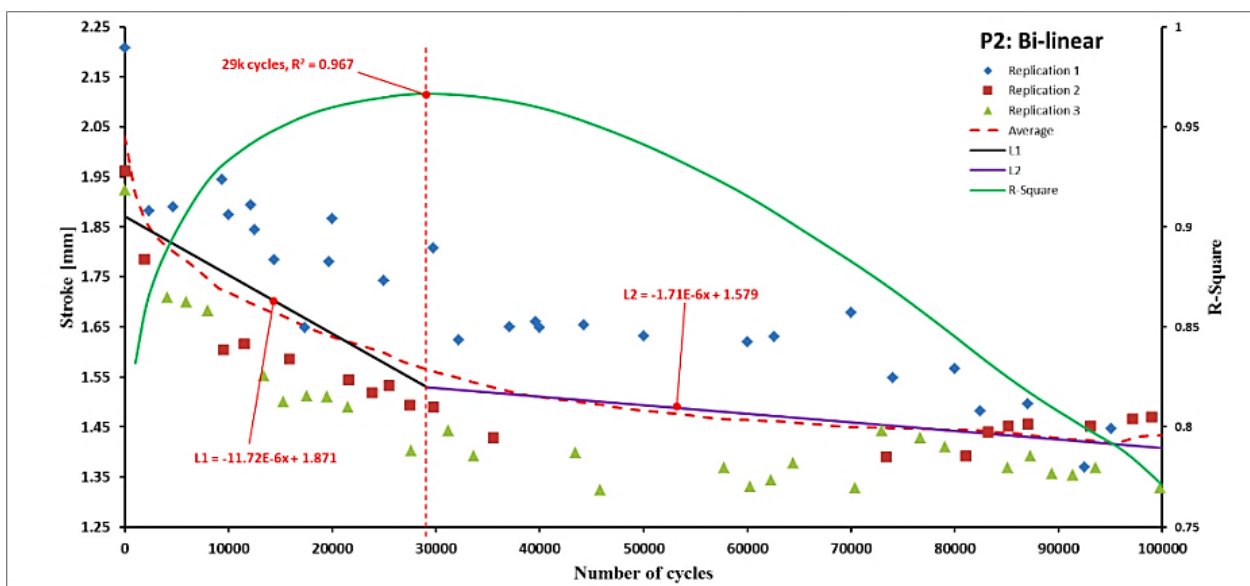


Figure 7.11 – Linear fit curve model

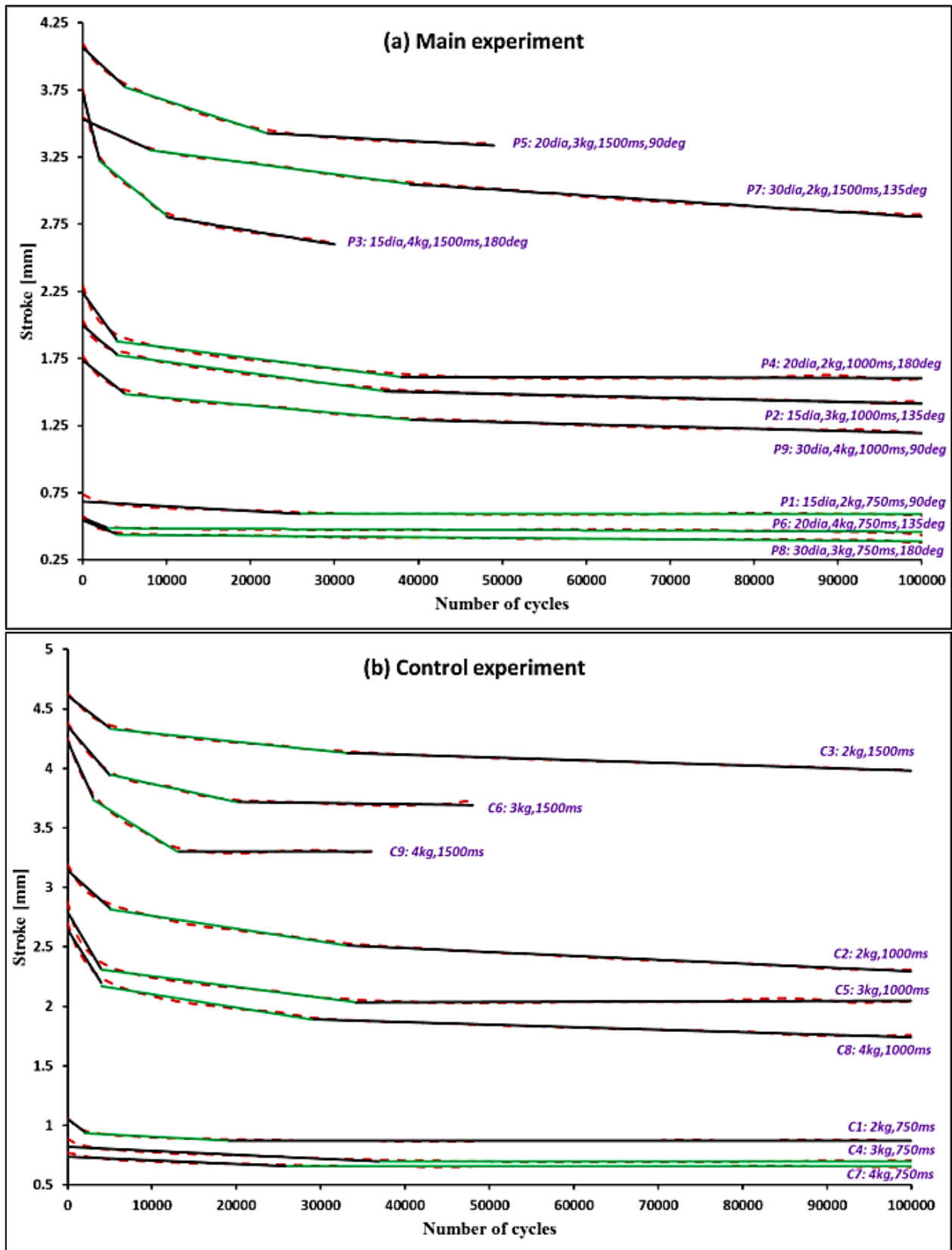


Figure 7.12 - Linear fit analysis on main and control experiments

Table 7.9 - Linear fit curve analysis results

Test	Bi-linear				Tri-Linear					
	Gradients (x10 ⁻⁶)		Intermediate point (x10 ³)	R ²	Gradients (x10 ⁻⁶)			Intermediate points (x10 ³)		R ²
	m1	m2	N _{int}		m1	m2	m3	N _{int1}	N _{int2}	
P1	-3.56	-0.03	26	0.903	-15.51	-2.10	0.01	5	32	0.983
P2	-11.72	-1.71	29	0.967	-52.76	-8.39	-1.44	4	36	0.992
P3	-130.47	-15.02	5	0.956	-249.04	-50.78	-10.19	2	10	0.995
P4	-14.82	-0.72	26	0.900	-86.75	-7.82	-0.13	4	38	0.985
P5	-29.95	-4.64	17	0.980	-58.01	-20.22	-3.40	5	22	0.996
P6	-25.55	-0.26	3	0.860	-25.55	-0.16	-1.69	3	85	0.943
P7	-12.43	-4.27	28	0.987	-28.15	-8.11	-4.01	8	39	0.998
P8	-25.23	-0.52	4	0.959	-30.90	-1.20	-0.39	3	29	0.978
P9	-28.00	-2.56	10	0.956	-49.31	-5.60	-1.61	5	39	0.992
Minimum			3.0	0.860	Minimum			2.0	10.0	0.943
Maximum			29.0	0.987	Maximum			8.0	85.0	0.998
Average			16.4	0.941	Average			4.3	36.7	0.985
Standard deviation			11.1	0.043	Standard deviation			1.7	20.5	0.017
C1	-13.93	-0.19	9	0.852	-39.86	-2.25	0.09	3	29	0.967
C2	-26.38	-3.94	16	0.975	-63.28	-10.80	-3.25	5	33	0.994
C3	-28.94	-2.96	11	0.968	-54.41	-7.21	-2.22	5	33	0.997
C4	-5.50	-1.32	19	0.984	-21.19	-3.19	-1.17	3	32	0.995
C5	-45.62	-1.31	11	0.864	-120.40	-9.08	0.21	4	34	0.979
C6	-60.59	-4.02	8	0.947	-82.33	-15.13	-0.95	5	20	0.992
C7	-2.89	-0.28	28	0.935	-9.21	-1.33	-0.08	7	47	0.987
C8	-52.57	-3.07	10	0.951	-111.88	-11.24	-2.12	4	29	0.992
C9	-74.88	-1.90	10	0.958	-155.97	-43.70	0.00	3	13	0.994
Minimum			8.0	0.852	Minimum			3.0	13.0	0.967
Maximum			28.0	0.984	Maximum			7.0	47.0	0.997
Average			13.6	0.937	Average			4.3	30.0	0.989
Standard deviation			6.5	0.047	Standard deviation			1.3	9.5	0.010

7.8.3 Visual and microscopy inspection on fracture surface

In a conventional wire rope drive element, fatigue cracks initiate at points that encounter the most damaging combination of tensile, bending, and contact stresses (Command, 1976b). In this work, the actuators were found with no damages (or wears) on the surface contacts between the sheave and drive element, and no movement shifting behaviour (i.e. no torsional movement). All fatigue fractures exhibit a crack initiation point (CP) in the region of the sheave tangent point, as indicated in Figure 7.6 (Gibson, 2001), and occurs at the surface with the largest bend radius (i.e. highest tensile bending stress). These cracks then propagate toward the sheave contact surface (i.e. smallest bend radius) until fracture occurs (Command, 1976b; Gibson, 2001). This outcome suggests that the ABS sheave successfully reduces contact stress and fretting, which, for conventional drive elements, results in a CP at the sheave contact surface (Gibson, 2001). Electron microscopy of SMA pulley actuator fracture surfaces (Figure 7.13b) shows similar fracture behaviour to previous BRF studies, i.e. where the crack always nucleate at the point on specimen surface with

highest tensile bending stress, which act as stress raisers during cyclic loading (Eggeler *et al.*, 2004).

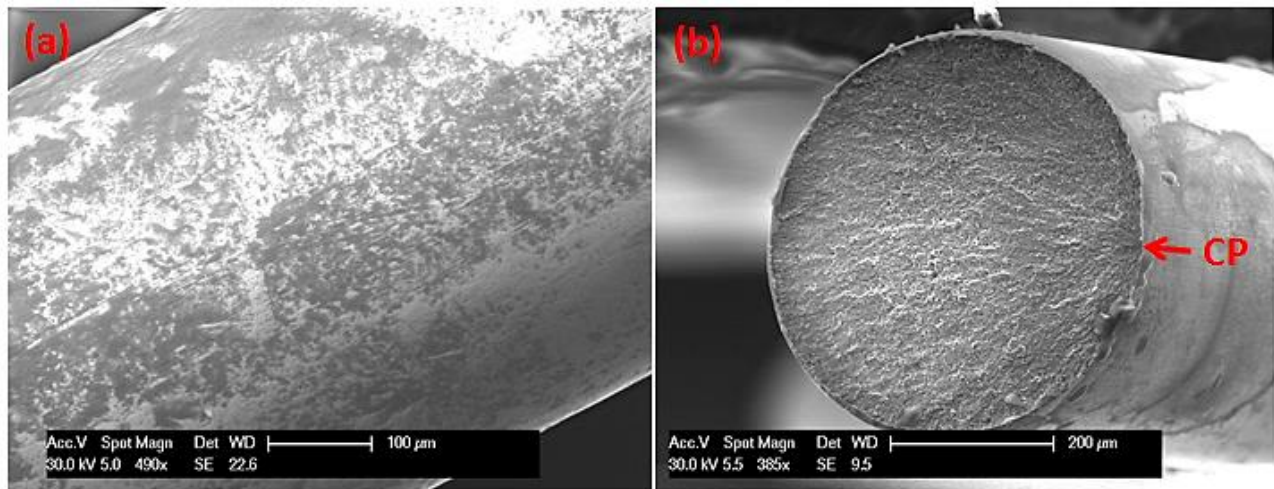


Figure 7.13 - SEM micrograph of the rupture surface of SMA actuator with a pulley system and the illustration of the fatigue crack growth from the crack initiation point (CP).

7.8.4 Taguchi method and ANOVA analysis

The results of L-9 Taguchi experiment for the main and control experiments are summarised in Table 7.10 and Table 7.11, respectively.

Table 7.10 - \bar{y} and S/N values for the main experiment

Test	Factors				Responses						\bar{y}		S/N _{LTB and STB}	
	\varnothing (mm)	W (g)	t_{act} (ms)	θ (°)	No. of cycles			Drift (mm)			No. of cycles	Drift (mm)	No. of cycles	Drift
					1	2	3	1	2	3				
P1	15	2000	750	90	100,000	100,000	100,000	0.17	0.17	0.16	100,000	0.167	100.00	15.56
P2	15	3000	1000	135	100,000	100,000	100,000	0.56	0.47	0.52	100,000	0.517	100.00	5.71
P3	15	4000	1500	180	35,381	30,043	37,944	1.16	1.13	1.17	34,456	1.153	90.62	-1.24
P4	20	2000	1000	180	100,000	100,000	100,000	0.67	0.64	0.62	100,000	0.643	100.00	3.83
P5	20	3000	1500	90	49,344	50,165	53,414	0.78	0.70	0.69	50,974	0.723	94.13	2.80
P6	20	4000	750	135	100,000	100,000	100,000	0.11	0.12	0.12	100,000	0.117	100.00	18.65
P7	30	2000	1500	135	100,000	100,000	100,000	0.41	0.41	0.47	100,000	0.430	100.00	7.31
P8	30	3000	750	180	100,000	100,000	100,000	0.17	0.13	0.16	100,000	0.153	100.00	16.23
P9	30	4000	1000	90	100,000	100,000	100,000	0.46	0.39	0.47	100,000	0.440	100.00	7.10

Table 7.11 - \bar{y} and S/N values for the control experiment

Test	Factors		Responses				\bar{y}		S/ N	
	W (g)	t_{act} (ms)	No. of cycles		Drift (mm)		No. of cycles	Drift (mm)	No. of cycles	Drift
			1	2	1	2				
C1	2000	750	100,000	100,000	0.27	0.15	100,000	0.210	100.00	13.21
C2	2000	1000	100,000	100,000	0.67	0.72	100,000	0.695	100.00	3.15
C3	2000	1500	100,000	100,000	0.54	0.48	100,000	0.510	100.00	5.83
C4	3000	750	100,000	100,000	0.19	0.17	100,000	0.180	100.00	14.88
C5	3000	1000	100,000	100,000	0.71	0.92	100,000	0.815	100.00	1.71
C6	3000	1500	48,135	65,803	0.67	0.79	56,969	0.730	94.80	2.70
C7	4000	750	100,000	100,000	0.10	0.16	100,000	0.130	100.00	17.50
C8	4000	1000	100,000	100,000	0.95	0.70	100,000	0.825	100.00	1.57
C9	4000	1500	36,936	46,021	1.11	1.03	41,479	1.070	92.20	-0.59

The effect of the pulley system on the structural and functional fatigue of SMA actuators was analysed by comparing the control experiment (i.e. SMA actuator with no pulley system) with the SMA-pulley system using one-way ANOVA (Table 7.12 and Table 7.14) show no significant difference at the 95% confidence level between the SMA-pulley system (main) and control experiments. Then the effect of variable pulley system configurations were further analysed with Taguchi and ANOVA to obtain the optimum fatigue performance for the system. The effect of each factor on mean and S/N ratio is summarised (Table 7.13 and Table 7.15) and presented graphically (Figure 7.14 and Figure 7.15) to examine the experimental results for optimum configurations selections. The influence of each factor and the variation interactions of the results were determined by ANOVA, where the importance of each factor can be measured by the ratio of factor-error variance, F and the contribution percentage of each factor on the response for both structural (Table 7.13) and functional fatigue (Table 7.15) conditions.

For this work, statistical analysis such as Taguchi and ANOVA for structural fatigue are not necessarily robust due the existence of an “undefined” number of cycles to failure for samples that survived the 1E6 runout condition. An alternative statistical approach for runout fatigue test such as logistic response function (Hosmer Jr, Lemeshow, & Sturdivant, 2013; SW Robertson *et al.*, 2015) is potentially inappropriate due to the insufficient number of test samples. Therefore, the acceptable analysis of SMA structural fatigue was limited to graphical interpretations and visual inspection. However, Taguchi and ANOVA analysis are still presented in this work, for future reference.

7.8.4.1 Structural fatigue analysis

Structural fatigue data was extracted from Table 7.10 and Table 7.11, and analysed for \bar{y} and S/N_{LTB} values (Table 7.12) and ANOVA (Table 7.13). In summary, the findings for structural fatigue at 95% confidence level are:

- Fatigue-life of SMA actuators for SMA-pulley system and control experiments reduces as the load and activation duration (i.e. strain) increases, which is consistent with previous studies (Eggeler *et al.*, 2004; Fumagalli *et al.*, 2009; Karhu & Lindroos, 2010; DC Lagoudas *et al.*, 2009; Mammano & Dragoni, 2011; W. Tang & Sandström, 1993; H. Tobushi *et al.*, 1998; Torra *et al.*, 2010).
- The fatigue life increases exponentially as the sheave diameter (i.e. diameter ratio) increases.
- The angle of wrap results suggest that fatigue life is compromised for larger wrap-angles, and optimised for the intermediate and low angles of wrap.
- The activation duration and load magnitude has a significant effect on the fatigue life of the SMA actuator with and without pulley system. However, the load effect on the fatigue life of SMA actuator is minor (similar to (Karhu & Lindroos, 2010)), and comparable with the pulley factors (e.g. sheave diameter and angle of wrap).
- There is no significant difference between the SMA-pulley system (main) and control experiments at the 95% confidence level (Table 7.12).
- ANOVA shows that: interaction between load and activation duration is significantly high; other interactions within the SMA-pulley system and for systems without pulleys system are insignificant at the 95% confidence level.

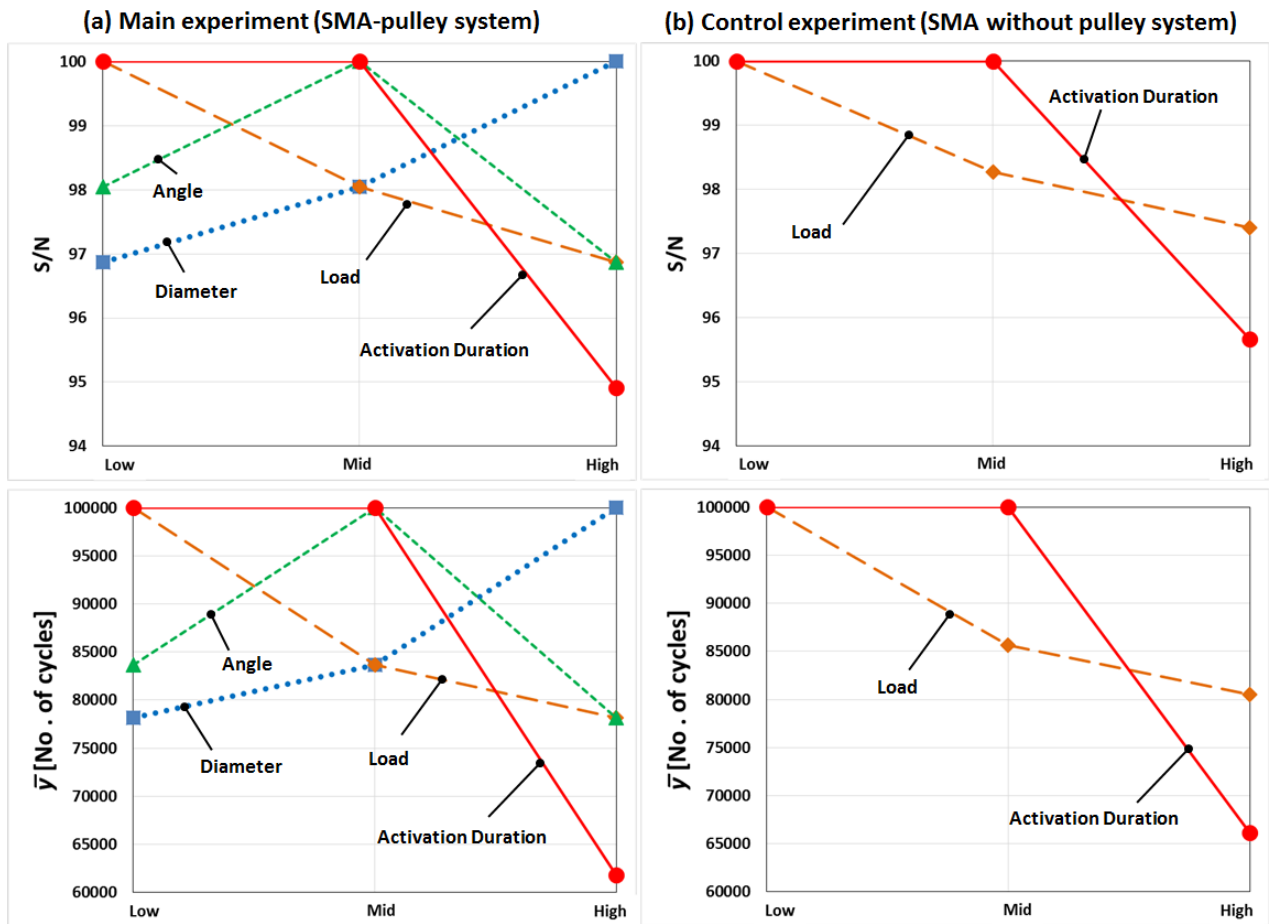


Figure 7.14 - Effect of controllable factors on \bar{y} and S/N_{LTB} for structural fatigue
(a) main and (b) control experiments

Table 7.12 - \bar{y} and S/N_{STB} values for all levels for main and control experiments for structural fatigue test

Factors	Levels	Main experiment (with pulley system)				Control experiment (without pulley system)				Main versus Control	
		\bar{y} (no. of cycles)	S/N_{LTB}	$\Delta S/N$	Rank	\bar{y} (no. of cycles)	S/N_{LTB}	$\Delta S/N$	Rank	P	Status
Sheave diameter, \varnothing (mm)	15	78,152	96.87								
	20	83,658	98.04	3.13	2					-	-
	30	100,000	100.00								
Load, W (g)	2000	100,000	100.00			100,000	100.00			1.00	Not Sig.
	3000	83,658	98.04	3.13	2	85,656	98.27	2.60	2	0.88	Not Sig.
	4000	78,152	96.87			80,493	97.40			0.89	Not Sig.
Activation duration, t_{act} (ms)	750	100,000	100.00			100,000	100.00			1.00	Not Sig.
	1000	100,000	100.00	5.08	1	100,000	100.00	4.33	1	1.00	Not Sig.
	1500	61,810	94.92			66,149	95.67			0.78	Not Sig.
Angle of wrap, θ (°)	90	83,658	98.04								
	135	100,000	100.00	3.13	2					-	-
	180	78,152	96.87								

‘Not Sig.’ indicates *no significant* difference between SMA-Pulley and control specimens with one-way ANOVA at 95% Confidence level and ‘Sig.’ is vice versa.

Table 7.13 - ANOVA on main and control experiments for structural fatigue test

<i>Factors</i>	<i>DOF</i>	<i>SS</i>	<i>MS</i>	<i>F</i>	<i>P</i>	<i>C [%]</i>	<i>Rank</i>
Main experiment							
Sheave diameter	2	2324129088.07	1162064544.04	500.87	<0.05	14.74	2
Load	2	2324129088.07	1162064544.04	500.87	<0.05	14.74	2
Activation duration	2	8750805680.07	4375402840.04	1885.89	<0.05	55.51	1
Angle of wrap	2	2324129088.07	1162064544.04	500.87	<0.05	14.74	2
Within (Interactions)	18	41761318.67	2320073.26	1.00	0.500	0.26	
TOTAL	26	15764954262.96				100.00	
Control experiment							
Load	2	1225864114.11	612932057.06	27.95	<0.05	14.49	2
Activation duration	2	4583515669.44	2291757834.72	104.52	<0.05	54.19	1
<u>Within (Interactions)</u>							
Load * Activation duration	4	2451728228.22	612932057.06	27.95	<0.05	28.99	
Other interactions	9	197347724.50	21927524.94	1.00	0.50	2.33	
Total within	13	2649075952.72	203775073.29			31.32	
TOTAL	17	8458455736.28				100.00	
Acronyms: DOF = Degree of freedom, SS = Sum of Square, MS = Mean of Square, F = F-statistic, P = P-value, C = contribution percentage							

7.8.4.2 Functional fatigue analysis

Functional fatigue data was extracted from Table 7.10 and Table 7.11 and analysed for \bar{y} and S/N_{STB} values (Table 7.14) and ANOVA (Table 7.15). In summary, the findings for structural fatigue at 95% confidence level are:

- In general, there is no significant difference at the 95% confidence level between the main and the control experiments (Table 7.14). The exception is the test at 1000ms (P-value = 0.0013).
- An increase in sheave diameter (i.e. diameter ratio) improves the functional fatigue of SMA-pulley system
- The angle of wrap results suggest that functional fatigue is compromised for larger wrap-angles, and optimised for intermediate and low angles of wrap.
- Within the SMA-pulley system and control systems, all factors are of significance to functional fatigue.
- The load is the least influential factor for the pulley system and the control experiment (i.e. ranked last by Taguchi and ANOVA), where the mean drift increased with the increasing load.
- With reference to Figure 7.15, load tends to follow the activation duration trends, and apparently influences the activation duration (i.e. influence the transformation temperatures (DC Lagoudas *et al.*, 2009; S. Stoeckel & Simpson, 1992). This finding was attested by ANOVA (Table 7.15), where the interaction between activation duration and load was significant. Increases in load increases the A_s and delay the activation initiation-time.
- Similar to previous structural fatigue analysis, ANOVA showed that the interaction between load and activation duration was significant at the 95% level (Table 7.15).

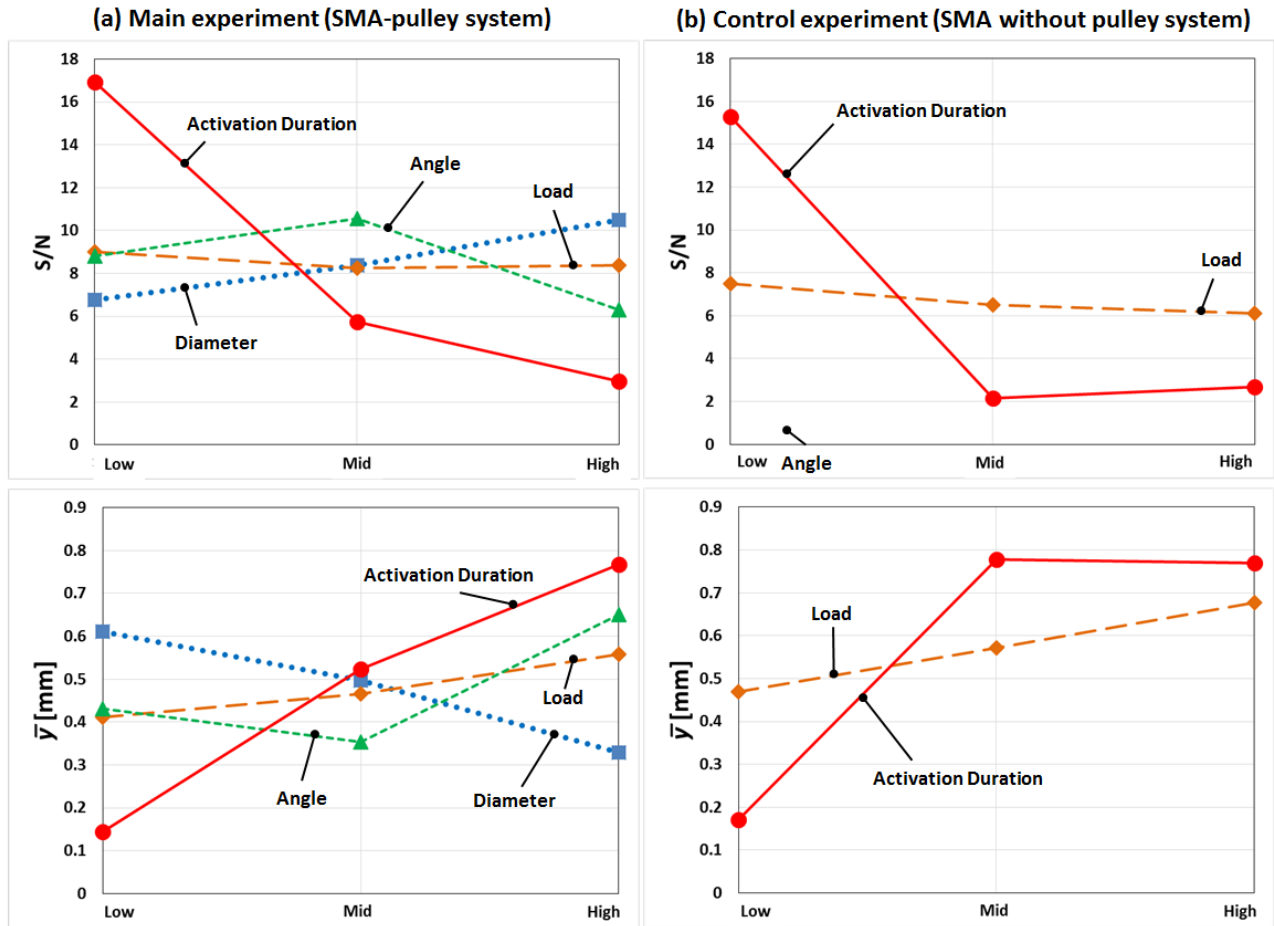


Figure 7.15 - Effect of control factors on \bar{y} and S/N_{STB} for the functional fatigue (a) main and (b) control experiments

Table 7.14 - \bar{y} and S/N_{STB} values for all levels for main and control experiments for functional fatigue test

Factors	Level <i>s</i>	Main experiment (with pulley system)				Control experiment (without pulley system)				Main versus Control	
		\bar{Y} (mm)	S/N_{STB}	$\Delta S/N$	Rank	\bar{Y} (mm)	S/N_{STB}	$\Delta S/N$	Rank	P	Status
Sheave diameter, \varnothing (mm)	15	0.61	6.68								
	20	0.49	8.43	3.54	3			-		-	-
	30	0.34	10.22								
Load, <i>W</i> (g)	2000	0.41	8.90			0.47	7.40			0.64	Not Sig.
	3000	0.46	8.25	0.73	4	0.58	6.43	1.24	2	0.48	Not Sig.
	4000	0.57	8.17			0.68	6.16			0.62	Not Sig.
Activation duration, t_{act} (ms)	750	0.15	16.82			0.17	15.20			0.14	Not Sig.
	1000	0.53	5.55	13.86	1	0.78	2.14	13.05	1	<0.05	Sig.
	1500	0.77	2.96			0.77	2.65			0.99	Not Sig.
Angle of wrap, θ (°)	90	0.44	8.49								
	135	0.35	10.56	4.29	2			-		-	-
	180	0.65	6.27								

‘Not Sig.’ indicates *no significant* difference between SMA-Pulley and control specimens with one-way ANOVA at 95% Confidence level and ‘Sig.’ is vice versa.

Table 7.15 - ANOVA on main and control experiments for functional fatigue test

Factors	DOF	SS	MS	F	P	C [%]	Rank
Main experiment							
Sheave diameter	2	0.3327	0.1663	163.90	<0.05	12.49	3
Load	2	0.1149	0.0574	56.61	<0.05	4.31	4
Activation duration	2	1.7832	0.8916	878.59	<0.05	66.96	1
Angle of wrap	2	0.4139	0.2069	203.93	<0.05	15.54	2
Within	18	0.0183	0.0010	1.00	0.50	0.69	
TOTAL	26	2.6629					
Control experiment							
Load	2	0.1240	0.0620	7.35	<0.05	6.65	2
Activation duration	2	1.4442	0.7221	85.57	<0.05	77.39	1
<u>Within (Interactions)</u>							
Load * Activation duration	4	0.2218	0.0555	6.57	<0.05	11.89	
Other interactions	9	0.0760	0.0084	1.00	0.50	4.07	
Total within	13	0.2978	0.0229			15.96	
TOTAL	17	1.8660				100.00	
Acronyms: DOF = Degree of freedom, SS = Sum of Square, MS = Mean of Square, F = F-statistic, P = P-value, C = contribution percentage							

7.8.5 SMA-pulley system optimum configurations and confirmation test

The Taguchi method and ANOVA identified that the activation duration had the highest effect or contribution percentage to the SMA functional fatigue for both systems. Taguchi and ANOVA ranked the factors from the highest to lowest as follows: activation duration, angle of wrap, sheave diameter, and load. Based on the experimental outcomes of this work with Taguchi method and ANOVA, it is recommended to apply the largest sheave diameter at 135° wrap-angle, with minimal load and activation duration. A confirmation experiment was conducted to verify these findings as recommended by Taguchi's DOE practitioners (Taguchi, 1987), and the results are summarised in Table 7.16 (with two repetitions). This result confirms that the highest observed functional fatigue performance can be achieved with these recommended configurations.

Table 7.16 - Confirmation test with optimum configuration for structural and functional fatigue of SMA-pulley system

Sheave diameter	Factors			No. of cycles	Test No.	Stroke (mm)			Drift after 3E4 cycles
	Load	Activation duration	Angle of wrap			1st cycle	3E4 cycles	1E5 cycles	
Ø30mm	2000g/96.8MPa	750ms	135°	100,000	1	0.63mm	0.52mm	0.48mm	0.11mm
					2	0.68mm	0.56mm	0.51mm	0.12mm

7.10 Commercially optimal SMA-pulley configuration test

Previous analysis had drawn the optimal configurations of the SMA-pulley system for structural and functional fatigue performances. However, the desired optimal configurations are limited by commercial needs. Large sheave diameter and low loads improve the fatigue performance of SMA-pulley system, but excessive sheave diameter may compromise available packaging space, and low loads reduce commercial utility. Therefore, the SMA-pulley systems were configured according to the following commercially beneficial configuration:

- Activation duration: 1000ms activation duration is recommended by the manufacturer for many commercial applications for the type of actuator used in this work (Table 7.4). However, the optimal stroke performance below the overheating level could be estimated with a numerical model (Mohd Jani *et al.*, 2015b).
- Applied load: the highest level of load (4000grams) was selected due to highest load preference in many commercial actuator applications (highest work density). The maximum allowable stress and duration limits can be obtained from the manufacturer data.
- Sheave diameter and wrap angle: Lowest level of sheave diameter (Ø15mm) and highest level of wrap-angle (180°) are recommended for compact and small space commercial applications (Figure 7.2).

Table 7.17 - Commercially optimal SMA-pulley system summary

Sheave diameter	Factors			No. of cycles	Test No.	Stroke (mm)			Drift after 3E4 cycles
	Load	Activation duration	Angle of wrap			1 st cycle	3E4 cycles	1E5 cycles	
Ø15mm	4000g/193.6MPa	1000ms	180°	100,000	1	1.69mm	1.19mm	1.09mm	0.50mm
					2	1.57mm	1.16mm	1.05mm	0.41mm

The results from these tests confirmed that SMA actuator with the commercially optimal pulley configurations is expected to survive in excess of 1E5 cycles, which is sufficient for consumer and automotive products (Fumagalli *et al.*, 2009; D. Homma, 2004). The recommended stroke for this setup is about 1% strain (1mm for 100mm length of SMA actuator). However, higher or optimal strain could be achieved with higher activation duration until the austenite final temperature, A_f .

7.12 Conclusion

This work shows that within the SMA-pulley system experiments, all selected pulley system design factors are statistically significant to both functional and structural fatigue:

- The application of a pulley system tends to reduce the stroke performance (i.e. functional fatigue) of SMA actuators. Taguchi and ANOVA rank the contribution order of examined factors for functional fatigue from highest to the lowest as: activation duration, angle of wrap, sheave diameter and applied load. The activation duration has the highest effect on functional fatigue for SMA systems (either with or without pulley), and the load (or applied stress) has the lowest observed effect. Functional fatigue of SMA-pulley systems is enhanced as activation duration are reduced, angle of wrap is at the low to intermediate-level, sheave diameter (i.e. diameter ratio) is increased and the load is reduced.
- Taguchi and ANOVA rank actuation duration as the most significant contributor to structural fatigue, followed by all other pulley-design parameters with similar contribution effect. This outcome highlights the need for robust and readily applicable models of SMA response in order (for example the novel contributions of Chapter 5) to ensure that SMA actuation duration is appropriate for the specific design application.

Based on these observations, confirmation experiments were completed for SMA pulleys systems with: suggested optimal configurations; and, configurations optimal considering automotive design imperatives. These confirmation experiments provide a statistically significant basis for the implementation of such systems in commercial applications. Generally, the SMA deformation rate tends to asymptote towards some constant value as N increases. This work proposes a novel bi- and tri-linear model that is found to characterise the observed functional fatigue with a high degree of correlation. Fatigue failure was only observed for an activation duration of 1500ms (i.e. actuator being heated in excess of the complete transformation, $>A_f$). In all cases, structural fatigue occurs at $N > 3E4$ cycles, which is compatible with the outcomes of similar studies where the recommended activation duration (or strain) and load are exceeded (Dynalloy Inc., 2007; Eggeler *et al.*, 2004; Fumagalli *et al.*, 2009; Mammano & Dragoni, 2011; H. Tobushi *et al.*, 1998); and are in agreement with (Rao & Srinivasa, 2013), where the deformation rate stabilised and the BRF rupture rate reduces in excess of $1E4$ cycles (Eggeler *et al.*, 2004). SMA actuators are expected to achieve superior stability at lower (or partial) transformation, in particular within RPT (W. Tang & Sandström, 1993; H. Tobushi *et al.*, 1996; H. Tobushi *et al.*, 1998), and higher stress level increases the dislocation of density rate (Karhu & Lindroos, 2010).

8. Conclusion

The demand for Shape Memory Alloy (SMA) applications has steadily increased in numerous commercial fields, particularly in biomedical, aerospace, robotics and automotive domains (Chapter 2). However, although extensive effort has been directed towards SMA research, and thousands of worldwide patents have been issued, the numbers of commercially successful applications are relatively low. This limited commercialisation is in part due to the technical challenges inherent to the available SMA materials, as well as to challenges encountered by design engineers, including limited availability of: readily applied design models; relevant fundamental insights; and, associated design data. For example, specific identified limitations that may stymie SMA commercialisation include:

- Potential lack of connectivity between the research outcomes of material scientists and the pragmatic requirements of engineering designers
- Lack of: design knowledge for understanding the technical requirements of SMAs; and, limited design methods and tools available to deploy SMAs in a robust manner to achieve the commercial application requirements of durability and positional stability
- Potential lack of 'smart marketing' of the commercial capabilities of SMA applications to key engineering design personnel
- Technical limitations of SMAs, associated with: usable strain, actuation frequency, controllability, and energy efficiency
- Potentially high material cost (of high surface area to volume geometries) due to relatively small commercial sales volumes of these relatively new SMA forms
- Relative lack of SMA research from an engineering design perspective; thereby resulting in a lack of design procedures, guidelines and tools to assist engineers in developing SMA applications
- Lack of readily applied models that are compatible with computer-based design and analysis methods, which are essential to enhancing the SMA design process, in particular for preliminary studies and validation of high risk and/or expensive projects

8.1 Contribution by research theme

These identified limitations provide the motivation for commercially relevant research to assist in the design of SMA actuators. Based on the thesis roadmap presented in Chapter 1, and associated literature review and analysis (Chapters 2 to 4) the following research themes were defined:

- Research Theme 1: Design methods to resolve SMA actuator limitations
- Research Theme 2: Development of simple and practical numerical models for SMA actuator response
- Research Theme 3: Data for SMA linear actuator design

The specific research contributions of this thesis are summarised below according to the associated research theme.

8.1.1 Research Theme 1: Design methods to resolve SMA actuator limitations

Applying highly conductive fluidic cooling media is one of the most effective ways to increase the cooling performance of SMA actuators. A novel investigation of the transient thermal response of cylindrically lagged thermal systems was conducted. This work provides previously unavailable design guidance for scenarios that are known to be transient, and to study the effect of transient heating on cylindrically lagged systems, as is required for the design of thermally lagged SMA linear actuators. Specific outcomes include:

- Quantification of the critical and crossover radii of cylindrically for cylindrically lagged thermal systems subject to a transient heating scenario
- Identification that the critical radius stabilizes more quickly than the crossover radius in response to intermittent heating
- Identification of distinct zones (and appropriate SMA design strategies) of transient thermal behaviour of cylindrically lagged thermal systems
- Novel conclusions between the steady-state and transient response of the critical and crossover radii
- Identification that the average heat transfer rate is independent of actuation period, and varies linearly with duty-cycle, thereby reducing computational cost by enabling a single simulation to be extrapolated to other scenarios of interest

SMA-pulley systems provide an important design approach to enable mechanical advantage (increase the force and stroke capacity) and reduce packaging space. Despite the design advantages of SMA-pulley systems, there appears to be no formal investigation of the effect of pulley system design parameters on SMA structural or functional fatigue. Specific contributions of this work include:

- The predictive models developed within Research Theme 2 (below) were applied to correctly predict the behaviour of SMA actuator systems subject to variable load and activation duration conditions
- For the identified load and activation duration condition, Taguchi methods and ANOVA were applied to characterise the influence of SMA-pulley system design parameters on SMA functional and structural fatigue
- Based on identified variables of interest, combined with commercial imperatives of actuator load and packaging envelope, fatigue design data was generated for the design of commercially optimal SMA pulley configurations
- A novel multi-linear-fit model was developed and proposed for SMA functional fatigue and found to robustly characterise the observed response

8.1.2 Research Theme 2: Development of simple and practical numerical models for SMA actuator response

This research has identified that enhanced SMA design and analysis tools are essential to the development of innovative and reliable SMA applications; and to minimise development time, cost and risk. Although numerous analytical and numerical models have been developed, existing models may be overly complex for application at the engineering design phase; whereby: thermomechanical problems are solved by separating the single phases (austenite or martensite phases) and transition phase (austenite-martensite phase) with multiple models; and, require numerous prerequisite experimental coefficients and equations. To address this impracticability, novel analytical and numerical models have been developed. Specific research contributions are outlined below:

- A robust and readily applied 1-D FDE model has been developed for transient heat transfer analysis of cylindrical system (e.g. lagged SMA linear actuator)
- Novel 1-D numerical models (analytical and FDE) are developed with advantages in practical applicability over existing methods
- These methods are extended to including novel latent heat models, and phase transitions effects
- Simulation capabilities are extended to accommodate the thermomechanical behaviour of SMA linear actuators under variable ambient and mechanical conditions

8.1.3 Research Theme 3: Data for SMA linear actuator design

This research has identified that the availability of methods, tools and data suitable to assist design engineers in developing SMA applications is often limited; and that SMA research is often directed towards the associated metallurgical properties of SMAs, rather than the associated design perspective. A number of pertinent limitations were identified and responded to within this work:

- A systematic SMA actuator designing process is proposed, and numerous SMA design approaches and techniques are compiled and categorised to assist designers in effectively developing SMA applications, including reference to:
 - Primary technical objectives of SMA actuator design: force, displacement and bandwidth
 - Considerations and embodiments for linear and rotary motion types
 - Design requirements and application selection factors for: material, loading configurations and geometry
 - Categorisation of primary SMA functions (i.e. free recovery, constrained recovery, actuator and superelasticity) and associated basic SMA actuator designs (one-directional, bias-force and antagonist)
 - Summary of applied design approaches and techniques to enhance SMA actuator performance, including: pulley system, parallel and serial SMA design, telescopic systems, active and passive cooling, and electronic controllers
- The study of heat transfer on cylindrical systems allows direct guidance for the design of cylindrically lagged SMA linear actuators in either transient or quasi-static cases for a given heat transfer scenario. Furthermore, opportunities to reduce computational cost in the prediction of heat transfer behaviour have been identified.
- Simple charts for prediction of SMA activation time versus Joule heating; and deactivation time versus convective heat transfer coefficient have been implemented for direct application by SMA design teams.
- Systematic investigation of the effect of pulley system parameters on structural and functional fatigue of SMA linear actuators with Taguchi and ANOVA provides previously unavailable insight for the design of generalised SMA-pulley systems
- By generating statistically significant fatigue design data for a commercially optimal SMA pulley configurations, this work provides the requisite design data for the commercial application of a specific, commercially relevant, SMA-pulley system

8.2 Future work

Research and development trends of SMA actuators within automotive, aerospace, robotics and biomedical domains are documented Chapter 2 and 3. Although these contributions are reasonably well established, further research prospects exist, for example the following general opportunities for SMA research contribution:

- New materials (including composites and hybrid SMMs), fabrication technologies and treatment processes for SMAs, which are more stable, more durable and can be utilised in a broad range of industries.
- More efficient and effective information platforms for knowledge sharing within SMM communities.
- Robust computational models of SMA behaviour, especially associated with functional and structural fatigue.
- Development of new design approaches or guidelines for the creation of novel SMA applications, in existing and new markets.
- Development of integrated actuator systems (with compact, fast and intelligent controllers).
- Combinations of SMA with various SMMs (i.e. SMHs and SMCs) to enhance material performance (e.g. higher damping capacity and strength, active functionality, multiple-state changing and self-healing capability).

In relation to the specific contributions of this work, the following future work is proposed:

- Extension of the developed numerical models and cylindrical-lagged design study:
 - To apply recent constitutive models to predict wider range of environmental and mechanical conditions, including load and thermally induced stresses
 - To consider phase heterogeneity due to the non-isothermal phase change
 - Simulation with various Joule heating patterns
 - To apply the developed models into FEM and FVM
 - To extend the models for complex geometries and non-uniformity problems
- To develop versatile activation and deactivation charts as a function of variable factors such as h , T_{∞} , D_{SMA} , σ_0 and SMA type. These charts are proposed to be standard documents supplied by SMA manufacturers, as simple and fast guideline to assist SMA developers and designers in their SMA development process.
- Extension of the structural and functional fatigue study:
 - To include thermal-cycling function for solving fatigue problems
 - Development of simplified prediction model for structural and functional fatigue, based on the multi-linear fit curve analysis

This thesis has contributed to the publications of Table 8.1.

Table 8.1 – Summary of publications with associated chapters in thesis

Publication	Abstract
<i>The critical and crossover radii on transient heating</i> , S Huang, J Mohd Jani, M Leary, A Subic, Applied Thermal Engineering 60(1), 325-334, 2013	For cylindrical and spherical heat transfer systems, it is imperative that the radius of thermal material is matched to the associated heat transfer objective. For systems that intend to maximize heat transfer, the critical radius defines the optimal radius for a specific scenario. For systems that intend to minimize heat transfer, the crossover radius defines the radius required to achieve an equal heat transfer rate to the uninsulated scenario; with any further increase in radii resulting in a monotonic reduction in the associated heat transfer rate. The critical radius is well defined for the steady-state scenario. In recent literature, the steady-state crossover radius has also received attention; however, the literature does not provide clarity for the transient scenario. This work overcomes this identified limitation by quantifying the crossover and critical radii of a transient cylindrical system, allowing novel conclusions to be drawn between the steady-state and transient scenarios. In particular, this work identifies that the cycle-average heat transfer rate can stabilize to a quasi-static value in response to transient heating.
<i>A review of shape memory alloy research, applications and opportunities</i> , J Mohd Jani, M Leary, A Subic, MA Gibson, Materials & Design 56, 1078-1113, 2014	Shape memory alloys (SMAs) belong to a class of shape memory materials (SMMs), which have the ability to 'memorise' or retain their previous form when subjected to certain stimulus such as thermomechanical or magnetic variations. SMAs have drawn significant attention and interest in recent years in a broad range of commercial applications, due to their unique and superior properties; this commercial development has been supported by fundamental and applied research studies. This work describes the attributes of SMAs that make them ideally suited to actuators in various applications, and addresses their associated limitations to clarify the design challenges faced by SMA developers. This work provides a timely review of recent SMA research and commercial applications, with over 100 state-of-the-art patents; which are categorised against relevant commercial domains and rated according to design objectives of relevance to these domains (particularly automotive, aerospace, robotic and biomedical). Although this work presents an extensive review of SMAs, other categories of SMMs are also discussed; including a historical overview, summary of recent advances and new application opportunities.
<i>Numerical modeling of Shape Memory Alloy linear actuator</i> , J Mohd Jani, S Huang, M Leary, A Subic, Computational Mechanics 53(3), 443-461, 2015	The demand for shape memory alloy (SMA) actuators in high-technology applications is increasing; however, there exist technical challenges to the commercial application of SMA actuator technologies, especially associated with actuation duration. Excessive activation duration results in actuator damage due to overheating while excessive deactivation duration is not practical for high-frequency applications. Analytical and finite difference equation models were developed in this work to predict the activation and deactivation durations and associated SMA thermomechanical behaviour under variable environmental and design conditions. Relevant factors, including latent heat effect, induced stress and material property variability are accommodated. An existing constitutive model was integrated into the proposed models to generate custom SMA stress-strain curves. Strong agreement was achieved between the proposed numerical models and experimental results; confirming their applicability for predicting the behaviour of SMA actuators with variable thermomechanical conditions.
<i>Fatigue of Ni-Ti SMA-pulley system using Taguchi and ANOVA</i> , J Mohd Jani, M Leary, A Subic, Smart Materials & Structures, 25(5), 057001, 2016	Shape memory alloy (SMA) actuators can be integrated with a pulley system to provide mechanical advantage and to reduce packaging space; however, there appears to be no formal investigation of the effect of a pulley system on SMA structural or functional fatigue. In this work, cyclic testing was conducted on Nickel-Titanium (NiTi) SMA actuators on a pulley system and a control experiment (without pulley). Both structural and functional fatigues were monitored until fracture, or a maximum of 1E5 cycles were achieved for each experimental condition. The Taguchi method and analysis of the variance (ANOVA) were used to optimise the SMA-pulley system configurations. In general, one-way ANOVA at the 95% confidence level showed no significant difference between the structural or functional fatigue of SMA-pulley actuators and SMA actuators without pulley. Within the sample of SMA-pulley actuators, the effect of activation duration had the greatest significance for both structural and functional fatigue, and the pulley configuration (angle of wrap and sheave diameter) had a greater statistical significance than load magnitude for functional fatigue. This work identified that structural and functional fatigue performance of SMA-pulley systems is optimised by maximising sheave diameter and using an intermediate wrap-angle, with minimal load and activation duration. However, these parameters may not be compatible with commercial imperatives. A test was completed for a commercially optimal SMA-pulley configuration. This novel observation will be applicable to many areas of SMA-pulley system applications development.
<i>Shape memory alloy applications in automotive</i> , J Mohd Jani, M Leary, A Subic, Applied Mechanics and Materials 663, 248-253, 2014	Shape memory alloy (SMA) actuators have drawn much attention and interest due to their unique and superior properties, and are expected to be equipped in many modern vehicles at competitive market prices. The key advantage is that SMA actuators do not require bulky and complicated mechanical design to function, where the active element (e.g. SMA wire or spring) can be deformed by applying minimal external force and will retain to their previous form when subjected to certain stimuli such as thermomechanical or magnetic changes. This paper describes the SMA attributes that make them ideally suited as actuators in automotive applications and to address their limitations, feasibilities and prospects.
<i>Analysis of convective heat transfer coefficient on shape memory alloy actuator under various ambient temperatures with finite difference method</i> , J Mohd Jani, S Huang, M Leary, A Subic, Applied Mechanics and Materials 736, 127-133, 2015	The demand for shape memory alloy (SMA) actuators for technical applications is steadily increasing; however, SMA may have poor deactivation time due to relatively slow convective cooling. Convection heat transfer mechanism plays a critical role in the cooling process, where an increase of air circulation around the SMA actuator (i.e. forced convection) provides a significant improvement in deactivation time compared to the natural convection condition. The rate of convective heat transfer, either natural or forced, is measured by the convection heat transfer coefficient, which may be difficult to predict theoretically due to the numerous dependent variables. In this work, a study of free convective cooling of linear SMA actuators was conducted under various ambient temperatures to experimentally determine the convective heat transfer coefficient. A finite difference equation (FDE) was developed to simulate SMA response, and calibrated with the experimental data to obtain the unknown convective heat transfer coefficient, h . These coefficients are then compared with the available theoretical equations, and it was found that Eisakhani <i>et. al</i> model provides good agreement with the Experiment-FDE calibrated results. Therefore, FDE is reasonably useful to estimate the convective heat transfer coefficient of SMA actuator experiments under various conditions, with a few identified limitations (e.g. exclusion of other associative heat transfer factors).

9. References

- Aase, J. H., Browne, A. L., Johnson, N. L., & Ulicny, J. C. (2006). US Patents 7059664B2.
- Abrahamsson, P., & Bjiimemo, R. (1994, 31 August - 4 September 1993). *The need for product design tools in shape memory technology*. Paper presented at the 3rd IUMRS International Conference on Advanced Materials, Sunshine City, Ikebukuro, Tokyo, Japan.
- Abrahamsson, P., & Møster, E. (1997). Demands on Shape Memory Alloys from the Application Designer's Point of View. *J. Phys. IV France*, 07(C5), C5-667-C665-672.
- Achenbach, M. (1989). A model for an alloy with shape memory. *International Journal of Plasticity*, 5(4), 371-395. doi:10.1016/0749-6419(89)90023-5
- Aerospace, T. (2013). Single crystal shape memory alloys. Retrieved from <http://www.tiniaerospace.com/smacrystal.html>
- Ahn, K. K., & Kha, N. B. (2008). Modeling and control of shape memory alloy actuators using Preisach model, genetic algorithm and fuzzy logic. *Mechatronics*, 18(3), 141-152. doi:10.1016/j.mechatronics.2007.10.008
- Airoidi, G., Riva, G., & Vanelli, M. (1995). Superelasticity and shape memory effect in NiTi orthodontic wires. *Journal de physique. IV*, 5(8), C8-1205.
- Alacqua, S., Capretti, G., Biasiotto, M., & Zanella, A. (2010). US Patent 7823955B2.
- Alex, V., Colin, S., & Shashank, P. (2011). A biomimetic robotic jellyfish (Robojelly) actuated by shape memory alloy composite actuators. *Bioinspiration & Biomimetics*, 6(3), 036004.
- Alexander, P. W., Brown, J. H., & Zolno, A. (2011). US Patents 7963600B2.
- Allie, D. E., Hebert, C. J., & Walker, C. M. (2004). Nitinol stent fractures in the SFA. *Endovascular Today*, (July/August 2004), 22-29. Retrieved from Endovascular Today website: <http://bmctoday.net/evtoday/2004/08/>
- Allston, B. K., Knebel, A. M., & Salemi, M. R. (2000). US Patents 6019113A.
- Altaii, K., & Thomas, B. (2010). US Patent 7692091B2.
- An, L., Huang, W. M., Fu, Y. Q., & Guo, N. Q. (2008). A note on size effect in actuating NiTi shape memory alloys by electrical current. *Materials & Design*, 29(7), 1432-1437. doi:10.1016/j.matdes.2007.09.001
- Anand, N., Acharya, P., Agrawal, V., Banerjee, S., Parmar, N., & Kothari, R. (2014). Adaptive Numerical and Computational Methods for Temperature Profiling of a Cylindrical Nuclear Fuel Rod. *International Journal of Engineering and Technology*, 6(4), 315.
- Andreasen, G. F. (1977). US Patents 4037324.
- Andreasen, G. F., & Hilleman, T. B. (1971). An evaluation of 55 cobalt substituted Nitinol wire for use in orthodontics. *The Journal of the American Dental Association*, 82(6), 1373-1375.
- Andrianesis, K., & Tzes, A. (2008, 19-22 Oct. 2008). *Design of an anthropomorphic prosthetic hand driven by Shape Memory Alloy actuators*. Paper presented at the Biomedical Robotics and Biomechatronics, 2008. BioRob 2008. 2nd IEEE RAS & EMBS International Conference on.
- Angioni, S. L., Meo, M., & Foreman, A. (2011). Impact damage resistance and damage suppression properties of shape memory alloys in hybrid composites—a review. *Smart Materials and Structures*, 20(1), 013001.

- Angueira, C. E., & Kadakia, S. C. (1997). Esophageal stents for inoperable esophageal cancer: which to use? *The American journal of gastroenterology*, 92(3), 373.
- Asada, H. H., Cho, K.-J., & Roy, B. (2005). US Patents 2005/0253425A1.
- Asada, H. H., Cho, K.-J., & Selden, B. (2007). US Patents 7188473B1.
- Asch, M. R. (2002). Initial Experience in Humans with a New Retrievable Inferior Vena Cava Filter¹. *Radiology*, 225(3), 835-844.
- Ashby, F. (2011). *Materials Selection in Mechanical Design*: Elsevier/Butterworth-Heinemann.
- Ashrafiuon, H., Eshraghi, M., & Elahinia, M. H. (2006). Position Control of a Three-link Shape Memory Alloy Actuated Robot. *Journal of Intelligent Material Systems and Structures*, 17(5), 381-392.
- Ashurst, G. R. (2002). US Patent 6427712B1.
- ASTM. (2014). Standard Test Method for Conducting Rotating Bending Fatigue Tests of Solid Round Fine Wire. West Conshohocken, PA: ASTM International.
- Auguet, C., Isalgue, A., Lovey, F. C., Pelegrina, J. L., Ruiz, S., & Torra, V. (2007). Metastable effects on martensitic transformation in SMA Part 3 - Tentative temperature effects in a NiTi alloy. *Journal of thermal analysis and calorimetry*, 89(2), 537-542.
- Auguet, C., Isalgue, A., Torra, V., Lovey, F. C., & Pelegrina, J. L. (2008). Metastable effects on martensitic transformation in SMA Part 7 - Aging problems in NiTi. *Journal of thermal analysis and calorimetry*, 92(1), 63-71.
- Auguet, C., Isalgué, A., Lovey, F. C., Martorell, F., & Torra, V. (2007). Metastable effects on martensitic transformation in SMA Part 4 - Thermomechanical properties of CuAlBe and NiTi observations for dampers in family houses. *Journal of thermal analysis and calorimetry*, 88(2), 537-548.
- Auricchio, F., & Lubliner, J. (1997). A uniaxial model for shape-memory alloys. *International Journal of Solids and Structures*, 34(27), 3601-3618. doi:10.1016/S0020-7683(96)00232-6
- Baer, G., Wilson, T. S., Matthews, D. L., & Maitland, D. J. (2007). Shape-memory behavior of thermally stimulated polyurethane for medical applications. *Journal of Applied Polymer Science*, 103(6), 3882-3892. doi:10.1002/app.25567
- Balta, J. A., Simpson, J., Michaud, V., Manson, J. A. E., & Schrooten, J. (2001). Embedded shape memory alloys confer aerodynamic profile adaptivity. *Smart Materials Bulletin*, 2001(12), 8-12. doi:10.1016/S1471-3918(01)80094-0
- Barnes, B., Brei, D., Luntz, J., & LaVigna, C. (2007). *Development of an antagonistic SMA actuator for instar rifle stabilization system*. Paper presented at the International Mechanical Engineering Congress and Exposition 2005 (IMECE 2005), Orlando, FL, USA.
- Bathe, K.-J. (2006). *Finite element procedures*: Klaus-Jurgen Bathe.
- Baumbick, R. J. (2000). US Patents 6151897.
- Baz, A., Imam, K., & McCoy, J. (1990). Active vibration control of flexible beams using shape memory actuators. *Journal of Sound and Vibration*, 140(3), 437-456. doi:10.1016/0022-460X(90)90760-W
- Behl, M., & Lendlein, A. (2007). Shape-memory polymers. *Materials Today*, 10(4), 20-28. doi:10.1016/S1369-7021(07)70047-0
- Bejan, A. (1993). *Heat Transfer* (1 ed.). USA: John Wiley & Sons.

- Bekker, A., & Brinson, L. C. (1998). Phase diagram based description of the hysteresis behavior of shape memory alloys. *Acta Materialia*, 46(10), 3649-3665. doi:10.1016/S1359-6454(97)00490-4
- Bellin, I., Kelch, S., Langer, R., & Lendlein, A. (2006). Polymeric triple-shape materials. *Proceedings of the National Academy of Sciences*, 103(48), 18043-18047.
- Bellini, A., Colli, M., & Dragoni, E. (2009). Mechatronic design of a shape memory alloy actuator for automotive tumble flaps: A case study. *IEEE Transactions on Industrial Electronics*, 56(7), 2644-2656. doi:10.1109/tie.2009.2019773
- Berendt, C. J. (2007). EP Patent 1,762,633.
- Bergamasco, M., Dario, P., & Salsedo, F. (1990). Shape memory alloy microactuators. *Sensors and Actuators A: Physical*, 21(1-3), 253-257. doi:10.1016/0924-4247(90)85049-A
- Bergamasco, M., Salsedo, F., & Dario, P. (1989, 14-19 May 1989). *A linear SMA motor as direct-drive robotic actuator*. Paper presented at the Robotics and Automation, 1989. Proceedings., 1989 IEEE International Conference on.
- Bergman, T. L., Lavine, A. S., Incropera, F. P., & DeWitt, D. P. (2011). *Fundamentals of heat and mass transfer* (7 ed.): John Wiley & Sons.
- Berry, M., & Garcia, E. (2008). Bio-inspired shape memory alloy actuated hexapod robot. 69281M-69281M. doi:10.1117/12.776540
- Beyer, J., & Mulder, J. H. (1994). *Recent Developments in High Temperature Shape Memory Alloys*. Paper presented at the MRS Proceedings.
- Bhattacharyya, A., Lagoudas, D. C., Wang, Y., & Kinra, V. K. (1995). On the role of thermoelectric heat transfer in the design of SMA actuators: theoretical modeling and experiment. *Smart Materials and Structures*, 4(4), 252.
- Biasiotto, M., Butera, F., & Alacqua, S. (2005). US Patent 2005/0195064A1.
- Bidaux, J.-E., Månson, J.-A., & Gotthardt, R. (1996). *Active stiffening of composite materials by embedded shape-memory-alloy fibres*. Paper presented at the MRS Proceedings.
- Biesiekierski, A., Wang, J., AH Gepreel, M., & Wen, C. (2012). A new look at biomedical Ti-based shape memory alloys. *Acta Biomaterialia*, 8(5), 1661-1669. doi:10.1016/j.actbio.2012.01.018
- Bigelow, G., Padula, S., II, Garg, A., Gaydosch, D., & Noebe, R. (2010). Characterization of Ternary NiTiPd High-Temperature Shape-Memory Alloys under Load-Biased Thermal Cycling. *Metallurgical and Materials Transactions A*, 41(12), 3065-3079. doi:10.1007/s11661-010-0365-5
- Bil, C., Massey, K., & Abdullah, E. J. (2013). Wing morphing control with shape memory alloy actuators. *Journal of Intelligent Material Systems and Structures*, 24(7), 879-898.
- Birman, V. (1997). Review of mechanics of shape memory alloy structures. *Applied Mechanics Reviews*, 50, 629.
- Bogue, R. (2009). Shape-memory materials: a review of technology and applications. *Assembly Automation*, 29(3), 214-219.
- Bohan, S. M. (2009). US Patent 7503444B2.
- Bonacina, C., Comini, G., Fasano, A., & Primicerio, M. (1973). Numerical solution of phase-change problems. *International Journal of Heat and Mass Transfer*, 16(10), 1825-1832. doi:10.1016/0017-9310(73)90202-0

- Borroni-Bird, C. E. (1997, March 03, 1997). *Smarter vehicles*. Paper presented at the Smart Structures and Materials 1997: Industrial and Commercial Applications of Smart Structures Technologies, San Diego, CA.
- Box, G. (1988). Signal-to-noise ratios, performance criteria, and transformations. *Technometrics*, 30(1), 1-17.
- Box, G. E. P., & Hunter, J. S. (1961). The 2k-p Fractional Factorial Designs Part I. *Technometrics*, 3(3), 311-351. doi:10.2307/1266725
- Boyd, J. G., & Lagoudas, D. C. (1996). A thermodynamical constitutive model for shape memory materials. Part I. The monolithic shape memory alloy. *International Journal of Plasticity*, 12(6), 805-842. doi:10.1016/S0749-6419(96)00030-7
- Brailovski, V., Prokoshkin, S., Terriault, P., & Trochu, F. (2003). *Shape memory alloys: fundamentals, modeling and applications* (V. Brailovski Ed.): Université du Québec. École de Technologie Supérieure.
- Brailovski, V., Trochu, F., & Daigneault, G. (1996). Temporal characteristics of shape memory linear actuators and their application to circuit breakers. *Materials & Design*, 17(3), 151-158. doi:10.1016/S0261-3069(96)00049-0
- Branco, J. F., Pinho, C. T., & Figueiredo, R. A. (2001). A dimensionless analysis of radial heat conduction with variable external convection boundary conditions. *International Communications in Heat and Mass Transfer*, 28(4), 489-497. doi:10.1016/S0735-1933(01)00253-6
- Brei, D., Redmond, J., Wilmot, N. A., Browne, A. L., Johnson, N. L., & Jones, G. L. (2006). US Patent 7063377B2.
- Breidert, J., & Welp, E. (2002). *Actuator Development Using a Knowledge Base*. Paper presented at the Proceedings of the 8th International Conference on New Actuators (ACTUATOR), Bremen, Germany.
- Brian, S., Kyujin, C., & Asada, H. H. (2006). Segmented shape memory alloy actuators using hysteresis loop control. *Smart Materials and Structures*, 15(2), 642.
- Brinson, L. C. (1993). One-Dimensional Constitutive Behavior of Shape Memory Alloys: Thermomechanical Derivation with Non-Constant Material Functions and Redefined Martensite Internal Variable. *Journal of Intelligent Material Systems and Structures*, 4(2), 229-242. doi:10.1177/1045389x9300400213
- Browne, A. L., Aase, J. H., Johnson, N. L., & Keefe, A. C. (2007). US Patent 7275846B2.
- Browne, A. L., Alexander, P. W., Mankame, N., Usoro, P., Johnson, N. L., Aase, J., . . . Herrera, G. (2011, 2 - 4 November 2011). *SMA heat engines: Advancing from a scientific curiosity to a practical reality*. Paper presented at the Smart materials, structures and NDT in Aerospace, Montreal, Quebec, Canada.
- Browne, A. L., Buravalla, V. R., & Johnson, N. L. (2007). US Patent 7188498B2.
- Browne, A. L., & Johnson, N. L. (2005). US Patents 6910714B2.
- Browne, A. L., & Johnson, N. L. (2009). US Patents 7498926B2.
- Browne, A. L., Johnson, N. L., Chernoff, A. B., Kramarczyk, M. A., Ukpai, U. I., Ulicny, J. C., & Jones, G. L. (2011). US Patent 7900986B2.
- Browne, A. L., Johnson, N. L., Khoury, J. Y., Alexander, P. W., & Carpenter, M. G. (2009). US Patents 7556313B2.
- Browne, A. L., Johnson, N. L., & Kramarczyk, M. A. (2006). US Patent 7029044B2.
- Browne, A. L., Johnson, N. L., Mankame, N. D., Barvosa-carter, W., Bucknor, N. K., Henry, C. P., . . . Keefe, A. C. (2009). US Patent 2009/0045042A1.

- Browne, A. L., Johnson, N. L., Mankame, N. D., Ulicny, J. C., Jones, G. L., & O'Kane, J. C. (2005). US Patent 2005/0199455A1.
- Browne, A. L., Johnson, N. L., Rober, K. B., Voss, M. A., Juechter, T. J., & Moss, E. D. (2009). US Patents US007607717B2.
- Browne, A. L., Johnson, N. L., & Sears, I. G. (2011). US Patents 7997632B2.
- Browne, A. L., Johnson, N. L., Zavattieri, P. D., Ukpai, U. I., Ulicny, J. C., Cafeo, J. A., . . . Xiujie Gao. (2010). US Patent 7758121B2.
- Browne, A. L., Mankame, N. D., Johnson, N. L., & Keefe, A. C. (2007). US Patents 7284786B2.
- Browne, A. L., Stauffer, L. E., Mathieu, R. J., Szczerba, J. F., & Johnson, N. L. (2009). US Patents 7631915B2.
- Bruckheimer, E., Judelman, A. G., Bruckheimer, S. D., Tavori, I., Naor, G., & Katzen, B. T. (2003). In Vitro Evaluation of a Retrievable Low-Profile Nitinol Vena Cava Filter. *Journal of Vascular and Interventional Radiology*, 14(4), 469-474. doi:10.1097/01.RVI.0000064863.65229.C3
- Brugger, D., Kohl, M., Hollenbach, U., Kapp, A., & Stiller, C. (2006). Ferromagnetic shape memory microscanner system for automotive applications. *International Journal of Applied Electromagnetics and Mechanics*, 23(1), 107-112.
- Buchanan, H. C., & Victor, K. R. (1991). US Patents 5062175.
- Buehler, W. J., Gilfrich, J. V., & Wiley, R. C. (1963). Effect of low-temperature phase changes on the mechanical properties of alloys near composition TiNi. *Applied Physics*, 34(5), 1475 - 1477.
- Buehler, W. J., & Wang, F. E. (1968). A summary of recent research on the nitinol alloys and their potential application in ocean engineering. *Ocean Engineering*, 1(1), 105-108. doi:10.1016/0029-8018(68)90019-X
- Bundhoo, V., Haslam, E., Birch, B., & Park, E. J. (2009). A shape memory alloy-based tendon-driven actuation system for biomimetic artificial fingers, part I: design and evaluation. *Robotica*, 27(01), 131-146.
- Bunget, G., & Seelecke, S. (2009). *Actuator placement for a bio-inspired bone-joint system based on SMA*.
- Butera, F. (2008). Shape memory actuators for automotive applications. *Advanced Materials and Processes*, 166(3), 37.
- Butera, F. (2010). EP Patent 2,171,183.
- Butera, F., Alacqua, S., & Zanella, A. (2006). EP Patent 1,726,467.
- Butera, F., Coda, A., & Vergani, G. (2007). Shape memory actuators for automotive applications. *nanotec IT newsletter*, (Number 8 June 2007), 12-16. Retrieved from nanotec IT website: <http://www.nanotec.it/newsletter/NewsletterGiugno07.pdf#page=12>
- CK Chun, S. O. P. (2000). A fixed-grid finite difference method for phase change problems. *Numerical Heat Transfer, Part B: Fundamentals*, 38(1), 59-73. doi:10.1080/10407790050131561
- Caldwell, D. G., & Taylor, P. M. (1988). *Artificial muscles as robotic actuators*. Paper presented at the IFAC Robot control conference (Syroc 88), Karlsruhe, Germany.
- Caldwell, N., Gutmark, E., & Ruggeri, R. (2007). Heat transfer model for blade twist actuator system. *Journal of thermophysics and heat transfer*, 21(2), 352-360.

- Calkins, F. T., & Mabe, J. H. (2010). Shape memory alloy based morphing aerostructures. *Journal of Mechanical Design*, 132, 111012.
- Campbell, D., Lake, M. S., Scherbarth, M. R., Nelson, E., & Six, R. W. (2005, 18 - 21 April 2005). *Elastic memory composite material: an enabling technology for future furlable space structures*. Paper presented at the 46th AIAA/ASME/ASCE/AHS/ASC structures, structural dynamics and materials conference, Austin, TX, USA.
- Carman, G. P., Mitrovic, M., & Pulliam, W. J. (2004). US Patent 2006/0110211A1.
- Carpenter, B., & Lyons, J. (2001). EO-1 technology validation report: Lightweight flexible solar array experiment. *NASA/GSFC*. Last updated: August, 8.
- Carpenter, B. F., & Draper, J. L. (2000). US Patents 6149742.
- Carreras, G., Casciati, F., Casciati, S., Isalgue, A., Marzi, A., & Torra, V. (2011). Fatigue laboratory tests toward the design of SMA portico-braces. *Smart Struct Syst*, 7, 41-57.
- Carreras, G., Isalgue, A., Torra, V., Lovey, F. C., & Soul, H. (2008). Metastable effects on martensitic transformation in SMA part 5 - Fatigue-life and detailed hysteresis behavior in NiTi and Cu-based alloys. *Journal of thermal analysis and calorimetry*, 91(2), 575-579.
- Carslaw, H., & Jaeger, J. J. C. (1959). *Conduction of heat in solids*: Oxford University Press London.
- Carter, A. J., Scott, D., Laird, J. R., Bailey, L., Kovach, J. A., Hoopes, T. G., . . . Virmani, R. (1998). Progressive vascular remodeling and reduced neointimal formation after placement of a thermoelastic self-expanding nitinol stent in an experimental model. *Catheterization and Cardiovascular Diagnosis*, 44(2), 193-201. doi:10.1002/(SICI)1097-0304(199806)44:2<193::AID-CCD13>3.0.CO;2-O
- Cederström, J., & Van Humbeeck, J. (1995). Relationship Between Shape Memory Material Properties and Applications. *J. Phys. IV France*, 05(C2), C2-335-C332-341.
- Cekirge, S., Weiss, J. P., Foster, R. G., Neiman, H. L., & McLean, G. K. (1993). Percutaneous Retrieval of Foreign Bodies: Experience with the Nitinol Goose Neck Snare. *Journal of Vascular and Interventional Radiology*, 4(6), 805-810. doi:10.1016/S1051-0443(93)71978-8
- Cepolina, F., & Michelini, R. C. (2004, 23-26 March 2004). *Robots in medicine: A survey of in-body nursing aids - Introductory overview and concept design hints*. Paper presented at the 35th International Symposium on Robotics 2004 (ISR2004), Paris, France.
- Chan, C. W., Man, H. C., & Cheng, F. T. (2013). Fatigue behavior of laser-welded NiTi wires in small-strain cyclic bending. *Materials Science and Engineering: A*, 559, 407-415. doi:10.1016/j.msea.2012.08.119
- Chan, K. C., Godman, M. J., Walsh, K., Wilson, N., Redington, A., & Gibbs, J. L. (1999). Transcatheter closure of atrial septal defect and interatrial communications with a new self expanding nitinol double disc device (Amplatzer septal occluder): multicentre UK experience. *Heart*, 82(3), 300-306.
- Chang, L. C., & Read, T. A. (1951). Behavior of the elastic properties of AuCd. *Trans. Met. Soc. AIME*, 191, 47.
- Chang-jun, Q., Pei-sun, M., & Qin, Y. (2004). A prototype micro-wheeled-robot using SMA actuator. *Sensors and Actuators A: Physical*, 113(1), 94-99. doi:10.1016/j.sna.2004.01.017

- Chaplin, C. (2008). *Interactive fatigue in wire rope applications*. Paper presented at the Symposium on Mechanics of Slender Structures (MoSS 2008).
- Charney, J. G., Fjörtoft, R., & Von Neumann, J. (1950). Numerical integration of the barotropic vorticity equation. *Tellus A*, 2(4).
- Chee Siong, L., Yokoi, H., & Arai, T. (2005a, 2-6 Aug. 2005). *Improving heat sinking in ambient environment for the shape memory alloy (SMA)*. Paper presented at the Intelligent Robots and Systems, 2005. (IROS 2005). 2005 IEEE/RSJ International Conference on.
- Chee Siong, L., Yokoi, H., & Arai, T. (2005b, 1-4 Sept 2005). *New Shape Memory Alloy Actuator: Design and Application in the Prosthetic Hand*. Paper presented at the 27th Annual International Conference of the Engineering in Medicine and Biology Society (IEEE-EMBS 2005), Shanghai, China.
- Chen, J., Sun, D. X., & Wu, C. F. J. (1993). A Catalogue of Two-Level and Three-Level Fractional Factorial Designs with Small Runs. *International Statistical Review / Revue Internationale de Statistique*, 61(1), 131-145. doi:10.2307/1403599
- Cheng, Y.-T., Ni, W., Lev, L. C., Lukitsch, M. J., Grummon, D. S., & Weiner, A. M. (2006). US Patent 7005195B2.
- Cheng, Y.-T., Ni, W., Lukitsch, M. J., Weiner, A. M., & Grummon, D. S. (2006). US Patent 7060140B2.
- Cheng, Y.-T., Ni, W., & Ulicny, J. C. (2004). US006766566B2. US Patent 6766566B2.
- Choi, J. Y. (2011). US Patents 7967098B2.
- Chonan, S., Jiang, Z. W., Tani, J., Orikasa, S., Tanahashi, Y., Takagi, T., . . . Tanikawa, J. (1997). Development of an artificial urethral valve using SMA actuators. *Smart Materials and Structures*, 6(4), 410.
- Choon, T. W., Salleh, A. S., Jamian, S., & Ghazai, M. I. (2007). Phase transformation temperatures for shape memory alloy wire. *ENFORMATIKA*, 19, 304-307.
- Choudhary, R. K., Theruvil, B., & Taylor, G. R. (2004). First metatarsophalangeal joint arthrodesis: A new technique of internal fixation by using memory compression staples. *The Journal of Foot and Ankle Surgery*, 43(5), 312-317. doi:10.1053/j.jfas.2004.07.003
- Churchill, S. W., & Bernstein, M. (1977). A Correlating Equation for Forced Convection From Gases and Liquids to a Circular Cylinder in Crossflow. *Journal of Heat Transfer*, 99(2), 300-306. doi:10.1115/1.3450685
- Churchill, S. W., & Chu, H. H. S. (1975). Correlating equations for laminar and turbulent free convection from a horizontal cylinder. *International Journal of Heat and Mass Transfer*, 18(9), 1049-1053. doi:10.1016/0017-9310(75)90222-7
- Clayton, P. (1993). Tribological behavior of a titanium-nickel alloy. *Wear*, 162–164, Part A(0), 202-210. doi:10.1016/0043-1648(93)90502-d
- Cleveland, M. A. (2008). US Patent 7367738B2.
- Clough, R. W. (2004). Early history of the finite element method from the view point of a pioneer. *International Journal for Numerical Methods in Engineering*, 60(1), 283-287. doi:10.1002/nme.962
- Coati, M., Marazzi, G., Marini, G., Rossi, G., Rossi, L., & Verturini, D. (2012). US Patent 8162942.
- Coats, L., & Bonhoeffer, P. (2007). New percutaneous treatments for valve disease. *Heart*, 93(5), 639-644.

- Coffee, C. L. (1993). US Patents 5211371.
- Colli, M., Bellini, A., Concari, C., Toscani, A., & Franceschini, G. (2006, 6-10 November 2006). *Current-controlled shape memory alloy actuators for automotive tumble flap*. Paper presented at the IECON 2006-32nd Annual Conference on IEEE Industrial Electronics, Paris.
- Collins, J. A., Busby, H. R., & Staab, G. H. (2010). *Mechanical Design of Machine Elements and Machines: A Failure Prevention Perspective*: Wiley.
- Colorado, J., Barrientos, A., Rossi, C., & Breuer, K. S. (2012). Biomechanics of smart wings in a bat robot: morphing wings using SMA actuators. *Bioinspiration & Biomimetics*, 7(3), 036006.
- Command, N. S. S. (1976a). *Design and engineering of wire-rope systems*. Retrieved from Washington DC, USA:
- Command, N. S. S. (1976b). *Wire-rope analysis and design data*. Retrieved from Washington DC, USA: <http://www.ntis.gov/search/product.aspx?ABBR=ADA955309>
- components, J. M. m. (2015). Nitinol Specification Guidelines. Retrieved from <http://jmmedical.com/resources/120/Nitinol-Specification-Guidelines.html>
- Condorelli, G. G., Bonaccorso, A., Smecca, E., Schäfer, E., Cantatore, G., & Tripi, T. R. (2010). Improvement of the fatigue resistance of NiTi endodontic files by surface and bulk modifications. *International Endodontic Journal*, 43(10), 866-873. doi:10.1111/j.1365-2591.2010.01759.x
- Contra, R., Dallolio, V., Franzoso, G., Gastaldi, D., & Vena, P. (2005). Biomechanical study of a pathologic lumbar functional spinal unit and a possible surgical treatment through the implant of an interspinous device.
- Core, R. A. (2010). US Patent 7716932B2.
- Corporation, T. SmartServo RC-1. Retrieved from <http://www.toki.co.jp/biometal/english/contents.php>
- Crank, J., & Nicolson, P. (1947). A practical method for numerical evaluation of solutions of partial differential equations of the heat-conduction type. *Mathematical Proceedings of the Cambridge Philosophical Society*, 43(01), 50-67. doi:10.1017/S0305004100023197
- Cross, N. (2008). *Engineering Design Methods: Strategies for Product Design* (4 ed.). West Sussex, England: John Wiley & Sons, Ltd.
- Cuschieri, A. (1991). Variable curvature shape- memory spatula for laparoscopic surgery. *Surgical Endoscopy*, 5(4), 179-181. doi:10.1007/BF02653258
- Cwikel, W., Willen, R., Stridbeck, H., Lillo-Gil, R., & Von Holstein, C. S. (1993). Self-expanding stent in the treatment of benign esophageal strictures: experimental study in pigs and presentation of clinical cases. *Radiology*, 187(3), 667-671.
- Czimmek, P. (2004). *Characterization of Magnetic Shape Memory Material*. Retrieved from http://asmeasternvirginia.tripod.com/member_education/2005/seminar05/asm_msm_czimmek.pdf
- Dahlgren, J. M., & Gelbart, D. (2009). US Patent 2009/0076597A1.
- Das, S. K. (2010). *Fundamentals of Heat and Mass Transfer*. Alpha Science International.
- Dauids, P. H. P., Groen, A. K., Rauws, E. A. J., Tytgat, G. N. J., & Huibregtse, K. (1992). Randomised trial of self-expanding metal stents versus polyethylene stents for distal malignant biliary obstruction. *The Lancet*, 340(8834-8835), 1488-1492. doi:10.1016/0140-6736(92)92752-2

- De la Flor, S., Urbina, C., & Ferrando, F. (2006). Constitutive model of shape memory alloys: Theoretical formulation and experimental validation. *Materials Science and Engineering: A*, 427(1–2), 112-122. doi:10.1016/j.msea.2006.04.008
- De Laurentis, K. J., & Mavroidis, C. (2002). Mechanical design of a shape memory alloy actuated prosthetic hand. *Technology and Health Care*, 10, 91-106.
- Decker, L. H. (1997). US Patents 5685721A.
- DeLaurentis, K. J., Mavroidis, C., & Pfeiffer, C. (2000). *Development of a Shape Memory Alloy Actuated Robotic Hand*. Paper presented at the Neural Networks.
- Descamps, O. (1991). The application of shape-memory alloys to sculpture. *JOM*, 43(3), 64-64. doi:10.1007/BF03220168
- Ditman, J. B., Bergman, L. A., & Tsao, T.-C. (1996). The design of extended bandwidth shape memory alloy actuators. *Journal of Intelligent Material Systems and Structures*, 7(6), 635-645.
- Dominique, C. G. (2003a). EP Patent 1,347,131.
- Dominique, C. G. (2003b). US 2003/0177974 A1. US Patent 2003/0177974A1.
- Donnellan, Q. A. (2005). *Design and testing of linear shape memory alloy actuator*. Retrieved from <http://tiims.tamu.edu/2005summerREU/papers/Donnellan.pdf>
- Dooley, B. A., Lasley, C. C., Mitchell, M. R., Steele, R. R., & Tittelbaugh, E. M. (2012). US Patents 8177927B2.
- Dotter, C. T., Buschmann, R. W., McKinney, M. K., & Rösch, J. (1983). Transluminally expandable nitinol coil stent grafting: preliminary report. *Radiology*, 147(1), 259-260.
- Duerig, T. (1990). *Applications of shape memory*. Paper presented at the Materials Science Forum.
- Duerig, T., Pelton, A., & Stöckel, D. (1999). An overview of nitinol medical applications. *Materials Science and Engineering: A*, 273–275(0), 149-160. doi:10.1016/S0921-5093(99)00294-4
- Duerig, T. W., & Pelton, A. R. (1994). Ti-Ni shape memory alloys *Materials Properties Handbook: Titanium Alloys* (pp. 1035-1048): Materials Park, OH: American Society for Metals.
- Duerig, T. W., Stockel, D., & Keeley, A. (1990). Actuator and work production devices. In T. W. Duerig, K. Melton, D. Stockel, & C. Wayman (Eds.), *Engineering Aspects of Shape Memory Alloys* (pp. 181-194): Butterworth-Heinemann, UK.
- Dunne, J. P., Hopkins, M. A., Baumann, E. W., Pitt, D. M., & White, E. V. (1999, 1999). *Overview of the SAMPSON smart inlet*. Paper presented at the 6th Annual International Symposium on Smart Structures and Materials Conference.
- Dynalloy. (2006). Dynalloy Newsletters(April 2006). Retrieved from <http://www.dynalloy.com/Newsletters.php>
- Dynalloy. (2007). Dynalloy Newsletters(May 2007). Retrieved from <http://www.dynalloy.com/Newsletters.php>
- Dynalloy Inc. (2007). Technical characteristics of Flexinol actuator wires. In U. Dynalloy Inc. (Ed.). Costa Mesa (CA).
- Eggeler, G., Hornbogen, E., Yawny, A., Heckmann, A., & Wagner, M. (2004). Structural and functional fatigue of NiTi shape memory alloys. *Materials Science and Engineering: A*, 378(1–2), 24-33. doi:10.1016/j.msea.2003.10.327

- Eisakhani, A., Ma, W., Gao, J., Culham, J. R., & Gorbet, R. (2011). *Natural convection heat transfer modelling of shape memory alloy wire*. Paper presented at the Smart materials, structures and NDT in aerospace, Montreal, Quebec, Canada.
- Elahinia, M. H., & Ahmadian, M. (2005). An enhanced SMA phenomenological model: II. The experimental study. *Smart Materials and Structures*, 14(6), 1309.
- Elisa, B., Pietro, V., Marco, Q., Arianna, M., & Paolo, D. (2009). Superelastic leg design optimization for an endoscopic capsule with active locomotion. *Smart Materials and Structures*, 18(1), 015001.
- Elwaleed, A. K., Mohamed, N. A., Nor, M. J. M., & Mustafa, M. M. (2007). A new concept of a linear smart actuator. *Sensors and Actuators A: Physical*, 135(1), 244-249. doi:10.1016/j.sna.2006.07.010
- Elzey, D. M., Sofla, A. Y. N., & Wadley, H. N. G. (2003, 2003). *A bio-inspired high-authority actuator for shape morphing structures*. Paper presented at the Smart structures and materials 2003 - Active Materials: Behavior and Mechanics.
- Engmann, E., & Asch, M. R. (1998). Clinical Experience with the Antecubital Simon Nitinol IVC Filter. *Journal of Vascular and Interventional Radiology*, 9(5), 774-778. doi:10.1016/S1051-0443(98)70390-2
- Erbstoesser, B., Armstrong, B., Taya, M., & Inoue, K. (2000). Stabilization of the shape memory effect in NiTi: an experimental investigation. *Scripta materialia*, 42(12), 1145-1150.
- Fan, J., Yu, W., & Zheng, R. (2009). US Patents 7591707B2.
- Fasching, A., Norwich, D., Geiser, T., & Paul, G. (2011). An Evaluation of a NiTiCo Alloy and its Suitability for Medical Device Applications. *Journal of Materials Engineering and Performance*, 20(4-5), 641-645. doi:10.1007/s11665-011-9845-z
- Featherstone, R., & Teh, Y. (2006). Improving the Speed of Shape Memory Alloy Actuators by Faster Electrical Heating. In M. Ang, Jr. & O. Khatib (Eds.), *Experimental Robotics IX* (Vol. 21, pp. 67-76): Springer Berlin Heidelberg.
- Fernandes, F. M. B., Mahesh, K. K., & Paula, A. d. S. (2013). Thermomechanical Treatments for Ni-Ti Alloys. In F. M. B. Fernandes (Ed.), *Shape Memory Alloys - Processing, Characterization and Applications*: InTech.
- Festo. (2013). BionicOpter – Inspired by dragonfly flight. Retrieved from http://www.festo.com/cms/en_corp/13165.htm
- Firstov, G. S., Van Humbeeck, J., & Koval, Y. N. (2006). High temperature shape memory alloys problems and prospects. *Journal of Intelligent Material Systems and Structures*, 17(12), 1041-1047.
- Forsythe, G. E., & Wasow, W. R. (1960). *Finite Difference Methods for Partial Differential Equations*. New York: John Wiley and Sons.
- Foss Jr, R. L., & Siebrecht, W. A. (1999). US Patents 6006522.
- Fries, A., & Hunter, W. G. (1980). Minimum Aberration 2k-p Designs. *Technometrics*, 22(4), 601-608. doi:10.2307/1268198
- Fu, Y., Du, H., Huang, W., Zhang, S., & Hu, M. (2004). TiNi-based thin films in MEMS applications: a review. *Sensors and Actuators A: Physical*, 112(2-3), 395-408. doi:10.1016/j.sna.2004.02.019
- Fujita, H. (1989). *Studies of micro actuators in Japan*. Paper presented at the IEEE International Conference on Robotic Automation, Institute of Industrial Science, Tokyo University. http://ieeexplore.ieee.org/xpls/abs_all.jsp?arnumber=100200

- Fujita, H., & Toshiyoshi, H. (1998). Micro actuators and their applications. *Microelectronics Journal*, 29(9), 637-640. doi:10.1016/S0026-2692(98)00027-5
- Fujun, P., Xin-Xiang, J., Yan-Ru, H., & Ng, A. (2005, 5-12 March 2005). *Application of Shape Memory Alloy Actuators in Active Shape Control of Inflatable Space Structures*. Paper presented at the Aerospace Conference, 2005 IEEE.
- Fulvio, P., Francesco, C., Michele, M., & Umberto, P. (2012). Multifunctional SMarT composite material for in situ NDT/SHM and de-icing. *Smart Materials and Structures*, 21(10), 105010.
- Fumagalli, L., Butera, F., & Coda, A. (2009). SmartFlex® NiTi Wires for Shape Memory Actuators. *Journal of Materials Engineering and Performance*, 18(5-6), 691-695.
- Funakubo, H., & Kennedy, J. B. (1987). *Shape memory alloys* (Vol. 1). New York: Taylor & Francis.
- Furuya, Y. (1996). Design and material evaluation of shape memory composites. *Intelligent material systems and structures*, 7(3), 321-330. doi:10.1177/1045389X9600700313
- Furuya, Y., Sasaki, A., & Taya, M. (1993). Enhanced mechanical properties of TiNi shape memory fiber/Al matrix composite. *JIM, Materials Transactions*, 34(3), 224-227.
- Furuya, Y., & Shimada, H. (1991). Shape memory actuators for robotic applications. *Materials & Design*, 12(1), 21-28. doi:10.1016/0261-3069(91)90088-L
- Gabriel, K. J., Mehregany, M., & Walker, J. A. (1989). US Patents 4864824.
- Gabriel, K. J., Trimmer, W. S. N., & Walker, J. A. (1987). US Patents 4700541.
- Gall, K., Tyber, J., Wilkesanders, G., Robertson, S. W., Ritchie, R. O., & Maier, H. J. (2008). Effect of microstructure on the fatigue of hot-rolled and cold-drawn NiTi shape memory alloys. *Materials Science and Engineering: A*, 486(1-2), 389-403. doi:10.1016/j.msea.2007.11.033
- Gall, K., Yakacki, C. M., Liu, Y., Shandas, R., Willett, N., & Anseth, K. S. (2005). Thermomechanics of the shape memory effect in polymers for biomedical applications. *Journal of Biomedical Materials Research Part A*, 73A(3), 339-348. doi:10.1002/jbm.a.30296
- Gambao, E., Hernando, M., & Brunete, A. (2005, 11-14 September 2005). *Multiconfigurabile inspection robots for low diameter canalizations*. Paper presented at the 22nd International Symposium on Automation and Robotics in Construction (ISARC 2005), Ferrara Italy.
- Gandhi, U. N. (2010). US Patent 7729828B2.
- Gao, X., Browne, A. L., Alexander, P. W., Johnson, N. L., & Brown, W. (2013). US2013/0011806 A. US Patents 2013/0011806A1.
- Garscha, M., Auernhammer, H., & Engelhardt, K. (2008). US Patents 2008/0271559A1.
- Gehm, R. (2007). Smart materials spur additional design possibilities. *Automotive Engineering International*, 46-47.
- Geraci, F., Cooper, J. E., & Amprikidis, M. (2003). Development of smart vortex generators. *Smart Structures and Materials 2003*, 5056, 1-8.
- Gheorghita, V., Gümpel, P., Strittmatter, J., Anghel, C., Heitz, T., & Senn, M. (2013). Using Shape Memory Alloys in Automotive Safety Systems *Proceedings of the FISITA 2012 World Automotive Congress* (Vol. 195, pp. 909-917): Springer Berlin Heidelberg.

- Ghosh, P., Rao, A., & Srinivasa, A. R. (2013). Design of multi-state and smart-bias components using Shape Memory Alloy and Shape Memory Polymer composites. *Materials & Design*, 44(0), 164-171. doi:10.1016/j.matdes.2012.05.063
- Gibson, P. T. (2001). Operational characteristics of ropes and cables. In J. F. Bash (Ed.), *Handbook of oceanographic winch, wire and cable technology* (3rd. ed.): National Science Foundation.
- Global, C. (2013). New Nickel Manganese Shape Memory Alloy Developed. *Success stories*. Retrieved from <http://www.crdglobal.org/news-and-events/success-stories/2013/02/21/new-nickel-manganese-shape-memory-alloy-developed>
- GM. (2013). Chevrolet Debuts Lightweight 'Smart Material' on Corvette. Retrieved from <http://media.gm.com/media/us/en/gm/news.detail.html/content/Pages/news/us/en/2013/Feb/0212-corvette.html>
- GmbH, T. (2013). TROX TJN jet nozzles – acoustically and technically optimised. Retrieved from http://www.troxtechnik.com/en/company/news/productnews/news_20130701/index.html
- Godard, O. J., Lagoudas, M. Z., & Lagoudas, D. C. (2003, 2003). *Design of space systems using shape memory alloys*. Paper presented at the Smart Structures and Materials.
- Goldstein, D., & Nguyen, T. D. (2000). US Patents 6041728.
- Gorbet, R. B., Morris, K. A., & Chau, R. C. C. (2009). Mechanism of bandwidth improvement in passively cooled SMA position actuators. *Smart Materials and Structures*, 18(9), 095013.
- Gottfried, H. W., Gnann, R., BrÄndle, E., Bachor, R., Gschwend, J. E., & Kleinschmidt, K. (1997). Treatment of high-risk patients with subvesical obstruction from advanced prostatic carcinoma using a thermosensitive mesh stent. *British Journal of Urology*, 80(4), 623-627. doi:10.1046/j.1464-410X.1997.00416.x
- Greninger, A. B., & Mooradian, V. G. (1938). Strain Transformation in Metastable Beta Copper-Zinc and Beta Copper-Ti Alloys. *AIME TRANS*, 128, 337-369.
- Grosskrueger, D. D., Carpenter, B. F., Easom, B. W., & Draper, J. L. (2000). US Patents 6024347.
- Group, T. M. S. (2015). Specifying NiTi materials. Retrieved from http://heim.ifi.uio.no/~mes/inf1400/COOL/Robot%20Prosjekt/Flexinol/specifying_niti_alloys.htm
- Gröber, H., & Erk, S. (1961). *Fundamentals of heat transfer*. McGraw-Hill.
- Gummin, M. A., Donakowski, W., & Gaines, G. (2007). USA Patent 7256518B2.
- Gummin, M. A., Donakowski, W., & Gaines, G. A. (2006). US Patents 7021055B2.
- Gurney, H. P., & Lurie, J. (1923). Charts for Estimating Temperature Distributions in Heating or Cooling Solid Shapes. *Industrial & Engineering Chemistry*, 15(11), 1170-1172. doi:10.1021/ie50167a028
- Gümpel, P., & Strittmatter, J. (2009). Smart materials: Opportunities and applications in some fields. *Australian Journal of Mechanical Engineering*, 7(1), 99.
- Habib, I. S. (1982). The effects of radiation, inclination and insulation opacity on the critical radius for radial heat transfer. *International Journal of Heat and Mass Transfer*, 25(10), 1607-1609. doi:10.1016/0017-9310(82)90040-0
- Haga, Y., Esashi, M., & Maeda, S. (2000, 23-27 Jan 2000). *Bending, torsional and extending active catheter assembled using electroplating*. Paper presented at the

- Micro Electro Mechanical Systems, 2000. MEMS 2000. The Thirteenth Annual International Conference on.
- Haga, Y., Makishi, W., Iwami, K., Totsu, K., Nakamura, K., & Esashi, M. (2005). Dynamic Braille display using SMA coil actuator and magnetic latch. *Sensors and Actuators A: Physical*, 119(2), 316-322.
- Haga, Y., Tanahashi, Y., & Esashi, M. (1998, 25-29 Jan 1998). *Small diameter active catheter using shape memory alloy*. Paper presented at the Micro Electro Mechanical Systems, 1998. MEMS 98. Proceedings., The Eleventh Annual International Workshop on.
- Hairer, E., Nørsett, S., & Wanner, G. (1993). *Solving Ordinary Difference Equations 1 - Nonstiff problems* (2nd ed.). Berlin: Springer.
- Hamaguchi, K., Tanii, J., & Kosaka, A. (2009). US Patent 7614228B2.
- Hara, F., Akazawa, H., & Kobayashi, H. (2001, 2001). *Realistic facial expressions by SMA driven face robot*. Paper presented at the Robot and Human Interactive Communication, 2001. Proceedings. 10th IEEE International Workshop on.
- Hartl, D. J., & Lagoudas, D. C. (2007). Aerospace applications of shape memory alloys. *Proceedings of the Institution of Mechanical Engineers, Part G: Journal of Aerospace Engineering*, 221(4), 535-552.
- Hartl, D. J., Lagoudas, D. C., Calkins, F. T., & Mabe, J. H. (2010). Use of a Ni60Ti shape memory alloy for active jet engine chevron application: I. Thermomechanical characterization. *Smart Materials and Structures*, 19(1), 015020.
- Hartl, D. J., Mooney, J. T., Lagoudas, D. C., Calkins, F. T., & Mabe, J. H. (2010). Use of a Ni60Ti shape memory alloy for active jet engine chevron application: II. Experimentally validated numerical analysis. *Smart Materials and Structures*, 19(1), 015021.
- Hashemi, M., & Schickel, D. (2011). US Patent 8011813B2.
- Hausegger, K. A., Cragg, A. H., Lammer, J., Lafer, M., Flückiger, F., Klein, G. E., . . . Pilger, E. (1994). Iliac artery stent placement: clinical experience with a nitinol stent. *Radiology*, 190(1), 199-202.
- Hautcoeur, A., & Eberthardt, A. (1997). US Patents 5640217.
- Hayashi, S. (1993). Properties and applications of polyurethane-series shape memory polymer. In K. Ashida & K. C. Frisch (Eds.), *International Progress in Urethanes* (1 ed., Vol. 6, pp. 90-115): CRC Press.
- He, Y. J., & Sun, Q. P. (2010). Frequency-dependent temperature evolution in NiTi shape memory alloy under cyclic loading. *Smart Materials and Structures*, 19(11), 115014.
- Heczko, O., & Straka, L. (2003). Temperature dependence and temperature limits of magnetic shape memory effect. *Journal of Applied Physics*, 94(11), 7139-7143. doi:10.1063/1.1626800
- Heisler, M. (1947). Temperature charts for induction and constant temperature heating. *Trans. ASME*, 69(3), 227-235.
- Henry, C. P. (2002). *Dynamic actuation properties of Ni-Mn-Ga ferromagnetic shape memory alloys*. (PhD), Massachusetts Institute of Technology, Massachusetts Institute of Technology. Retrieved from <http://dspace.mit.edu/handle/1721.1/8442>
- Heo, J.-H., & Chung, B.-J. (2012). Natural convection heat transfer on the outer surface of inclined cylinders. *Chemical Engineering Science*, 73(0), 366-372. doi:10.1016/j.ces.2012.02.012

- Himpens, J. (1993). Laparoscopic inguinal hernioplasty. *Surgical Endoscopy*, 7(4), 315-318. doi:10.1007/BF00725948
- Hines, A., Gausman, T. J., Glime, W. H., Hill, S. H., & Rigsby, B. S. (2001). US Patents 6247678B1.
- Hino, T., & Maeno, T. (2004). Development of a miniature robot finger with a variable stiffness mechanism using shape memory alloy.
- Hirose, S., Ikuta, K., & Sato, K. (1988). Development of a shape memory alloy actuator. Improvement of output performance by the introduction of a σ -mechanism. *Advanced robotics*, 3(2), 89-108.
- Hirose, S., Ikuta, K., & Umetani, Y. (1988). Development of shape-memory alloy actuators. Performance assessment and introduction of a new composing approach. *Advanced robotics*, 3(1), 3-16. doi:10.1163/156855389X00145
- Hisaaki, T., Kimio, K., Hiroyuki, I., & Cahoon, J. (1990). Basic Research on Shape Memory Alloy Heat Engine (Output Power Characteristics and Problems in Development). *JSME international journal*, 33-1(2), 263-268.
- Hodgson, D. E., Wu, M. H., & Biermann, R. J. (1990). Shape memory alloys *ASM Handbook* (Vol. 2, pp. 897-902): ASM International.
- Hoffman, J. D., & Frankel, S. (2001). *Numerical methods for engineers and scientists*: CRC press.
- Holman, J. P. (2009). *Heat Transfer* (10 ed.). New York, USA: McGraw-Hill.
- Homma, D. (1990). US Patent 4973024A.
- Homma, D. (2004). US Patent 6746552B2.
- Hong, D., & Priya, S. (2011). Twelve Degree of Freedom Baby Humanoid Head Using Shape Memory Alloy Actuators. *Journal of Mechanisms*, 3, 011008-011001.
- Hongjip, K., Yongsu, H., Dae-young, L., Jung-Ik, H., & Kyu-Jin, C. (2013). Sensorless displacement estimation of a shape memory alloy coil spring actuator using inductance. *Smart Materials and Structures*, 22(2), 025001.
- Honma, D., Miwa, Y., & Iguchi. (1985). Micro Robots and Micro Mechanisms Using Shape Memory Alloy to Robotic Actuators. *Robotic Systems*, 2(1), 3-25.
- Hoover, A. M., Steltz, E., & Fearing, R. S. (2008, 22-26 Sept. 2008). *RoACH: An autonomous 2.4g crawling hexapod robot*. Paper presented at the IEEE/RSJ International Conference on Intelligent Robots and Systems 2008 (IROS 2008).
- Hornbogen, E. (2004). Review Thermo-mechanical fatigue of shape memory alloys *Journal of Materials Science* (Vol. 39, pp. 385-399): Kluwer Academic Publishers.
- Hosmer Jr, D. W., Lemeshow, S., & Sturdivant, R. X. (2013). *Applied logistic regression* (Vol. 398): John Wiley & Sons.
- Hosoda, Y., Kojima, Y., Fujie, M., Honma, K., Iwamoto, T., Nakano, Y., & Kamejima, K. (1986). US Patents 4586335.
- Howe, R. D., Kontarinis, D. A., & Peine, W. J. (1995, 13-15 Dec 1995). *Shape memory alloy actuator controller design for tactile displays*. Paper presented at the Decision and Control, 1995., Proceedings of the 34th IEEE Conference on.
- Hu, J. (2007). *Shape memory polymers and textiles*. Cambridge, England: Woodhead Publishing Ltd.
- Hu, J., Zhu, Y., Huang, H., & Lu, J. (2012). Recent advances in shape-memory polymers: Structure, mechanism, functionality, modeling and applications. *Progress in Polymer Science*, 37(12), 1720-1763. doi:10.1016/j.progpolymsci.2012.06.001

- Huang, H. L., Park, S.-H., & Park, J.-O. (2008, 15 - 17 Oct 2008). *Shape Memory Alloy based Flower Robot*. Paper presented at the 39th International Symposium on Robotics 2008, Seoul, Korea.
- Huang, S., Leary, M., Ataalla, T., Probst, K., & Subic, A. (2012). Optimisation of Ni–Ti shape memory alloy response time by transient heat transfer analysis. *Materials & Design*, 35(0), 655-663. doi:10.1016/j.matdes.2011.09.043
- Huang, S., Mohd Jani, J., Leary, M., & Subic, A. (2013). The critical and crossover radii on transient heating. *Applied Thermal Engineering*, 60(1–2), 325-334. doi:10.1016/j.applthermaleng.2013.06.052
- Huang, W. (1999). Two-Way Behaviour of a Nitinol Torsion Bar. *Smart structures and materials 1999: 3-4 March, 1999, Newport Beach, California. Smart materials technologies*, 3675, 284.
- Huang, W. (2002). On the selection of shape memory alloys for actuators. *Materials & Design*, 23(1), 11-19.
- Huang, W., & Toh, W. (2000). Training two-way shape memory alloy by reheat treatment. *Materials Science Letters*, 19(17), 1549-1550. doi:10.1023/A:1006721022185
- Huang, W. M., Song, C. L., Fu, Y. Q., Wang, C. C., Zhao, Y., Purnawali, H., . . . Zhang, J. L. (2013). Shaping tissue with shape memory materials. *Advanced Drug Delivery Reviews*, 65(4), 515-535. doi:10.1016/j.addr.2012.06.004
- Huang, W. M., Yang, B., An, L., Li, C., & Chan, Y. S. (2005). Water-driven programmable polyurethane shape memory polymer: demonstration and mechanism. *Applied Physics Letters*, 86(11), 114105-114105.
- Huang, W. M., Zhao, Y., Wang, C. C., Ding, Z., Purnawali, H., Tang, C., & Zhang, J. L. (2012). Thermo/chemo-responsive shape memory effect in polymers: a sketch of working mechanisms, fundamentals and optimization. *Journal of Polymer Research*, 19(9), 1-34. doi:10.1007/s10965-012-9952-z
- Huettl, B., & Willey, C. (2000). *Design and Development of Miniature Mechanisms for Small Spacecraft*. Paper presented at the 14th AIAA/USU Small Satellite Conference, North Logan, UT, USA.
- Huitao, Y., Peisun, M., & Chongzhen, C. (2005, 29 July-1 Aug. 2005). *A novel in-pipe worming robot based on SMA*. Paper presented at the Mechatronics and Automation, 2005 IEEE International Conference.
- Humbeeck, J. V. (1999). Non-medical applications of shape memory alloys. *Materials Science and Engineering: A*(273-275), 134-148.
- Hunter, I. W., Hollerbach, J. M., & Ballantyne, J. (1991). A comparative analysis of actuator technologies for robotics. *Robotics Review*, 2.
- Iadicola, M. A., & Shaw, J. A. (2002). An experimental setup for measuring unstable thermo-mechanical behavior of shape memory alloy wire. *Journal of Intelligent Material Systems and Structures*, 13(2-3), 157-166.
- Icardi, U., & Ferrero, L. (2009). Preliminary study of an adaptive wing with shape memory alloy torsion actuators. *Materials & Design*, 30(10), 4200-4210. doi:10.1016/j.matdes.2009.04.045
- Idelsohn, S., Peña, J., Lacroix, D., Planell, J. A., Gil, F. J., & Arcas, A. (2004). Continuous mandibular distraction osteogenesis using superelastic shape memory alloy (SMA). *Journal of Materials Science: Materials in Medicine*, 15(4), 541-546. doi:10.1023/B:JMSM.0000021135.72288.8f

- Ikuta, K., Tsukamoto, M., & Hirose, S. (1988, 24-29 Apr 1988). *Shape memory alloy servo actuator system with electric resistance feedback and application for active endoscope*. Paper presented at the 1988 IEEE International Conference on Robotics and Automation.
- Imai, M. (1986). *Kaizen: The Key To Japan's Competitive Success*: McGraw-Hill Education.
- Incropera, F., & DeWitt, D. (1985). Introduction to heat transfer.
- Ingram, R. B. (1998). US Patents 5836066.
- Isalgue, A., Torra, V., Yawny, A., & Lovey, F. C. (2008). Metastable effects on martensitic transformation in SMA part 6 - The Clausius - Clapeyron relationship. *Journal of thermal analysis and calorimetry*, 91(3), 991-998.
- Iserles, A. (1996). *A First Course in the Numerical Analysis of Differential Equations*: Cambridge University Press.
- Jackson, C. M., Wagner, H. M., & Wasilewski, R. J. (1972). 55-Nitinol-The Alloy with a Memory: It's Physical Metallurgy Properties, and Applications. NASA SP-5110. *NASA Special Publication*, 5110.
- Jacot, A. D., Julien, G. J., & Clingman, D. J. (2000). US Patent 6065934.
- Jacot, A. D., Ruggeri, R. T., & Clingman, D. J. (2006). US Patents 7037076B2.
- Jahn, J., & Maennig, W.-W. (1997). Safe evaluation of fatigue data in the range of finite endurance. *International Journal of Fatigue*, 19(4), 335-344. doi:10.1016/S0142-1123(96)00075-8
- Jakobsen, H. A. (2014). Numerical Solution Methods *Chemical Reactor Modeling* (pp. 1089-1273): Springer International Publishing.
- Jaluria, Y., & Atluri, S. (1994). Computational heat transfer. *Computational Mechanics*, 14(5), 385-386. doi:10.1007/BF00377593
- Janke, L., Czaderski, C., Motavalli, M., & Ruth, J. (2005). Applications of shape memory alloys in civil engineering structures—Overview, limits and new ideas. *Materials and Structures*, 38(5), 578-592. doi:10.1007/BF02479550
- Jayender, J., Patel, R. V., Nikumb, S., & Ostojic, M. (2005, 15-15 Dec. 2005). *H_∞ Loop Shaping Controller for Shape Memory Alloy Actuators*. Paper presented at the Decision and Control, 2005 and 2005 European Control Conference. CDC-ECC '05. 44th IEEE Conference on.
- Jee, K. K., Han, J. H., Kim, Y. B., Lee, D. H., & Jang, W. Y. (2008). New method for improving properties of SMA coil springs. *European Physical Journal: Special Topics*, 158(1), 261-266. doi:10.1140/epjst/e2008-00685-y
- Jenko, E. J. (2009). US Patent 7632450B2.
- Johnson, A. D. (1992). US Patents 5119555.
- Johnson, A. D. (1998). *State-of-the-art of Shape Memory Actuators*. Paper presented at the 6th international conference on new actuators, Bremen, Germany.
- Johnson, A. D. (2009). US Patents 7540899B1.
- Johnson, A. D., Bokaie, M., & Martynov, V. (2006). US Patents 2008/0075557A1.
- Johnson, A. D., Bokaie, M., & Martynov, V. (2008). US Patents 7422403B1.
- Johnson, A. D., Bokaie, M., & Martynov, V. (2009). US Patents 7544257B2.
- Johnson, A. D., Martynov, V., Bokaie, M. D., & Gray, G. R. (2010). US Patents 7842143B2.

- Johnson, N. L., Browne, A. L., Strom, K. A., Brei, D., Barnes, B. M., & Luntz, J. E. (2011). US Patents 7963360B2.
- Johnson, R. W., Evans, J. L., Jacobsen, P., Thompson, J. R., & Christopher, M. (2004). The changing automotive environment: high-temperature electronics. *Electronics Packaging Manufacturing, IEEE Transactions on*, 27(3), 164-176. doi:10.1109/TEPM.2004.843109
- Jones, S. D., Campbell, J. P., & Janmey, R. M. (2010). US Patents 7833649B2.
- Jong, W.-R., Chen, S.-C., Tsai, H.-C., Chiu, C.-C., & Chang, H.-T. (2006). The geometrical effects of bumps on the fatigue life of flip-chip packages by Taguchi method. *Journal of reinforced plastics and composites*, 25(1), 99-114.
- Jun, H. Y., Rediniotis, O. K., & Lagoudas, D. C. (2007). Development of a fuel-powered shape memory alloy actuator system: II. Fabrication and testing. *Smart Materials and Structures*, 16(1), S95.
- Kahny, H., Huffz, M. A., & Heuer, A. H. (1998). The TiNi shape-memory alloy and its applications for MEMS. *Micromechanics and Microengineering*, 8(3), 213-221. doi:10.1088/0960-1317/8/3/007
- Kardas, D., Rust, W., Polley, G. A., & Fabian, T. (2007). Turning up the volume. *ADVANTAGE*, 4.
- Karhu, M., & Lindroos, T. (2010). Long-term behaviour of binary Ti–49.7 Ni (at.%) SMA actuators - the fatigue lives and evolution of strains on thermal cycling. *Smart Materials and Structures*, 19(11), 115019.
- Kate, M., Bettencourt, G., Marquis, J., Gerratt, A., Fallon, P., Kierstead, B., . . . Trimmer, B. (2008). *SoftBot: A soft-material flexible robot based on caterpillar biomechanics*. Tufts University, Medford, MA.
- Kato, I., & Smalley, A. (2012). *Toyota Kaizen Methods: Six Steps to Improvement*: CRC Press.
- Kauffman, G., & Mayo, I. (1997). The Story of Nitinol: The Serendipitous Discovery of the Memory Metal and Its Applications. *The Chemical Educator*, 2(2), 1-21. doi:10.1007/s00897970111a
- Kaufman, J. A., Geller, S. C., Brewster, D. C., Fan, C.-M., Cambria, R. P., LaMuraglia, G. M., . . . Waltman, A. C. (2000). Endovascular Repair of Abdominal Aortic Aneurysms. *American Journal of Roentgenology*, 175(2), 289-302. doi:10.2214/ajr.175.2.1750289
- Kennedy, D. K., Straub, F. K., Schetky, L. M., Chaudhry, Z. A., & Roznoy, R. (2000). Development of an SMA actuator for in-flight rotor blade tracking. 62-75. doi:10.1117/12.388858
- Kennedy, J. R., & Larson Jr, D. J. (1993). US Patents 5265456.
- Kennedy, K. R., Nathan, J. F., Hanlon, S. R., & Maue, H. W. (2010). US Patent 7775596B2.
- Kha, N. B., & Kyoung Kwan, A. (2006, 24-26 May 2006). *Position Control of Shape Memory Alloy Actuators by Using Self Tuning Fuzzy PID Controller*. Paper presented at the Industrial Electronics and Applications, 2006 1ST IEEE Conference on.
- Khan, M. I., Pequegnat, A., & Zhou, Y. N. (2013). Multiple Memory Shape Memory Alloys. *Advanced Engineering Materials*, 15(5), 386-393. doi:10.1002/adem.201200246
- Kheirikhah, M., Rabiee, S., & Edalat, M. (2011). A Review of Shape Memory Alloy Actuators in Robotics. In J. Ruiz-del-Solar, E. Chown, & P. Plöger (Eds.), *RoboCup*

2010: *Robot Soccer World Cup XIV* (Vol. 6556, pp. 206-217): Springer Berlin Heidelberg.

Khoury, R. K. (2002). US Patent 6478656.

Kilgore, J. T., & Robinson, B. S. (2000). US Patents 6039030A.

Kim, H. Y., Satoru, H., Kim, J. I., Hosoda, H., & Miyazaki, S. (2004). Mechanical properties and shape memory behavior of Ti-Nb alloys. *Materials transactions*, 45(7), 2443-2448.

Kim, S., Hawkes, E., Choy, K., Joldaz, M., Foley, J., & Wood, R. (2009, 10-15 Oct 2009). *Micro artificial muscle fiber using niti spring for soft robotics*. Paper presented at the IEEE/RSJ International Conference on Intelligent Robots and Systems, 2009 (IROS 2009), St. Louis, MO, USA.

Kirkby, E. L., Rule, J. D., Michaud, V. J., Sottos, N. R., White, S. R., & Manson, J.-A. E. (2008). Embedded Shape-Memory Alloy Wires for Improved Performance of Self-Healing Polymers. *Advanced Functional Materials*, 18(15), 2253-2260. doi:10.1002/adfm.200701208

Kitamura, K., Tobushi, H., Yoshimi, Y., Date, K., & Miyamoto, K. (2010). Fatigue Properties of Cast TiNi Shape-Memory Alloy Brain Spatula. *Journal of Solid Mechanics and Materials Engineering*, 4(6), 796-805.

Knebel, A. M., & Salemi, M. R. (2004). US Patents 6691977B2.

Knowles, G., & Bird, R. W. (2004). US Patent 6834835B1.

Ko, J., Jun, M. B., Gilardi, G., Haslam, E., & Park, E. J. (2011). Fuzzy PWM-PID control of cocontracting antagonistic shape memory alloy muscle pairs in an artificial finger. *Mechatronics*, 21(7), 1190-1202. doi:10.1016/j.mechatronics.2011.07.003

Kochure, P., & Nandurkar, K. (2012). Taguchi method and ANOVA: An approach for selection of process parameters of induction hardening of EN8 D steel.

Kohl, M. (2010). *Shape memory microactuators (microtechnology and MEMS)* (1 ed.). Heidelberg: Springer-Verlag Berlin.

Komatsu, K., Mori, T., & Takinami, M. (1994). US Patents 5335498.

Kourambas, J., Delvecchio, F. C., Munver, R., & Preminger, G. M. (2000). Nitinol stone retrieval-assisted ureteroscopic management of lower pole renal calculi. *Urology*, 56(6), 935-939.

Kruelevitch, P., Lee, A. P., Ramsey, P. B., Trevino, J. C., Hamilton, J., & Northrup, M. A. (1996). Thin film shape memory alloy microactuators. *Microelectromechanical Systems, Journal of*, 5(4), 270-282. doi:10.1109/84.546407

Krumme, J. F., & Dickinson, F. C. (2001). US Patents 6277033B1.

Kudva, J. N. (2004). Overview of the DARPA smart wing project. *Journal of Intelligent Material Systems and Structures*, 15(4), 261-267.

Kujala, S., Pajala, A., Kallioinen, M., Pramila, A., Tuukkanen, J., & Ryhänen, J. (2004). Biocompatibility and strength properties of nitinol shape memory alloy suture in rabbit tendon. *Biomaterials*, 25(2), 353-358. doi:10.1016/S0142-9612(03)00488-5

Kujala, S., Ryhänen, J., Jämsä, T., Danilov, A., Saaranen, J., Pramila, A., & Tuukkanen, J. (2002). Bone modeling controlled by a nickel–titanium shape memory alloy intramedullary nail. *Biomaterials*, 23(12), 2535-2543. doi:10.1016/S0142-9612(01)00388-X

- Kulkarni, M., & Nelson, K. (2006). Introduction of a new crossover radius for the guaranteed heat transfer reduction in radial thermal insulation systems. *Heat transfer engineering*, 27(7), 23-28.
- Kulkarni, M. R. (2004). Critical radius for radial heat conduction: a necessary criterion but not always sufficient. *Applied Thermal Engineering*, 24(7), 967-979. doi:10.1016/j.applthermaleng.2003.08.017
- Kumar, P. K., & Lagoudas, D. C. (2008). Introduction to Shape Memory Alloys *Shape Memory Alloys* (Vol. 1, pp. 1-51): Springer US.
- Kurdjumov, G. V., & Khandros, L. G. (1949). First reports of the thermoelastic behaviour of the martensitic phase of Au-Cd alloys. *Doklady Akademii Nauk SSSR*, 66, 211-213.
- Kuribayashi, K. (1986). A New Actuator of a Joint Mechanism Using TiNi Alloy Wire. *The International Journal of Robotics Research*, 4, 47-58. doi:10.1177/027836498600400404
- Kuribayashi, K. (1989, 20-22 Feb 1989). *Millimeter size joint actuator using shape memory alloy*. Paper presented at the Micro Electro Mechanical Systems, 1989, Proceedings, An Investigation of Micro Structures, Sensors, Actuators, Machines and Robots. IEEE.
- Kuribayashi, K. (1991). Improvement of the Response of an SMA Actuator Using a Temperature Sensor. *The International Journal of Robotics Research*, 10(1), 13-20. doi:10.1177/027836499101000102
- Kutlucinar, I. (2005a). US Patent 6938416B1.
- Kutlucinar, I. (2005b). US Patent 6915633B2.
- Kyu-Jin, C., Hawkes, E., Quinn, C., & Wood, R. J. (2008, 19-23 May 2008). *Design, fabrication and analysis of a body-caudal fin propulsion system for a microrobotic fish*. Paper presented at the Robotics and Automation, 2008. ICRA 2008. IEEE International Conference on.
- Laborde, J., Borenstein, N., Behr, L., Farah, B., & Fajadet, J. (2006). Percutaneous implantation of the corevalve aortic valve prosthesis for patients presenting high risk for surgical valve replacement. *EuroIntervention: journal of EuroPCR in collaboration with the Working Group on Interventional Cardiology of the European Society of Cardiology*, 1(4), 472.
- Lagoudas, D. C. (2010). *Shape memory alloys: Modeling and engineering applications* (1 ed.). New York: Springer.
- Lagoudas, D. C., & Bo, Z. (1999). Thermomechanical modeling of polycrystalline SMAs under cyclic loading, Part II: material characterization and experimental results for a stable transformation cycle. *International Journal of Engineering Science*, 37(9), 1141-1173. doi:10.1016/S0020-7225(98)00114-1
- Lagoudas, D. C., Machado, L. G., & Lagoudas, M. (2005, 2005). *Nonlinear vibration of a one-degree of freedom shape memory alloy oscillator: A numerical-experimental investigation*. Paper presented at the 46th AIAA / ASME / ASCE / AHS / ASC Structures, Structural Dynamics and Materials Conference, Austin, TX, USA.
- Lagoudas, D. C., Miller, D. A., Rong, L., & Kumar, P. K. (2009). Thermomechanical fatigue of shape memory alloys. *Smart Materials and Structures*, 18(8), 085021.
- Landis, G. A., & Jenkins, P. P. (1997, 29 Sep-3 Oct 1997). *Dust on Mars: Materials Adherence Experiment results from Mars Pathfinder*. Paper presented at the Photovoltaic Specialists Conference, 1997., Conference Record of the Twenty-Sixth IEEE.

- Lane, P. (2008). EP Patent 1,288,048.
- Langbein, S. (2009, 7-11 Sept 2009). *Development of standardised and integrated shape memory components in "one-module"-design*. Paper presented at the 8th European Symposium on Martensitic Transformations (ESOMAT 2009), Prague, Czech Republic.
- Langbein, S., & Czechowicz, A. (2012). Adaptive resetting of SMA actuators. *Journal of Intelligent Material Systems and Structures*, 23(2), 127-134.
- Langenhove, L. V., & Hertleer, C. (2004). Smart clothing: a new life. *International Journal of Clothing Science and Technology*, 16(1), 63-72. doi:10.1108/09556220410520360
- Lara-Quintanilla, A., & Bersee, H. E. N. (2015). Active Cooling and Strain-Ratios to Increase the Actuation Frequency of SMA Wires. *Shape Memory and Superelasticity*, 1-8. doi:10.1007/s40830-015-0038-8
- Larssen, J. V., & Calkins, F. T. (2010). US Patents 2010/0219288A1.
- Laster, Z., MacBean, A. D., Ayliffe, P. R., & Newlands, L. C. (2001). Fixation of a frontozygomatic fracture with a shape-memory staple. *British Journal of Oral and Maxillofacial Surgery*, 39(4), 324-325. doi:10.1054/bjom.2001.0633
- Laurentis, K. J. D., Fisch, A., Nikitczuk, J., & Mavroidis, C. (2002, May 2002). *Optimal design of shape memory alloy wire bundle actuators*. Paper presented at the International conference on Robotics & Automation, Washington DC, USA.
- Lawall, J. P., McQueen, D. K., Johnson, N. L., Browne, A. L., & Alexander, P. W. (2011). US Patent 7931337B2.
- Lawall, J. P., McQueen, D. K., Morris, S. E., Browne, A. L., Johnson, N. L., Thomas, S. D., & Strom, K. A. (2010). US Patents 7784819.
- Leary, M., Huang, S., Ataalla, T., Baxter, A., & Subic, A. (2013). Design of shape memory alloy actuators for direct power by an automotive battery. *Materials & Design*, 43(0), 460-466. doi:10.1016/j.matdes.2012.07.002
- Leary, M., Mac, J., Mazur, M., Schiavone, F., & Subic, A. (2010). Enhanced shape memory alloy actuators *Sustainable Automotive Technologies 2010* (pp. 183-190). Berlin Heidelberg: Springer-Verlag.
- Leary, M., Schiavone, F., & Subic, A. (2010). Lagging for control of shape memory alloy actuator response time. *Materials & Design*, 31(4), 2124-2128. doi:10.1016/j.matdes.2009.10.010
- Leary, M., Schiavone, F., Subic, A., & Miller, J. (2009). US Patents 2012/0048839A1.
- Lederlé, S. (2002). *Issues in the design of shape memory alloy actuators*. (MSc Master of Science), Massachusetts Institute of Technology, USA. Retrieved from <http://18.7.29.232/handle/1721.1/16830>
- Lee, C. J., & Mavroidis, C. (2002). *Analytical dynamic model and experimental robust and optimal control of shape-memory-alloy bundle actuators*. Paper presented at the ASME 2002 International Mechanical Engineering Congress and Exposition.
- Lee, S.-K., & Kim, B. (2008). Design parametric study based fabrication and evaluation of in-pipe moving mechanism using shape memory alloy actuators. *Journal of Mechanical Science and Technology*, 22(1), 96-102. doi:10.1007/s12206-007-1011-z
- Lelatko, J., & Morawiec, H. (2001). High temperature Cu-Al-Nb - based shape memory alloys. *J. Phys. IV France*, 11(PR8), Pr8-487-Pr8-492.

- Lendlein, A., Jiang, H., Jünger, O., & Langer, R. (2005). Light-induced shape-memory polymers. *Nature*, 434(7035), 879-882.
- Lendlein, A., & Kelch, S. (2002). Shape-Memory Polymers. *Angewandte Chemie International Edition*, 41(12), 2034-2057. doi:10.1002/1521-3773(20020617)41:12<2034::AID-ANIE2034>3.0.CO;2-M
- Leng, J., Lv, H., Liu, Y., & Du, S. (2008). Comment on "Water-driven programmable polyurethane shape memory polymer: Demonstration and mechanism"[Appl. Phys. Lett. 86, 114105 (2005)]. *Applied Physics Letters*, 92(20), 206105-206105.
- Leo, D. J., Weddle, C., Naganathan, G., & Buckley, S. J. (1998). Vehicular applications of smart material systems. 106-116. doi:10.1117/12.310625
- Levi, D. S., Kusnezov, N., & Carman, G. P. (2008). Smart materials applications for pediatric cardiovascular devices. *Pediatric research*, 63(5), 552-558.
- Lewis, G. (2008). Materials, fluid dynamics, and solid mechanics aspects of coronary artery stents: A state-of-the-art review. *Journal of Biomedical Materials Research Part B: Applied Biomaterials*, 86B(2), 569-590. doi:10.1002/jbm.b.31028
- Liang, C., & Rogers, C. (1997). One-dimensional thermomechanical constitutive relations for shape memory materials. *Journal of Intelligent Material Systems and Structures*, 8(4), 285-302.
- Liang, C., & Rogers, C. A. (1992). Design of Shape Memory Alloy Actuators. *Journal of Mechanical Design*, 114(2), 223-230. doi:10.1115/1.2916935
- Lim, G., Park, K., Sugihara, M., Minami, K., & Esashi, M. (1996). Future of active catheters. *Sensors and Actuators A: Physical*, 56(1-2), 113-121. doi:10.1016/0924-4247(96)01279-4
- Limache, A. C., & Idelsohn, S. R. (2007). On the development of finite volume methods for computational solid mechanics. *Mecánica Computacional*, 26(11), 827-843.
- Liu, C., Qin, H., & Mather, P. T. (2007). Review of progress in shape-memory polymers. *Journal of Materials Chemistry*, 17(16), 1543-1558.
- Liu, C. Y., & Liao, W. H. (2004, 22-26 Aug. 2004). *A Snake Robot Using Shape Memory Alloys*. Paper presented at the IEEE International Conference on Robotics and Biomimetics, 2004 (ROBIO 2004).
- Liu, Y. (2010). Some factors affecting the transformation hysteresis in Shape Memory Alloys. In H. R. Chen (Ed.), *Shape Memory Alloys: Manufacture, Properties and Applications* (pp. 361-369): Nova Science Publishers.
- Liu, Y., Lv, H., Lan, X., Leng, J., & Du, S. (2009). Review of electro-active shape-memory polymer composite. *Composites Science and Technology*, 69(13), 2064-2068. doi:10.1016/j.compscitech.2008.08.016
- Liwei, S., Shuxiang, G., & Asaka, K. (2010, 13-15 July 2010). *A novel jellyfish-like biomimetic microrobot*. Paper presented at the IEEE/ICME International Conference on Complex Medical Engineering (CME), 2010.
- Long, C. F. L., & Vezain, G. A. P. (1998). US Patents 5829253.
- Lortz, B. K., & Tang, A. (1998). US Patents 5722709.
- Lu, J., Liang, Z., & Qu, W. (2009, 12-14 Aug 2009). *Optimal Design of Rotating Actuators Made by Magnetically Controlled Shape Memory Alloy*.
- Luchetti, T., Zanella, A., Biasiotto, M., & Saccagno, A. (2009). Electrically Actuated Antiglare Rear-View Mirror Based on a Shape Memory Alloy Actuator. *Journal of Materials Engineering and Performance*, 18(5-6), 717-724. doi:10.1007/s11665-009-9487-6

- Luo, X., & Mather, P. T. (2013). Shape Memory Assisted Self-Healing Coating. *ACS Macro Letters*, 2(2), 152-156. doi:10.1021/mz400017x
- Luo, Y., Takagi, T., Maruyama, S., & Yamada, M. (2000). A shape memory alloy actuator using Peltier modules and R-phase transition. *Journal of Intelligent Material Systems and Structures*, 11(7), 503-511.
- Lv, H., Leng, J., Liu, Y., & Du, S. (2008). Shape-Memory Polymer in Response to Solution. *Advanced Engineering Materials*, 10(6), 592-595. doi:10.1002/adem.200800002
- Ma, J., & Karaman, I. (2010). Expanding the Repertoire of Shape Memory Alloys. *Science*, 327(5972), 1468-1469. doi:10.1126/science.1186766
- Ma, J., Karaman, I., & Noebe, R. D. (2010). High temperature shape memory alloys. *International Materials Reviews*, 55(5), 257-315.
- Ma, N., & Song, G. (2003). Control of shape memory alloy actuator using pulse width modulation. *Smart Materials and Structures*, 12(5), 712-719. doi:10.1088/0964-1726/12/5/007
- Ma, N., Song, G., & Lee, H. J. (2004). Position control of shape memory alloy actuators with internal electrical resistance feedback using neural networks. *Smart Materials and Structures*, 13(4), 777.
- Mabe, J. H., Calkins, F. T., Bushnell, G. S., & Bieniawski, S. R. (2011). US Patent 7878459B2.
- Macgregor, R., Szilagyi, A., & Von Behrens, P. (2004). WO Patent 2004097218.
- MacGregor, R., Szilagyi, A., & Von Behrens, P. E. (2008). US Patent 7350762B2.
- Machado, L. G., & Savi, M. A. (2003). Medical applications of shape memory alloys. *Brazilian Journal of Medical and Biological Research*, 36, 683-691.
- Maehara, K., & Chikaraishi, T. (1999). US Patents 5913736A.
- Maeno, T., & Hino, T. (2006, 14 - 16 Aug 2006). *Miniature five-fingered robot hand driven by shape memory alloy actuators*. Paper presented at the 12th International Conference on Robotics and Applications (IASTED) 2006, Honolulu, Hawaii, USA.
- Maghsoodloo, S., Ozdemir, G., Jordan, V., & Chen-Hsiu Huang. (2004). Strengths and Limitations of Taguchi's Contributions to Quality, Manufacturing, and Process Engineering.
- Mahtabi, M. J., Shamsaei, N., & Mitchell, M. R. (2015). Fatigue of Nitinol: The state-of-the-art and ongoing challenges. *Journal of the Mechanical Behavior of Biomedical Materials*, 50, 228-254. doi:10.1016/j.jmbbm.2015.06.010
- Majumdar, P. (2005). *Computational methods for heat and mass transfer* (1 ed.). New York, USA: Taylor & Francis.
- Maletta, C., Sgambitterra, E., Furguele, F., Casati, R., & Tuissi, A. (2012). Fatigue of pseudoelastic NiTi within the stress-induced transformation regime: a modified Coffin–Manson approach. *Smart Materials and Structures*, 21(11), 112001.
- Mammano, G. S., & Dragoni, E. (2011). Functional fatigue of shape memory wires under constant-stress and constant-strain loading conditions. *Procedia Engineering*, 10(0), 3692-3707. doi:10.1016/j.proeng.2011.04.607
- Mani, R., Lagoudas, D. C., & Rediniotis, O. K. (2003). MEMS-based active skin for turbulent drag reduction. *Smart Structures and Materials 2003*, 5056, 9-20.
- Manna, M. (1992). *A three dimensional high resolution compressible flow solver*. (PhD), Catholic Univ. of Louvain-Von Karman, Belgium.

- Mantovani, D. (2000). Shape memory alloys: Properties and biomedical applications. *JOM*, 52(10), 36-44. doi:10.1007/s11837-000-0082-4
- Manzo, J., Garcia, E., Wickenheiser, A., & Horner, G. C. (2005). Design of a shape-memory alloy actuated macro-scale morphing aircraft mechanism. 232-240. doi:10.1117/12.601372
- Mascaro, S. A., & Asada, H. H. (2003, 14-19 Sept. 2003). *Wet shape memory alloy actuators for active vasculated robotic flesh*. Paper presented at the Robotics and Automation, 2003. Proceedings. ICRA '03. IEEE International Conference on.
- Materials, A. S. f. T. (1983). *Annual Book of ASTM Standards*: American Society for Testing and Materials.
- Maynard, R. S. (1999). US Patents 5941249.
- Mc Knight, G. P., Massey, C., Herrera, G. A., Barvosa-Carter, W., Johnson, N. L., & Browne, A. L. (2008). US Patents 7429074B2.
- McDonald, P. (1971). *The computation of transonic flow through two-dimensional gas turbine cascades*. Paper presented at the ASME 1971 International Gas Turbine Conference and Products Show.
- McDonald Schetky, L. (1991). Shape memory alloy applications in space systems. *Materials & Design*, 12(1), 29-32. doi:10.1016/0261-3069(91)90089-M
- McWilliams, A. (2011). *Smart Materials and Their Applications: Technologies and Global Markets* (AVM023D). Retrieved from <http://www.bccresearch.com/market-research/advanced-materials/smart-materials-technologies-markets-avm023d.html>
- Meier, H., & Czechowicz, A. (2012). Computer-Aided Development and Simulation Tools for Shape-Memory Actuators. *Metallurgical and Materials Transactions A*, 43(8), 2882-2890. doi:10.1007/s11661-011-1020-5
- Meier, H., Czechowicz, A., Haberland, C., & Langbein, S. (2011). Smart control systems for smart materials. *Journal of Materials Engineering and Performance*, 20(4-5), 559-563. doi:10.1007/s11665-011-9877-4
- Mellor, B. (1989). Engineering properties of shape memory alloys. *Science and technology of Shape Memory Alloys Palma de Mallorca: Univ. Illes Balears*, 335-395.
- Melton, K. N. (1999). General applications of shape memory alloys and smart materials. In K. Otsuka & C. M. Wayman (Eds.), *Shape memory materials* (pp. 220-239): Cambridge University Press.
- Melton, K. N., & Mercier, O. (1979). Fatigue of NITi thermoelastic martensites. *Acta Metallurgica*, 27(1), 137-144. doi:10.1016/0001-6160(79)90065-8
- Melz, T., Seipel, B., Sielhorst, B., & Zimmerman, E. (2011). US Patent 7905517B2.
- Menciassi, A., Accoto, D., Gorini, S., & Dario, P. (2006). Development of a biomimetic miniature robotic crawler. *Autonomous Robots*, 21(2), 155-163. doi:10.1007/s10514-006-7846-9
- Menciassi, A., Gorini, S., Pernorio, G., & Dario, P. (2004, April 26-May 1, 2004). *A SMA actuated artificial earthworm*. Paper presented at the IEEE International Conference on Robotics and Automation, 2004 (ICRA'04).
- Meng, Q., Liu, Y., Yang, H., Shariat, B. S., & Nam, T.-h. (2012). Functionally graded NiTi strips prepared by laser surface anneal. *Acta Materialia*, 60(4), 1658-1668. doi:10.1016/j.actamat.2011.11.052
- Menon, C., & Sitti, M. (2005, 18-22 April 2005). *Biologically Inspired Adhesion based Surface Climbing Robots*. Paper presented at the IEEE International Conference on Robotics and Automation, 2005 (ICRA 2005).

- Merkin, J. (1977). Mixed convection from a horizontal circular cylinder. *International Journal of Heat and Mass Transfer*, 20(1), 73-77. doi:10.1016/0017-9310(77)90086-2
- Mertmann, M., & Vergani, G. (2008). Design and application of shape memory actuators. *European Physical Journal: Special Topics*, 158(1), 221-230. doi:10.1140/epjst/e2008-00679-9
- Mi, Z.-n., Gong, Z.-b., Qian, J.-w., Mi, Z.-w., & Shen, L.-y. (2001). Study on moving principle of colonoscopic robot. *Journal of Shanghai University (English Edition)*, 5(2), 143-146. doi:10.1007/s11741-001-0011-y
- Michael, A. D. (1995). The Effect of Stress Ageing on the Properties of Shape Memory Alloys. *J. Phys. IV France*, 05(C2), C2-349-C342-354. doi:10.1051/jp4:1995253
- Mieloszyk, M., Krawczuk, M., Zak, A., & Ostachowicz, W. (2010). An adaptive wing for a small-aircraft application with a configuration of fibre Bragg grating sensors. *Smart Materials and Structures*, 19(8), 085009.
- MigaMotors. Data sheets: Miga Motor Company.
- Mihálcz, I. (2001). Fundamental characteristics and design method for nickel-titanium shape memory alloy. *PERIODICA POLYTECHNICA SER. MECH. ENG.*, 45(1), 75-86.
- Mirzaeifar, R., DesRoches, R., Yavari, A., & Gall, K. (2012). Coupled thermo-mechanical analysis of shape memory alloy circular bars in pure torsion. *International Journal of Non-Linear Mechanics*, 47(3), 118-128. doi:10.1016/j.ijnonlinmec.2012.01.007
- Mishra, S. C., Kim, M. Y., Das, R., Ajith, M., & Uppaluri, R. (2009). Lattice Boltzmann Method Applied to the Analysis of Transient Conduction-Radiation Problems in a Cylindrical Medium. *Numerical Heat Transfer, Part A: Applications*, 56(1), 42-59. doi:10.1080/10407780903107162
- Mitteer, D. M. (2010). US Patent 7814810B2.
- Miyazaki, S., Imai, T., Igo, Y., & Otsuka, K. (1986). Effect of cyclic deformation on the pseudoelasticity characteristics of Ti-Ni alloys. *Metallurgical Transactions A*, 17(1), 115-120. doi:10.1007/BF02644447
- Miyazaki, S., & Ishida, A. (1999). Martensitic transformation and shape memory behavior in sputter-deposited TiNi-base thin films. *Materials Science and Engineering: A*, 273-275(0), 106-133. doi:10.1016/S0921-5093(99)00292-0
- Miyazaki, S., Kim, H. Y., & Hosoda, H. (2006). Development and characterization of Ni-free Ti-base shape memory and superelastic alloys. *Materials Science and Engineering: A*, 438-440(0), 18-24. doi:10.1016/j.msea.2006.02.054
- Miyazaki, S., Mizukoshi, K., Ueki, T., Sakuma, T., & Liu, Y. (1999). Fatigue life of Ti-50 at.% Ni and Ti-40Ni-10Cu (at.%) shape memory alloy wires. *Materials Science and Engineering: A*, 273-275(0), 658-663. doi:10.1016/S0921-5093(99)00344-5
- Miyazaki, S., Onoda, M., Okada, N., Fujii, Y., & Kim, H. Y. (2008). WO Patent 2,008,016,009.
- Mohamed Ali, M. S., & Takahata, K. (2010). Frequency-controlled wireless shape-memory-alloy microactuators integrated using an electroplating bonding process. *Sensors and Actuators A: Physical*, 163(1), 363-372. doi:10.1016/j.sna.2010.08.007
- Mohammad, T., Jeng-Jong, R., & Chuh, M. (2002). Thermal post-buckling and aeroelastic behaviour of shape memory alloy reinforced plates. *Smart Materials and Structures*, 11(2), 297.

- Mohd Jani, J., Huang, S., Leary, M., & Subic, A. (2015a). Analysis of convective heat transfer coefficient on shape memory alloy actuator under various ambient temperatures with finite difference method. *Applied Mechanics and Materials*, 736, 127-133. doi:10.4028/www.scientific.net/AMM.736.127
- Mohd Jani, J., Huang, S., Leary, M., & Subic, A. (2015b). Numerical modeling of shape memory alloy linear actuators. *Computational Mechanics*, 56(3), 443-461. doi:10.1007/s00466-015-1180-z
- Mohd Jani, J., Leary, M., & Subic, A. (2014). Shape memory alloys in automotive applications. *Applied Mechanics and Materials*, 663, 248-253. doi:10.4028/www.scientific.net/AMM.663.248
- Mohd Jani, J., Leary, M., & Subic, A. (2016). *Fatigue of Ni-Ti SMA-pulley system using Taguchi and ANOVA*. Smart Materials and Structures.
- Mohd Jani, J., Leary, M., Subic, A., & Gibson, M. A. (2014). A review of shape memory alloy research, applications and opportunities. *Materials & Design*, 56, 1078-1113. doi:10.1016/j.matdes.2013.11.084
- Mohr, R., Kratz, K., Weigel, T., Lucka-Gabor, M., Moneke, M., & Lendlein, A. (2006). Initiation of shape-memory effect by inductive heating of magnetic nanoparticles in thermoplastic polymers. *Proceedings of the National Academy of Sciences of the United States of America*, 103(10), 3540-3545.
- Mons, C. M. (2008). US Patents 2009/0056307A1.
- Morehead, J. H., & Harrington, H. E. (2007). US Patent 7296457B2.
- Morgan, N. B. (2004). Medical shape memory alloy applications - the market and its products. *Materials Science and Engineering: A*, 378(1-2), 16-23.
- Morgan, R. K., & Yaeger, J. R. (1985). US Patents 4524343.
- Mori, K., Okamoto, S., & Akimoto, M. (1995). Placement of the Urethral Stent Made of Shape Memory Alloy in Management of Benign Prostatic Hypertrophy for Debilitated Patients. *The Journal of Urology*, 154(3), 1065-1068. doi:10.1016/S0022-5347(01)66977-5
- Mori, T. (2011). *Taguchi Methods: Benefits, impacts, mathematics, statistics and applications* (S.-C. Tsai, Trans.). New York, USA: ASME Press.
- Mosley, M. J., & Mavroidis, C. (2000). *Design and dynamics of shape memory alloy wire bundle actuator*. Paper presented at the Design Engineering Technical Conference 2000, Baltimore, Maryland, USA.
- Mukherjee, R., & Christian, T. F. (1998). US Patents 5763979.
- Murphy, E. B., & Wudl, F. (2010). The world of smart healable materials. *Progress in Polymer Science*, 35(1-2), 223-251. doi:10.1016/j.progpolymsci.2009.10.006
- Nabijou, S., & Hobbs, R. E. (1994). Fatigue of wire ropes bent over small sheaves. *International Journal of Fatigue*, 16(7), 453-460. doi:10.1016/0142-1123(94)90195-3
- Nair, V. N., Abraham, B., MacKay, J., Box, G., Kacker, R. N., Lorenzen, T. J., . . . Jeff Wu, C. F. (1992). Taguchi's Parameter Design: A Panel Discussion. *Technometrics*, 34(2), 127-161. doi:10.1080/00401706.1992.10484904
- Nam, C., Chattopadhyay, A., & Kim, Y. (2002, March 17, 2002). *Application of shape memory alloy (SMA) spars for aircraft maneuver enhancement*. Paper presented at the Smart Structures and Materials: Smart Structures and Integrated Systems, San Diego, CA.

- Nam, T. H., Saburi, T., & Shimizu, K. (1990). Cu-content dependence of shape memory characteristics in Ti-Ni-Cu alloys. *Materials transactions*, 31(11), 959-967.
- Neugebauer, R., Bucht, A., Pagel, K., & Jung, J. (2010a). Numerical simulation of the activation behavior of thermal shape memory alloys. 76450J-76450J. doi:10.1117/12.847594
- Neugebauer, R., Bucht, A., Pagel, K., & Jung, J. (2010b). *Numerical simulation of the activation behavior of thermal shape memory alloys*.
- Ngo, E., Northwang, W. D., Cole, M. W., Hubbard, C., Hirsch, G., Mohanchandra, K. P., & Carman, G. P. (2004). *Fabrication of active thin films for vibration damping in MEMS devices for the next generation army munition systems*. Retrieved from
- Nishida, M., Tanaka, K., & Wang, H. O. (2006, 15-19 May 2006). *Development and control of a micro biped walking robot using shape memory alloys*. Paper presented at the IEEE International Conference on Robotics and Automation, 2006 (ICRA 2006).
- Niskanen, A. J., & Laitinen, I. (2013). Design and Simulation of a Magnetic Shape Memory (MSM) Alloy Energy Harvester. *Advances in Science and Technology*, 78, 58-62.
- Niskanen, J. D., Daniels, A. R., & Mrkovic, D. (2008). US Patents 7364211B2.
- Noebe, R., Gaydosh, D., Padula li, S., Garg, A., Biles, T., & Nathal, M. (2005). *Properties and potential of two (Ni,Pt)Ti alloys for use as high-temperature actuator materials*.
- Noebe, R. D., Draper, S. L., Nathal, M. V., & Garg, A. (2009). US Patents 7501032B1.
- Noebe, R. D., Quackenbush, T. R., & II, S. A. P. (2005). *Benchtop Demonstration of an Adaptive Chevron Completed Using a New High-Temperature Shape-Memory Alloy*. Retrieved from <http://www.grc.nasa.gov/WWW/RT/2005/RX/RX30A-noebe2.html>
- Novák, V., Šittner, P., Dayananda, G. N., Braz-Fernandes, F. M., & Mahesh, K. K. (2008). Electric resistance variation of NiTi shape memory alloy wires in thermomechanical tests: Experiments and simulation. *Materials Science and Engineering: A*, 481–482, 127-133. doi:10.1016/j.msea.2007.02.162
- Nudelman, I. L., Fuko, V., Greif, F., & Lelcuk, S. (2002). Colonic anastomosis with the nickel-titanium temperature-dependent memory-shape device. *The American Journal of Surgery*, 183(6), 697-701. doi:10.1016/S0002-9610(02)00857-7
- Ochonski, W. (2010). Application of shape memory materials in fluid sealing technology. *Industrial Lubrication and Tribology*, 62(2), 99-110.
- Odhner, L. U., & Asada, H. H. (2006). Sensorless temperature estimation and control of shape memory alloy actuators using thermoelectric devices. *Mechatronics, IEEE/ASME Transactions on*, 11(2), 139-144. doi:10.1109/TMECH.2006.871088
- Oehler, S. D., Hartl, D. J., Lopez, R., Malak, R. J., & Lagoudas, D. C. (2012). Design optimization and uncertainty analysis of SMA morphing structures. *Smart Materials and Structures*, 21(9), 094016.
- Oh, S.-R., Chang, S.-W., Lee, Y., Gu, Y., Son, W.-J., Lee, W., . . . Lim, S.-M. (2010). A comparison of nickel-titanium rotary instruments manufactured using different methods and cross-sectional areas: ability to resist cyclic fatigue. *Oral Surgery, Oral Medicine, Oral Pathology, Oral Radiology, and Endodontology*, 109(4), 622-628.
- Oku, M. (1993). US Patent 5242002.
- Olsen, T. W., Loftness, P. E., & Erdman, A. G. (2012). EP Patent 1,986,581B1.
- Otsuka, K., & Ren, X. (1999). Recent developments in the research of shape memory alloys. *Intermetallics*, 7(5), 511-528.

- Otsuka, K., & Wayman, C. (1999). *Shape memory materials*. Cambridge: Cambridge University Press.
- Ozisik, M. N. (1987). *Basic Heat Transfer*. R.E. Krieger Publishing Company.
- Ozisik, N. (1994). *Finite difference methods in heat transfer* (1 ed.). Boca Raton: CRC.
- O'toole, K. T., & McGrath, M. M. (2007, 2007). *Mechanical design and theoretical analysis of a four fingered prosthetic hand incorporating embedded SMA bundle actuators*. Paper presented at the World Academy of Science, Engineering and Technology.
- Pappas, P., Bollas, D., Parthenios, J., Dracopoulos, V., & Galiotis, C. (2007). Transformation fatigue and stress relaxation of shape memory alloy wires. *Smart Materials and Structures*, 16(6), 2560.
- Patankar, S. (1980). *Numerical heat transfer and fluid flow*. USA: Hemisphere Publishing Corporation.
- Pattabi, M., & Murari, M. S. (2015). Effect of Cold Rolling on Phase Transformation Temperatures of NiTi Shape Memory Alloy. *Journal of Materials Engineering and Performance*, 24(2), 556-564. doi:10.1007/s11665-014-1344-6
- Peffer, A., Denoyer, K., Fosness, E., & Sciulli, D. (2000, 2000). *Development and transition of low-shock spacecraft release devices*. Paper presented at the IEEE Aerospace Conference Proceedings, 2000.
- Pelton, A. R. (2011). Nitinol Fatigue: A Review of Microstructures and Mechanisms. *Journal of Materials Engineering and Performance*, 20(4-5), 613-617. doi:10.1007/s11665-011-9864-9
- Pelton, A. R., Fino-Decker, J., Vien, L., Bonsignore, C., Saffari, P., Launey, M., & Mitchell, M. R. (2013). Rotary-bending fatigue characteristics of medical-grade Nitinol wire. *Journal of the Mechanical Behavior of Biomedical Materials*, 27, 19-32. doi:10.1016/j.jmbbm.2013.06.003
- Pelton, A. R., Schroeder, V., Mitchell, M. R., Gong, X.-Y., Barney, M., & Robertson, S. W. (2008). Fatigue and durability of Nitinol stents. *Journal of the Mechanical Behavior of Biomedical Materials*, 1(2), 153-164. doi:10.1016/j.jmbbm.2007.08.001
- Perkins, J., & Hodgson, D. (1990). The two-way shape memory effect. *Butterworth-Heinemann, Engineering Aspects of Shape Memory Alloys(UK)*, 1990, 195-206.
- Perkins, J., Hodgson, D., Duerig, T. W., Melton, K. N., Stockel, D., & Wayman, C. M. (1990). Engineering Aspects of Shape Memory Alloys. *British Library*, 195.
- Perry, P. D., & Veinotte, A. (2006). US Patents 7089919B2.
- Petrini, L., & Migliavacca, F. (2011). Biomedical Applications of Shape Memory Alloys. *Journal of Metallurgy*, 2011. doi:10.1155/2011/501483
- Pfeifer, R., Müller, C. W., Hurschler, C., Kaierle, S., Wesling, V., & Haferkamp, H. (2013). Adaptable Orthopedic Shape Memory Implants. *Procedia CIRP*, 5(0), 253-258. doi:10.1016/j.procir.2013.01.050
- Pieczyska, E., Tobushi, H., Date, K., & Miyamoto, K. (2010). Torsional Deformation and Fatigue Properties of TiNi SMA Thin Strip For Rotary Driving Element. *Journal of Solid Mechanics and Materials Engineering*, 4(8), 1306-1314.
- Pitt, D., Dunne, J., White, E., & Garcia, E. (2001, 16-20 Apr 2001). *SAMPSON smart inlet SMA powered adaptive lip design and static test*. Paper presented at the 42nd AIAA Structures, Structural Dynamics, and Materials Conference, Seattle, WA, USA.
- Pittaccio, S., Viscuso, S., Rossini, M., Magoni, L., Pirovano, S., Villa, E., . . . Molteni, F. (2009). SHADE: A shape-memory-activated device promoting ankle dorsiflexion.

Journal of Materials Engineering and Performance, 18(5), 824-830.
doi:10.1007/s11665-009-9405-y

- Pitts, D., & Sissom, L. E. (2002). *Schaum's outline of theory and problems of heat transfer* (2 ed.): Beijing: Science Press.
- Poczek, M., Maspes, F., Masala, S., Squillaci, E., Assegnati, G., Moraldi, A., & Simonetti, G. (1996). Palliative treatment of neoplastic strictures by self-expanding nitinol Strecker stent. *European Radiology*, 6(2), 230-235. doi:10.1007/BF00181157
- Poletti, P. A., Becker, C. D., Prina, L., Ruijs, P., Bounameaux, H., Didier, D., . . . Terrier, F. (1998). Long-term results of the Simon nitinol inferior vena cava filter. *European Radiology*, 8(2), 289-294. doi:10.1007/s003300050382
- Porter, G. A., Liaw, P. K., Tiegs, T. N., & Wu, K. H. (2001). Fatigue and fracture behavior of nickel–titanium shape-memory alloy reinforced aluminum composites. *Materials Science and Engineering: A*, 314(1–2), 186-193. doi:10.1016/S0921-5093(00)01915-8
- Porter, W. W. (1996). US Patents 5581441.
- Potapov, P. L., & Da Silva, E. P. (2000). Time Response of Shape Memory Alloy Actuators. *Journal of Intelligent Material Systems and Structures*, 11(2), 125-134. doi:10.1106/xh1h-fh3q-1yex-4h3f
- Prahlad, H., & Chopra, I. (2001, 2001). *Design of a variable twist tilt-rotor blade using shape memory alloy (SMA) actuators*. Paper presented at the 8th Annual International Symposium on Smart Structures and Materials.
- Prashant Reddy, G., & Gupta, N. (2010). Material selection for microelectronic heat sinks: An application of the Ashby approach. *Materials & Design*, 31(1), 113-117. doi:10.1016/j.matdes.2009.07.013
- Predki, W., & Bauer, B. (2010). Concept of a start-up clutch with nickel-titanium shape memory alloys. *Forschung im Ingenieurwesen*, 74(1), 41-47.
- Price, A. D., Jnifene, A., & Naguib, H. E. (2007). Design and control of a shape memory alloy based dexterous robot hand. *Smart Materials and Structures*, 16(4), 1401.
- Pugh, S. (1991). *Total design: Integrated methods for successful product engineering*. Essex, England: Addison-Wesley Publisher Ltd.
- Qian, H., Li, H., Song, G., Chen, H., Ren, W., & Zhang, S. (2010). *Seismic vibration control of civil structures using shape memory alloys: A review*. Paper presented at the ASCE Earth and Space 2010: Engineering, Science, Construction, and Operations in Challenging Environments.
- Qiu, J., Tani, J., Osanai, D., & Urushiyama, Y. (2001). *High-speed actuation of shape memory alloy*. Paper presented at the Smart Materials and MEMS.
- Raghavan, J., Bartkiewicz, T., Boyko, S., Kupriyanov, M., Rajapakse, N., & Yu, B. (2010). Damping, tensile, and impact properties of superelastic shape memory alloy (SMA) fiber-reinforced polymer composites. *Composites Part B: Engineering*, 41(3), 214-222. doi:10.1016/j.compositesb.2009.10.009
- Rajan, G. P., Eikelboom, R. H., Anandacoomaraswamy, K. S., & Atlas, M. D. (2005). In vivo performance of the Nitinol shape-memory stapes prosthesis during hearing restoration surgery in otosclerosis: A first report. *Journal of Biomedical Materials Research Part B: Applied Biomaterials*, 72B(2), 305-309. doi:10.1002/jbm.b.30165
- Raju, G. S., & Gajula, L. (2004). Endoclips for GI endoscopy. *Gastrointestinal Endoscopy*, 59(2), 267-279.

- Rao, A., & Srinivasa, A. R. (2013). *Experiments on functional fatigue of thermally activated shape memory alloy springs and correlations with driving force intensity*.
- Ratna, D., & Karger-Kocsis, J. (2008). Recent advances in shape memory polymers and composites: a review. *Journal of Materials Science*, 43(1), 254-269. doi:10.1007/s10853-007-2176-7
- Ren, J., & Liew, K. M. (2005). Meshfree modelling and characterisation of thermomechanical behaviour of NiTi alloys. *Engineering analysis with boundary elements*, 29(1), 29-40.
- Renz, R., & Kramer, J. (1997). US Patents 5687958.
- Rey, N. M., Miller, R. M., Tillman, T. G., Rukus, R. M., & Kettle, J. L. (2006). US Patents 7004047B2.
- Reynaerts, D. (1995). *Control methods and actuation technology for whole-hand dexterous manipulation*. (PhD), Katholieke Universiteit Leuven, Katholieke Universiteit Leuven, Belgium. (D/1995/5769/2)
- Reynaerts, D., & Brussel, H. V. (1998). Design aspect of shape memory actuators. *Mechatronics*, 8(6), 635-656. doi:10.1016/S0957-4158(98)00023-3
- Reynaerts, D., Peirs, J., & Van Brussel, H. (1996, 26 - 28 June 1996). *Design of a shape memory actuated gastro-intestinal intervention system*. Paper presented at the 5th International Conference on New Actuators, Bremen, Germany.
- Richman, R. H., Rao, A. S., & Kung, D. (1995). Cavitation erosion of NiTi explosively welded to steel. *Wear*, 181–183, Part 1(0), 80-85. doi:10.1016/0043-1648(95)90011-x
- Richtmyer, R. D., & Morton, K. W. (1994). *Difference methods for initial-value problems* (2 ed. Vol. 1). Malabar, Fla.: Krieger Publishing Co.
- Rober, K. B., Browne, A. L., Johnson, N. L., & Aase, J. H. (2010). US Patents 7686382B2.
- Robert, G. L. (1997). Recent developments in smart structures with aeronautical applications. *Smart Materials and Structures*, 6(5), R11.
- Robertson, S. W., Launey, M., Shelley, O., Ong, I., Vien, L., Senthilnathan, K., . . . Pelton, A. R. (2015). A statistical approach to understand the role of inclusions on the fatigue resistance of superelastic Nitinol wire and tubing. *Journal of the Mechanical Behavior of Biomedical Materials*, 51, 119-131. doi:10.1016/j.jmbbm.2015.07.003
- Robertson, S. W., Pelton, A. R., & Ritchie, R. O. (2012). Mechanical fatigue and fracture of Nitinol. *International Materials Reviews*, 57(1), 1-37. doi:10.1179/1743280411Y.0000000009
- Roh, J.-H., Han, J.-H., & Lee, I. (2005). *Finite element analysis of adaptive inflatable structures with SMA strip actuator*. Paper presented at the Smart Structures and Materials 2005: Smart Structures and Integrated Systems.
- Romanelli, M. J., & Otterstedt, P. J. (1990). US Patents 4899543.
- Romano, R., & Tannuri, E. A. (2009). Modeling, control and experimental validation of a novel actuator based on shape memory alloys. *Mechatronics*, 19(7), 1169-1177.
- Ross, R. J. (1993a). US Patents 5273116.
- Ross, R. J. (1993b). US Patents 5199497.
- Ross, R. J. (1993c). US Patents 5215145.
- Rossi, P., Bezzi, M., Rossi, M., Adam, A., Chetty, N., Roddie, M. E., . . . Boguth, L. (1994). *Metallic Stents in Malignant Biliary Obstruction: Results of a Multicenter European*

Study of 240 Patients. *Journal of Vascular and Interventional Radiology*, 5(2), 279-285. doi:10.1016/S1051-0443(94)71483-4

Rudduck, D., Blattmann, L., & Brown, S. (2007). WO Patent 2,007,068,034.

Rudduck, D., Goldspink, L. R., Ng, N. A., Blattmann, L. D., Park, J. R., Kelliher, C. G., & Farren-Price, E. D. (2009). US Patent 7610783B2.

Russell, R. A., & Gorbet, R. B. (1995, 21-27 May 1995). *Improving the response of SMA actuators*. Paper presented at the IEEE International Conference on Robotics and Automation, 1995.

Ryhänen, J., Kallioinen, M., Tuukkanen, J., Junila, J., Niemelä, E., Sandvik, P., & Serlo, W. (1998). In vivo biocompatibility evaluation of nickel-titanium shape memory metal alloy: Muscle and perineural tissue responses and capsule membrane thickness. *Biomedical Materials Research*, 41(3), 481–488. doi:10.1002/(SICI)1097-4636(19980905)41:3<481::AID-JBM19>3.0.CO;2-L

Saadat, S., Salichs, J., Noori, M., Hou, Z., Davoodi, H., Bar-on, I., . . . Masuda, A. (2002). An overview of vibration and seismic applications of NiTi shape memory alloy. *Smart Materials and Structures*, 11(2), 218.

Sahatjian, R. A. (1990). US Patents 4909510.

Sahin, A., & Kalyon, M. (2004). The critical radius of insulation in thermal radiation environment. *Heat and mass transfer*, 40(5), 377-382. doi:10.1007/s00231-003-0471-7

Sampson, R. (1987). US Patent 4706330.

Sanders, A. E., Sanders, J. O., & More, R. B. (1994). US Patent 5290289.

Sanders, J. O., Sanders, A. E., More, R., & Ashman, R. B. (1993). A preliminary investigation of shape memory alloys in the surgical correction of scoliosis. *Spine*, 18(12), 1640-1646.

Sarbu, I., & Popina, O. (2001). Numerical analysis with finite and boundary elements of thermal fields in steady state regime. *ARPJ Journal of Engineering and Applied Sciences*, 6(2), 13-23.

Sattapan, B., Palamara, J. E. A., & Messer, H. H. (2000). Torque During Canal Instrumentation Using Rotary Nickel-Titanium Files. *Journal of Endodontics*, 26(3), 156-160. doi:10.1097/00004770-200003000-00007

Schaffer, J. E., & Plumley, D. L. (2009). Fatigue Performance of Nitinol Round Wire with Varying Cold Work Reductions. *Journal of Materials Engineering and Performance*, 18(5-6), 563-568. doi:10.1007/s11665-009-9363-4

Schiedeck, F., & Mojrzisch, S. (2011). Design of a robust control strategy for the heating power of shape memory alloy actuators at full contraction based on electric resistance feedback. *Smart Materials and Structures*, 20(4), 045002.

Schmerling, M. A., Wilkov, M. A., Sanders, A. E., & Woosley, J. E. (1976). Using the shape recovery of nitinol in the Harrington rod treatment of scoliosis. *Journal of Biomedical Materials Research*, 10(6), 879-892. doi:10.1002/jbm.820100607

Schroeder, T. A., & Wayman, C. M. (1977). The two-way shape memory effect and other "training" phenomena in Cu-Zn single crystals. *Scripta metallurgica*, 11(3), 225-230. doi:10.1016/0036-9748(77)90058-8

Schron, J. H., & Summers, J. L. (1998). 834380. EP Patent 834,380.

Scirè Mammano, G., & Dragoni, E. (2014). Functional fatigue of Ni–Ti shape memory wires under various loading conditions. *International Journal of Fatigue*, 69(0), 71-83. doi:10.1016/j.ijfatigue.2012.03.004

- Selden, B., Cho, K., & Asada, H. H. (2006). Segmented shape memory alloy actuators using hysteresis loop control. *Smart Materials and Structures*, 15(2), 642.
- Sepulveda, A., Muñoz, R., Lovey, F. C., Auguet, C., Isalgue, A., & Torra, V. (2007). Metastable effects on martensitic transformation in SMA Part 2 - The grain growth effects in Cu-Al-Be alloy. *Journal of thermal analysis and calorimetry*, 89(1), 101-107.
- Seri, L. (1995, 7-9 Feb 1995). *Optimum design and selection of heat sinks*. Paper presented at the Semiconductor Thermal Measurement and Management Symposium, 1995. SEMI-THERM XI., Eleventh Annual IEEE.
- Shah, T. K., Corboy, G. W., & William Russell Kraft, II. (2008). US Patents 7464634B1.
- Shahin, A. R., Meckl, P. H., Jones, J. D., & Thrasher, M. A. (1994). Enhanced cooling of shape memory alloy wires using semiconductor 'heat pump' modules. *Journal of Intelligent Material Systems and Structures*, 5(1), 95-104.
- Shaw, G., Prince, T., Snyder, J., Willett, M., & Lisy, F. (2009). US Patent 7587944B1.
- Sherwin, Y., & Ulmer, D. G. (2004). US Patent 6796408B2.
- Shiotsu, A., Yamanaka, M., Matsuyama, Y., Nakanishi, H., Hara, Y., Tsuboi, T., . . . Hirai, S. (2005, 29 Nov - 1 Dec 2005). *Crawling and jumping soft robot KOHARO*. Paper presented at the 36th International Symposium on Robotics (ISR 2005), Tokyo, Japan.
- Shiraishi, Y., Yambe, T., Saijo, Y., Sato, F., Tanaka, A., Yoshizawa, M., . . . Homma, D. (2007, 22-26 Aug. 2007). *Morphological Approach for the Functional Improvement of an Artificial Myocardial Assist Device using Shape Memory Alloy Fibres*. Paper presented at the 29th Annual International Conference of the IEEE Engineering in Medicine and Biology Society, 2007 (EMBS 2007).
- Shmilovich, A., Yadlin, Y., Smith, D. M., & Clark, R. W. (2010). US Patent 7669785B2.
- Si, H.-M., Cho, C., & Kwahk, S.-Y. (2003). A hybrid method for casting process simulation by combining FDM and FEM with an efficient data conversion algorithm. *Journal of Materials Processing Technology*, 133(3), 311-321. doi:10.1016/S0924-0136(02)01008-7
- Silverbrook, K. (2003). US Patents 6557977.
- Simon, M., Kaplow, R., Salzman, E., & Freiman, D. (1977). A vena cava filter using thermal shape memory alloy experimental aspects. *Radiology*, 125(1), 89-94.
- Singh, J. K., & Alpas, A. T. (1995). Dry sliding wear mechanisms in a Ti50Ni47Fe3 intermetallic alloy. *Wear*, 181-183, 302-311.
- Singh, K., & Chopra, I. (2002, 2002). *Design of an improved shape memory alloy actuator for rotor blade tracking*. Paper presented at the Smart Structures and Materials.
- Smith, C., Villanueva, A., Joshi, K., Tadesse, Y., & Priya, S. (2011). Working principle of bio-inspired shape memory alloy composite actuators. *Smart Materials and Structures*, 20(1), 012001.
- Smith, G. D. (1985). *Numerical solution of partial differential equations: finite difference methods*: Oxford University Press.
- Smith, J. E., Pertl, F. A., Angle, II, Gerald, M., Yarborough, C. N., Nawrocki, A. J., . . . Williams, K. A. (2012). US Patent 2012/0003090A1.
- Smith, J. M., & Stein, H. (2008). Endoscopic placement of multiple artificial chordae with robotic assistance and nitinol clip fixation. *The Journal of thoracic and cardiovascular surgery*, 135(3), 610-614. doi:10.1016/j.jtcvs.2007.10.041

- Sofla, A. Y. N., Elzey, D. M., & Wadley, H. N. G. (2008). Cyclic degradation of antagonistic shape memory actuated structures. *Smart Materials and Structures*, 17(2), 025014. doi:10.1088/0964-1726/17/2/025014
- Sofla, A. Y. N., Meguid, S. A., Tan, K. T., & Yeo, W. K. (2010). Shape morphing of aircraft wing: Status and challenges. *Materials & Design*, 31(3), 1284-1292. doi:10.1016/j.matdes.2009.09.011
- Song, C. (2010). History and current situation of shape memory alloys devices for minimally invasive surgery. *Open Medical Devices Journal*, 2(1), 24-31.
- Song, C., Frank, T., & Cuschieri, A. (2005). Shape memory alloy clip for compression colonic anastomosis. *Journal of biomechanical engineering*, 127(2), 351.
- Song, G., & Ma, N. (2012). US Patents 8245516.
- Song, G., Ma, N., & Li, H. N. (2006). Applications of shape memory alloys in civil structures. *Engineering Structures*, 28(9), 1266-1274. doi:10.1016/j.engstruct.2005.12.010
- Song, G., Patil, D., Kocurek, C., & Bartos, J. (2010). Applications of shape memory alloys in offshore oil and gas industry: a review. *Proc. Earth and Space 2010—Engineering, Science, Construction, and Operations in Challenging Environments (Honolulu, HI, USA, 14–17 March 2010)*, 366.
- Spaggiari, A., Mammano, G. S., & Dragoni, E. (2012). Optimum Mechanical Design of Binary Actuators Based on Shape Memory Alloys. In G. Berselli, R. Vertechy, & G. Vassura (Eds.), *Smart Actuation and Sensing Systems - Recent Advances and Future Challenges* (pp. 716). Croatia: InTech.
- Sparrow, E. M., & Kang, S. S. (1985). Two-dimensional heat transfer and critical radius results for natural convection about an insulated horizontal cylinder. *International Journal of Heat and Mass Transfer*, 28(11), 2049-2060. doi:10.1016/0017-9310(85)90098-5
- Sparrow, E. M., & Lee, L. (1976). Analysis of mixed convection about a horizontal cylinder. *International Journal of Heat and Mass Transfer*, 19(2), 229-232. doi:10.1016/0017-9310(76)90118-6
- Sreekumar, M., Nagarajan, T., & Singaperumal, M. (2009). Application of trained NiTi SMA actuators in a spatial compliant mechanism: Experimental investigations. *Materials & Design*, 30(8), 3020-3029. doi:10.1016/j.matdes.2008.12.017
- Sreekumar, M., Nagarajan, T., Singaperumal, M., Zoppi, M., & Molfino, R. (2007). Critical review of current trends in shape memory alloy actuators for intelligent robots. *Industrial Robot: An International Journal*, 34(4), 285-294.
- Stalmans, R., Van Humbeeck, J., & Delaey, L. (1991). Training and the 2 way memory effect in copper based shape memory alloys. *Journal de physique iv*, 1(C4), 403-408.
- Stephen, J. F., George, B., & Stefan, S. (2013). Design and fabrication of a bat-inspired flapping-flight platform using shape memory alloy muscles and joints. *Smart Materials and Structures*, 22(1), 014011.
- Stirling, L., Yu, C.-H., Miller, J., Hawkes, E., Wood, R., Goldfield, E., & Nagpal, R. (2011). Applicability of shape memory alloy wire for an active, soft orthotic. *Journal of Materials Engineering and Performance*, 20(4-5), 658-662.
- Stoeckel, D. (1990). Shape memory actuators for automotive applications. *Materials & Design*, 11(6), 302-307.

- Stoeckel, D., & Tinschert, F. (1991). *Temperature Compensation with Thermovisible Rate Springs in Automatic Transmissions* (910805). Retrieved from <http://www.nitinol.com/media/reference-library/057.pdf>
- Stoeckel, D., & Waram, T. (1992, January 13, 1992). *Use of Ni-Ti shape memory alloys for thermal sensor-actuators*. Paper presented at the Active and Adaptive Optical Components, San Diego, CA, USA.
- Stoeckel, S., & Simpson, J. (1992). *Actuation and control with shape memory alloys*. Paper presented at the Proc. Conf. on Active Materials and Adaptive Structures.
- Strelec, J. K., Lagoudas, D. C., Khan, M. A., & Yen, J. (2003). Design and implementation of a shape memory alloy actuated reconfigurable airfoil. *Journal of Intelligent Material Systems and Structures*, 14(4-5), 257-273.
- Strittmatter, J., & Gümpel, P. (2011). Long-time stability of Ni-Ti-shape memory alloys for automotive safety systems. *Journal of Materials Engineering and Performance*, 20(4-5), 506-510. doi:10.1007/s11665-011-9848-9
- Strittmatter, J., Gümpel, P., & Zhigang, H. (2009). Long-time stability of shape memory actuators for pedestrian safety system. *J. Achiev. Mater. Manuf. Eng.*, 34(1), 23-30.
- Stöckel, D. (1995). *The Shape Memory Effect: Phenomenon, Alloys, Applications*. Paper presented at the Shape memory alloys for power systems (EPRI).
- Sugiyama, Y., & Hirai, S. (2006). Crawling and Jumping by a Deformable Robot. *The International Journal of Robotics Research*, 25(5-6), 603-620.
- Sun, L., & Huang, W. M. (2009). Nature of the multistage transformation in shape memory alloys upon heating. *Metal Science and Heat Treatment*, 51(11-12), 573-578. doi:10.1007/s11041-010-9213-x
- Sun, L., Huang, W. M., Ding, Z., Zhao, Y., Wang, C. C., Purnawali, H., & Tang, C. (2012). Stimulus-responsive shape memory materials: A review. *Materials & Design*, 33(0), 577-640. doi:10.1016/j.matdes.2011.04.065
- Sun, L., Huang, W. M., Wang, C. C., Ding, Z., Zhao, Y., Tang, C., & Gao, X. Y. (2013). Polymeric shape memory materials and actuators. *Liquid Crystals*, 1-13. doi:10.1080/02678292.2013.805832
- Sunkil, P., Kyo-in, K., Seoung Min, B., Jeong Youp, P., Si Young, S., & Dongil 'Dan', C. (2008). A novel microactuator for microbioscopy in capsular endoscopes. *Journal of Micromechanics and Microengineering*, 18(2), 025032.
- Suzuki, M. (1986). US Patents 4626085.
- Swain, M. V. (1986). Shape memory behaviour in partially stabilized zirconia ceramics.
- Swenson, S. R. (1992). US Patent 5127228.
- Tack, J., Gevers, A.-M., & Rutgeerts, P. (1998). Self-expandable metallic stents in the palliation of rectosigmoidal carcinoma: a follow-up study. *Gastrointestinal Endoscopy*, 48(3), 267-271. doi:10.1016/S0016-5107(98)70189-0
- Tadesse, Y. (2013). *Electroactive polymer and shape memory alloy actuators in biomimetics and humanoids*.
- Tadesse, Y., Thayer, N., & Priya, S. (2010). Tailoring the response time of shape memory alloy wires through active cooling and pre-stress. *Journal of Intelligent Material Systems and Structures*, 21(1), 19-40.
- Taguchi, G. (1987). *The System of Experimental Design: Engineering Methods to Optimize Quality and Minimize Cost* (L. W. Tung, Trans.). USA: UNIPUB/Kraus International Publications.

- Taguchi, G., & Clausing, D. (1990). Robust Quality. *Harvard Business Review*, 65-75.
- Takahashi, M. (2009). US Patent 2009/0302708A1.
- Takeda, K., Mitsui, K., Tobushi, H., Levintant-Zayonts, N., & Kucharski, S. (2013). Influence of nitrogen ion implantation on deformation and fatigue properties of TiNi shape-memory alloy wire. *Archives of Mechanics*, 65(5), 391-405.
- Tam, L. M., & Ghajar, A. J. (2006). Transitional Heat Transfer in Plain Horizontal Tubes. *Heat transfer engineering*, 27(5), 23-38. doi:10.1080/01457630600559538
- Tamura, H., Mitose, K., & Suzuki, Y. (1995). Fatigue properties of Ti-Ni shape memory alloy springs. *Journal de physique. IV*, 5(8), C8-617.
- Tanaka, K. (1986). A thermomechanical sketch of shape memory effect: one-dimensional tensile behavior. *Res Mechanica*, 18, 251-263.
- Tanaka, M., Hirano, K., Goto, H., Namima, T., Uchi, K., Jiang, Z. W., . . . Chonan, S. (1999). Artificial SMA valve for treatment of urinary incontinence: upgrading of valve and introduction of transcutaneous transformer. *Bio-Medical Materials and Engineering*, 9(2), 97-112.
- Tanaka, Y., Himuro, Y., Kainuma, R., Sutou, Y., Omori, T., & Ishida, K. (2010). Ferrous Polycrystalline Shape-Memory Alloy Showing Huge Superelasticity. *Science*, 327(5972), 1488-1490. doi:10.1126/science.1183169
- Tang, C., Huang, W. M., Wang, C. C., & Purnawali, H. (2012). The triple-shape memory effect in NiTi shape memory alloys. *Smart Materials and Structures*, 21(8), 085022.
- Tang, W., & Sandström, R. (1993). Analysis of the influence of cycling on TiNi shape memory alloy properties. *Materials & Design*, 14(2), 103-113.
- Tao, T., Liang, Y.-C., & Taya, M. (2006). Bio-inspired actuating system for swimming using shape memory alloy composites. *International Journal of Automation and Computing*, 3(4), 366-373. doi:10.1007/s11633-006-0366-4
- Taya, M., Cheng, V., Sugandi, H., Liang, Y., Chen, H., & Wang, C.-Y. (2010). US007688168B2. US Patent 7688168B2.
- Taya, M., Wada, T., Chen, H.-h., Kusaka, M., Cheng, V., & Wang, C. (2010). US007810326B2. US Patent 7810326B2.
- Teh, Y. H. (2008). *Fast, accurate force and position control of Shape Memory Alloy actuators*. (Doctor of Philosophy), The Australian National University, Canberra.
- Tellinen, J., Suorsa, I., Jääskeläinen, A., Aaltio, I., & Ullakko, K. (2002). *Basic properties of magnetic shape memory actuators*. Paper presented at the Proc. of 8th Int. Conf. on Actuator, Bremen, Germany.
- Terauchi, M., Zenba, K., Shimada, A., & Fujita, M. (2006, 18-21 Oct. 2006). *Controller Design on the Fingerspelling Robot Hand using Shape Memory Alloy*. Paper presented at the SICE-ICASE, 2006. International Joint Conference.
- Terzo, G. (2006). Taking the Pulse of the Stent Market. *Investment Dealers' Digest*, 72, 12.
- Testa, C., Leone, S., Ameduri, S., & Concilio, A. (2005). Feasibility study on rotorcraft blade morphing in hovering. 171-182. doi:10.1117/12.600975
- Thanopoulos, M. D. B. D., Laskari, M. D. C. V., Tsaousis, M. D. G. S., Zarayelyan, M. D. A., Vekiou, M. D. A., & Papadopoulos, M. D. G. S. (1998). Closure of Atrial Septal Defects With the Amplatzer Occlusion Device: Preliminary Results. *Journal of the American College of Cardiology*, 31(5), 1110-1116. doi:10.1016/S0735-1097(98)00039-4
- Thoma, P. E., Kao, M.-Y., & Schmitz, D. M. (1995). US Patents 5419788.

- Thrasher, M. A., Shahin, A. R., Meckl, P. H., & Jones, J. D. (1994). Efficiency analysis of shape memory alloy actuators. *Smart Materials and Structures*, 3(2), 226.
- Tobushi, H., Ikai, A., Yamada, S., Tanaka, K., & LExcellent, C. (1996). Thermomechanical properties of TiNi shape memory alloy. *Le Journal de Physique IV*, 6(C1), C1-385. doi:10.1051/jp4:1996137
- Tobushi, H., Kitamura, K., Yoshimi, Y., Miyamoto, K., & Mitsui, K. (2011, 2011). *Mechanical Properties of Cast Shape Memory Alloy for Brain Spatula*.
- Tobushi, H., Yamada, S., Hachisuka, T., & Hashimoto, T. (1998). Cyclic Deformation and Fatigue of a TiNi Shape-Memory Alloy Wire Subjected to Rotating Bending. *Journal of Engineering Materials and Technology*, 120(1), 64-70. doi:10.1115/1.2806839
- Torra, V., Auguet, C., Isalgue, A., Lovey, F. C., Sepulveda, A., & Soul, H. (2010). Metastable effects on martensitic transformation in SMA Part 8 - Temperature effects on cycling. *Journal of thermal analysis and calorimetry*, 102(2), 671-680.
- Torra, V., Pelegrina, J. L., Isalgue, A., & Lovey, F. C. (2005). Metastable effects on martensitic transformation in SMA Part 1 - Recoverable effects by the action of thermodynamic forces in parent phase. *Journal of thermal analysis and calorimetry*, 81(1), 131-135.
- Torrizi, L. (1999). The NiTi superelastic alloy application to the dentistry field. *Bio-Medical Materials and Engineering*, 9(1), 39-47.
- Trimmer, B. A., Takesian, A., Sweet, B., Rogers, C. B., Hake, D. C., & Rogers, D. J. (2006, 2-5 May 2006). *Caterpillar locomotion: a new model for soft-bodied climbing and burrowing robots*. Paper presented at the 7th International Symposium on Technology and Mine problem, Monterey, California, USA.
- Tsuchiya, K., Tsutsumi, A., Ohtsuka, H., & Umemoto, M. (2004). Modification of Ni-Mn-Ga ferromagnetic shape memory alloy by addition of rare earth elements. *Materials Science and Engineering: A*, 378(1-2), 370-376. doi:10.1016/j.msea.2003.11.076
- Tsui, K.-L. (1992). An overview of Taguchi method and newly developed statistical methods for robust design. *IIE Transactions*, 24(5), 44-57. doi:10.1080/07408179208964244
- Tuissi, C. M. a. E. S. a. F. F. a. R. C. a. A. (2012). Fatigue of pseudoelastic NiTi within the stress-induced transformation regime: a modified Coffin-Manson approach. *Smart Materials and Structures*, 21(11), 112001.
- Tuna, C., Solomon, J. H., Jones, D. L., & Hartmann, M. J. Z. (2012, 25-30 March 2012). *Object shape recognition with artificial whiskers using tomographic reconstruction*. Paper presented at the Acoustics, Speech and Signal Processing (ICASSP), 2012 IEEE International Conference on.
- Tung, A. T., Park, B.-H., Liang, D. H., & Niemeyer, G. (2008). Laser-machined shape memory alloy sensors for position feedback in active catheters. *Sensors and Actuators A: Physical*, 147(1), 83-92. doi:10.1016/j.sna.2008.03.024
- Turner, M., Clough, R., Martin, H., & Topp, L. (1956). Stiffness and Deflection Analysis of Complex Structures. *Journal of the Aeronautical Sciences*, 23(9), 805-823. doi:10.2514/8.3664
- Tyagi, S., Singh, S., Mukhopadhyay, S., & Kaul, U. A. (2003). Self-and balloon-expandable stent implantation for severe native coarctation of aorta in adults. *The American heart journal*, 146(5), 920-928.
- Uchino, K. (1989). Recent topics of ceramic actuators how to develop new ceramic devices. *Ferroelectrics*, 91(1), 281-292. doi:10.1080/00150198908015745

- Uflacker, R., & Robison, J. (2001). Endovascular treatment of abdominal aortic aneurysms: a review. *European Radiology*, 11(5), 739-753. doi:10.1007/s003300000747
- Ullakko, K., Huang, J. K., Kantner, C., O'Handley, R. C., & Kokorin, V. V. (1996). Large magnetic-field-induced strains in Ni₂MnGa single crystals. *Applied Physics Letters*, 69(13), 1966-1968. doi:10.1063/1.117637
- Ullakko, K., Huang, J. K., Kokorin, V. V., & O'Handley, R. C. (1997). Magnetically controlled shape memory effect in Ni₂MnGa intermetallics. *Scripta materialia*, 36(10), 1133-1138. doi:10.1016/S1359-6462(96)00483-6
- Ullakko, K., Sasaki, K., & Müllner, P. (2013). US2013/0091954A1. US Patent 2013/0091954A1.
- Vaidyanathan, R. (2000). Shape-Memory Alloys *Kirk-Othmer Encyclopedia of Chemical Technology*. John Wiley & Sons, Inc.
- VDH Zijnen, B. G. (1956). Modified correlation formulae for the heat transfers by natural and by forced convection from horizontal cylinders. *Applied Scientific Research, Section A*, 6(2-3), 129-140. doi:10.1007/BF03185032
- Van Humbeeck, J. (1997). Shape memory materials: state of the art and requirements for future applications. *Le Journal de Physique IV*, 7(C5), C5-3.
- Van Humbeeck, J., Chandrasekaran, M., & Delaey, L. (1991). Shape memory alloys: materials in action. *Endeavour*, 15(4), 148-154. doi:10.1016/0160-9327(91)90119-V
- Vasquez, J. A., & Garrod, T. C. (2008). US Patent 7424978B2.
- Veers, P. S. (1996). Statistical considerations in fatigue. In S. R. Lampman & N. DiMaterio (Eds.), *Fatigue and Fracture* (Vol. 19, pp. 295-302). Materials Park, OH 44073-0002, USA: ASM International.
- Velázquez, R., & Pissaloux, E. (2012). Modelling and Temperature Control of Shape Memory Alloys with Fast Electrical Heating. *International Journal of Mechanics and Control*, 13(02), 1-8.
- Velázquez, R., Pissaloux, E., Szewczyk, J., & Hafez, M. (2005, 2005). *Miniature shape memory alloy actuator for tactile binary information display*. Paper presented at the 2005 IEEE International Conference on Robotics and Automation (ICRA 2005).
- Vernon, L. B., & Vernon, H. M. (1941). US2234993.
- Vinograd, I., Klin, B., Brosh, T., Weinberg, M., Flomenblit, Y., & Nevo, Z. (1994). A new intratracheal stent made from nitinol, an alloy with "shape memory effect". *The Journal of thoracic and cardiovascular surgery*, 107(5), 1255-1261.
- Voit, W., Ware, T., Dasari, R. R., Smith, P., Danz, L., Simon, D., . . . Gall, K. (2010). High-Strain Shape-Memory Polymers. *Advanced Functional Materials*, 20(1), 162-171.
- Vollach, S., & Shilo, D. (2010). The Mechanical Response of Shape Memory Alloys Under a Rapid Heating Pulse. *Experimental Mechanics*, 50(6), 803-811. doi:10.1007/s11340-009-9320-z
- Voller, V. R., Cross, M., & Markatos, N. C. (1987). An enthalpy method for convection/diffusion phase change. *International Journal for Numerical Methods in Engineering*, 24(1), 271-284. doi:10.1002/nme.1620240119
- Von Behrens, P. E., & Fairbanks, D. M. (2006). US007017345B2. US Patent 7017345 B2.
- Wada, K., & Liu, Y. (2005). Shape recovery of NiTi shape memory alloy under various pre-strain and constraint conditions. *Smart Materials and Structures*, 14(5), S273.

- Wagner, M., Frenzel, J., & Eggeler, G. (2006). *Evolution of microstructural parameters during cycling of NiTi and their effect on mechanical and thermal memory*. Paper presented at the SMST-2004: Proceedings of the International Conference on Shape Memory and Superelastic Technologies.
- Wagner, M. F. X., Nayan, N., & Ramamurty, U. (2008). Healing of fatigue damage in NiTi shape memory alloys. *Journal of Physics D: Applied Physics*, 41(18), 185408.
- Walak, S. (2007). US Patents 2007/0200656 A1.
- Walker, J. (2008). *Fundamental of Physics* (8 ed.). USA: John Wiley & Sons Inc.
- Walsh, K. P., & Maadi, I. M. (2000). The Amplatz septal occluder. *Cardiology in the Young*, 10(05), 493-501M493 - 410.1017/S1047951100008180.
- Wang, B., Han, J., & Sun, Y. (2012). A finite element/finite difference scheme for the non-classical heat conduction and associated thermal stresses. *Finite Elements in Analysis and Design*, 50, 201-206.
- Wang, C. C., Huang, W. M., Ding, Z., Zhao, Y., & Purnawali, H. (2012). Cooling-/water-responsive shape memory hybrids. *Composites Science and Technology*, 72(10), 1178-1182. doi:10.1016/j.compscitech.2012.03.027
- Wang, C. C., Huang, W. M., Ding, Z., Zhao, Y., Purnawali, H., Zheng, L. X., . . . He, C. B. (2012). Rubber-like shape memory polymeric materials with repeatable thermal-assisted healing function. *Smart Materials and Structures*, 21(11), 115010.
- Wang, W. Y., Cooper, S. G., & Eberhardt, S. C. (1999). Use of a nitinol gooseneck snare to open an incompletely expanded over-the-wire stainless steel Greenfield filter. *AJR. American journal of roentgenology*, 172(2), 499-500.
- Wang, Z. G., Zu, X. T., Feng, X. D., Lin, L. B., Zhu, S., You, L. P., & Wang, L. M. (2003). Design of TiNi alloy two-way shape memory coil extension spring. *Materials Science and Engineering: A*, 345.
- Wang, Z. G., Zu, X. T., Feng, X. D., Zhu, S., Bao, J. W., & Wang, L. M. (2004). Characteristics of two-way shape memory TiNi springs driven by electrical current. *Materials & Design*, 25(8), 699-703.
- Waram, T. (1993). *Actuator Design Using Shape Memory Alloys* (2nd (metric) ed.): Hamilton, Ont. : T.C. Waram.
- Weber, A. (2010). Smart materials have a bright future. Retrieved from <http://www.assemblymag.com/articles/87695-smart-materials-have-a-bright-future>
- Webster, P. J., Ziebeck, K. R. A., Town, S. L., & Peak, M. S. (1984). Magnetic order and phase transformation in Ni₂MnGa. *Philosophical Magazine B*, 49(3), 295-310.
- Weems, W. (2000). US Patent 6129181A.
- Wellman, P. S., Peine, W. J., Favalora, G., & Howe, R. D. (1997). *Mechanical Design and Control of a High-Bandwidth Shape Memory Alloy Tactile Display*. Paper presented at the 1997 International Symposium on Experimental Robotics, Barcelona, Spain.
- Welp, E. G., & Breidert, J. (2004). Knowledge and Method Base for Shape Memory Alloys. *Materialwissenschaft und Werkstofftechnik*, 35(5), 294-299. doi:10.1002/mawe.200400745
- Wever, D., Elstrodt, J., Veldhuizen, A., & v Horn, J. (2002). Scoliosis correction with shape-memory metal: results of an experimental study. *European Spine Journal*, 11(2), 100-106. doi:10.1007/s005860100347
- White, P. M. (2001). US Patent 6257593B1.
- White, P. M. (2002). US Patents 6435519B1.

- White, P. M. (2008). US Patents 7407440B2.
- Widdle, R. D., Grimshaw, M. T., Crosson-Elturan, K. S., Mabe, J. H., Calkins, F. T., Gravatt, L. M., & Shome, M. (2009). US Patent 2011/0030380A1.
- Wilkes, K., Liaw, P., & Wilkes, K. (2000). The fatigue behavior of shape-memory alloys. *JOM*, 52(10), 45-51. doi:10.1007/s11837-000-0083-3
- Willey, C. E., Huettl, B., & Hill, S. W. (2001). *Design and development of a miniature mechanisms tool-kit for micro spacecraft*. Paper presented at the 35 th Aerospace Mechanisms Symposium.
- Williams, E., & Elahinia, M. H. (2008). An automotive SMA mirror actuator: Modeling, design, and experimental evaluation. *Journal of Intelligent Material Systems and Structures*, 19(12), 1425-1434. doi:10.1177/1045389x07087328
- Williams, E. A., Shaw, G., & Elahinia, M. (2010). Control of an automotive shape memory alloy mirror actuator. *Mechatronics*, 20(5), 527-534. doi:10.1016/j.mechatronics.2010.04.002
- Williams, K. A., Chiu, G. T., & Bernhard, R. J. (2000). Controlled continuous tuning of an adaptively tunable vibration absorber incorporating shape memory alloys. 564-575. doi:10.1117/12.388800
- Williams, P. L. (2001). US Patents 6242841 B1.
- Winzek, B., Schmitz, S., Rumpf, H., Sterzl, T., Ralf Hassdorf, Thienhaus, S., . . . Quandt, E. (2004). Recent developments in shape memory thin film technology. *Materials Science and Engineering: A*, 378(1-2), 40-46.
- Witold, S., Annick, M., Shunichi, H., L'Hocine, Y., & Jean, R. (2007). Medical applications of shape memory polymers. *Biomedical Materials*, 2(1), S23.
- Wood, J. H. (2007). EP Patent 1,817,489.
- Wood, J. H., & Dunne, J. P. (2008). US Patent 7340883B2.
- Wu, M. H., & Schetky, L. M. (2000). *Industrial applications for Shape Memory Alloys*. Paper presented at the International Conference on Shape Memory and Superelastic Technologies, Pacific Grove, California, USA.
- Wu, M. H., & Schetky, L. M. (2000). *Industrial applications for shape memory alloys*. Paper presented at the International Conference on Shape Memory and Superelastic Technologies, Pacific Grove, California, USA.
- Wu, T. (1999). US Patents 5862995.
- Xie, T. (2010). Tunable polymer multi-shape memory effect. *Nature*, 464(7286), 267-270.
- Yachia, D. (1993, 1993). [The use of urethral stents for the treatment of urethral strictures].
- Yamada, A., Shiraishi, Y., Sugai, T. K., Miura, H., Shiga, T., Hashem, M. O., . . . Homma, D. (2013). Preliminary Design of the Mechanical Circulation Assist Device for Fontan Circulation using Shape Memory Alloy Fibers. In M. Long (Ed.), *World Congress on Medical Physics and Biomedical Engineering May 26-31, 2012, Beijing, China* (Vol. 39, pp. 119-121): Springer Berlin Heidelberg.
- Yanagihara, K., Mizuno, H., Wada, H., & Hitomi, S. (1997). Tracheal Stenosis Treated With Self-Expanding Nitinol Stent. *The Annals of Thoracic Surgery*, 63(6), 1786-1789. doi:10.1016/S0003-4975(97)00369-X
- Yang, K. (2010). US Patent 7795823B2.
- Yang, R.-J., Le, J. J., Chou, C., & Tzou, H.-S. (2007). US Patent 7278679 B2.

- Young Pyo, L., Byungkyu, K., Moon Gu, L., & Jong-Oh, P. (2004, 26 April-1 May 2004). *Locomotive mechanism design and fabrication of biomimetic micro robot using shape memory alloy*. Paper presented at the IEEE International Conference on Robotics and Automation, 2004 (ICRA 2004).
- Yson, A. P., & Messinger, R. H. (2008). US Patent 7464548B2.
- Zhang, C., Zee, R. H., & Thoma, P. E. (1996, 1996). *Development of Ni-Ti based shape memory alloys for actuation and control*. Paper presented at the Energy Conversion Engineering Conference 1996 (IECEC 96).
- Zhang, L., Zhao, J. M., Liu, L. H., & Wang, S. Y. (2012). Hybrid finite volume/ finite element method for radiative heat transfer in graded index media. *Journal of Quantitative Spectroscopy and Radiative Transfer*, 113(14), 1826-1835. doi:10.1016/j.jqsrt.2012.04.020
- Zhenlong, W., Guanrong, H., Yangwei, W., Jian, L., & Wei, D. (2008). Embedded SMA wire actuated biomimetic fin: a module for biomimetic underwater propulsion. *Smart Materials and Structures*, 17(2), 025039.
- Zider, R. B., & Krumme, J. F. (1988). US Patents 4772112.
- Zienkiewicz, O., & Cheung, Y. (1965). Finite elements in the solution of field problems. *Engineer*, 507-510.
- Zimmer, G., & Zimmer, M. (2006). WO Patent 2006/063566A1.
- Zychowicz, R. (1992). US Patents 5166832.
- Çengel, Y. A., & Ghajar, A. J. (2011). *Heat and mass transfer: Fundamentals & applications*. New York, USA: McGraw-Hill.
- Ölander, A. (1932). An electrochemical investigation of solid cadmium-gold alloys. *American Chemical Society*, 54(10), 3819-3833. doi:10.1021/ja01349a004

10. Appendices

Appendix A. SMA actuators

ACTUATORS AND MOTORS			
Description	Remarks	Year	Inventor / Researcher
Self-regulating actuator that cut-off the power when reach its stroke. Also protect actuator and connected mechanism from damage due to jam or malfunction	Linear type. Self-regulated	1985	(R. K. Morgan & Yaeger, 1985)
An actuator with multiple SMA wires arranged around a resilient member (such as spring) to increase bandwidth	Linear type	1986	(Hosoda <i>et al.</i> , 1986)
A temperature traction device suited to closing doors automatically following a short delay after opening	Linear type	1987	(Sampson, 1987)
An actuator comprising of a SMA wire and control element rotate to different section by applying various selective voltage. Aimed primarily for robotics but is deemed more widely applicable	Rotary type	1987	(Gabriel, Trimmer, & Walker, 1987)
An actuator consisting of two concentric tubes of SMA, torsional along their longitudinal axis, with the ends constrained relative to one another to provide two stable positions and smooth motion between the two with more describes uniform heating, thus deliver maximum work output per unit volume with minimal power consumption for activation	Rotary type. Bi-directional	1992	(Swenson, 1992)
A micro-actuation system in which able to move freely with a stroke in the range of 1 to 500µm	Linear type. Folding	1994	(Komatsu, Mori, & Takinami, 1994)
An invention for increasing the life of a SMA actuator by maintaining a martensite strain on the SMA element at < 3%	Linear/Rotary type. Control strain	1995	(Thoma <i>et al.</i> , 1995)
An actuation system to control multiple SMA elements in a matrix configuration that reduces the electrical connections by 50%.	Control system	1998	(Mukherjee & Christian, 1998)
A linear actuator to translate an object from one position to another by the action of a SMA flat spring attached at one end to a heating device and to the object at the other end	Linear type	1999	(Foss Jr & Siebrecht, 1999)
An actuator consists of SMA strips (coiled into springs) and SMA springs that produce a constant force from applied heat. Can rotate either a clockwise or anti-clockwise depending on which spring is activated	Rotary type	2000	(Weems, 2000)
A rotary actuator which can provide either small or large amounts of torque and is able to operate in both directions using a single SMA member	Rotary type	2000	(Arthur Dean Jacot, Julien, & Clingman, 2000)
A rotary drive system that incorporates SMA elements for use in a motorised camera	Rotary type	2001	(P. L. Williams, 2001)
A method of designing a SMA actuator to enhance service life (more than 100k cycles), with limited tensile stress (100 MPa)	Enhance life cycle	2004	(Dai Homma, 2004)
An actuator with two stable working positions that will switch between these positions upon sequential activation of a SMA element, and maintained until the next activation cycle	Two states switch	2005	(Biasiotto, Butera, & Alacqua, 2005)
A rotary actuator composed of a SMA torque tube connected with a bias superelastic return spring	Rotary type	2006	(A. Dean Jacot <i>et al.</i> , 2006)
Several linear and rotational actuators with combination of SMA elements to create a long output stroke from as compact unit	Linear and Rotary types	2006, 2007	(MA Gummin <i>et al.</i> , 2007; Mark A. Gummin, Donakowski, & Gaines, 2006)
An actuator assembly with several protection mechanisms and variable return force to impart motion in an output shaft	Linear type	2006	(Von Behrens & Fairbanks, 2006)
A linear actuator with several SMA members in tubular shape and are set coaxially to provide a telescopic extension	Linear type	2008	(Yson & Messinger, 2008)
A turn-actuator with a tensile element made of three SMA elements, which are fixed to a rotational element in such a way it can rotates in both direction	Rotary type	2008	(Garscha, Auernhammer, & Engelhardt, 2008)
A SMA linear actuator with a SMA wire, two moving bodies and two bias springs positioned in a cylinder	Linear type	2009	(Takahashi, 2009)
A SMA linear actuator shielded/lagged with conductive material for faster actuation response	Enhance cooling	2009	(Martin Leary <i>et al.</i> , 2009)
A torque actuator incorporating SMA and MSMA composites	Rotary type	2010	(Taya, Wada, <i>et al.</i> , 2010)
A linear actuator design based on MSMA composites (A hybrid electromagnet and a permanent magnet to activate FSMA spring)	Linear type	2010	(Taya, Cheng, <i>et al.</i> , 2010)
An SMA wire actuator made in a series to increase applied load	Linear type	2010	(Butera, 2010)
A solar tracking mechanism driven by SMA motor	Linear type	2010	(Altaii & Thomas, 2010)
An actuator device with sliding elements and thermal conduction to base to improve response time	Linear type	2010	(K. Yang, 2010)
A device and method for controlling a phase transformation temperature of a shape memory alloy. Developed by Dynalloy and GM	Control system	2013	(Gao, Browne, Alexander, Johnson, & Brown, 2013)

Appendix B. Bonding and joining

FASTENERS, SEALS, CONNECTORS AND CLAMPS			
Description	Remarks	Year	Inventor / Researcher
A pre-tensioned SMA actuator for high loads and long period idling applications (e.g. clamping mechanism for space station)	Clamps	1990	(Romanelli & Otterstedt, 1990)
A device for the non-explosive separation of coupled components with SMA element in a controlled fashion	Release mech	1992	(Alfred D. Johnson, 1992)
A metal to metal seal for use in a wellbore that incorporates a SMA element	Seals	1993	(Ross, 1993c)
A method to enhance fatigue lifetime around holes formed in structural members through cold working using a tool or an interference fit fastener fabricated from SMA material.	Fasteners	1993	(J. R. Kennedy & Larson Jr, 1993)
A heat operated release mechanism with SMA element that is controllable to allow a heat exchanger (on PCB Board) to be held firmly in place and to be withdrawn when so desired	Release mech. PCB application	1996	(W. W. Porter, 1996)
A novel clamping device incorporating a SMA element for the easy clamping and release of a work piece	Release/Clamp mech	1998	(Schron & Summers, 1998)
An effective connection between two components by simple relative motion, with one of the components being a super-elastic material	Fasteners	2001	(Patrick Michel White, 2001)
A sealing assembly that incorporates a flat washer gasket made of a super-elastic alloy that deforms elastically to seal between two connecting members when the sealing surfaces are fully engaged	Seals	2002	(Patrick Michel White, 2002)
A releasable fastener system comprising a series of loops (composed of a fibre that has a non-axisymmetric coating of a SMA) that when pressed together they interlock to form a releasable engagement	Fasteners	2004	(Cheng, Ni, & Ulicny, 2004)
A system consists of two release mechanism of different structure states (pseudoelastic and martensite-austenite).	Release mech	2004	(Carman, Mitrovic, & Pulliam, 2004)
To improve adhesion between two dissimilar metals (such as a hard CrN coating and aluminium) with interlayer of SMA material between them by compensating the mismatches of mechanical	Fasteners	2006	(Cheng, Ni, Lev, <i>et al.</i> , 2006)
Devices and methods for fasteners (such as bolts) made of single crystal SMA capable of adjusting the tension in the assembly.	Fasteners	2006	(AD Johnson, Bokaie, & Martynov, 2006)
SMA as fastening system for instrument panels, e.g. in a motor vehicle which can improve the fixing or releasing of trim panel and can change the approach to dashboard design	Fasteners	2007	(Rudduck, Blattmann, & Brown, 2007)
A torque transmitting coupling assembly incorporates an elongated shaft member made of a super-elastic alloy, which lock two members together in a fixed relative position upon activation	Fasteners	2008	(Patrick M. White, 2008)
A device and method for holding components together and permanently deforms a bolt to adjust the components to a pre-determined distance without being fully detached fully by selective activation of SMA element	Fasteners	2008	(AD Johnson, Bokaie, & Martynov, 2008)
Several types of fastener, fastener systems and fastener assemblies using SMA elements	Fasteners	2009	(Rudduck <i>et al.</i> , 2009)
A ratchet mechanism with SMA	Clamps	2011	(N. L. Johnson <i>et al.</i> , 2011)

Appendix C. Industrial and manufacturing

INDUSTRIAL AND MANUFACTURING			
Description	Remarks	Year	Inventor / Researcher
A SMA wire as its driving source to open or close the linear valve	Valve	1990	(Homma, 1990)
A linearly actuated valve with SMA wire that is inexpensive, lightweight and constructed from as few parts as possible	Valve	1993	(Coffee, 1993)
A fluid control valves with SMA element	Valve	2001	(Hines, Gausman, Glime, Hill, & Rigsby, 2001)
An invention for a press brake tool holder with SMA actuator for the clamping force	Press brake tool	2007	(Morehead & Harrington, 2007)
Same tool/die to form different geometries with changeable SMA surface	Tool and Die	2007	(AL Browne, Buravalla, & Johnson, 2007)
A resettable thermal valve for fluid flow control using a SMA actuator that permits the valve to move from an open to a closed position when heated to a predetermined temperature	Valve	2008	(Vasquez & Garrod, 2008)
To control the gas flow rate (flow controller) with SMA by varying aperture size (rotary motion) of the frame	Valve	2008	(MacGregor, Szilagyi, & Von Behrens, 2008)
Adjusting the nozzle tip height and hot runner seals in an injection moulding machine effectively and efficiently with SMA element	Injection moulding	2009	(Jenko, 2009)

Appendix D. SMA material and process and material improvements

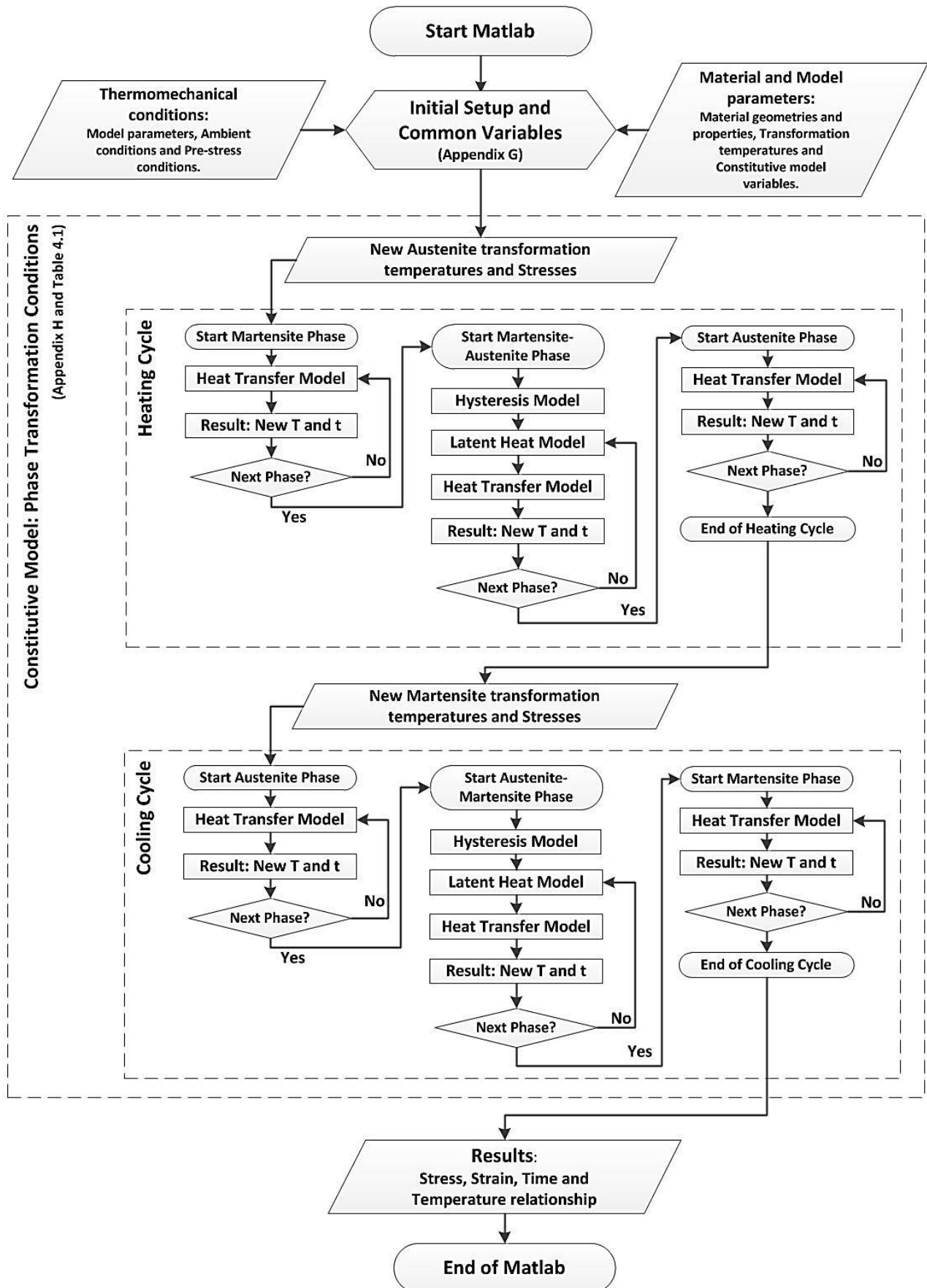
SMA PROCESS AND MATERIAL IMPROVEMENTS			
Description	Remarks	Year	Inventor / Researcher
Producing a two-way SME from one-way memory material by deforming the material into a predetermined shape and then work hardening, such as through shot peening	Transform OWSME to TWSME	1998	(Ingram, 1998)
A process ("training") for conditioning a SMA by cold working and annealing prior to force application/release cycling at a temperature above the martensitic-austenitic transformation finish temperature, but below the maximum temperature at which the austenitic-martensitic transformation will be effected by the force application, to yields greater control over the forward and reverse transformation temperatures and therefore produces a reduction in the hysteresis variability	Reduce hysteresis variability	2000	(B. F. Carpenter & Draper, 2000)
A novel SMA (Ti50Ni47Fe3) which responds to changes in ambient temperature over a narrower temperature range (~2°C) by taking advantage of a transition to the R-phase rather than the martensite phase to reduce hysteresis effects. A specific application for such an actuator is to control an anti-freeze plug for opening a drainage hole in a condensate collector pan of an air conditioner when the ambient temperature approaches freezing	SMA material with narrow temperature range	2002	(Ashurst, 2002)
An apparatus to improve the control and operating efficiency of a SMA device by using a thermoelectric (TEC) material to pump heat between the SMA and a heat sink	SMA improvement with TEC	2006	(A. Dean Jacot <i>et al.</i> , 2006)
A method of preparing nitinol for use in manufacturing instruments with improved fatigue resistance by subjecting the nitinol to a strain and thermal cycling process (between a cold bath of about 0°C to 10°C and a hot bath of about 100°C to 180°C for a minimum of about five cycles)	Improve fatigue resistance	2007	(Berendt, 2007)
A system of a multitude SMA segments, which are linked together but controlled separately to generate co-ordinated gross movement as well as independent fine movements with a minimum of complexity	SMA controller system	2007	(Harry Haruhiko Asada, Cho, & Selden, 2007)
SMA actuator manufacturing system	Manufacture SMA	2009	(Hamaguchi, Tanii, & Kosaka, 2009)
A range of compositions in the Ni-Ti-Pt SMA for high temperature (above 100°C), high force, narrow hysteresis and produce a high specific work output.	HTSMA	2009	(Ronald D Noebe <i>et al.</i> , 2009)
A method of forming single crystal thin film SMA by the specific heat treatment of an amorphous sputter deposits. The single crystal SMA exhibits greater recovery, constant force deflection, wider transition temperature range and a narrow loading hysteresis	Thin film SMA forming	2009	(AD Johnson, 2009)
Shape-setting methods for the fabrication of devices made from single crystal Cu-Ni-Al SMA	Cu-Ni-Al SMA shape-setting method	2009	(AD Johnson, Bokaie, & Martynov, 2009)
"Hyperelastic" SMA single crystal material which is capable of a recoverable strain of 9% (and in exceptional circumstances as large as 22%). These SMAs exhibit no creep or gradual change during repeated cycling because there are no grain boundaries (Cu-Al-X, where X may be Ni, Fe, Co or Mn)	Hyperelastic SMA	2010	(Alfred David Johnson, Martynov, Bokaie, & Gray, 2010)
A ferrous-based SMA known as NCATB alloy has exhibited maximum superelastic strain of about 13.5% and a very high tensile strength of 1200MPa	Fe-based SMA. Higher strain and strength	2010	(Y. Tanaka <i>et al.</i> , 2010)
Adding cobalt (Co) as ternary elements into NiTi alloys has proven to increase the plateau stress (i.e. 'stiffness') of NiTi alloys by 35%, which is important for medical applications	NiTiCo SMA. Increase stiffness of material	2011	(Fasching, Norwich, Geiser, & Paul, 2011)
'Programming' process to enable NiTi SMA to perform Triple-SME	Transform OWSME to Triple-SME	2012	(C. Tang <i>et al.</i> , 2012)
Researchers from University of Western Australia and Gyeongsang National University developed novel methods of preparing single material NiTi SMA to exhibit "four-way" SME via laser annealing and thermal diffusion annealing	Four ways SME NiTi SMA	2012	(Meng, Liu, Yang, Shariat, & Nam, 2012)
NiMn FSMA can be used for actuation, sensing, magnetic refrigeration, active tissue scaffolding and energy harvesting	FSMA	2013	(Global, 2013)
Multiple shapes of SMA at various temperatures could be achieved by using a new process, namely Multiple Memory Material Technology (MMMT). These new breeds of smart materials are called Multiple Memory Materials (MMMs)	Multiple Shapes SMA	2013	(Khan <i>et al.</i> , 2013)
A single-crystal SMA (SCSMA) made of CuAlNi that exhibits significantly better performance over NiTi SMA. This new alloy is capable to operate at more than 200°C, fully resettable (repeatable with 100% recovery), may be operable for up to one million of cycles, provide significantly greater strain recovery (9%), wider transition temperature range (-270°C to +250°C), and very narrow loading hysteresis (< 25°C)	CuAlNi SCSMA. Better performance than NiTi SMA	2013	(Aerospace, 2013)

Appendix E. Miscellaneous SMA applications

MISCELLANEOUS			
Description	Remarks	Year	Inventor / Researcher
An invention for a subterranean wellbore tool with SMA actuator	Wellbore tool	1993	(Ross, 1993a, 1993b)
A refreshable braille cell display uses a single moving part per tactile element (with SMA actuators) gives users access to full computer generated screens of text and graphical information in real time	Braille	1997	(Decker, 1997)
A golf ball with SMA layer to provide an effect of tightening the core, thus improving the ball's resiliency, resulting an increased travel distance	Golf ball	1999	(Maehara & Chikaraishi, 1999)
A control tab installed at the trailing edge of the stern planes of a submarine, by a remote control actuator system with two SMA cables	Submarine	2000	(Goldstein & Nguyen, 2000)
A striking face for golf clubs with SMA material with capability to change patterns to create a sweet spot on the striking face of the club	Golf club	2001	(Krumme & Dickinson, 2001)
Application of SMA as ejecting drops mechanism	Ink jet printer	2003	(Silverbrook, 2003)
To recover surface damage from mechanical contact by activating a SMA surface either as a complete entity or as a protective coating	Material surface	2006	(Cheng, Ni, Lukitsch, Weiner, & Grummon, 2006)
SMA actuator to vary the exit nozzle fan flaps of a gas turbine engine to improve performance and efficiency	Gas turbine	2006	(Rey <i>et al.</i> , 2006)
The invention of a two-way actuated shape memory composite material (SMA is bonded to another elastic metal)	SMA composites	2007	(Walak, 2007)
A cold-launch system with one or more stages of SMA actuators to accelerate material to a required launch velocity	Cold-launcher	2008	(Shah, Corboy, & William Russell Kraft, 2008)
SMA underwire assembly for use in a brassiere	Fashion/Brassiere	2009	(Fan, Yu, & Zheng, 2009)
SMA elements to modify blade surface of wind turbines to improve aerodynamics	Wind turbine	2012	(J. E. Smith <i>et al.</i> , 2012)
SMA to automatically adjust the jet nozzle of an air-condition system	Air-condition jet nozzle	2013	(GmbH, 2013)

Appendix F. Numerical model structure of complete solution for Matlab

The structure of numerical solution for Matlab in this study is illustrated in the chart below. Selection of appendices G to N is required to complete the Matlab code.



Appendix G. Matlab code: initial setup and variables

```
%#####  
%% Description: This code is for the initial setup and variable definitions for most  
%% of the operation codes used in this study  
%% Inputs: Ambient conditions, Joule heating current, SMA geometry, Spring  
parameters,  
%% Pre-stress load, Material properties, Constitutive variables.  
%% Outputs: Initial variables for model calculations (analytical or FDE)  
%% Prepared by Jaronie, 14Sep2015  
  
% Model parameters  
t_heat = 17.9; %Max heating duration in sec  
t_cool = 41.7; %Max cooling duration in sec  
T_max = 400; % Material max temp in degC  
  
ISMA = 2.0; % Resistive current in A  
  
Zheta0 = 1; % Initial martensite fraction (1=100% to 0=0%)  
  
% Ambient conditions  
T_amb = 30; % Ambient temperature in degC  
h = 50.8; % Convective heat transfer coefficient in W/m2.K  
  
%Pre-stress conditions (for Bias-spring scenario)  
Sigma00 = 90.6081942026475; % Pre-Stress condition in MPa  
Kspring = 0.00266; %Spring constant in MN/m,  
%for deadweight condition, apply dead-weight Eq.4.15.  
  
%Material geometry  
DSMA = 0.000508; % diameter in m  
LSMA = 0.1; % Length in m  
  
%Material properties (e.g. Dynalloy 70LT) – with phase change  
LH = 24180; % Latent heat of transformation in J/kg  
  
rhoSMA_m = 6450; % density in kg/m3 (Martensite)  
rhoSMA_a = 6450; % density in kg/m3 (Austenite)  
  
kSMA_m = 8; % conductivity of material (Martensite) in W/m.K  
kSMA_a = 18; % conductivity of material (Austenite) in W/m.K  
  
cSMA_m = 322.4; % specific heat of material (Martensite) in J/kgK  
cSMA_a = 322.4; % specific heat of material (Austenite) in J/kgK  
  
rSMA_m = 0.00000076; % Martensite resistivity in micro-ohm.m  
rSMA_a = 0.00000084; % Austenite resistivity in micro-ohm.m  
  
EModulus_m = 28000; % Young modulus in MPa (Martensite)  
EModulus_a = 75000; % Young modulus in MPa (Austenite)  
  
EpsilonL = 0.04; % Maximum recovery strain  
  
AS = 68; % Austenite start temperature (As)
```

```

AF = 78;      % Austenite final temperature (Af)
MS = 52;      % Martensite start temperature (Ms)
MF = 42;      % Martensite final temperature (Mf)

%Constitutive model variables
Theta_m = 0.55; %Thermoelastic tensor in MPa/K (Martensite phase)
Theta_a = 0.55; %Thermoelastic tensor in MPa/K (Austenite phase)

C_AS = 7;     % stress influence coefficient in MPa/K (As)
C_AF = 7;     % stress influence coefficient in MPa/K (Af)
C_MS = 2.5;   % stress influence coefficient in MPa/K (Ms)
C_MF = 10.0;  % stress influence coefficient in MPa/K (Mf)

% Variables calculation (Liang & Roger, 1997)
aA = pi/(AF-AS);
aM = pi/(MS-MF);
bAS = -aA/C_AS;
bAF = -aA/C_AF;
bMS = -aM/C_MS;
bMF = -aM/C_MF;

Ax = (pi*DSMA^2)/4; %Calculate cross-sectional area in m2
Asf = pi*DSMA*LSMA; %Calculate surface area in m2
Vol = Ax*LSMA; %Calculate volume in m3
Mass = rhoSMA_m*Vol; %Calculate mass in kg

I_density = ISMA/Ax; %Calculate current density in A/m2

% Transformation tensor in MPa, (Eq. 4.12) (Liang & Roger, 1997)
Omega_m = -EpsilonL*EModulus_m; % Martensite
Omega_a = -EpsilonL*EModulus_a; % Austenite

% Constitutive equation constant for bias-spring scenario (Eq. 4.17) (Liang & Roger, 1997)
Constant_m = 1+((Ax*EModulus_m)/(Kspring*LSMA)); %Martensite phase
Constant_a = 1+((Ax*EModulus_a)/(Kspring*LSMA)); %Austenite phase
% For deadweight condition, apply dead-weight Eq.4.15, or change both constants = 1

EpsilonRes = Zeta0 * EpsilonL; % Martensite residual strain (Liang & Roger, 1997)

FSMA0 = Sigma00*Ax; %Initial Force in MN

%%% Optional: To check Bi <<1
Bi = (h*DSMA)/(4*kSMA_m); % (Eq. 4.6)
if(Bi <= 0.1)&&(I_density <= 100000000)

    fprintf(1,'\nBi = %6.4f is within range (Bi<= 0.1)',Bi);
    %fprintf(1,'\nDiffusivity = %6.8f m2/s',alphaSMA);
    fprintf(1,'\nCurrent density = %6.3f A/m2',I_density);
    fprintf(1,'\nh = %4.2f W/m2.K',h);
    fprintf(1,'\nSimulation proceed...\n');
else
    fprintf(1,'\nEither Bi = %6.4f (Bi > 0.1)',Bi);
    fprintf(1,'\nor the Current density (I_density > 10^8 A/m2) = %6.3f A/m2',I_density);

```

```

fprintf(1,'\nSimulation cancelled...\n');
Break;

end

% Initial variables
tt = 0; % Starting from t=0 second
TSMA = T_amb; % Starting from ambient temperature

%MATRIX PREPARATION
TableDATA(1,1) = tt; % Initial TableDATA for time
TableDATA(1,2) = TSMA; % Initial TableDATA for Temperature
TableDATA(1,3) = 1; % Initial TableDATA for Martensite fraction
TableDATA(1,4) = Sigma00; % Initial TableDATA for Stress
TableDATA(1,5) = 0; % Initial TableDATA for Strain

%##### END #####

```

Appendix H. Matlab code: Liang and Roger constitutive model for SMA linear actuator

```
#####
%% Description: Constitutive model with Liang and Roger model (Liang & Roger, 1997)
%% Inputs: Initial setup and parameters from Appendix F
%% Outputs: Pre-stress influenced transformation temperatures, material phase transition
variables
%%          and martensite phase fraction.
%% Prepared by Jaronie, 14Sep2015

% Initial variables
Sigma = Sigma00; % Starting with pre-stress
Epsilon0 = EpsilonRes + (Sigma00/EModulus_m); % Initial strain (Liang & Roger,
1997)

% Phases triggers
Trig1 = 0;
Trig2 = 0;
Trig3 = 0;

% ##### HEATING CYCLE begin #####
i=2;
Sigma=Sigma00;

% New austenite transformation temperatures and stresses (Liang & Roger, 1997)
AS_new = round(((C_AS*AS - ((Theta_m/Constant_m)*TSMA)+Sigma))/...
    /(C_AS - (Theta_m/Constant_m))); % (Eq. 4.18)
SigmaAS=((Theta_m/Constant_m)*(AS_new-MF))+Sigma; % (Eq. 4.19)
AF_new=round(((aA*AS) -(bAF*SigmaAS)+(bAF*(Omega_a/Constant_a)... % (Eq. 4.20)
    *(Epsilon0/EpsilonL))+ (bAF*(Theta_a/Constant_a)*AS_new) + pi)/(aA +
bAF*(Theta_a/Constant_a)));

%++++ Add LOOP VARIABLE for HEATING CYCLE here
% Analytical (Appendix I) or FDE (Appendix J to Appendix N)

% PHASE TRANSFORMATION CONDITIONS (refer Table 4.1)
% Below As (Martensite phase)
if(TSMA < AS_new)
    if(Trig1 == 0) %Trigger1
        Trig1 = 1;
        T0 = TSMA;
        Zheta0 = 1;
        Sigma0 = Sigma;
    end

% Phase variables
Zheta = 1;
rhoSMA = rhoSMA_m;
cSMA = cSMA_m;
rSMA = rSMA_m;
kSMA = kSMA_m;
Theta = Theta_m;
```

```

EModulus = EModulus_m;
LHT = 0;

```

```

% Af and above (Austenite phase)
elseif(TSMA >= AF_new)

```

```

    if(Trig3 == 0) %Trigger3
        Trig3 = 1;
        t_AF = tt;
        Temp_AF = TSMA;
        T0 = TSMA;
        Zheta0 = Zheta;
        Sigma0 = Sigma;
        SigmaAF = Sigma;
    end

```

```

    % Phase variables
    Zheta = 0;
    rhoSMA = rhoSMA_a;
    cSMA = cSMA_a;
    rSMA = rSMA_a;
    kSMA = kSMA_a;
    Theta = Theta_a;
    EModulus = EModulus_a;
    LHT = 0;

```

```

% Between As and Af (Martensite-Austenite phase)
else

```

```

    if(Trig2 == 0) %Trigger t_AS
        Trig2 = 1;
        Temp_AS = TSMA;
        t_AS = tt;
        T0 = TSMA;
        Zheta0 = Zheta;
        Sigma0 = Sigma;
        SigmaAF = Sigma;
    end

```

```

    % Phase variables

```

```

    Zheta = (Zheta0/2)*(cos((pi/(AF_new-AS_new))*((TSMA-AS_new))) + 1); % (Eq.
4.26)

```

```

    rhoSMA = (rhoSMA_m*Zheta)+(rhoSMA_a*(1-Zheta));
    rSMA = (rSMA_m*Zheta)+(rSMA_a*(1-Zheta)); % (Eq. 6.4)
    Theta = (Theta_m*Zheta)+(Theta_a*(1-Zheta));
    EModulus = (EModulus_m*Zheta)+(EModulus_a*(1-Zheta));
    % cSMA and kSMA embedded into latent heat models

```

```

    % ++++Add LATENT HEAT MODEL for HEATING CYCLE here
    % Analytical (Appendix I) or FDE (Appendix J to Appendix N)

```

```

end

```

```

% ++++ Add HEAT TRANSFER MODEL for HEATING CYCLE here
% Analytical (Appendix I) or FDE (Appendix J to Appendix N)

```

```
% CONSTITUTIVE MODEL calculation for stress and strain, refer Section 4.3.3.1
Constant = 1+((Ax*EModulus)/(Kspring*LSMA));   %(Eq. 4.17)
Omega = -EpsilonL*EModulus;                   %(Eq. 4.12)
Sigma = (((Theta*(TSMA - T0)))+(Omega*(Ztheta-Ztheta0)))/Constant) + Sigma0;   %(Eq. 4.15)
Epsilon = (Sigma - Sigma00)/(Kspring*LSMA/Ax);   %(Eq. 4.16)
```

```
% DATA SAVING
```

```
TableDATA(i,1) = tt;   % Time in s
TableDATA(i,2) = TSMA_mean;   % SMA Mean Temperature in C
TableDATA(i,3) = Ztheta;   % Martensite fraction
TableDATA(i,4) = Sigma;   % Stress in MPa
TableDATA(i,5) = Epsilon;   % Strain in %
```

```
%End of cycle when reach t_heat
```

```
if(tt>=t_heat)
```

```
    break;
```

```
end
```

```
%++++ Add VARIABLE INCREMENT CODE here (Temperature or time)
```

```
% Analytical (Appendix I) or FDE (Appendix J to Appendix N)
```

```
i=i+1;
```

```
end %End of LOOP VARIABLES
```

```
%##### End of HEATING CYCLE #####
```

```
%Reset triggers
```

```
Trig1 = 0;
```

```
Trig2 = 0;
```

```
Trig3 = 0;
```

```
%##### COOLING CYCLE begin #####
```

```
%Sigma is the last Sigma from previous cycle
```

```
% New martensite transformation temperatures and stresses (Liang & Roger, 1997: Eqs. 50, 51 and 54)
```

```
MS_new = round((aM*MF - (bMS*Sigma) + (bMS*(Theta_a/Constant_a)*TSMA)+ pi)/...
    (aM + bMS*(Theta_a/Constant_a)));   % (Eq. 4.22)
```

```
SigmaMS = Sigma + ((Theta_a/Constant_a)*(MS_new - TSMA));   % (Eq. 4.23)
```

```
MF_new = round(((aM*MF)-(bMF*SigmaMS)-(bMF*(Omega_m/Constant_m)*...
    (1-Ztheta)))+(bMF*(Theta_m/Constant_m)*MS_new))/...
    (aM + bMF*(Theta_m/Constant_m)));   % (Eq. 4.24)
```

```
SigmaMF = ((Theta_m/Constant_m)*(MF_new-MF))+((Omega_m/Constant_m)*(1-
    Ztheta))+SigmaMS;
    % (Eq. 4.25)
```

```
%++++ Add LOOP VARIABLE for COOLING CYCLE here
```

```
% Analytical (Appendix I) or FDE (Appendix J to Appendix N)
```

```
% PHASE TRANSFORMATION CONDITIONS (refer Table 4.1)
```

```
% Above Ms (Austenite phase)
```

```
if(TSMA > MS_new)
```

```
    if(Trig1 == 0)   %Trigger1
```



```

    Trig1 = 1;
    T0 = TSMA;
    Zheta0 = Zheta;
    Sigma0 = Sigma;
end

%Zheta = 0;

rhoSMA = rhoSMA_a;
cSMA = cSMA_a;
rSMA = rSMA_a;
kSMA = kSMA_a;
LHT = 0;

%Constitutive model variables
Theta = Theta_a;
EModulus = EModulus_a;

elseif(TSMA<=MF_new)

    if(Trig3 == 0) %Trigger3
        Trig3 = 1;
        t_MF = tt;
        Temp_MF = TSMA;
        %T0 = MF_new;
        T0 = TSMA;
        Zheta0 = Zheta;
        Sigma0 = Sigma;
    end

    %Zheta = 1;

    rhoSMA = rhoSMA_m;
    cSMA = cSMA_m;
    rSMA = rSMA_m;
    kSMA = rSMA_m;
    LHT = 0;

%Constitutive model variables
    Theta = Theta_m;
    EModulus = EModulus_m;

else

    if(Trig2 == 0) %Trigger2
        Trig2 = 1;
        t_MS = tt;
        Temp_MS = TSMA;
        T0 = TSMA;
        Zheta0 = Zheta;
        Sigma0 = Sigma;
        MS_new = T0;
    end

```

```

    Zheta = ((1-Zheta0)/2)*(cos((pi/(MS_new-MF_new))*((TSMA-
MF_new))))+((1+Zheta0)/2);   %(Eq. 4.27)
    rhoSMA = (rhoSMA_m*Zheta)+(rhoSMA_a*(1-Zheta));
    rSMA = (rSMA_m*Zheta)+(rSMA_a*(1-Zheta));   %(Eq. 6.4)
    Theta = (Theta_m*Zheta)+(Theta_a*(1-Zheta));
    EModulus = (EModulus_m*Zheta)+(EModulus_a*(1-Zheta));
    % cSMA and kSMA embedded into latent heat models

    %++++ Add LATENT HEAT MODEL for COOLING CYCLE here
    % Analytical (Appendix I) or FDE (Appendix J to Appendix N)

end

%++++ Add HEAT TRANSFER MODEL for COOLING CYCLE here
% Analytical (Appendix I) or FDE (Appendix J to Appendix N)

% CONSTITUTIVE MODEL calculation for stress and strain, refer Section 4.3.3.1
Constant = 1+((Ax*EModulus)/(Kspring*LSMA));   %(Eq. 4.17)
Omega = -EpsilonL*EModulus;   %(Eq. 4.12)
Sigma = (((Theta*(TSMA - T0)))+(Omega*(Zheta-Zheta0)))/Constant + Sigma0;   %(Eq.
4.15)
Epsilon = (Sigma - Sigma00)/(Kspring*LSMA/Ax);   %(Eq. 4.16)

%DATA SAVING
TableDATA(i,1) = tt;   % Time in s
TableDATA(i,2) = TSMA_mean;   % SMA Mean Temperature in C
TableDATA(i,3) = Zheta;   % Martensite fraction
TableDATA(i,4) = Sigma;   % Stress in MPa
TableDATA(i,5) = Epsilon;   % Strain in %

%End of cycle when reach t_cool
if(tt>=t_cool+t_heat)
    break;
end

%++++ Add VARIABLE INCREMENT CODE here (Temperature or time)
% Analytical (Appendix I) or FDE (Appendix J to Appendix N)
i=i+1;

end %End of LOOP VARIABLES
##### End of COOLING CYCLE #####

%Reset triggers
Trig1 = 0;
Trig2 = 0;
Trig3 = 0;

```

```

%#### PLOT FINAL RESULTS
% Plot results in 4 subplots
figure('Name','Numerical Model')

subplot(4,1,1) %Stress versus Time
plot(TableDATA(i,1),TableDATA(:,4),'b-');
title('Stress versus Time')
axis auto
grid,xlabel('Time (s)'),ylabel('Stress (MPa)')

subplot(4,1,2) %Strain versus Time
plot(TableDATA(i,1),TableDATA(:,5),'b-');
title('Strain versus Time')
axis auto
grid,xlabel('Time (s)'),ylabel('Strain (%)')

subplot(4,1,3) %Stress versus Strain
plot(TableDATA(i,5),TableDATA(:,4),'b-');
title('Stress versus Strain')
axis auto
grid,xlabel('Strain (%)'),ylabel('Stress (MPa)')

subplot(4,1,4) %mean Temp versus Time
plot(TableDATA(i,1),TableDATA(:,2),'b-');
title('Mean temperature versus Time')
axis auto
grid,xlabel('Time (s)'),ylabel('Temperature (degC)')

%##### END #####

```

Appendix I. Matlab code: Analytical heat transfer model for SMA linear actuator

```
%% Description: This code is for the analytical model solution of this study.
%% Requirement: Initial codes and constitutive model from Appendices G and H.
%% Inputs: Initial setup and parameters from Appendix F
%%           and variables from constitutive model (Pre-stress influenced transformation
temperatures,
%%           material phase transition variables and martensite phase fraction).
%% Outputs: Temperature versus Time data in TableDATA.
%% Prepared by Jaronie, 14Sep2015

% Model parameters
dT = 0.005; %Temperature incremental value

##### HEATING CYCLE code begin
TSMA = T_amb + dT;

%+++++ LOOP VARIABLES
for j=dT:dT:(T_max-T_amb) %Loop with increase of dT until T_max, resulting new tt
    TSMA_mean=TSMA;

% ++++++ Analytical LATENT HEAT MODEL (Eq. 7.9)
% Add into Constitutive model (Appendix H), (also refer Shahin, 1994)
LHT = ((pi*LH)/(2*(AF_new-AS_new)))*(sin(pi*((TSMA-AS_new)/(AF_new-AS_new))));
cSMA = 0;
kSMA = (kSMA_m*Zeta)+(kSMA_a*(1-Zeta)); % (Eq. 7.21)

% ++++++ Analytical HEAT TRANSFER MODEL (Eq. 6.11)
tc = (rhoSMA*Vol*dT*(cSMA+LHT))/(((ISMA^2)*(rSMA*LSMA/Ax))-(h*Asf*(TSMA-
T_amb)));
tt = tt + tc;

%+++++ VARIABLE INCREMENT CODE
TSMA = TSMA + dT;
##### HEATING CYCLE code end

##### COOLING CYCLE code begin
%+++++ LOOP VARIABLES
for k=dT:dT:(TSMA-T_amb) %Loop with decrease of dT until T_amb, resulting new tt
    TSMA_mean=TSMA;

%+++++ Analytical LATENT HEAT MODEL (Eq. 7.10)
% Add into Constitutive model (Appendix H), (also refer Shahin, 1994)
LHT = ((pi*LH)/(2*(MS_new-MF_new)))*(sin(pi*((TSMA-MF_new)/(MS_new-MF_new))));
cSMA = 0;
kSMA = (kSMA_m*Zeta)+(kSMA_a*(1-Zeta)); % (Eq. 7.21)

%+++++ Analytical HEAT TRANSFER MODEL (Eq. 7.11)
tc = (rhoSMA*Vol*-dT*(cSMA+LHT))/(0-(h*Asf*(TSMA-T_amb)));
tt = tt + tc;

%+++++ VARIABLE INCREMENT CODE
TSMA = TSMA - dT;
##### COOLING CYCLE code end
```

Appendix J. General Matlab code of FDM heat transfer model for SMA linear actuator

```
%% Description: General heat transfer model code for FDM
%% Requirement: Initial codes and constitutive model from Appendices G and H.
%% Inputs: Initial setup and parameters from Appendix G
%%          and variables from constitutive model.
%% Outputs: Temperature versus Time data in TableDATA.
%% Prepared by Jaronie, 14Sep2015

%FDE time and space steps size
dr=0.00001; %Space step size
dt=0.001; %Time step size

%Setup nodes
I=floor(t_cool/dt); % Time nodes
J=floor(DSMA/(2*dr)); % Space nodes
TSMA=T_amb*ones(1,J+1);

%##### HEATING CYCLE code begin
%++++ LOOP VARIABLE for HEATING CYCLE
while (dt*(i-1)<=t_heat) %Loop increase until t_heat

%++++ FDE LATENT HEAT MODEL (cSMA and kSMA manipulation, refer Section
7.4.3.1)
dTh = (AF_new-AS_new)/2;
cSMA = (((pi*LH)/(4*dTh))*sin(pi*((mean(TSMA(1,:))-AS_new)/(AF_new-AS_new)))); %
Eq. 7.19
kSMA = (kSMA_m*Zheta)+(kSMA_a*(1-Zheta)); %Eq. 7.21

%++++ FDE HEAT TRANSFER MODEL for HEATING CYCLE
alphaSMA=kSMA/(rhoSMA*cSMA); %SMA thermal diffusivity in m2/s (Section
4.4.1.1)
Fo=((alphaSMA*dt)/(dr^2))*ones(1,J+1); % Fourier number (Section 4.1.1)
RSMA=(rSMA*LSMA)/Ax; % Resistance in Ohm
GSMA=(ISMA^2*RSMA*(dr^2))/(Vol*kSMA); % Heat generation rate (Eqs.7.12 and
7.15)
%Convective cooling rate (Eqs. 7.13 and 7.15)
CHSMA=(TSMA(1,J+1)-T_amb)*((2*(dr^2)*h)/((DSMA/2)*kSMA));

%++++ Add the MATRIX FORM of selected FDE model here (refer Section 4.4.1.5)

%++++ VARIABLE INCREMENT CODE
tt=tt+dt;
%##### HEATING CYCLE code end

%#### COOLING CYCLE code begin
%++++ LOOP VARIABLE for HEATING CYCLE
while (dt*(i-1)<=t_cool+t_heat) %Loop increases until t_heat+t_cool

%++++ FDE LATENT HEAT MODEL (cSMA and kSMA manipulation, refer Section
7.4.3.1)
dTc = (MS_new-MF_new)/2;
cSMA = (((pi*LH)/(4*dTh))*sin(pi*((mean(TSMA(1,:))-MF_new)/(MS_new-MF_new)))); %
Eq. 7.19
```

$k_{SMA} = (k_{SMA_m} \cdot \text{Zheta}) + (k_{SMA_a} \cdot (1 - \text{Zheta}))$; %Eq. 7.21

%++++ FDE HEAT TRANSFER MODEL for COOLING CYCLE

$\alpha_{SMA} = k_{SMA} / (\rho_{SMA} \cdot c_{SMA})$; %SMA thermal diffusivity in m²/s (Section 4.4.1.1)

$Fo = ((\alpha_{SMA} \cdot dt) / (dr^2)) \cdot \text{ones}(1, J+1)$; % Fourier number (Section 4.4.1.1)

$R_{SMA} = (r_{SMA} \cdot L_{SMA}) / A_x$; % Resistance in Ohm

$G_{SMA} = 0$; % No heat generation

%Convective cooling rate (Eqs. 7.13 and 7.15)

$CH_{SMA} = (T_{SMA}(1, J+1) - T_{amb}) \cdot ((2 \cdot (dr^2) \cdot h) / ((DSMA/2) \cdot k_{SMA}))$;

%++++ Add the MATRIX FORM of selected FDE model here (refer Figure 4.8 and Table 4.1)

%++++ VARIABLE INCREMENT CODE

$tt = tt + dt$;

%##### COOLING CYCLE code end

Appendix K. Forward (Explicit) FDM code for Matlab

%% Description: MATRIX FORM for Forward (Explicit) FDE model

%% Inputs: Initial SMA temperature for each nodes.

%% Outputs: New SMA temperatures for each nodes.

%% Prepared by Jaronie, 14Sep2015

%% Refer Figure 4.8 and Table 4.1 in Section 4.4.1.5

% Matrix A

for k=2:J

 A(k,k-1)=Fo(1,k-1);

 A(k,k)=1-(2*Fo(1,k));

 A(k,k+1)=Fo(1,k+1);

end

%Boundary condition on r=0

A(1,1)=1;

% Boundary condition on r=rsma

A(J+1,J)=-1; %or 0

A(J+1,J+1)=1;

% Matrix B (known nodes)

% boundary conditions $0 \leq r < r_{sma}$

for k=1:J+1

 B(k,1) = TSMA(1,k)+((Fo(1,1)*(GSMA-CHSMA))); %Refer Appendix N for Fo, GSMA
 and CHSMA

end

% FDE solution (unknown nodes in Matrix D)

D=AB;

Appendix L. Backward (Implicit) FDM code for Matlab

%% Description: MATRIX FORM for Backward (Implicit) FDE model

%% Inputs: Initial SMA temperature for each nodes.

%% Outputs: New SMA temperatures for each nodes.

%% Prepared by Jaronie, 14Sep2015

%% Refer Figure 4.8 and Table 4.1 in Section 4.4.1.5

% Matrix A

for k=2:J

 A(k,k-1)=-Fo(1,k-1);

 A(k,k)=1+(2*Fo(1,k));

 A(k,k+1)=-Fo(1,k+1);

end

%Boundary condition on r=0

A(1,1)=1;

% Boundary condition on r=rsma

A(J+1,J)=-1; %or 0

A(J+1,J+1)=1;

% Matrix D (known nodes)

% boundary conditions $0 \leq r < r_{sma}$

for k=1:J+1

 D(k,1) = TSMA(1,k)+((Fo(1,1)*(GSMA-CHSMA))); %Refer Appendix N for Fo, GSMA
and CHSMA

end

% FDE solution (unknown nodes in Matrix B)

B=A\D;

Appendix M. Central (Crank-Nicholson) FDM code for Matlab

%% Description: MATRIX FORM for central (Crank-Nicholson) FDE model

%% Inputs: Initial SMA temperature for each nodes.

%% Outputs: New SMA temperatures for each nodes.

%% Prepared by Jaronie, 14Sep2015

%% Refer Figure 4.8 and Table 4.1 in Section 4.4.1.5

% Matrix A

for k=2:J

 A(k,k-1)=-Fo/2(1,k-1);

 A(k,k)=1+Fo(1,k);

 A(k,k+1)=-Fo/2(1,k+1);

end

% Matrix C

for k=2:J

 A(k,k-1)=Fo/2(1,k-1);

 A(k,k)=1-Fo(1,k);

 A(k,k+1)=Fo/2(1,k+1);

end

%Boundary condition on r=0

A(1,1)=1;

% Boundary condition on r=rsma

A(J+1,J)=-1; %or 0

A(J+1,J+1)=1;

% Matrix D (known nodes)

% boundary conditions $0 \leq r < r_{sma}$

for k=1:J+1

 D(k,1) = TSMA(1,k)+((Fo(1,1)*(GSMA-CHSMA))); %Refer Appendix N for Fo, GSMA
and CHSMA

end

% FDE solution (unknown nodes in Matrix B)

R=C*D; %Solving right-hand side matrix

%If necessary, apply boundary conditions on Matrix R(1) and R(J+1)

B=A\R %Solving Matrix B

Appendix N. Alternative Matlab code of FDM model for SMA linear actuator

```
%% Description: Alternative FDE model for heat transfer model
%% Requirement: Initial codes and constitutive model from Appendix G and Appendix H.
%% Inputs: Initial setup and parameters from Appendix G
%%           and variables from constitutive model (Pre-stress influenced transformation
temperatures,
%%           material phase transition variables and martensite phase fraction).
%% Outputs: Temperature versus Time data in TableDATA.
%% Prepared by Jaronie, 14Sep2015

##### HEATING CYCLE begin
%Generate MATRIX FORM (refer Figure 4.8 and Table 4.1 in Section 4.4.1.5)
%Applying Explicit FDE with Joule Heating and convective cooling

% Matrix A
for k=2:J
    A(k,k-1)=-Fo(1,k-1);
    A(k,k)=1+(2*Fo(1,k));
    A(k,k+1)=-Fo(1,k+1);
end

%Boundary condition on r=0
A(1,1)=1;

% Boundary condition on r=rsma
A(J+1,J)=-1;
A(J+1,J+1)=1;

% Matrix B
% boundary conditions  $0 \leq r < r_{sma}$ 
for k=1:J+1
    B(k,1) = TSMA(1,k)+((Fo(1,1)*(GSMA-CHSMA)));
end

% FDE solution
X=A\B;
TSMA(1,:)=X(1,:); %new TSMA
TSMA_mean=mean(X(1,:)); % new mean temperature

%VARIABLE INCREMENT CODE
Tt=tt+dt;
##### HEATING CYCLE end

#### COOLING CYCLE begin
%Generate MATRIX FORM (refer Figure 7.4)
%Applying alternative Crank-Nicholson FDE with Joule Heating and convective cooling
% Matrix A
for k=2:J
    A(k,k-1)=Fo(1,k)*(2*(k-1)-1);
    A(k,k)=-4*(k-1)*(Fo(1,k)+1);
    A(k,k+1)=Fo(1,k)*(2*(k-1)+1);
end
```

%Boundary condition on $r=0$

$A(1,1)=1;$

$A(1,2)=1;$

$B(1,1)=0;$

% Boundary condition on $r=r_{sma}$

$A(J+1,J)=-1;$

$A(J+1,J+1)=((dr \cdot h)/kSMA)+1;$

$B(J+1,1)=(dr \cdot h \cdot Ta)/kSMA;$

```

% boundary conditions  $0 < r < r_{sma}$ 
for k=2:J
    B(k,1)=-Fo(1,k)*(2*(k-1)-1)*TSMA(1,k-1)+4*(k-1)*(Fo(1,k)-1)*TSMA(1,k)...
    -Fo(1,k)*(2*(k-1)+1)*TSMA(1,k+1);
end

% FDE solution
X=A\B;
X=X';

TSMA(1,:)=X(1,:); %new TSMA
TSMA_mean=mean(X(1,:)); % new mean temperature

%VARIABLE INCREMENT CODE
tt=tt+dt;
##### COOLING CYCLE end

```

Appendix O. SMA response charts with simplified analytical model

%% Description: SMA response charts with simplified analytical model (Refer Section 7.4.5)

%% Inputs: Initial setup and parameters, and variables from constitutive model
%% (Pre-stress influenced transformation temperatures,
%% material phase transition variables and martensite phase fraction).

%% Outputs: Activation and deactivation response charts

%% Prepared by Jaronie, 28Oct2015

clear all; close all; clc;

%Resistive heating (for heating response chart under natural convection)

%ISMA_min = 1.00;

ISMA_max = 21.00;

ISMA_inc = 0.5;

%Force convection (for cooling response chart)

h_min = 40;

h_max = 500;

h_inc = 5;

%Ambient temperature in K

T_amb_min = 20;

T_amb_max = 60;

T_amb_inc = 10;

%Material geometry

DSMA = 0.000508; % diameter in m 0.000508, 0.000254

LSMA = 0.1; % Length in m

%Material properties

rhoSMA_m = 6450; % density in kg/m3

rhoSMA_a = 6450; % density in kg/m3

kSMA_m = 8; % W/m.K conductivity of material (Martensite)

kSMA_a = 18; % W/m.K conductivity of material (Austenite)

cSMA_m = 322.4; % J/kgK specific heat of material (Martensite)

cSMA_a = 322.4; % J/kgK specific heat of material (Austenite)

rSMA_m = 0.00000076; % Martensite resistivity in micro-ohm.m

rSMA_a = 0.00000084; % Austenite resistivity in micro-ohm.m

EModulus_m = 28000; % Young modulus in MPa (Martensite)

EModulus_a = 75000; % Young modulus in MPa (Austenite)

Theta_m = 0.55; %Thermoelastic tensor in MPa/K (Martensite)

Theta_a = 0.55; %Thermoelastic tensor in MPa/K (Austenite)

EpsilonL = 0.04; %Maximum recovery strain

%Transformation temperatures

AS = 68 + Kelvin; % Austenite start temperature

```

AF = 78 + Kelvin; % Austenite final temperature
MS = 52 + Kelvin; % Martensite start temperature
MF = 42 + Kelvin; % Martensite final temperature

LH = 24180; %Latent heat of transformation in J/kg (24180)

%Pre-Stress conditions
Sigma00 = 5; % Pre-Stress condition in MPa (Measured with Dead weight or Spring)
          %90.6081942026475 (30);73.378713969694(40);74.2806804964444
(50);
Kspring = 0.00266; %Spring constant in MN/m (0.00266,0.00268, 0.00253)

C_AS = 10;
C_AF = 10;
C_MS = 10;
C_MF = 10;

%Calculate variables
%Calculate Cross-section area in m2
Ax = (pi*DSMA^2)/4;

%Calculate Surface area in m2
Asf = pi*DSMA*LSMA;

%Calculate Volume in m3
Vol = Ax*LSMA;

%Calculate mass in kg
Mass = rhoSMA_a*Vol;

%Transformation tensor in MPa
Omega_m = -EpsilonL*EModulus_m;
Omega_a = -EpsilonL*EModulus_a;

K_m = 1+((Ax*EModulus_m)/(Kspring*LSMA));
K_a = 1+((Ax*EModulus_a)/(Kspring*LSMA));

%Intial variables
%I_density = ISMA/Ax; %Current density in A/m2
%I_density = ISMA/(Ax*(1000^2)); %Current density in A/mm2

fprintf(1,'\nSimulation begin...\n');

%%%%%%%%%%%%%
%Heating cycle begin

T_amb = T_amb_min;
N = 1;
N_max = ((T_amb_max-T_amb_min)/T_amb_inc)+1;

% Plot graph Temp vs Time
title_str1 = sprintf('SMA response charts, D=%gmm, natural convection',DSMA*1000);
figure('Name','Activation Response Chart')

```

```

PlotColor = jet(N_max); %Plot change color

subplot(2,1,1)

fprintf(1,'\nT_amb=%g degC, Sigma00=%g MPa\n',T_amb,Sigma00);

fprintf(1,'\nJ-Chart begin...');

while(N<=N_max)

% h based on Eisakhani correlation equation
A_ek = 0.113;
n_ek = 0.113;
C_ek = 0.610; %Vertical = 0.610

%load Material data
load('MATERIALS_DATA');

%Air Properties to calculate h
k_air =interp1(Air(:,1),Air(:,4),T_amb); %air thermal conductivity in W/m.K
g_acc = 9.81; % gravitational acceleration in m/s2
Pr=interp1(Air(:,1),Air(:,7),T_amb); % Prandtl number
beta=interp1(Air(:,1),Air(:,6),T_amb); % Expansion Coeff in 1/K
nu=interp1(Air(:,1),Air(:,5),T_amb); %Kinematic

%Calculate h
Gr = (g_acc*(DSMA^3)*beta*(AF_new-T_amb))/(nu^2); %Grashof number
Ra = Pr*Gr; %Rayleigh number
h=(k_air/DSMA)*(A_ek+(C_ek*(Ra^n_ek))); %convective heat transfer rate

%Biot number
Bi = (h*DSMA)/(4*kSMA_m);

%New transformation temperatures and stresses, based on Liang and Roger
AS_new=round((((AS*C_AS)-((Theta_m/K_m)*T_amb)+Sigma00)/(C_AS-
(Theta_m/K_m))));
SigmaAS_new=((Theta_m/K_m)*(AS_new-MF))+Sigma00;
AF_new=round((((AF*C_AF)-((Theta_a/K_a)*AS_new)-(Omega_a/K_a)+SigmaAS_new)/...
(C_AF-(Theta_a/K_a))));
SigmaAF_new=((Theta_a/K_a)*(AF_new-AS_new))-(Omega_a/K_a)+SigmaAS_new;

MS_new=round((((MS*C_MS)-((Theta_a/K_a)*AF_new)+SigmaAF_new)/(C_MS-
(Theta_a/K_a))));
SigmaMS_new=((Theta_a/K_a)*(MS_new-AF_new))+SigmaAF_new;
MF_new=round((((MF*C_MF)-
((Theta_m/K_m)*MS_new)+(Omega_m/K_m)+SigmaMS_new)/...
(C_MF-(Theta_m/K_m))));
SigmaMF_new=((Theta_m/K_m)*(MF_new-MF_new))+(Omega_m/K_m)+SigmaMS_new;

%Resistivity
RSMA_m = rSMA_m*LSMA/Ax;
RSMA_a = rSMA_a*LSMA/Ax;
RSMA_t = 0.5*(rSMA_m+rSMA_a)*LSMA/Ax;

```

```

%Saving Data Table
Table(1,N) = T_amb; %Ambient Temp
Table(2,N) = Sigma00; %Pre-Stress in MPa
Table(3,N) = AS; %AS in C
Table(4,N) = AF; %AF in C
Table(5,N) = MS; %MS in C
Table(6,N) = MF; %MF in C
Table(7,N) = AS_new; %AS_new in C
Table(8,N) = AF_new; %AF_new in C
Table(9,N) = MS_new; %MS_new in C
Table(10,N) = MF_new; %MF_new in C
Table(11,N) = SigmaAS_new; %SigmaAS_new in MPa
Table(12,N) = SigmaAF_new; %SigmaAF_new in MPa
Table(13,N) = SigmaMS_new; %SigmaMS_new in MPa
Table(14,N) = SigmaMF_new; %SigmaMF_new in MPa

%Minimum current requirement
ISMA_min = sqrt((h*Asf*(AF_new+AS_new-(2*T_amb)))/(RSMA_m+RSMA_a));
ISMA = round(ISMA_min/ISMA_inc)*ISMA_inc;

ISMA=ISMA_min;

i=1;
while(ISMA<=ISMA_max) % Current density loop

    fprintf(1,'\nI=%g A, Ta= %g degC, h=%g W/m2K,...',ISMA,T_amb,h);

    dt_AS = (rhoSMA_m*Vol*(cSMA_m*(AS_new-T_amb)))/((((ISMA^2)*RSMA_m))-
    ((h*Asf*(0.5*(T_amb+AS_new)-T_amb))));
    dt_AF = dt_AS + (rhoSMA_m*Vol*LH)/((((ISMA^2)*RSMA_t))-...
    ((h*Asf*(0.5*(AS_new+AF_new)-T_amb))));

    JChart(i,1,N)=ISMA; %current A
    JChart(i,2,N)=ISMA/(Ax*1000000); %current density in A/mm2
    JChart(i,3,N)=dt_AS;
    JChart(i,4,N)=dt_AF;

    i=i+1;
    ISMA = ISMA + ISMA_inc;

    fprintf(1,'\nAS_new=%g degC, AF_new=%g degC,...',AS_new,AF_new);
    fprintf(1,'\ndt_AS=%g s, dt_AF=%g s,...\n',dt_AS,dt_AF);

end

%Plot new data
if(N_max==1)
    loglog(JChart(:,2,N),JChart(:,4,N),'r-');
else
    loglog(JChart(:,2,N),JChart(:,4,N),'color',PlotColor(N,:));
end

hold on;

```



```

Legend1{N,1}=sprintf('T_a = %.2f degC',T_amb); %Added

T_amb = T_amb + T_amb_inc;
N=N+1;
end

%Identify dt_min & dt_max
% dt1_min = min(HTable(:,2,N_max));
% dt1_max = max(HTable(:,2,1));

%Summarise activation plot1
hold off
%title(title_str1,'FontWeight','bold','FontSize',14)
axis auto
%axis [J_min J_max dt1_min dt1_max]
grid
xlabel('Current density, J [A/mm^2]','FontWeight','bold','FontSize',12);
ylabel('Activation duration, dt [s]','FontWeight','bold','FontSize',12);
legend(Legend1)
%% Heating cycle chart End
%%%%%%%%%%%%%%%%%%%%%%%%%%%%%%%%%%%%%%%%%%%%%%%%%%%%%%%%%%%%%%%%%%%%%%%%

%%%%%%%%%%%%%%%%%%%%%%%%%%%%%%%%%%%%%%%%%%%%%%%%%%%%%%%%%%%%%%%%%%%%%%%%
%Cooling cycle begin
T_amb = T_amb_min;
N = 1;
N_max = ((T_amb_max-T_amb_min)/T_amb_inc)+1;

% Plot graph Temp vs Time
%title_str2 = sprintf('SMA deactivation response chart, D=%gmm',DSMA*1000);
%figure('Name','Deactivation Response Chart')
% PlotColor = jet(N_max); %Plot change color
subplot(2,1,2)

while(N<=N_max)
%Bi
Bi = (h*DSMA)/(4*kSMA_m);

fprintf(1,'\nH-Chart begin...');

%chart begin
h = h_min;

i=1;
while(h<=h_max) % Convective cooling loop

    fprintf(1,'\nTa=%g degC, h=%g W/m2K...',T_amb,h);

    dt_MS = (rhoSMA_a*Vol*((cSMA_a*(MS_new-AF_new)))/...
        (-h*Asf*(0.5*(MS_new+AF_new)-T_amb)));
    dt_MF = dt_MS + (rhoSMA_a*Vol*(-LH))/...
        (-h*Asf*(0.5*(MF_new+MS_new)-T_amb)));

```

```

fprintf(1,'\ndt_MS=%g s, dt_MF=%g s,...\n',dt_MS,dt_MF);

HChart(i,1,N)=h;
HChart(i,2,N)=dt_MS;
HChart(i,3,N)=dt_MF;

i=i+1;
h = h + h_inc;
end
%Plot new data
if(N_max==1)
    loglog(HChart(:,1,N),HChart(:,3,N),'r-');
else
    loglog(HChart(:,1,N),HChart(:,3,N),'color',PlotColor(N,:));
end

hold on;
Legend2{N,1}=sprintf('T_a = %.2f degC',T_amb); %Added

T_amb = T_amb + T_amb_inc;
N=N+1;
end

%Identify dt_min & dt_max
% dt2_min = min(CTable(:,2,1));
% dt2_max = max(CTable(:,2,N_max));

%Summarise activation plot2
hold off
%title(title_str2,'FontWeight','bold','FontSize',14)
axis auto
%axis [h_min h_max dt2_min dt2_max]
grid
xlabel('Convective heat transfer coefficient, h
[W/mm^2K]','FontWeight','bold','FontSize',12);
ylabel('Deactivation duration, dt [s]','FontWeight','bold','FontSize',12);
legend(Legend2)

fprintf(1,'\nSimulation end...\n');

```

Appendix P. Taguchi's L9 orthogonal array, for 4 factors and 3 levels (L9)

Test No.	Factor 1	Factor 2	Factor 3	Factor 4
1	Level 1	Level 1	Level 1	Level 1
2	Level 1	Level 2	Level 2	Level 2
3	Level 1	Level 3	Level 3	Level 3
4	Level 2	Level 1	Level 2	Level 3
5	Level 2	Level 2	Level 3	Level 1
6	Level 2	Level 3	Level 1	Level 2
7	Level 3	Level 1	Level 3	Level 2
8	Level 3	Level 2	Level 1	Level 3
9	Level 3	Level 3	Level 2	Level 1

Appendix Q. Full-factorial DOE, for 4 factors and 3 levels (3⁴)

Test No.	Factor 1	Factor 2	Factor 3	Factor 4	Test No.	Factor 1	Factor 2	Factor 3	Factor 4
1	Level 1	Level 1	Level 1	Level 1	42	Level 2	Level 2	Level 2	Level 3
2	Level 1	Level 1	Level 1	Level 2	43	Level 2	Level 2	Level 3	Level 1
3	Level 1	Level 1	Level 1	Level 3	44	Level 2	Level 2	Level 3	Level 2
4	Level 1	Level 1	Level 2	Level 1	45	Level 2	Level 2	Level 3	Level 3
5	Level 1	Level 1	Level 2	Level 2	46	Level 2	Level 3	Level 1	Level 1
6	Level 1	Level 1	Level 2	Level 3	47	Level 2	Level 3	Level 1	Level 2
7	Level 1	Level 1	Level 3	Level 1	48	Level 2	Level 3	Level 1	Level 3
8	Level 1	Level 1	Level 3	Level 2	49	Level 2	Level 3	Level 2	Level 1
9	Level 1	Level 1	Level 3	Level 3	50	Level 2	Level 3	Level 2	Level 2
10	Level 1	Level 2	Level 1	Level 1	51	Level 2	Level 3	Level 2	Level 3
11	Level 1	Level 2	Level 1	Level 2	52	Level 2	Level 3	Level 3	Level 1
12	Level 1	Level 2	Level 1	Level 3	53	Level 2	Level 3	Level 3	Level 2
13	Level 1	Level 2	Level 2	Level 1	54	Level 2	Level 3	Level 3	Level 3
14	Level 1	Level 2	Level 2	Level 2	55	Level 3	Level 1	Level 1	Level 1
15	Level 1	Level 2	Level 2	Level 3	56	Level 3	Level 1	Level 1	Level 2
16	Level 1	Level 2	Level 3	Level 1	57	Level 3	Level 1	Level 1	Level 3
17	Level 1	Level 2	Level 3	Level 2	58	Level 3	Level 1	Level 2	Level 1
18	Level 1	Level 2	Level 3	Level 3	59	Level 3	Level 1	Level 2	Level 2
19	Level 1	Level 3	Level 1	Level 1	60	Level 3	Level 1	Level 2	Level 3
20	Level 1	Level 3	Level 1	Level 2	61	Level 3	Level 1	Level 3	Level 1
21	Level 1	Level 3	Level 1	Level 3	62	Level 3	Level 1	Level 3	Level 2
22	Level 1	Level 3	Level 2	Level 1	63	Level 3	Level 1	Level 3	Level 3
23	Level 1	Level 3	Level 2	Level 2	64	Level 3	Level 2	Level 1	Level 1
24	Level 1	Level 3	Level 2	Level 3	65	Level 3	Level 2	Level 1	Level 2
25	Level 1	Level 3	Level 3	Level 1	66	Level 3	Level 2	Level 1	Level 3
26	Level 1	Level 3	Level 3	Level 2	67	Level 3	Level 2	Level 2	Level 1
27	Level 1	Level 3	Level 3	Level 3	68	Level 3	Level 2	Level 2	Level 2
28	Level 2	Level 1	Level 1	Level 1	69	Level 3	Level 2	Level 2	Level 3
29	Level 2	Level 1	Level 1	Level 2	70	Level 3	Level 2	Level 3	Level 1
30	Level 2	Level 1	Level 1	Level 3	71	Level 3	Level 2	Level 3	Level 2
31	Level 2	Level 1	Level 2	Level 1	72	Level 3	Level 2	Level 3	Level 3
32	Level 2	Level 1	Level 2	Level 2	73	Level 3	Level 3	Level 1	Level 1
33	Level 2	Level 1	Level 2	Level 3	74	Level 3	Level 3	Level 1	Level 2
34	Level 2	Level 1	Level 3	Level 1	75	Level 3	Level 3	Level 1	Level 3
35	Level 2	Level 1	Level 3	Level 2	76	Level 3	Level 3	Level 2	Level 1
36	Level 2	Level 1	Level 3	Level 3	77	Level 3	Level 3	Level 2	Level 2
37	Level 2	Level 2	Level 1	Level 1	78	Level 3	Level 3	Level 2	Level 3
38	Level 2	Level 2	Level 1	Level 2	79	Level 3	Level 3	Level 3	Level 1
39	Level 2	Level 2	Level 1	Level 3	80	Level 3	Level 3	Level 3	Level 2
40	Level 2	Level 2	Level 2	Level 1	81	Level 3	Level 3	Level 3	Level 3
41	Level 2	Level 2	Level 2	Level 2					

Appendix R. Fractional-factorial DOE (resolution IV), for 4 factors and 3 levels ($3_{IV}^{(4-1)}$)

Test No.	Factor 1	Factor 2	Factor 3	Factor 4	Test No.	Factor 1	Factor 2	Factor 3	Factor 4
1	Level 1	Level 1	Level 1	Level 1	15	Level 2	Level 2	Level 3	Level 2
2	Level 1	Level 1	Level 2	Level 2	16	Level 2	Level 3	Level 1	Level 1
3	Level 1	Level 1	Level 3	Level 3	17	Level 2	Level 3	Level 2	Level 2
4	Level 1	Level 2	Level 1	Level 2	18	Level 2	Level 3	Level 3	Level 3
5	Level 1	Level 2	Level 2	Level 3	19	Level 3	Level 1	Level 1	Level 3
6	Level 1	Level 2	Level 3	Level 1	20	Level 3	Level 1	Level 2	Level 1
7	Level 1	Level 3	Level 1	Level 3	21	Level 3	Level 1	Level 3	Level 2
8	Level 1	Level 3	Level 2	Level 1	22	Level 3	Level 2	Level 1	Level 1
9	Level 1	Level 3	Level 3	Level 2	23	Level 3	Level 2	Level 2	Level 2
10	Level 2	Level 1	Level 1	Level 2	24	Level 3	Level 2	Level 3	Level 3
11	Level 2	Level 1	Level 2	Level 3	25	Level 3	Level 3	Level 1	Level 2
12	Level 2	Level 1	Level 3	Level 1	26	Level 3	Level 3	Level 2	Level 3
13	Level 2	Level 2	Level 1	Level 3	27	Level 3	Level 3	Level 3	Level 1
14	Level 2	Level 2	Level 2	Level 1					

Appendix S. Linear curve fit analysis on experimental data

Test	Single-Line			Bi-linear						Tri-Linear								
	L1		R ²	L1		L2		N _{int} (x10 ³)	R ²	L1		L2		L3		Intermediate points (x10 ³)		R ²
	m (x10 ⁻⁶)	c		m1 (x10 ⁻⁶)	c1	m2 (x10 ⁻⁶)	c2			m1 (x10 ⁻⁶)	c1	m2 (x10 ⁻⁶)	c2	m3 (x10 ⁻⁶)	c3	N _{int1}	N _{int2}	
P1	-0.62	0.636	0.468	-3.56	0.685	-0.03	0.595	26	0.903	-15.51	0.727	-2.10	0.659	0.01	0.591	5	32	0.983
P2	-3.78	1.726	0.771	-11.72	1.871	-1.71	1.579	29	0.967	-52.76	1.996	-8.39	1.810	-1.44	1.558	4	36	0.992
P3	-24.90	3.220	0.732	-130.47	3.618	-15.02	3.014	5	0.956	-249.04	3.726	-50.78	3.323	-10.19	2.905	2	10	0.995
P4	-3.09	1.830	0.559	-14.82	2.029	-0.72	1.663	26	0.900	-86.75	2.240	-7.82	1.910	-0.13	1.618	4	38	0.985
P5	-11.79	3.804	0.800	-29.95	3.984	-4.64	3.552	17	0.980	-58.01	4.066	-20.22	3.873	-3.40	3.503	5	22	0.996
P6	-0.35	0.491	0.468	-25.55	0.564	-0.26	0.486	3	0.860	-25.55	0.564	-0.16	0.482	-1.69	0.612	3	85	0.943
P7	-5.84	3.337	0.926	-12.43	3.454	-4.27	3.226	28	0.987	-28.15	3.533	-8.11	3.367	-4.01	3.205	8	39	0.998
P8	-0.67	0.450	0.642	-25.23	0.545	-0.52	0.440	4	0.959	-30.90	0.551	-1.20	0.454	-0.39	0.431	3	29	0.978
P9	-3.35	1.481	0.795	-28.00	1.689	-2.56	1.427	10	0.956	-49.31	1.736	-5.60	1.513	-1.61	1.356	5	39	0.992
C1	-0.53	0.902	0.308	-13.93	1.005	-0.19	0.878	9	0.852	-39.86	1.045	-2.25	0.927	0.09	0.858	3	29	0.967
C2	-5.42	2.782	0.839	-26.38	3.042	-3.94	2.674	16	0.975	-63.28	3.143	-10.80	2.869	-3.25	2.620	5	33	0.994
C3	-3.91	4.323	0.809	-28.94	4.552	-2.96	4.258	11	0.968	-54.41	4.611	-7.21	4.368	-2.22	4.204	5	33	0.997
C4	-1.72	0.793	0.901	-5.50	0.845	-1.32	0.765	19	0.984	-21.19	0.878	-3.19	0.818	-1.17	0.754	3	32	0.995
C5	-2.94	2.250	0.430	-45.62	2.641	-1.31	2.139	11	0.864	-120.40	2.792	-9.08	2.346	0.21	2.027	4	34	0.979
C6	-8.57	4.001	0.611	-60.59	4.312	-4.02	3.850	8	0.947	-82.33	4.355	-15.13	4.022	-0.95	3.738	5	20	0.992
C7	-0.774	0.698	0.682	-2.89	0.736	-0.28	0.663	28	0.935	-9.21	0.764	-1.33	0.706	-0.08	0.647	7	47	0.987
C8	-4.58	2.125	0.678	-52.57	2.528	-3.07	2.023	10	0.951	-111.88	2.645	-11.24	2.215	-2.12	1.953	4	29	0.992
C9	-16.03	3.716	0.555	-74.88	4.086	-1.90	3.355	10	0.958	-155.97	4.227	-43.70	3.869	0.00	3.302	3	13	0.994

Acronyms: m = gradient, N_{int} = Intermediate point, L = Linear segments

Appendix T. Curve-fitting code for Matlab

%% Description: Curve-fitting analysis code for functional fatigue SMA
%% Inputs: SMA stroke versus Number of cycles data: Data(N,stroke)
%% Outputs: Single, Bi- and Tri- Linear curves
%% Prepared by Jaronie, 14Sep2015

```
clear all; clc; close all;
```

```
Data = 'C1'; %dataset name
```

```
datastr = [Data,'Data'];
```

```
titlestr = [Data,' Results'];
```

```
figstr = Data;
```

```
load(datastr); %Load C1 dataset, consist of 3 responses: C1_R1, C1_R2, and C1_R3
```

```
%#####
```

```
% Generate average data from 3 responses
```

```
Nmin = 1; % 1st cycle number
```

```
Nmax = 100000; % Last cycle number
```

```
Nstep = 1000; % Cycle steps
```

```
%Using interpolate
```

```
xx=[0:Nstep:Nmax]; %Generate cycle steps from Nmin to Nmax
```

```
xx(1,1)=Nmin;
```

```
InterpolateData(:,1)=xx; %Saving the Cycles data into first Column
```

```
nx=(Nmax/Nstep)+1; %number of cycles steps
```

```
% interpolate choices: nearest, linear, spline, pchip, cubic, v5cubic
```

```
% saving interpolated data
```

```
%interpolated from Response1 data into column 2
```

```
InterpolateData(:,2) = interp1(C1_R1(:,1),C1_R1(:,2),xx,'cubic');
```

```
%interpolated from Response2 data into column 3
```

```
InterpolateData(:,3) = interp1(C1_R2(:,1),C1_R2(:,2),xx,'cubic');
```

```
%interpolated from Response3 data into column 4
```

```
InterpolateData(:,4) = interp1(C1_R3(:,1),C1_R3(:,2),xx,'cubic');
```

```
% saving average Data into column 5
```

```
for m = 1:nx
```

```
InterpolateData(m,5) =
```

```
(InterpolateData(m,2)+InterpolateData(m,3)+InterpolateData(m,4))/3;
```

```
end
```

```
% saving smoothed-average data into column 6
```

```
InterpolateData(:,6) = smooth(InterpolateData(:,5),0.5,'moving');
```

```
% NEW average data from 3 responses into new x1 and y1 tables
```

```
x1 = InterpolateData(:,1);
```

```
y1 = InterpolateData(:,6);
```

```
nx = size(x1,1);
```

```
%#####
```

```

%%%%% single linear
s1 = polyfit(x1,y1,1);
s1_fit = s1(1)*x1 + s1(2);

%R-Square
s1_resid = y1 - s1_fit;
SS_resid_s1 = sum(s1_resid.^2);
SS_total_s1 = (length(y1)-1)*var(y1);
Rsquare_s1 = 1 - (SS_resid_s1/SS_total_s1);
s1(1,3) = Rsquare_s1; %R-Square for single line
%%%%%

%#####
%%% bi-linear
%Prelocate Data Tables
Bi_L1 = x1;
Bi_L2 = x1;
Results = zeros(3,11);

for i=2:nx

    N_intermediate1 = i;

    % 1st line
    x1_bi=x1(1:N_intermediate1);
    y1_bi=y1(1:N_intermediate1);

    p1_bi = polyfit(x1_bi,y1_bi,1);
    y1_fit_bi = p1_bi(1)*x1_bi + p1_bi(2);

    % 2nd Line
    x2_bi=x1(N_intermediate1:end);
    y2_bi=y1(N_intermediate1:end);

    p2_bi = polyfit(x2_bi,y2_bi,1);
    y2_fit_bi = p2_bi(1)*x2_bi + p2_bi(2);

    %R-Square
    y1_resid_bi = y1_bi - y1_fit_bi;
    y2_resid_bi = y2_bi - y2_fit_bi;
    Bi_resid = vertcat(y1_resid_bi,y2_resid_bi);
    Bi_SS_resid = sum(Bi_resid.^2);
    Bi_SS_total = (length(y1)-1)*var(y1);
    Rsquare_bi = 1 - (Bi_SS_resid/Bi_SS_total);

    %RL analysis table
    Bi_TableRL(i,1)= x1(i,1);
    Bi_TableRL(i,2)= Bi_SS_resid;
    Bi_TableRL(i,3)= Bi_SS_total;
    Bi_TableRL(i,4)= Rsquare_bi;

    %Saving data into Bi-Linear Data Tables
    Bi_L1(1:N_intermediate1,N_intermediate1) = y1_fit_bi;
    Bi_L2(N_intermediate1:end,N_intermediate1) = y2_fit_bi;

```



```

Bi_Poly(i,1) = N_intermediate1;
Bi_Poly(i,2) = x1(N_intermediate1,1);
Bi_Poly(i,3) = p1_bi(1);
Bi_Poly(i,4) = p1_bi(2);
Bi_Poly(i,5) = p2_bi(1);
Bi_Poly(i,6) = p2_bi(2);
Bi_Poly(i,7) = Rsquare_bi;

end

%identify the optimum intermediate point for bi-linear
index_int_bi = find(max(Bi_TableRL(:,4))== Bi_TableRL(:,4));
xmax_bi = Bi_TableRL(index_int_bi,1);
ymax_bi = Bi_TableRL(index_int_bi,4);

% #####
% tri-linear
%Prelocate Data Tables
Tri_L1 = x1;
Tri_L2 = x1;
Tri_L3 = x1;

k=1;

for i=2:nx

    N_intermediate1 = i;

    % 1st line
    x1_tri=x1(1:N_intermediate1);
    y1_tri=y1(1:N_intermediate1);

    p1_tri = polyfit(x1_tri,y1_tri,1);
    y1_fit_tri = p1_tri(1)*x1_tri + p1_tri(2);

    % 2nd Line
    for j=N_intermediate1+1:nx
        N_intermediate2 = j;

        x2_tri=x1(N_intermediate1:N_intermediate2);
        y2_tri=y1(N_intermediate1:N_intermediate2);

        p2_tri = polyfit(x2_tri,y2_tri,1);
        y2_fit_tri = p2_tri(1)*x2_tri + p2_tri(2);

        %3rd Line
        x3_tri=x1(N_intermediate2:end);
        y3_tri=y1(N_intermediate2:end);

        p3_tri = polyfit(x3_tri,y3_tri,1);
        y3_fit_tri = p3_tri(1)*x3_tri + p3_tri(2);
    end
end

```

```

%R-Square
y1_resid_tri = y1_tri - y1_fit_tri;
y2_resid_tri = y2_tri - y2_fit_tri;
y3_resid_tri = y3_tri - y3_fit_tri;
Tri_resid = vertcat(y1_resid_tri,y2_resid_tri,y3_resid_tri);
Tri_SS_resid = sum(Tri_resid.^2);
Tri_SS_total = (length(y1)-1)*var(y1);
Rsquare_tri = 1 - (Tri_SS_resid/Tri_SS_total);

```

```

%RL analysis table
Tri_TableRL(k,1)= x1(i,1);
Tri_TableRL(k,2)= x1(j,1);
Tri_TableRL(k,3)= Tri_SS_resid;
Tri_TableRL(k,4)= Tri_SS_total;
Tri_TableRL(k,5)= Rsquare_tri;

```

```

%Saving data into Data Tables
Tri_L1(1:N_intermediate1,k+1) = y1_fit_tri;
Tri_L2(N_intermediate1:N_intermediate2,k+1) = y2_fit_tri;
Tri_L3(N_intermediate2:end,k+1) = y3_fit_tri;

```

```

Tri_Poly(k,1) = N_intermediate1;
Tri_Poly(k,2) = N_intermediate2;
Tri_Poly(k,3) = x1(N_intermediate1,1);
Tri_Poly(k,4) = x1(N_intermediate2,1);
Tri_Poly(k,5) = p1_tri(1);
Tri_Poly(k,6) = p1_tri(2);
Tri_Poly(k,7) = p2_tri(1);
Tri_Poly(k,8) = p2_tri(2);
Tri_Poly(k,9) = p3_tri(1);
Tri_Poly(k,10) = p3_tri(2);
Tri_Poly(k,11) = Rsquare_tri;

```

```

k=k+1;

```

```

end

```

```

end

```

```

%identify the optimum intermediate points for tri-linear
index_int_tri = find(max(Tri_TableRL(:,5))== Tri_TableRL(:,5));
xmax_tri(1,1) = Tri_TableRL(index_int_tri,1);
xmax_tri(1,2) = Tri_TableRL(index_int_tri,2);
ymax_tri = Tri_TableRL(index_int_tri,5);

```

```

% #####
% Plot Results into 3 subplots
figure('name',figstr)
subplot(3,1,1)
plot(x1(:,1),y1(:,1),'r--')
hold on

```

```

%plot single line
plot(x1,s1_fit,'k-', 'lineWidth',2)
hold off
legend('Average','L1','location','northeast')
xlabel('Number of cycles','FontWeight','bold','FontSize',12)
ylabel('Stroke [mm]','FontWeight','bold','FontSize',12);
title([titlestr,': Single line, R^2=',num2str(Rsquare_s1)],'FontWeight','bold','FontSize',14);

%plot bi-linear
subplot(3,1,2)
plot(x1(:,1),y1(:,1),'r--')
hold on
plot(Bi_L1(1:index_int_bi,1),Bi_L1(1:index_int_bi,index_int_bi),'k-', 'lineWidth',2)
plot(Bi_L2(index_int_bi:end,1),Bi_L2(index_int_bi:end,index_int_bi),'k-', 'lineWidth',2)
hold off
legend('Average','L1','L2','location','northeast')
xlabel('Number of cycles','FontWeight','bold','FontSize',12)
ylabel('Stroke [mm]','FontWeight','bold','FontSize',12);
title(['Bi-Linear, R^2=',num2str(Bi_Poly(index_int_bi,7))],'FontWeight','bold','FontSize',14);

%plot tri-linear
subplot(3,1,3)
plot(x1(:,1),y1(:,1),'r--')
hold on
plot(Tri_L1(1:Tri_Poly(index_int_tri,1),1),Tri_L1(1:Tri_Poly(index_int_tri+1,1),index_int_tri+1),'k-', 'lineWidth',2)
plot(Tri_L2(Tri_Poly(index_int_tri,1):Tri_Poly(index_int_tri,2),1),Tri_L2(Tri_Poly(index_int_tri,1):Tri_Poly(index_int_tri,2),index_int_tri+1),'k-', 'lineWidth',2)
plot(Tri_L3(Tri_Poly(index_int_tri,2):end,1),Tri_L3(Tri_Poly(index_int_tri,2):end,index_int_tri+1),'k-', 'lineWidth',2)
hold off
legend('Average','L1','L2','L3','location','northeast')
xlabel('Number of cycles','FontWeight','bold','FontSize',12)
ylabel('Stroke [mm]','FontWeight','bold','FontSize',12);
title(['Tri-Linear, R^2=',num2str(Tri_Poly(index_int_tri,11))],'FontWeight','bold','FontSize',14);

%##### END #####

```

Appendix U. Air properties

Data table for "MATERIAL_DATA.mat"

T [°C]	ρ_D [kg/m ³]	c_p [kJ/kgK]	k [W/mK]	ν [x10 ⁻⁶ m ² /s]	β [x10 ⁻³ K ⁻¹]	Pr
-150	2.793	1.026	0.012	3.08	8.21	0.76
-100	1.980	1.009	0.016	5.95	5.82	0.74
-50	1.534	1.005	0.020	9.55	4.51	0.73
0	1.293	1.005	0.024	13.30	3.67	0.72
20	1.205	1.005	0.026	15.11	3.43	0.71
40	1.127	1.005	0.027	16.97	3.20	0.71
60	1.067	1.009	0.029	18.90	3.00	0.71
80	1.000	1.009	0.030	20.94	2.83	0.71
100	0.946	1.009	0.031	23.06	2.68	0.70
120	0.898	1.013	0.033	25.23	2.55	0.70
140	0.854	1.013	0.034	27.55	2.43	0.70
160	0.815	1.017	0.036	29.85	2.32	0.69
180	0.779	1.022	0.037	32.29	2.21	0.69
200	0.746	1.026	0.039	34.63	2.11	0.69
250	0.675	1.034	0.042	41.17	1.91	0.68
300	0.616	1.047	0.045	47.85	1.75	0.68
350	0.566	1.055	0.049	55.05	1.61	0.68
400	0.524	1.068	0.052	62.53	1.49	0.68
-150	2.793	1.026	0.012	3.08	8.21	0.76